

# **Contractive Annulation — A Strategy for the Synthesis of Small, Strained Cyclophanes**

by

© Sourav Biswas

A thesis submitted to the  
School of Graduate Studies  
in partial fulfillment of the requirements  
for the degree of Doctor of Philosophy

Department of Chemistry

Memorial University

March 2022

St. John's

Newfoundland

*Dedicated to:*

**My Family and Friends**

*Without their support, none of this would have been possible*

## Abstract

Since the inception of cyclophane chemistry, chemists have been fascinated by the pursuit of ever-smaller and more strained cyclophanes owing to the unusual chemical and physical properties that arise in such systems. The strained nature of these systems poses synthetic challenges and the level of challenge escalates with the level of strain in the cyclophanes. As the degree of strain increases, so does the synthetic challenge and a variety of inventive synthetic approaches to small, strained cyclophanes have been developed.

Chapter 1 introduces some important underlying concepts in the area of cyclophane chemistry. A brief summary of different general strategies for the synthesis of cyclophanes is presented. Overall, Chapter 1 serves as a prelude to the subsequent Chapters.

Chapter 2 focuses on the development of a new three-stage strategy (contractive annulation) for the synthesis of highly strained cyclophanes that would be very difficult or impossible to access using existing synthetic approaches. The viability of the contractive annulation strategy has been demonstrated by a nine-step synthesis of a strained [2.1]cyclophane from commercially available [2.2]paracyclophane. X-ray crystallographic analysis of the [2.1]cyclophane pointed toward a strained cyclophane framework. The strained nature of the cyclophane was further corroborated by theoretical calculations.

Chapter 3 describes the results of the two-directional application of the contractive annulation strategy on [2.2]paracyclophane. As revealed by X-ray crystallographic analysis, the product of the two-directional contractive annulation, a [1.1]cyclophane, was found to have a short interplanar distance. The [1.1]cyclophane is the hitherto smallest member of the [m.n]naphthalenophane family. As expected, DFT calculations indicated that the [1.1]cyclophane

is more strained than the [2.1]cyclophane reported in Chapter 2. The emission behavior of the [1.1]cyclophane was tentatively ascribed to an intramolecular excimer formation mechanism.

Chapter 4 describes studies on the synthesis and physical properties of [2.2]paracyclophane/9-alkylfluorene hybrids, wherein a solvent-assisted rearrangement reaction of a [2.2]paracyclophane moiety bearing cyclopentadienone was discovered. The rearrangement could be avoided by generating the cyclopentadienone under mild conditions and using benzyne as dienophiles to afford the targeted cyclophanes. One of the [2.2]paracyclophane/9-alkylfluorene hybrids (containing a triphenylene moiety) was found to exhibit dual fluorescence emission.

Chapter 5 highlights the synthetic utility of two of the intermediates featured in the synthesis of the [2.1]cyclophane in Chapter 2. One of the intermediates was transformed into [2.2]paracyclophane/quinoxaline hybrids over two steps (oxidation/condensation reactions). An attempt to use the other intermediate for a multistep synthesis of a [2.1]cyclophane bearing a perylene moiety failed. However, the last step of the synthesis met with a serendipitous rearrangement reaction under Scholl reaction conditions to afford an unusual [2.1]cyclophane featuring a 1,1'-binaphthalene moiety. Two plausible mechanistic pathways that have resemblance to those of the Scholl reaction have been delineated to account for the formation of the unexpected [2.1]cyclophane.

## Acknowledgements

Firstly, I would like to thank my supervisor, Prof. Dr. Graham J. Bodwell, for giving me the opportunity to join his research group. I would like to convey my sincere gratitude to him for providing me with wonderful projects which I have thoroughly enjoyed. I truly admire his ability to invoke meaningful and insightful discussion on every aspect of organic chemistry, which is indeed very influential. I have been extremely fortunate to have a supervisor who cared so much about my work and who responded to my queries so promptly. He always emphasizes on “paying attention to detail”, which in turn has been very helpful as I have progressed in my program. I would also like to thank Dr. Bodwell for organizing the Summer Organic Chemistry Conference on Everybody's Research (SOCCER) conferences, which gave me opportunities to interact with distinguished professors from other universities.

I express my gratitude to the members of my supervisory committee, Dr. Sunil V. Pansare and Dr. Karen Hattenhauer, for providing me with their valuable comments and suggestions during supervisory committee meetings. I would also like to extend my thanks to Dr. Yuming Zhao for his scientific discussions and research collaboration. I would also like to appreciate Dr. Huck K. Grover for his fruitful suggestions during the past “Grover–Bodwell” group meetings.

I would like to thank the present and former members of the Bodwell group for their immense help during my PhD studies. Specially, I would like to thank Dr. Parisa Ghods Ghasemabadi (former member) for guiding me in my initial days to complete essential paperwork before starting lab work. Thanks to Dr. Joshua C. Walsh (former member) for often bringing up interesting topics, which led to invigorating discussions. Sometimes, these discussions helped me to easily identify some of my weaknesses (some of the basic concepts in organic chemistry) and made me brush up on the fundamentals. I really admire the teaching skills of Dr. Marc R.

MacKinnon (former member), who was always energetic and confident while explaining science. I would also like to thank Mr. Simon D. Brake (current member), who taught me how to maintain a lab notebook properly. We had a lot of fun in the lab, which helped to alleviate stress and motivate me. I would also to extend my gratitude to Mr. Ryan N. Warren (current member) for taking care of our group so nicely. Support from group members of other laboratories at Memorial University of Newfoundland is greatly appreciated.

The services of C-CART and CREAT at Memorial University of Newfoundland that are indispensable to the progress of research are greatly appreciated. I would like to thank Dr. Celine Schneider (NMR analysis), Dr. Stefana Egli (mass spectral analysis), and Dr. Jian-Bin Lin (X-ray crystallography) for their assistance in the characterization of the compounds presented in this thesis. The financial support from the School of Graduate Studies (SGS), Chemistry Department, and the Natural Sciences and Engineering Research Council of Canada (NSERC) is gratefully acknowledged.

Finally, I would like to convey my respect and gratitude to my parents. Without their support, I could not have completed my doctoral work. I express my love and admiration to my girlfriend, Ms. Sanghita Biswas, for her continual companionship and support. I would also like to thank my friends, Dr. Ayan Dasgupta, Mr. Sankarsan Biswas, and Mr. Anupam Das, for guiding me in the right direction during my PhD program. I would also like to thank my cousin, Mr. Santu Mandal, for welcoming me to Canada and helping me find accommodation in St. John's, NL. I can not thank my former and current housemates enough for their help whenever needed.

## Table of Contents

|                                   |  |      |
|-----------------------------------|--|------|
| Dedication                        |  | ii   |
| Abstract                          |  | iii  |
| Acknowledgements                  |  | v    |
| Table of Contents                 |  | vii  |
| List of Figures                   |  | xiii |
| List of Schemes                   |  | xvi  |
| List of Tables                    |  | xxi  |
| List of Abbreviations and Symbols |  | xxii |
| <br>                              |  |      |
| Chapter 1                         | Introduction   | 1    |
| 1.1                               | Cyclophane Chemistry   | 1    |
|                                   | 1.1.1 General Synthetic Strategies for the Synthesis of Cyclophanes                                    | 2    |
| 1.2                               | [ <i>n</i> ]Cyclophanes  | 4    |
|                                   | 1.2.1 [ <i>n</i> ]Paracyclophanes  | 5    |
|                                   | 1.2.2 [ <i>n</i> ]Metacyclophanes  | 7    |
|                                   | 1.2.3 Bending an Aromatic System   | 8    |
|                                   | 1.2.3.1 Bend Angles  | 8    |
|                                   | 1.2.3.2 Strain Energy  | 9    |
|                                   | 1.2.4 Synthesis of [ <i>n</i> ]Para- and [ <i>n</i> ]Metacyclophanes Utilizing Different Strategies    | 9    |
|                                   | 1.2.4.1 Synthesis of [ <i>n</i> ]Para- and [ <i>n</i> ]Metacyclophanes Utilizing the Type I Strategies | 10   |

|           |         |   |    |
|-----------|---------|---|----|
|           | 1.2.4.2 | Synthesis of an $[n]$ Paracyclophane Utilizing the Type II Strategy   | 13 |
|           | 1.2.4.3 | Synthesis of $[n]$ Para- and $[n]$ Metacyclophanes Utilizing the Type III Strategy  | 14 |
| 1.3       |         | $[m.n]$ Cyclophanes   | 18 |
|           | 1.3.1   | $[2.2]$ Paracyclophane  | 20 |
|           | 1.3.2   | Nomenclature and Stereochemical Descriptors for Chiral $[2.2]$ Paracyclophane Derivatives   | 20 |
|           | 1.3.3   | Transannular Interactions   | 23 |
|           | 1.3.4   | <i>pseudo-gem</i> Directing Effect  | 27 |
|           | 1.3.5   | Synthesis of $[m.n]$ Cyclophanes  | 30 |
|           | 1.3.5.1 | Synthesis of $[m.n]$ Cyclophanes Utilizing Type I Strategies  | 30 |
|           | 1.3.5.2 | Synthesis of $[m.n]$ Cyclophanes Utilizing the Type II Strategy   | 33 |
|           | 1.3.5.3 | Synthesis of $[m.n]$ Cyclophanes Utilizing the Type III Strategy  | 35 |
| 1.4       |         | Summary   | 38 |
| 1.5       |         | References  | 39 |
| Chapter 2 |         | Contractive Annulation: A Strategy for the Synthesis of Small, Strained Cyclophanes and Its Application in the Synthesis of $[2](6,1)$ Naphthaleno $[1]$ paracyclophane | 44 |

|           |   |     |
|-----------|---|-----|
| 2.1       | Introduction  | 45  |
| 2.2       | Objective   | 46  |
| 2.3       | Results and Discussion  | 47  |
| 2.3.1     | Synthesis   | 48  |
| 2.3.1.1   | First Attempted Route toward the Synthesis of<br>[2](6,1)Naphthaleno[1]paracyclophane ( <b>2.12</b> )               | 53  |
| 2.3.1.2   | Successful Synthesis of<br>[2](6,1)Naphthaleno[1]paracyclophane ( <b>2.12</b> )                                     | 58  |
| 2.3.2     | X-Ray Crystallographic Analysis   | 62  |
| 2.3.3     | Strain Energy (SE) and Nucleus-Independent Chemical Shifts<br>(NICS) Calculations by Computational Methods          | 65  |
| 2.3.4     | NMR Analysis  | 66  |
| 2.3.5     | UV/Vis Absorption and Fluorescence Spectroscopy   | 69  |
| 2.4       | Conclusions   | 71  |
| 2.5       | Experimental Section  | 71  |
| 2.6       | References  | 94  |
|           | Appendix 1  | 98  |
| Chapter 3 | Synthesis of [1](1,6)Naphthaleno[1](1,6)naphthalenophane by Double<br>Contractive Annulation of [2.2]Paracyclophane | 142 |
| 3.1       | Introduction  | 143 |
| 3.2       | Objective   | 143 |
| 3.3       | Results and Discussion  | 145 |

|            |   |     |
|------------|---|-----|
| 3.3.1      | Synthesis   | 145 |
| 3.3.2      | X-Ray Crystallographic Analysis   | 155 |
| 3.3.3      | Density Functional Theory (DFT) Calculations  | 157 |
| 3.3.4      | NMR Analysis  | 161 |
| 3.3.5      | UV/Vis Absorption and Fluorescence Spectroscopy   | 163 |
| 3.3.6      | Cyclic Voltammetry  | 165 |
| 3.4        | Conclusions   | 166 |
| 3.5        | Experimental Section  | 167 |
| 3.6        | References  | 180 |
| Appendix 2 |   | 182 |
|            |   |     |
| Chapter 4  | Synthesis of [2.2]Paracyclophane/9-Alkylfluorene Hybrids and the<br>Discovery of a Solvent-assisted Rearrangement | 240 |
| 4.1        | Introduction  | 241 |
| 4.2        | Objective   | 243 |
| 4.3        | Results and Discussion  | 244 |
| 4.3.1      | Synthesis   | 244 |
| 4.3.2      | Reaction Mechanism of the Rearrangement of Cyclopentadienone<br><b>4.11</b> to Cyclophane <b>4.18</b>             | 253 |
| 4.3.3      | X-Ray Crystallographic Analysis   | 258 |
| 4.3.4      | NMR Analysis  | 258 |
| 4.3.5      | UV/Vis Absorption and Fluorescence Spectroscopy   | 262 |
| 4.4        | Conclusions   | 264 |

|            |   |     |
|------------|---|-----|
| 4.5        | Experimental Section  | 266 |
| 4.6        | References  | 278 |
| Appendix 3 |   | 282 |
|            |   |     |
| Chapter 5  | Synthetic Utility of a [2.2]Paracyclophane-derived Tetralone and Indanone                 | 340 |
| 5.1        | Introduction  | 340 |
| 5.2        | Objective   | 341 |
| 5.3        | Results and Discussion  | 344 |
| 5.3.1      | Synthesis   | 345 |
| 5.3.1.1    | Attempted Synthesis of Cyclophane <b>5.9</b>  | 345 |
| 5.3.1.2    | Synthesis of Quinoxalines <b>5.14a</b> and <b>5.27</b>                                    | 346 |
| 5.3.1.3    | Attempted Synthesis of Benzopentalenophanes <b>5.18</b><br>and <b>5.19</b>                | 348 |
| 5.3.2      | Proposed Reaction Mechanisms  | 350 |
| 5.3.2.1    | Proposed Mechanism for the Formation of Cyclophane<br><b>5.25</b> under Scholl Conditions | 350 |
| 5.3.2.2    | Proposed Mechanism for the Formation of Cyclophane<br><b>5.31</b> under Acidic Conditions | 353 |
| 5.3.3      | X-Ray Crystallographic Analysis   | 353 |
| 5.3.4      | NMR Analysis  | 355 |
| 5.4        | Future Outlook  | 356 |
| 5.5        | Conclusions   | 359 |
| 5.6        | Experimental Section  | 359 |



## List of Figures

|                    |   |    |
|--------------------|---|----|
| <b>Figure 1.1</b>  | [ <i>n</i> ]Cyclophanes with different bridging patterns  | 1  |
| <b>Figure 1.2</b>  | A few selected examples of cyclophanes  | 2  |
| <b>Figure 1.3</b>  | Structures of [ <i>n</i> ]metacyclophanes <b>1.17–1.20</b> , <b>1.22–1.24</b> , and dimer <b>1.21</b>   | 7  |
| <b>Figure 1.4</b>  | Bend angles in a [ <i>n</i> ]paracyclophane (left) and a [ <i>n</i> ]metacyclophane (right)   | 9  |
| <b>Figure 1.5</b>  | [ <i>m.n</i> ]Cyclophanes with different bridging patterns  | 19 |
| <b>Figure 1.6</b>  | Transannular distances in [2.2]paracyclophane ( <b>1.4</b> )  | 20 |
| <b>Figure 1.7</b>  | Mono- and disubstituted chiral [2.2]paracyclophane derivatives <b>1.66–1.75</b>   | 22 |
| <b>Figure 1.8</b>  | Numbering for the [2.2]paracyclophane backbone and stereochemical descriptors for [2.2]paracyclophane derivatives   | 23 |
| <b>Figure 1.9</b>  | Structures of [4.4]paracyclophane ( <b>1.77</b> ) and [6.6]paracyclophane ( <b>1.78</b> )   | 24 |
| <b>Figure 1.10</b> | Selected example of a planar chiral [2.2]paracyclophane-based ligand  | 30 |
| <b>Figure 2.1</b>  | Two views of naphthalenophane <b>2.12</b> in the crystal with 50% displacement ellipsoids   | 63 |
| <b>Figure 2.2</b>  | Structures of comparison compounds <b>2.47–2.49</b>   | 64 |
| <b>Figure 2.3</b>  | Strain energies of <b>2.11–2.12</b> and NICS values for <b>2.12</b>   | 66 |
| <b>Figure 2.4</b>  | 300 MHz <sup>1</sup> H NMR spectrum of <b>2.12</b> in CDCl <sub>3</sub>   | 66 |
| <b>Figure 2.5</b>  | Experimental (blue) and calculated (red) [M06-2X/6-311+G(2d,p)] chemical shifts for cyclophanes <b>2.11</b> , <b>2.12</b> , and <b>2.13</b>   | 69 |
| <b>Figure 2.6</b>  | (A) Normalized UV/vis absorption spectra of <b>2.12</b> measured in different organic solvents, and TD-M06-2X/Def2TZVP calculated absorption spectrum of (red bar graph). (B) Contour plots and eigenvalues of frontier | 70 |

molecular orbitals of **2.12** (M06-2X/Def2TZVP). (C) Fluorescence spectra of **2.12** in CH<sub>2</sub>Cl<sub>2</sub> ( $\lambda_{\text{exc}} = 350$  nm)

- Figure 3.1** Four views of the structure of [1.1]naphthalenophane **3.3** with 50% displacement ellipsoids. CCDC 2105261 contains the crystallographic data for **3.3** 157
- Figure 3.2** (A) MEP map of **3.3**. (B) Non-covalent interaction (NCI) plot of **3.3** (isovalue = 0.50 a.u.). Calculations were performed at the M06-2x/Def2SVP level of theory 158
- Figure 3.3** DFT-calculated NICS values for the naphthalene units in **3.3**, **3.32**, and **3.33** 159
- Figure 3.4** Numbering of the protons in [1.1]naphthalenophane **3.3** 162
- Figure 3.5** 300 MHz <sup>1</sup>H NMR spectrum of **3.3** in CDCl<sub>3</sub> 163
- Figure 3.6** (A) UV/vis absorption and fluorescence ( $\lambda_{\text{exc}} = 350$  nm,  $\Phi_{\text{F}} = 0.033$ ) spectra of **3.3** measured in cyclohexane. TD-DFT simulated UV/vis spectrum (red color bar graph) calculated at the M06/Def2-TZVPP level (cyclohexane). (B) Contour plots for FMOs of **3.3** calculated at M06-2X/Def2SVP level 164
- Figure 3.7** Cyclic voltammograms of (A) 1,6-dimethylnaphthalene (**3.32**) and (B) [1.1]naphthalenophane **3.3** measured in CH<sub>3</sub>CN. Experimental conditions: electrolyte: *n*-Bu<sub>4</sub>NBF<sub>4</sub>, 0.1 M, working electrode: glassy carbon, reference electrode: Ag/AgCl, counter electrode: Pt wire. Scan rate = 0.5 V/s 165
- Figure 4.1** Recently reported PAHs **4.1–4.3** synthesized using the Diels–Alder / Scholl approach 241
- Figure 4.2** Aromatic regions ( $\delta_{\text{H}} = 8.0\text{--}5.9$  ppm and  $\delta_{\text{C}} = 137\text{--}123$  ppm) of the HSQC spectrum of cyclophane **4.18** 245

- Figure 4.3** Optimized geometries of **TS-1**, **TS-2**, **IM-1**, and **TS-3** and energy profiles 257  
for the potential energy surface of the ethanol-assisted rearrangement  
pathway in the gas phase (red) and in ethanol (blue)
- Figure 4.4** Crystal structures of cyclophanes **4.11**, **4.20**, and **4.22** with 50% 260  
displacement ellipsoids
- Figure 4.5** VT-NMR (500 MHz, C<sub>2</sub>D<sub>2</sub>Cl<sub>4</sub>) spectra of cyclophane **4.22** (aromatic and 262  
methine protons)
- Figure 4.6** Normalized electronic absorption spectra of **4.18** (red solid line), **4.11** 264  
(black solid line), **4.20** (blue solid line) and **4.22** (solid green line) in  
dichloromethane, and emission spectra of **4.20** (blue broken line) and **4.22**  
(green broken line) in dichloromethane ( $\lambda_{\text{exc}}$  (**4.20**) = 320 nm;  $\lambda_{\text{exc}}$  (**4.22**) =  
350 nm)
- Figure 5.1** X-ray crystal structure of **5.25** (non-hydrogen atoms are represented by 354  
displacement ellipsoids at the 50% probability level)

## List of Schemes

|                    |   |    |
|--------------------|---|----|
| <b>Scheme 1.1</b>  | Strategies for the synthesis of cyclophanes   | 3  |
| <b>Scheme 1.2</b>  | Structures of [ <i>n</i> ]paracyclophanes ( <i>n</i> = 4–6) <b>1.10</b> , <b>1.15</b> , and <b>1.16</b> ; valence isomerization of <b>1.9</b> and <b>1.14</b> to <b>1.10</b> and <b>1.15</b> , respectively | 6  |
| <b>Scheme 1.3</b>  | Synthesis [10]paracyclophane ( <b>1.28</b> ) by Cram and co-workers. Inset: failed Wurtz coupling for the generation of [8]paracyclophane ( <b>1.30</b> )   | 10 |
| <b>Scheme 1.4</b>  | Synthesis [8]metacyclophane ( <b>1.34</b> ) by Hubert and Dale  | 11 |
| <b>Scheme 1.5</b>  | Syntheses of [8]paracyclophane <b>1.38</b> and [7]paracyclophane <b>1.39</b> by Allinger and co-workers   | 12 |
| <b>Scheme 1.6</b>  | Synthesis of [7]metacyclophane ( <b>1.41</b> ) by Misumi and co-workers   | 12 |
| <b>Scheme 1.7</b>  | Synthesis of [7]paracyclophane ( <b>1.48</b> ) by Jones Jr. and co-workers  | 13 |
| <b>Scheme 1.8</b>  | Synthesis of [5]paracyclophane ( <b>1.15</b> ) and its rearrangement to benzocycloheptene ( <b>1.50</b> ) by Bickelhaupt, Tobe, and co-workers  | 15 |
| <b>Scheme 1.9</b>  | Trifluoroacetic acid-catalyzed rearrangement of [6]paracyclophane ( <b>1.16</b> )   | 15 |
| <b>Scheme 1.10</b> | Synthesis of [4]paracyclophane derivative <b>1.57</b> by Tsuji and co-workers   | 17 |
| <b>Scheme 1.11</b> | Synthesis of 8,11-dichloro[5]metacyclophane ( <b>1.62</b> ) by Bickelhaupt and co-workers   | 18 |
| <b>Scheme 1.12</b> | Complexation of AlCl <sub>3</sub> with monoacetylated paracyclophanes <b>1.79</b> , <b>1.83</b> , and <b>1.85</b>   | 25 |
| <b>Scheme 1.13</b> | The <i>pseudo-gem</i> effect in bromination of 4-methoxycarbonyl[2.2]paracyclophane ( <b>1.87</b> )   | 28 |
| <b>Scheme 1.14</b> | Synthesis of <i>pseudo-gem</i> diamine <b>1.95</b>  | 28 |

|                    |  |    |
|--------------------|--|----|
| <b>Scheme 1.15</b> | Synthesis of [2.2.2](1,2,4)cyclophane ( <b>1.100</b> ) from 4-acetyl[2.2]paracyclophane ( <b>1.79</b> )  | 29 |
| <b>Scheme 1.16</b> | Synthesis of [2.2]naphthalenophane <b>1.103</b> by Baker and co-workers  | 30 |
| <b>Scheme 1.17</b> | Synthesis of [2.2](3,11)dibenzo[ <i>c,l</i> ]chrysenophane ( <b>1.108</b> ) by Matsubara and co-workers. Inset: conversion of cyclophanediene <b>1.110</b> to infinitene <b>1.111</b> under photochemical conditions | 32 |
| <b>Scheme 1.18</b> | Synthesis of [3.3]cyclophane <b>1.119</b> by Bodwell and co-workers  | 34 |
| <b>Scheme 1.19</b> | Synthesis of [3.3]metacyclophane ( <b>1.124</b> ) by Semmelheck and co-workers   | 35 |
| <b>Scheme 1.20</b> | Synthesis of [1.1]paracyclophane ( <b>1.133</b> ) by Tsuji and co-workers  | 36 |
| <b>Scheme 1.21</b> | 8-Step synthesis of [1.1]paracyclophane <b>1.134</b> by Tsuji and co-workers   | 38 |
| <b>Scheme 2.1</b>  | Existing aromatization-based approach to the syntheses of highly strained cyclophanes and selected examples of its use   | 45 |
| <b>Scheme 2.2</b>  | Contractive annulation strategy for simultaneously growing the aromatic component of a cyclophane and contracting its bridge   | 47 |
| <b>Scheme 2.3</b>  | Contractive annulation of [2.2]paracyclophane ( <b>2.11</b> )  | 47 |
| <b>Scheme 2.4</b>  | Synthesis of indanone <b>2.19</b> from [2.2]paracyclophane ( <b>2.11</b> )   | 50 |
| <b>Scheme 2.5</b>  | Preparation of $\alpha$ -diazoketone <b>2.23</b> from 4-acetyl[2.2]paracyclophane ( <b>2.13</b> )  | 51 |
| <b>Scheme 2.6</b>  | Conversion of indanone <b>2.19</b> to methylindene <b>2.27</b>   | 53 |
| <b>Scheme 2.7</b>  | Synthesis of diol <b>2.33</b> from indanone <b>2.19</b>  | 56 |
| <b>Scheme 2.8</b>  | Acid-catalyzed ring opening reaction leading to <b>2.36</b> and <b>2.37</b> . Inset: mechanism for the ring opening reaction   | 58 |

|                    |  |     |
|--------------------|--|-----|
| <b>Scheme 2.9</b>  | 4-Step synthesis of dihydronaphthalene <b>2.46</b> from indanone <b>2.19</b>   | 59  |
| <b>Scheme 2.10</b> | Monitoring the progress of the dehydrogenation of <b>2.46</b> by <sup>1</sup> H NMR spectroscopy   | 60  |
| <b>Scheme 3.1</b>  | Contractive annulation for the synthesis of [2](6,1)naphthaleno[1]paracyclophane ( <b>3.2</b> )  | 143 |
| <b>Scheme 3.2</b>  | Possible products from the double contractive annulation of [2.2]paracyclophane ( <b>3.1</b> ). Inset: selected examples of [1.1]paracyclophanes   | 145 |
| <b>Scheme 3.3</b>  | 4-Step synthesis of diacetyl[2.2]paracyclophane <b>3.14</b> from [2.2]paracyclophane ( <b>3.1</b> ). Inset: structures of dibromo[2.2]paracyclophanes <b>3.15–3.17</b> , and 4-acetyl[2.2]paracyclophane ( <b>3.18</b> ) | 147 |
| <b>Scheme 3.4</b>  | Synthesis of the key intermediate <b>3.21</b> from diacetyl[2.2]paracyclophane <b>3.14</b>   | 148 |
| <b>Scheme 3.5</b>  | Synthesis of bis(dihydronaphthalene) <b>3.26</b> from bis(indanone) <b>3.21</b> over four steps. Inset: structure of diketone <b>3.27</b>  | 150 |
| <b>Scheme 3.6</b>  | Attempted cycloaddition of [1.1]naphthalenophane <b>3.3</b> . Inset: formation of cage hydrocarbon <b>3.31</b> from [2.2]naphthalenophane <b>3.30</b> under photochemical conditions                                     | 155 |
| <b>Scheme 4.1</b>  | Double aldol condensation of 2,3-butanedione ( <b>4.4</b> ) with 1,3-diphenylacetone ( <b>4.5</b> )  | 243 |
| <b>Scheme 4.2</b>  | Intended synthesis of [2.2]paracyclophane-PAH hybrid <b>4.15</b>   | 244 |
| <b>Scheme 4.3</b>  | Serendipitous synthesis of cyclophane <b>4.18</b>  | 246 |

|                    |  |     |
|--------------------|--|-----|
| <b>Scheme 4.4</b>  | Two-step conversion of dione <b>4.10</b> to cyclophane <b>4.18</b>   | 248 |
| <b>Scheme 4.5</b>  | Attempted synthesis of fluorene-containing cyclophane <b>4.14</b>  | 248 |
| <b>Scheme 4.6</b>  | Reactions of cyclopentadienone <b>4.11</b> with <i>in-situ</i> generated arynes  | 249 |
| <b>Scheme 4.7</b>  | Hopf and co-workers' attempt to synthesize nanographenophane <b>4.24</b>   | 251 |
| <b>Scheme 4.8</b>  | Attempted synthesis of compound <b>4.33</b>  | 253 |
| <b>Scheme 4.9</b>  | Initially considered mechanism for the formation of cyclophane <b>4.18</b><br>under aldol condensation conditions  | 254 |
| <b>Scheme 4.10</b> | Control experiment with dione <b>4.10</b> and 2-phenylacetophenone ( <b>4.43</b> ) to<br>shed light on the mechanism of the formation of cyclophane <b>4.18</b>  | 255 |
| <b>Scheme 4.11</b> | Different pathways for the rearrangement of cyclopentadienone <b>4.11</b> to<br>cyclophane <b>4.18</b>   | 256 |
| <b>Scheme 5.1</b>  | Scholl reaction of 1,1'-binaphthalene ( <b>5.1</b> ) for the synthesis of perylene<br>( <b>5.2</b> ). Inset: structure of the perylene bisimide (PBI) unit   | 341 |
| <b>Scheme 5.2</b>  | Intended synthesis of [2](1,4)perylene[1]paracyclophane <b>5.9</b>   | 342 |
| <b>Scheme 5.3</b>  | Proposed route to [2.2]paracyclophane/quinoxaline hybrids <b>5.14</b>  | 343 |
| <b>Scheme 5.4</b>  | Proposed synthesis of benzopentalenophanes. Inset: structures of<br>pentalene ( <b>5.20</b> ), benzopentalene ( <b>5.21</b> ), and dibenzo[ <i>a,e</i> ]pentalene<br>( <b>5.22</b> ), and pentalenes <b>5.23</b> and <b>5.24</b> | 344 |
| <b>Scheme 5.5</b>  | Serendipitous synthesis of cyclophane <b>5.25</b> over three steps from $\alpha$ -<br>tetralone <b>5.4</b>   | 346 |
| <b>Scheme 5.6</b>  | Successful and attempted condensation reactions of dione <b>5.13</b> with<br>different diamines  | 347 |

- Scheme 5.7** Three-step transformation of allenyl aryl ketone **5.28** into 349  
dibenzopentalenes **5.30** by Miao, Ren, and co-workers
- Scheme 5.8** Reduction of cyclophane **5.16** followed by attempted Wagner–Meerwein 350  
rearrangement under Brønsted/Lewis acidic conditions
- Scheme 5.9** Proposed pathways for the formation of cyclophane **5.25** under Scholl 352  
conditions
- Scheme 5.10** Possible mechanism for the formation of cyclophane **5.31** from 353  
cyclophane **5.17** in the presence of *p*-TsOH
- Scheme 5.11** Potential utility of dihydronaphthalene **5.6** for the synthesis of 358  
[2.1]cyclophanes **5.43a–b** and **5.46a–d** over two steps. Inset: numbering  
for pyrene (**5.47**)

## List of Tables

|                  |  |     |
|------------------|--|-----|
| <b>Table 1.1</b> | Substituent-dependent chemical shifts of the aromatic protons in 4-substituted [2.2]paracyclophane derivatives | 26  |
| <b>Table 2.1</b> | Optimization of C–H insertion reaction conditions  | 52  |
| <b>Table 2.2</b> | Screening of reaction conditions for the dehydrogenation of dihydronaphthalene <b>2.46</b>                     | 62  |
| <b>Table 2.3</b> | Experimentally determined values of $\alpha$ , $\beta$ and $\alpha+\beta$ for <b>2.12</b>                      | 64  |
| <b>Table 3.1</b> | Conditions screened for the dehydrogenation of hydrocarbon <b>3.26</b>   | 152 |
| <b>Table 3.2</b> | Comparison of the NICS values for compounds <b>3.3</b> , <b>3.32</b> , and <b>3.33</b>                         | 161 |
| <b>Table 4.1</b> | Attempted Scholl and photocyclization reactions for the synthesis of cyclophane <b>4.15</b>                    | 250 |
| <b>Table 5.1</b> | Experimentally determined values of $\alpha$ , $\beta$ and $\alpha+\beta$ for <b>5.25</b>                      | 355 |

## List of Abbreviations and Symbols

|            |   |
|------------|---|
| Ac         | acetyl                                    |
| ASE        | aromatic stabilization energy             |
| APPI       | atmospheric pressure photo ionization     |
| °C         | degree centigrade                         |
| <i>ca.</i> | circa                                     |
| calcd      | calculated                                |
| CIP        | Cahn–Ingold–Prelog                        |
| cm         | centimeter(s)                             |
| COSY       | correlation spectroscopy                  |
| CPL        | circularly polarized luminescence         |
| d          | doublet                                   |
| DBU        | 1,8-diazabicyclo[5.4.0]undec-7-ene        |
| 1,2-DCE    | 1,2-dichloroethane                        |
| DDQ        | 2,3-dichloro-5,6-dicyano-1,4-benzoquinone |
| DFT        | density functional theory                 |
| DMAD       | dimethyl acetylenedicarboxylate           |
| DMF        | <i>N,N</i> -dimethylformamide             |
| DMSO       | dimethyl sulfoxide                        |
| Et         | ethyl                                     |
| EWG        | electron withdrawing group                |
| equiv      | equivalent(s)                             |
| g          | gram(s)                                   |

|                  |   |
|------------------|---|
| $G^\ddagger$     | free energy of activation               |
| H                | hour(s)                                 |
| HMBC             | heteronuclear multiple bond correlation |
| $^1\text{H}$ NMR | proton nuclear magnetic resonance       |
| HOMO             | highest occupied molecular orbital      |
| HRMS             | high-resolution mass spectroscopy       |
| HSQC             | heteronuclear single quantum coherence  |
| Hz               | Hertz                                   |
| IEDDA            | inverse electron demand Diels–Alder     |
| $J$              | coupling constant (Hz) (in NMR)         |
| K                | degrees Kelvin                          |
| kcal             | kilocalorie                             |
| LDA              | lithium diisopropylamine                |
| LiHMDS           | lithium hexamethyldisilazide            |
| LUMO             | lowest unoccupied molecular orbital     |
| m                | multiplet                               |
| <i>m-</i>        | <i>meta</i>                             |
| MEP              | molecular electrostatic potential       |
| mg               | milligram(s)                            |
| mL               | milliliter(s)                           |
| mmHg             | millimetres of mercury                  |
| min              | minute(s)                               |
| mp               | melting point                           |

|            |   |
|------------|---|
| Me         | methyl  |
| MO         | molecular orbital                               |
| mol        | mole(s)   |
| MHz        | megahertz                                       |
| $m/z$      | mass to charge ratio                            |
| NBO        | natural bond orbital                            |
| nm         | nanometer(s)                                    |
| NMR        | nuclear magnetic resonance                      |
| NOESY      | nuclear Overhauser effect spectroscopy          |
| NICS       | nucleus-independent chemical shift              |
| <i>p</i> - | <i>para</i>                                     |
| PBI        | perylene bisimide                               |
| PCC        | pyridinium chlorochromate                       |
| PAH        | polynuclear aromatic hydrocarbon                |
| Pd/C       | palladium/charcoal                              |
| Ph         | phenyl  |
| $pK_a$     | acid dissociation constant at logarithmic scale |
| ppm        | parts per million                               |
| rt         | room temperature                                |
| q          | quartet   |
| $R_f$      | retention factor                                |
| RDG        | reduced density gradient                        |
| s          | singlet   |

|                |   |
|----------------|---|
| $SE$           | strain energy                                   |
| $S_N2$         | bimolecular substitution nucleophilic           |
| $T_c$          | coalescence temperature                         |
| TCNE           | tetracyanoethylene                              |
| $t_{1/2}$      | half-life                                       |
| TLC            | thin-layer chromatography                       |
| Tf             | trifluoromethanesulfonyl                        |
| Ts             | 4-toluenesulfonyl or tosyl                      |
| TD-DFT         | time-dependent density functional theory        |
| THF            | tetrahydrofuran                                 |
| THF- $d_8$     | deuterated THF                                  |
| TFA            | trifluoroacetic acid                            |
| TPP            | tetraphenylporphyrin                            |
| UV/vis         | ultraviolet visible                             |
| VT-NMR         | variable temperature nuclear magnetic resonance |
| $\delta$       | chemical shift                                  |
| $\Delta\delta$ | difference in chemical shift                    |
| $\Delta\nu_0$  | difference in frequency at $T_c$                |
| $\phi$         | fluorescence quantum yield                      |

## Chapter 1: Introduction

### 1.1 Cyclophane Chemistry

Cyclophanes are a diverse class of molecules consisting of one or more aromatic units (*e.g.* benzene) bridged by one or more aliphatic units, wherein the aliphatic part connects two non-adjacent positions of the aromatic ring. In the case of benzene, two bridging patterns are possible, namely *para* (1,4) and *meta* (1,3) (Figure 1.1). The *ortho* (1,2) bridging pattern can be viewed as ring fusion, so orthocyclophanes do not normally appear in the discussions of cyclophane chemistry. The scope of cyclophane chemistry is limitless because a cyclophane can possess any type and any number of aromatic rings, as well as multiple bridges of any length and atom type.<sup>1</sup>

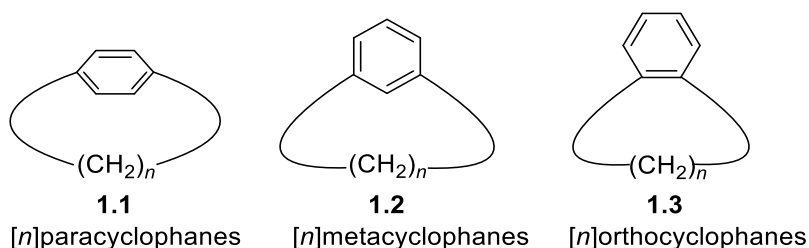


**Figure 1.1:** [*n*]Cyclophanes with different bridging patterns.

The isolation of [2.2]paracyclophane (**1.4**), the quintessential cyclophane, by Brown and Farthing in 1949 and Cram's ensuing cogent synthesis marked the dawn of cyclophane chemistry.<sup>2,3</sup> Since its inception, cyclophane chemistry has attracted a great deal of attention from the synthetic community for several reasons, including, aesthetically pleasing and unusual structures, synthetic challenges, the emergence of unusual physical and chemical properties as a result of strain and nonplanarity in the aromatic systems, and opportunities to study rudimentary phenomena, such as aromaticity, conformational behaviour, host-guest interactions,  $\pi$ - $\pi$  interactions *etc.* To briefly illustrate the structural diversity, a few selected examples of cyclophanes (**1.4–1.8**) are depicted in Figure 1.2.<sup>4</sup>

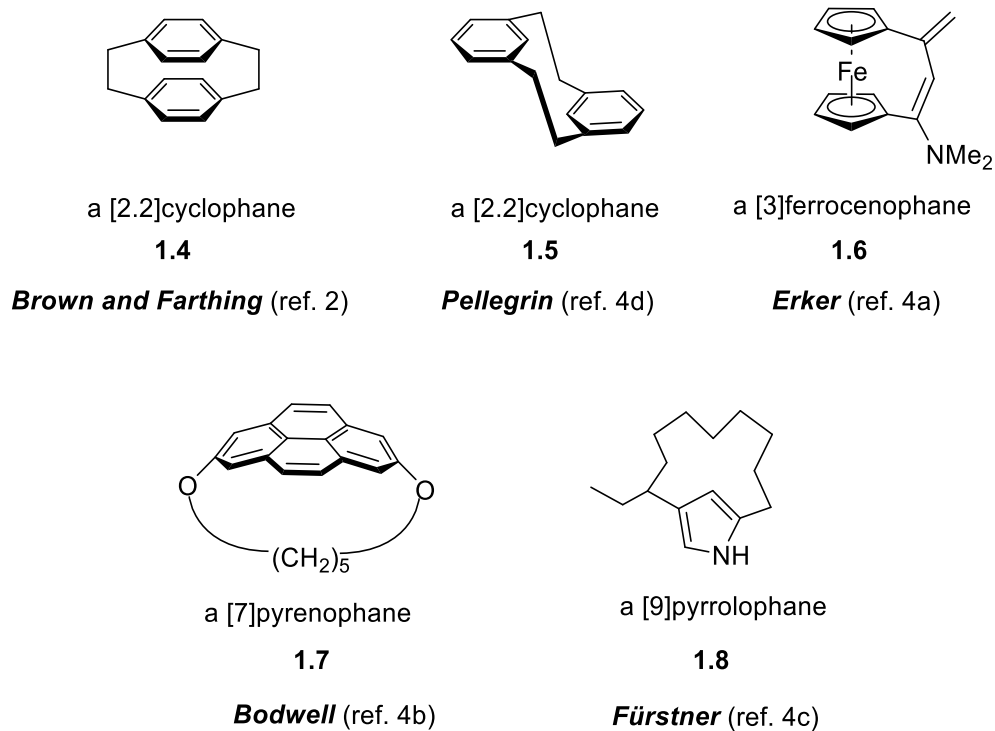
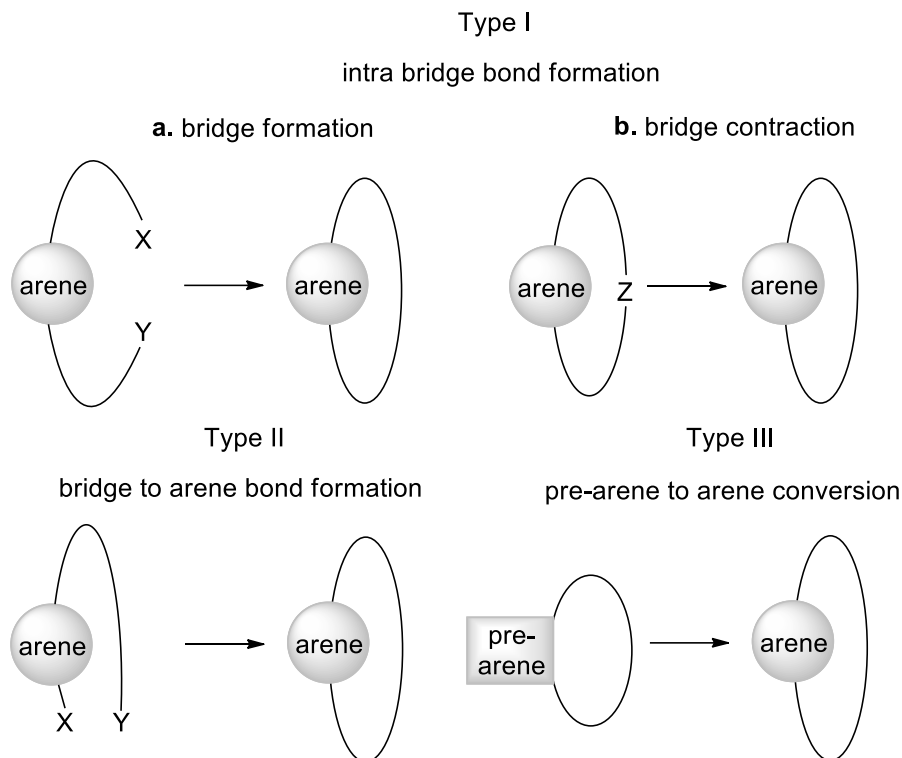


**Figure 1.2:** A few selected examples of cyclophanes.

### 1.1.1 General Synthetic Strategies for the Synthesis of Cyclophanes

The breadth of the synthetic methodology utilized in the synthesis of cyclophanes is far less than the diversity in cyclophane structure. From a strategic viewpoint, cyclophane syntheses can largely be divided according to the nature of the cyclophane-forming step (Scheme 1.1).

Type I strategies, which entail the formation of a bond between two atoms in a bridge, can in turn be divided into two subsets (Type I-a and Type I-b). A new bond can form during a new bridge formation (Type I-a), or contraction of an existing bridge can also lead to the formation of a new bond between two atoms of the bridge (Type I-b). A downside of Type I approaches is that they can only offer moderately strained cyclophanes.<sup>5</sup> The main reasons for this are as follows.



**Scheme 1.1:** Strategies for the synthesis of cyclophanes.

Formation of a bond that becomes part of the bridge can result in the distortion of the aromatic system out of planarity, which is an energetically demanding process. Unless the bond-forming reaction is sufficiently exergonic, even a low level of strain can cause the desired intramolecular reaction to become thermodynamically unfavorable. Furthermore, the requirement for an ordered transition state can render an intramolecular reaction more entropically challenging than its intermolecular counterpart. For the aforementioned reasons, Type I strategies are inefficacious for the synthesis of highly strained cyclophanes.<sup>6</sup>

The Type II strategy involves the formation of a bond between an aromatic unit and an atom of the bridge. Akin to the Type I strategies, reactions that fall under Type II are also intramolecular and suffer from the same pitfalls. It is worthy of note that Type II approaches have not been employed commonly and this strategy has only proved to be effective for the generation of cyclophanes with little or no strain.<sup>7</sup>

The Type III strategy banks on the generation of a bridged aromatic system from a bridged “pre-arene” in the cyclophane-forming step. This strategy is superior to the others for a number of reasons. First, the pre-arene has a shape that easily accommodates the bridge, so the construction of the pre-arene does not have the challenge of generating strained synthetic intermediates. Second, the bridged pre-arene already has all the necessary skeletal atoms in it, so its conversion to a bridged arene (cyclophane), typically via elimination or pericyclic reactions, avoids competing intermolecular reactions. Finally, conversion of the pre-arene into the corresponding arene is accompanied by the gain of a considerable amount of aromatic stabilization energy (ASE), which serves to counterbalance the developing strain. This strategy is the only one that has been successful in achieving the synthesis of highly-strained cyclophanes.<sup>8</sup> The implementation of several ingenious synthetic methods corresponding to each of the strategies discussed above is described in the following sections.

## 1.2 [*n*]Cyclophanes

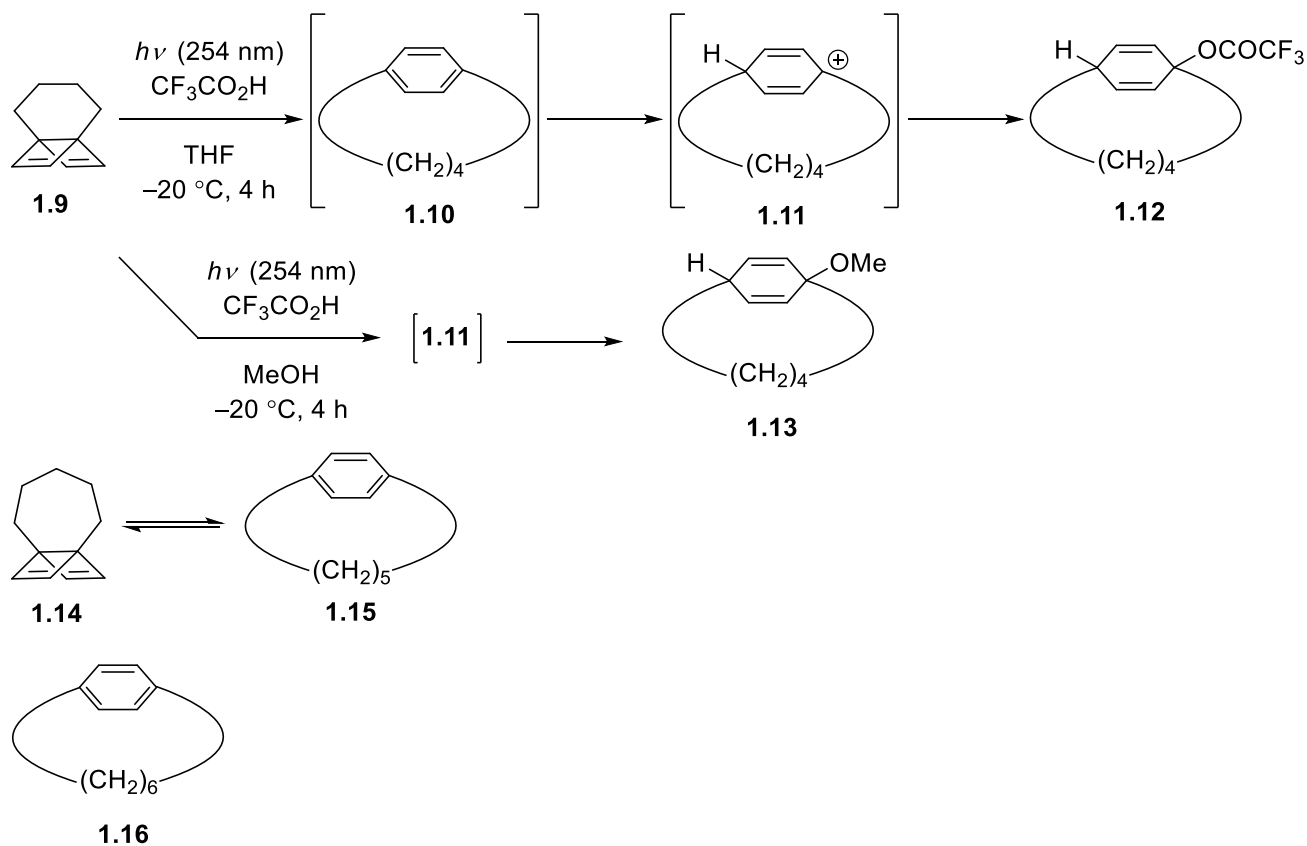
[*n*]Cyclophanes represent the simplest class of cyclophanes, which consist of one aromatic unit and one bridge (*n* denotes the number of skeletal atoms in the bridge). Below a particular value of *n*, the variation of the length or nature of the bridge directly influences the conformation of the aromatic unit and this renders this class of cyclophanes especially interesting. Most notably, systematic changes in the bridge cause systematic changes in the shape of the aromatic unit. This enables the study of how incremental changes in structure affect the physical and chemical properties of the arene. Almost without exception, the incorporation of any aromatic system into an [*n*]cyclophane can be used as a means to distort the aromatic system from its lowest energy conformation. This is as true for innately planar aromatic systems, such as benzene, as it is for innately nonplanar systems, such as helicenes or buckybowls.

### 1.2.1 [*n*]Paracyclophanes

Benzene is the quintessential aromatic system and is undoubtedly the most common system to have been integrated into cyclophanes. Bridging of the two most remote positions, 1 and 4, of benzene can result in the greatest distortion of the benzene ring from planarity, producing an [*n*]paracyclophane. The ensuing [*n*]paracyclophanes (**1.1**) have captivated the attention of synthetic chemists since 1954 when Cram and Allinger<sup>9</sup> first reported their initial work on this family of compounds.<sup>10</sup>

The main objective of the study was to prepare some smaller homologues to examine how far the benzene ring can be deformed from planarity and the resulting consequences on the physical and chemical properties of the aromatic system. The benzene ring in the [*n*]paracyclophanes with  $n > 10$  is virtually planar owing to the presence of a sufficiently long and flexible bridge. Consequently, the spectroscopic and chemical properties are similar to those of 1,4-dialkylbenzenes. In contrast, the [*n*]paracyclophanes with  $n \leq 10$  exhibit physical and chemical properties that change significantly as *n* becomes smaller. [6]Paracyclophane (**1.16**) (Scheme 1.2) is the smallest isolable member of this family.<sup>11</sup> The next lower homologue is [5]paracyclophane (**1.15**) (Scheme 1.2), which exists in equilibrium with its Dewar benzene isomer **1.14**.<sup>12</sup> In contrast, the generation of [4]paracyclophane (**1.10**) (Scheme 1.2) was inferred from trapping experiments at  $-20\text{ }^{\circ}\text{C}$  (Scheme 1.2).<sup>13</sup> Photoirradiation of Dewar benzene **1.9** generated [4]paracyclophane **1.10**, which under the acidic reaction conditions underwent protonation of the bridgehead carbon atom to produce arenium intermediate **1.11**. This followed by an attack of the trifluoroacetate counter anion afforded cyclohexadiene **1.12**. Under the same photochemical conditions, the replacement of the solvent from THF to methanol resulted in the formation of cyclohexadiene **1.13** *via* the intermediacy of **1.11**. Later, Tsuji and co-workers were able to detect

the generation of **1.10** in a matrix at  $-196\text{ }^{\circ}\text{C}$  by UV/vis spectroscopy.<sup>14</sup> The instability of **1.10** and **1.15** stems from their proclivity



**Scheme 1.2:** Structures of [n]paracyclophanes ( $n = 4-6$ ) **1.10**, **1.15**, and **1.16**; valence isomerization of **1.9** and **1.14** to **1.10** and **1.15**, respectively.

for undergoing addition reactions at the bridgehead positions, resulting in the release of strain (*vide infra*). The longest wavelength band in the absorption spectra of the [n]paracyclophanes with  $n < 10$  exhibit a gradual red shift as the length of the bridge decreases, which is congruent with the computationally predicted narrowing of the HOMO–LUMO energy gap.<sup>10b</sup> For example, the longest absorption band for cyclophane **1.15** appears at 330 nm, which is 34 nm red-shifted compared to that for cyclophane **1.16** (296 nm). The UV/vis absorption spectrum of cyclophane **1.10** shows the longest absorption band at 340 nm, which is in accord with the “red shift” trend.

## 1.2.2 [*n*]Metacyclophanes

Bridging of the 1 and 3 positions of benzene can also result in the distortion of the benzene ring from planarity. The resulting cyclophanes are known as [*n*]metacyclophanes (**1.2**). Akin to the [*n*]paracyclophanes, the stability of [*n*]metacyclophanes decreases as the length of the bridge becomes smaller.

The benzene ring in [9]metacyclophane (**1.20**) is essentially planar. [5]Metacyclophane (**1.18**) (Figure 1.3) is hitherto the smallest isolable member of this family.<sup>15</sup> Compared to bench-stable [6]metacyclophane (**1.19**) (Figure 1.3), **1.18** showcases considerably higher reactivity.<sup>16</sup> In fact, [5]metacyclophane (**1.18**) undergoes polymerization slowly at room

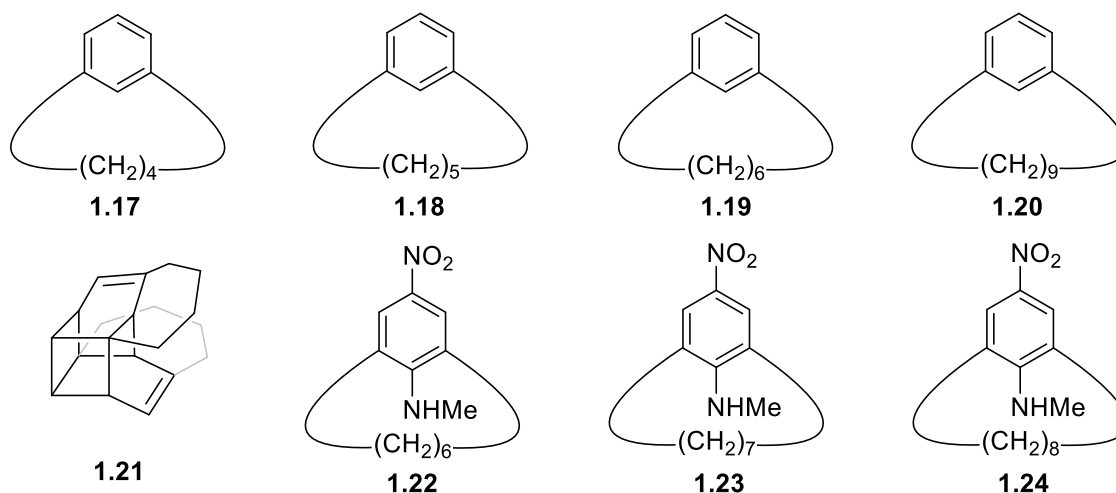


**Figure 1.3:** Structures of [*n*]metacyclophanes **1.17–1.20**, **1.22–1.24**, and dimer **1.21**.

temperature upon standing.<sup>15</sup> Until now, [4]metacyclophane (**1.17**) (Figure 1.3), a highly strained cyclophane, has not been isolated and characterized. However, the generation of the cyclophane as a short-lived species has been illustrated by isolation of the dimer **1.21** (Figure 1.3), which arises from an intermolecular [4+2]/intramolecular [2+2] sequence.<sup>17</sup> As the benzene ring becomes more bent (as *n* becomes smaller), a red shift of the longest wavelength band is observed for the

[*n*]metacyclophanes **1.22–1.24**.<sup>18</sup> The UV/vis absorption spectra of **1.22–1.24** in dichloromethane show the longest wavelength bands at 418, 408, and 398 nm, respectively.

### 1.2.3 Bending an Aromatic System

When an aromatic unit in a small cyclophane is forced out of planarity, the structural changes must be quantified in such a way as to allow for correlations between structure and the changes in chemical and physical properties. The changes in the energy of both the aromatic system and the cyclophane as a whole must also be considered. A brief discussion centred on these points is presented below.

#### 1.2.3.1 Bend Angles

The most salient facet of a strained [*n*]cyclophane is the out-of-plane bending of the aromatic unit into a boat-like conformation. The level of distortion of the aromatic unit from planarity is commonly represented by the two parameters,  $\alpha$  and  $\beta$ . The bend angle  $\alpha$  is defined as the smallest angle (envelope flap angle) formed by the planes C2-C1-C6 and C2-C3-C5-C6 in the case of an [*n*]paracyclophane (Figure 1.4a) and by the planes C11-C12-C13 and C10-C11-C13-C14 in the case of an [*n*]metacyclophane (Figure 1.4b). The other bending angle  $\beta$  is defined as the smallest angle formed by the plane C2-C1-C6 and the line formed by the bridgehead and benzylic carbon atoms C1 and C7 in the case of an [*n*]paracyclophane and by the plane C10-C11-C13-C14 and the line formed by C11-C16 in the case of an [*n*]metacyclophane. As bending of the aromatic ring in an [*n*]metacyclophane gives rise to a less symmetrical arene structure than in an [*n*]paracyclophane, there is an additional bend angle  $\gamma$  (another envelope flap angle, Figure 1.4b) similar to the bend angle  $\alpha$  in the case of an [*n*]metacyclophane. The bend angle  $\gamma$  is defined as the smallest angle formed by the planes C10-C9-C14 and C10-C11-C13-C14. For an

[*n*]paracyclophane (any *para*-substituted ring), the local distortion at a bridgehead carbon atom is expressed by the sum of  $\alpha + \beta$ . Whereas, for an [*n*]metacyclophane (any *meta*-substituted ring), the three angles  $\alpha$ ,  $\beta$ , and  $\gamma$  describe the overall bend.

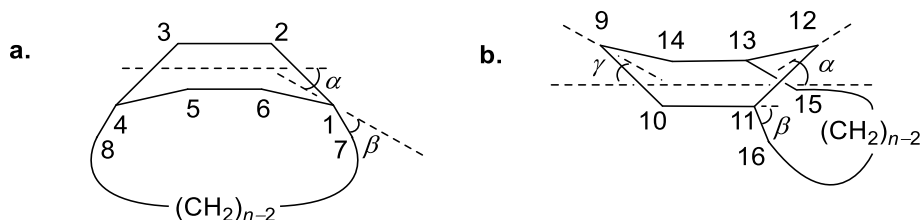


**Figure 1.4:** Bend angles in a [*n*]paracyclophane (left) and a [*n*]metacyclophane (right).

### 1.2.3.2 Strain Energy

In small [*n*]cyclophanes, as the benzene unit is forced to embrace a non-planar conformation, maintaining ideal geometries for all of the carbon atoms (*sp*<sup>2</sup>- and *sp*<sup>3</sup>-hybridized) becomes unattainable, which means that strain energy (*SE*) comes into play. Bockisch and co-workers described the total strain energy (*SE*<sub>tot</sub>) as “the difference between the heats of formation of the (strained) molecule and a fictitious unstrained molecule” (Equation 1) during their theoretical studies of the [*n*]paracyclophanes and their valence isomers.<sup>19</sup>

$$SE_{\text{tot}} = \Delta H_{f,\text{strained}}^0 - \Delta H_{f,\text{unstrained}}^0 \quad \text{eqn. 1}$$

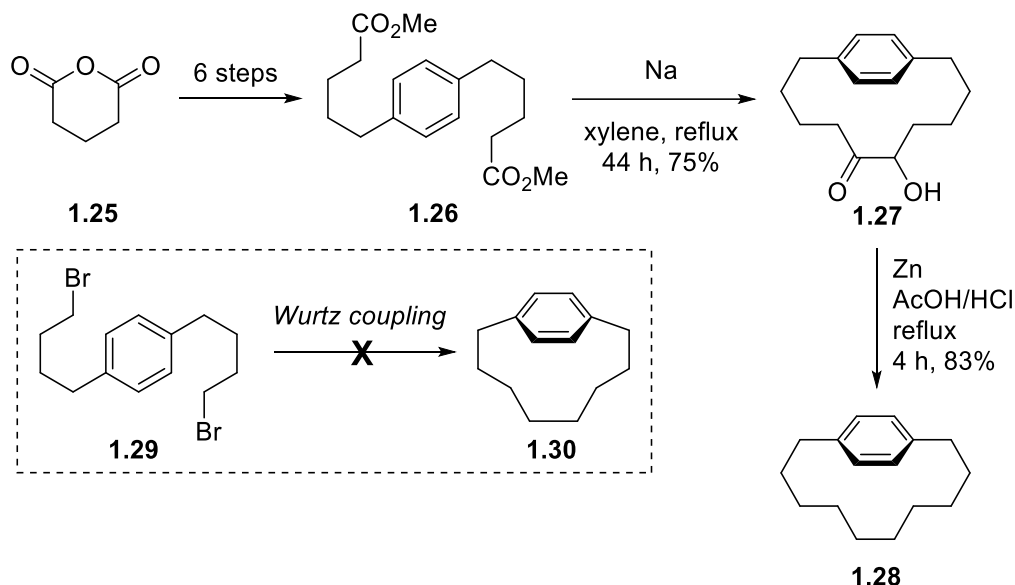
The strain in any molecule is spread out over the entire molecule in a way that minimizes the total strain. In [*n*]cyclophanes, the total strain energy (*SE*<sub>tot</sub>) can be represented by the sum of the strain energies of the ring and the bridge, *i.e.*  $SE_{\text{tot}} = SE_{\text{ring}} + SE_{\text{bridge}}$ , where *SE*<sub>ring</sub> corresponds to the energy required to deform the aromatic system and *SE*<sub>bridge</sub> corresponds to the energy required to distort (stretch) the alkyl bridge from its ideal geometry.

### 1.2.4 Synthesis of [*n*]Para- and [*n*]Metacyclophanes Utilizing Different Strategies

In the last few decades, a myriad of cyclophanes have been synthesized mainly using the previously mentioned three strategies, as discussed in Section 1.1.1. A very few selected examples are discussed below showcasing the power and limitations of the strategies.

#### 1.2.4.1 Synthesis of [*n*]Para- and [*n*]Metacyclophanes Utilizing the Type I Strategies

An elegant example of the use of the Type I-a strategy can be found in the Cram and co-workers' synthesis of [10]paracyclophane (**1.28**) from commercially abundant and inexpensive glutaric anhydride (**1.25**) (Scheme 1.3).<sup>20</sup> The key intermediate **1.26** was obtained from **1.25** over six steps. Subsequently, an intramolecular acyloin condensation reaction furnished hydroxyketone

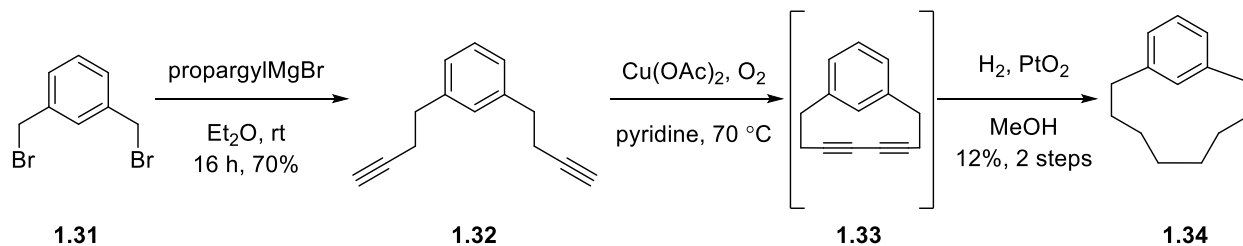


**Scheme 1.3:** Synthesis [10]paracyclophane (**1.28**) by Cram and co-workers. Inset: failed Wurtz coupling for the generation of [8]paracyclophane (**1.30**).

**1.27** (75%). Lastly, exhaustive reduction of the keto as well as the hydroxy groups produced **1.28** (83%). In this regard, it is worth mentioning that no reports can be found in the literature for the preparation of smaller [*n*]paracyclophanes using the aforementioned approach (acyloin

condensation). An attempt to synthesize [8]paracyclophane (**1.30**) employing Wurtz coupling of dibromide **1.29** in an intramolecular setting met with failure (Scheme 1.3, inset).

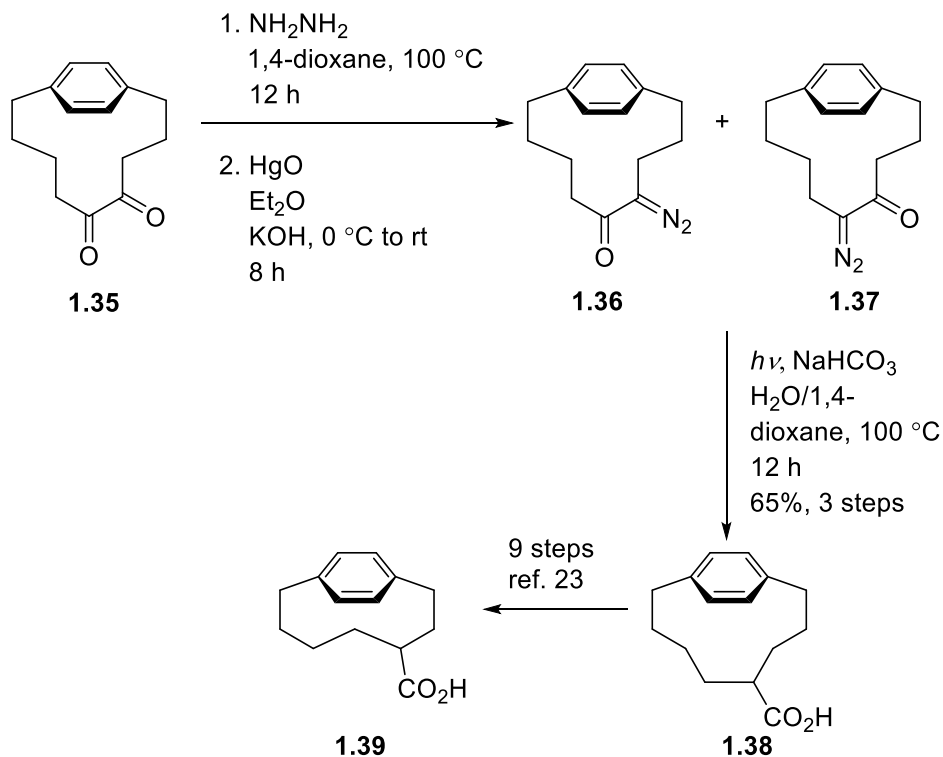
The synthesis of [8]metacyclophane (**1.34**) by Hubert and Dale in 1963 represents another example of application of the Type I-a strategy (Scheme 1.4).<sup>21</sup> The first step was a double nucleophilic substitution reaction of dibromo-*m*-xylene **1.31** with propargylmagnesium bromide (the Grignard reagent derived from propargyl bromide) to yield diyne **1.32**. Exposure of **1.32** to Glaser coupling reaction conditions led to the formation of the precursor (**1.33**) to the targeted metacyclophane **1.34**. Hydrogenation of the triple bonds using Adams' catalyst (PtO<sub>2</sub>) finally furnished **1.34**. Taking into account the 8% yield over 3 steps and the fact that **1.33** is not an especially strained system, the likelihood of using Glaser coupling for the synthesis of smaller [*n*]metacyclophanes is slim.



**Scheme 1.4:** Synthesis [8]metacyclophane (**1.34**) by Hubert and Dale.

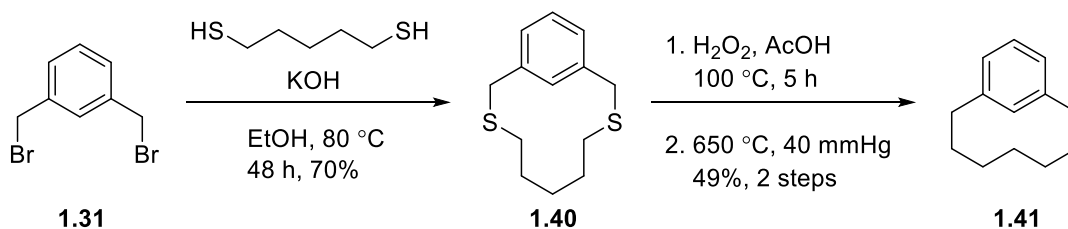
Allinger and co-workers accomplished the synthesis of [8]paracyclophane **1.38** using the Type I-b strategy (Scheme 1.5).<sup>22</sup> The synthesis began with the formation of a mixture of the regioisomeric  $\alpha$ -diazoketones **1.36** and **1.37** from an advanced starting material, diketone **1.35** by treatment with hydrazine followed by oxidation of the intermediate monohydrazones with mercuric oxide. Irradiation of the mixture of **1.36** and **1.37** with a 275 W sun lamp at 100 °C effected a Wolff rearrangement and delivered 4-carboxy[8]paracyclophane (**1.38**) in 65% yield over three steps. Carboxylic acid **1.38** then served as a starting material for the synthesis of the next lower homologue **1.39**.<sup>23</sup> At this point, it is not known whether the photochemical Wolff

rearrangement is powerful enough to enable the synthesis of the next lower homologue because there is no report of any attempt to do so. Perhaps, another iteration of the 9-step synthetic sequence of reactions was thwarted by the unavailability of a sufficient quantity of **1.39**.



**Scheme 1.5:** Syntheses of [8]paracyclophane **1.38** and [7]paracyclophane **1.39** by Allinger and co-workers.

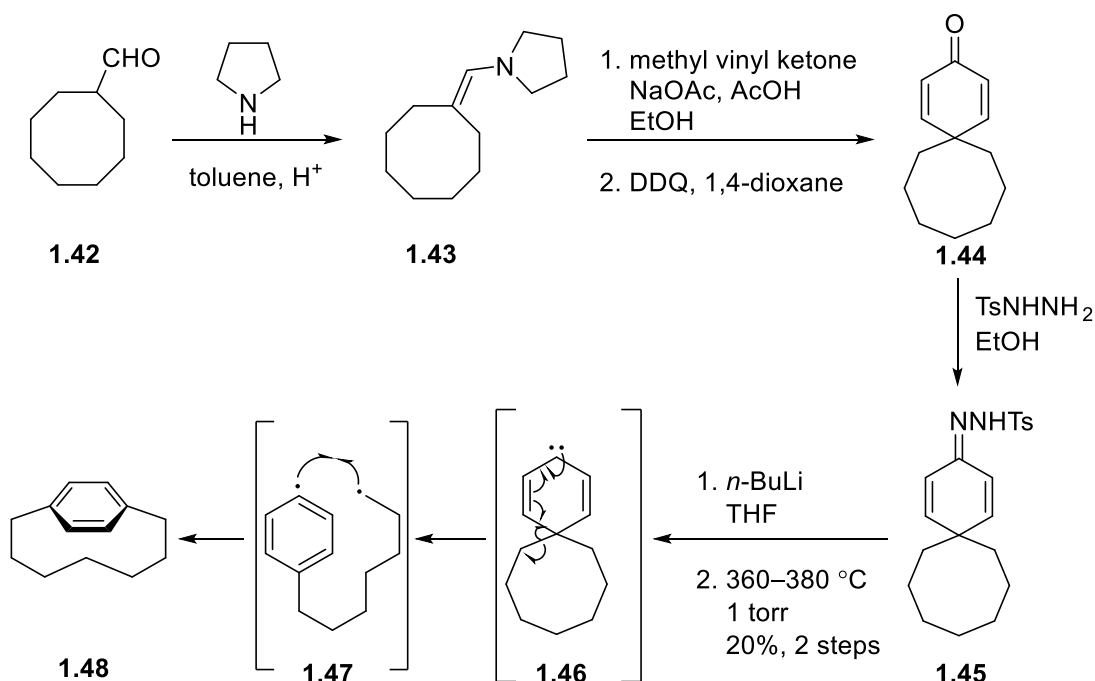
In 1978, Misumi and co-workers reported the synthesis of [7]metacyclophane (**1.41**), which entails the Type I-b strategy (Scheme 1.6).<sup>24</sup> Coupling between dibromide **1.31** and 1,5-pentanedithiol in the presence of  $\text{KOH}$  proceeded smoothly to produce disulfide **1.40** (70%). Subsequent oxidation of **1.40** into the corresponding sulfone followed by flash vacuum pyrolysis provided **1.41** (49%, 2 steps).



**Scheme 1.6:** Synthesis of [7]metacyclophane (**1.41**) by Misumi and co-workers.

### 1.2.4.2 Synthesis of an $[n]$ Paracyclophane Utilizing the Type II Strategy

As discussed earlier, the Type II strategy is not effective for the generation of highly strained cyclophanes. At best, this strategy can be exploited to generate cyclophanes with only relatively low strain. Therefore, there is a paucity of examples in the literature showing the successful use of it for the synthesis of  $[n]$ cyclophanes. In this regard, Jones Jr. and co-workers' synthesis of [7]paracyclophane (**1.48**) features the Type II strategy (Scheme 1.7).<sup>25</sup> Although it might be tempting to classify the synthesis (*vide infra*) under the Type III strategy as a “pre-arene” can be spotted in the precursor (**1.45**) to **1.48**, the absence of any bridge in **1.45** precludes that notion. Enamine **1.43** was obtained by condensation of cyclooctanecarbaldehyde (**1.42**) with pyrrolidine. A Robinson annulation between **1.43** and methyl vinyl ketone (MVK) proceeded to give an enone (not shown), which upon treatment with DDQ furnished the divinyl ketone **1.44**.



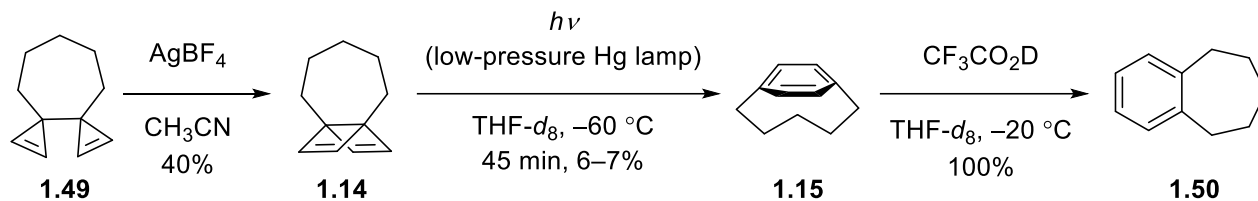
**Scheme 1.7:** Synthesis of [7]paracyclophane (**1.48**) by Jones Jr. and co-workers.

Reaction of **1.44** with tosyl hydrazide afforded hydrazone **1.45**. Abstraction of the nitrogen-bound proton with *n*-BuLi to generate the corresponding salt followed by the application of high temperature and low pressure resulted in the formation of **1.48**. The conversion from **1.45** to **1.48** proceeds via the intermediacy of spirocarbene **1.46**, which undergoes C–C bond cleavage to generate the reactive diradical **1.47**. Finally, recombination of the radicals intramolecularly yields [7]paracyclophane (**1.48**).

#### 1.2.4.3 Synthesis of [*n*]Para- and [*n*]Metacyclophanes Utilizing the Type III Strategy

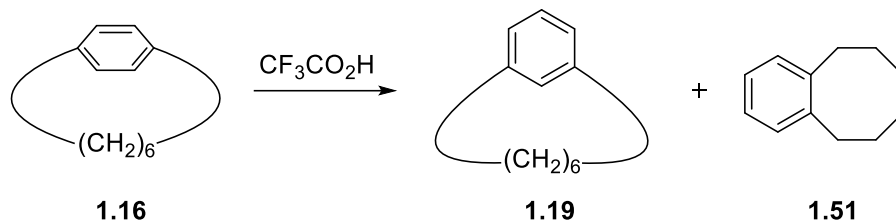
As mentioned earlier, the Type III strategy, which involves the generation of non-planar aromatics from bridged “pre-arene”, benefits mostly from the gain of aromatic stabilization energy (ASE)/resonance energy. The success or failure of the final step (arene-forming reaction) banks on the magnitude of the developing strain and the ASE. In this context, bridged Dewar benzenes have served as excellent synthetic precursors for the preparation of [*n*]cyclophanes with high strain. In addition to the gain of *ca.* 30 kcal/mol of ASE from the valence isomerization of a Dewar benzene to benzene, this transformation is also accompanied by a substantial degree of strain relief as two conjoined cyclobutene rings are turned into a six-membered ring.

In 1985, Bickelhaupt, Tobe, and co-workers documented the synthesis of [5]paracyclophane (**1.15**), which showcase the utilization of the Type III strategy (Scheme 1.8).<sup>12</sup> Silver tetrafluoroborate-catalyzed isomerization of the bis(spiro-cyclopropene) **1.49** to the Dewar benzene **1.14** and its ensuing irradiation with a low-pressure mercury lamp at low temperature led to the formation of **1.15**, the existence of which was evidenced by low temperature <sup>1</sup>H NMR and UV spectroscopic studies. Prolonged irradiation or elevation of the temperature of its THF-*d*<sub>8</sub> solution to 0 °C resulted in complete decomposition. Rearrangement of **1.15** to benzocycloheptene (**1.50**) took place upon treatment of a THF-*d*<sub>8</sub> solution of **1.15** with deuterated trifluoroacetic acid.



**Scheme 1.8:** Synthesis of [5]paracyclophane (**1.15**) and its rearrangement to benzocycloheptene (**1.50**) by Bickelhaupt, Tobe, and co-workers.

Tobe and co-workers also came across a similar outcome when [6]paracyclophane (**1.16**) was treated with trifluoroacetic acid (Scheme 1.9).<sup>11</sup> Worthy of note is that **1.16** provided some [6]metacyclophane (**1.19**) besides the corresponding benzocyclooctene (**1.51**). In the case of [5]paracyclophane (**1.15**), the formation of [5]metacyclophane (**1.18**) was not observed. Tobe and co-workers also reported a few [5]paracyclophane derivatives taking the advantage of the “Dewar benzene to benzene” transformation.<sup>26</sup> Nevertheless, to date, no report of an isolable [5]paracyclophane with noticeable lifetime at ambient temperature appears in the literature.

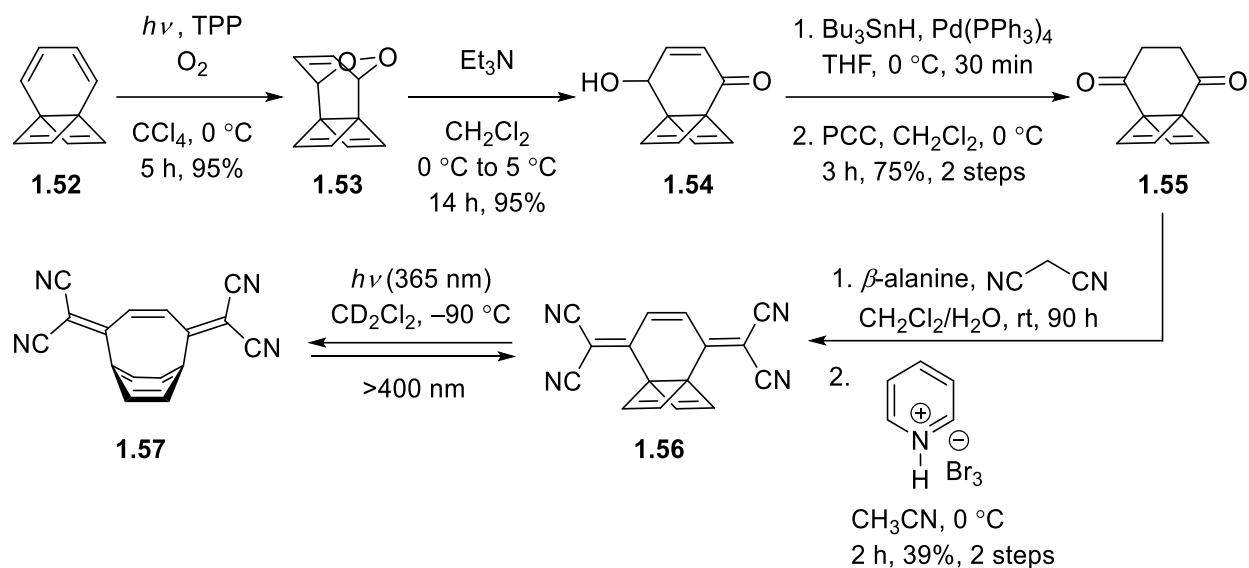


**Scheme 1.9:** Trifluoroacetic acid-catalyzed rearrangement of [6]paracyclophane (**1.16**).

If the bridge of **1.15** is shortened by one carbon atom, the resulting cyclophane is [4]paracyclophane (**1.10**). Based on the observations by Bickelhaupt and co-workers in the synthesis of **1.15**,<sup>12</sup> the synthesis of **1.10** poses a formidable challenge. Early work toward this goal revealed the formation of this desired cyclophane **1.10** in a matrix at a temperature as low as  $-196\text{ }^\circ\text{C}$ .<sup>14</sup> For **1.10**, unlike **1.15**, the Dewar benzene isomer is favored over the benzene isomer (energy difference =  $9 \pm 4$  kcal/mol).<sup>27</sup> Furthermore, depending on the level of theory, the calculated strain energy (*SE*) of **1.10** is 91–108 kcal/mol,<sup>27</sup> which is exceedingly high compared

to the Schleyer and co-workers' calculations of the RE/ASE for benzene, which was estimated to be *ca.* 33 kcal/mol.<sup>28</sup> The prime challenge to the isolation or even observation of the highly bent aromatic system is the inclination of its bridgehead carbon atoms to undergo reactions with reagents/protic solvents that helps to alleviate the inherent strain to a large extent.

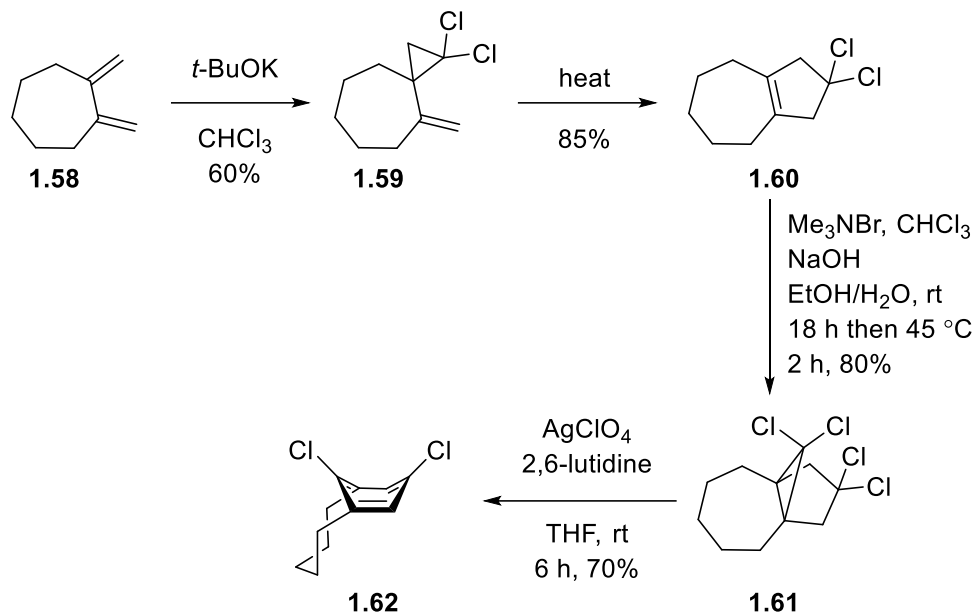
Tsuji offered a great solution to the aforementioned problem and reported the synthesis of [4]paracyclophane derivative **1.57** with a half-life ( $t_{1/2}$ ) of *ca.* 12 min (Scheme 1.10).<sup>29</sup> The logic behind the decoration of the derivative is that the introduction of bulky substituents like dicyanomethylene near the bridgehead positions would sterically block the approach of reagents and this would in turn allow for the complete characterization of such a deformed aromatic system. The synthesis started with treatment of tetraene **1.52** with singlet oxygen under photochemical conditions to give endoperoxide **1.53** via a Diels-Alder cycloaddition. Subsequently, enone **1.54** was formed upon subjection of a dichloromethane solution of **1.53** to triethylamine. The conjugated double bond (alkene) was reduced under radical reaction conditions with tributyltin hydride and Pd(PPh<sub>3</sub>)<sub>4</sub> and subsequent oxidation of the hydroxyl group furnished diketone **1.55**. Knoevenagel condensation between **1.55** and malononitrile using  $\beta$ -alanine as catalyst followed by a reaction sequence consisting of bromination/dehydrobromination with pyridinium bromide perbromide provided the Dewar benzene **1.56**. When a deuterated dichloromethane solution of **1.56** was irradiated at 365 nm at -90 °C, a broad absorption band between 270 and 420 nm developed, hinting at the formation of a distorted benzene ring (formation of **1.57**), and the bands between 300–390 nm, attributed to the Dewar isomer, disappeared. As a result of the reversal behavior of the photochemical reaction, irradiation of the incipient species at a wavelength higher than 400 nm resulted in the formation of **1.56**. The cyclophane proved to be stable enough to allow acquisition of a <sup>1</sup>H NMR spectrum at -75 °C.



**Scheme 1.10:** Synthesis of [4]paracyclophane derivative **1.57** by Tsuji and co-workers.

In an attempt to discern more about the [4]paracyclophane system, Tsuji and co-workers reported the synthesis of other [4]paracyclophane derivatives bearing even bulkier groups.<sup>29a</sup> It is worth mentioning that although the benzene rings of the [4]paracyclophane derivatives are highly bent, nucleus-independent chemical shift (NICS) and diamagnetic susceptibility exaltation calculations suggest that a significant amount of aromaticity is retained by the distorted benzene rings. For example, the NICS value for the benzene ring in **1.57** was estimated to be  $-8.1$ , which is comparable to  $-9.7$  for benzene.

Bickelhaupt and co-workers' report on the synthesis of 8,11-dichloro[5]metacyclophane (**1.62**) also features the application of the Type III strategy (Scheme 1.11).<sup>30</sup> One-fold cyclopropanation of diene **1.58** with dichlorocarbene (generated *in situ* by treatment of



**Scheme 1.11:** Synthesis of 8,11-dichloro[5]metacyclophane (**1.62**) by Bickelhaupt and co-workers.

chloroform with potassium *tert*-butoxide) afforded dichloride **1.59**, which underwent vinylcyclopropane rearrangement upon heating to produce dichloride **1.60**. Another cyclopropanation took place when **1.60** was exposed to dichlorocarbene (generated *in situ* using a slightly different set of conditions), providing [5.3.1]propellane **1.61**. At this stage, the highly strained tricyclic system of **1.61** contains all the carbon atoms present in **1.62**. Finally, treatment of **1.61** with silver perchlorate and 2,6-lutidine resulted in a Grob-type fragmentation followed by dehydrochlorination (mechanism not shown) to afford [5]metacyclophane **1.62**. This cyclophane, to date, represents the smallest isolable metacyclophane with an X-ray structure. Later, Bickelhaupt reported a few syntheses of [5]metacyclophanes,<sup>31</sup> but employment of this strategy toward the synthesis of [4]metacyclophane (**1.17**) led to the formation of only the Dewar benzene isomer.<sup>32</sup>

### 1.3 [*m.n*]Cyclophanes

$[m.n]$ Cyclophanes consist of two aromatic units connected by two bridges of equal ( $m = n$ ) or different lengths ( $m \neq n$ ). This family of compounds has captivated the attention of chemists from various disciplines owing to their usefulness in polymer chemistry, materials chemistry,

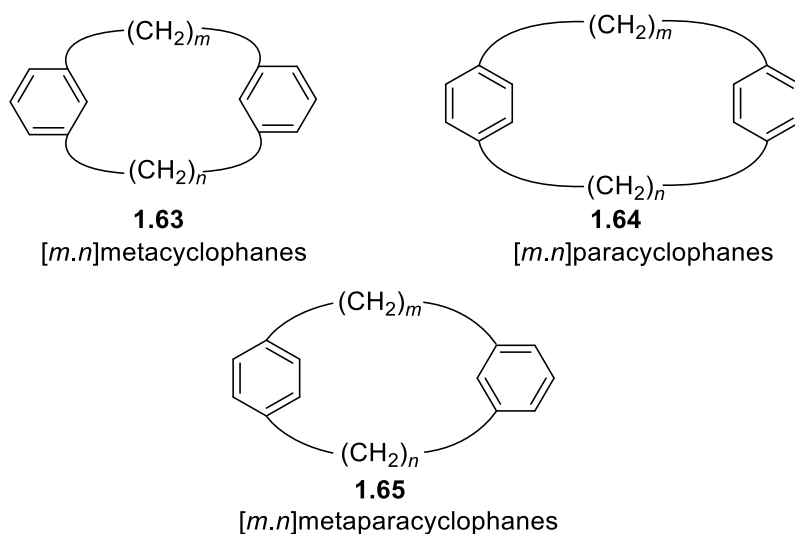


**Figure 1.5:**  $[m.n]$ Cyclophanes with different bridging patterns.

and asymmetric catalysis.<sup>10b,33</sup> Naturally occurring  $[m.n]$ cyclophanes have also motivated synthetic organic chemists working in the field of total synthesis of natural products.<sup>34</sup> Undoubtedly, benzene is the most common aromatic system to have been integrated into  $[m.n]$ cyclophanes. The three common connectivity patterns for  $[m.n]$ cyclophanes (**1.63–1.65**) bearing two benzene rings are depicted in Figure 1.5. However,  $[m.n]$ metaparacyclophanes (**1.65**) are underexplored,<sup>35</sup> whereas the most thoroughly-studied  $[m.n]$ cyclophanes are the  $[m.n]$ paracyclophanes (**1.64**).<sup>10b</sup> [2.2]Paracyclophane derivatives have been the most popular among the  $[m.n]$ paracyclophanes as evidenced by the vast body of literature dedicated to this one system.<sup>36</sup> The ensuing Chapters will describe the syntheses and properties of some novel, structurally usual and interesting cyclophanes, all of which can be traced back to

[2.2]paracyclophane (**1.4**). This being the case, the remainder of this Chapter will focus primarily on the discussion of the various unusual features of [2.2]paracyclophane and its derivatives.

### 1.3.1 [2.2]Paracyclophane

The two short ethano bridges connecting the *para*-positions of the two cofacially stacked benzene rings in [2.2]paracyclophane (**1.4**), forces the two aromatic rings to be bent out of planarity. The free rotation of these “bent and battered”<sup>37</sup> benzene rings is not possible without rupture of a bridge due to their proximity. Thermal cleavage of the bridge(s) occurs only above 180 °C, which results in thermal isomerization of certain [2.2]paracyclophane derivatives.<sup>38</sup> The distance between the centroids of the two rings in **1.4** is 3.09 Å (Figure 1.6), which is less than the van der Waals distance of 3.40 Å observed between the two adjacent layers in graphite.<sup>39</sup> The benzene rings in **1.4** adopt a shallow boat-like conformation, which renders the distance between the two bridgehead carbon atoms on the opposite benzene rings, as indicated in Figure 1.6, even shorter (2.78 Å). [2.2]Paracyclophane derivatives showcase unusual chemical reactivities due to both their distorted rings and unique transannular interactions (*vide infra*, Section 1.3.3) within the framework. For example, the reaction of **1.4** with chromium hexacarbonyl has a first order rate constant that is approximately 25% greater than the rate constant for the reaction of *p*-xylene with chromium hexacarbonyl.<sup>40</sup>

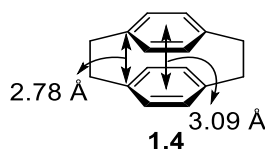


**Figure 1.6:** Transannular distances in [2.2]paracyclophane (**1.4**).

### 1.3.2 Nomenclature and Stereochemical Descriptors for Chiral [2.2]Paracyclophane Derivatives

Monosubstituted [2.2]paracyclophane derivatives are inherently chiral. The substituent can reside either on one of the benzene rings or one of the bridges. If the benzene ring is substituted, the derivative (**1.66**) is chiral owing to the presence of a chiral plane (Figure 1.7).<sup>41</sup> On the other hand, when the bridge is substituted, the corresponding derivative (**1.67**) is chiral owing to the possession of a center of chirality. For disubstituted [2.2]paracyclophane derivatives, one aryl substituent with respect to another can be placed at the three available positions on the same ring, leading to the three isomeric [2.2]paracyclophane derivatives **1.68–1.70**. The prefixes *ortho*-, *meta*-, and *para*- are generally included in their names to mention the relative positions of the two substituents. These derivatives are chiral when X and Y are different substituents. If X and Y are the same substituent, a plane of symmetry can be found in each of these derivatives, rendering them achiral. Disubstituted [2.2]paracyclophane derivatives, in which both rings are substituted, can be chiral or achiral. In this scenario, distribution of the substituents leads to four isomeric derivatives (**1.71–1.74**). Among these, the *pseudo-gem* isomer **1.71** and *pseudo-para* isomer **1.72** are chiral if X and Y are different. When X = Y, **1.71** and **1.72** become achiral as they possess a plane of symmetry and a point of inversion, respectively. The other two isomers **1.73** (*pseudo-ortho*) and **1.74** (*pseudo-meta*) are always chiral. Although rare, the two elements of chirality, namely, a plane of chirality and a center of chirality can be found in disubstituted [2.2]paracyclophanes. An example of such a type (*syn-latero*) of chiral disubstituted [2.2]paracyclophane (**1.75**) is shown in Figure 1.7.

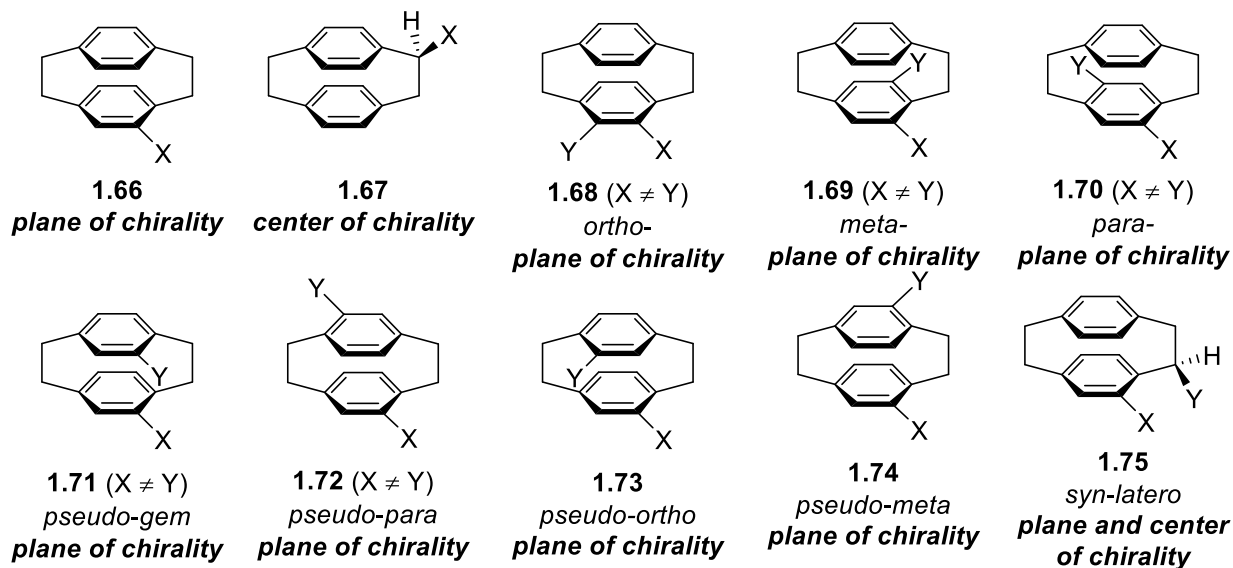


**Figure 1.7:** Mono- and disubstituted chiral [2.2]paracyclophane derivatives **1.66–1.75**.

Like any other racemic chiral compounds, a racemic planar chiral [2.2]paracyclophane derivative also exists as a 1:1 mixture of two enantiomers, denoted by  $R_p$  and  $S_p$ , where p stands for planar chirality.<sup>33b,42</sup> In order to assign the descriptors, first, a chiral plane has to be identified. The plane with a maximum number of atoms is considered to be the chiral plane. Next task is to ascertain a pilot atom, which is the closest out-of-plane atom (if more than one substituent is present in the chiral plane, the atom closest to the substituent of higher priority according to the Cahn–Ingold–Prelog (CIP) system is preferred). Numbering starts from this pilot atom and follows the way shown in Figure 1.8. It is worth mentioning that for the sake of numbering and assigning stereochemical descriptors, it is best to consider each benzene ring and the two connecting benzylic carbon atoms to be coplanar. Once the pilot atom has been identified, the three adjacent atoms of the chiral plane are marked with the letters a, b, and c (in case of more than one choice, CIP priority rules are followed). If  $a \rightarrow b \rightarrow c$  shows a clockwise orientation, when viewed from the pilot atom, the descriptor is  $R_p$  (**1.76**). Similarly,  $S_p$  (**1.66**) represents a counterclockwise orientation of  $a \rightarrow b \rightarrow c$ . However, substituents on both rings gives rise to more

complex scenarios. In these cases, two separate pilot atoms are chosen with respect to two chiral planes, and the same rules described above are applied. Compound **1.71** (Figure 1.8) is such an example, which helps understand the rules more clearly. Considering that X has a higher precedence than Y according to the CIP system, **1.71** is ( $4S_p, 13R_p$ ) configured.

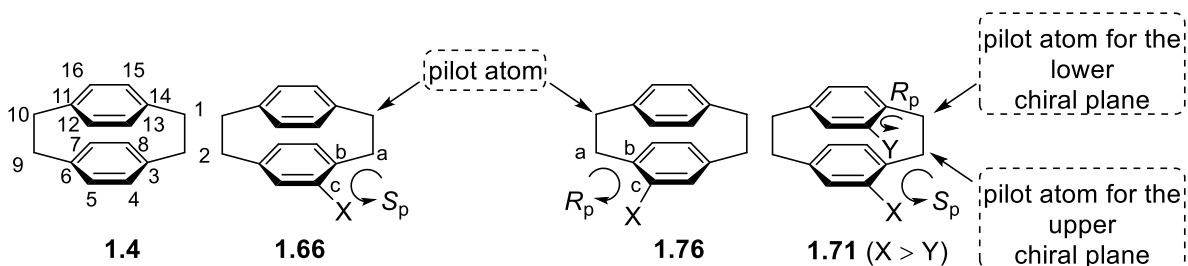


**Figure 1.8:** Numbering for the [2.2]paracyclophane backbone and stereochemical descriptors for [2.2]paracyclophane derivatives.

### 1.3.3 Transannular Interactions

Through-space interactions between the aromatic systems of  $[m.n]$ paracyclophanes, often referred to “transannular interactions” cause the two systems to tend to behave as one.<sup>43</sup> The magnitude of this interaction depends mainly on the distance between the two rings. Various spectroscopic observations and unique reactivities offered by this class of cyclophanes support the existence of these interactions.

The correlation between the magnitude of interactions with the size of the  $[m.n]$ paracyclophane can be easily understood from the kinetic studies performed by Cram and co-workers pertaining to the relative rates for acylation of [6.6]paracyclophane (**1.78**) (Figure 1.9), [4.4]paracyclophane (**1.77**) (Figure 1.9), and [2.2]paracyclophane (**1.4**).<sup>44</sup> From these studies, it was found that the relative rates of monoacylation of **1.78**, **1.77**, and **1.4** were 1, 1.6, and 29, respectively. The interpretation of these results is that the benzene rings in **1.4** are close enough to show strong interactions. This results in a mutual enhancement of electron density of the two rings, thereby leading to an increase in the reaction rate. Cyclophane **1.77** poses an intermediate

situation, wherein, the weak interactions between the two benzene rings translates into the sluggishness of its reaction compared to **1.4**. On the other hand, the benzene rings in **1.78** are too far apart (on time average) to exert an appreciable degree of transannular interactions on one another, accounting for the slowest rate of monoacylation.

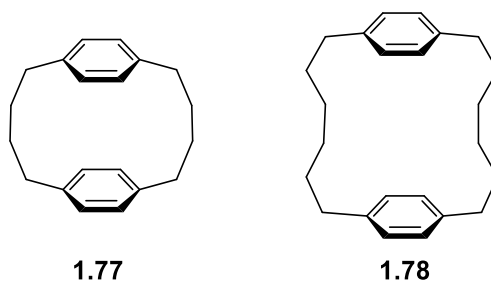
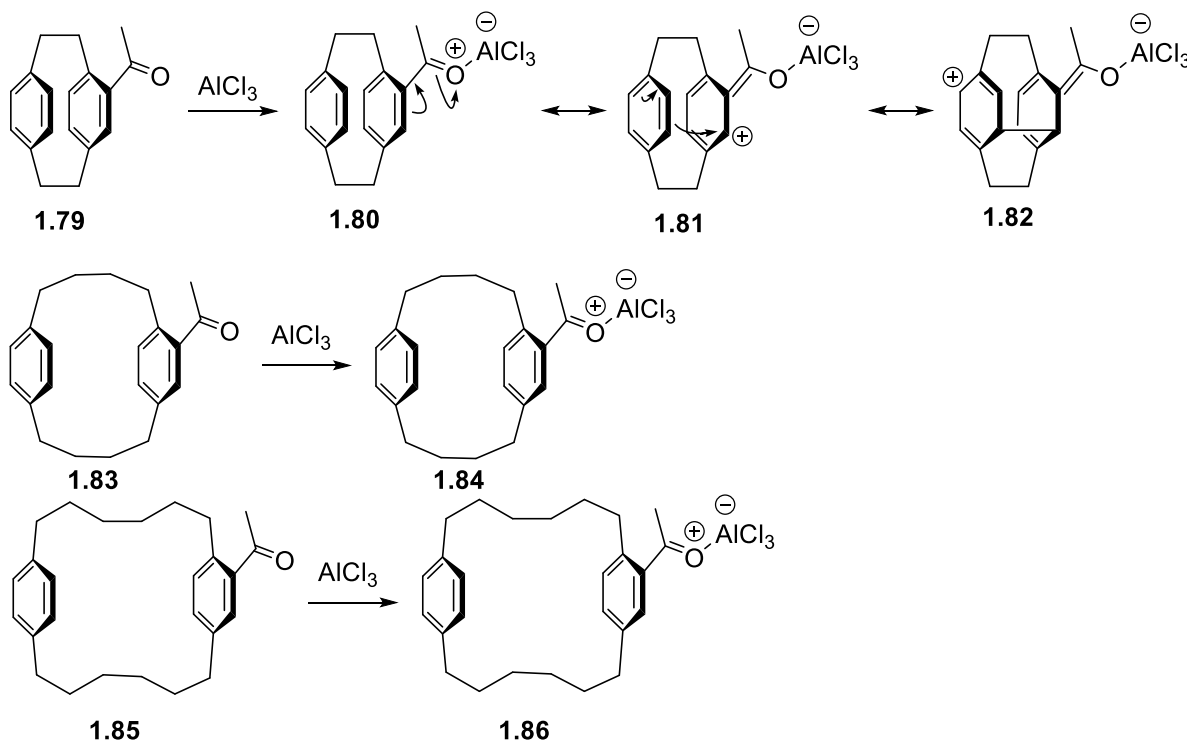


**Figure 1.9:** Structures of [4.4]paracyclophane (**1.77**) and [6.6]paracyclophane (**1.78**).

The ease with which the second acylation proceeds (in the unsubstituted ring) follows a completely reverse order, but this also can be explained in terms of transannular interactions.<sup>44</sup> Although there is no report in the literature discussing the relative rates of reaction for the second acylation, qualitative information about the rates can be obtained from the outcome of the acylation reactions of **1.4**, **1.77**, and **1.78**.<sup>45</sup> The involvement of the Lewis acid–base adducts **1.80**, **1.84**, and **1.86**, resulting from the complexation of aluminum chloride (Lewis acidic catalyst for the Friedel–Crafts acylation reactions) with 4-acetyl[2.2]paracyclophane (**1.79**), 6-acetyl[4.4]paracyclophane (**1.83**), and 8-acetyl[6.6]paracyclophane (**1.85**), respectively, was invoked to interpret the observed behavior (Scheme 1.12). The distribution of the positive charge to both rings in **1.80** as shown by two resonance structures **1.81** and **1.82** are possible only when transannular interactions are considered. Complex **1.82** represents a resonance structure in which the unsubstituted ring of **1.80** becomes electron deficient. This renders the second acylation formidable. None of the isomeric diacetyl[2.2]paracyclophanes were detected and the major product under the Friedel–Crafts acylation conditions was **1.79** (71%).<sup>45a</sup> Under the acylation conditions, cyclophane **1.77** afforded

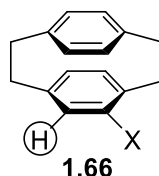
**1.83** (88%) as the major product along with a mixture of diacetylated [4.4]paracyclophanes (7%), the regioisomerism of which was not determined.<sup>45b</sup> The low yield of the diacetylated products was presumably due to the weaker interactions between the two benzene rings (than the interactions in **1.80**) in the corresponding Lewis acid–base adduct **1.84**. In **1.86**, the distance between the two benzene rings is too large to exhibit an appreciable degree of interactions. Hence, the second acylation could take place smoothly in the unsubstituted ring under Friedel–Crafts conditions to furnish two diacetylated products.<sup>45c</sup> Each of the products contains two isomers that can readily interconvert by rotation of an aromatic ring. The product that contained the interconverting *pseudo-para* and *pseudo-ortho* diacetylated [2.2]paracyclophanes was isolated in 32% yield. The product that contained the interconverting *pseudo-meta* and *pseudo-gem* diacetylated [2.2]paracyclophanes was isolated in 31% yield.



**Scheme 1.12:** Complexation of AlCl<sub>3</sub> with monoacetylated paracyclophanes **1.79**, **1.83**, and **1.85**.

The effect of a substituent on one ring to the other, also known as “transannular substituent effects” is also evident from the inspection of the  $^1\text{H}$  NMR spectra of a few 4-substituted [2.2]paracyclophane derivatives.<sup>46</sup> The proton next to the substituent in 4-substituted [2.2]paracyclophane derivatives (**1.66**) stands apart from all other aromatic protons (Table 1.1). The chemical shift of this proton is very sensitive to the electronic nature of the substituent. As expected, the proton adjacent to an electron-withdrawing substituent ( $\text{NO}_2$  or Ac) (Table 1.1, Entries 2 and 3) resonates at significantly lower field than that adjacent to an electron-donating substituent (Et or OMe) (Table 1.1, Entries 4 and 5). Due to the overlap of some of the signals, the signals for the remaining six protons could not be assigned with a high level of confidence. Consequently, the chemical shift corresponding to the “center of gravity” of the remaining six aromatic protons was used as a probe to note the effect of the substituent. As can be seen from the

**Table 1.1:** Substituent-dependent chemical shifts of the aromatic protons in 4-substituted [2.2]paracyclophane derivatives.



| Entry | Substituent (X) | Chemical Shift of <i>ortho</i> -H (Circled) <sup>a</sup> | Center of Gravity of Chemical Shifts of Other Ar-H <sup>a</sup> |
|-------|-----------------|--|---|
| 1     | H               | 6.38 ppm   | 6.38 ppm  |
| 2     | $\text{NO}_2$   | 7.11 ppm   | 6.51 ppm  |
| 3     | Ac              | 6.78 ppm   | 6.40 ppm  |
| 4     | Et              | 6.00 ppm   | 6.28 ppm  |
| 5     | MeO             | 5.44 ppm   | 6.24 ppm  |

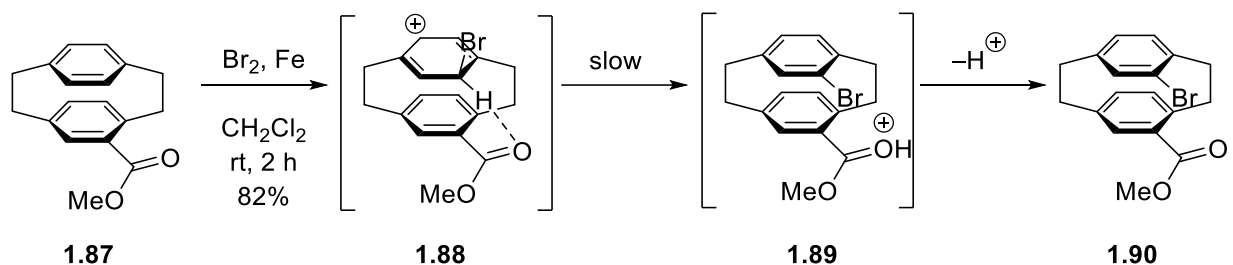
<sup>a</sup>60 MHz NMR instrument

chemical shift values in Table 1.1, the center of gravity moves to lower field with increasing electron-withdrawing character of X (Table 1.1, Entries 2 and 3) and moves higher field with increasing electron-donating character of X (Table 1.1, Entries 4 and 5).

### 1.3.4 *pseudo-gem* Directing Effect

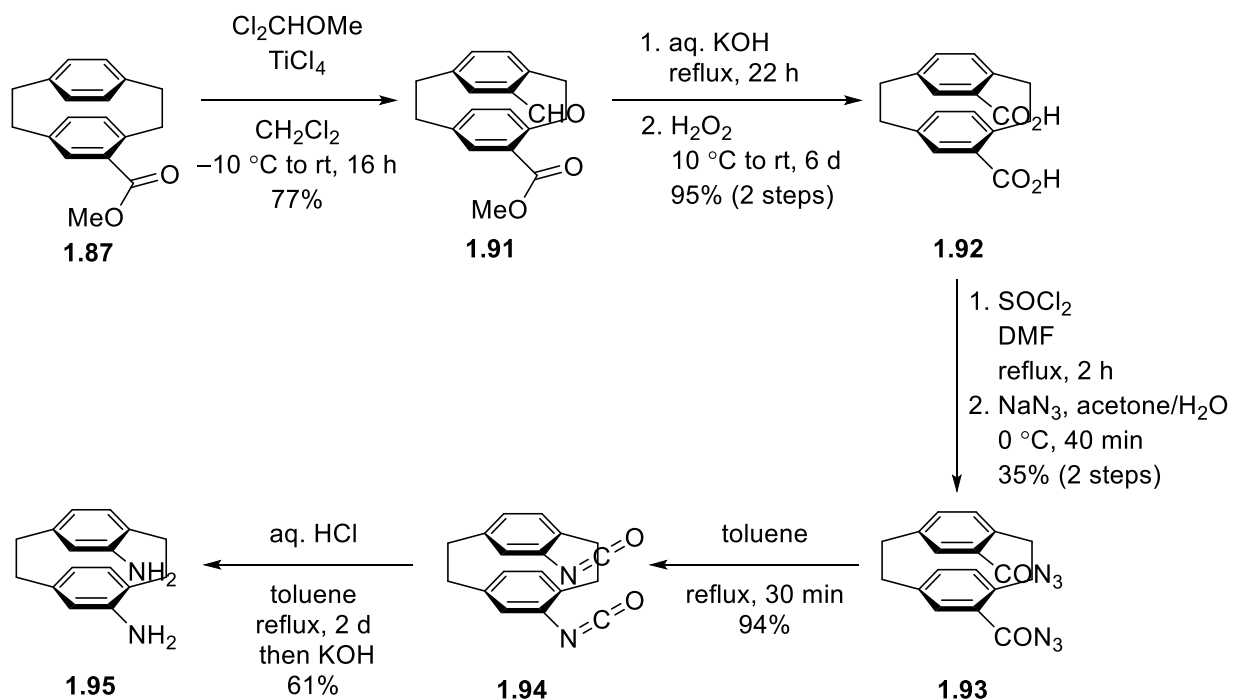
One of the most important and noteworthy intramolecular effects in [2.2]paracyclophanes is the *pseudo-gem* effect.<sup>10b</sup> Herein, two electrophilic substitution reactions of 4-methoxycarbonyl[2.2]paracyclophane (**1.87**) are presented (*vide infra*), which illustrates the directing effect by the selective synthesis of the *pseudo-gem*-difunctionalized [2.2]paracyclophanes.

Bromination of 4-methoxycarbonyl[2.2]paracyclophane (**1.87**) afforded the *pseudo-gem* bromide **1.90** (82%) as the major product (Scheme 1.13).<sup>47</sup> Cram and co-workers explained this high regioselectivity by proposing the *in-situ* formation of the cationic intermediate **1.88**. In **1.88**, the hydrogen atom connected to the same carbon atom as the bromine atom is suitably oriented toward the most basic oxygen atom of the ester functionality. This orientation facilitates the intramolecular proton transfer to the oxygen atom leading to **1.89**. An alternative explanation involving the complexation of the basic oxygen atom to the electrophile and an ensuing delivery of the electrophile to the *pseudo-gem* position of the unsubstituted ring can not be completely ruled out. Worthy of note is that cationic intermediates other than **1.88** could also be considered, but none can benefit from the subsequent “intramolecular proton delivery process”.



**Scheme 1.13:** The *pseudo-gem* effect in bromination of 4-methoxycarbonyl[2.2]paracyclophane (**1.87**).

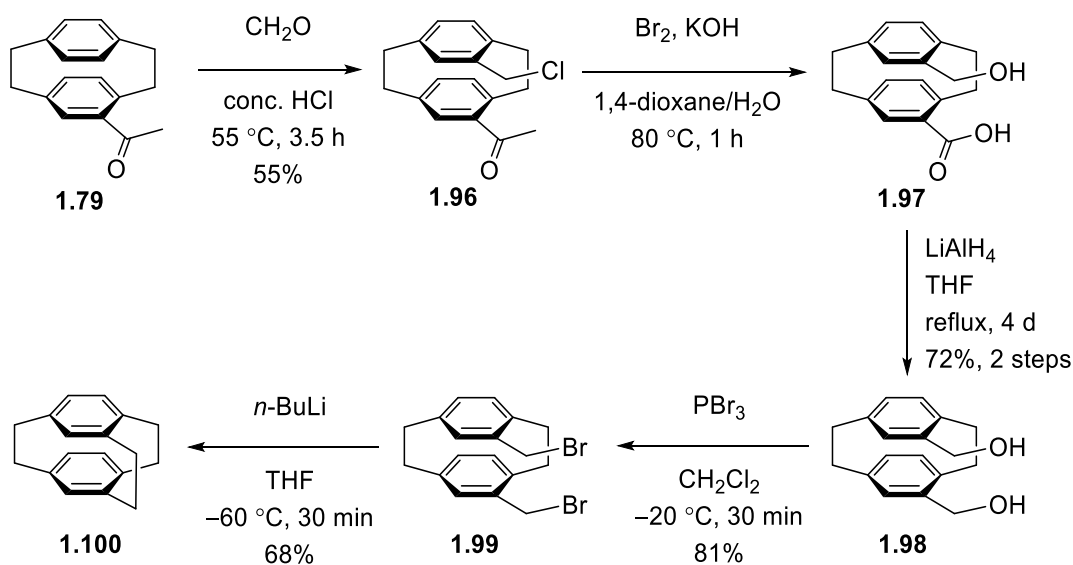
The synthesis of diamine **1.95** involves an intermediate (**1.91**), which was synthesized by taking advantage of the *pseudo-gem* effect (Scheme 1.14).<sup>48</sup> Rieche formylation of **1.87** yielded the *pseudo-gem* effect-dictated aldehyde ester **1.91** (77%), which was converted into bis(carboxylic acid) **1.92** over two steps. Treatment of **1.92** with  $\text{SOCl}_2$  led to the formation of the corresponding bis(acid chloride) (not shown) *in situ*, which was further converted to the corresponding bis(acyl azide) **1.93**. Heating a solution of **1.93** in toluene at reflux resulted in the production of diisocyanate **1.94** as a bench-stable solid by Curtius rearrangement. Finally, hydrolysis of **1.94** afforded diamine **1.95**.



**Scheme 1.14:** Synthesis of *pseudo-gem* diamine **1.95**.

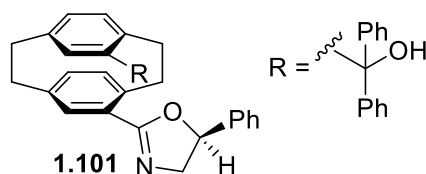
There are three important aspects of the *pseudo-gem* effect. Firstly, the control of regioselectivity in the functionalization of the opposite ring can be exploited in the target-oriented synthesis of structurally complex cyclophanes, which would be rather difficult to access by conventional synthetic methods, as demonstrated by the synthesis of diamine **1.95** (Scheme 1.14).

Secondly, the effect offers a platform for the introduction of additional bridges into the [2.2]paracyclophane backbone. The preparation of [2.2.2](1,2,4)cyclophane (**1.100**) (Scheme 1.15) represents such an example.<sup>49</sup> Chloromethylation of 4-acetyl[2.2]paracyclophane (**1.79**) took place at the *pseudo-gem* position, affording the corresponding cyclophane **1.96** (55%). Oxidation of **1.96** with bromine under basic conditions furnished carboxylic acid **1.97**, which was reduced with LiAlH<sub>4</sub> to give diol **1.98** (72%, 2 steps). Bromination of **1.98** with PBr<sub>3</sub> afforded bis(bromomethyl)[2.2]paracyclophane **1.99** (81%). Finally, treatment of **1.99** with *n*-BuLi resulted in the formation of a new bridge, leading to **1.100** (68%).



**Scheme 1.15:** Synthesis of [2.2.2](1,2,4)cyclophane (**1.100**) from 4-acetyl[2.2]paracyclophane (**1.79**).

Thirdly, the *pseudo-gem* effect has been instrumental in the synthesis of multifunctionalized chiral [2.2]paracyclophane derivatives, the vast majority of which have gained increasing interest in asymmetric synthesis as ligands.<sup>50</sup> Oxazolinylcyclophane **1.101** (Figure 1.10) represents such a planar chiral ligand that has proved to be useful in the enantioselective addition of diethylzinc to benzaldehydes to form the corresponding benzyl alcohols in high levels of enantioselectivity.<sup>50b</sup>



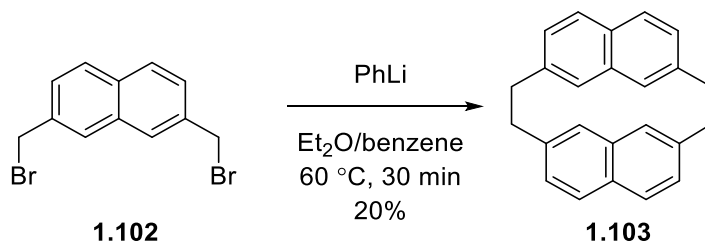
*ligand used in the enantioselective addition of diethylzinc to aldehydes  
ee upto 95% (ref. 50b)*

**Figure 1.10:** Selected example of a planar chiral [2.2]paracyclophane-based ligand.

### 1.3.5 Synthesis of [m.n]Cyclophanes

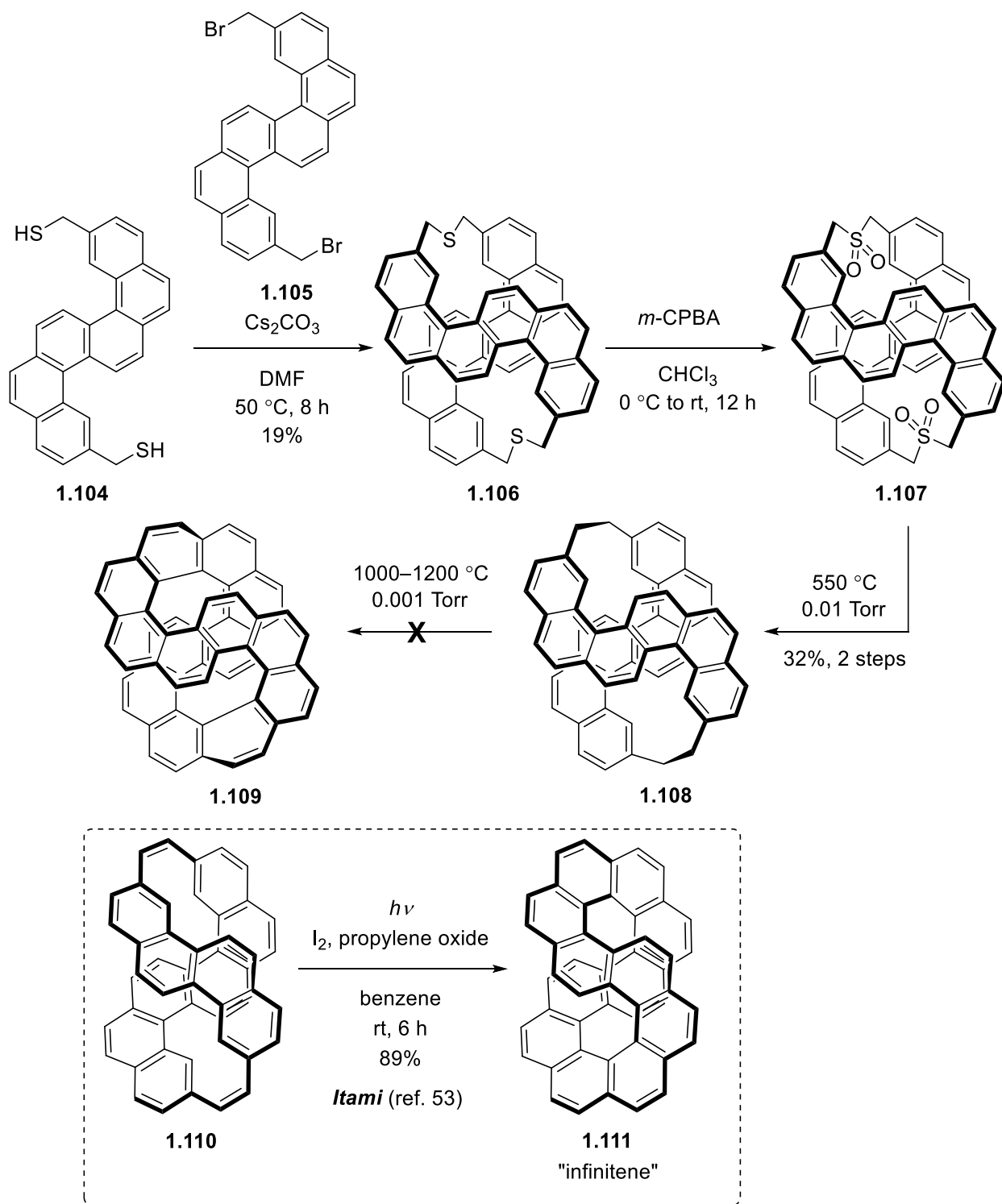
#### 1.3.5.1 Synthesis of [m.n]Cyclophanes Utilizing Type I Strategies

The Wurtz coupling remains one of the oldest synthetic methods to forge a new C–C bond in organic synthesis. Baker and co-workers' synthesis of [2.2]naphthalenophane **1.103** demonstrates the use of the Type I-a strategy (Section 1.1.1) by employing a Wurtz coupling reaction (Scheme 1.16).<sup>51</sup> Treatment of 2,7-bis(bromomethyl)naphthalene (**1.102**) with phenyllithium (prepared *in situ* from bromobenzene and lithium) afforded **1.103** in low yield (20%).



**Scheme 1.16:** Synthesis of [2.2]naphthalenophane **1.103** by Baker and co-workers.

The synthesis of [2.2](3,11)dibenzo[*c,l*]chrysenophane (**1.108**) was achieved by using a Type I-b strategy (Scheme 1.17).<sup>52</sup> Reaction of dithiol **1.104** with 3,11-bis(bromomethyl)dibenzo[*c,l*]chrysene (**1.105**) under basic conditions afforded dithiacyclophane **1.106** in low yield (19%). Compound **1.106** was transformed into disulfone **1.107** by oxidation with *m*-CPBA. Pyrolysis of **1.107** delivered **1.108** (32%, 2 steps). Unfortunately, this cyclophane could not be converted into the figure eight-shaped polynuclear aromatic hydrocarbon (PAH) **1.109**. Very recently, a similar cyclophane **1.110** was reported by Itami and co-workers using a similar synthetic approach and it was successfully converted into the topologically interesting PAH “infinifene” **1.111** (Scheme 1.17, inset) by a two-fold Mallory reaction.<sup>53</sup>

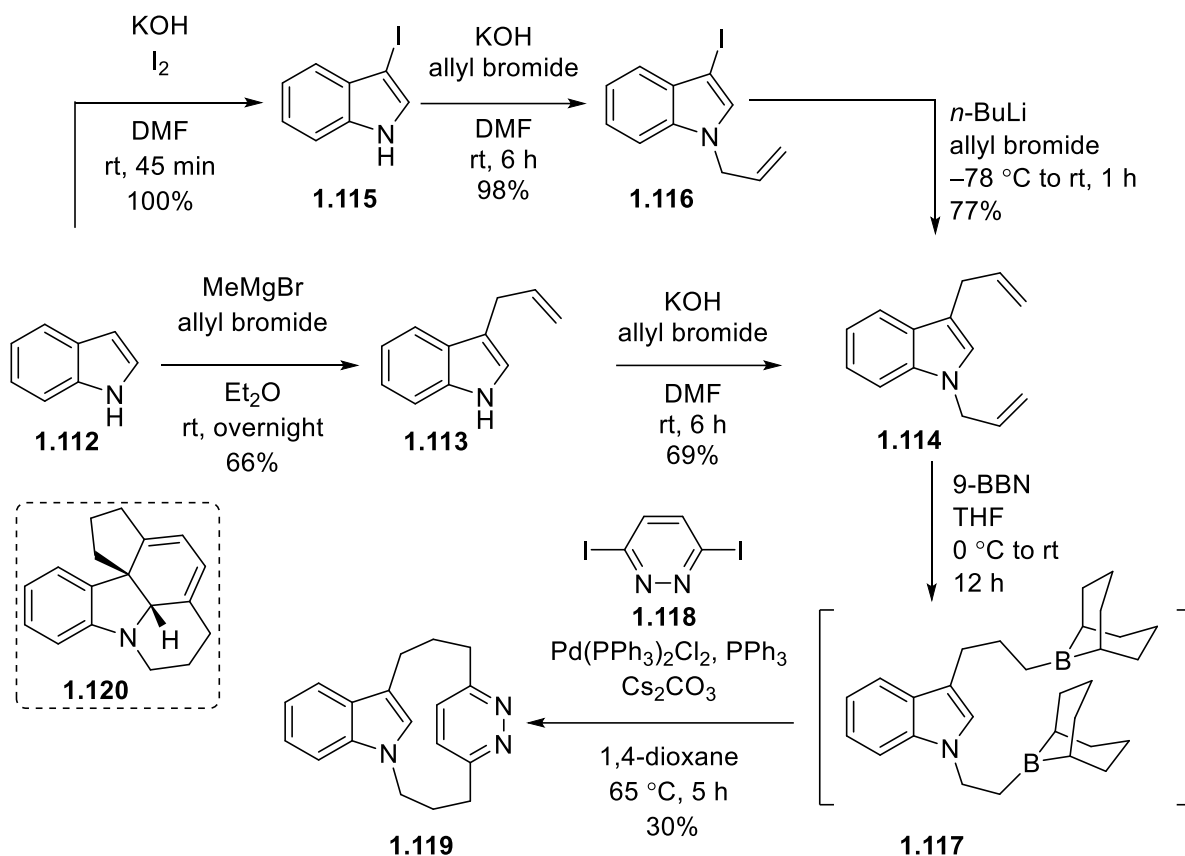


**Scheme 1.17:** Synthesis of [2.2](3,11)dibenzo[*c,l*]chrysenophane (**1.108**) by Matsubara and co-workers.

Inset: conversion of cyclophanediene **1.110** to infinitene **1.111** under photochemical conditions.

### 1.3.5.2 Synthesis of [*m.n*]Cyclophanes Utilizing the Type II Strategy

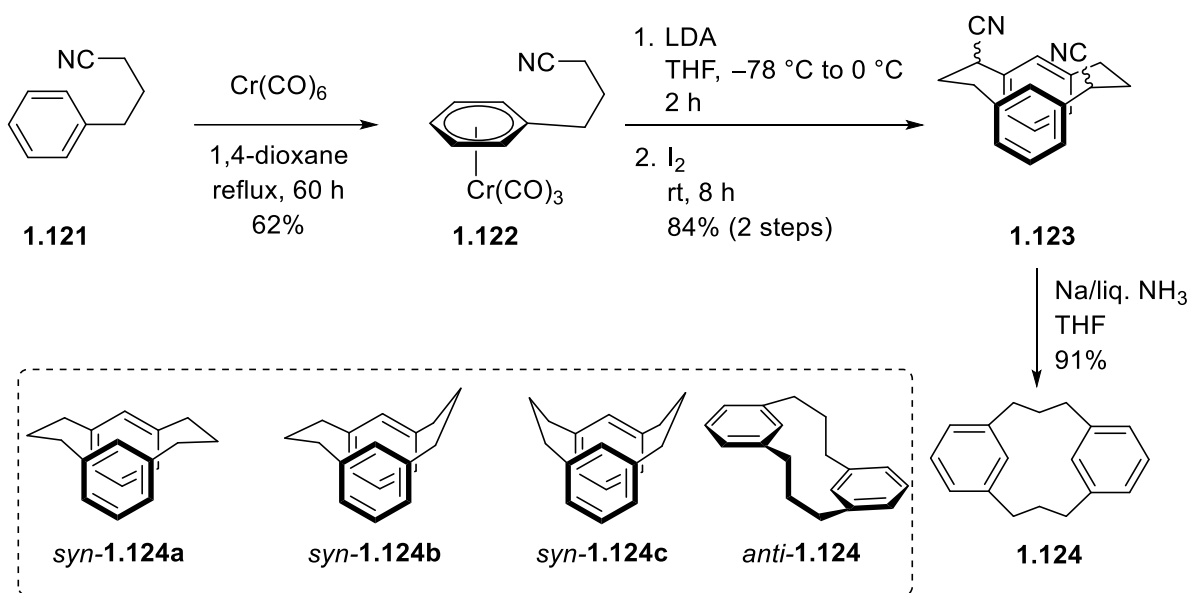
In 2001, the Bodwell group reported an elegant synthesis of [3](3,6)pyridazino[3](1,3)indolophane (**1.119**) from commercially available indole (**1.112**) (Scheme 1.18).<sup>54</sup> Strategically, the last step of the synthesis falls under the Type II strategy. 1,3-Diallylindole (**1.114**) was prepared from **1.112** *via* two different routes. The first route consists of two steps. C3 allylated indole **1.113** was obtained by treatment of **1.112** with MeMgBr followed by allyl bromide. The choice of the base MeMgBr is important for the C3 selectivity because the magnesium counterion reduces the nucleophilicity of the nitrogen atom in the *in-situ* generated salt by strong coordination. Treatment of **1.113** with KOH followed by allyl bromide resulted in *N*-allylation to afford **1.114**. The second route commences with the preparation of 3-iodoindole (**1.115**) from **1.112**. The iodination reaction led to the formation of **1.115** quantitatively, which was *N*-allylated to give **1.116** in a near quantitative yield (98%). Subjection of **1.116** to a lithiation/allylation protocol furnished the required 1,3-diallylindole (**1.114**). The overall yield for the first route was 46%. The overall yield was significantly improved to 75% following the second route. Treatment of **1.114** with 9-BBN presumably afforded the organoborane species **1.117**, which without isolation was reacted with 3,6-diiodopyridazine (**1.118**) under Suzuki–Miyaura cross-coupling conditions to give the [3.3]cyclophane **1.119** (30%). In this regard, it is noteworthy that the synthesis of **1.119** is the first example wherein the Suzuki–Miyaura reaction has been used for the preparation of a [3.3]cyclophane. The synthetic utility of **1.119** was foreshadowed by its conversion to the pentacycle **1.120** (Scheme 1.18, inset) through an inverse electron demand Diels–Alder (IEDDA) reaction. The pentacyclic product has immense potential as a precursor to be utilized in the synthesis of a wide variety of indole alkaloids.



**Scheme 1.18:** Synthesis of [3.3]cyclophane **1.119** by Bodwell and co-workers.

Using the Type II strategy, Semmelheck and co-workers completed a concise 4-step synthesis of [3.3]metacyclophane (**1.124**) (Scheme 1.19) from phenylbutyronitrile (**1.121**).<sup>7</sup> Coordination of a transition metal to the  $\pi$ -system of an arene renders the aromatic system substantially electron deficient, which allows for the addition of nucleophiles on the aromatic system. The effect of activation by transition metals in the nucleophilic attack to arenes is well preceded in the literature.<sup>55</sup> The synthesis of **1.124** delineated below involves the use of such a transition metal-assisted strategy. Reaction of **1.121** with chromium hexacarbonyl in 1,4-dioxane at reflux afforded tricarbonylchromium complex(0) **1.122** (62%). Treatment of **1.122** with LDA followed by decomplexation with iodine (oxidative conditions) afforded 1,10-dicyano[3.3]metacyclophane (**1.123**) as a mixture of isomers. The two cyano groups were cleaved

by subjecting **1.123** to reductive conditions (Na/liq. NH<sub>3</sub>), providing **1.124** in excellent yield (91%). The X-ray crystal structure of **1.124** reveals a chair-chair conformation (*syn*-**1.124a**). Molecular mechanics calculations suggested that *syn*-**1.124a** was more stable than *syn*-**1.124b**, *syn*-**1.124c**, and *anti*-**1.124** by 0.60, 1.07, and 6.57 kcal/mol, respectively.

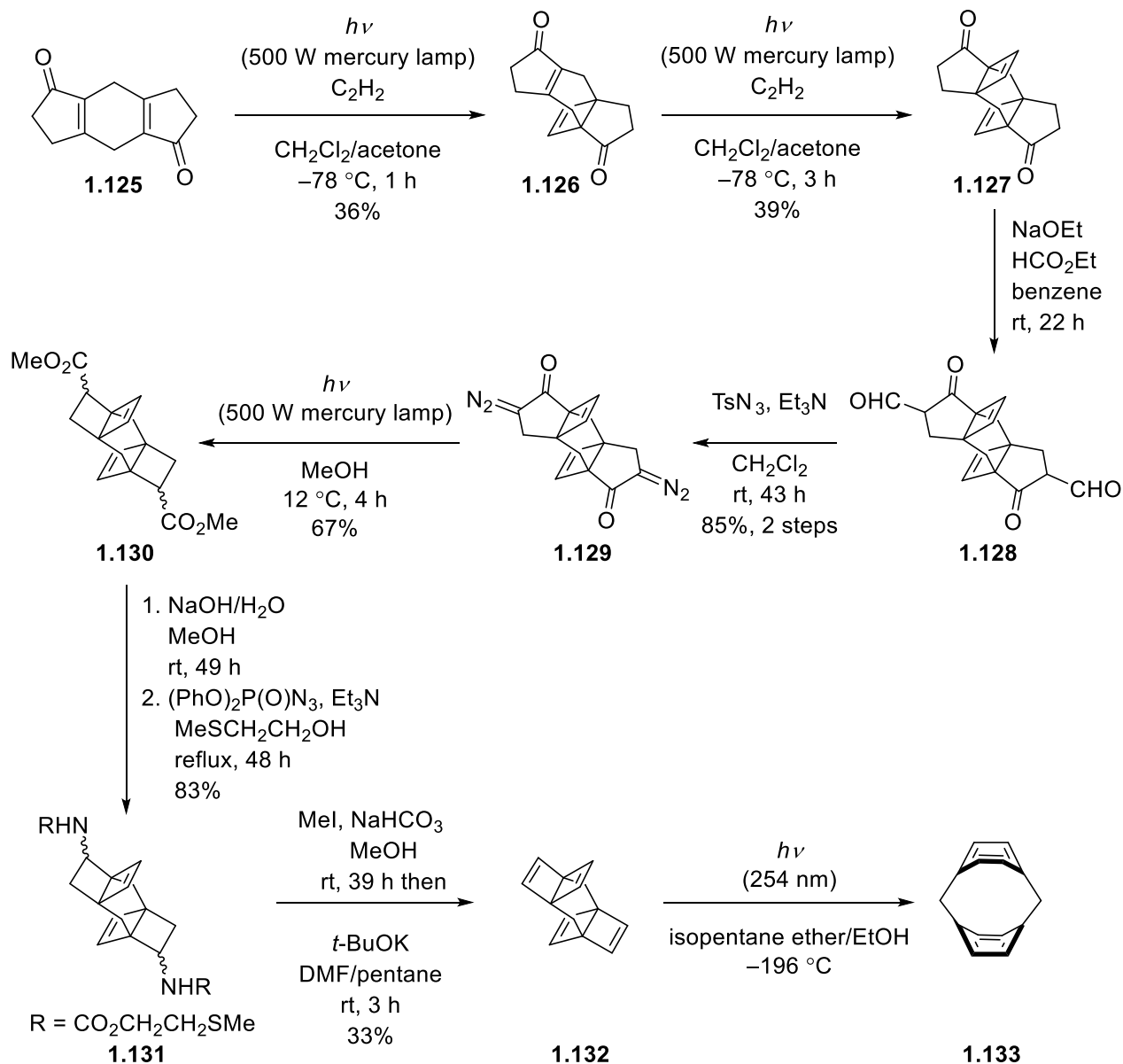


**Scheme 1.19:** Synthesis of [3.3]metacyclophane (**1.124**) by Semmelheck and co-workers.

### 1.3.5.3 Synthesis of [*m.n*]Cyclophanes Utilizing the Type III Strategy

In addition to the synthesis of highly strained [*n*]cyclophanes, the type III strategy discussed in Section 1.1.1 has been also successful in gaining access to small, strained [*m.n*]cyclophanes, as demonstrated by the synthesis of [1.1]paracyclophane (**1.133**) below.

The synthesis of **1.133** commenced with the photochemical [2+2] cycloaddition between the advanced starting material, tricyclic diketone **1.125** and acetylene to afford diketone **1.126**



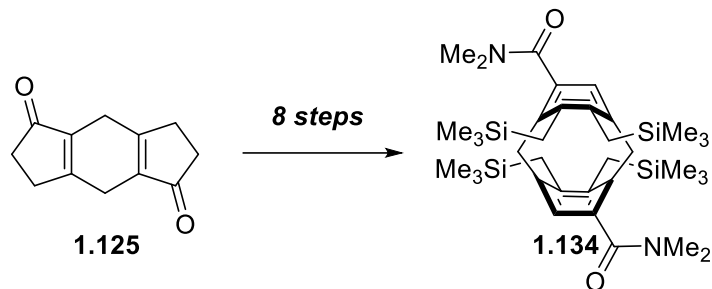
**Scheme 1.20:** Synthesis of [1.1]paracyclophane (**1.133**) by Tsuji and co-workers.

(36%) as a major product along with diketone **1.127** (12%) (Scheme 1.20).<sup>56</sup> Compound **1.127**, resulting from a two-fold [2+2] cycloaddition, was a key intermediate in the synthesis. To obtain synthetically useful quantities of **1.127**, **1.126** was subjected to a further [2+2] cycloaddition reaction under the same conditions. Treatment of **1.127** with NaOEt/HCO<sub>2</sub>Et led to the formation of bis(ketoaldehyde) **1.128** presumably with the enol tautomers. Subsequently, a deformylative

diazo transfer reaction of **1.128** furnished bis(diazoketone) **1.129** (85%, 2 steps). The five-membered rings in **1.129** were contracted under Wolff rearrangement conditions to afford diester **1.130** as a mixture of three stereoisomers. Hydrolysis of **1.130** afforded a mixture of the corresponding carboxylic acids. Exposure of the mixture to diphenyl phosphoryl azide in the presence of Et<sub>3</sub>N as a base resulted in the formation of the corresponding mixture of isocyanates, which was trapped with 2-(methylthio)ethanol to yield carbamate **1.131**. Compound **1.131** was converted into the corresponding quaternary salt, which underwent a double elimination reaction upon treatment with *t*-BuOK to afford bis(Dewar benzene) **1.132**. It should be noted that each of the steps from **1.129** to **1.131** gave rise to the corresponding product as a mixture of stereoisomers. No attempts were made to separate the stereoisomers in any of the steps. Irradiation of a glassy mixture of **1.132** in isopentane/ether/EtOH with a 254 nm light source led to the generation of **1.133**, which was discerned from the changes in UV/vis spectrum of the reaction mixture. The absorption spectrum of **1.133** showed no sign of degradation for a few hours at -20 °C. The sufficient stability also allowed measurement of its <sup>1</sup>H NMR spectrum. The calculated overall bend ( $\alpha+\beta$ ) in the benzene rings of **1.133** was estimated to be approximately 50.0°, which is significantly smaller than that calculated (67.9°) for [4]paracyclophane (**1.10**), although comparable to that (52.2°) calculated for [5]paracyclophane (**1.15**).<sup>57</sup> Depending on the level of theory, the calculated strain energy of **1.133** is 93–128 kcal/mol.

Later, Tsuji and co-workers reported the preparation of the [1.1]paracyclophane derivative **1.134**, which is stable enough to be isolated at room temperature (Scheme 1.21).<sup>58</sup> The kinetic stabilization provided by the bulky trimethylsilyl groups near the bridgehead carbon atoms mainly contributes to the improved stability of **1.134** compared to **1.133**. The logic for introducing the bulky groups in **1.134** mirrors that used in the synthesis of the kinetically stabilized

[4]paracyclophane derivative **1.57** (Section 1.2.4.3). The trimethylsilyl groups sterically shield the bridgehead carbon atoms from the approach of reagents or protic solvents. The sequence of reactions in the synthesis of **1.134** is very similar to that exploited in the synthesis of the thermally labile parent [1.1]paracyclophane (**1.133**). The most remarkable facet of this work is that the authors were able to obtain X-ray crystallographic data for **1.134**. The average total bending angle ( $\alpha+\beta$ ) was determined to be  $49.8^\circ$  from the crystallographic data, which is very close to the calculated total bend for **1.133** and [5]paracyclophane (**1.15**). The value of  $49.8^\circ$  remains the largest experimentally obtained ( $\alpha+\beta$ ) value for a paracyclophane.



**Scheme 1.21:** 8-Step synthesis of [1.1]paracyclophane **1.134** by Tsuji and co-workers.

## 1.4 Summary

The degree of bend in the aromatic system(s) of cyclophanes modulate their chemical and physical properties. In general, cyclophanes with shorter bridges are more strained than the ones with longer bridges. The common approaches for accessing cyclophanes fall under three categories (Type I, Type II, and Type III). The Type III approaches are the ones that have been successful in gaining access to highly strained cyclophanes. The success of the type III approach relies on the gain of aromatic stabilization energy (ASE) that accompanies the generation of the new aromatic system. The synthesis of a few selected examples of  $[n]$ cyclophanes and  $[m.n]$ cyclophanes have been discussed, showcasing the power and limitations of the Type I–III approaches. Although the Type III strategy has been relied upon for the generation of highly strained cyclophanes, it is still

quite limited in terms of the structural types it has been able to deliver. There remains considerable scope for improvement and/or the development of new strategies that can fill the gap.

## 1.5 References

1. Ghasemabadi, P. G.; Yao, T.; Bodwell, G. J. *Chem. Soc. Rev.* **2015**, *44*, 6494–6518.
2. Brown, C. J.; Farthing, A. C. *Nature* **1949**, *164*, 915–916.
3. Cram, D. J.; Steinberg, H. *J. Am. Chem. Soc.* **1951**, *73*, 5691–5704.
4. (a) Liptau, P.; Knüppel, S.; Kehr, G.; Kataeva, O.; Fröhlich, R.; Erker, G. *J. Organomet. Chem.* **2001**, *637–639*, 621–630. (b) Bodwell, G. J.; Bridson, J. N.; Houghton, T. J.; Kennedy, J. W. J.; Mannion, M. R. *Chem. Eur. J.* **1999**, *5*, 1823–1827. (c) Fürstner, A.; Szillat, H. F.; Gabor, B.; Mynott, R. *J. Am. Chem. Soc.* **1998**, *120*, 8305–8314. (d) Pellegrin, M. M. *Recl. Trav. Chim. Pays-Bas* **1899**, *18*, 457–465.
5. (a) Bodwell, G. J.; Ernst, L.; Haenel, M.; Hopf, H. *Angew. Chem. Int. Ed. Engl.* **1989**, *28*, 455–456. (b) Staab, H. A.; Kirrstetter, R. G. H. *Liebigs Ann. Chem.* **1979**, 886–898.
6. Bodwell, G. J.; Ernst, L.; Hopf, H. *Chem. Ber.* **1989**, *122*, 1013–1016.
7. Semmelhack, M. F.; Harrison, J. J.; Young, D. C.; Gutiérrez, A.; Rafii, S.; Clardy, J. *J. Am. Chem. Soc.* **1985**, *107*, 7508–7514.
8. Tsuji, T.; Ohkita, M.; Kawai, H. *Bull. Chem. Soc. Jpn.* **2002**, *75*, 415–433.
9. Cram, D. J.; Allinger, N. L.; Steinberg, H. *J. Am. Chem. Soc.* **1954**, *76*, 6132–6141.
10. (a) Ghasemabadi, P. G.; Yao, T.; Bodwell, G. J. *Chem. Soc. Rev.* **2015**, *44*, 6494–6518. (b) *Modern Cyclophane Chemistry*; Gleiter, R., Hopf, H., Eds.; Wiley-VCH: Weinheim, 2004.
11. Tobe, Y.; Ueda, K.; Kakiuchi, K.; Odaira, Y.; Kai, Y.; Kasai, N. *Tetrahedron* **1986**, *42*, 1851–1858.

12. Jenneskens, L. W.; de Kanter, F. J. J.; Kraakman, P. A.; Turkenburg, L. A. M.; Koolhaas, W. E.; de Wolf, W. H.; Bickelhaupt, F.; Tobe, Y.; Kakiuchi, K.; Odaira, Y. *J. Am. Chem. Soc.* **1985**, *107*, 3716–3717.
13. Kostermans, G. B. M.; Bobeldijk, M.; de Wolf, W. H.; Bickelhaupt, F. *J. Am. Chem. Soc.* **1987**, *109*, 2471–2475.
14. (a) Tsuji, T.; Nishida, S. *J. Chem. Soc. Chem. Commun.* **1987**, 1189–1190. (b) Tsuji, T.; Nishida, S. *J. Am. Chem. Soc.* **1988**, *110*, 2157–2164.
15. Turkenburg, L. A. M.; Blok, P. M. L.; de Wolf, W. H.; Bickelhaupt, F. *Tetrahedron Lett.* **1981**, *22*, 3317–3320.
16. Jenneskens, L. W.; de Boer, H. J. R.; de Wolf, W. H.; Bickelhaupt, F. *J. Am. Chem. Soc.* **1990**, *112*, 8941–8949.
17. Kostermans, G. B. M.; van Dansink, P.; de Wolf, W. H.; Bickelhaupt, F. *J. Am. Chem. Soc.* **1987**, *109*, 7887–7888.
18. Shuvalov, V. Y.; Eltsov, I. V.; Tumanov, N. A.; Boldyreva, E. V.; Nefedov, A. A.; Sagitullina, G. P. *Eur. J. Org. Chem.* **2017**, 5410–5416.
19. Bockisch, F.; Rayez, J. C.; Liotard, D.; Duguay, B. *J. Comput. Chem.* **1992**, *13*, 1047–1056.
20. Cram, D. J.; Daeniker, H. U. *J. Am. Chem. Soc.* **1954**, *76*, 2743–2752.
21. Hubert, A. J.; Dale, J. *J. Chem. Soc.* **1963**, 86–93.
22. Newton, M. G.; Walter, T. J.; Allinger, N. L. *J. Am. Chem. Soc.* **1973**, *95*, 5652–5658.
23. Allinger, N. L.; Walter, T. J. *J. Am. Chem. Soc.* **1972**, *94*, 9267–9268.
24. Otsubo, T.; Misumi, S. *Synth. Commun.* **1978**, *8*, 285–289.
25. Wolf, A. D.; Kane, V. V.; Levin, R. H.; Jones Jr., M. *J. Am. Chem. Soc.* **1973**, *95*, 1680.
26. Tobe, Y.; Kaneda, T.; Kakiuchi, K.; Odaira, Y. *Chem. Lett.* **1985**, 1301–1304.

27. Ma, B.; Sulzbach, H. M.; Remington, R. B.; Schaefer III, H. F. *J. Am. Chem. Soc.* **1995**, *117*, 8392–8400.
28. Schleyer, P. v. R.; Pühlhofer, F. *Org. Lett.* **2002**, *4*, 2873–2876.
29. (a) Tsuij, T.; Okuyama, M.; Ohkita, M.; Kawai, H.; Suzuki, T. *J. Am. Chem. Soc.* **2003**, *125*, 951–961. (b) Okuyama, M.; Tsuji, T. *Angew. Chem. Int. Ed. Engl.* **1997**, *36*, 1085–1087.
30. van Straten, J. W.; de Wolf, W. H.; Bickelhaupt, F. *Tetrahedron Lett.* **1977**, *18*, 4667–4670.
31. Turkenburg, L. A. M.; de Wolf, W. H.; Bickelhaupt, F.; Cofino, W. P.; Lammertsma, K. *Tetrahedron Lett.* **1983**, *24*, 1821–1824.
32. Turkenburg, L. A. M.; van Straten, J. W.; de Wolf, W. H.; Bickelhaupt, F. *J. Am. Chem. Soc.* **1980**, *102*, 3256–3257.
33. (a) Morisaki, Y.; Chujo, Y. *Angew. Chem. Int. Ed.* **2006**, *45*, 6430–6437. (b) Gibson, S. E.; Knight, J. D. *Org. Biomol. Chem.* **2003**, *1*, 1256–1269.
34. Gulder, T.; Baran, P. S. *Nat. Prod. Rep.* **2012**, *29*, 899–934.
35. (a) Patel, S.; Dais, T. N.; Plieger, P. G.; Rowlands, G. J. *Beilstein J. Org. Chem.* **2021**, *17*, 1518–1526. (b) Shimizu, T.; Hita, K.; Paudel, A.; Tanaka, J.; Yamato, T. *J. Chem. Res.* **2009**, 244–247. (c) Vögtle, F.; Neumann, P. *Synthesis* **1973**, *2*, 85–103.
36. (a) Hassan, Z.; Spuling, E.; Knoll, D. M.; Bräse, S. *Angew. Chem. Int. Ed.* **2020**, *59*, 2156–2170. (b) Hassan, Z.; Spuling, E.; Knoll, D. M.; Lahann, J.; Bräse, S. *Chem. Soc. Rev.* **2018**, *47*, 6947–6963. (c) Paradies, J. *Synthesis* **2011**, 3749–3766.
37. Cram, D. J.; Cram, J. M. *Acc. Chem. Res.* **1971**, *4*, 204–213.
38. (a) Reich, H. J.; Cram, D. J. *J. Am. Chem. Soc.* **1969**, *91*, 3517–3526. (b) Reich, H. J.; Cram, D. J. *J. Am. Chem. Soc.* **1967**, *89*, 3078–3080.

39. Rathnayake, R. M. N. M.; Duignan T. T.; Searles D. J.; Zhao, X. S. *Phys. Chem. Chem. Phys.* **2021**, *23*, 3063–3070.
40. Dyson, P. J.; Humphrey, D. G.; McGrady, J. E.; Suman, P.; Tocher, D. *J. Chem. Soc., Dalton Trans.* **1997**, 1601–1606.
41. Eliel, E. L.; Wilen, S. H. *Stereochemistry of Organic Compounds*; Wiley: New York, 1994; pp 1166–1170.
42. Cahn, R. S.; Ingold, C. K.; Prelog, V. *Angew. Chem. Int. Ed. Engl.* **1966**, *5*, 385–415.
43. Boschi, R.; Schmidt, W. *Angew. Chem. Int. Ed. Engl.* **1973**, *12*, 402–404.
44. Cram, D. J.; Wechter, W. J.; Kierstead, R. W. *J. Am. Chem. Soc.* **1958**, *80*, 3126–3132.
45. (a) Cram, D. J.; Allinger, N. L. *J. Am. Chem. Soc.* **1955**, *77*, 6289–6294. (b) Cram, D. J.; Kierstead, R. W. *J. Am. Chem. Soc.* **1955**, *77*, 1186–1190. (c) Cram, D. J.; Abell, J. *J. Am. Chem. Soc.* **1955**, *77*, 1179–1186.
46. Singer, L. A.; Cram, D. J. *J. Am. Chem. Soc.* **1963**, *85*, 1080–1084.
47. Reich, H. J.; Cram, D. J. *J. Am. Chem. Soc.* **1969**, *91*, 3505–3516.
48. Zitt, H.; Dix, I.; Hopf, H.; Jones, P. G. *Eur. J. Org. Chem.* **2002**, 2298–2307.
49. Truesdale, E. A.; Cram, D. J. *J. Am. Chem. Soc.* **1973**, *95*, 5825–5827.
50. (a) Rozenberg, V. I.; Antonov, D. Y.; Sergeeva, E. V.; Vorontsov, E. V.; Starikova, Z. A.; Fedyanin, I. V.; Schulz, C.; Hopf, H. *Eur. J. Org. Chem.* **2003**, 2056–2061. (b) Wu, X.-W.; Hou, X.-L.; Dai, L.-X.; Tao, J.; Cao, B.-X.; Sun, J. *Tetrahedron: Asymmetry* **2001**, *12*, 529–532.
51. Baker, W.; McOmie, J. F. W.; Warburton, W. K. *J. Chem. Soc.* **1952**, 2991–2993.
52. Matsubara, H.; Yano, K.; Yamamoto, K. *Polycyclic Aromat. Compd.* **2001**, *19*, 165–177.

53. Krzeszewski, M.; Ito, H.; Itami, K. *J. Am. Chem. Soc.* **2021**, DOI: 10.1021/jacs.1c10807. (b)  
Krzeszewski, M.; Ito, H.; Itami, K. *ChemRxiv* **2021**, DOI: 10.33774/chemrxiv-2021-pcwcc.
54. (a) Bodwell, G. J.; Li, J. *Org. Lett.* **2002**, *4*, 127–130. (b) Li, J. PhD Dissertation, Memorial  
University of Newfoundland, 2002.
55. Pape, A. R.; Kaliappan, K. P.; Kündig, E. P. *Chem. Rev.* **2000**, *100*, 2917–2940.
56. Tsuji, T.; Ohkita, M.; Konno, T.; Nishida, S. *J. Am. Chem. Soc.* **1997**, *119*, 8425–8431.
57. Grimme, S. *J. Am. Chem. Soc.* **1992**, *114*, 10542–10547.
58. Kawai, H.; Suzuki, T.; Ohkita, M.; Tsuji, T. *Angew. Chem. Int. Ed.* **1998**, *37*, 817–819.

## **Chapter 2: Contractive Annulation: A Strategy for the Synthesis of Small, Strained Cyclophanes and Its Application in the Synthesis of [2](6,1)Naphthaleno[1]paracyclophane**

### **Statement of Co-Authorship**

The majority of this chapter has been published in *Angew. Chem. Int. Ed.* **2019**, 58, 9166–9170.

Authors: Sourav Biswas, Christopher S. Qiu, Prof. Louise N. Dawe, Prof. Yuming Zhao, and Prof. Graham J. Bodwell.

Sourav Biswas (listed as 1<sup>st</sup> author): Performed the synthetic work, physical data collection, data analysis, and contributed significantly to the preparation of the manuscript.

Christopher S. Qiu: Calculated the strain energies of [2.2]paracyclophane (**2.11**) and [2](6,1)naphthaleno[1]paracyclophane (**2.12**) by DFT calculations.

Louise N. Dawe: Solved the crystal structure of [2](6,1)naphthaleno[1]paracyclophane (**2.12**) and provided a publishable crystal structure report.

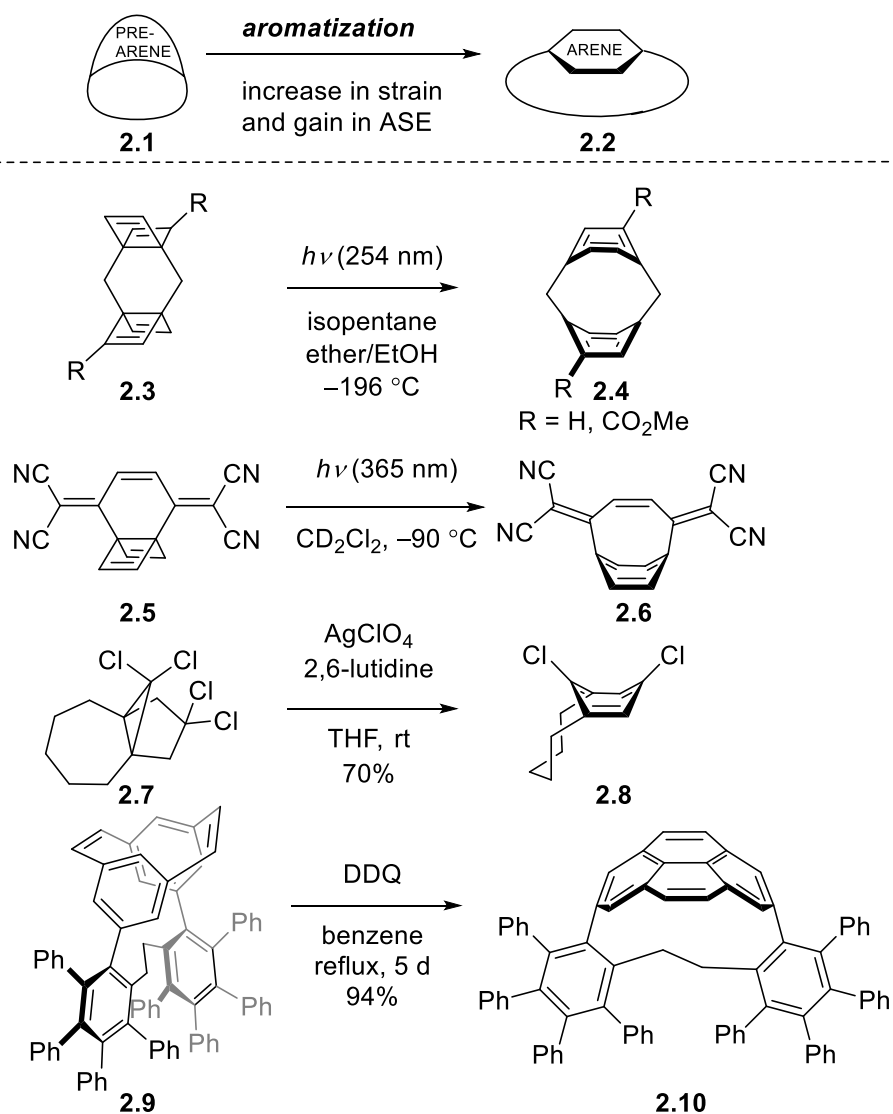
Yuming Zhao: Performed all computational calculations, interpreted the results, contributed to writing of the corresponding sections of the manuscript.

Graham J. Bodwell: Principal investigator (PI) of the work, who led the project and majorly contributed to the interpretation/analysis of data and writing of the manuscript.

The article has been reproduced in this chapter in an adapted form that includes the contributions of all the co-authors for the purpose of a complete discussion.

## 2.1 Introduction

Ever since the early days of cyclophane chemistry, the pursuit of ever-smaller and more strained cyclophanes has been of interest owing to the unusual chemical and physical properties that arise in such systems. As the degree of strain increases, so does the synthetic challenge and a variety of inventive synthetic approaches to small, strained cyclophanes have been developed. From a strategic perspective, all of these approaches fall under the same general strategy (Type III



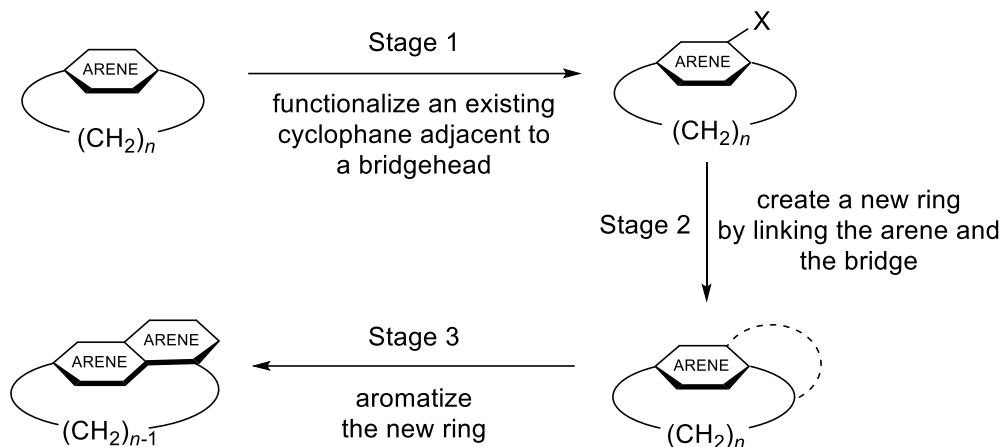
**Scheme 2.1:** Existing aromatization-based approach to the syntheses of highly strained cyclophanes and selected examples of its use.

strategy, Chapter 1), which is the only one that has been found to be effective in gaining access to the most highly-strained cyclophanes. It involves the conversion of a bridged, nonplanar “pre-arene” (**2.1**) into the corresponding cyclophane (**2.2**) *via* some sort of aromatization reaction (Scheme 2.1). Using this approach, only benzene and pyrene have been bent to the limits of stability, as exemplified by cyclophanes **2.4**,<sup>1</sup> **2.6**,<sup>2</sup> **2.8**<sup>3</sup> and **2.10**,<sup>4</sup> which were generated from bridged Dewar benzenes **2.3** and **2.5**, propellane **2.7**, and bridged [2.2]metacyclophane-1,9-diene **2.9**, respectively. The details of the syntheses of **2.4** (R = H), **2.6**, and **2.8** have been discussed in Chapter 1. All other strategies for the synthesis of cyclophanes,<sup>5</sup> *i.e.* those based on macrocyclization or ring contraction, fail when called upon to deliver highly-strained systems. The success of the arene-forming strategy is attributable to the gain of aromatic stabilization energy (ASE) during the cyclophane-forming reaction, which serves to counterbalance the concomitant increase in strain. The initial results on the conception and realization of a new strategy for the synthesis of highly-strained cyclophanes are presented in this chapter.

## 2.2 Objective

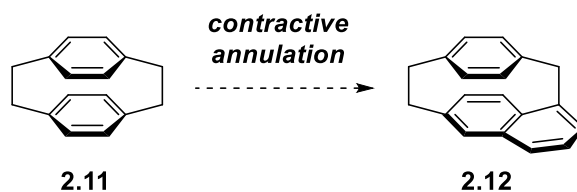
Although the strategy involving the conversion of a “pre-arene” to an “arene” has been relied upon for the generation of highly strained cyclophanes, it is still quite limited in terms of the structural types it has been able to deliver. This offered an opportunity for the development a new strategy. The new strategy consists of a three-stage process, which commences with an existing cyclophane (Scheme 2.2). The first step is to functionalize the aromatic system at a position adjacent to one of the bridgeheads. This is followed by synthetic manipulation that leads to the formation of a new ring linking the arene to the neighbouring benzylic position. Finally, the new ring is aromatized to afford a new cyclophane, in which the aromatic system has been enlarged by one new benzenoid ring and the bridge has been contracted by one carbon atom. The term “contractive

annulation” captures the essence of this approach. As in the existing arene-forming strategy, the gain of ASE in the final step is meant to play a role in offsetting the increase in strain.



**Scheme 2.2:** Contractive annulation strategy for simultaneously growing the aromatic component of a cyclophane and contracting its bridge.

To test the contractive annulation strategy, [2.2]paracyclophane (**2.11**) was chosen as a starting material. In addition to its ready availability, relatively low cost and well-understood chemistry, every non-quaternary aromatic position is adjacent to a bridgehead, so fulfillment of Stage 1 should not be complicated by issues of regioselectivity. The successful application of the contractive annulation strategy on **2.11** could provide [2](6,1)naphthaleno[1]paracyclophane (**2.12**), which was expected to be more strained than **2.11** (Scheme 2.3).



**Scheme 2.3:** Contractive annulation of [2.2]paracyclophane (**2.11**).

## 2.3 Results and Discussion

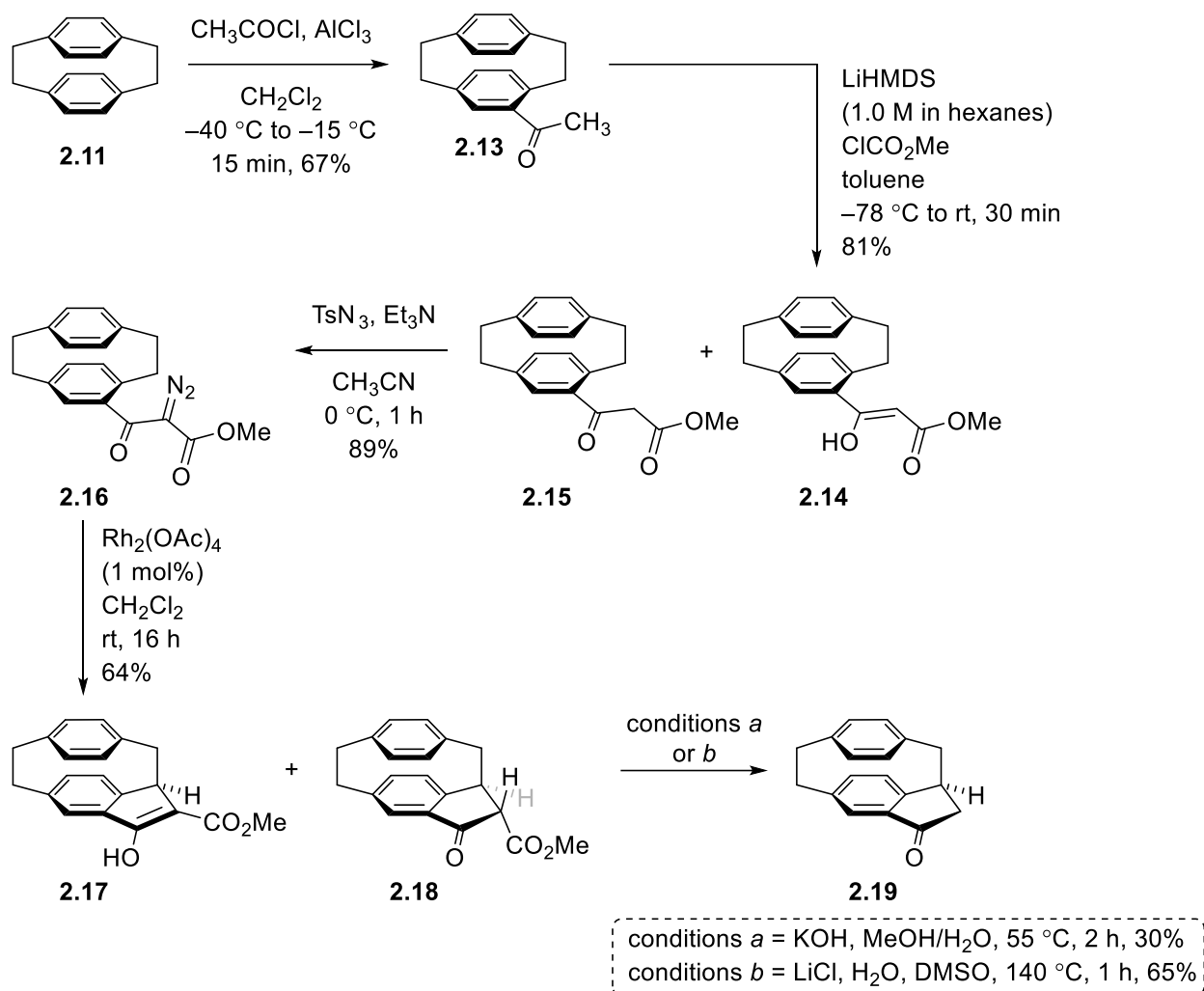
With regard to Stage 2, there does not appear to be any precedent among the large body of literature on the chemistry of [2.2]paracyclophane for the formation of a covalent link between one of the

benzene rings and an adjacent bridge. As a first step in this direction, methodology for the functionalization of a bridge atom adjacent to an aryl substituent was sought. Directed metalation reactions have achieved this objective on two occasions,<sup>6</sup> but the prospects for using the resulting functionality to quickly install a six-membered all-carbon ring did not appear to be good. Thus, an alternative way of approaching Stage 2 was devised and this involved the use of an intramolecular carbene C–H insertion reaction.

### 2.3.1 Synthesis

Accordingly, to accomplish the fulfillment of Stage 1, [2.2]paracyclophane (**2.11**) was acylated under Friedel-Crafts conditions to afford 4-acetyl[2.2]paracyclophane (**2.13**) (67%) (Scheme 2.4).<sup>7</sup> For the aforementioned C–H insertion reaction, a diazo functionality needed to be installed next to the carbonyl group in **2.13**. The Regitz diazo transfer reaction is one of the frequently utilized reactions for the installation of a diazo functionality in 1,3-dicarbonyl compounds.<sup>8</sup> With an aim to convert **2.13** to a  $\beta$ -keto ester, **2.13** was treated with LiHMDS to generate the corresponding enolate *in situ*, which was trapped with methyl chloroformate to give an inseparable *ca.* 89:11 mixture of  $\beta$ -keto ester **2.15** and its enol tautomer **2.14** (81%). To set the stage for the key insertion reaction, subjection of the mixture of **2.14** and **2.15** to Regitz diazo transfer conditions afforded  $\alpha$ -diazo- $\beta$ -keto ester **2.16** (89%). Although, the involvement of the ester functionality in the reaction sequence might seem redundant, there are two possible benefits of its incorporation. Firstly, the attachment of an ester group to the methyl carbon of **2.13** would be expected to increase the acidity of the resulting methylene protons ( $\alpha$ -to the keto group) significantly, which in turn should facilitate the installation of the diazo group in the diazo transfer reaction. Secondly, in general,  $\alpha$ -diazo- $\beta$ -keto esters are known to be more thermally stable than  $\alpha$ -diazoketones.<sup>9</sup> The greater

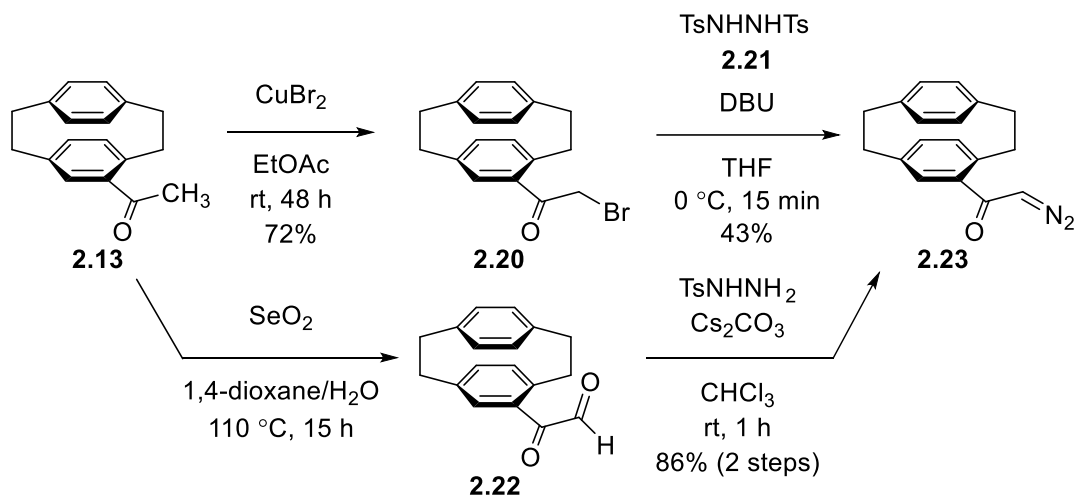
stability of  $\alpha$ -diazo- $\beta$ -keto esters is attributed to the electron-withdrawing ability of the ester groups. This in turn makes the handling of  $\alpha$ -diazo- $\beta$ -keto esters safer than that of  $\alpha$ -diazoketones. Gratifyingly, **2.16** underwent C–H insertion reaction in the presence of 1 mol% of  $\text{Rh}_2(\text{OAc})_4$  to furnish a *ca.* 83:17 mixture of  $\beta$ -keto ester **2.18** and the enol tautomer **2.17** (64%). The stereochemistry of the  $\alpha$ -carbon atom to both the keto and the ester groups in **2.18** was tentatively assigned based on the experimentally observed small coupling constant ( $J = 0.8$  Hz) between the two methine protons of the five-membered ring ( $\delta = 4.30$  and  $3.65$  ppm). Inspection of molecular models reveals that the H–C–C–H dihedral angle in **2.18** is close to  $90^\circ$ , whereas the corresponding angle in its epimer (not shown) is *ca.*  $30^\circ$ . Increasing the loading of the catalyst  $\text{Rh}_2(\text{OAc})_4$  to 2% did not improve the yield, rather led to a diminished yield (52%). To remove the ester functionality, the mixture of **2.17** and **2.18** was subjected to classical decarboxylation conditions (Scheme 2.4, conditions *a*,) to afford indanone **2.19** (30%). Exposure of the mixture of **2.17** and **2.18** to Krapcho dealkoxycarbonylation conditions (Scheme 2.4, conditions *b*) led to the formation of **2.19** in moderate yield (65%).



**Scheme 2.4:** Synthesis of indanone **2.19** from [2.2]paracyclophane (**2.11**).

After checking the viability of the C–H insertion reaction, focus was next turned to prepare  $\alpha$ -diazoketone **2.23** from 4-acetyl[2.2]paracyclophane (**2.13**) (Scheme 2.5). If successful, this would shorten the step count from **2.13** to **2.19**, which could perhaps improve the overall yield. Bromination<sup>10</sup> of **2.13** with  $\text{CuBr}_2$  resulted in the formation of  $\alpha$ -bromoketone **2.20** (72%). Treatment of **2.20** with *N,N'*-ditosylhydrazine (**2.21**) in the presence of DBU as base afforded  $\alpha$ -diazoketone **2.23** (43%) as a pale yellow solid. Compound **2.23** was found to be stable in the solid state for several months under ambient conditions. The overall yield in going from **2.13** to **2.23** (31%) was rather low, so the use of a different reaction sequence was investigated. Ketone **2.13**

was converted into glyoxal **2.22** (presumably as a mixture with its hydrate) under Riley oxidation conditions,<sup>11</sup> which upon reaction with tosyl hydrazide in the presence of Cs<sub>2</sub>CO<sub>3</sub> produced **2.23**. The overall yield for this two-step sequence was 86%.

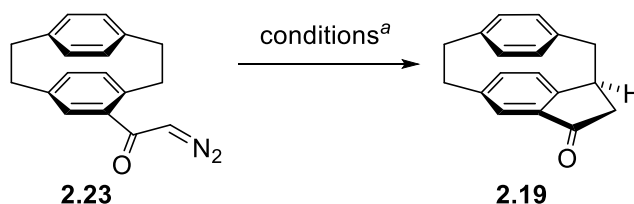


**Scheme 2.5:** Preparation of  $\alpha$ -diazoketone **2.23** from 4-acetyl[2.2]paracyclophane (**2.13**).

The influence of several reaction parameters (catalyst, solvent, and temperature) for the intramolecular C–H insertion reaction of  $\alpha$ -diazoketone **2.23** was examined. The results are depicted in Table 2.1. Reaction carried out with 2 mol% of Rh<sub>2</sub>(OAc)<sub>4</sub> in CH<sub>2</sub>Cl<sub>2</sub> at room temperature afforded **2.19** in 51% yield (Table 2.1, Entry 1). Reduction of the catalyst loading to 1 mol% had practically no effect on the yield, furnishing **2.19** in essentially same yield (52%) (Table 2.1, Entry 2). The yield was slightly improved when the reaction was performed at 40 °C (Table 2.1, Entry 3). A significant increase in yield (64%) was observed when the temperature was decreased to 0 °C (Table 2.1, Entry 4). Changing the solvent from CH<sub>2</sub>Cl<sub>2</sub> to 1,2-dichloroethane or  $\alpha,\alpha,\alpha$ -trifluorotoluene led to diminished yields (Table 2.1, Entries 5 and 6). Among the rest of the conditions screened (Table 2.1, Entries 7–10), the set of conditions of Entry 8 was found to be as effective as the conditions of Entry 4. However, when Rh<sub>2</sub>(oct)<sub>4</sub> was used as the catalyst, in both cases (Entries 8 and 9), purification of **2.19** by silica gel column

chromatography became problematic as the catalyst coeluted with **2.19** as evident from visual observation (a green colored band was found to coelute with a yellow band). Hence, Entry 4 proved to be the optimal set of conditions for the C–H insertion reaction. Worthy of note is that the insertion reaction under the “Entry 4” conditions was amenable to a gram-scale synthesis of indanone **2.19** without a significant deterioration in yield (*cf.* 62% yield on a 7.6 mmol scale).

**Table 2.1:** Optimization of C–H insertion reaction conditions.

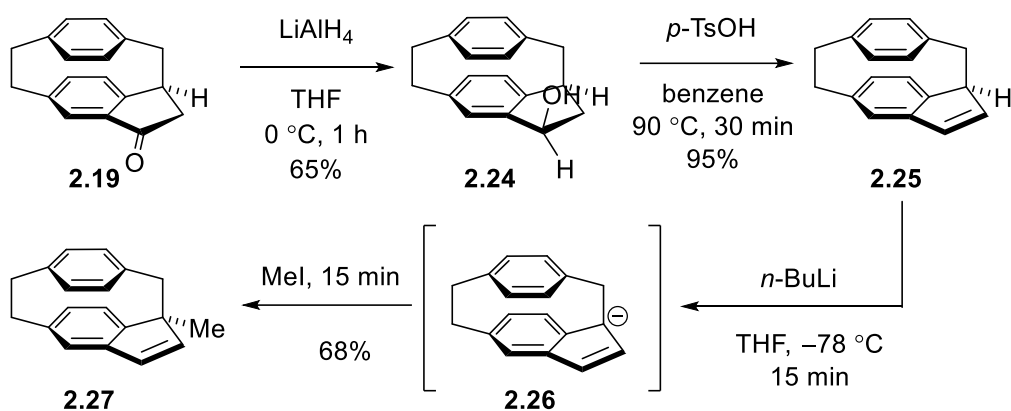


| Entry | Catalyst                           | Cat. Loading | Solvent                         | Temperature | Time   | Yield <sup>b</sup> |
|-------|------------------------------------|--------------|---------------------------------|-------------|--------|--------------------|
| 1     | Rh <sub>2</sub> (OAc) <sub>4</sub> | 2 mol%       | CH <sub>2</sub> Cl <sub>2</sub> | rt          | 30 min | 51%                |
| 2     | Rh <sub>2</sub> (OAc) <sub>4</sub> | 1 mol%       | CH <sub>2</sub> Cl <sub>2</sub> | rt          | 30 min | 52%                |
| 3     | Rh <sub>2</sub> (OAc) <sub>4</sub> | 1 mol%       | CH <sub>2</sub> Cl <sub>2</sub> | 40 °C       | 30 min | 54%                |
| 4     | Rh <sub>2</sub> (OAc) <sub>4</sub> | 1 mol%       | CH <sub>2</sub> Cl <sub>2</sub> | 0 °C        | 45 min | 64%                |
| 5     | Rh <sub>2</sub> (OAc) <sub>4</sub> | 1 mol%       | 1,2-DCE                         | 0 °C        | 45 min | 59%                |
| 6     | Rh <sub>2</sub> (OAc) <sub>4</sub> | 1 mol%       | PhCF <sub>3</sub>               | 0 °C        | 60 min | 53%                |
| 7     | Rh <sub>2</sub> (TFA) <sub>4</sub> | 1 mol%       | CH <sub>2</sub> Cl <sub>2</sub> | 0 °C        | 45 min | 55%                |
| 8     | Rh <sub>2</sub> (oct) <sub>4</sub> | 1 mol%       | CH <sub>2</sub> Cl <sub>2</sub> | 0 °C        | 45 min | 61% <sup>c</sup>   |
| 9     | Rh <sub>2</sub> (oct) <sub>4</sub> | 1 mol%       | CH <sub>2</sub> Cl <sub>2</sub> | rt          | 30 min | 59% <sup>c</sup>   |
| 10    | Rh <sub>2</sub> (esp) <sub>2</sub> | 1 mol%       | CH <sub>2</sub> Cl <sub>2</sub> | rt          | 30 min | 57%                |

<sup>a</sup>Reaction conditions: **2.23** (0.18 mmol), catalyst (as per table), solvent (4 mL). <sup>b</sup>Isolated yields. <sup>c</sup>Coeluted catalyst is present as impurity. Rh<sub>2</sub>(TFA)<sub>4</sub> = rhodium(II) trifluoroacetate dimer. Rh<sub>2</sub>(oct)<sub>4</sub> = rhodium(II) octanoate dimer. Rh<sub>2</sub>(esp)<sub>2</sub> = bis[rhodium( $\alpha,\alpha',\alpha',\alpha'$ -tetramethyl-1,3-benzenedipropionic acid)].

Indanone **2.19** was reduced with LiAlH<sub>4</sub> to afford indanol **2.24** (65%) as a single diastereomer (Scheme 2.6). The stereochemistry could not be determined unambiguously, but it

is highly likely that the hydride is delivered from the less hindered bottom face of the carbonyl group to give the isomer shown. Acid-catalyzed dehydration of **2.24** led to the formation of indene **2.25** (95%). Indene **2.25** is an interesting system in that deprotonation of it would deliver the corresponding indenide **2.26**, wherein the indene moiety would follow Hückel's  $4N+2$  rule ( $N = 2$ ) and thereby would become aromatic. The successful preparation of **2.26** would serve as the first proof of principle of the contractive annulation strategy because the transformation of [2.2]paracyclophane (**2.11**) to **2.26** would meet all the requirements of "Stage 1–3". In fact, treatment of **2.25** with *n*-BuLi followed by methyl iodide provided methylindene **2.27** (68%), which implies the intermediacy of **2.26**.



**Scheme 2.6:** Conversion of indanone **2.19** to methylindene **2.27**.

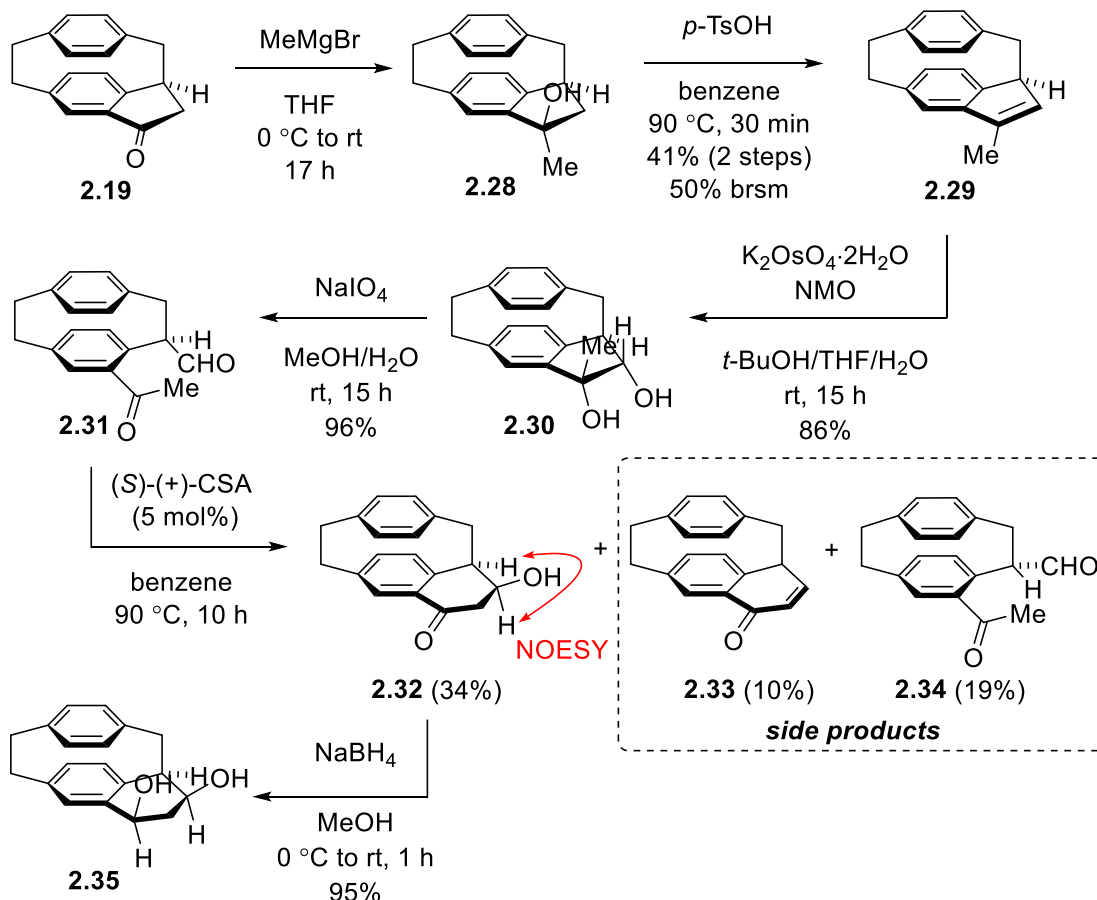
### 2.3.1.1 First Attempted Route toward the Synthesis of [2](6,1)Naphthaleno[1]paracyclophane (**2.12**)

Having indanone **2.19** in hand, the transformation of it into [2](6,1)naphthaleno[1]paracyclophane (**2.12**) was explored. Since the newly created arene-bridge link was a five-membered ring, ring-expansion was then required to establish a suitable framework for Stage 3. Grignard reaction of **2.19** with MeMgBr afforded a *ca.* 71:29 mixture of indanol **2.28** and the unreacted starting material **2.19** (Scheme 2.7) as judged from the  $^1\text{H}$  NMR spectrum of the crude reaction mixture. As for the

reduction of **2.19** to **2.24** (Scheme 2.6), in this case, the reagent (MeMgBr) likely attacked the carbonyl group of **2.19** from the bottom face to give the stereoisomer shown. Prolonging the reaction time or adding an excess of MeMgBr did not lead to complete consumption of **2.19**. This is likely due to competitive deprotonation of **2.19** by MeMgBr to provide the corresponding enolate, which would then be unreactive toward 1,2-addition of the Grignard reagent. Surprisingly, the starting material **2.28** and the product **2.19** were found to have the same  $R_f$  value ( $R_f = 0.27$  in 20% ethyl acetate/hexanes). A variety of other solvent systems of varying polarity were screened for TLC analysis, but none of them brought about meaningful separation. No further attempts (*e.g.* recrystallization) were made and the crude mixture was subjected to dehydration conditions to give indene **2.29** (41%, 2 steps). Column chromatographic purification also resulted in 17% recovery of the unreacted indanone **2.19**. Upjohn dihydroxylation<sup>12</sup> of **2.29** afforded the vicinal diol **2.30**, wherein both hydroxyl groups are on the same side of the five-membered ring. Although not determined unequivocally, the reagent presumably approached from the less-hindered bottom face of **2.29**, which placed the hydroxyl groups as shown in the structure of **2.30**. Oxidative cleavage of **2.30** with NaIO<sub>4</sub> provided ketoaldehyde **2.31** in excellent yield (96%). An acid-catalyzed intramolecular aldol reaction of **2.31** afforded  $\beta$ -hydroxytetralone **2.32** (34%). The stereochemistry at the carbon atom bearing the hydroxyl group was not unambiguously determined. Attempts to grow crystals suitable for X-ray analysis failed. A NOESY experiment showed a correlation between the methine proton on the bridge and the one on the OH-bearing carbon atom, but this would also be expected for the epimer of **2.32**. The chemical shift of the methine proton bound to the OH-bearing carbon was calculated by DFT computational methods at the GIAO-B3LYP/6-311+G(2d,p) level of theory for both **2.32** and its epimer. The methine proton in question was calculated to resonate at  $\delta = 4.31$  ppm for **2.32** and  $\delta$

= 3.84 ppm for its epimer (see Appendix 1) according to the DFT calculations. Careful analysis of the  $^1\text{H}$  NMR spectrum revealed that the methine proton on the OH-bearing carbon atom appeared as an apparent td at  $\delta$  4.78 ppm. The difference ( $\Delta\delta$ ) between the experimentally observed chemical shift value of 4.78 ppm and DFT-calculated value of 4.31 ppm is 0.47 ppm, whereas the difference between ( $\Delta\delta$ ) the experimentally observed chemical shift value of 4.78 ppm and DFT-calculated value of 3.84 ppm is 0.94 ppm. The smaller chemical shift difference of 0.47 ppm supported the notion that compound **2.32** as opposed to the epimer of **2.32** was the product formed in the aldol reaction. DFT-calculations at the M06-2X/Def2SVP level of theory also revealed that **2.32** was thermodynamically more stable than its epimer by 0.3 kcal/mol.

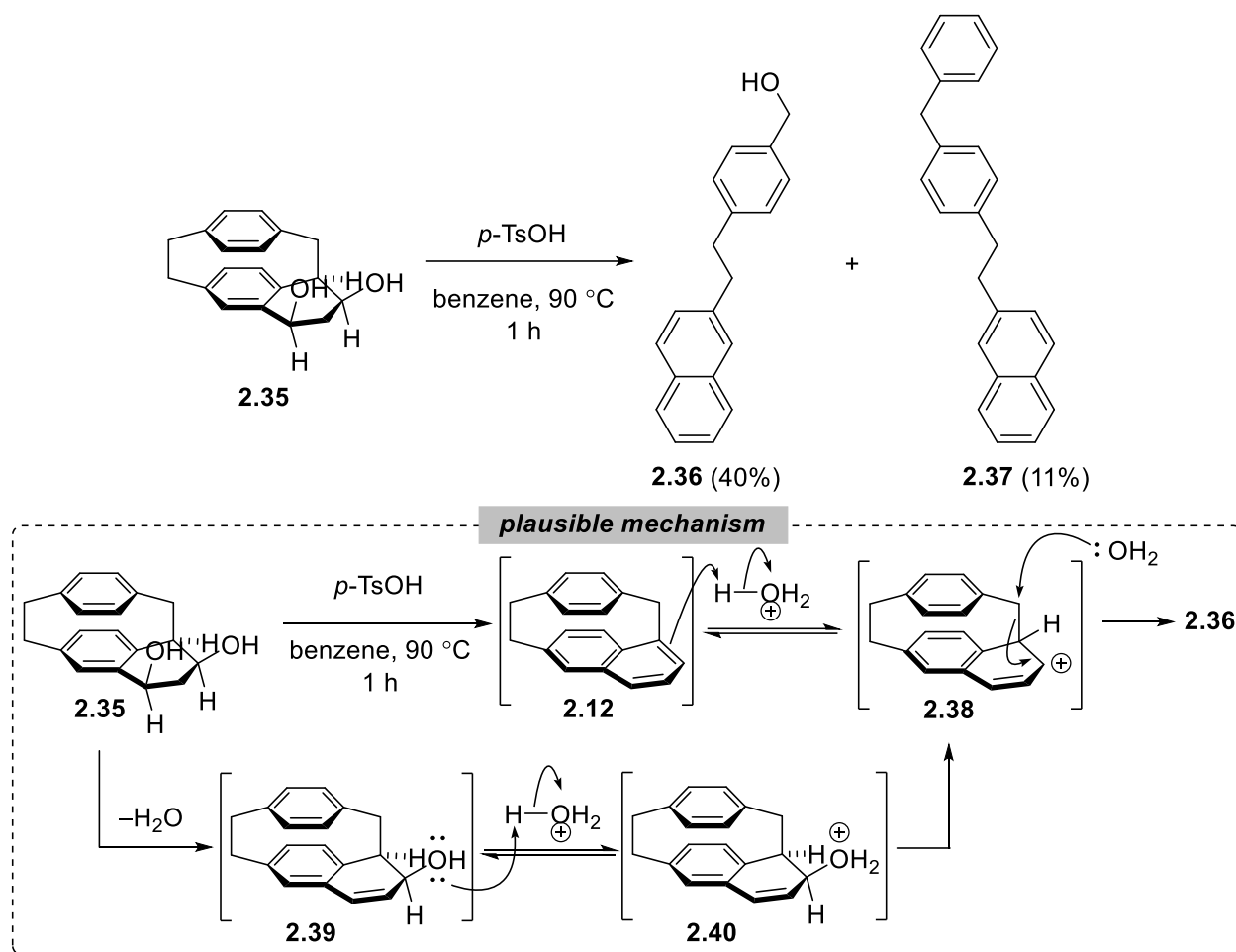
The low yield of **2.32** could be rationalized by considering two undesired reactions, the evidence for which was gleaned from the experimental outcome. Firstly, under the reaction conditions, **2.32** underwent dehydration to afford enone **2.33** (10%). Secondly, an acid-catalyzed epimerization at the methine carbon atom of the bridge in **2.31** led to the formation of ketoaldehyde **2.34** (19%).  $\beta$ -Hydroxytetralone **2.32** was reduced with  $\text{NaBH}_4$ , which presumably attacked from the bottom face of the carbonyl group, affording diol **2.35** (95%). This set the platform for Stage 3.



**Scheme 2.7:** Synthesis of diol **2.33** from indanone **2.19**.

Diol **2.35** contains all the necessary carbon atoms that are present in cyclophane **2.12**. A two-fold dehydration of **2.35** was deemed to afford **2.12**. Unfortunately, subsection of **2.35** to dehydration conditions (catalytic amount of *p*-TsOH) resulted in the rupture of the cyclophane framework and furnished 4-[2-(2-naphthalenyl)ethyl]benzyl alcohol (**2.36**) and diphenylmethane **2.37** in 40% and 11% yields, respectively (Scheme 2.8). A plausible mechanism accounting for the formation of **2.36** is delineated below (Scheme 2.8, inset). A double elimination of water *via* two successive E1 reactions was the expected pathway from **2.35** to form **2.12**, and this may indeed have occurred. Upon closer examination, the benzylic alcohol would be expected to be involved in the elimination first due to the more stable benzylic carbocation intermediate. Protonation of the remaining OH group and loss of water would then afford allylic alcohol **2.39**. Protonation of

**2.12** under the acidic reaction conditions would be expected to occur selectively at the bridgehead carbon ( $\alpha$ -carbon) of the naphthalene moiety to regenerate the carbocation intermediate **2.38** because it would cause more strain relief than protonation at any other naphthalene  $\alpha$ -position. The CH<sub>2</sub>–CH bond in **2.38** appears to be aligned with the adjacent empty *p*-orbital of the allylic carbocation moiety. Nucleophilic attack by water at the neighboring benzylic carbon atom in an S<sub>N</sub>2-like reaction leads to C–C bond cleavage to furnish **2.36**. The overall process from **2.12** to **2.36** is a retro-Friedel–Crafts alkylation reaction. Instead of water, an attack of the solvent (benzene) as nucleophile followed by loss of a proton from the resulting arenium ion intermediate (not shown) results in the formation of **2.37**. Attempts to convert the hydroxyl groups of **2.35** into better leaving groups by tosylation or mesylation and a subsequent two-fold elimination reaction in the presence of a base (Et<sub>3</sub>N or DBU) to obtain **2.12** met with failure.

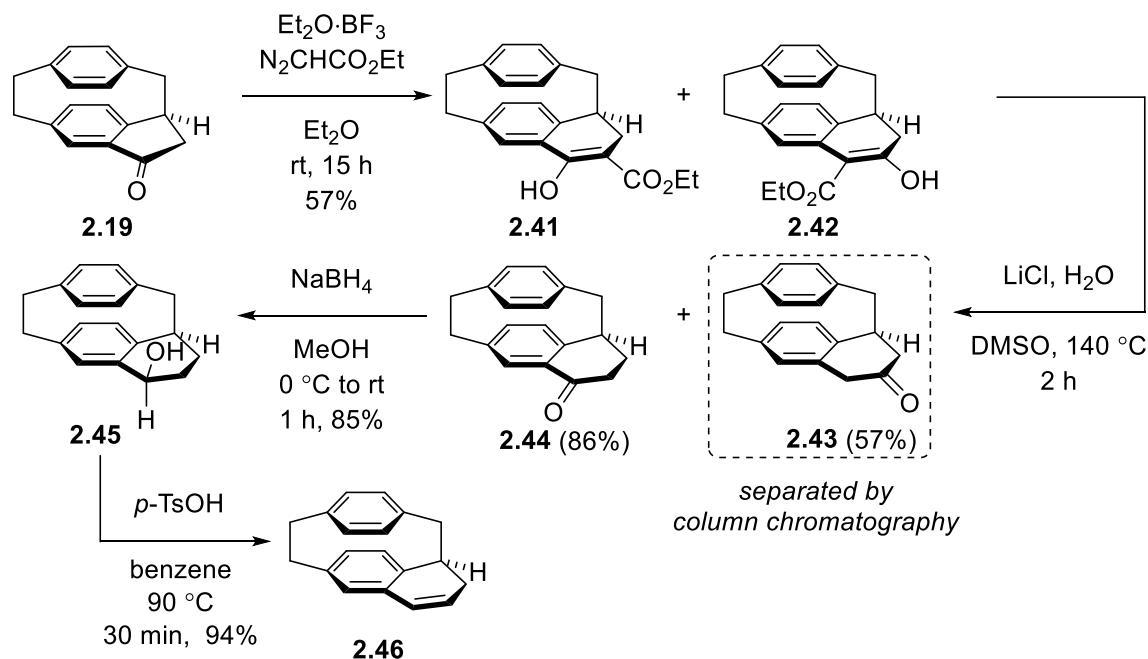


**Scheme 2.8:** Acid-catalyzed ring opening reaction leading to **2.36** and **2.37**. Inset: mechanism for the ring opening reaction.

### 2.3.1.2 Successful Synthesis of [2](6,1)Naphthaleno[1]paracyclophane (**2.12**)

The inaccessibility of **2.12** following the previous route (*vide supra*) prompted the investigation of a different route. Reaction of indanone **2.19** with ethyl diazoacetate in the presence of  $\text{Et}_2\text{O} \cdot \text{BF}_3$  led to a one-step ring expansion,<sup>13</sup> affording an inseparable *ca.* 93:7 mixture of enol esters **2.41** and **2.42**. Subjection of this mixture to Krapcho dealkoxycarbonylation conditions provided  $\alpha$ -tetralone **2.44** (46%, 2 steps from **2.19**) and  $\beta$ -tetralone **2.43** (2%, 2 steps from **2.19**), which were separated by column chromatography. Based on a 93:7 ratio of enol esters **2.41** and **2.42**, the individual yields of **2.44** and **2.43** in the Krapcho dealkoxycarbonylation are 86% and 57%,

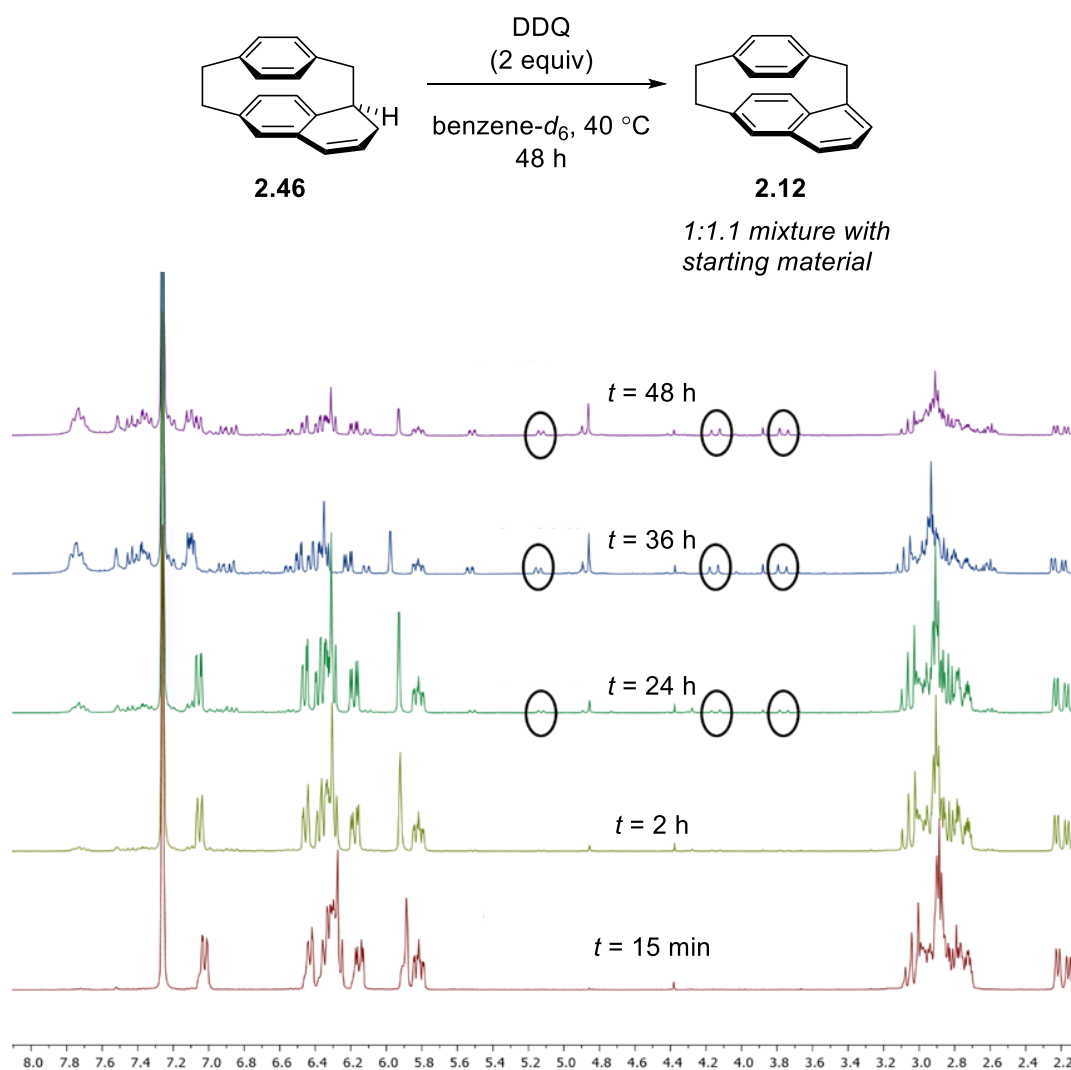
respectively. Stage 3 of the contractive annulation strategy was initiated by reduction of **2.44** with  $\text{NaBH}_4$ , which afforded tetralol **2.45** (85%) as the single diastereomer shown. The stereochemistry was assigned tentatively based on the expectation that the reducing agent attacked the carbonyl group from the less hindered bottom face of the carbonyl group. Dehydration of **2.45** in the presence of a catalytic amount of *p*-TsOH furnished dihydronaphthalene **2.46** (94%).



**Scheme 2.9:** 4-Step synthesis of dihydronaphthalene **2.46** from indanone **2.19**.

After synthesizing dihydronaphthalene **2.46**, a dehydrogenation reaction was used to obtain the targeted cyclophane **2.12**. Compounds **2.46** and **2.12** were expected to have very close  $R_f$  values, which could provide misleading information about the progress of the dehydrogenation reaction by thin-layer chromatographic (TLC) analysis. Hence, the progress of the reaction of **2.46** with 2 equivalents of DDQ (oxidant) in deuterated benzene as solvent was monitored by  $^1\text{H}$  NMR spectroscopy at different time intervals (Scheme 2.10). The  $^1\text{H}$  NMR spectrum recorded after 24 h displayed a newly developed pair of mutually coupled doublets ( $J = 14.2$  Hz) at 4.17 ppm and 3.79 ppm (AB system) attributable to the two diastereotopic methano-bridge protons of **2.12**.

Additionally, several newly developed high-field aromatic signals were observed in the  $^1\text{H}$  NMR spectrum, which were also expected for **2.12**. The highest field signal for an aromatic proton appeared at 5.14 ppm. As the reaction progressed for another 12 h ( $t = 36$  h), the new signals had grown in intensity and at  $t = 48$  h, virtually no change of the relative intensity of the signals for the product compared to the starting material (**2.46**) was observed, suggesting very little to no progress of the reaction after  $t = 36$  h.



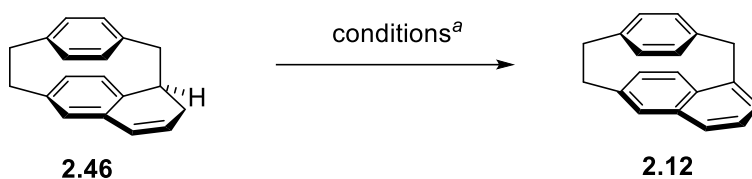
**Scheme 2.10:** Monitoring the progress of the dehydrogenation of **2.46** by  $^1\text{H}$  NMR spectroscopy.

A brief optimization of the reaction conditions revealed that the dehydrogenation reaction did not proceed at room temperature with 3 equiv of DDQ in benzene (Table 2.2, Entry 1). Elevation of the temperature to 40 °C with no change in the amount of DDQ and the solvent afforded **2.12** in 14% yield (Table 2.2, Entry 2). A further increase of the temperature to 80 °C had a deleterious effect on the yield of **2.12** (8%) (Table 2.2, Entry 3). The use of 5.0 equiv of DDQ as oxidant significantly shortened the reaction time and led to a slight increase in the yield (Table 2.2, Entry 4). It was surmised that the quinol (resulting from reduction of DDQ) that was formed in these reactions as a byproduct might be acidic ( $pK_{a1}=3.9$  and  $pK_{a2}=6.1$  as predicted by DFT calculations)<sup>14</sup> enough to trigger a retro-Friedel–Crafts reaction of **2.12**. This could be a major reason for the low yields (Table 2.2, Entries 1–4). The addition of a base could prove to be beneficial as the base would convert the quinol to the corresponding phenolate, and this would suppress the undesired decomposition pathway of **2.12**. In fact, the use of  $K_2CO_3$  as an additive led to a slight increase in yield (Table 2.2, Entry 5). The formation of **2.12** was completely shut down upon changing the solvent from benzene to more polar solvents, such as  $CH_2Cl_2$  and 1,2-DCE (Table 2.2, Entries 6 and 7). In both cases, TLC analysis indicated the formation of only baseline material.

An alternative two-step protocol (bromination/elimination reactions) was also examined for the conversion of **2.46** to **2.12**. Bromination of **2.46** followed by a two-fold elimination reaction with *t*-BuOK as base resulted in the formation of **2.12** in 11% yield. All of the DDQ-mediated reactions in benzene were much cleaner and the isolation of **2.12** was straightforward and easy. The use of  $Et_3N$ -neutralized silica gel or neutral alumina in lieu of commercially available normal phase silica gel as the stationary phase for the column chromatographic purification of **2.12** was examined to check if the acidic nature of the stationary phase had contributed to the isolated low

yield of **2.12** (Table 2.2, Entry 5). The isolated yields of 17% and 20% following the use of Et<sub>3</sub>N-neutralized silica gel and neutral alumina, respectively, as stationary phase, were comparable to the yield of 19% (Table 2.2, Entry 5) following the use of commercially available silica gel. Cyclophane **2.12** is stable both in the solid state for months and in solution (benzene, dichloromethane, chloroform, and ethyl acetate) for at least two weeks under ambient conditions.

**Table 2.2:** Screening of reaction conditions for the dehydrogenation of dihydronaphthalene **2.46**.



| Entry | Conditions   | Yield <sup>b</sup> |
|-------|--|--------------------|
| 1     | DDQ (3.0 equiv), benzene, rt, 27 h   | no reaction        |
| 2     | DDQ (3.0 equiv), benzene, 40 °C, 30 h  | 14%                |
| 3     | DDQ (3.0 equiv), benzene, 80 °C, 18 h  | 8%                 |
| 4     | DDQ (5.0 equiv), benzene, 40 °C, 20 h  | 16%                |
| 5     | DDQ (5.0 equiv), K <sub>2</sub> CO <sub>3</sub> (5.0 equiv), benzene, 40 °C, 20 h  | 19%                |
| 6     | DDQ (5.0 equiv), K <sub>2</sub> CO <sub>3</sub> (5.0 equiv), CH <sub>2</sub> Cl <sub>2</sub> , rt, 6 h                             | not detected       |
| 7     | DDQ (5.0 equiv), K <sub>2</sub> CO <sub>3</sub> (5.0 equiv), 1,2-DCE, rt, 6 h  | not detected       |
| 8     | Br <sub>2</sub> (2.1 equiv), CHCl <sub>3</sub> , 0 °C to rt, 18 h; after work up, <i>t</i> -BuOK (2.5 equiv), THF, 0 °C to rt, 3 h | 11% <sup>c</sup>   |

<sup>a</sup>Reaction conditions: **2.46** (0.41 mmol), reagent (as per table), solvent (10 mL). <sup>b</sup>Isolated yields. <sup>c</sup>*ca.* 90% pure by <sup>1</sup>H NMR analysis.

### 2.3.2 X-Ray Crystallographic Analysis

Crystals suitable for X-ray crystallographic analysis were grown by diffusion of acetonitrile into a solution of **2.12** in chloroform.<sup>15</sup> In addition to the experimentally-determined structure (Figure

2.1), a gas-phase structure of **2.12** was calculated (Def2TZVP/M062X)<sup>16</sup> and the calculated structure agrees very well with the observed structure.

Key structural features of [2.2]paracyclophane (**2.11**) are the face-to-face orientation of the two benzene rings, the boat-shaped benzene rings and their proximity. As a consequence of the contractive annulation of **2.11**, the benzene deck in naphthalenophane **2.12** no longer has a

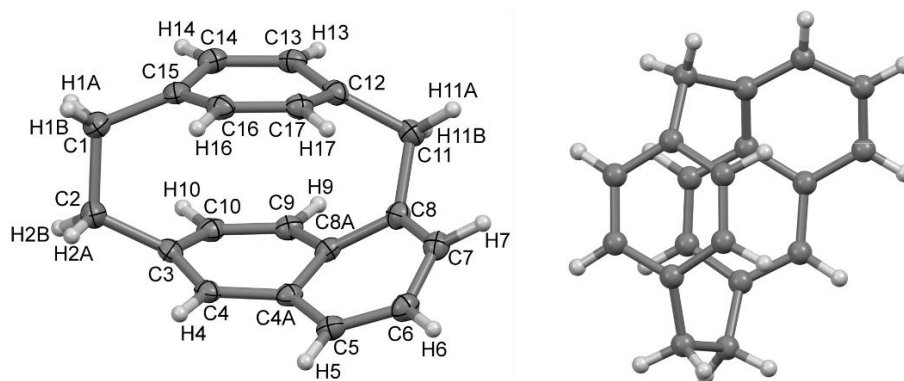


**Figure 2.1:** Two views of naphthalenophane **2.12** in the crystal with 50% displacement ellipsoids.

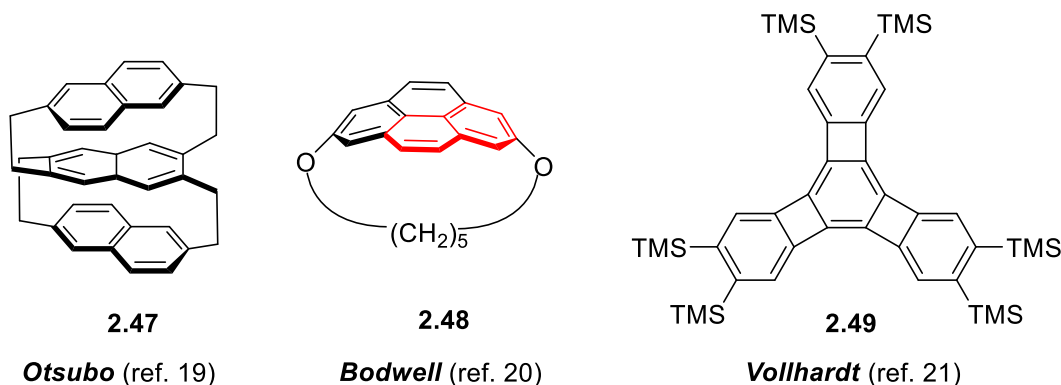
perfect face-to-face orientation with the six-membered ring below it. Instead, the centroid of the benzene ring is closer to the C9–C10 centroid (3.01 Å) than it is to the centroid of the six-membered ring beneath it (3.17 Å).

As discussed in Chapter 1, the angles  $\alpha$  and  $\beta$  are normally used to describe the distortion from planarity of bent benzene rings and their sum can be used as a measure of local distortion. For [2.2]paracyclophane (**2.11**),  $\alpha = 12.6^\circ$ ,  $\beta = 11.2^\circ$  and  $\alpha + \beta = 23.8^\circ$ .<sup>17</sup> For **2.12**, there are four sets of  $\alpha$  and  $\beta$  associated with the four bridgehead carbon atoms C3, C8, C12, and C15 (Table 2.3). The average values of  $\alpha$ ,  $\beta$  and  $\alpha + \beta$  are significantly greater than those of **2.11**, which shows that the additional strain in **2.12** is distributed around the molecule. As indicated by the  $\alpha + \beta$  values, there is a higher degree of local distortion in the vicinity of the bridgeheads of the one-carbon bridge (C8 and C12).

**Table 2.3:** Experimentally determined values of  $\alpha$ ,  $\beta$  and  $\alpha+\beta$  for **2.12**.

| Bridgehead | $\alpha$ | $\beta$  | $\alpha+\beta$ |
|------------|----------|----------|----------------|
| C(3)       | 16.4(3)° | 10.0(3)° | 26.4(4)°       |
| C(8)       | 11.7(3)° | 18.9(3)° | 30.6(4)°       |
| C(12)      | 13.3(3)° | 15.4(3)° | 28.7(4)°       |
| C(15)      | 13.2(3)° | 9.4(3)°  | 22.6(4)°       |
| Average    | 13.7(3)° | 13.4(3)° | 27.1(4)°       |

While the benzene ring in **2.12** is boat-shaped, the naphthalene system is highly twisted,<sup>18</sup> as measured by the torsion angles C3–C10–C7–C6 [35.2(2)°] and C10–C3–C6–C7 [35.0(2)°]. These values exceed that of the central naphthalene unit in triple-decker naphthalenophane **2.47**<sup>19</sup> (32°; the previously most-twisted naphthalene system in a naphthalenophane) and are just shy of the embedded naphthalene system in pyrenophane **2.48** (37°; the most distorted pyrene system for which there is a crystal structure) (Figure 2.2).<sup>20</sup>

**Figure 2.2:** Structures of comparison compounds **2.47–2.49**.

A small bond alternation was observed in the benzene deck favoring the Kekulé structure shown throughout this chapter. Starting with the C12–C13 bond, the observed bond lengths are 1.389(4), 1.401(3), 1.385(4), 1.404(4), 1.385(4) and 1.400(4) Å. The bond length differences ( $\Delta d$ )

between adjacent bonds range from 0.011 to 0.019 Å and average 0.015 Å, which exceeds three standard deviations (0.012 Å). The bond alternation is also predicted in the calculated structure, where  $\Delta d = 0.012$  Å. The magnitude of  $\Delta d$  is much less than what has been observed in benzene rings fused to three small rings, such as tris(benzocyclobutadieno)benzene **2.49** ( $\Delta d_{\text{avg}} = 0.159$  Å),<sup>21</sup> but the benzene ring in **2.12** is merely a 1,4-disubstituted system. In this regard, it is worth noting that a kinetically stabilized analog of [4]paracyclophane derivative **2.6**<sup>22</sup> has unequal bond lengths, but not bond alternation.

The bond lengths in the naphthalene system are within normal ranges,<sup>23</sup> except for C4–C4a [1.438(3) Å] and C8–C8a [1.437(3) Å], which are a little longer than the corresponding bonds in naphthalene (1.420 Å).<sup>23</sup> The stretching of these bonds is presumably a consequence of their location on the bridgehead-to-bridgehead pathway (C3 to C8).

The ethano bridge in **2.12** has bond lengths [1.521(3), 1.586(4) and 1.513(3) Å] and angles [113.9(2) and 113.7(2)°] that closely resemble those in **2.11** (1.511 and 1.593 Å; 113.7°).<sup>17</sup> The C15–C1–C2–C3 torsion angle is 9.5°, which makes the C1–C2 bond somewhat less eclipsed than its fully eclipsed counterpart in **2.11**.<sup>17</sup> The methano bridge (C11) has a compressed C–C–C bond angle of 104.73(19)° and the two bonds lengths [1.542(3) and 1.537(3) Å] are a little elongated.

### **2.3.3 Strain Energy (SE) and Nucleus-Independent Chemical Shifts (NICS) Calculations by Computational Methods**

One of the aims of the contractive annulation strategy is that it should bring about a substantial increase in strain energy. To evaluate the extent to which this objective was achieved, the strain energies of **2.11** (25.6 kcal/mol) and **2.12** (44.1 kcal/mol) were calculated at the M06-2X/Def2TZVP level of theory (Figure 2.3).<sup>16</sup> The 18.5 kcal/mol increase in strain corresponds to a 72% absolute increase. However, taking the number of skeletal atoms into account, the strain

energy increases from 1.60 kcal/mol per carbon atom in **2.11** to 2.32 kcal/mol per carbon atom in **2.12**, a 45% overall increase. By either measure, the increase in strain is indeed substantial.

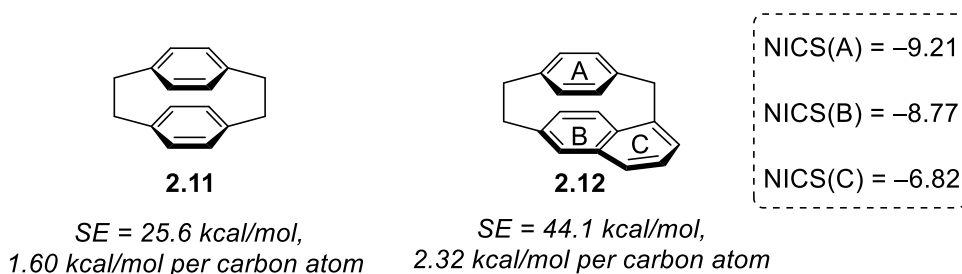


**Figure 2.3:** Strain energies of **2.11**–**2.12** and NICS values for **2.12**.

The calculated NICS values of the nonplanar aromatic systems in **2.12** (Figure 2.3) are consistent with high retention of aromaticity. The somewhat lower value in the newly-installed ring (C) is consistent with it being the one having the bridgehead associated with the highest local distortion from planarity [ $\alpha+\beta$  involving C8 = 30.6(4)°, Table 2.3].

### 2.3.4 NMR Analysis

The slippage of the two aromatic systems away from a perfect face-to-face arrangement causes the aromatic protons of **2.12** to be spread out over a rather broad range ( $\delta$  7.32 to 4.97 ppm) (Figures 2.4).

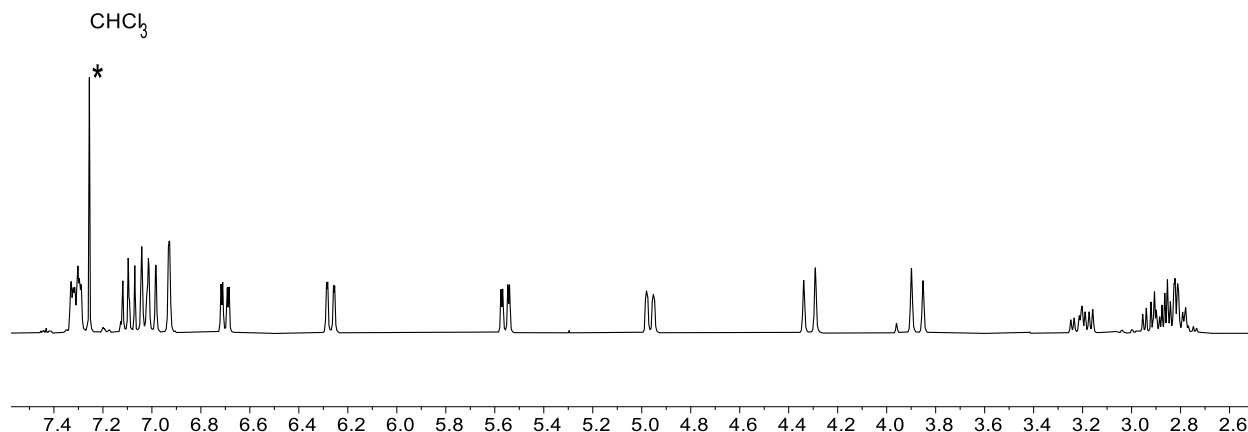


**Figure 2.4:** 300 MHz <sup>1</sup>H NMR spectrum of **2.12** in CDCl<sub>3</sub>.

The assignments of the proton and carbon resonances of **2.12** were corroborated by 1D and 2D NMR (COSY, HSQC, HMBC, and NOESY) experiments. All the 1D and 2D NMR spectra are shown in Appendix 1 (*vide infra*). A detailed description of how the assignments were made is given below. The numbering of protons in the description indicates that of the protons of the crystal structure (*vide supra*, Figure 2.1). All but the five quaternary carbon atoms, namely C3, C8, C8A, C12, and C15, could be assigned unequivocally. The closeness of some of the quaternary signals rendered it difficult to spot cross-peaks from the HMBC spectrum, thereby thwarting the assignments of the signals.

1. H4 is the only aromatic proton that will be a singlet or narrow doublet (d). A slightly broadened singlet is observed at 6.93 ppm. Assignment: H4 = 6.93 ppm.
2. H4 shows a HSQC cross peak to 126.6. Assignment: C4 = 126.6.
3. The signal at 6.93 ppm shows a weak COSY cross-peak to the doublet of doublets (dd) at 6.28 ppm. This is consistent with meta coupling. Assignment: H10 = 6.28 ppm.
4. The signal at 6.28 ppm shows a strong COSY cross-peak to a part (the right-hand side) of the multiplet (m) at 7.13–6.99 ppm. This is consistent with ortho coupling. Assignment: H9 = 7.13–6.99 ppm (rhs).
5. H10 shows a HSQC cross peak to 133.3 ppm. Assignment: C10 = 133.3 ppm.
6. H9 shows a HSQC cross peak to 129.6 ppm. Assignment: C9 = 129.6 ppm.
7. The doublets at 4.32 and 3.88 must be the geminal protons on C11. Both show a HSQC cross peak to 44.0 ppm. Assignment: C11 = 44.0 ppm.
8. The highest field aromatic signal at 4.97 ppm must be the one situated over the naphthalene ring. Assignment: H17 = 4.97 ppm.

9. H17 shows a strong COSY cross-peak to the signal at 5.56 ppm. This is consistent with ortho coupling. Assignment: H16 = 5.56 ppm.
10. H17 shows a weak COSY cross-peak to the right hand side of the multiplet (m) at 7.34–7.29 ppm. This is consistent with meta coupling. Assignment: H13 = 7.39–7.29 ppm (rhs).
11. H17 shows a HSQC cross peak to 132.6 ppm. Assignment: C17 = 132.6 ppm.
12. H13 shows a HSQC cross peak to 134.8 ppm. Assignment: C13 = 134.8 ppm.
13. H16 shows a HSQC cross peak to 132.9 ppm. Assignment: C16 = 132.9 ppm.
14. H16 shows a weak COSY cross-peak to the doublet of doublets (dd) at 6.71 ppm. This is consistent with meta coupling. Assignment: H14 = 6.71 ppm.
15. H14 shows a HSQC cross peak to 130.5 ppm. Assignment: C14 = 130.5 ppm.
16. The left-hand side of the multiplet (m) at 7.13–6.99 ppm shows cross peaks to the left-hand side of the multiplet (m) at 7.34–7.29 ppm and to the middle of the multiplet (m) at 7.13–6.99 ppm. Assignment: H6 = 7.13–6.99 ppm (lhs).
17. H6 shows a HSQC cross peak to 124.2 ppm. Assignment: C6 = 124.2 ppm.
18. C11 shows a HMBC cross peak to the middle of the multiplet (m) at 7.13–6.99 ppm. Assignment: H7 = 7.13–6.99 ppm (middle).
19. H7 shows a HSQC cross peak to 124.4 ppm. Assignment: C7 = 124.4 ppm.
20. H6 shows a strong COSY cross peak to the left-hand side of the multiplet (m) at 7.34–7.29 ppm. Assignment: H5 = 7.34–7.29 ppm (lhs).
21. H5 shows a HSQC cross peak to 124.9 ppm. Assignment: C5 = 124.9 ppm.
22. H4 shows an HMBC cross peak to 34.8 ppm. Assignment: C2 = 34.8 ppm. C1 must therefore be 32.3 ppm.

23. C2 shows a HSQC cross peak to the doublet of doublet of doublets (ddd) at 3.21 ppm.

Assignment: One of the H2A or H2B = 3.21 ppm.

24. The signal at 148.1 ppm shows HMBC cross peaks to H14, H16, and both H11A and H11B.

Assignment: C12 = 148.1 ppm.

25. The signal at 146.8 ppm shows HMBC cross peaks to H6, H9, and both H11A and H11B (one strong, one very weak). Assignment: C4A = 146.8 ppm.

For the benzene ring, the signals for C13–H ( $\delta$ 7.31 ppm) and C14–H ( $\delta$ 6.71 ppm) resonate at *ca.* 0.8 and 0.2 ppm lower field, respectively, than the analogous protons in **2.11** ( $\delta$ 6.48 ppm) and **2.13** ( $\delta$ 6.51 ppm) (Figure 2.5).<sup>24</sup> In contrast, the signals for C16–H ( $\delta$ 5.56 ppm) and C17–H ( $\delta$ 4.97 ppm) are observed at substantially higher field than the corresponding protons in **2.11** ( $\delta$ 6.48 ppm) and even **2.13** ( $\delta$ 5.66 ppm). C10–H ( $\delta$  6.28 ppm) is also observed at significantly higher field than its counterpart in **2.13** ( $\delta$ 6.80 ppm).

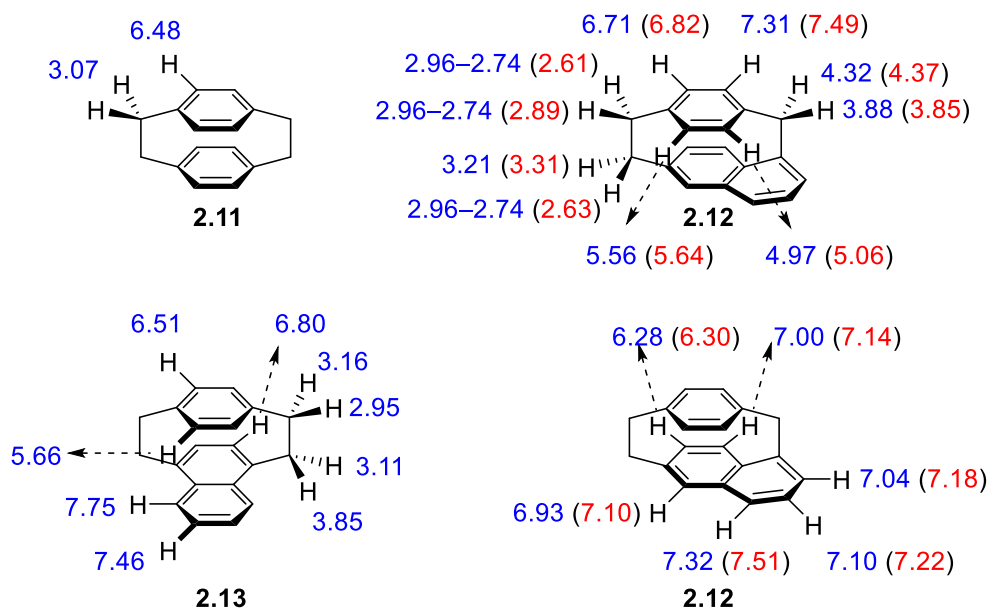


**Figure 2.5:** Experimental (blue) and calculated (red) [M06-2X/6-311+G(2d,p)] chemical shifts for cyclophanes **2.11**, **2.12**, and **2.13**.

### 2.3.5 UV/Vis Absorption and Fluorescence Spectroscopy

The absorption spectrum of naphthalenophane **2.12** was measured in four solvents, ranging from nonpolar (cyclohexane) to polar (acetonitrile) and they show nearly identical features, indicating a negligible solvatochromic effect (Figure 2.6A). There are two prominent peaks at *ca.* 225 and 255 nm, and a weak, broad band envelope ranging from 300 to 375 nm. TD-DFT calculations predict that the lowest-energy absorption band is due mainly to the HOMO to LUMO transition, while the peak at 250 nm is due to HOMO-1 to LUMO and HOMO to LUMO+1 transitions (see Appendix 1). The naphthalene unit makes the major contribution to the frontier molecular orbitals (Figure 2.6B), and the calculated HOMO-LUMO gap is 6.40 eV. The lowest-energy band of **2.12** is red-shifted compared to those of [2.2]paracyclophane (**2.11**) ( $\lambda_{\text{max}}$  (CH<sub>2</sub>Cl<sub>2</sub>) = 287, 305 nm)<sup>25</sup> and naphthalenophane **2.13** ( $\lambda_{\text{max}}$  (95% EtOH) = 300, 310 nm).<sup>26</sup> The red shift in going from **2.13** (less distorted naphthalene system) to **2.12** (more distorted naphthalene system) is consistent with the continual red shift observed in the [*n*]paracyclophanes as *n* becomes smaller.<sup>27</sup> The distortion of the naphthalene system in **2.12** may also be responsible for the weakly emissive nature of **2.12** ( $\lambda_{\text{max}}$  = 405 nm,  $\phi$  = 0.036, *cf.* 0.23 for naphthalene<sup>28</sup>).

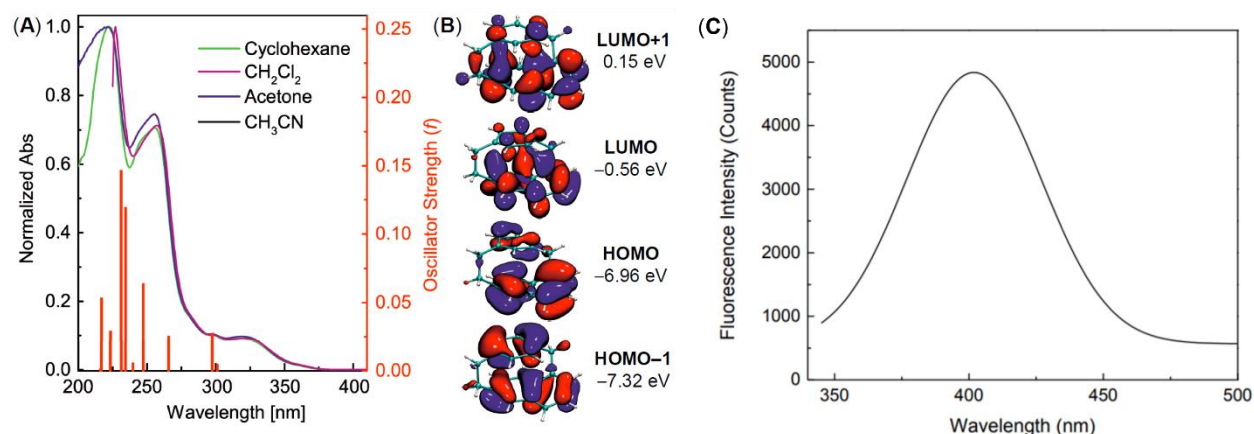


**Figure 2.6:** (A) Normalized UV/vis absorption spectra of **2.12** measured in different organic solvents, and TD-M06-2X/Def2TZVP calculated absorption spectrum of (red bar graph). (B) Contour plots and eigenvalues of frontier molecular orbitals of **2.12** (M06-2X/Def2TZVP). (C) Fluorescence spectra of **2.12** in CH<sub>2</sub>Cl<sub>2</sub> ( $\lambda_{\text{exc}}$  = 350 nm).

## 2.4 Conclusions

In conclusion, the new contractive annulation strategy for the synthesis of small, strained cyclophanes has been successfully applied to the conversion of [2.2]paracyclophane (**2.11**) (SE = 25.6 kcal/mol) into [2](6,1)naphthaleno[1]paracyclophane (**2.12**) (SE = 44.1 kcal/mol) using a 9-step synthetic pathway. Structural distortions in **2.12** are spread around the molecule, but are more pronounced in the vicinity of the one-carbon bridge. If successful, two-directional contractive annulation of **2.11** should lead to a [1.1]cyclophane. In the next chapter (Chapter 3), results pertaining to the synthesis of the [1.1]cyclophane will be discussed. Examples of [1.1]cyclophanes are extremely rare in the literature, presumably reflecting the difficulties associated with the synthesis of highly strained structures. The feasibility of the developed strategy also bodes well for its potential application in the synthesis of hitherto unknown, structurally interesting larger aromatic systems.

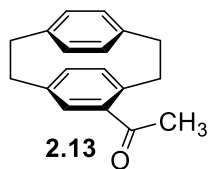
## 2.5 Experimental Section

### General

Reactions were performed under a balloon containing nitrogen gas unless otherwise indicated. All reactions were performed with oven-dried (120 °C) glassware. ACS grade chloroform was used for the reaction as solvent. ACS grade benzene was distilled from calcium hydride and stored over 3 Å molecular sieves. Commercial DDQ was recrystallized from benzene prior to use. Solvents were removed from reaction mixtures under reduced pressure using a rotary evaporator. Chromatographic separations were achieved using Silicycle silica gel 60, particle size of 40–63 μm. Column dimensions are recorded as height × diameter. Thin-layer chromatography (TLC) was performed using precoated plastic-backed POLYGRAM® SIL G/UV254 silica gel plates with

a layer thickness of 200  $\mu\text{m}$ . Compounds on TLC plates were visualized using a UV lamp (254 and 365 nm) or cerium molybdate stain (Hanessian's stain). Melting points were recorded using an OptiMelt automated melting point instrument and are uncorrected. Infrared (IR) spectra were recorded using neat samples on a Bruker Alpha spectrometer.  $^1\text{H}$  and  $^{13}\text{C}$  NMR spectra were recorded on Bruker AVANCE spectrometers at 300 MHz or 500 MHz and 75 MHz, respectively. Chemical shifts of the NMR spectra are reported relative to the residual solvent peak ( $\text{CDCl}_3$ :  $\delta$  7.26 ppm for  $^1\text{H}$  NMR,  $\delta$  77.16 ppm for  $^{13}\text{C}$  NMR;  $\text{DMSO}-d_6$ :  $\delta$  2.50 ppm for  $^1\text{H}$  NMR,  $\delta$  39.52 ppm for  $^{13}\text{C}$  NMR). UV/vis absorption spectra were recorded on a Varian Cary 6000i spectrophotometer. The fluorescence spectrum was recorded on a Photon Technology International (PTI) QuantaMaster spectrofluorometer. High resolution mass spectrometry (HRMS) data were obtained using an Agilent 6200 series instrument, employing a TOF mass analyzer.

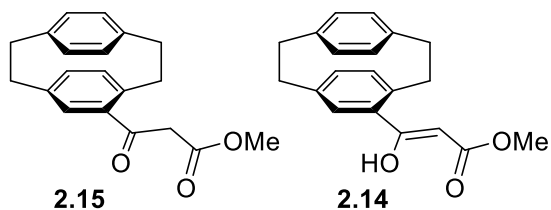
#### 4-Acetyl[2.2]paracyclophane (**2.13**)<sup>7</sup>



A solution of acetyl chloride (5.50 mL, 76.8 mmol) and aluminum chloride (9.21 g, 69.1 mmol) in dichloromethane (15 mL) was added to a stirred  $-40\text{ }^\circ\text{C}$  (dry ice/acetonitrile) solution of [2.2]paracyclophane (**11**) (8.00 g, 38.4 mmol) in dichloromethane (50 mL). The cold bath was removed and the resulting mixture was stirred for 15 min as it warmed to  $-15\text{ }^\circ\text{C}$ . The mixture was acidified with 6 M hydrochloric acid solution (10 mL) and stirred vigorously until it was colorless. The reaction mixture was diluted with dichloromethane (30 mL) and the layers were separated. The aqueous layer was extracted with dichloromethane (30 mL) and the combined organic layers were washed with saturated sodium bicarbonate solution (100 mL), washed with water ( $2 \times 100\text{ mL}$ ), dried over  $\text{Na}_2\text{SO}_4$ , filtered and

concentrated under reduced pressure. The residue was subjected to column chromatography (15 × 8.5 cm, 10% ethyl acetate/hexanes) to afford **2.13** (6.43 g, 67%) as a white solid.  $R_f = 0.32$  (10% ethyl acetate/hexanes); mp 110–112 °C (lit. mp<sup>7</sup> 109–110 °C); <sup>1</sup>H NMR (300 MHz, CDCl<sub>3</sub>)  $\delta$  6.93 (d,  $J = 1.8$  Hz, 1H), 6.66 (dd,  $J = 7.8, 1.6$  Hz, 1H), 6.57–6.46 (m, 4H), 6.38 (dd,  $J = 7.9, 1.8$  Hz, 1H), 4.03–3.90 (m, 1H), 3.25–3.10 (m, 4H), 3.07–2.99 (m, 2H), 2.86 (ddd,  $J = 12.6, 8.4, 8.4$ , Hz, 1H), 2.47 (s, 3H); <sup>13</sup>C NMR (75 MHz, CDCl<sub>3</sub>)  $\delta$  200.4, 141.7, 140.5, 139.9, 139.3, 138.0, 136.6, 136.5, 134.3, 133.2, 133.0, 132.2, 131.3, 36.2, 35.34, 35.31, 35.1, 28.9; IR  $\nu$  2951 (w), 2921 (m), 2887 (w), 2850 (w), 1679 (s), 1321 (m), 1265 (s), 853 (m), 615 (s) cm<sup>-1</sup>; HRMS [APPI(+)] calcd for C<sub>18</sub>H<sub>19</sub>O [M+H]<sup>+</sup> 251.1436, found 251.1427.

#### **$\beta$ -Keto Ester **2.15** and Enol Tautomer **2.14****

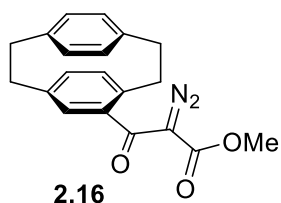


A 1.0 M solution of lithium hexamethyldisilazide (5.60 mL, 5.57 mmol) in hexanes was added to a stirred -78 °C (dry ice/acetone) solution of 4-acetyl[2.2]paracyclophane (**2.13**) (0.450 g, 1.80

mmol) in dry toluene (15 mL). The reaction mixture was stirred for 5 min at the same temperature, after which methyl chloroformate (0.15 mL, 2.0 mmol) was added into the mixture. The cold bath was removed, and the resulting mixture was stirred for 30 min as it warmed to rt. The reaction was quenched with the addition of a saturated aqueous NH<sub>4</sub>Cl solution (20 mL). The reaction mixture was diluted with ethyl acetate (10 mL) and the layers were separated. The aqueous layer was extracted with ethyl acetate (2 × 15 mL). The combined organic layers were washed with water (2 × 50 mL), dried over Na<sub>2</sub>SO<sub>4</sub>, filtered, and concentrated under reduced pressure. The residue was subjected to column chromatography (15 × 4.5 cm, 10% ethyl acetate/hexanes) to afford a *ca.* 89:11 mixture (<sup>1</sup>H NMR analysis) of **2.15** and **2.14** (0.448 g, 81%) as a white solid.

$R_f = 0.23$  (10% ethyl acetate/hexanes); mp 130–133 °C;  $^1\text{H NMR}$  (300 MHz,  $\text{CDCl}_3$ ) for **2.15**:  $\delta$  6.91 (d,  $J = 1.8$  Hz, 1H), 6.69 (dd,  $J = 7.7, 1.9$  Hz, 1H), 6.57–6.48 (m, 4H), 6.36 (dd,  $J = 7.9, 1.9$  Hz, 1H), 3.95 (ddd,  $J = 13.0, 9.3, 2.5$  Hz, 1H), 3.93, 3.70 (AB system,  $J = 15.4$  Hz, 2H), 3.80 (s, 3H), 3.27–2.97 (m, 6H), 2.85 (ddd,  $J = 12.6, 9.4, 7.4$  Hz, 1H); distinguishable signals for **2.14**:  $\delta$  12.45 (s, 1H), 6.73 (d,  $J = 2.0$  Hz, 1H), 6.44 (br d,  $J = 7.9$  Hz, 1H), 5.37 (s, 1H), 3.83 (s, 3H);  $^{13}\text{C NMR}$  (75 MHz,  $\text{CDCl}_3$ ) for **2.15**:  $\delta$  194.2, 168.4, 142.7, 140.4, 140.2, 139.3, 137.2, 136.8, 136.6, 134.0, 133.1, 133.0, 132.3, 131.4, 52.6, 47.4, 36.2, 35.3, 34.9 (one signal fewer than expected); distinguishable signals for **2.14**:  $\delta$  174.5, 139.9, 139.7, 139.5, 136.4, 135.2, 134.8, 132.9, 132.7, 131.9, 129.3, 90.4, 51.5, 35.5, 35.4, 35.3; IR  $\nu$  2932 (w), 1733 (s), 1672 (s), 1327(s), 1165 (s), 997 (m), 723 (m)  $\text{cm}^{-1}$ ; HRMS [APPI-(+)] calcd for  $\text{C}_{20}\text{H}_{21}\text{O}_3$   $[\text{M}+\text{H}]^+$  309.1491, found 309.1474.

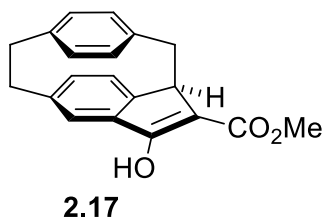
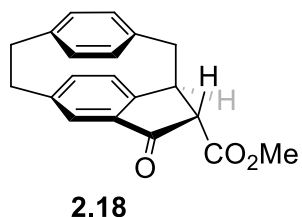
### $\alpha$ -Diazo- $\beta$ -keto Ester **2.16**



Tosyl azide (0.315 g, 1.60 mmol) was added to a stirred 0 °C (ice/water) suspension of a mixture of  $\beta$ -keto ester **2.15** and its enol tautomer **2.14** (0.410 g, 1.33 mmol) in dry acetonitrile (15 mL). Then triethylamine (0.22 mL, 1.6 mmol) was added dropwise to the mixture at 0 °C (ice/water) and the resulting mixture was stirred at the same temperature for 1 h. The majority of the solvent was evaporated under reduced pressure. The reaction mixture was diluted with ethyl acetate (25 mL) and water (25 mL). The layers were separated and the aqueous layer was extracted with ethyl acetate (2  $\times$  20 mL). The combined organic layers were washed with water (2  $\times$  50 mL), washed with saturated aqueous NaCl solution (50 mL), dried over  $\text{Na}_2\text{SO}_4$ , filtered, and concentrated under reduced pressure. The residue was subjected to column chromatography (15  $\times$  4.5 cm, 7–15% ethyl acetate/hexanes) to afford **2.16** (0.394 g, 89%) as an off-white solid.  $R_f = 0.25$  (10% ethyl acetate/hexanes); mp 87–90 °C;  $^1\text{H NMR}$  (300 MHz,  $\text{CDCl}_3$ )  $\delta$  6.76 (br d,  $J = 8.0$  Hz, 1H), 6.65–6.62 (m, 2H), 6.59–6.53

(m, 2H), 6.50 (d,  $J = 8.3$  Hz, 1H), 6.34 (br d,  $J = 8.1$  Hz, 1H), 3.75 (s, 3H), 3.42–2.88 (m, 8H);  $^{13}\text{C}$  NMR (75 MHz,  $\text{CDCl}_3$ )  $\delta$  186.2, 161.7, 139.9, 139.7, 139.5, 139.4, 136.7, 135.8, 134.5, 132.8, 132.7, 132.3, 131.9, 131.7, 75.5, 52.4, 35.8, 35.2, 34.4; IR  $\nu$  3013 (w), 2928 (w), 2852 (w), 2127 (s), 1733 (s), 1683 (m), 1309 (s), 1097 (m), 739 (w)  $\text{cm}^{-1}$ ; HRMS [APPI-(+)] calcd for  $\text{C}_{20}\text{H}_{18}\text{N}_2\text{O}_3$   $[\text{M}]^+$  334.1317, found 334.1397; calcd for  $\text{C}_{20}\text{H}_{19}\text{O}_3$   $[\text{M}+\text{H}-\text{N}_2]^+$  307.1334, found 307.1326.

### **$\beta$ -Keto Ester **2.18** and Enol Tautomer **2.17****

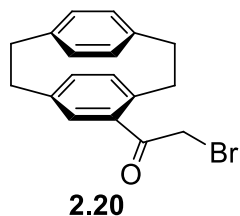


$\text{Rh}_2(\text{OAc})_4$  (0.0048 g, 0.011 mmol) was added to a stirred room temperature solution of  $\alpha$ -diazo- $\beta$ -keto ester **2.16** (0.360 g, 1.08 mmol) in dichloromethane (20 mL). The

resulting mixture was stirred for 16 h. Then the solvent was removed under reduced pressure and the residue was directly subjected to column chromatography (15 cm  $\times$  3.5 cm, 10% ethyl acetate/hexanes) to afford a *ca.* 83:17 mixture of **2.18** and **2.17** (0.210 g, 64%) as a waxy off-white solid.  $R_f = 0.30$  (10% ethyl acetate/hexanes);  $^1\text{H}$  NMR (300 MHz,  $\text{CDCl}_3$ ) signals for **2.18**:  $\delta$  6.92–6.83 (m, 3H), 6.55 (d,  $J = 8.0$  Hz, 1H), 6.51–6.45 (m, 2H), 6.42 (d,  $J = 8.0$  Hz, 1H), 4.30 (t,  $J = 4.4$  Hz, 1H), 3.76 (s, 3H), 3.65 (d,  $J = 0.8$  Hz, 1H), 3.29–3.21 (m, 4H), 3.10–2.94 (m, 2H); distinguishable signals for **2.17**: 10.55 (br s, 1H), 6.75 (dd,  $J = 7.7, 1.8$  Hz, 1H), 6.65–6.60 (m, 3H), 6.20 (dd,  $J = 7.9, 2.0$  Hz, 1H), 4.19 (d,  $J = 7.1$  Hz, 1H), 4.01–3.93 (m, 4H), 3.41–3.33 (m, 2H), 2.91–2.82 (m, 1H);  $^{13}\text{C}$  NMR (75 MHz,  $\text{CDCl}_3$ ) signals for **2.18**:  $\delta$  199.0, 169.1, 156.4, 143.6, 141.1, 140.9, 138.1, 137.5, 135.6, 133.0, 132.9, 130.0, 129.1, 128.2, 63.4, 53.0, 46.0, 44.3, 35.5, 35.3; distinguishable signals for **2.17**:  $\delta$  145.8, 141.4, 140.1, 139.3, 136.1, 136.0, 135.8, 132.2, 132.1, 131.2, 128.7, 125.9, 122.2, 105.3, 58.4, 51.5, 46.5, 40.1, 35.2; IR  $\nu$  2933 (w), 1732 (s), 1683

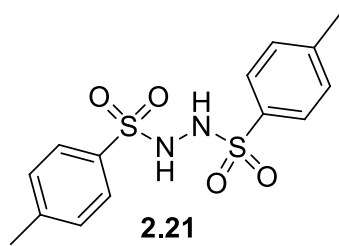
(s), 1437 (m), 1312 (m), 737 (w)  $\text{cm}^{-1}$ ; HRMS [APPI-(+)] calcd for  $\text{C}_{20}\text{H}_{19}\text{O}_3$   $[\text{M}+\text{H}]^+$  307.1334, found 307.1320.

### $\alpha$ -Bromoketone **2.20**<sup>29</sup>



$\text{CuBr}_2$  (0.161 g, 0.719 mmol) was added to a stirred room temperature solution of 4-acetyl[2.2]paracyclophane (**2.13**) (0.150 g, 0.599 mmol) in ethyl acetate (5 mL). The resulting mixture was stirred for 48 h. Then the reaction mixture was passed through a small pad of Celite<sup>®</sup>. The filter cake was thoroughly washed with ethyl acetate (20 mL) and then the solvent was removed under reduced pressure. The residue was subjected to column chromatography (18 cm  $\times$  2.5 cm, 4–6% ethyl acetate/hexanes) to afford **2.20** (0.142 g, 72%) as a white solid.  $R_f = 0.42$  (10% ethyl acetate/hexanes); mp 114–116  $^\circ\text{C}$  (lit. mp<sup>29</sup> 115–116  $^\circ\text{C}$ );  $^1\text{H}$  NMR (300 MHz,  $\text{CDCl}_3$ )  $\delta$  6.97 (d,  $J = 1.8$  Hz, 1H), 6.71 (dd,  $J = 7.8, 1.8$  Hz, 1H), 6.59–6.50 (m, 4H), 6.39 (dd,  $J = 7.9, 1.8$  Hz, 1H), 4.38, 4.17 (AB system,  $J = 12.2$  Hz, 2H), 3.88 (ddd,  $J = 12.4, 9.8, 2.3$  Hz, 1H), 3.31–3.13 (m, 4H), 3.07–2.97 (m, 2H), 2.88 (ddd,  $J = 12.6, 9.7, 7.0$  Hz, 1H);  $^{13}\text{C}$  NMR (75 MHz,  $\text{CDCl}_3$ )  $\delta$  193.0, 143.1, 140.3, 140.2, 139.3, 137.5, 136.8, 134.9, 133.8, 133.01, 132.95, 132.5, 131.4, 36.2, 35.3, 35.2, 35.0, 33.2; IR  $\nu$  2930 (w), 2853 (w), 1694 (s), 1212 (m), 994 (m), 721 (m)  $\text{cm}^{-1}$ ; HRMS [APPI-(+)] calcd for  $\text{C}_{18}\text{H}_{17}^{79}\text{BrO}$   $[\text{M}]^+$  328.0463, found 328.0466; calcd for  $\text{C}_{18}\text{H}_{17}^{81}\text{BrO}$   $[\text{M}]^+$  330.0442, found 330.0456.

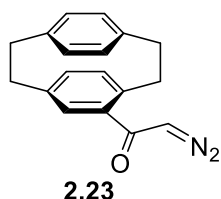
### *N,N'*-Ditosylhydrazine (**2.21**)<sup>30</sup>



**2.21** was synthesized in 84% yield from the reaction of tosyl chloride and tosyl hydrazide in the presence of pyridine as base following a literature procedure.<sup>30</sup>  $R_f = 0.40$  (50% ethyl acetate/hexanes); mp 217–219  $^\circ\text{C}$  (dec.) [lit. mp<sup>30</sup> 212–215  $^\circ\text{C}$  (dec.)];  $^1\text{H}$  NMR (300 MHz,

DMSO-*d*<sub>6</sub>)  $\delta$  9.58 (s, 2H), 7.66–7.63 (AA'BB' half-spectrum, 4H), 7.40–7.37 (AA'BB' half-spectrum, 4H), 2.40 (s, 6H); <sup>13</sup>C NMR (75 MHz, CDCl<sub>3</sub>)  $\delta$  143.5, 135.5, 129.5, 127.8, 21.1; HRMS [APPI-(+)] calcd for C<sub>14</sub>H<sub>16</sub>N<sub>2</sub>NaO<sub>4</sub>S<sub>2</sub> [M+Na]<sup>+</sup> 363.0449, found 363.0449.

### $\alpha$ -Diazoketone **2.23**



4-Acetyl[2.2]paracyclophane (**2.13**) (2.50 g, 9.99 mmol) was added to a stirred 50 °C solution of selenium dioxide (1.66 g, 15.0 mmol) in 1,4-dioxane/deionized water (60 mL, 10:1 v/v). The resulting mixture was then heated at 110 °C for 15 h. Then the reaction mixture was cooled to room temperature, filtered through a small pad of Celite<sup>®</sup>, washed with ethyl acetate (30 mL), concentrated under reduced pressure, diluted with ethyl acetate (50 mL), washed with water (50 mL), and saturated aqueous NaCl solution (50 mL). The organic layer was dried over Na<sub>2</sub>SO<sub>4</sub>, concentrated under reduced pressure and the residue was subjected to column chromatography (10 cm × 5.5 cm, 40% ethyl acetate/hexanes) to afford **2.22** (2.84 g) as a yellow oil. *R*<sub>f</sub> = 0.50–0.82 (40% ethyl acetate/hexanes); <sup>1</sup>H NMR (300 MHz, CDCl<sub>3</sub>)  $\delta$  9.63 (s), the remainder of the spectrum is complex; IR  $\nu$  3427 (br, w), 2928 (m), 2893 (w), 2854 (w), 1671 (s), 1550 (m), 1276 (m), 1096 (m), 991 (m), 733 (m), 611 (w) cm<sup>-1</sup>; HRMS [APPI-(+)] calcd for C<sub>18</sub>H<sub>17</sub>O<sub>2</sub> [M+H]<sup>+</sup> 265.1229, found 265.1228.

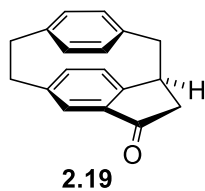
Tosyl hydrazide (2.10 g, 11.3 mmol) and cesium carbonate (10.5 g, 32.2 mmol) were added to a stirred room temperature solution of **2.22** (2.84 g) in chloroform (100 mL). The resulting mixture was stirred at the same temperature for 1 h. Water (100 mL) was added to the reaction mixture and stirred vigorously for 5 min. The layers were separated and the aqueous layer was further extracted with chloroform (2 × 50 mL). The combined organic layers were washed with saturated aqueous NaCl solution (2 × 150 mL), dried over Na<sub>2</sub>SO<sub>4</sub>, filtered, and concentrated under

reduced pressure. The residue was subjected to column chromatography (15 cm × 5.5 cm, 10–15% ethyl acetate/hexanes) to afford **2.23** (2.37 g, 86% over two steps) as a yellow solid.  $R_f = 0.33$  (15% ethyl acetate/hexanes); mp 127–128 °C (dec.);  $^1\text{H NMR}$  (300 MHz,  $\text{CDCl}_3$ )  $\delta$  6.67–6.61 (m, 3H), 6.55–6.50 (m, 3H), 6.39 (dd,  $J = 7.9, 1.5$  Hz, 1H), 5.44 (s, 1H), 3.87–3.80 (m, 1H), 3.31–2.84 (m, 7H);  $^{13}\text{C NMR}$  (75 MHz,  $\text{CDCl}_3$ )  $\delta$  188.6, 140.11, 140.10, 140.0, 139.2, 136.8, 136.3, 136.1, 132.8, 132.7, 132.5, 131.8, 131.6, 55.6, 35.5, 35.2, 35.17, 35.15; IR  $\nu$  3064 (m), 2927 (m), 2851 (w), 2095 (s), 1589 (s), 1351 (s), 1016 (m), 877 (m), 716 (m), 634 (m)  $\text{cm}^{-1}$ ; HRMS [APPI-(+)] calcd for  $\text{C}_{18}\text{H}_{17}\text{O}$   $[\text{M}+\text{H}-\text{N}_2]^+$  249.1280, found 249.1281 ( $[\text{M}]^+$  and  $[\text{M}+\text{H}]^+$  peaks were not observed).

$\alpha$ -Diazoketone **2.23** was also synthesized following a different reaction. The procedure for the reaction is described below.

A solution of DBU (0.23 mL, 1.5 mmol) in THF (5 mL) was added dropwise to a stirred 0 °C (ice/water) mixture of *N,N'*-Ditosylhydrazine (**2.21**) (0.155 g, 0.456 mmol) and  $\alpha$ -bromoketone **2.20** (0.100 g, 0.304 mmol) in THF (5 mL) over 5 min. The reaction mixture was further stirred for 10 min at the same temperature. An aqueous saturated sodium bicarbonate solution (10 mL) was added to the reaction mixture and the mixture was stirred for 5 min as it warmed to room temperature. The majority of the solvent was removed under reduced pressure. The reaction mixture was diluted with ethyl acetate (20 mL) and water (20 mL). The layers were separated and the aqueous layer was further extracted with ethyl acetate ( $2 \times 15$  mL). The combined organic layers were washed with saturated aqueous NaCl solution ( $2 \times 50$  mL), dried over  $\text{Na}_2\text{SO}_4$ , filtered, and concentrated under reduced pressure. The residue was subjected to column chromatography (15 cm × 2.5 cm, 10–13% ethyl acetate/hexanes) to afford **2.23** (0.036 g, 43%) as a yellow solid.

### Indanone 2.19



$\text{Rh}_2(\text{OAc})_4$  (0.034 g, 0.076 mmol) was added to a stirred 0 °C solution of  $\alpha$ -diazoketone **2.23** (2.10 g, 7.60 mmol) in dichloromethane (150 mL). The resulting mixture was stirred at the same temperature for 30 min. The reaction mixture was cooled to room temperature and the solvent was removed under reduced pressure. The residue was directly subjected to column chromatography (18 cm  $\times$  5.5 cm, 10–20% ethyl acetate/hexanes) to afford **2.19** (1.17 g, 62%) as a pale yellow solid.  $R_f = 0.27$  (20% ethyl acetate/hexanes); mp 184–186 °C;  $^1\text{H}$  NMR (300 MHz,  $\text{CDCl}_3$ )  $\delta$  6.85–6.82 (m, 3H), 6.54 (dd,  $J = 7.7, 1.8$  Hz, 1H), 6.49–6.46 (m, 2H), 6.40 (dd,  $J = 7.8, 1.7$  Hz, 1H), 4.01 (ddd,  $J = 8.1, 5.8, 2.3$  Hz, 1H), 3.34–2.93 (m, 7H), 2.56 (dd,  $J = 18.7, 0.6$  Hz, 1H);  $^{13}\text{C}$  NMR (75 MHz,  $\text{CDCl}_3$ )  $\delta$  206.6, 156.3, 143.0, 140.8, 140.3, 139.4, 138.0, 135.5, 132.94, 132.91, 129.9, 128.3, 127.7, 46.8, 44.9, 41.4, 35.6, 35.3; IR  $\nu$  2918 (m), 2851 (w), 1697 (s), 1592 (m), 1408 (m), 1219 (m), 1203 (m), 846 (m), 717 (m), 663 (m), 637 (w), 629 (w)  $\text{cm}^{-1}$ ; HRMS [APPI-(+)] calcd for  $\text{C}_{18}\text{H}_{17}\text{O}$   $[\text{M}+\text{H}]^+$  249.1279, found 249.1284.

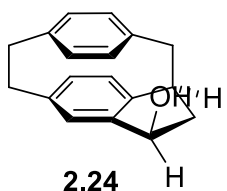
Indanone **2.19** was also synthesized following another two different reactions. The procedures for those reactions are described below.

A 1.0 M aqueous solution of potassium hydroxide (3.25 mL, 3.25 mmol) was added to a stirred room temperature solution of a mixture of  $\beta$ -Keto ester **2.18** and its enol tautomer **2.17** (0.100 g, 0.326 mmol) in methanol (5 mL). The resulting mixture was heated at 55 °C for 2 h. After cooling the reaction mixture to room temperature, the majority of the solvents was removed. The reaction mixture was diluted by the addition of ethyl acetate (15 mL) and water (15 mL). The layers were separated and the aqueous layer was further extracted with ethyl acetate (2  $\times$  15 mL). The combined organic layers were washed with saturated aqueous NaCl solution (2  $\times$  50 mL), dried over  $\text{Na}_2\text{SO}_4$ , filtered, and concentrated under reduced pressure. The residue was subjected

to column chromatography (15 cm × 2.5 cm, 15–20% ethyl acetate/hexanes) to afford **2.19** (0.024 g, 30%) as a pale yellow solid.

Lithium chloride (0.028 g, 0.65 mmol) and water (0.10 mL, 5.2 mmol) were added to a stirred room temperature solution of a mixture of  $\beta$ -Keto ester **2.18** and its enol tautomer **2.17** (0.100 g, 0.326 mmol) in dimethyl sulfoxide (6 mL). The resulting mixture was heated at 140 °C for 1 h. The reaction mixture was cooled to room temperature, poured into ice-cold water (30 mL), and stirred for 5 min. Ethyl acetate (30 mL) was added to the mixture and the layers were separated. The aqueous layer was extracted with ethyl acetate (3 × 30 mL) and the combined organic layers were washed with water (2 × 100 mL), washed with saturated aqueous NaCl solution (100 mL), dried over Na<sub>2</sub>SO<sub>4</sub>, filtered, and concentrated under reduced pressure. The residue was subjected to column chromatography (18 cm × 2.5 cm, 15% ethyl acetate/hexanes) to afford **2.19** (0.053 g, 65%) as a pale yellow solid.

### Indanol 2.24

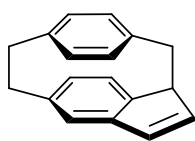


Lithium aluminum hydride (0.046 g, 1.2 mmol) was added to a stirred 0 °C (ice/water) solution of indanone **2.19** (0.150 g, 0.604 mmol) in THF (10 mL).

The resulting mixture was stirred at the same temperature for 1 h. To quench the reaction, a saturated aqueous solution of Rochelle's salt (potassium sodium tartrate) (10 mL) was added at the same temperature to the reaction mixture. The resulting mixture was stirred for 15 min after which the majority of the solvent was evaporated under reduced pressure. The reaction mixture was then diluted with ethyl acetate (20 mL) and water (15 mL). The layers were separated and the aqueous layer was extracted with ethyl acetate (2 × 15 mL). The combined organic layers were washed with water (2 × 50 mL), washed with saturated aqueous NaCl solution (50 mL), dried over Na<sub>2</sub>SO<sub>4</sub>, filtered, and concentrated under reduced pressure. The residue was

subjected to column chromatography (15 cm × 2.5 cm, 20–25% ethyl acetate/hexanes) to afford **2.24** (0.098 g, 65%) as a white solid.  $R_f = 0.59$  (40% ethyl acetate/hexanes); mp 163–165 °C;  $^1\text{H}$  NMR (300 MHz,  $\text{CDCl}_3$ )  $\delta$  6.86 (dd,  $J = 8.1, 2.0$  Hz, 1H), 6.61 (dd,  $J = 7.8, 2.0$  Hz, 1H), 6.56–6.51 (m, 3H), 6.48 (dd,  $J = 7.8, 2.0$  Hz, 1H), 6.43 (dd,  $J = 8.0, 2.0$  Hz, 1H), 5.08 (ddd,  $J = 10.1, 6.8, 3.4$  Hz, 1H), 3.77 (ddd,  $J = 9.7, 7.3, 2.5$  Hz, 1H), 3.23–2.97 (m, 7H), 2.27 (d,  $J = 7.1$  Hz, 1H), 1.96 (dt,  $J = 15.2, 3.0$  Hz, 1H);  $^{13}\text{C}$  NMR (75 MHz,  $\text{CDCl}_3$ )  $\delta$  144.6, 143.1, 141.7, 140.6, 139.0, 134.7, 134.3, 133.1, 132.6, 129.8, 129.1, 127.2, 75.6, 46.8, 45.5, 42.5, 36.0, 35.4; HRMS [APPI(+)] calcd for  $\text{C}_{18}\text{H}_{17}$   $[\text{M}+\text{H}-\text{H}_2\text{O}]^+$  233.1330, found 233.1320.

### Indene **2.25**



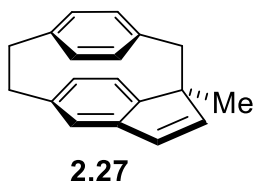
**2.25**

*p*-Toluenesulfonic acid (0.0026 g, 0.015 mmol) was added to a stirred room temperature solution of indanol **2.24** (0.075 g, 0.30 mmol) in benzene (5 mL).

The reaction flask was equipped with a Barrett apparatus and the resulting mixture was heated at 90 °C for 30 min. After cooling to room temperature, saturated sodium bicarbonate solution (10 mL) was added to the reaction mixture and stirring was continued for 5 min. Ethyl acetate (10 mL) was added to the mixture and the layers were separated. The aqueous layer was extracted with ethyl acetate (2 × 10 mL) and the combined organic layers were washed with water (30 mL), washed with saturated aqueous NaCl solution (30 mL), dried over  $\text{Na}_2\text{SO}_4$ , filtered, and concentrated under reduced pressure. The residue was subjected to column chromatography (10 cm × 2.5 cm, hexanes) to afford **2.25** (0.066 g, 95%) as a white solid.  $R_f = 0.54$  (1% ethyl acetate/hexanes); mp 149–150 °C;  $^1\text{H}$  NMR (300 MHz,  $\text{CDCl}_3$ )  $\delta$  6.78 (dd,  $J = 7.9, 2.0$  Hz, 1H), 6.66–6.54 (m, 4H), 6.46 (dd,  $J = 5.4, 2.2$  Hz, 1H), 6.36 (dd,  $J = 7.8, 2.0$  Hz, 1H), 6.25 (s, 1H), 6.08 (dd,  $J = 7.9, 2.0$  Hz, 1H), 4.03 (dd,  $J = 7.4, 1.9$  Hz, 1H), 3.22–2.79 (m, 6H);  $^{13}\text{C}$  NMR (75 MHz,  $\text{CDCl}_3$ )  $\delta$  146.7, 145.0, 140.6, 139.8, 138.3, 135.6, 135.2, 133.8, 132.02, 132.00, 130.6,

128.0, 126.2, 120.9, 52.1, 38.7, 35.7, 35.4; IR  $\nu$  2919 (m), 2852 (w), 756 (m), 720 (m)  $\text{cm}^{-1}$ ; HRMS [APPI-(+)] calcd for  $\text{C}_{18}\text{H}_{17}$   $[\text{M}+\text{H}]^+$  233.1330, found 233.1324.

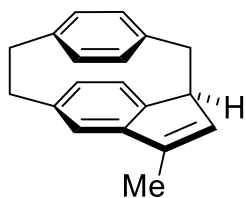
### Methylindene **2.27**



A 1.45 M solution of *n*-butyllithium (0.18 mL, 0.26 mmol) in hexanes was added dropwise to a stirred  $-78\text{ }^{\circ}\text{C}$  (dry ice/acetone) solution of indene **2.25** (0.050 g, 0.22 mmol) in THF (3 mL). Immediately after the addition of *n*-butyllithium, the color of the mixture turned purple, indicating the formation of the corresponding indenide. The resulting mixture was stirred at the same temperature for 15 min. Then a solution of iodomethane (0.034 g, 0.24 mmol) in THF (1 mL) was added to the reaction mixture and the resulting mixture was stirred for another 15 min at  $-78\text{ }^{\circ}\text{C}$ . A saturated  $\text{NH}_4\text{Cl}$  solution (2 mL) was added dropwise to the mixture to quench the reaction. The majority of the solvent was removed under reduced pressure and the mixture was diluted with ethyl acetate (10 mL) and water (10 mL). The layers were separated and the aqueous layer was extracted with ethyl acetate ( $2 \times 10\text{ mL}$ ). The combined organic layers were washed with water (30 mL), washed with saturated aqueous NaCl solution (30 mL), dried over  $\text{Na}_2\text{SO}_4$ , filtered, and concentrated under reduced pressure. The residue was subjected to column chromatography (15 cm  $\times$  2.0 cm, 0–1% ethyl acetate/hexanes) to afford **2.27** (0.036 g, 68%) as an off-white solid.  $R_f = 0.35$  (1% ethyl acetate/hexanes); mp 105–107  $^{\circ}\text{C}$ ;  $^1\text{H NMR}$  (300 MHz,  $\text{CDCl}_3$ )  $\delta$  6.82 (dd,  $J = 7.9, 2.0\text{ Hz}$ , 1H), 6.61 (dd,  $J = 7.8, 2.0\text{ Hz}$ , 1H), 6.56 (dd,  $J = 7.7, 1.5\text{ Hz}$ , 1H), 6.53 (d,  $J = 7.7\text{ Hz}$ , 1H), 6.52 (d,  $J = 5.4\text{ Hz}$ , 1H), 6.31 (dd,  $J = 7.8, 1.9\text{ Hz}$ , 1H), 6.30 (d,  $J = 5.4\text{ Hz}$ , 1H), 6.17 (br s, 1H), 6.12 (dd,  $J = 7.9, 2.0\text{ Hz}$ , 1H), 3.23–3.11 (m, 3H), 2.97–2.78 (m, 2H), 2.71 (d,  $J = 12.4\text{ Hz}$ , 1H), 1.61 (s, 3H);  $^{13}\text{C NMR}$  (75 MHz,  $\text{CDCl}_3$ )  $\delta$  148.7, 146.1, 143.8, 140.6, 139.8, 136.4, 135.8, 132.1, 132.0, 131.5, 130.1, 126.2, 125.6,

120.8, 58.3, 47.5, 35.7, 35.4, 20.6; IR  $\nu$  2921 (m), 2851 (w), 936 (w), 888 (w), 773 (m), 724 (m)  $\text{cm}^{-1}$ ; HRMS [APPI-(+)] calcd for  $\text{C}_{19}\text{H}_{18}$   $[\text{M}]^+$  246.1409, found 246.1400.

### Indene **2.29**



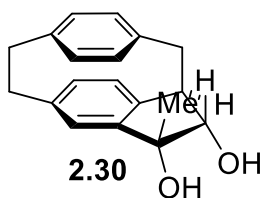
**2.29**

A 2.50 M solution of methylmagnesium bromide (2.42 mL, 6.04 mmol) in diethyl ether was added dropwise to a stirred 0 °C (ice/water) solution of indanone **2.19** (0.500 g, 2.01 mmol) in THF (20 mL). The cold bath was removed and the reaction mixture was stirred for 17 h as it warmed to room temperature. Then the reaction mixture was cooled to 0 °C (ice/water) and saturated  $\text{NH}_4\text{Cl}$  solution (10 mL) was added and stirred for 5 min. The majority of the solvent was evaporated under reduced pressure and the reaction mixture was diluted with ethyl acetate (50 mL) and water (50 mL). The layers were separated and the aqueous layer was extracted with ethyl acetate ( $2 \times 30$  mL). The combined organic layers were washed with water (100 mL), saturated  $\text{NaCl}$  solution ( $2 \times 100$  mL), dried over  $\text{Na}_2\text{SO}_4$ , filtered, and concentrated under reduced pressure to afford an inseparable *ca.* 71:29 ( $^1\text{H}$  NMR analysis) mixture of **2.28** and unreacted **2.19** (0.529 g) as a beige solid.  $R_f = 0.27$  (20% ethyl acetate/hexanes).

*p*-Toluenesulfonic acid (0.017 g, 0.10 mmol) was added to a stirred room temperature suspension of a mixture of **2.28** and unreacted **2.19** (0.529 g) in benzene (10 mL). The reaction flask was equipped with a Barrett apparatus and the resulting mixture was heated at 90 °C for 30 min. After cooling to room temperature, saturated sodium bicarbonate solution (10 mL) was added to the reaction mixture and stirring was continued for 5 min. Ethyl acetate (15 mL) was added to the mixture and the layers were separated. The aqueous layer was extracted with ethyl acetate ( $2 \times 20$  mL) and the combined organic layers were washed with water (50 mL), washed with saturated aqueous  $\text{NaCl}$  solution (50 mL), dried over  $\text{Na}_2\text{SO}_4$ , filtered, and concentrated under reduced

pressure. The residue was subjected to column chromatography (12 cm × 3.5 cm, hexanes) to afford **2.29** (0.203 g, 41% over two steps) as a white solid and **2.19** (0.091 g, 18% recovery) as a pale yellow solid.  $R_f = 0.32$  (1% ethyl acetate/hexanes); mp 132–134 °C;  $^1\text{H NMR}$  (300 MHz,  $\text{CDCl}_3$ )  $\delta$  6.64 (dd,  $J = 7.8, 2.0$  Hz, 2H), 6.61–6.55 (m, 2H), 6.35 (dd,  $J = 7.8, 1.9$  Hz, 1H), 6.19 (br s, 1H), 6.11–6.07 (m, 2H), 3.98 (ddd,  $J = 7.2, 3.7, 1.8$  Hz, 1H), 3.26–2.78 (m, 6H), 2.07 (t,  $J = 1.6$  Hz, 3H) (Note: The  $^1\text{H NMR}$  signal at  $\delta = 6.64$  ppm consists of two sets of accidentally degenerate doublet of doublets);  $^{13}\text{C NMR}$  (75 MHz,  $\text{CDCl}_3$ )  $\delta$  148.2, 145.6, 141.7, 140.5, 139.9, 136.0, 135.2, 133.2, 132.1, 131.2, 130.5, 127.6, 124.0, 120.6, 50.8, 39.8, 35.8, 35.5, 12.8; IR  $\nu$  2922 (m), 2854 (w), 901 (m), 842 (m), 791 (s), 719 (m)  $\text{cm}^{-1}$ ; HRMS [APPI-(+)] calcd for  $\text{C}_{19}\text{H}_{19}$  [M+H] $^+$  247.1487, found 247.1481.

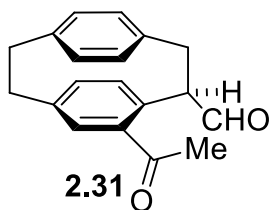
### Diol **2.30**



$\text{K}_2\text{OsO}_4 \cdot 2\text{H}_2\text{O}$  (0.0087 g, 0.024 mmol) was added to a stirred room temperature mixture of indene **2.29** (0.195 g, 0.792 mmol) and *N*-methylmorpholine *N*-oxide (NMO) (0.185 g, 1.58 mmol) in *tert*-butyl alcohol/THF/deionized water (10 mL, 8:10:1 v/v). The resulting mixture was stirred for 17 h, after which a saturated aqueous solution of sodium sulfite (10 mL) was added into the reaction mixture. The majority of the solvents was removed under reduced pressure. The reaction mixture was diluted with ethyl acetate (20 mL) and water (20 mL). The layers were separated and the aqueous layer was extracted with ethyl acetate (2 × 20 mL). The combined organic layers were washed with saturated aqueous NaCl solution (50 mL), dried over  $\text{Na}_2\text{SO}_4$ , filtered, and concentrated under reduced pressure. The residue was subjected to column chromatography (15 cm × 3.5 cm, 50–60% ethyl acetate/hexanes) to afford **2.30** (0.190 g, 86%) as an off-white solid.  $R_f = 0.34$  (60% ethyl acetate/hexanes); mp 133–136 °C;  $^1\text{H NMR}$  (300 MHz,  $\text{CDCl}_3$ )  $\delta$  6.61 (dd,  $J = 7.5, 1.9$  Hz,

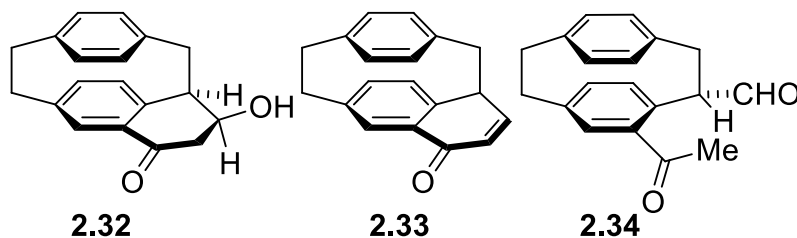
1H), 6.57–6.49 (m, 4H), 6.46 (s, 1H), 6.29 (dd,  $J = 8.0, 2.0$  Hz, 1H), 4.31 (dd,  $J = 7.9, 2.7$  Hz, 1H), 3.61 (dd,  $J = 7.6, 2.7$  Hz, 1H), 3.39–3.35 (m, 2H), 3.18–2.97 (m, 5H), 1.74 (s, 4H) (Note: The  $^1\text{H}$  NMR signal at  $\delta = 1.74$  ppm consists of two accidentally degenerate singlets);  $^{13}\text{C}$  NMR (75 MHz,  $\text{CDCl}_3$ )  $\delta$  145.9, 143.4, 141.1, 140.1, 138.8, 136.0, 134.6, 133.1, 132.3, 131.2, 127.7, 126.1, 86.2, 78.7, 55.5, 43.8, 35.5, 35.3, 22.4; IR  $\nu$  3332 (br, w), 2915 (w), 1391 (w), 1046 (s), 893 (m), 847 (m), 721 (w)  $\text{cm}^{-1}$ ; HRMS [APPI-(+)] calcd for  $\text{C}_{19}\text{H}_{19}\text{O}$   $[\text{M}+\text{H}]^+$  263.1436, found 263.1423.

### Ketoaldehyde **2.31**



Sodium metaperiodate (0.172 g, 0.803 mmol) was added to a stirred room temperature suspension of diol **2.30** (0.150 g, 0.535 mmol) in methanol/deionized water (20 mL, 5:1 v/v). The resulting mixture was stirred for 15 h. The majority of the solvents was removed under reduced pressure. The reaction mixture was diluted with ethyl acetate (30 mL) and water (30 mL). The layers were separated and the aqueous layer was extracted with ethyl acetate ( $2 \times 20$  mL). The combined organic layers were washed with saturated aqueous NaCl solution (70 mL), dried over  $\text{Na}_2\text{SO}_4$ , filtered, and concentrated under reduced pressure. The residue was subjected to column chromatography (10 cm  $\times$  2.5 cm, 30% ethyl acetate/hexanes) to afford **2.31** (0.143 g, 96%) as a white solid.  $R_f = 0.33$  (30% ethyl acetate/hexanes); mp 191–193  $^\circ\text{C}$  (dec.);  $^1\text{H}$  NMR (300 MHz,  $\text{CDCl}_3$ )  $\delta$  9.91 (s, 1H), 7.02 (d,  $J = 1.9$  Hz, 1H), 6.81 (dd,  $J = 8.1, 1.7$  Hz, 1H), 6.68 (d,  $J = 7.8$  Hz, 1H), 6.57–6.54 (m, 1H), 6.50–6.42 (m, 3H), 3.80–3.74 (m, 1H), 3.61 (dd,  $J = 13.0, 9.2$ , 1H), 3.39 (dd,  $J = 13.0, 8.2$ , 1H), 3.29–3.00 (m, 4H), 2.48 (s, 3H);  $^{13}\text{C}$  NMR (75 MHz,  $\text{CDCl}_3$ )  $\delta$  199.7, 198.6, 141.9, 139.4, 138.9, 138.8, 137.4, 137.0, 136.9, 136.1, 133.9, 133.4, 131.9, 131.2, 62.3, 36.1, 35.2, 35.1, 27.6; IR  $\nu$  2928 (w), 2855 (w), 1710 (s), 1664 (s), 1268 (m), 856 (w), 727 (m)  $\text{cm}^{-1}$ ; HRMS [APPI-(+)] calcd for  $\text{C}_{19}\text{H}_{19}\text{O}_2$   $[\text{M}+\text{H}]^+$  279.1385, found 279.1390.

**$\beta$ -Hydroxytetralone 2.32, Enone 2.33, and Ketoaldehyde 2.34**



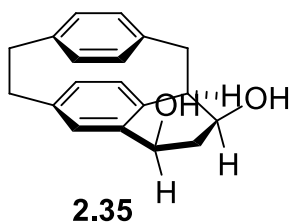
(*S*)-(+)-Camphorsulfonic acid (0.0050 g, 0.020 mmol) was added to a stirred room temperature suspension of ketoaldehyde **2.31** (0.110 g, 0.395 mmol) in benzene (15 mL). The resulting mixture was heated at 90 °C for 10 h. The reaction mixture was cooled to room temperature and was diluted with ethyl acetate (20 mL) and water (20 mL). The layers were separated and the aqueous layer was extracted with ethyl acetate (2 × 20 mL). The combined organic layers were washed with saturated aqueous NaCl solution (50 mL), dried over Na<sub>2</sub>SO<sub>4</sub>, filtered, and concentrated under reduced pressure. The residue was subjected to column chromatography (18 cm × 2.5 cm, 10–40% ethyl acetate/hexanes) to afford **2.32** (0.037 g, 34%) as a pale pink viscous oil, **2.33** (0.010 g, 10%) as a beige solid, **2.34** (0.021 g, 19%) as a yellow waxy solid, and unreacted **2.31** (0.017 g, 15% recovery) as an off-white solid.

**2.32:** *R*<sub>f</sub> = 0.29 (50% ethyl acetate/hexanes); <sup>1</sup>H NMR (300 MHz, CDCl<sub>3</sub>) δ 7.14 (d, *J* = 2.0 Hz, 1H), 6.75 (dd, *J* = 7.8, 2.0 Hz, 1H), 6.62 (d, *J* = 7.9 Hz, 2H), 6.53 (d, *J* = 8.0 Hz, 1H), 6.43–6.38 (m, 2H), 4.78 (td, *J* = 8.9, 4.6 Hz, 1H), 3.79 (dt, *J* = 10.6, 4.1 Hz, 1H), 3.43 (dd, *J* = 13.9, 3.5 Hz, 1H), 3.20–3.07 (m, 5H), 3.00 (br d, *J* = 8.8, Hz, 2H), 2.31 (br s, 1H) (*Note: Each of the <sup>1</sup>H NMR signals at δ = 6.62 and 3.00 ppm consists of two accidentally degenerate doublets*); <sup>13</sup>C NMR (75 MHz, CDCl<sub>3</sub>) δ 196.7, 143.6, 142.3, 140.0, 139.2, 139.0, 134.7, 134.3, 133.44, 133.38, 132.8, 131.7, 131.4, 68.8, 47.9, 42.9, 35.3, 35.2, 34.0; IR ν 3395 (br, w), 2926 (w), 1663 (s), 1416 (w), 1093 (m), 889 (s), 733 (w) cm<sup>-1</sup>; HRMS [APPI-(+)] calcd for C<sub>19</sub>H<sub>19</sub>O<sub>2</sub> [M+H]<sup>+</sup> 279.1385, found 279.1377.

**2.33:**  $R_f = 0.42$  (20% ethyl acetate/hexanes); mp 117–119 °C;  $^1\text{H NMR}$  (300 MHz,  $\text{CDCl}_3$ )  $\delta$  7.04 (dd,  $J = 7.5, 2.2$  Hz, 1H), 6.87 (dd,  $J = 7.8, 1.7$  Hz, 1H), 6.85–6.80 (m, 2H), 6.59–6.56 (m, 2H), 6.13 (dd,  $J = 9.6, 5.2$  Hz, 1H), 5.91 (d,  $J = 1.9$  Hz, 1H), 5.65 (dd,  $J = 7.9, 1.7$  Hz, 1H), 3.41 (ddt,  $J = 8.7, 5.2, 1.2$  Hz, 1H), 3.14–3.03 (m, 3H), 2.93 (d,  $J = 12.6$ , 1H), 2.52 (ddd,  $J = 12.5, 10.5, 8.1$  Hz, 1H), 2.21 (ddd,  $J = 12.5, 10.5, 7.9$  Hz, 1H);  $^{13}\text{C NMR}$  (75 MHz,  $\text{CDCl}_3$ )  $\delta$  204.9, 140.2, 139.5, 136.6, 135.5, 132.7, 132.2, 130.3, 129.8, 129.6, 129.20, 129.16, 128.7, 127.2, 125.3, 51.8, 39.5, 36.8, 34.9; IR  $\nu$  2921 (w), 1685 (m), 1092 (s), 882 (s)  $\text{cm}^{-1}$ ; HRMS [APPI(+)] calcd for  $\text{C}_{19}\text{H}_{17}\text{O}$   $[\text{M}+\text{H}]^+$  261.1279, found 261.1277.

**2.34:**  $R_f = 0.29$  (30% ethyl acetate/hexanes);  $^1\text{H NMR}$  (300 MHz,  $\text{CDCl}_3$ )  $\delta$  10.05 (s, 1H), 7.06 (d,  $J = 1.9$  Hz, 1H), 6.66 (dd,  $J = 7.9, 1.9$  Hz, 1H), 6.58–6.53 (m, 2H), 6.51 (d,  $J = 7.7$ , 1H), 6.32–6.27 (m, 2H), 5.43 (dd,  $J = 10.0, 4.1$  Hz, 1H), 3.70 (dd,  $J = 13.3, 4.1$ , 1H), 3.23 (dd,  $J = 13.0, 9.6$  Hz, 1H), 3.18–3.05 (m, 4H), 2.53 (s, 3H);  $^{13}\text{C NMR}$  (75 MHz,  $\text{CDCl}_3$ )  $\delta$  200.9, 200.3, 141.2, 139.2, 139.1, 138.7, 137.6, 135.5, 135.2, 134.2, 133.7, 132.8, 132.5, 132.0, 56.7, 35.2, 35.0, 33.8, 29.1; IR  $\nu$  2927 (w), 1717 (s), 1672 (s), 1267 (m), 894 (m), 732 (s)  $\text{cm}^{-1}$ ; HRMS [APPI(+)] calcd for  $\text{C}_{19}\text{H}_{19}\text{O}_2$   $[\text{M}+\text{H}]^+$  279.1385, found 279.1380.

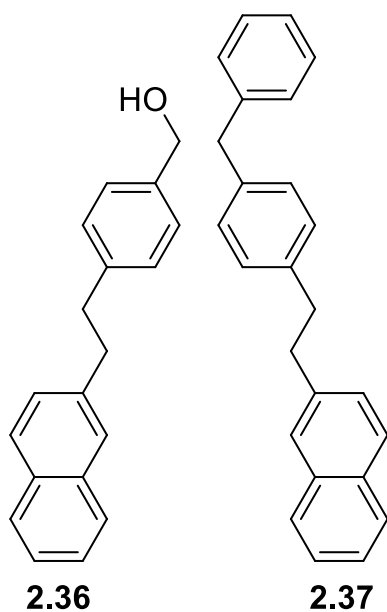
### Diol 2.35



Sodium borohydride (0.0079 g, 0.21 mmol) was added to a stirred 0 °C (ice/water) solution of  $\beta$ -hydroxytetralone **2.32** (0.0292 g, 0.105 mmol) in methanol (3 mL). The cold bath was removed and the resulting mixture was stirred for 1 h as it warmed to room temperature. After cooling to 0 °C, water (5 mL) was added to the reaction mixture. The majority of the solvent was removed under reduced pressure. The remaining mixture was diluted with ethyl acetate (20 mL) and water (20 mL). The layers were separated and the aqueous layer was extracted with ethyl

acetate (2 × 15 mL). The combined organic layers were washed with saturated aqueous NaCl solution (50 mL), dried over Na<sub>2</sub>SO<sub>4</sub>, filtered, and concentrated under reduced pressure. The residue was subjected to column chromatography (12 cm × 1.5 cm, 70–80% ethyl acetate/hexanes) to afford **2.35** (0.0279 g, 95%) as a white solid. *R*<sub>f</sub> = 0.28 (80% ethyl acetate/hexanes); mp 166–168 °C; <sup>1</sup>H NMR (300 MHz, CDCl<sub>3</sub>) δ 6.76 (br s, 1H), 6.61–6.54 (m, 2H), 6.49 (br d, *J* = 8.1 Hz, 1H), 6.46–6.44 (m, 2H), 6.42 (d, *J* = 7.7 Hz, 1H), 4.68 (dd, *J* = 10.5, 6.9, 1H), 4.44 (dt, *J* = 12.0, 4.5, 1H), 3.67–3.62 (m, 1H), 3.30 (dd, *J* = 13.8, 2.9 Hz, 1H), 3.21–2.97 (m, 5H), 2.50–2.31 (m, 2H), 1.89 (br s, 2H) (Note: The <sup>1</sup>H NMR signal at δ = 1.89 consists of two accidentally degenerate broad singlets); <sup>13</sup>C NMR (75 MHz, CDCl<sub>3</sub>) δ 141.2, 139.8, 139.4, 138.3, 134.8, 133.9, 133.7, 133.44, 133.39, 132.9, 132.7, 128.5, 69.2, 68.7, 48.3, 38.0, 36.1, 35.6, 35.3; IR ν 3389 (br, w), 3357 (br, w), 2922 (w), 1092 (s), 891 (s) cm<sup>-1</sup>; HRMS [APPI-(+)] calcd for C<sub>19</sub>H<sub>19</sub>O [M+H-H<sub>2</sub>O]<sup>+</sup> 263.1436, found 263.1419.

#### 4-[2-(2-Naphthalenyl)ethyl]benzyl Alcohol (**2.36**) and Diphenylmethane **2.37**



*p*-Toluenesulfonic acid (0.0012 g, 0.0072 mmol) was added to a stirred room temperature suspension of **2.35** (0.0201 g, 0.0717 mmol) in benzene (3 mL). The reaction flask was equipped with a Barrett apparatus and the resulting mixture was heated at 90 °C for 1 h. After cooling to room temperature, saturated sodium bicarbonate solution (5 mL) was added to the reaction mixture and stirring was continued for 5 min. Ethyl acetate (10 mL) was added to the mixture and the layers were separated. The aqueous layer was extracted with ethyl acetate (2 × 15 mL) and the

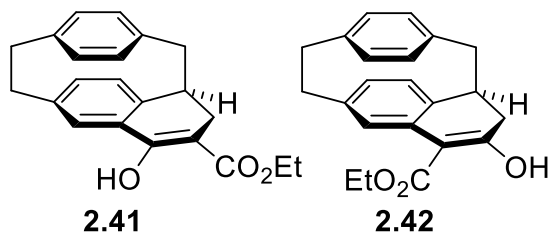
combined organic layers were washed with water (30 mL), washed with saturated aqueous NaCl

solution (30 mL), dried over Na<sub>2</sub>SO<sub>4</sub>, filtered, and concentrated under reduced pressure. The residue was subjected to column chromatography (15 cm × 1.0 cm, 0–25% ethyl acetate/hexanes) to afford **2.36** (0.0075 g, 40%) and **2.37** (0.0025 g, 11%) as a beige and a white solid, respectively.

**2.36:** *R*<sub>f</sub> = 0.30 (30% ethyl acetate/hexanes); mp 114–116 °C; <sup>1</sup>H NMR (500 MHz, CDCl<sub>3</sub>) δ 7.81 (d, *J* = 7.6 Hz, 1H), 7.78–7.76 (m, 2H), 7.62 (s, 1H), 7.47–7.41 (m, 2H), 7.34 (dd, *J* = 8.4, 1.8 Hz, 1H), 7.29 (d, *J* = 7.8 Hz, 2H), 7.21 (d, *J* = 7.8 Hz, 2H), 4.67 (s, 2H), 3.11–3.07 (AA'BB' half-spectrum, 2H), 3.04–3.00 (AA'BB' half-spectrum, 2H); <sup>13</sup>C NMR (75 MHz, CDCl<sub>3</sub>) δ 141.4, 139.3, 138.7, 133.8, 132.2, 128.9, 128.0, 127.8, 127.6, 127.5, 127.3, 126.6, 126.1, 125.3, 65.4, 38.2, 37.6; IR ν 3311 (br, w), 2924 (w), 2857 (w), 1508 (w), 1007 (m), 821 (s) cm<sup>-1</sup>; HRMS [APPI(+)] calcd for C<sub>19</sub>H<sub>18</sub>O [M]<sup>+</sup> 262.1358, found 262.1350.

**2.37:** *R*<sub>f</sub> = 0.38 (1% ethyl acetate/hexanes); <sup>1</sup>H NMR (500 MHz, CDCl<sub>3</sub>) δ 7.81 (d, *J* = 7.5 Hz, 1H), 7.77–7.75 (m, 2H), 7.60 (s, 1H), 7.46–7.40 (m, 2H), 7.34 (dd, *J* = 8.4, 1.8 Hz, 1H), 7.30–7.27 (m, 2H), 7.21–7.18 (m, 3H), 7.15–7.10 (m, 4H), 3.96 (s, 2H), 3.08–3.04 (AA'BB' half-spectrum, 2H), 3.00–2.96 (AA'BB' half-spectrum, 2H); <sup>13</sup>C NMR (75 MHz, CDCl<sub>3</sub>) δ 141.5, 139.6, 139.5, 138.9, 133.8, 132.2, 129.08, 129.05, 128.7, 128.6, 128.0, 127.8, 127.6, 127.5, 126.6, 126.2, 126.0, 125.3, 41.7, 38.3, 37.6; IR ν 2921 (w), 1233 (w), 891 (s) cm<sup>-1</sup>; HRMS [APPI(+)] calcd for C<sub>25</sub>H<sub>22</sub> [M]<sup>+</sup> 322.1722, found 322.1699. *Note: The melting point of 2.37 could not be obtained due to the unavailability of a sufficient quantity of the material.*

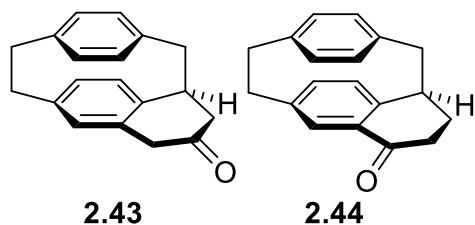
### Enol Esters **2.41** and **2.42**



Et<sub>2</sub>O·BF<sub>3</sub> (1.30 g, 10.1 mmol) was added to a stirred room temperature suspension of indanone **2.19** (0.500 g, 2.01 mmol) in diethyl ether (35 mL). The resulting mixture was stirred at this temperature for

5 min, during which the majority of the solid was dissolved. A solution of ethyl diazoacetate (1.15 g, 10.1 mmol) in diethyl ether (5 mL) was added to the mixture and the resulting mixture was stirred at room temperature for 15 h. Water (30 mL) was added dropwise to the reaction mixture and the layers were separated. The aqueous layer was extracted with diethyl ether (30 mL) and the combined organic layers were washed with saturated aqueous NaCl solution (2 × 50 mL), dried over Na<sub>2</sub>SO<sub>4</sub>, filtered, and concentrated under reduced pressure. The residue was subjected to column chromatography (15 cm × 5.5 cm, 0–4% ethyl acetate/hexanes) to afford a *ca.* 93:7 (<sup>1</sup>H NMR analysis) mixture of **2.41** and **2.42** (0.383 g, 57%) as a yellow solid. *R*<sub>f</sub> = 0.44 (5% ethyl acetate/hexanes); mp 132–138 °C; <sup>1</sup>H NMR (300 MHz, CDCl<sub>3</sub>) major isomer **2.41**: δ 12.61 (s, 1H), 6.97 (d, *J* = 1.8 Hz, 1H), 6.75–6.72 (m, 1H), 6.65 (dd, *J* = 7.7, 1.8 Hz, 1H), 6.51–6.48 (m, 3H), 6.42–6.39 (m, 1H), 4.34 (q, *J* = 7.1 Hz, 2H), 3.36–2.75 (m, 9H), 1.40 (t, *J* = 7.1 Hz, 3H); distinguishable signals for minor isomer **2.42**: δ 13.85 (s, 1H), 7.13 (d, *J* = 1.4 Hz, 1H), 6.78 (dd, *J* = 7.9, 1.9 Hz, 1H), 4.59–4.40 (m, 2H), 2.62 (dd, *J* = 17.3, 1.1 Hz, 1H), 1.51 (t, *J* = 7.1 Hz, 3H); <sup>13</sup>C NMR (75 MHz, CDCl<sub>3</sub>) major isomer **2.41**: δ 173.9, 165.2, 141.1, 140.5, 140.1, 140.0, 135.3, 133.3, 133.1, 132.5, 131.83, 131.80, 130.8, 130.0, 94.4, 60.7, 41.8, 39.8, 35.6, 35.4, 29.4, 14.5; distinguishable signals for minor isomer **2.42**: δ 133.2, 132.3, 130.6, 129.4, 128.9, 61.3, 41.6, 39.9, 38.2, 36.1, 35.6; IR ν 2978 (w), 2929 (m), 2850 (w), 1636 (s), 1611 (m), 1585 (s), 1561 (m), 1252 (s), 1185 (m), 1082 (m), 808 (m), 634 (m) cm<sup>-1</sup>; HRMS [APPI-(+)] calcd for C<sub>22</sub>H<sub>23</sub>O<sub>3</sub> [M+H]<sup>+</sup> 335.1647, found 335.1632.

#### **β-Tetralone 2.43 and α-Tetralone 2.44**



Lithium chloride (0.088 g, 2.1 mmol) and water (0.15 mL, 8.4 mmol) were added to a stirred room temperature solution of a *ca.* 93:7 mixture of **2.41** and **2.42** (0.350 g,

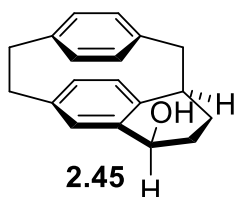
1.05 mmol) in dimethyl sulfoxide (10 mL). The resulting mixture was stirred at 140 °C for 2 h. The reaction mixture was cooled to room temperature, poured into ice-cold water (30 mL) and stirred for 5 min. Ethyl acetate (50 mL) was added to the mixture and the layers were separated. The aqueous layer was extracted with ethyl acetate (3 × 20 mL) and the combined organic layers were washed with water (2 × 100 mL), washed with saturated aqueous NaCl solution (100 mL), dried over Na<sub>2</sub>SO<sub>4</sub>, filtered, and concentrated under reduced pressure. The residue was subjected to column chromatography (18 cm × 5.5 cm, 5–15% ethyl acetate/hexanes) to afford **2.43** (0.011 g, 57% based on the amount of **2.42** in the 93:7 mixture of **2.41** and **2.42**) as a pale orange solid and **2.44** (0.219 g, 86% based on the amount of **2.41** in the 93:7 mixture of **2.41** and **2.42**) as a yellow oil that solidified on standing in a freezer.

**2.43:**  $R_f = 0.53$  (20% ethyl acetate/hexanes); mp 131–134 °C; <sup>1</sup>H NMR (300 MHz, CDCl<sub>3</sub>)  $\delta$  6.61–6.56 (m, 2H), 6.52 (dd,  $J = 7.9, 1.7$  Hz, 1H), 6.49 (d,  $J = 8.2$  Hz, 1H), 6.46 (dd,  $J = 7.9, 2.1$  Hz, 1H), 6.40 (dd,  $J = 7.9, 2.0$  Hz, 1H), 6.07 (s, 1H), 3.78–3.71 (m, 1H), 3.50, 3.41 (AB system,  $J = 20.9$  Hz, 2H), 3.38 (dd,  $J = 13.6, 10.6$  Hz, 1H), 3.17–2.96 (m, 5H), 2.78 (ddd,  $J = 14.6, 2.4, 0.9$  Hz, 1H), 2.65 (dd,  $J = 13.6, 3.7$  Hz, 1H); <sup>13</sup>C NMR (75 MHz, CDCl<sub>3</sub>)  $\delta$  209.6, 141.3, 140.0, 139.0, 136.3, 135.0, 133.9, 133.6, 133.5, 132.6, 132.4, 131.5, 128.5, 48.3, 45.6, 43.0, 42.7, 35.43, 35.37; IR  $\nu$  2921 (m), 2850 (w), 1708 (s), 1392 (w), 871 (w), 713 (m), 645 (m) cm<sup>-1</sup>; HRMS [APPI(+)] calcd for C<sub>19</sub>H<sub>18</sub>O [M]<sup>+</sup> 262.1358, found 262.1347.

**2.44:**  $R_f = 0.45$  (20% ethyl acetate/hexanes); <sup>1</sup>H NMR (300 MHz, CDCl<sub>3</sub>)  $\delta$  7.16 (d,  $J = 1.9$  Hz, 1H), 6.68 (dd,  $J = 7.8, 1.9$  Hz, 1H), 6.60 (dd,  $J = 7.9, 1.6$  Hz, 1H), 6.56–6.50 (m, 2H), 6.45 (dd,  $J = 8.1, 1.6$  Hz, 1H), 6.40 (dd,  $J = 8.1, 1.5$  Hz, 1H), 3.58 (ddd,  $J = 10.4, 6.8, 3.4$  Hz, 1H), 3.41 (dd,  $J = 13.2, 10.7$  Hz, 1H), 3.20–2.94 (m, 6H), 2.75 (ddd,  $J = 5.3, 2.2, 0.8$  Hz, 1H), 2.70–2.54 (m, 1H), 2.27–2.19 (m, 1H); <sup>13</sup>C NMR (75 MHz, CDCl<sub>3</sub>)  $\delta$  198.2, 146.3, 141.4, 140.1, 139.6, 138.7,

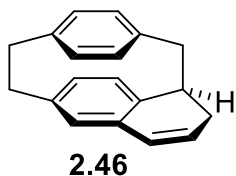
135.4, 133.6, 133.3, 133.0, 132.7, 131.6, 131.5, 40.8, 40.2, 35.4, 35.3, 34.0, 29.8; IR  $\nu$  2924 (m), 2857 (w), 1672 (s), 1592 (m), 1408 (m), 1280 (w), 1226 (w), 1036 (w), 645 (w)  $\text{cm}^{-1}$ ; HRMS [APPI-(+)] calcd for  $\text{C}_{19}\text{H}_{19}\text{O}$   $[\text{M}+\text{H}]^+$  263.1436, found 263.1437.

### Tetralol **2.45**



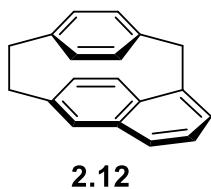
Sodium borohydride (0.043 g, 1.1 mmol) was added to a stirred 0 °C (ice/water) solution of tetralone **2.44** (0.200 g, 0.762 mmol) in methanol (10 mL). The cold bath was removed and the resulting mixture was stirred for 1 h as it warmed to room temperature. After cooling to 0 °C, water (5 mL) was added to the reaction mixture. The majority of the solvent was removed under reduced pressure. The remaining mixture was diluted with ethyl acetate (20 mL) and water (10 mL). The layers were separated and the aqueous layer was extracted with ethyl acetate (2 × 10 mL). The combined organic layers were washed with saturated aqueous NaCl solution (50 mL), dried over  $\text{Na}_2\text{SO}_4$ , filtered, and concentrated under reduced pressure. The residue was subjected to column chromatography (15 cm × 4.5 cm, 10–25% ethyl acetate/hexanes) to afford **2.45** (0.171 g, 85%) as a white solid.  $R_f$  = 0.50 (30% ethyl acetate/hexanes); mp 144–147 °C;  $^1\text{H}$  NMR (300 MHz,  $\text{CDCl}_3$ )  $\delta$  6.77 (s, 1H), 6.60–6.53 (m, 3H), 6.44 (dd,  $J$  = 8.2, 1.7 Hz, 1H), 6.37 (dd,  $J$  = 7.7, 1.7 Hz, 1H), 6.33 (d,  $J$  = 7.7 Hz, 1H), 4.68–4.60 (m, 1H), 3.46 (ddd,  $J$  = 10.3, 6.5, 3.4 Hz, 1H), 3.31 (dd,  $J$  = 13.1, 10.5 Hz, 1H), 3.20–3.01 (m, 4H), 2.90 (dd,  $J$  = 13.1, 2.5 Hz, 1H), 2.40–2.25 (m, 2H), 2.23–2.14 (m, 1H), 2.13–1.95 (m, 1H), 1.87 (d,  $J$  = 6.7 Hz, 1H);  $^{13}\text{C}$  NMR (75 MHz,  $\text{CDCl}_3$ )  $\delta$  140.1, 139.89, 139.86, 139.3, 137.5, 133.2, 133.1, 133.01, 133.00, 132.9, 128.1, 69.9, 44.0, 41.0, 35.6, 35.4, 30.1, 29.5 (one signal fewer than expected); IR  $\nu$  3276 (br, m), 2924 (m), 2848 (m), 1593 (m), 1076 (m), 1045 (s), 899 (s), 719 (s), 627 (m)  $\text{cm}^{-1}$ ; HRMS [APPI-(+)] calcd for  $\text{C}_{19}\text{H}_{19}$   $[\text{M}+\text{H}-\text{H}_2\text{O}]^+$  247.1487, found 247.1488 ( $[\text{M}]^+$  and  $[\text{M}+\text{H}]^+$  peaks were not observed).

## Dihydronaphthalene **2.46**



*p*-Toluenesulfonic acid (0.005 g, 0.03 mmol) was added to a stirred room temperature solution of tetralol **2.45** (0.150 g, 0.567 mmol) in benzene (10 mL). The reaction flask was equipped with a Barrett apparatus and the resulting mixture was heated at 90 °C for 30 min. After cooling to room temperature, saturated sodium bicarbonate solution (10 mL) was added to the reaction mixture and stirring was continued for 5 min. Ethyl acetate (15 mL) was added to the mixture and the layers were separated. The aqueous layer was extracted with ethyl acetate (2 × 10 mL) and the combined organic layers were washed with water (30 mL), washed with saturated aqueous NaCl solution (30 mL), dried over Na<sub>2</sub>SO<sub>4</sub>, filtered, and concentrated under reduced pressure. The residue was subjected to column chromatography (10 cm × 2.5 cm, 0–4% ethyl acetate/hexanes) to afford **2.46** (0.130 g, 94%) as a white solid. *R*<sub>f</sub> = 0.28 (3% ethyl acetate/hexanes); mp 156–157 °C; <sup>1</sup>H NMR (300 MHz, CDCl<sub>3</sub>) δ 6.96 (dd, *J* = 7.9, 1.9 Hz, 1H), 6.52 (dd, *J* = 7.9, 1.8 Hz, 1H), 6.47 (dd, *J* = 7.6, 1.7 Hz, 1H), 6.42–6.38 (m, 3H), 6.21 (dd, *J* = 9.5, 3.1 Hz, 1H), 6.05 (d, *J* = 1.6 Hz, 1H), 5.96 (ddd, *J* = 9.1, 6.4, 2.4 Hz, 1H), 3.28–2.93 (m, 7H), 2.89–2.80 (m, 1H), 2.46 (dd, *J* = 17.7, 6.0 Hz, 1H); <sup>13</sup>C NMR (75 MHz, CDCl<sub>3</sub>) δ 140.3, 140.1, 139.8, 136.2, 135.9, 133.3, 132.9, 132.52, 132.50, 132.0, 131.5, 129.9, 129.6, 126.0, 42.0, 39.7, 35.53, 35.50, 33.3; IR ν 3029 (w), 2944 (w), 2919 (m), 2849 (w), 2829 (w), 1481 (w), 810 (m), 754 (m), 706 (s) cm<sup>-1</sup>; HRMS [APPI-(+)] calcd for C<sub>19</sub>H<sub>19</sub> [M+H]<sup>+</sup> 247.1487, found 247.1497.

## [2](6,1)Naphthaleno[1]paracyclophane (**2.12**)



DDQ (0.464 g, 2.05 mmol) and anhydrous K<sub>2</sub>CO<sub>3</sub> (0.283 g, 2.05 mmol) were added to a stirred nitrogen-purged room temperature solution of **2.46** (0.100 g, 0.409 mmol) in dry benzene (10 mL). The resulting mixture was heated at 40

°C for 20 h. After cooling to room temperature, water (10 mL) was added to the reaction mixture and stirred for 5 min. Ethyl acetate (20 mL) was added to the mixture and two layers were separated. The aqueous layer was extracted with ethyl acetate (3 × 10 mL) and the combined organic layers were washed with saturated aqueous NaCl solution (50 mL), dried over Na<sub>2</sub>SO<sub>4</sub>, filtered, and concentrated under reduced pressure. The residue was subjected to column chromatography (15 cm × 2.5 cm, 0–3% ethyl acetate/hexanes) to afford **2.12** (0.019 g, 19%) as an off-white solid. *R*<sub>f</sub> = 0.32 (3% ethyl acetate/hexanes); mp 115–117 °C (dec.); <sup>1</sup>H NMR (300 MHz, CDCl<sub>3</sub>) δ 7.34–7.29 (m, 2H), 7.13–6.99 (m, 3H), 6.93 (s, 1H), 6.71 (dd, *J* = 7.8, 2.1 Hz, 1H), 6.28 (dd, *J* = 8.6, 1.3 Hz, 1H), 5.56 (dd, *J* = 8.4, 2.1 Hz, 1H), 4.97 (ddd, *J* = 8.4, 1.6, 1.0 Hz, 1H), 4.32, 3.88 (AB system, *J* = 14.2 Hz, 2H), 3.21 (ddd, *J* = 13.1, 9.5, 3.9 Hz, 1H), 2.96–2.74 (m, 3H); <sup>13</sup>C NMR (75 MHz, CDCl<sub>3</sub>) δ 148.1, 146.8, 137.4, 136.8, 135.7, 134.8, 134.1, 133.3, 132.9, 132.6, 130.5, 129.6, 126.6, 124.9, 124.4, 124.2, 44.0, 34.8, 32.3; IR ν 3049 (w), 2952 (w), 2919 (m), 2848 (w), 1723 (w), 1485 (m), 887 (m), 880 (m), 754 (s), 706 (m), 656 (m), 591 (m) cm<sup>-1</sup>; HRMS [APPI-(+)] calcd for C<sub>19</sub>H<sub>16</sub> [M]<sup>+</sup> 244.1252, found 244.1258.

## 2.6 References

1. (a) Tsuji, T.; Ohkita, M.; Konno, T.; Nishida, S. *J. Am. Chem. Soc.* **1997**, *119*, 8425–8431.  
(b) Tsuji, T.; Ohkita, M.; Nishida, S. *J. Am. Chem. Soc.* **1993**, *115*, 5284–5285.
2. (a) Tsuji, T.; Okuyama, M.; Ohkita, M.; Kawai, H.; Suzuki, T. *J. Am. Chem. Soc.* **2003**, *125*, 951–961. (b) Okuyama, M.; Ohkita, M.; Tsuji, T. *Chem. Commun.* **1997**, 1277–1278. (c) Okuyama, M.; Tsuji, T. *Angew. Chem. Int. Ed. Engl.* **1997**, *36*, 1085–1087.
3. (a) van Straten, J. W.; de Wolf, W. H.; Bickelhaupt, F. *Tetrahedron Lett.* **1977**, *18*, 4667–4670.

4. (a) Zhang, B.; Zhao, Y.; Bodwell, G. J. *Can. J. Chem.* **2017**, *95*, 460–481. (b) Zhang, B.; Zhao, Y.; Bodwell, G. J. *Synlett* **2016**, *27*, 2113–2116.
5. Ghasemabadi, P. G.; Yao, T.; Bodwell, G. J. *Chem. Soc. Rev.* **2015**, *44*, 6494–6518.
6. (a) Enders, M.; Friedmann, C. J.; Plessow, P. N.; Bihlmeier, A.; Nieger, M.; Klopper, W.; Bräse, S. *Chem. Commun.* **2015**, *51*, 4793–4795. (b) Focken, T.; Hopf, H.; Snieckus, V.; Dix, I.; Jones, P. G. *Eur. J. Org. Chem.* **2001**, 2221–2228.
7. Truesdale, E. A.; Cram, D. J. *J. Org. Chem.* **1980**, *45*, 3974–3981.
8. (a) Regitz, M.; Maas, G. *Diazo Compounds, Properties, and Synthesis*; Academic Press: New York, 1986. (b) Regitz, M. *Angew. Chem. Int. Ed. Engl.* **1967**, *6*, 733–749.
9. (a) Mortén, M.; Henum, M.; Bonge-Hansen, T. *Beilstein J. Org. Chem.* **2016**, *12*, 1590–1597. (b) Doyle, M. P.; McKervey, M. A.; Ye, T. *Modern Catalytic Methods for Organic Synthesis with Diazo Compounds: From Cyclopropanes to Ylides*; John Wiley & Sons: New York, 1998.
10. (a) Aeluri, R.; Alla, M.; Polepalli, S.; Jain, N. *Eur. J. Med. Chem.* **2015**, *100*, 18–23. (b) King, L. C.; Ostrum, G. K. *J. Org. Chem.* **1964**, *29*, 3459–3461.
11. Samanta, S.; Mondal, S.; Hajra, A. *Org. Biomol. Chem.* **2018**, *16*, 1088–1092.
12. Tatton, M. R.; Simpson, I.; Donohoe, T. J. *Chem. Commun.* **2014**, *50*, 11314–11316.
13. Honda, T.; Ishige, H.; Nagase, H. *J. Chem. Soc., Perkin Trans. 1* **1994**, 3305–3310.
14. Morency, M.; Néron, S.; Iftimie, R.; Wuest, J. D. *J. Org. Chem.* **2021**, *86*, 14444–14460.
15. CCDC 1906402 contains the supplementary crystallographic data for compound **2.12**. These data can be obtained free of charge from The Cambridge Crystallographic Data Centre.
16. The M06-2X functional was chosen for the DFT and TD-DFT calculations because of its reliable performance in computing ground- and excited state geometries and energies. See:

- (a) Zhao, Y.; Truhlar, D. G. *Theor. Chim. Acc.* **2008**, *120*, 215–241. (b) Mardirossian, N.; Head-Gordon, M. *J. Chem. Theory Comput.* **2016**, *12*, 4303–4325. (c) Leang, S. S.; Zahariev, F.; Gordona, M. S. *J. Chem. Phys.* **2012**, *136*, 104101. (d) Jacquemin, D.; Perpète, E. A.; Ciofini, I.; Adamo, C.; Valero, R.; Zhao, Y.; Tuhlar, D. G. *J. Chem. Theory Comput.* **2010**, *6*, 2071–2085.
17. Hope, H.; Bernstein, J.; Trueblood, K. N. *Acta Crystallogr. Sect. B* **1972**, *28*, 1733–1743.
18. Pascal, R. A., Jr. *Chem. Rev.* **2006**, *106*, 4809–4819.
19. Otsubo, T.; Aso, Y.; Ogura, F.; Misumi, S.; Kawamoto, A.; Tanaka, J. *Bull. Chem. Soc. Jpn.* **1989**, *62*, 164–170.
20. Bodwell, G. J.; Bridson, J. N.; Houghton, T. J.; Kennedy, J. W. J.; Mannion, M. R. *Chem. Eur. J.* **1999**, *5*, 1823–1827.
21. Diercks, R.; Vollhardt, K. P. C. *J. Am. Chem. Soc.* **1986**, *108*, 3150–3152.
22. Kawai, H.; Suzuki, T.; Ohkita, M.; Tsuji, T. *Chem. Eur. J.* **2000**, *6*, 4177–4187.
23. From a search of the CCDC, 31 structures of naphthalene were found with R1 < 7.5%. Mean values of these 31 structures (see Appendix 1, Table A1-9) were used as the reference bond lengths for naphthalene.
24. Dodziuk, H.; Szymanski, S.; Jazwinski, J.; Ostrowski, M.; Demissie, T. B.; Ruud, K.; Kus, P.; Hopf, H.; Lin, S.-T. *J. Phys. Chem. A* **2011**, *115*, 10638–10649.
25. Nurmukhametov, R. N.; Shapovalov, A. V.; Antonov, D. Yu. *J. Appl. Spectrosc.* **2016**, *83*, 27–34.
26. Cram, D. J.; Dalton, C. K.; Knox, G. R. *J. Am. Chem. Soc.* **1963**, *85*, 1088–1093.
27. Rademacher, P. In *Modern Cyclophane Chemistry*, Gleiter, R., Hopf, H., Eds.; Wiley-VCH: Weinheim, 2004; pp 275–310.

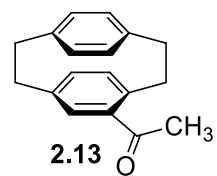
28. Berlman, I. B. *Handbook of Fluorescence Spectra of Aromatic Molecules*, Academic Press, New York, 1971.
29. Sarbu, L. G.; Bahrin, L. G.; Jones, P. G.; Birsa, L. M.; Hopf, H. *Beilstein J. Org. Chem.* **2015**, *11*, 1917–1921.
30. Kaupang, Å.; Bonge-Hansen, T. *Beilstein J. Org. Chem.* **2013**, *9*, 1407–1413.

## **Appendix 1**

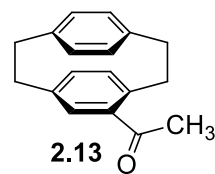
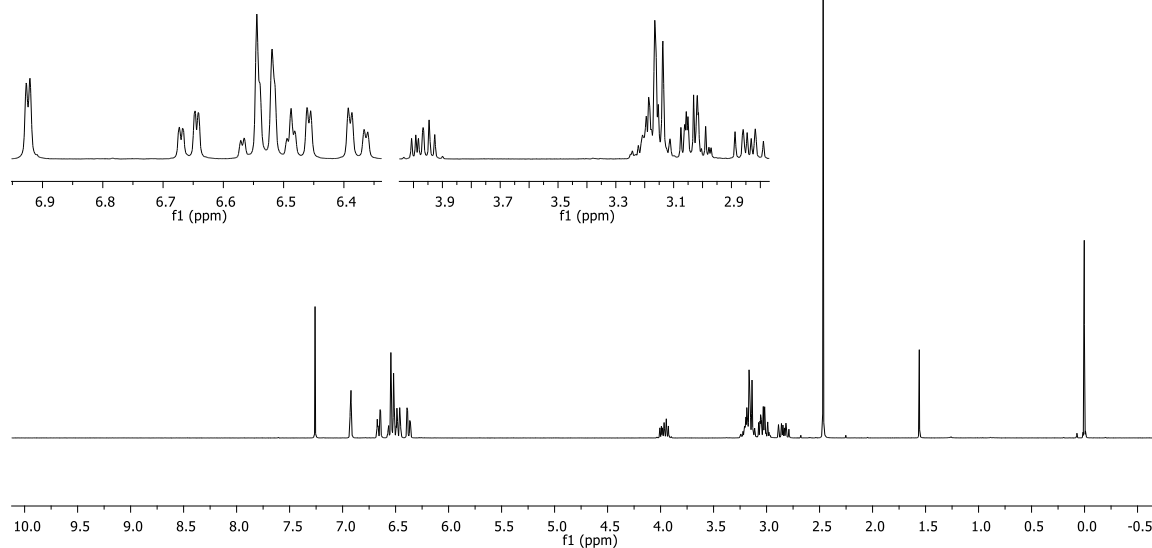
**$^1\text{H}$ ,  $^{13}\text{C}$  NMR Spectra, Two-Dimensional NMR Spectra, X-ray Crystallographic Data, and Computational Data for**

## **Chapter 2**

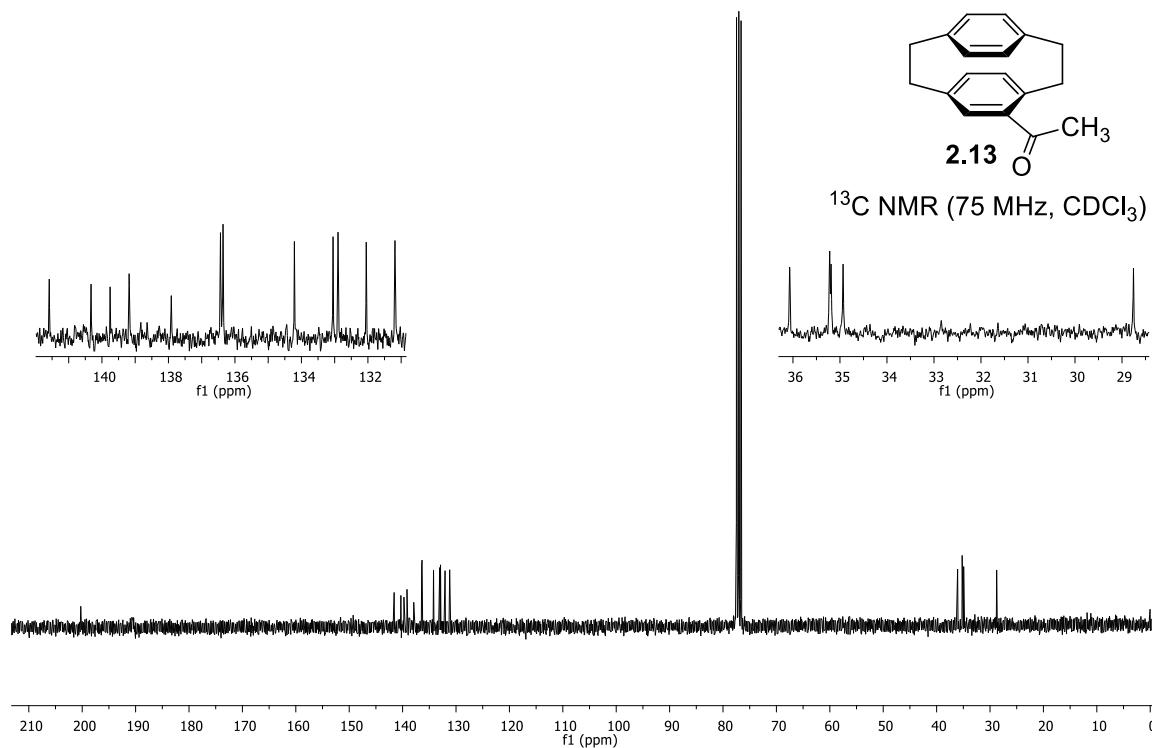
# 1. $^1\text{H}$ and $^{13}\text{C}$ NMR Spectra

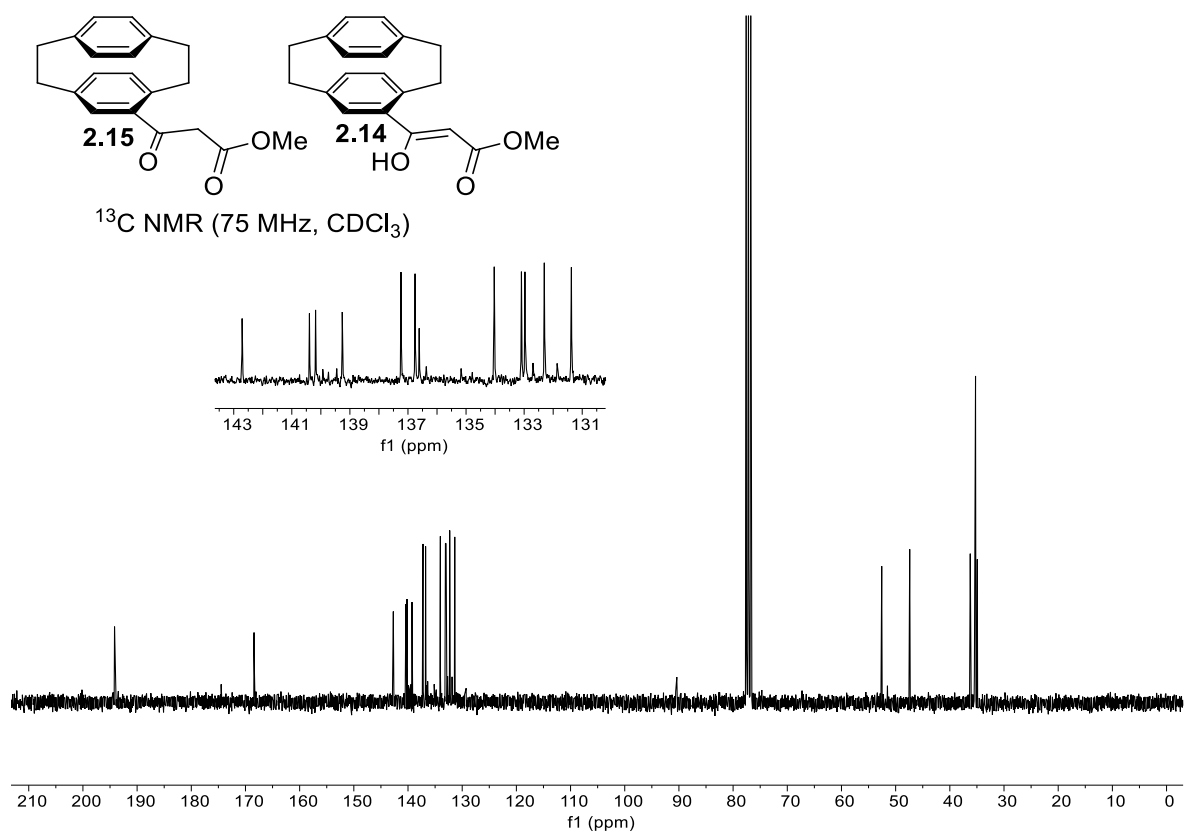
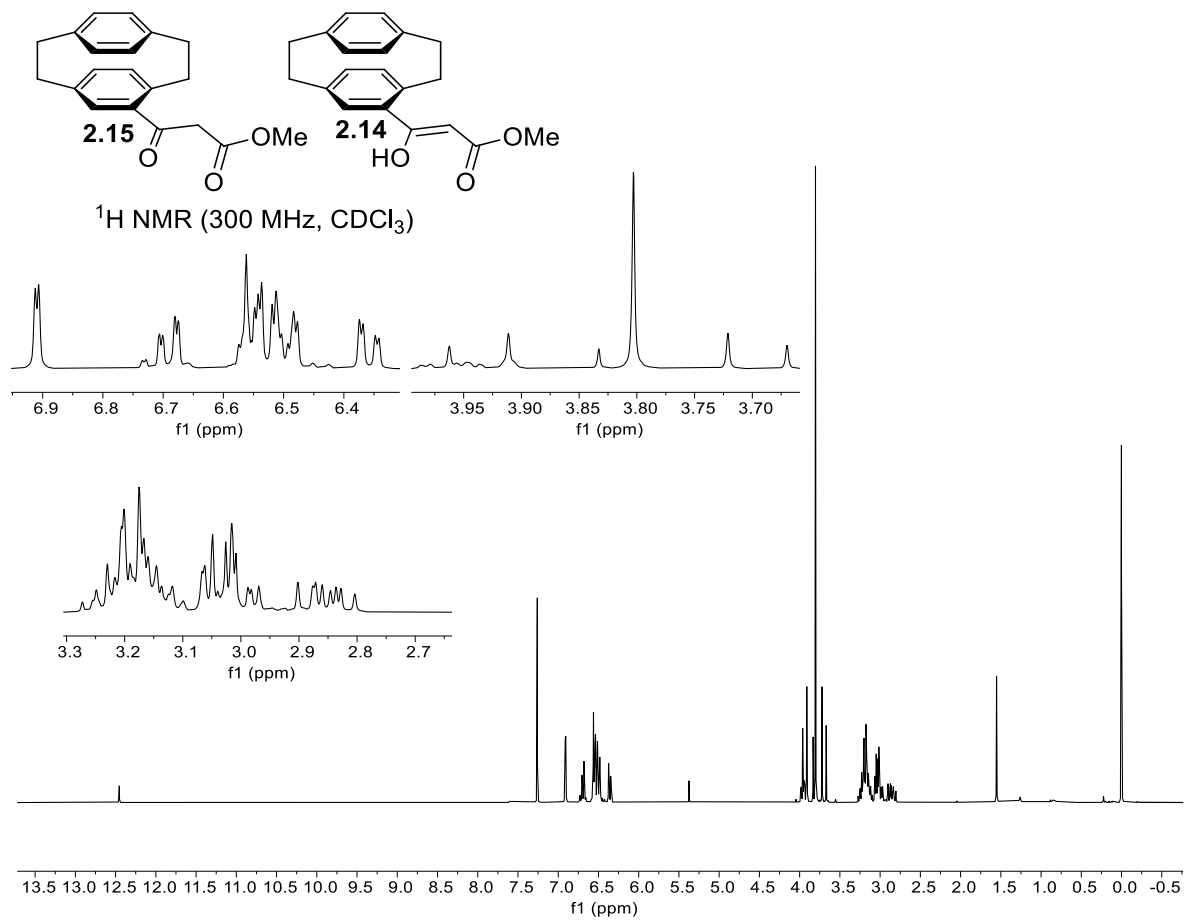


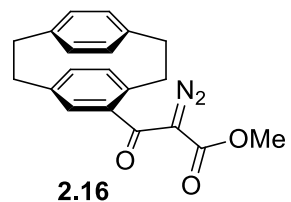
$^1\text{H}$  NMR (300 MHz,  $\text{CDCl}_3$ )



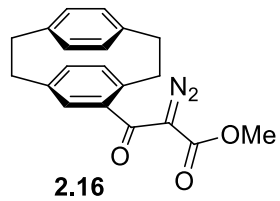
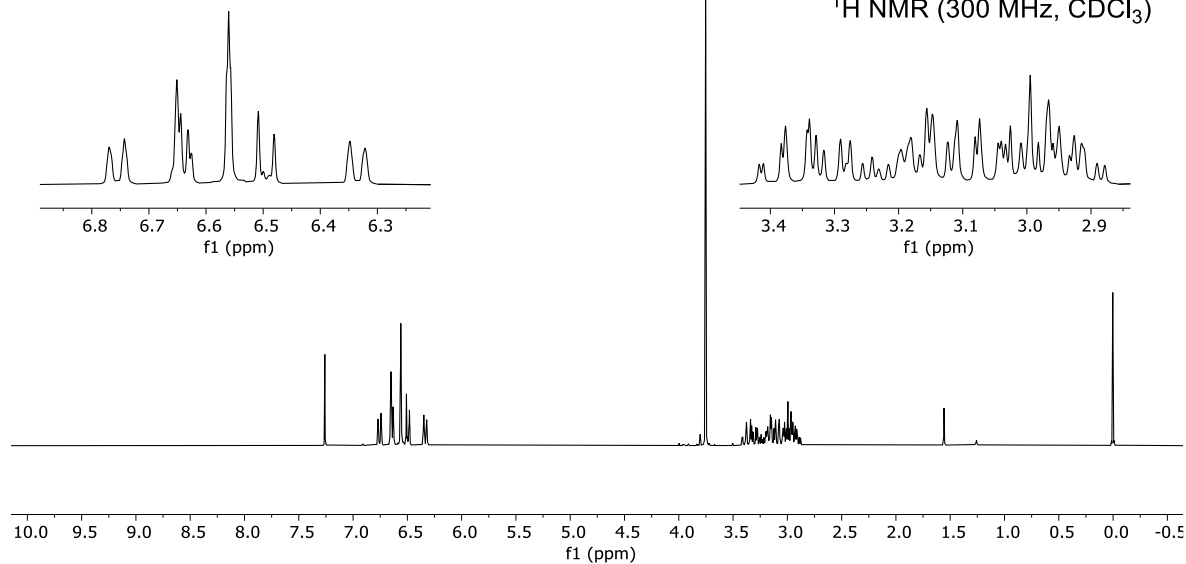
$^{13}\text{C}$  NMR (75 MHz,  $\text{CDCl}_3$ )



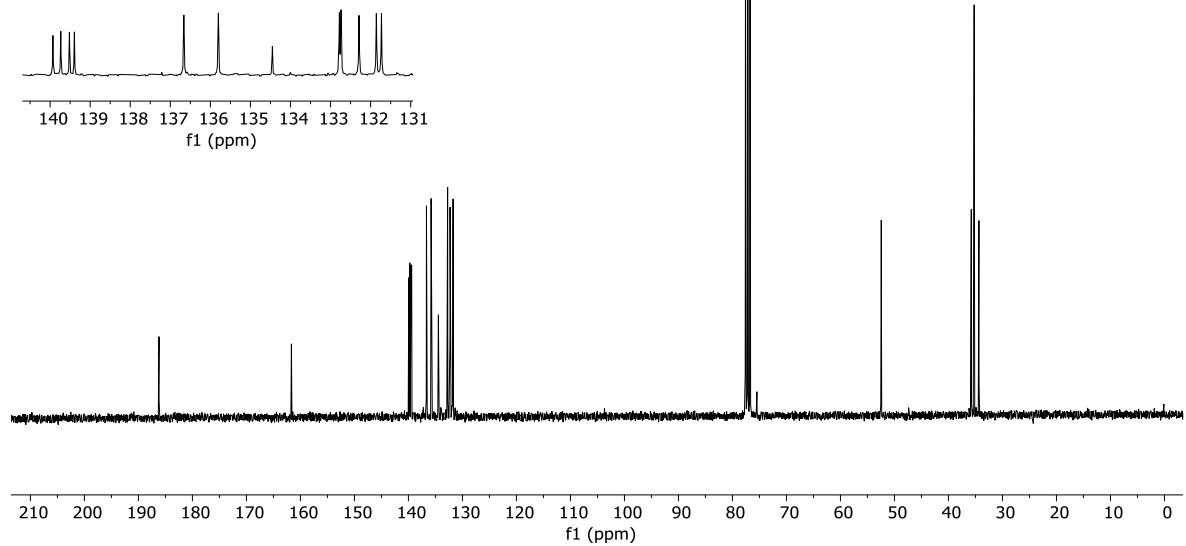


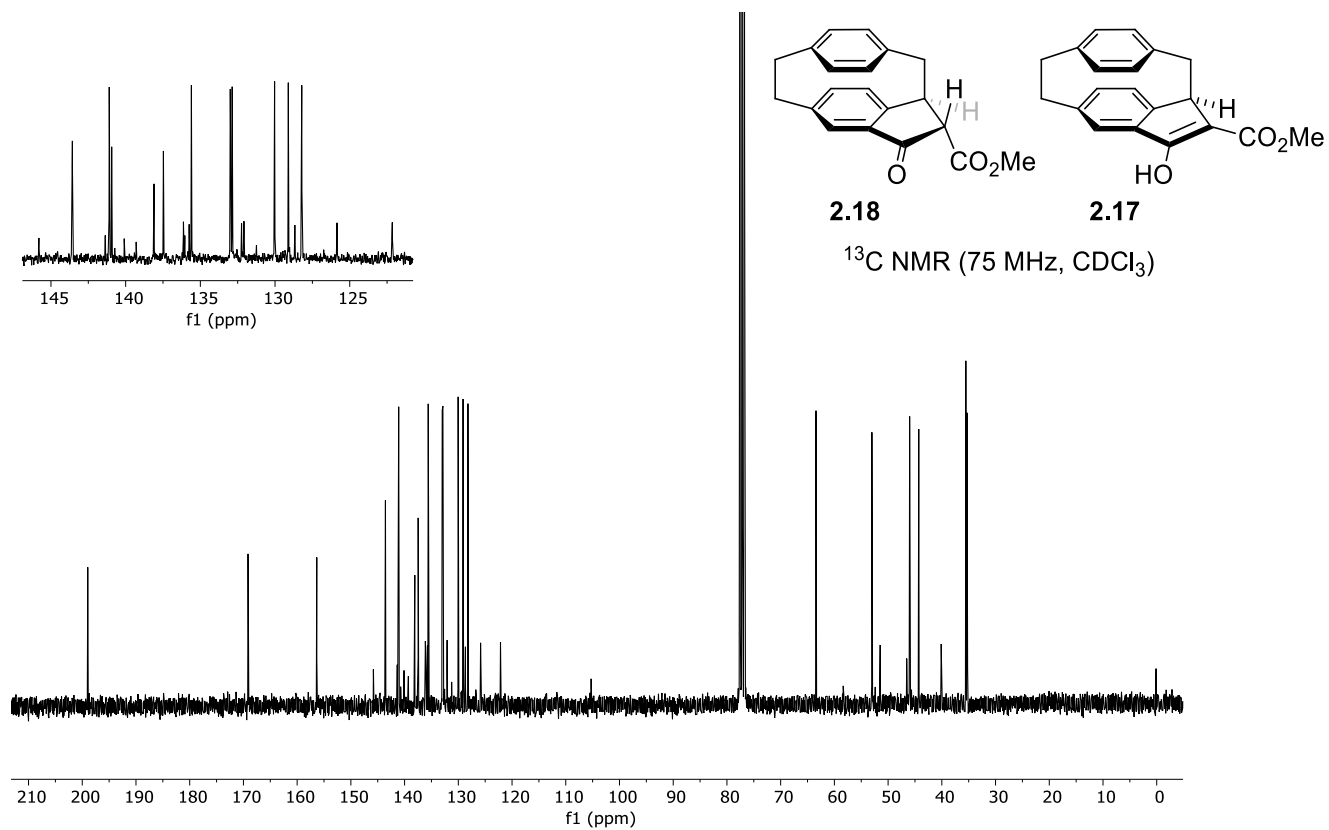
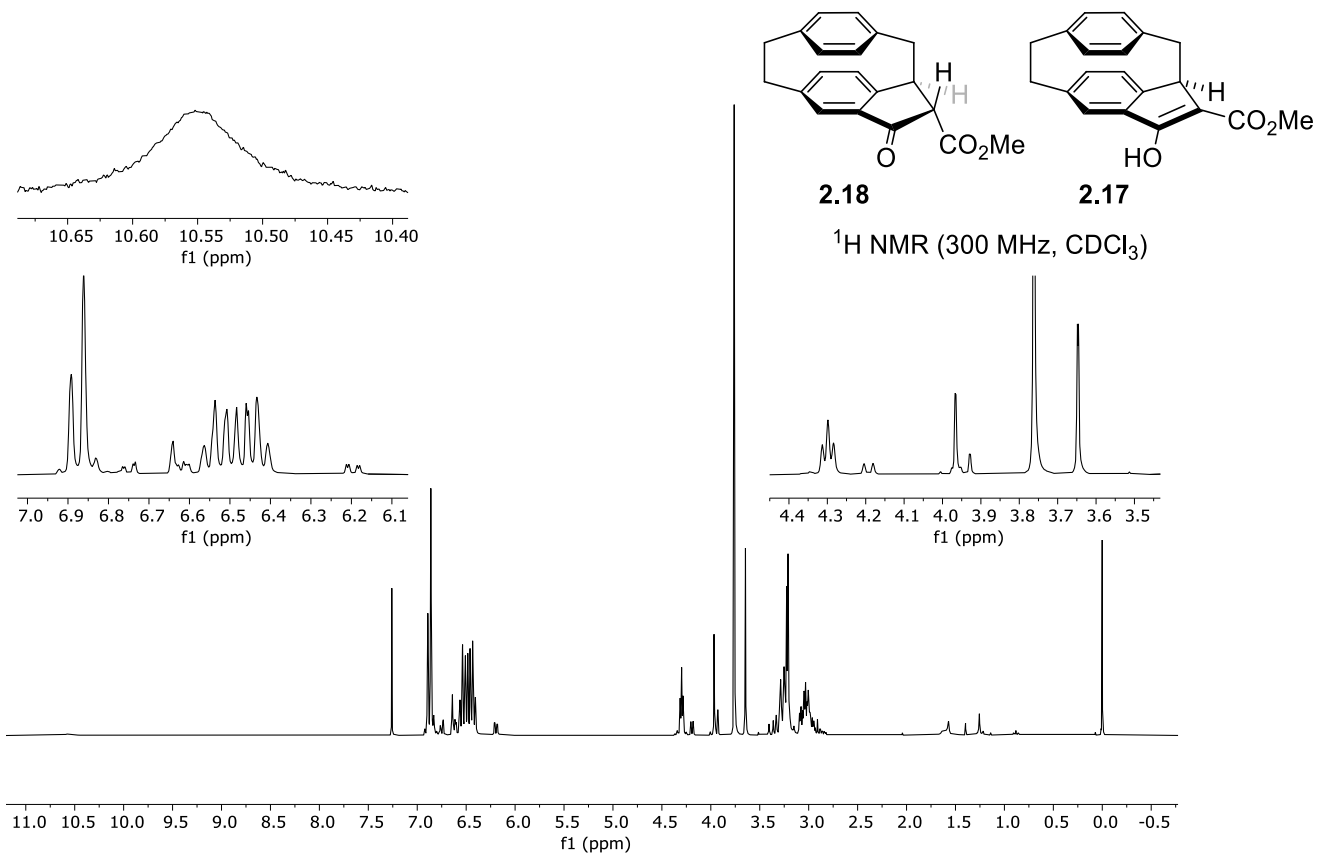


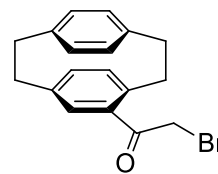
$^1\text{H}$  NMR (300 MHz,  $\text{CDCl}_3$ )



$^{13}\text{C}$  NMR (75 MHz,  $\text{CDCl}_3$ )

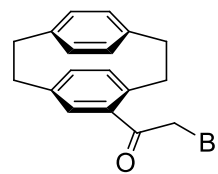
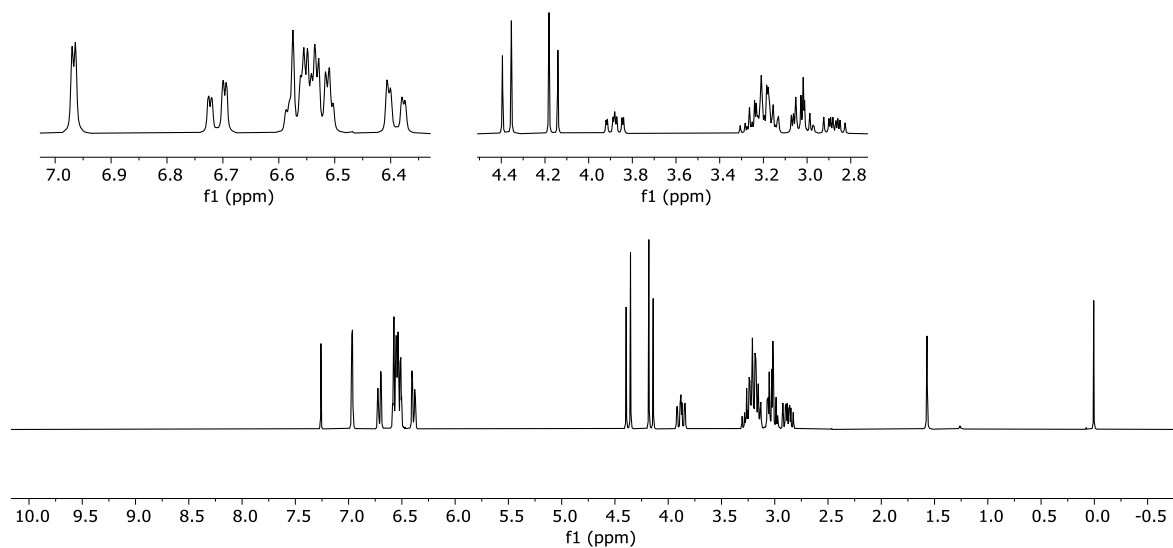






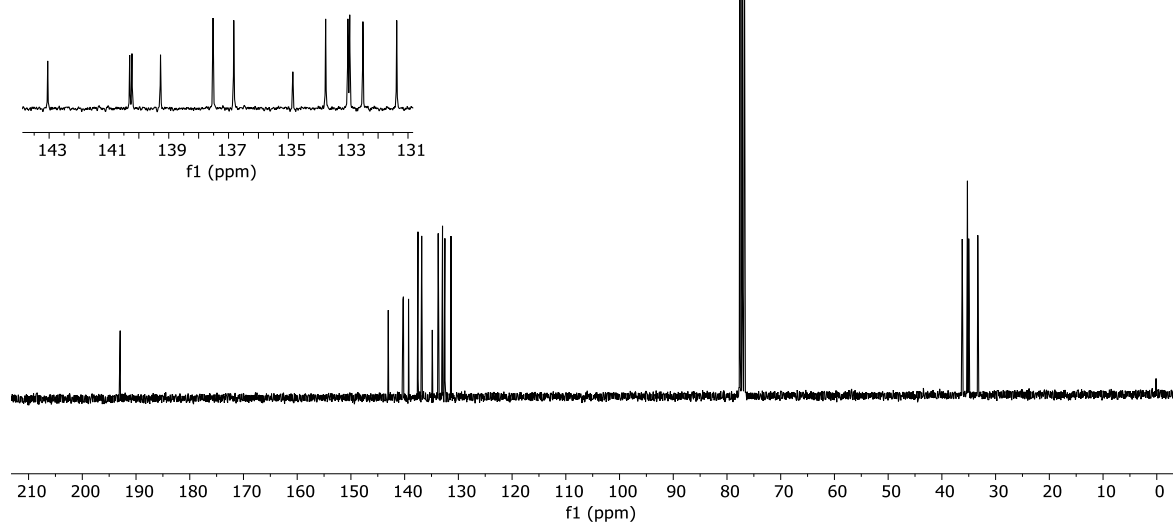
**2.20**

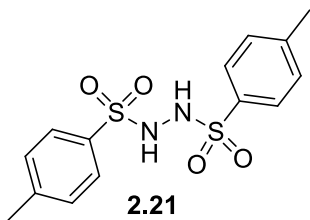
$^1\text{H}$  NMR (300 MHz,  $\text{CDCl}_3$ )



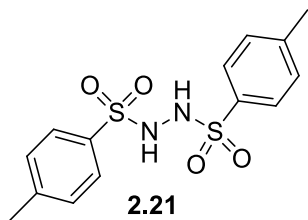
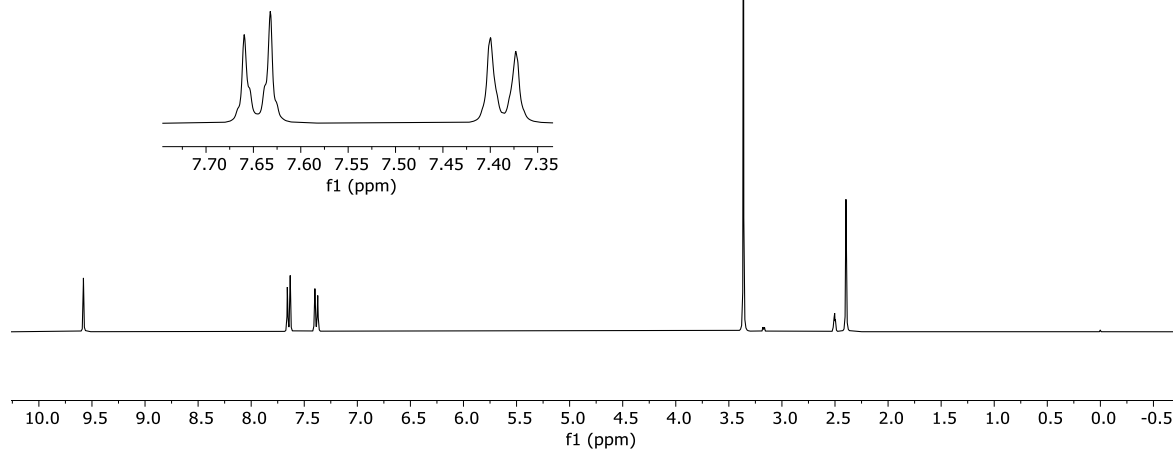
**2.20**

$^{13}\text{C}$  NMR (75 MHz,  $\text{CDCl}_3$ )

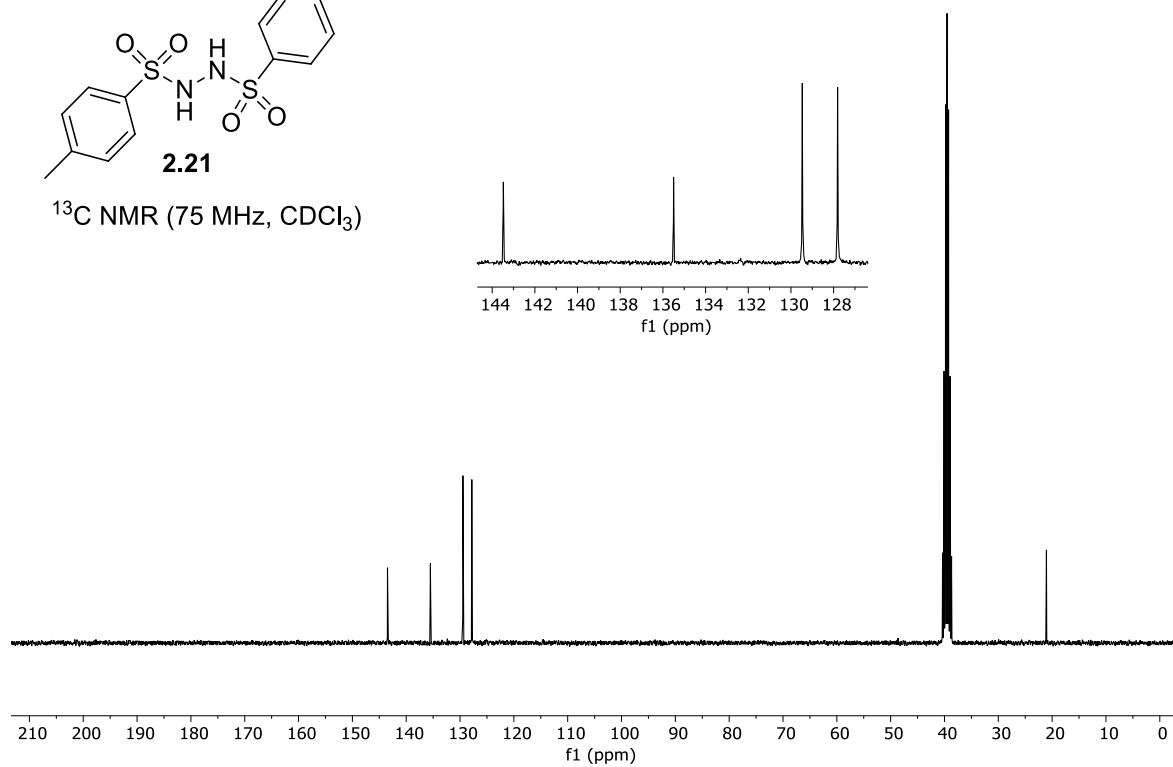


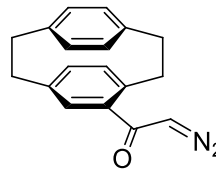


$^1\text{H}$  NMR (300 MHz,  $\text{CDCl}_3$ )



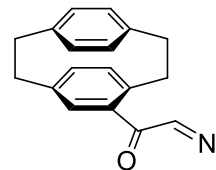
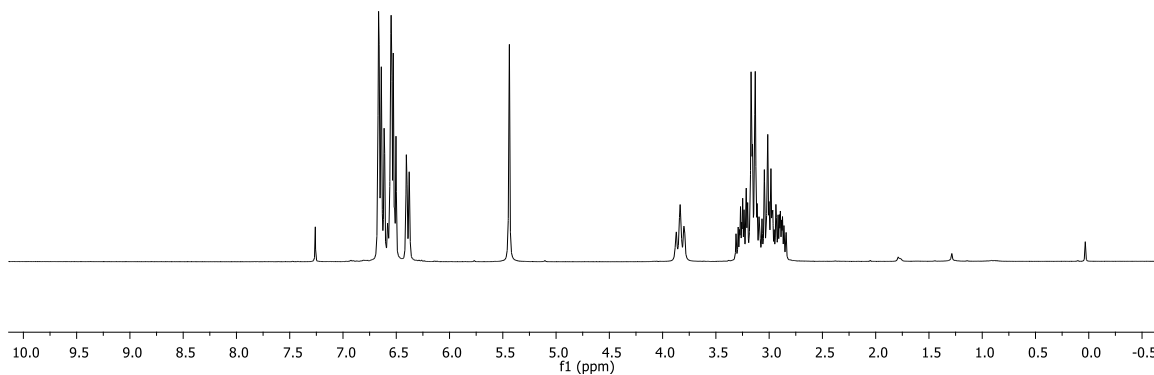
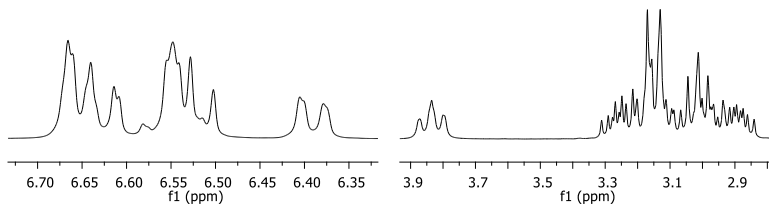
$^{13}\text{C}$  NMR (75 MHz,  $\text{CDCl}_3$ )





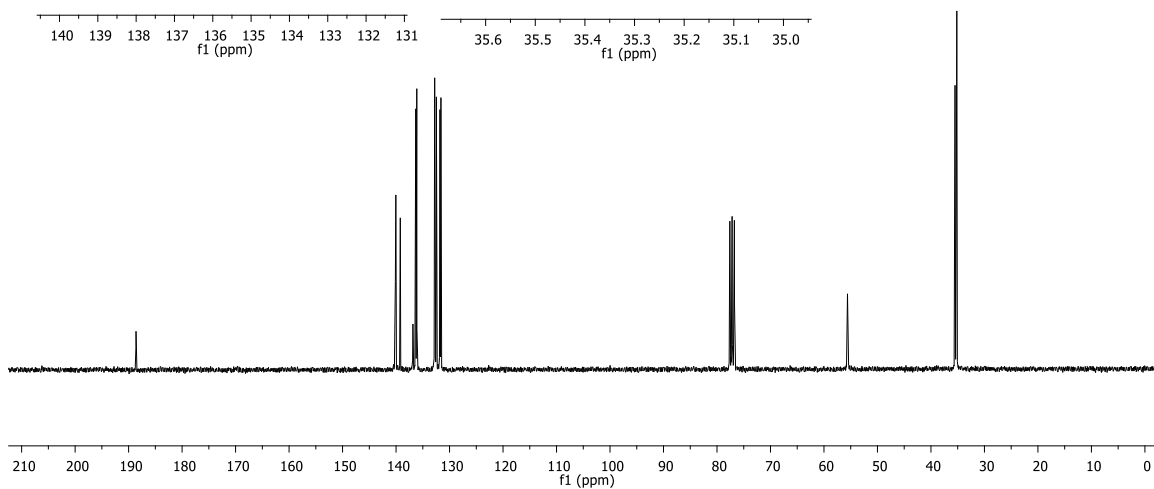
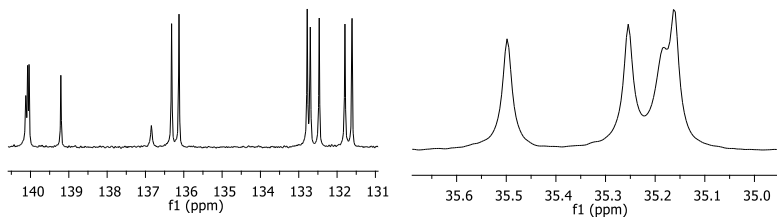
**2.23**

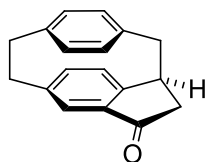
$^1\text{H}$  NMR (300 MHz,  $\text{CDCl}_3$ )



**2.23**

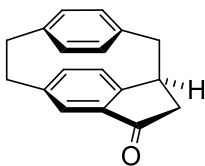
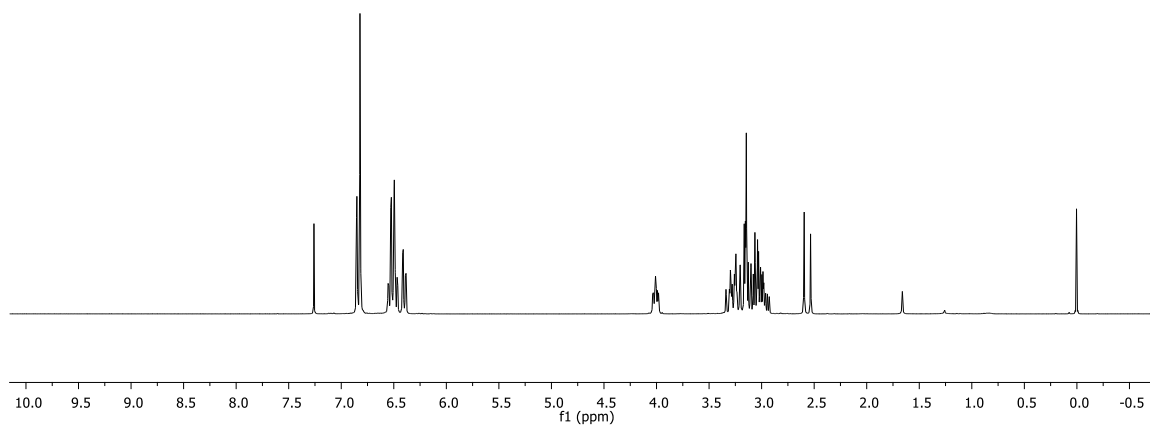
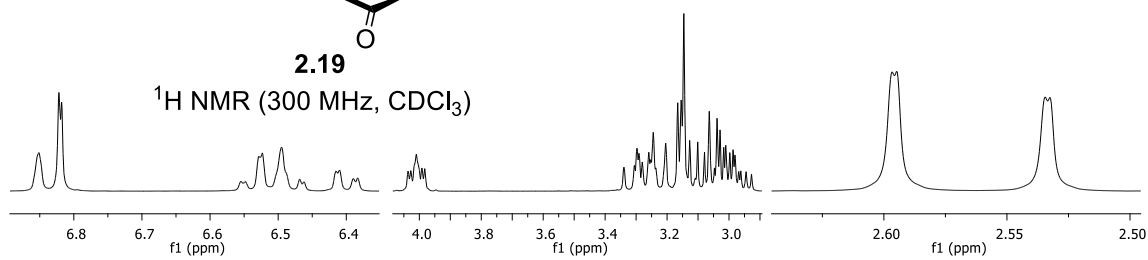
$^{13}\text{C}$  NMR (75 MHz,  $\text{CDCl}_3$ )





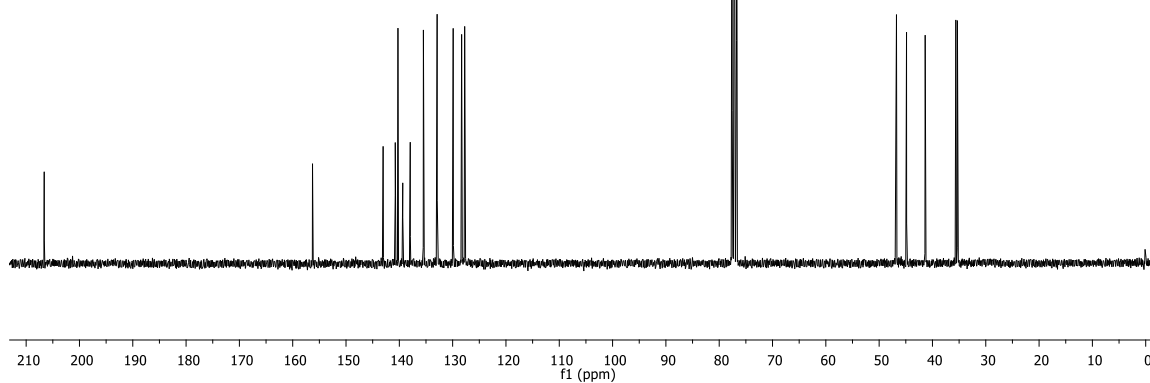
2.19

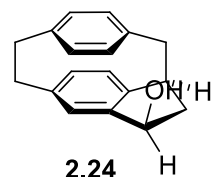
$^1\text{H}$  NMR (300 MHz,  $\text{CDCl}_3$ )



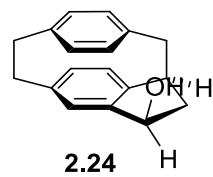
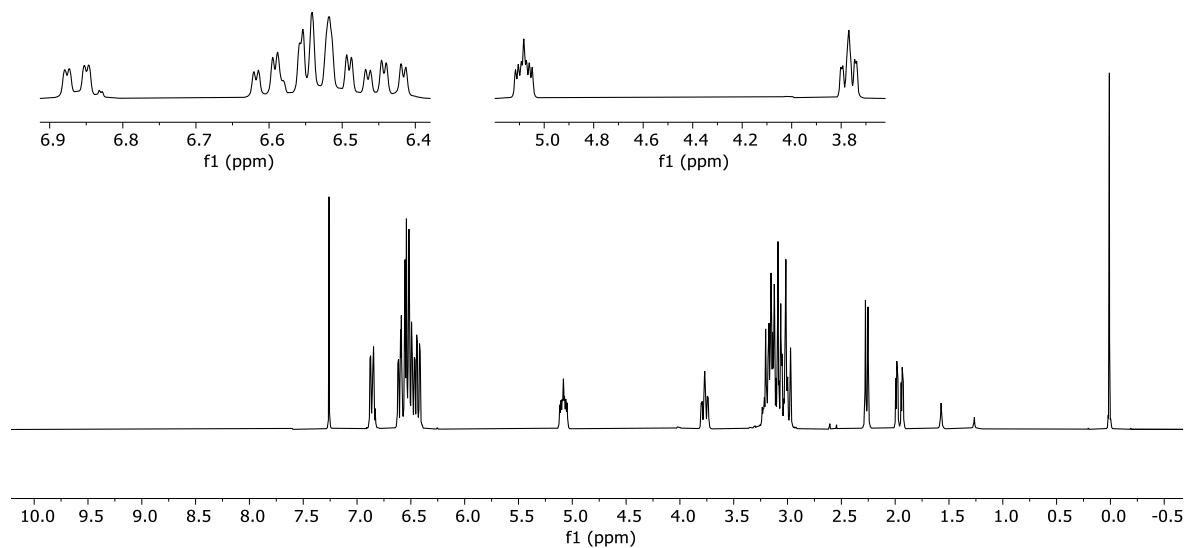
2.19

$^{13}\text{C}$  NMR (75 MHz,  $\text{CDCl}_3$ )

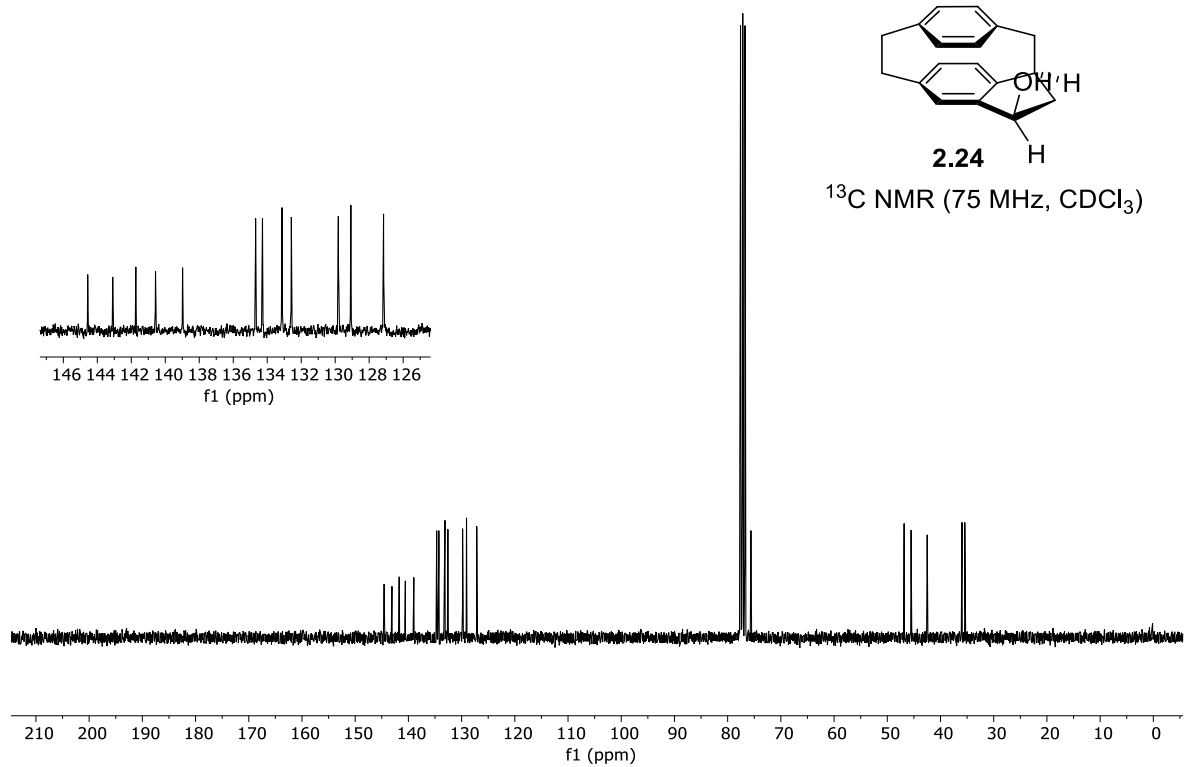


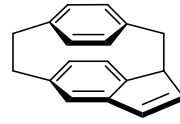


<sup>1</sup>H NMR (300 MHz, CDCl<sub>3</sub>)



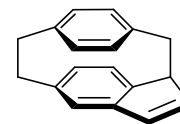
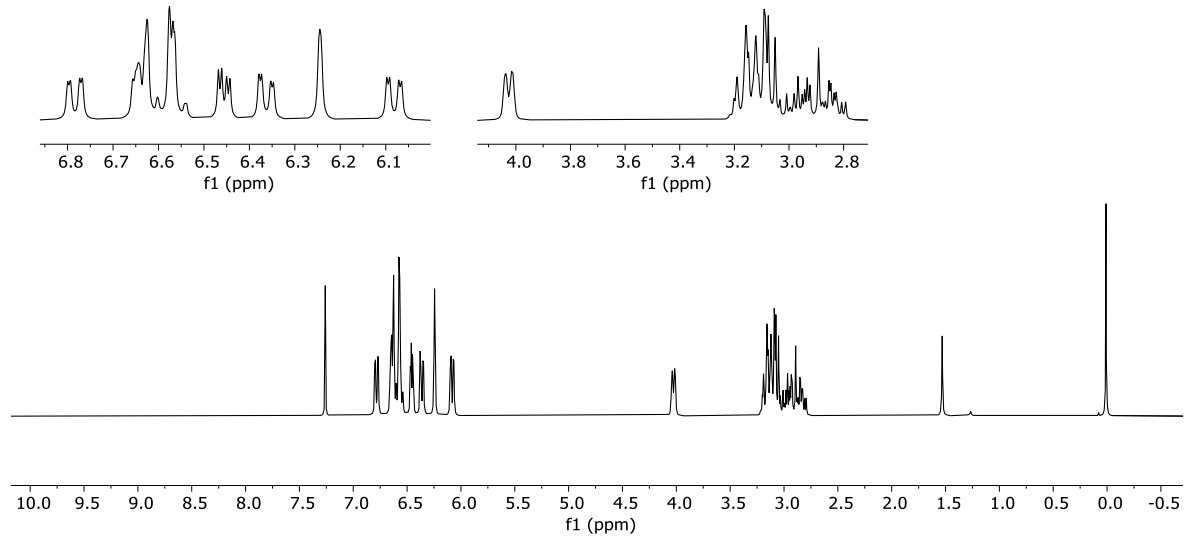
<sup>13</sup>C NMR (75 MHz, CDCl<sub>3</sub>)





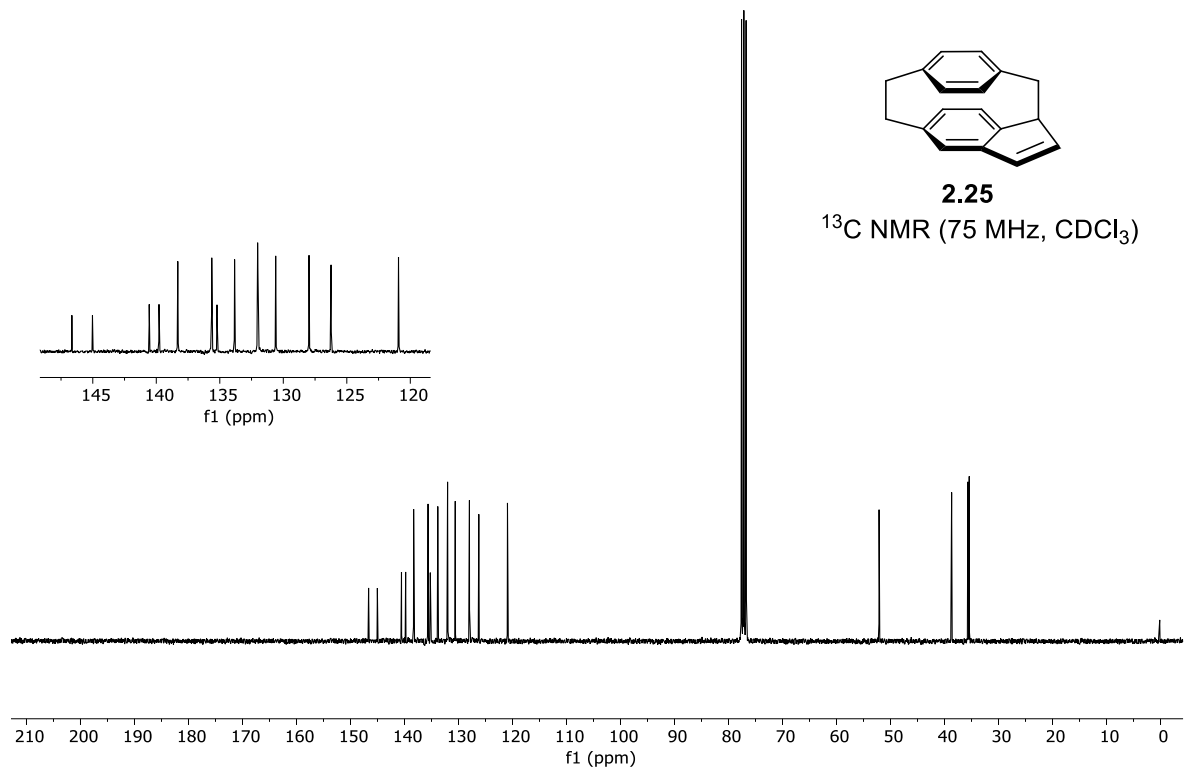
**2.25**

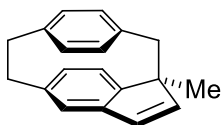
$^1\text{H}$  NMR (300 MHz,  $\text{CDCl}_3$ )



**2.25**

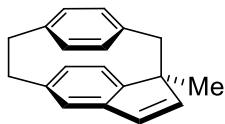
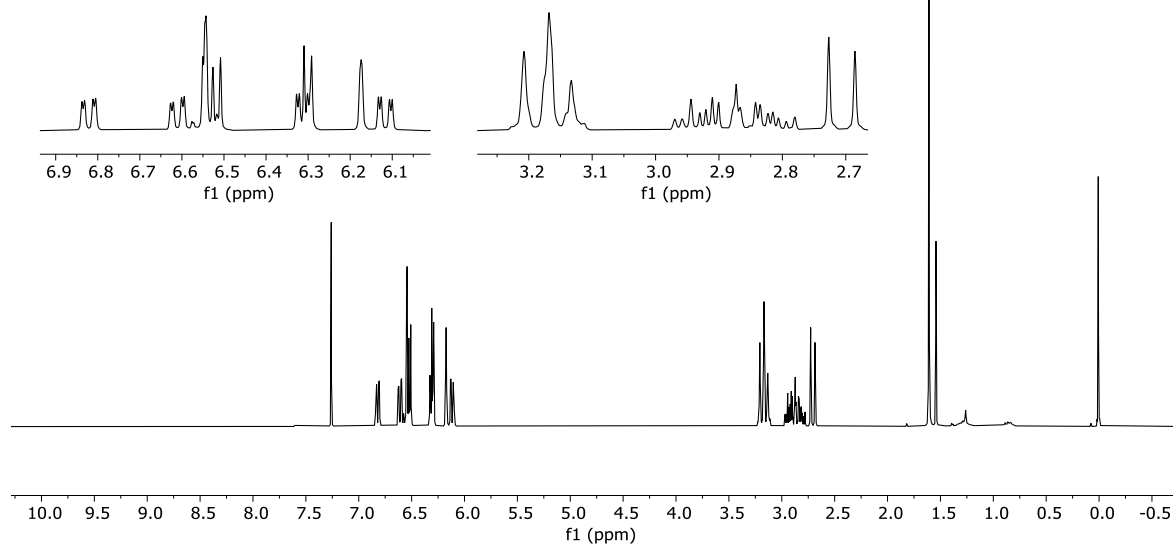
$^{13}\text{C}$  NMR (75 MHz,  $\text{CDCl}_3$ )





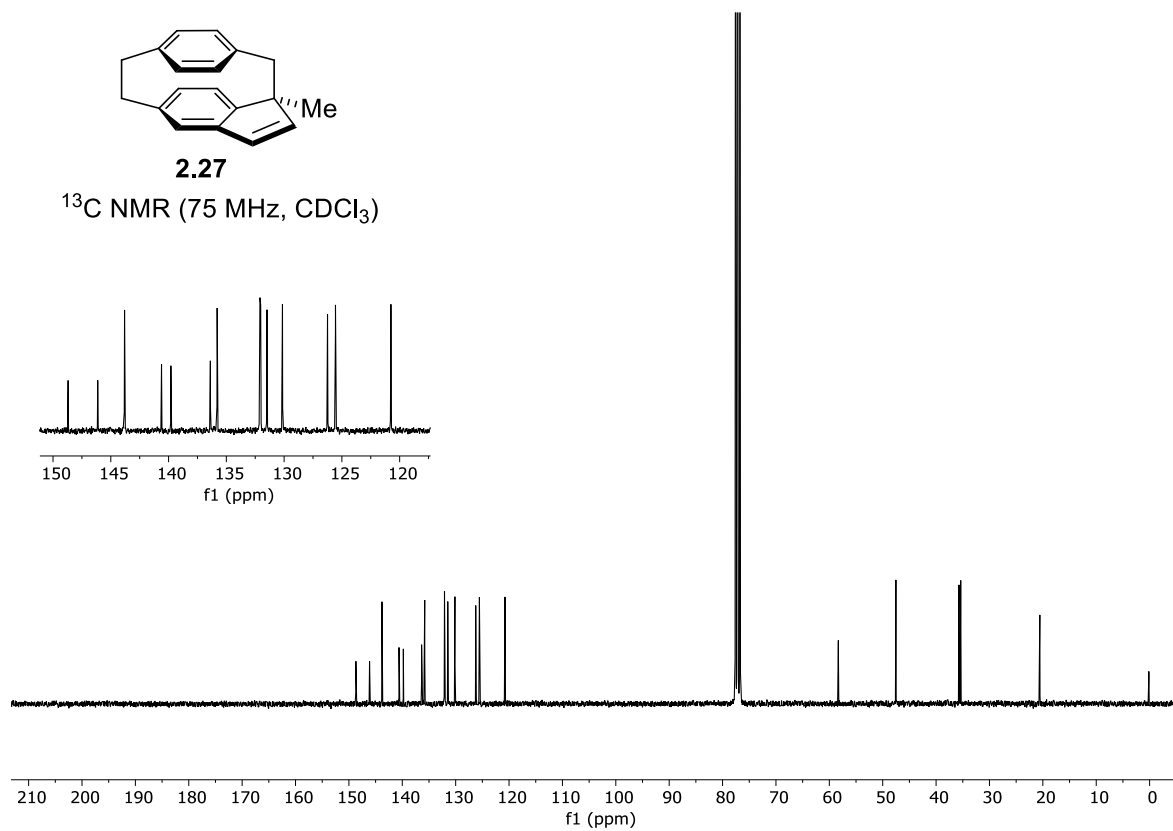
**2.27**

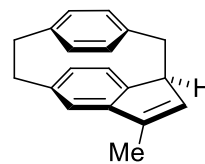
$^1\text{H NMR}$  (300 MHz,  $\text{CDCl}_3$ )



**2.27**

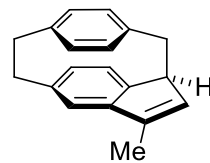
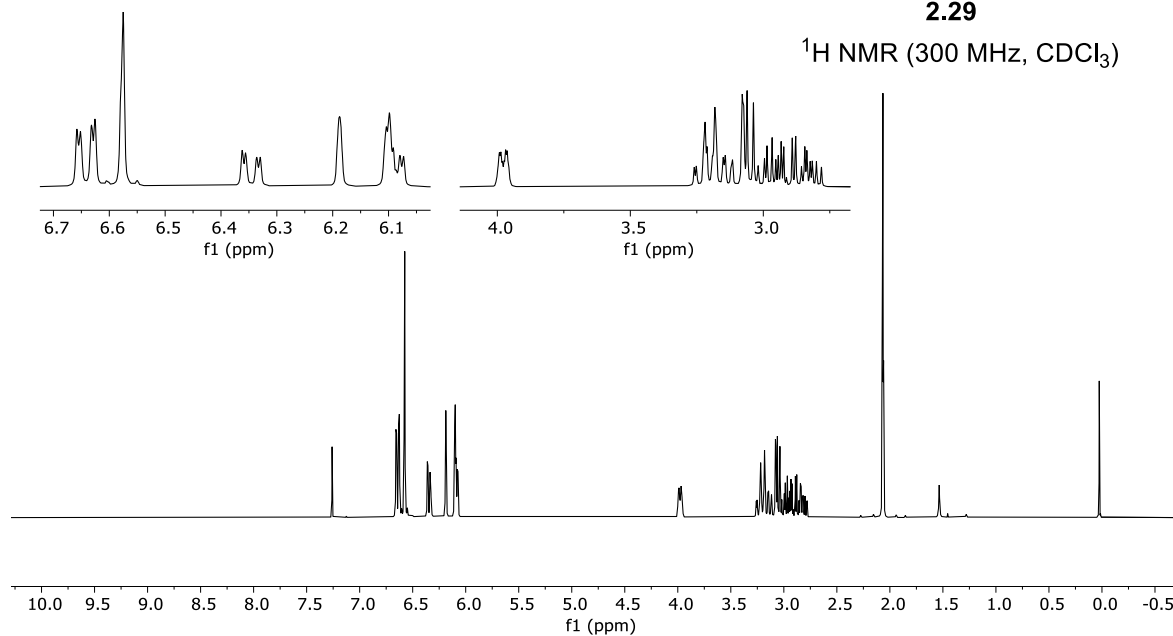
$^{13}\text{C NMR}$  (75 MHz,  $\text{CDCl}_3$ )





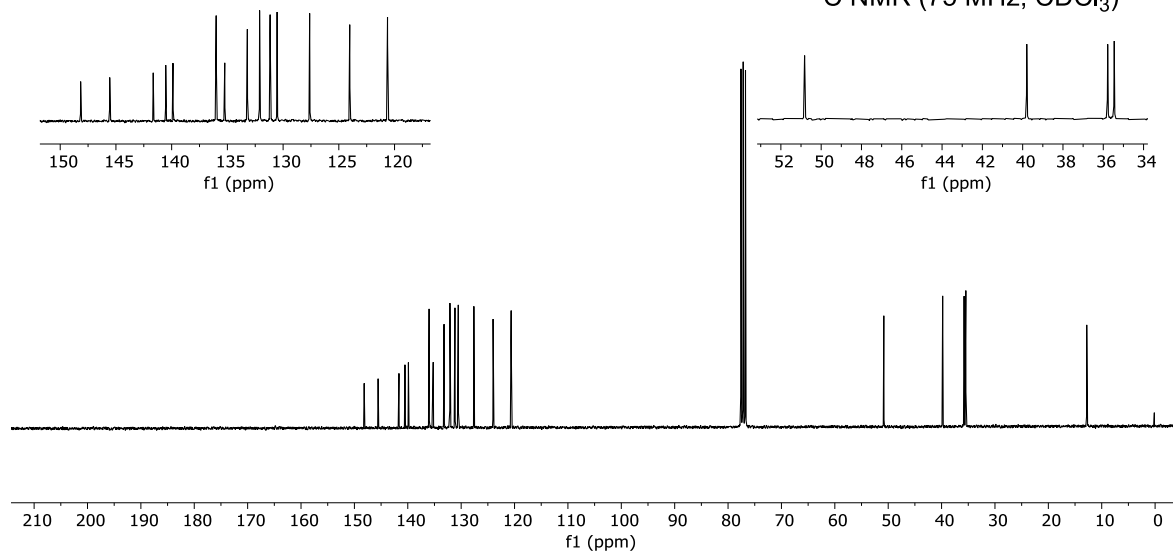
**2.29**

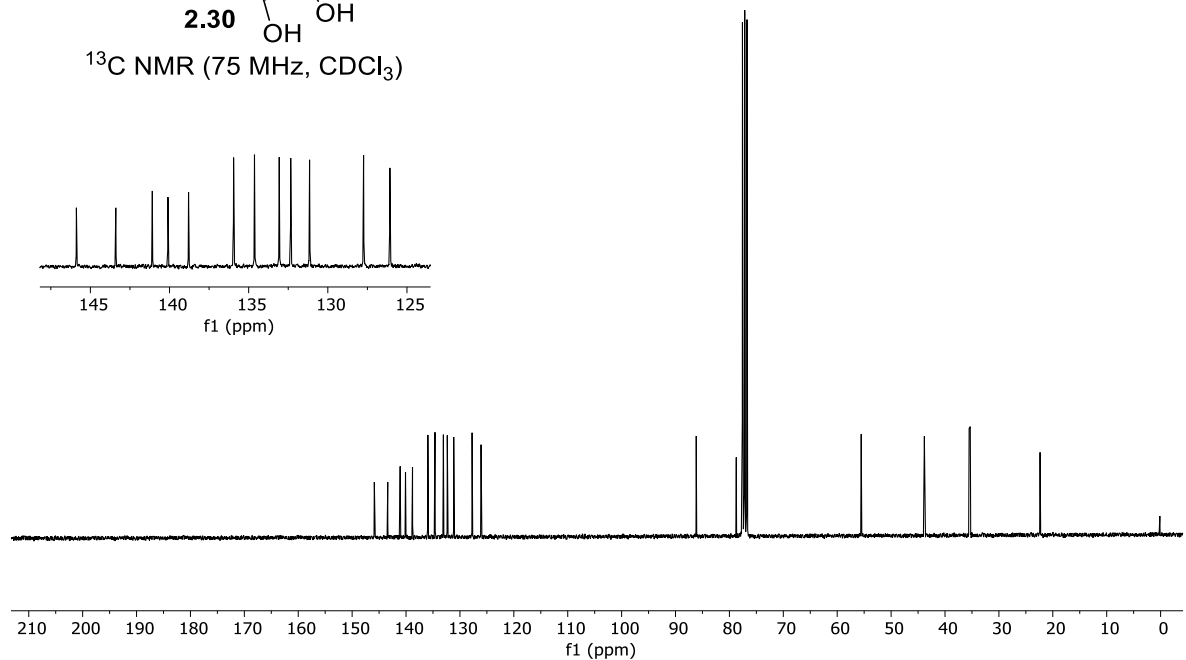
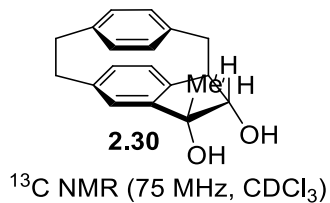
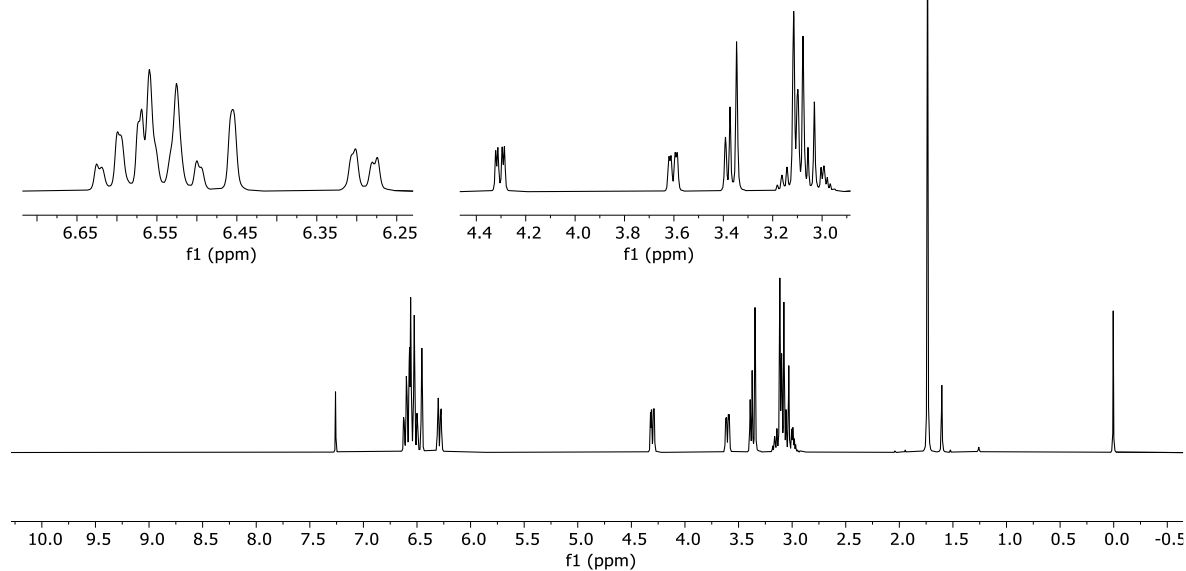
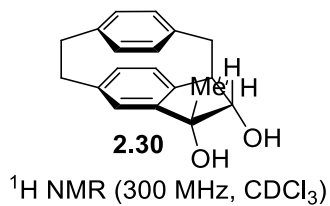
$^1\text{H NMR}$  (300 MHz,  $\text{CDCl}_3$ )

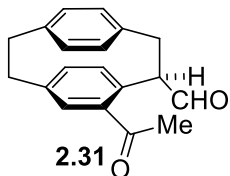


**2.29**

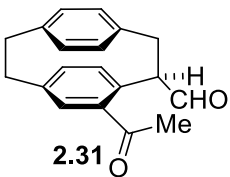
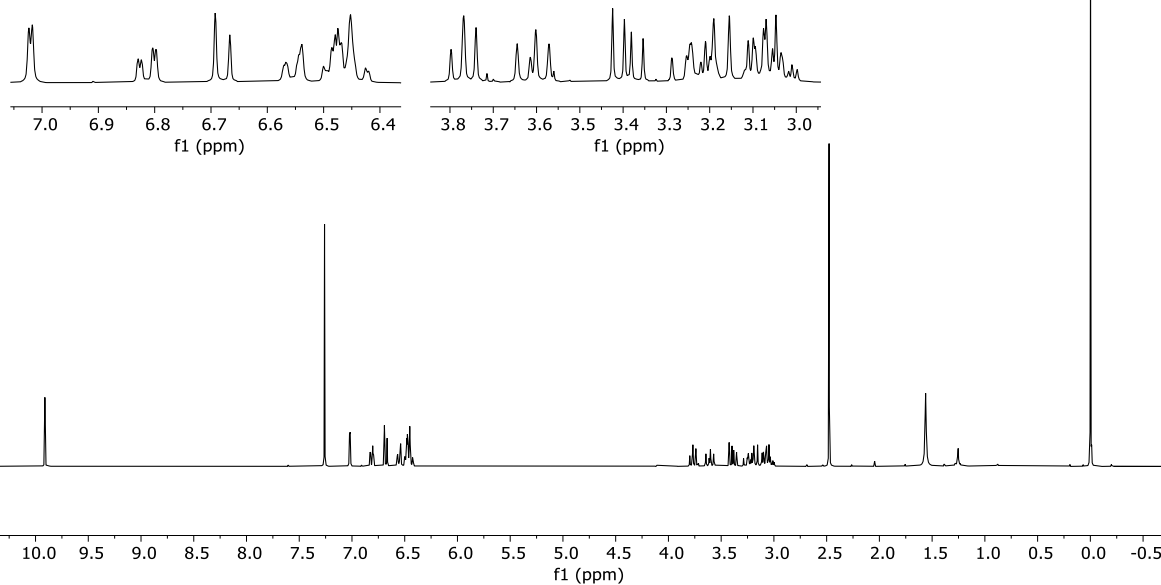
$^{13}\text{C NMR}$  (75 MHz,  $\text{CDCl}_3$ )



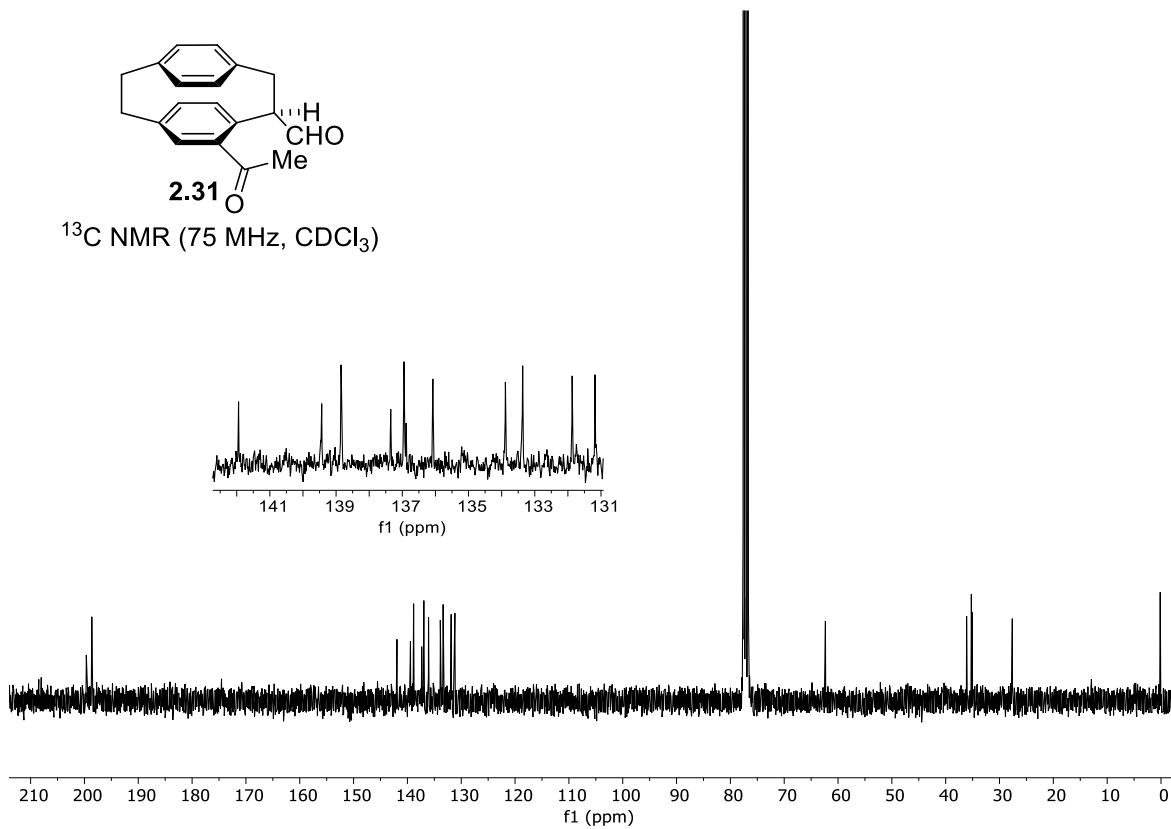


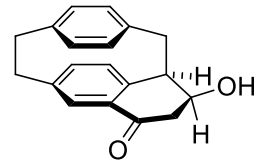


<sup>1</sup>H NMR (300 MHz, CDCl<sub>3</sub>)



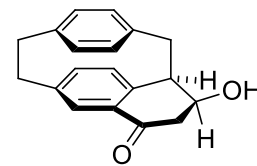
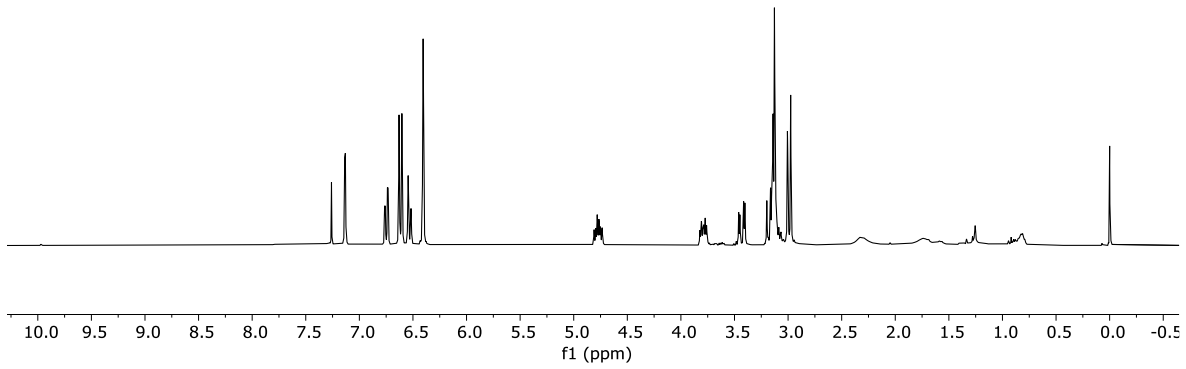
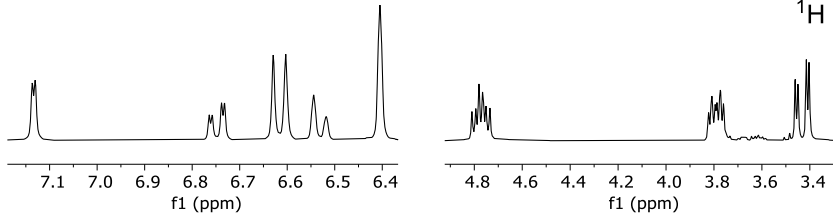
<sup>13</sup>C NMR (75 MHz, CDCl<sub>3</sub>)





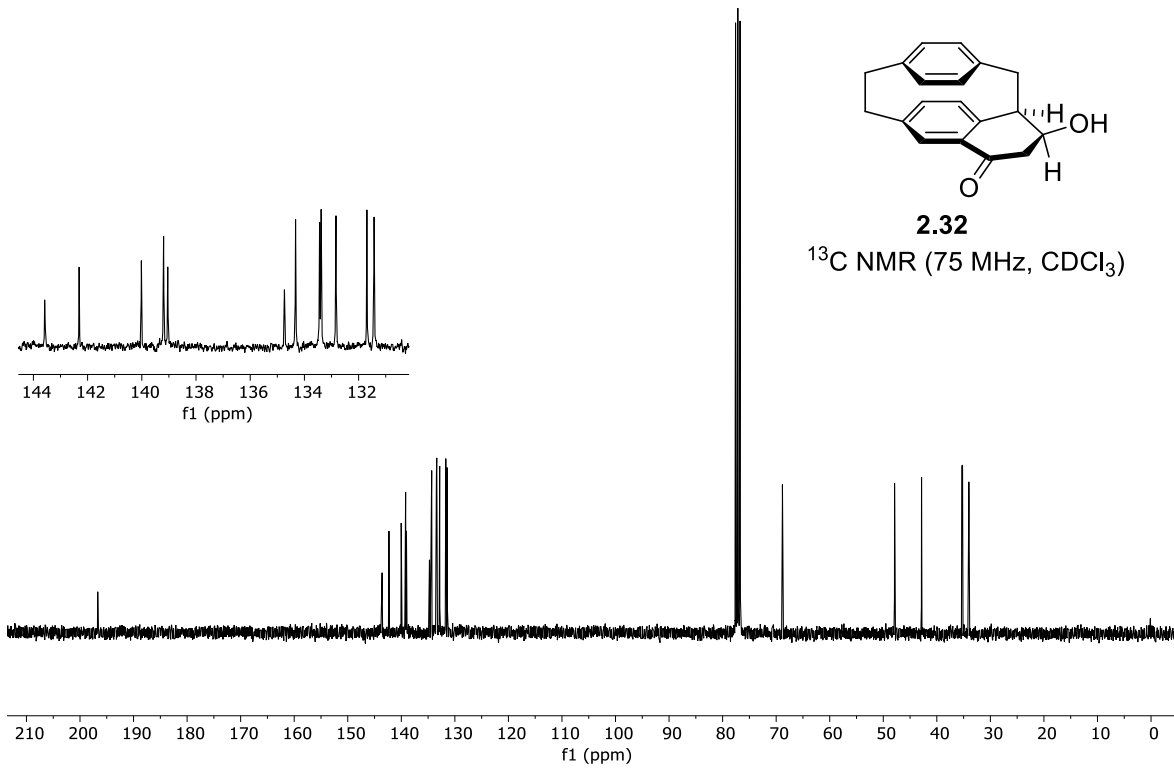
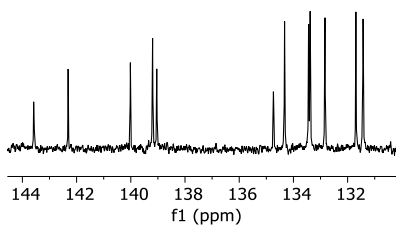
**2.32**

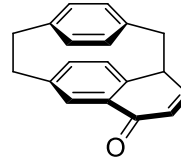
<sup>1</sup>H NMR (300 MHz, CDCl<sub>3</sub>)



**2.32**

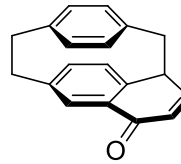
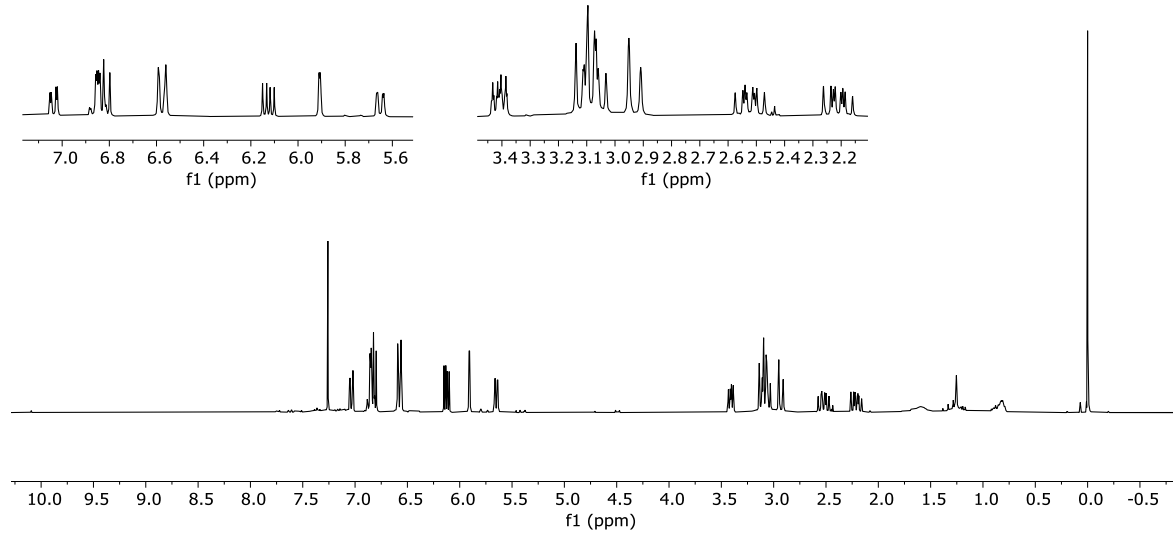
<sup>13</sup>C NMR (75 MHz, CDCl<sub>3</sub>)





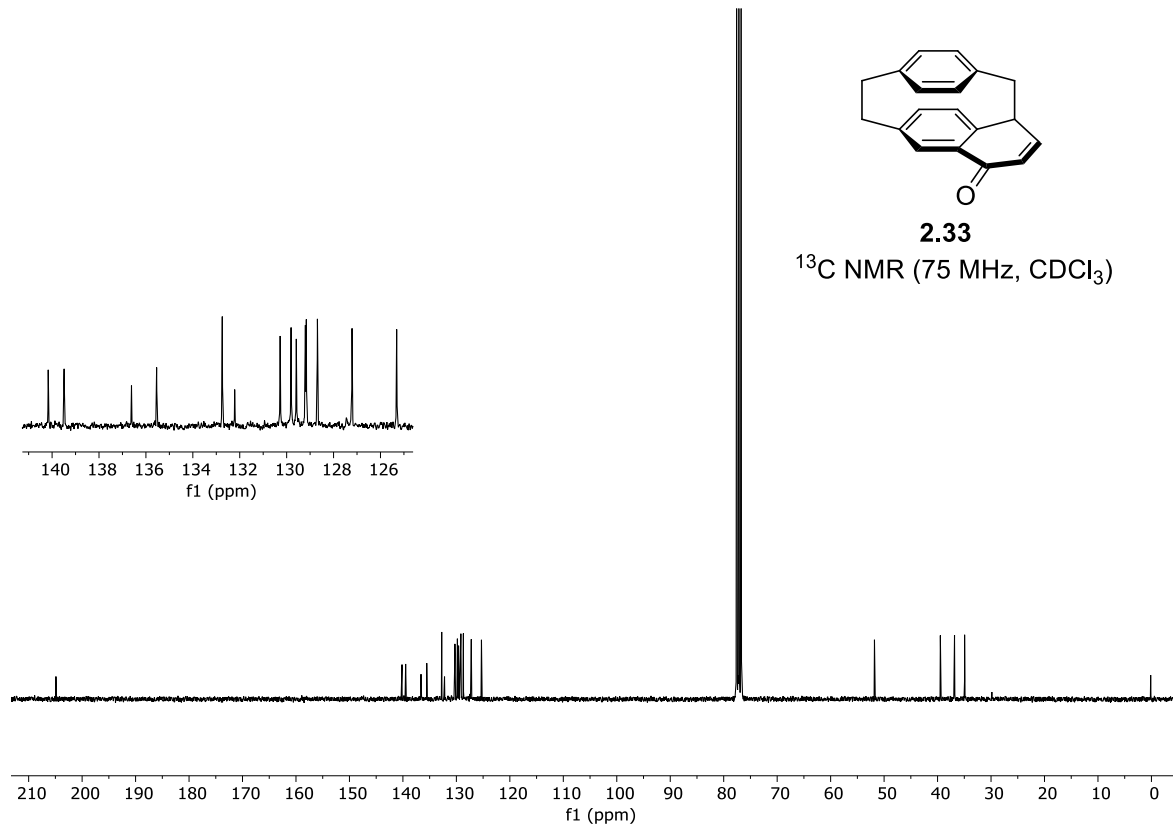
**2.33**

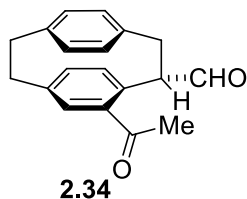
<sup>1</sup>H NMR (300 MHz, CDCl<sub>3</sub>)



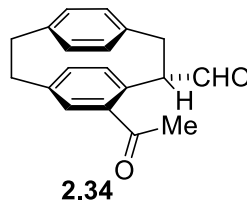
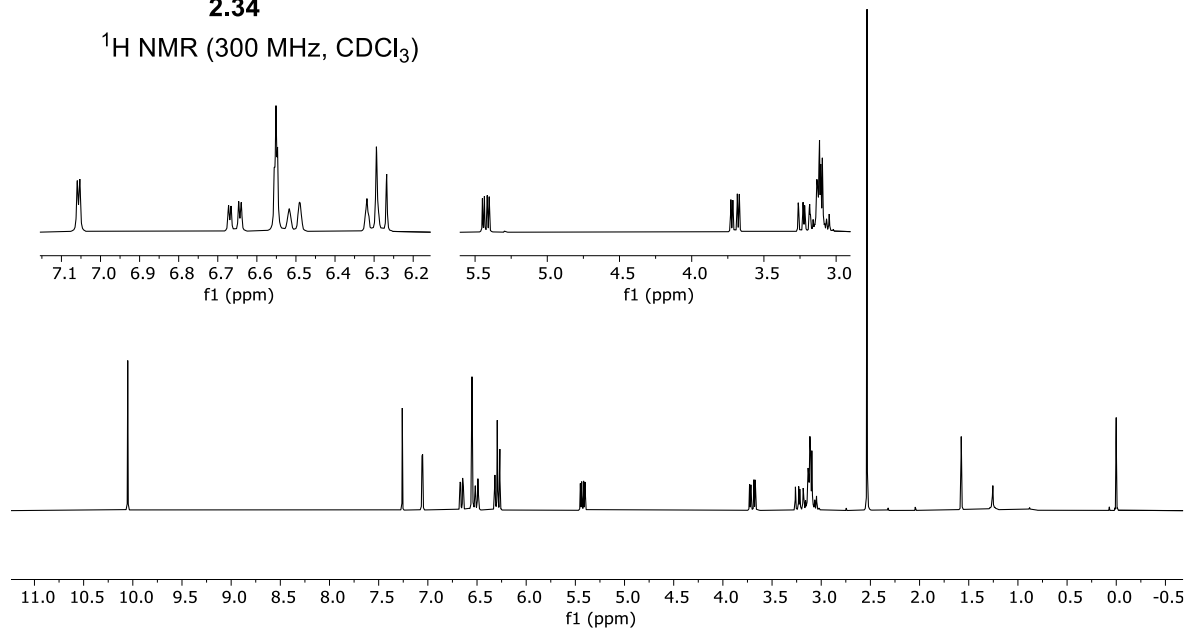
**2.33**

<sup>13</sup>C NMR (75 MHz, CDCl<sub>3</sub>)

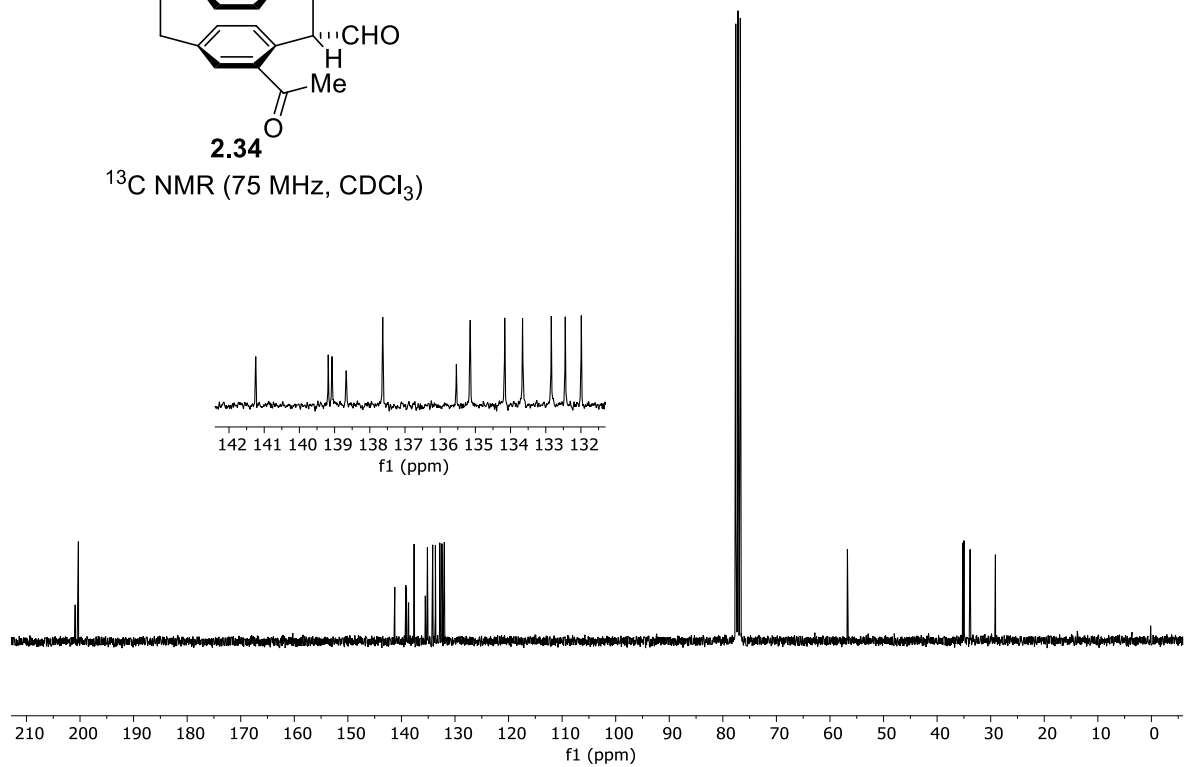


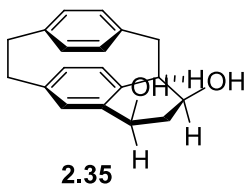


<sup>1</sup>H NMR (300 MHz, CDCl<sub>3</sub>)

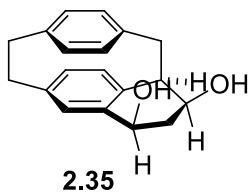
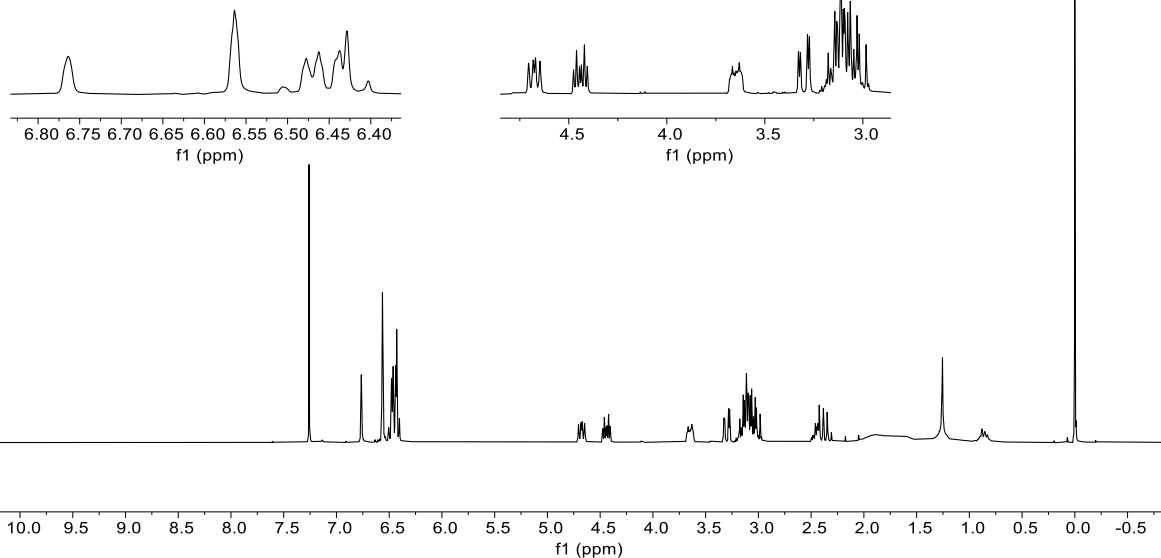


<sup>13</sup>C NMR (75 MHz, CDCl<sub>3</sub>)

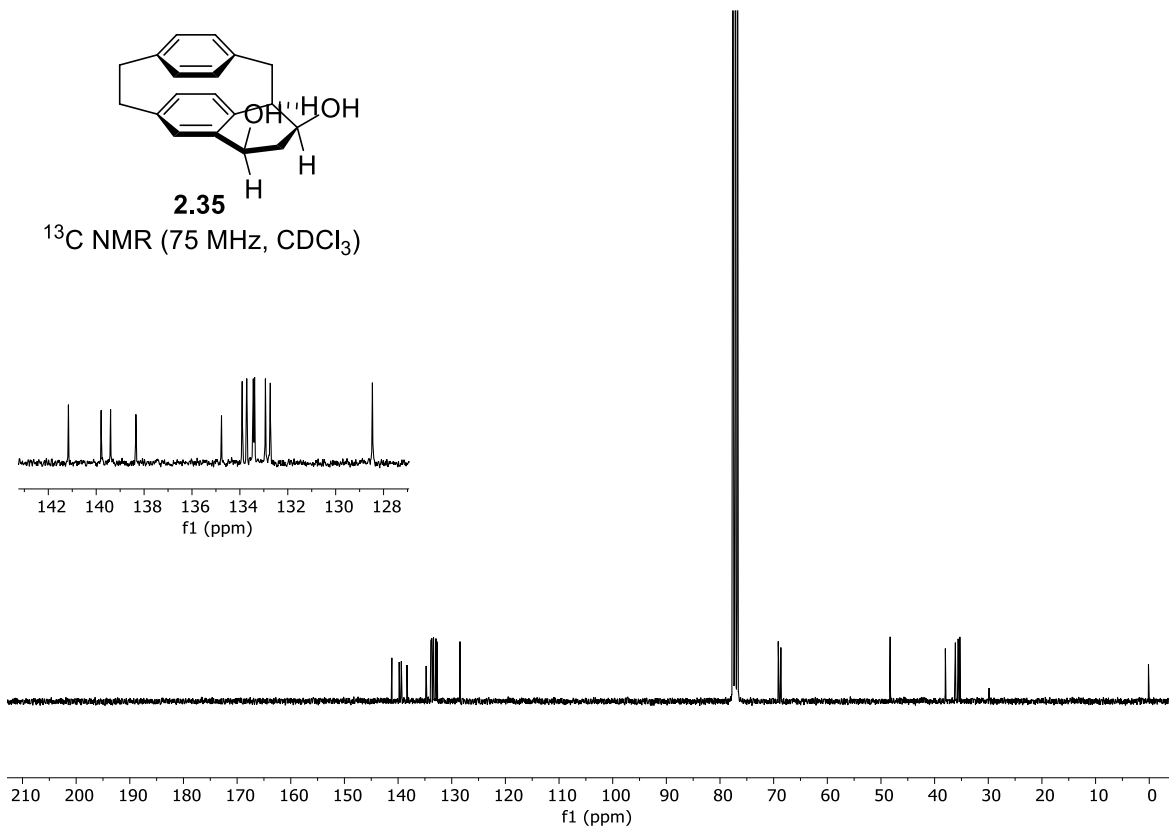


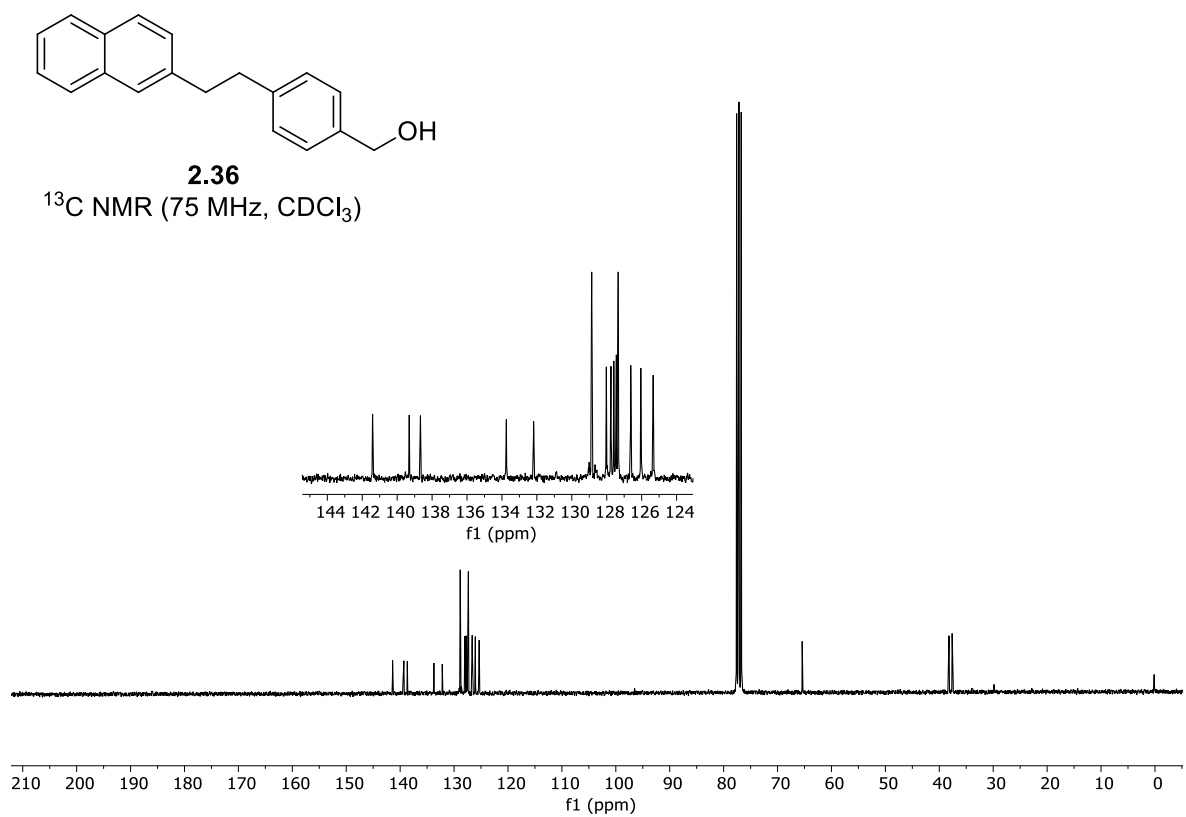
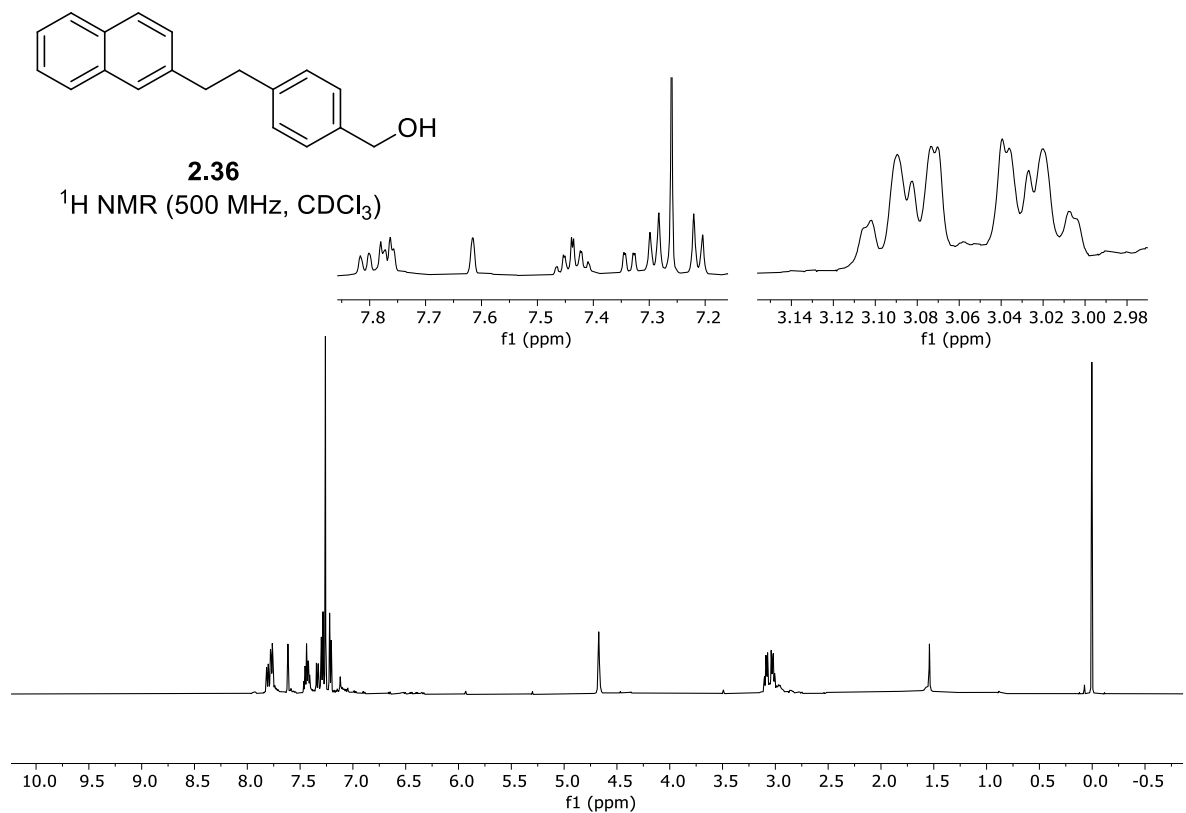


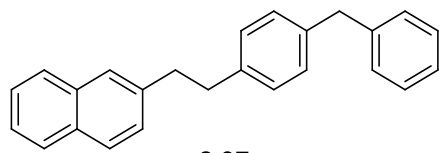
<sup>1</sup>H NMR (300 MHz, CDCl<sub>3</sub>)



<sup>13</sup>C NMR (75 MHz, CDCl<sub>3</sub>)

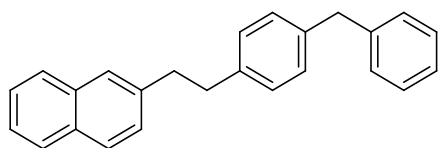
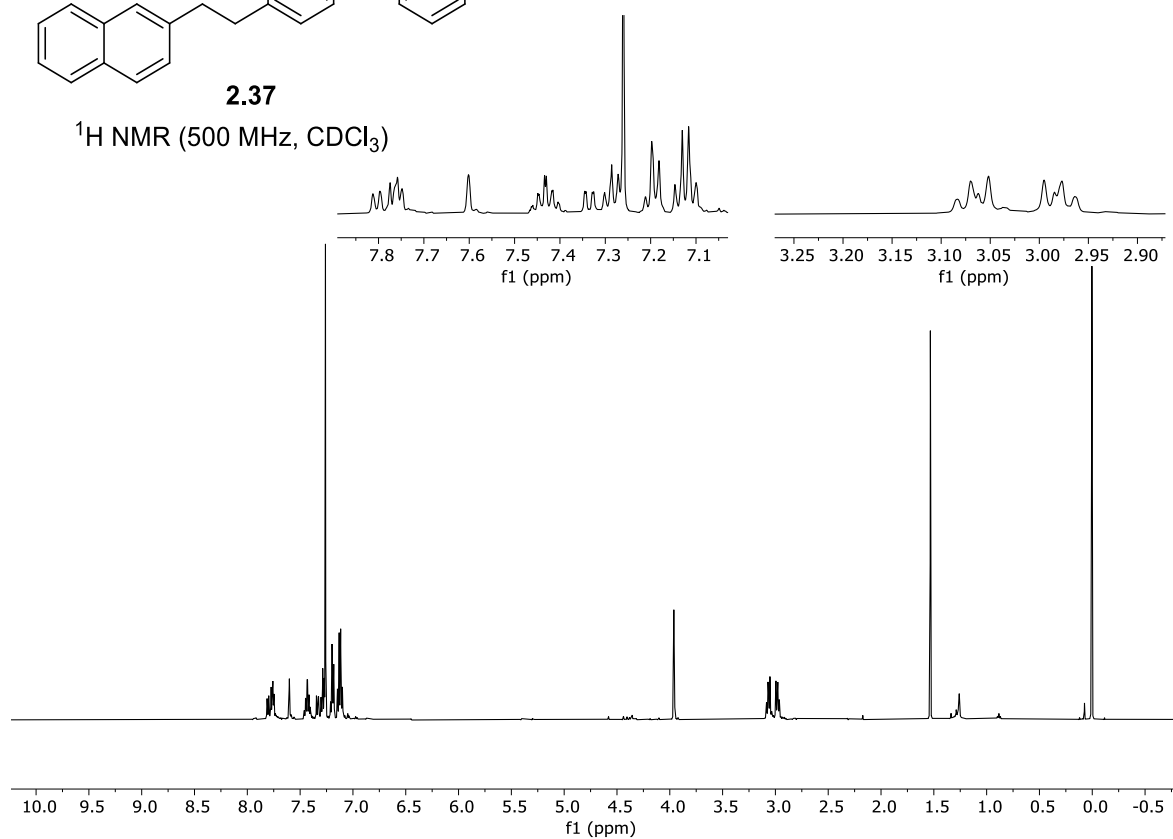






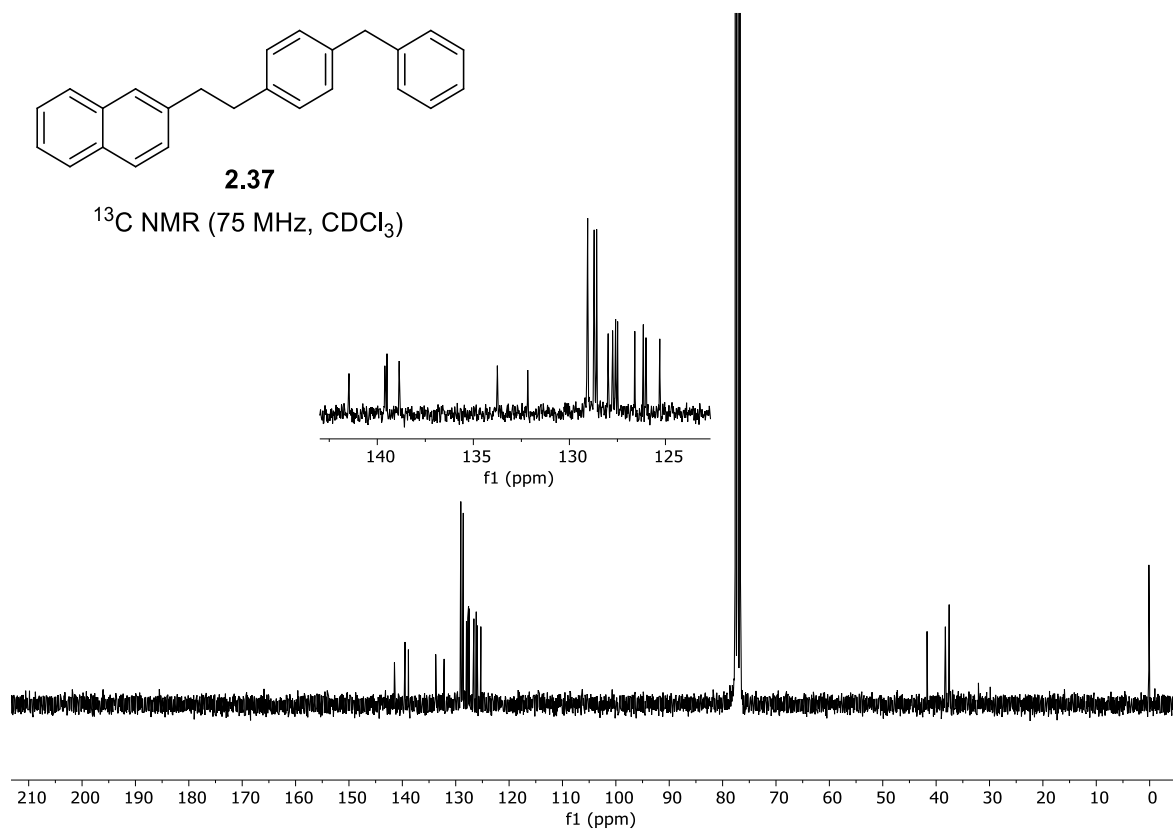
**2.37**

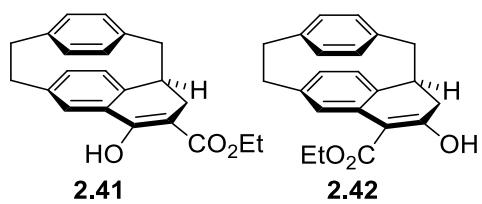
<sup>1</sup>H NMR (500 MHz, CDCl<sub>3</sub>)



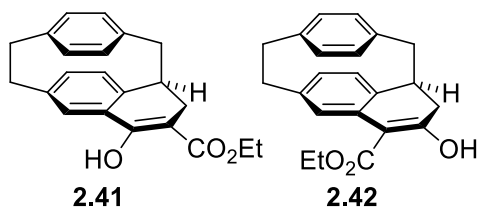
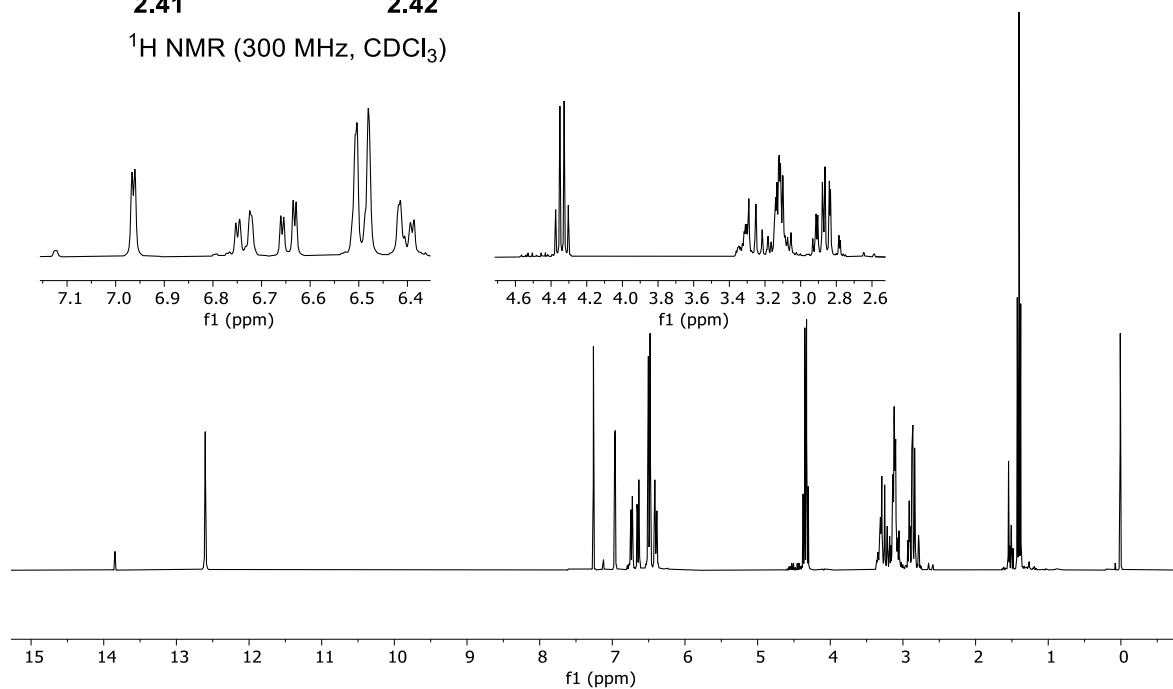
**2.37**

<sup>13</sup>C NMR (75 MHz, CDCl<sub>3</sub>)

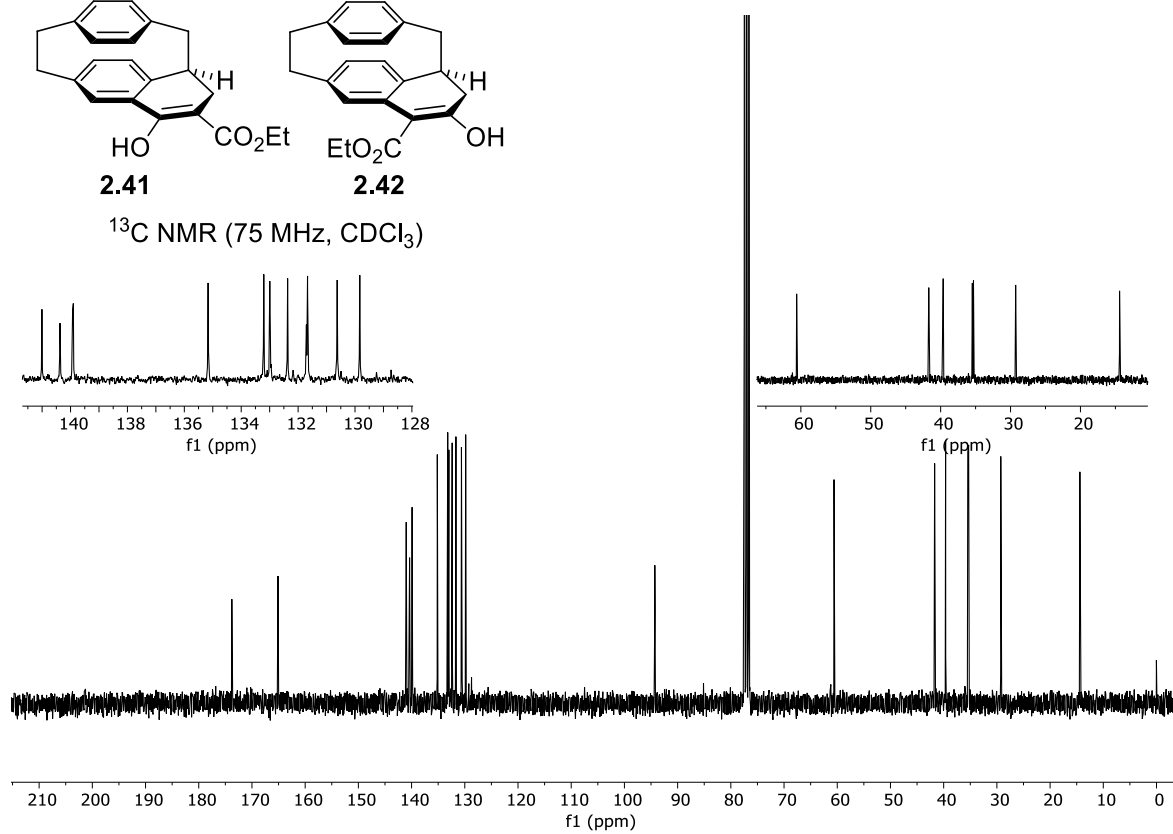


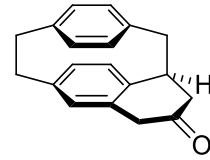


$^1\text{H NMR}$  (300 MHz,  $\text{CDCl}_3$ )



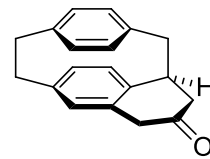
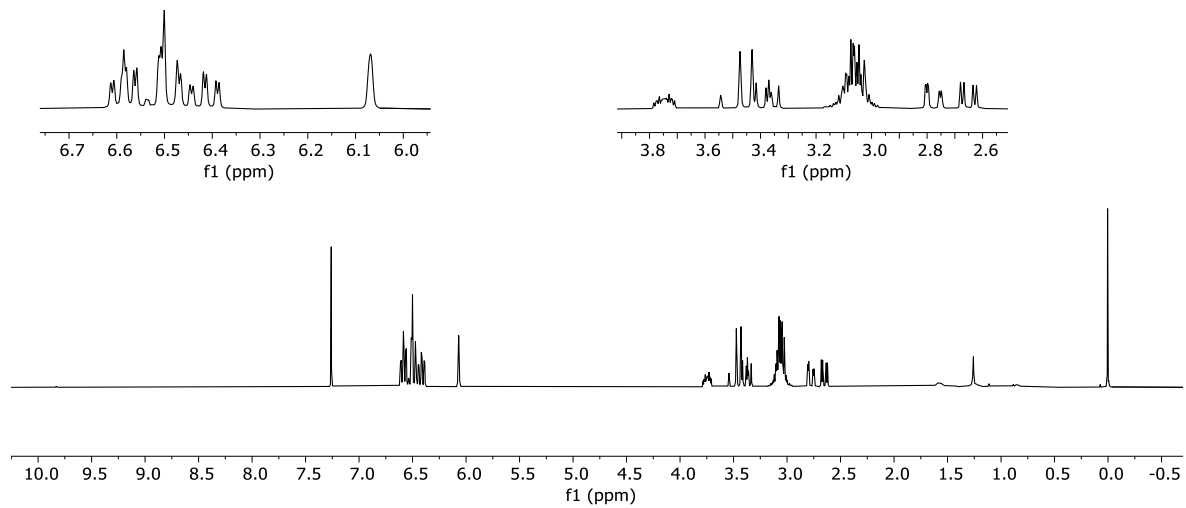
$^{13}\text{C NMR}$  (75 MHz,  $\text{CDCl}_3$ )





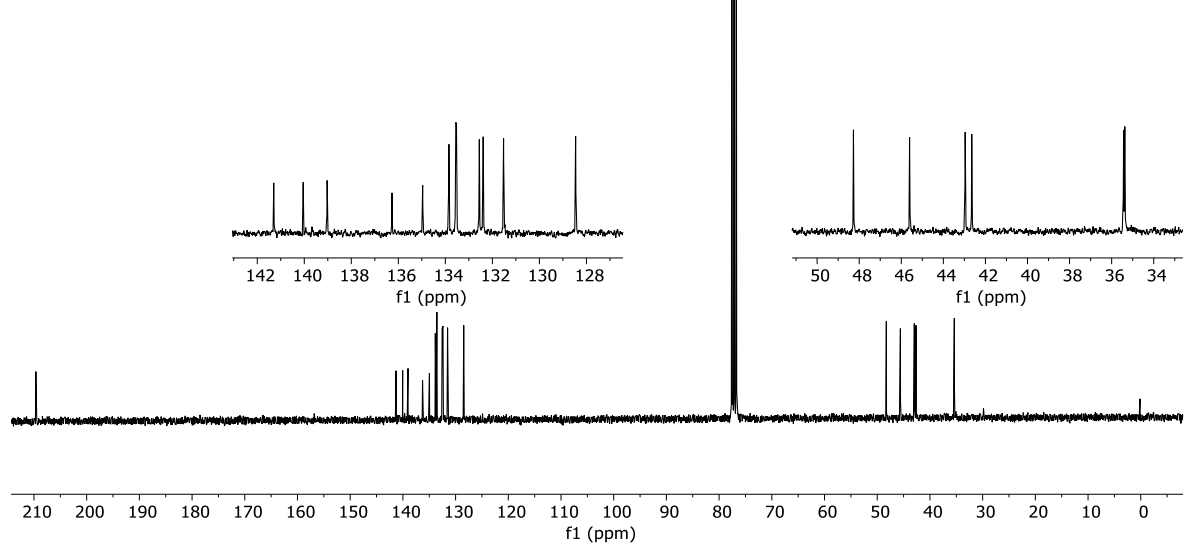
**2.43**

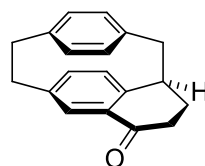
<sup>1</sup>H NMR (300 MHz, CDCl<sub>3</sub>)



**2.43**

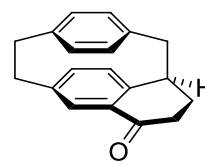
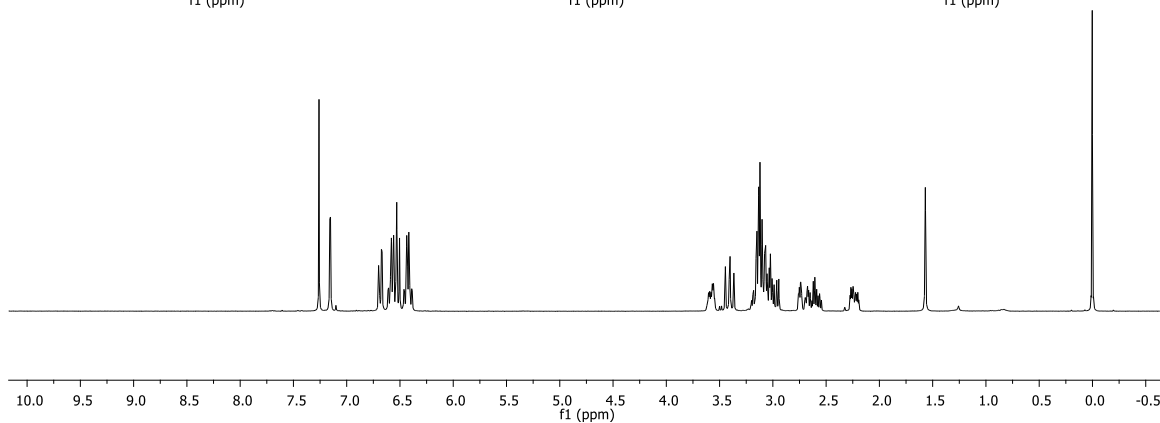
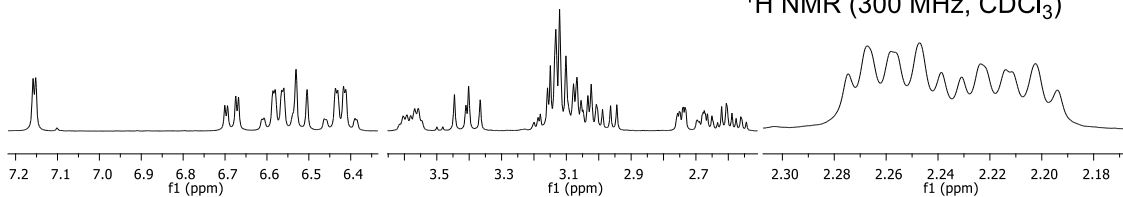
<sup>13</sup>C NMR (75 MHz, CDCl<sub>3</sub>)





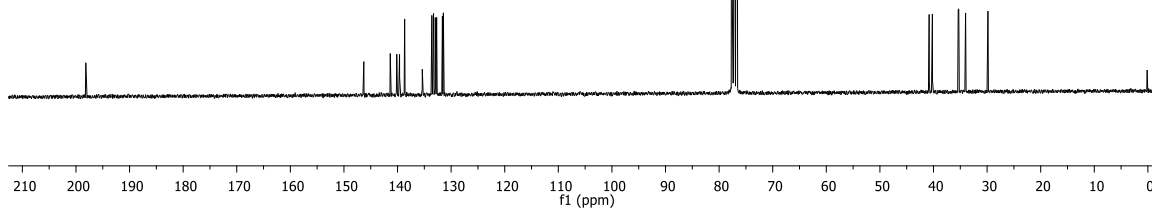
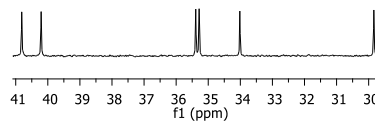
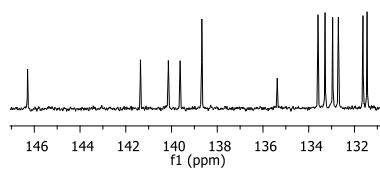
**2.44**

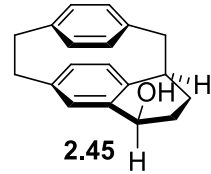
<sup>1</sup>H NMR (300 MHz, CDCl<sub>3</sub>)



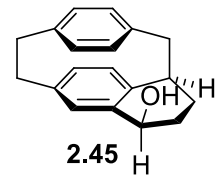
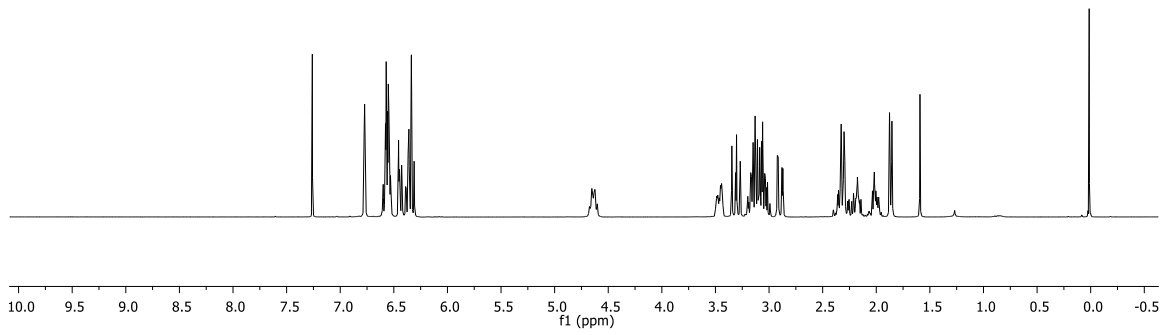
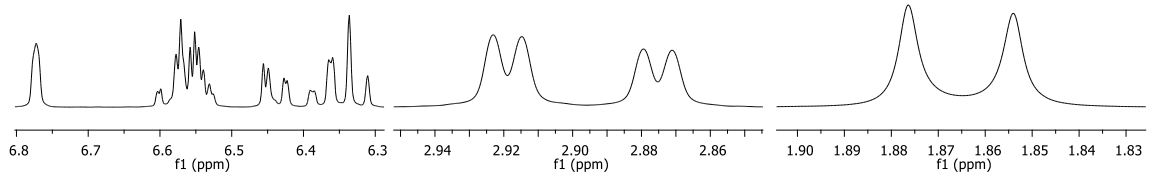
**2.44**

<sup>13</sup>C NMR (75 MHz, CDCl<sub>3</sub>)

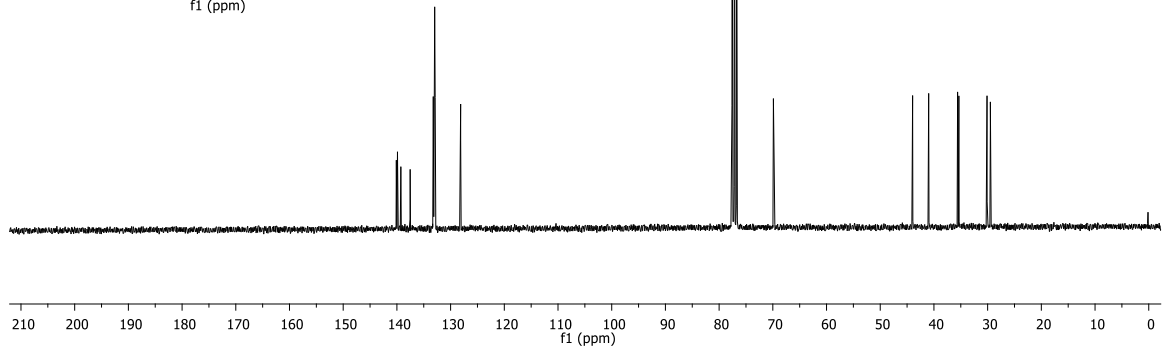
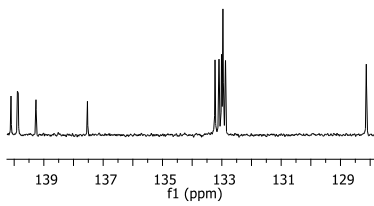




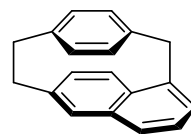
<sup>1</sup>H NMR (300 MHz, CDCl<sub>3</sub>)



<sup>13</sup>C NMR (75 MHz, CDCl<sub>3</sub>)

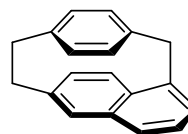
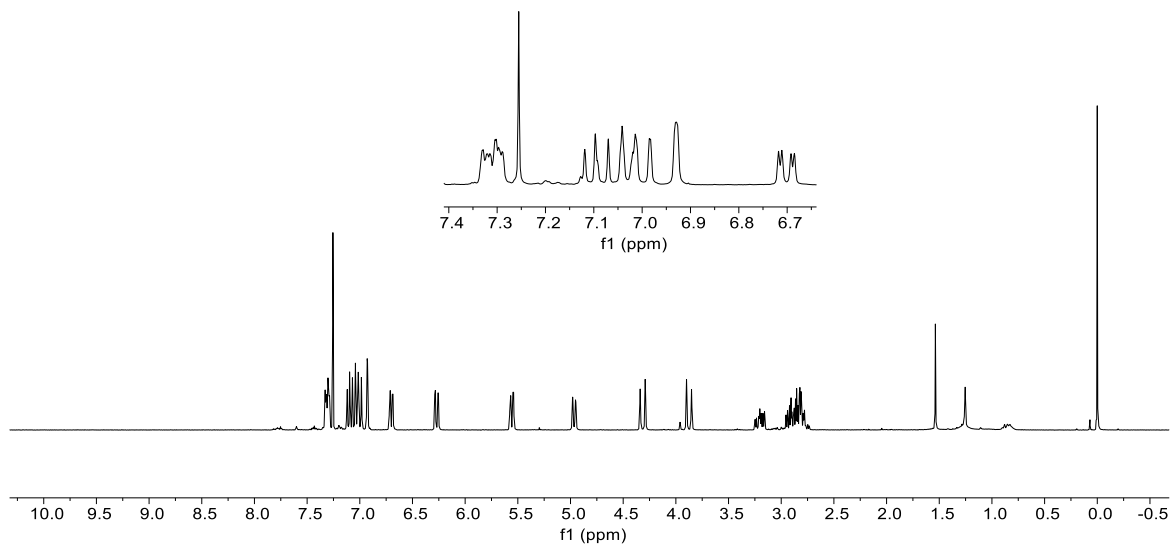






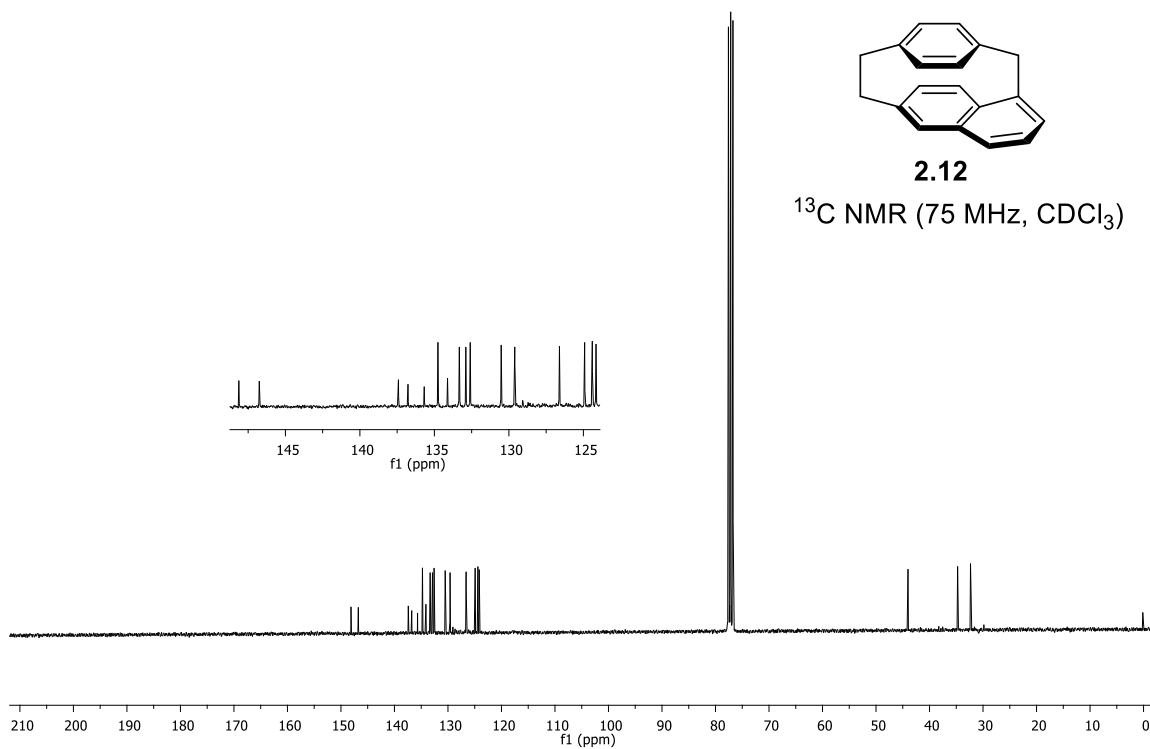
**2.12**

$^1\text{H}$  NMR (300 MHz,  $\text{CDCl}_3$ )

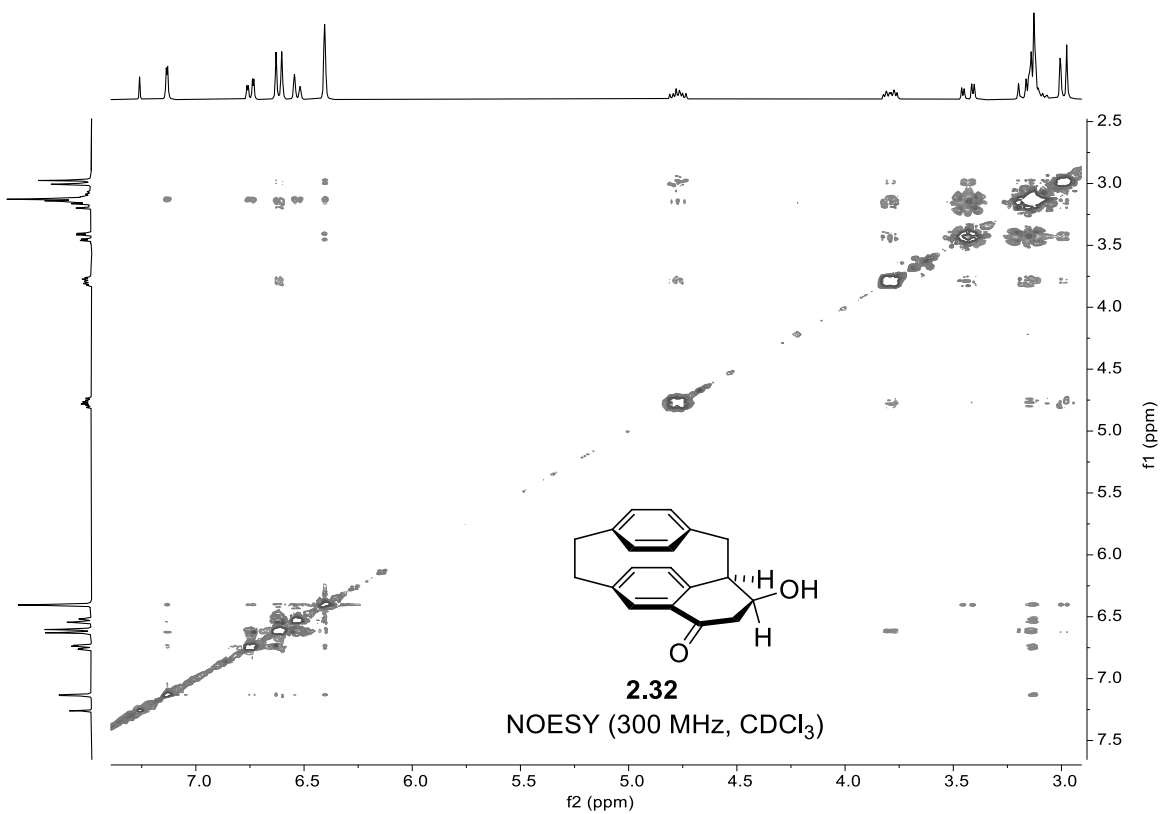
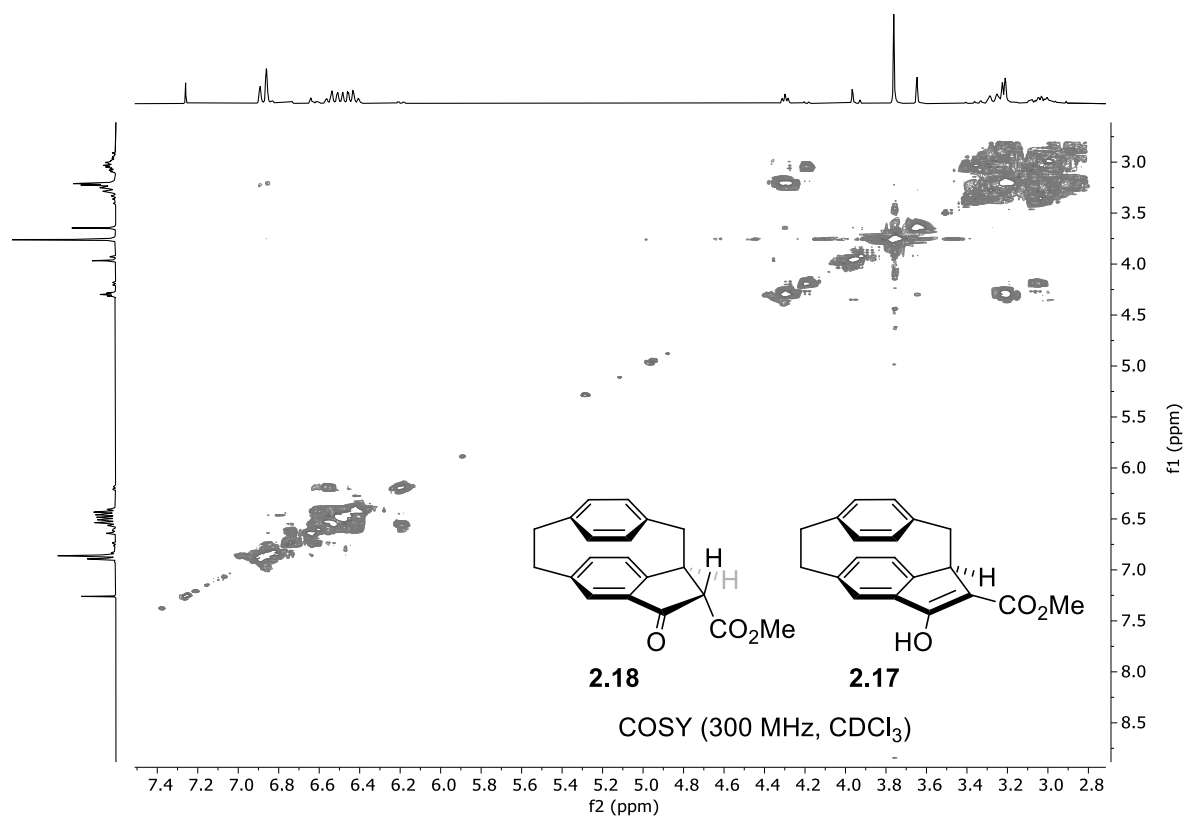


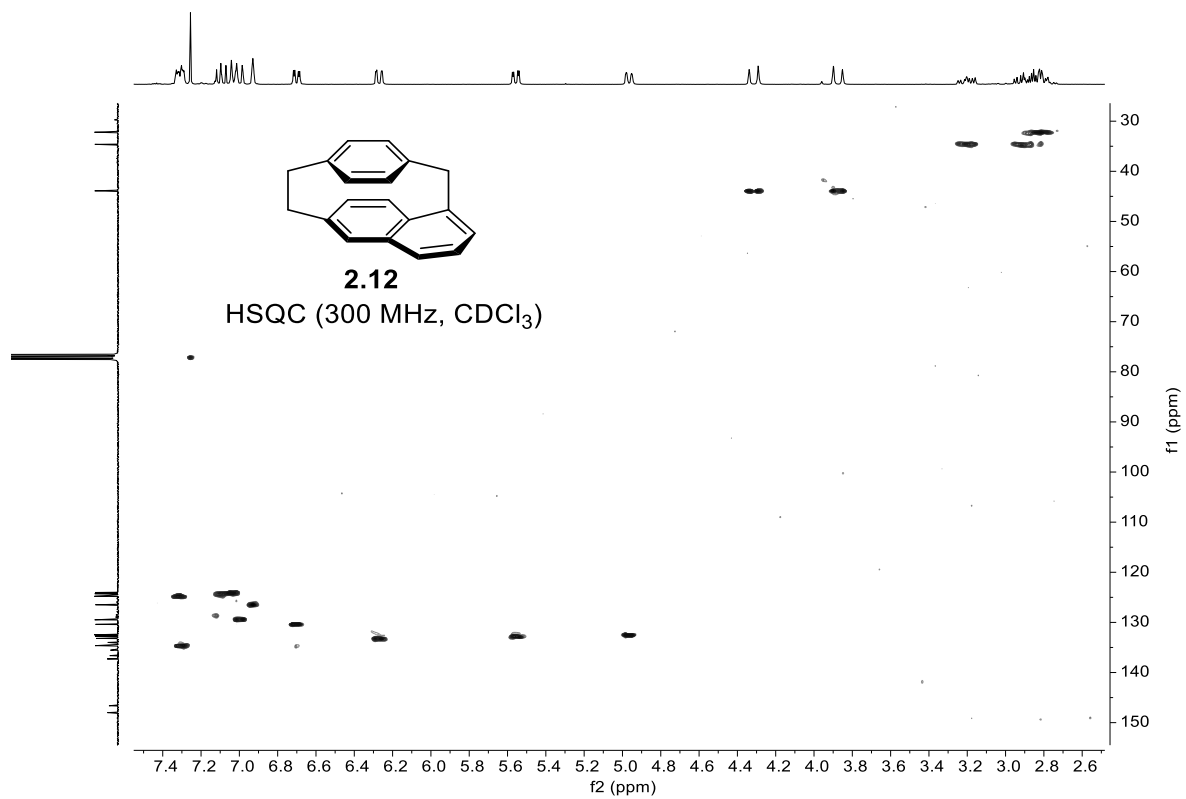
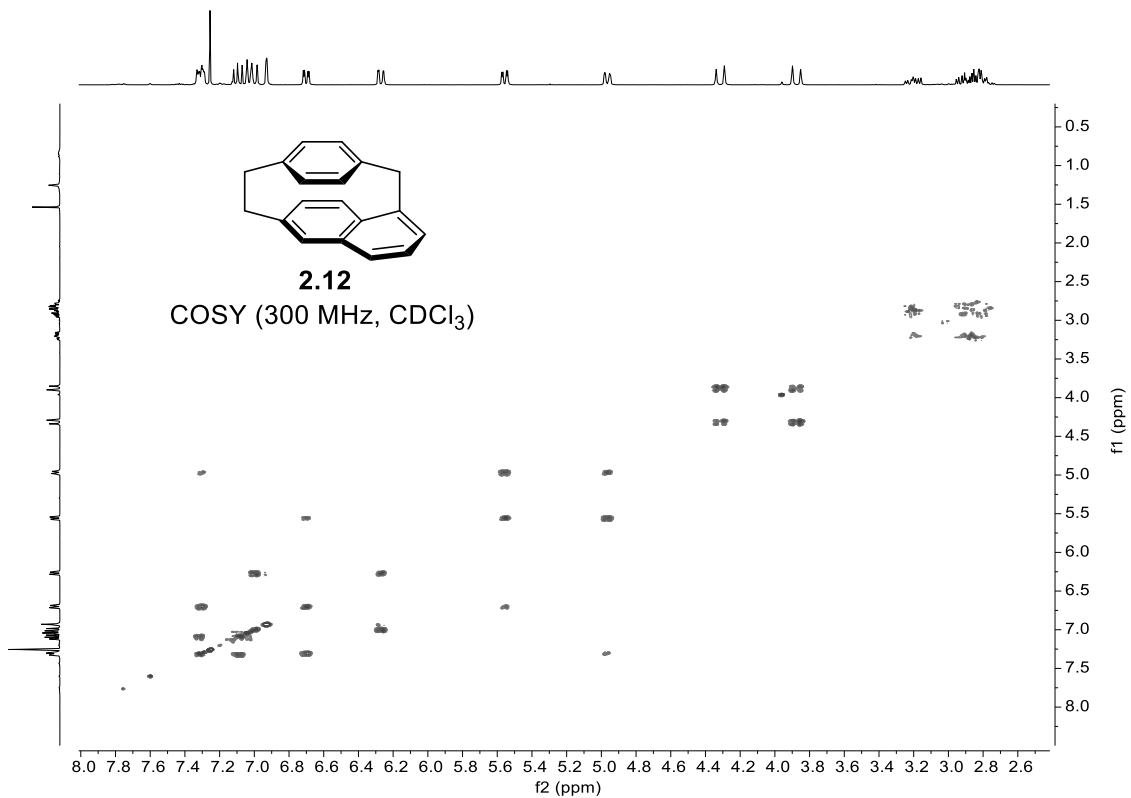
**2.12**

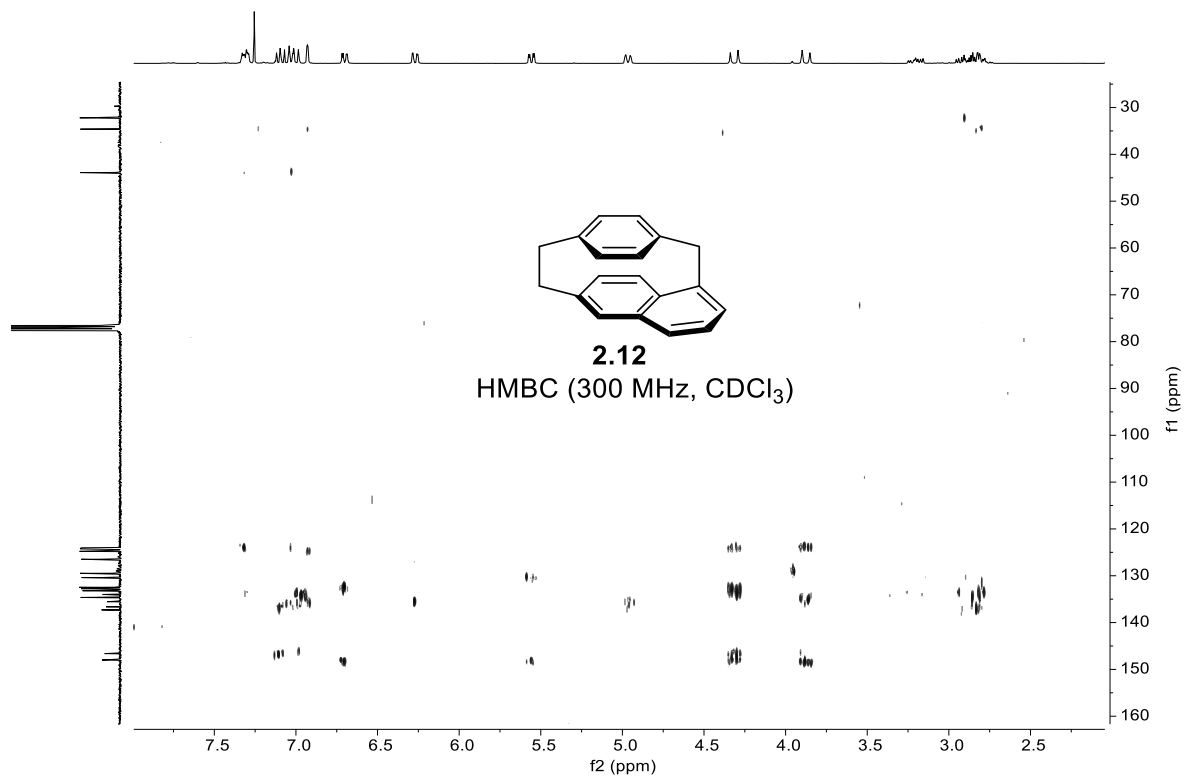
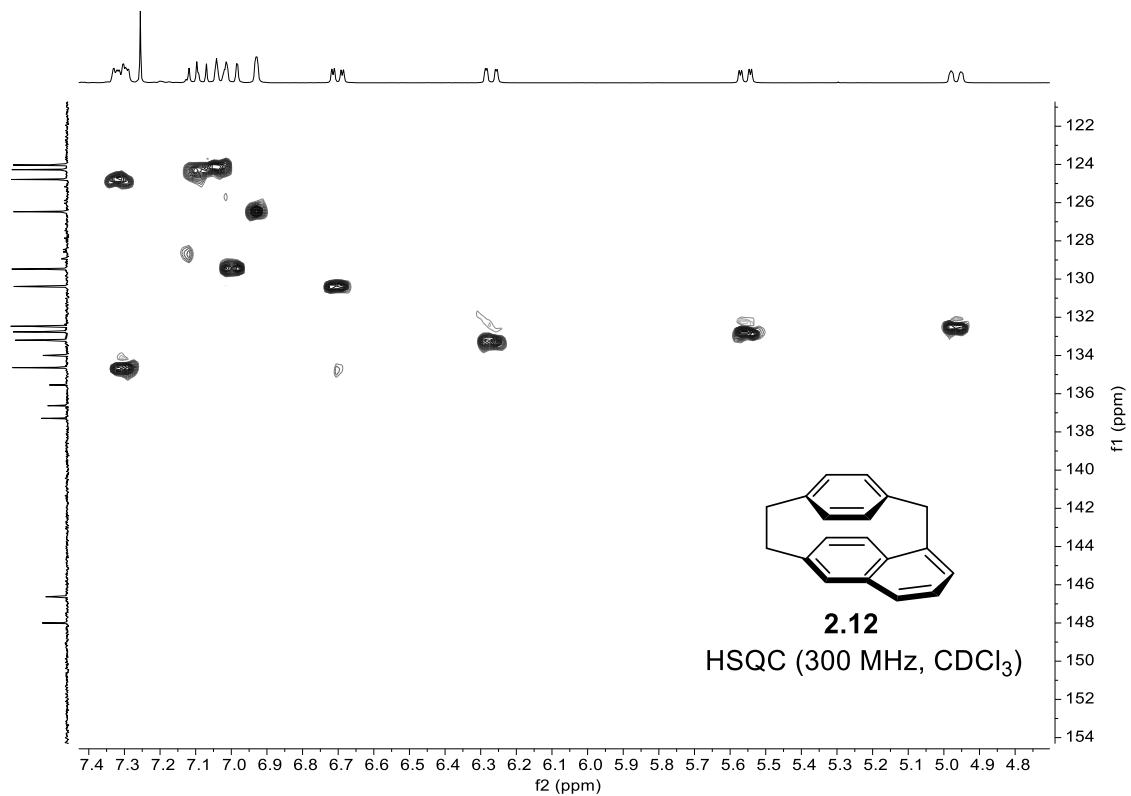
$^{13}\text{C}$  NMR (75 MHz,  $\text{CDCl}_3$ )

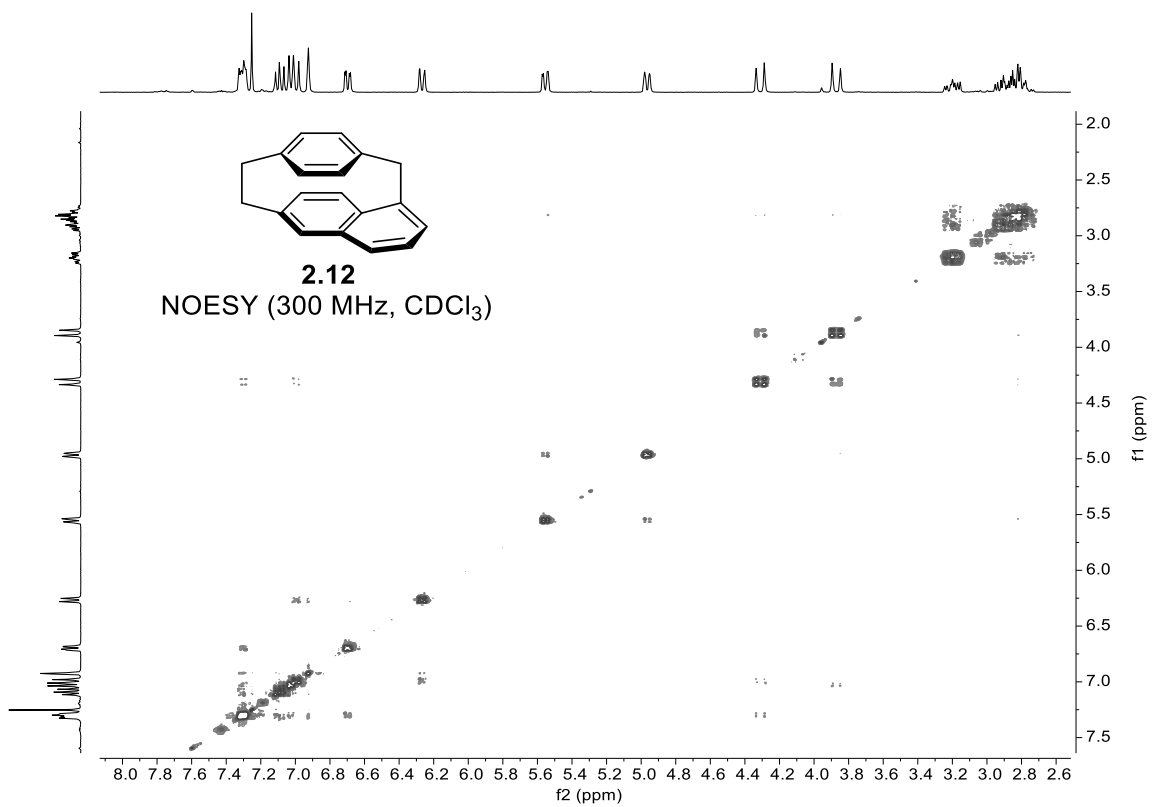
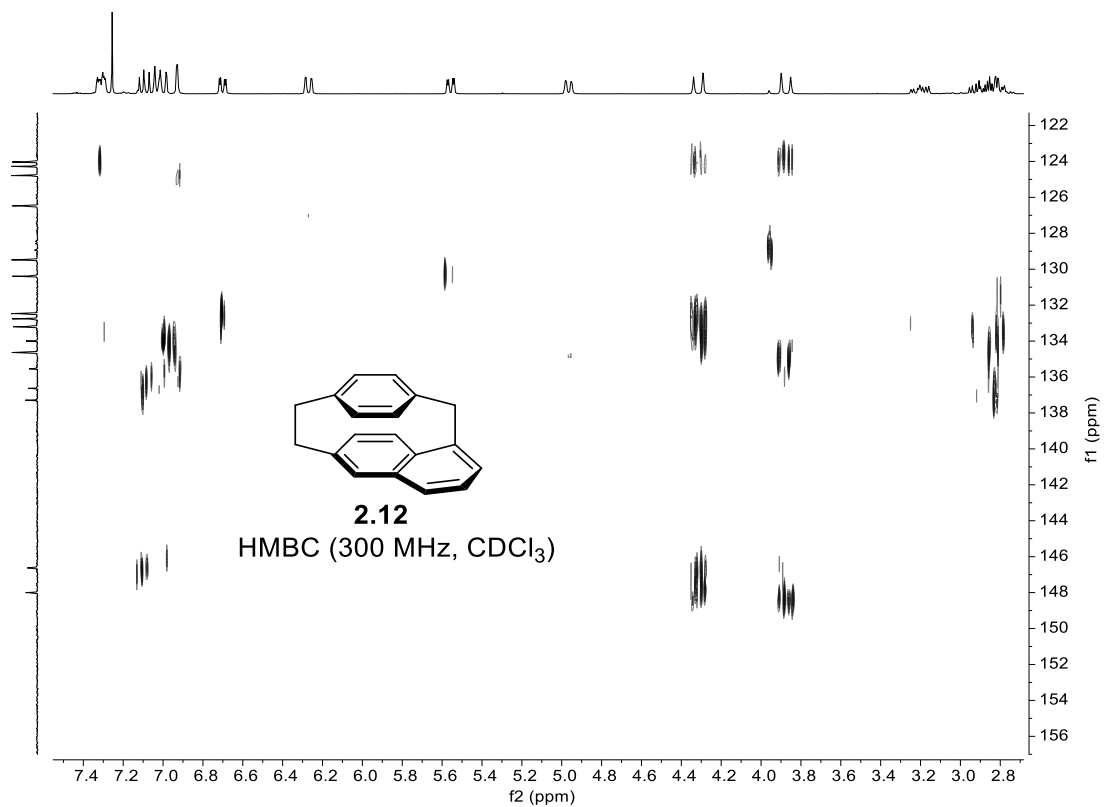


## 2. Two-Dimensional NMR Spectra









### 3. Crystal Structure Determination for Compound 2.12

Sample:       MUN1118

X-ray Structure Report

for

Dr. G. Bodwell

Prepared by

Louise N. Dawe, PhD

Department of Chemistry and Biochemistry

Wilfrid Laurier University

Science Building  
75 University Ave. W.  
Waterloo, ON, ON

ldawe@wlu.ca

November 15, 2018

#### Introduction

Data collection was performed by Mr. Adam Beaton, Memorial University of Newfoundland.

All H-atoms with an  $sp^2$  parent C were introduced in calculated positions and refined with their displacement parameter riding on the parent atom, and all with a same distance restraint. All other H-atoms were introduced in calculated positions and refined on a riding model. All non-hydrogen atoms were introduced in difference map positions and refined anisotropically.

The absolute structure parameter is meaningless because the compound is a weak anomalous scatterer. This was further investigated with PLATON's Bijvoet-pair analysis, which gave:

Hooft  $y = -0.3(13)$  and

$P2(\text{true}) = 0.607$ ;

$P3(\text{true}) = 0.406$ ;

$P3(\text{rac-twin}) = 0.330$ ;

$P3(\text{false}) = 0.263$

(which further confirms that no conclusions can be drawn based on Flack  $x$  or Hooft  $y$ , since this is a light atom structure that was collected with an Mo radiation source, which was the only source available in the home lab.)

### Experimental

A suitable crystal of  $C_{19}H_{16}$  was selected and collected on a Rigaku Saturn 70 diffractometer. The crystal was kept at 100.0 K during data collection. Using Olex2 [1], the structure was solved with the ShelXT [2] structure solution program using Intrinsic Phasing and refined with the ShelXL [3] refinement package using Least Squares minimisation.

1. Dolomanov, O.V., Bourhis, L.J., Gildea, R.J, Howard, J.A.K. & Puschmann, H. (2009), *J. Appl. Cryst.* 42, 339-341.
2. Sheldrick, G.M. (2015). *Acta Cryst.* A71, 3-8.
3. Sheldrick, G.M. (2015). *Acta Cryst.* C71, 3-8.

### Crystal Structure Determination

**Crystal Data** for  $C_{19}H_{16}$  ( $M = 244.32$  g/mol): orthorhombic, space group  $Pna2_1$  (no. 33),  $a = 18.9371(4)$  Å,  $b = 9.1172(2)$  Å,  $c = 7.2212(2)$  Å,  $V = 1246.76(5)$  Å<sup>3</sup>,  $Z = 4$ ,  $T = 100(2)$  K,  $\mu(\text{MoK}\alpha) = 0.073$  mm<sup>-1</sup>,  $D_{\text{calc}} = 1.302$  g/cm<sup>3</sup>, 17356 reflections measured ( $4.958^\circ \leq 2\theta \leq 54.202^\circ$ ), 2748 unique (2624 with  $I > 2\sigma(I)$ )  $R_{\text{int}} = 0.0525$ ,  $R_{\text{sigma}} = 0.0290$ ) which were used in all calculations. The final  $R_1$  was 0.0438 ( $I > 2\sigma(I)$ ) and  $wR_2$  was 0.1059 (all data).

**MUN1118****Table A1-1:** Crystal data and structure refinement for MUN1118.

|   |  |
|---|--|
| Identification code                         | MUN1118  |
| Empirical formula                           | C <sub>19</sub> H <sub>16</sub>  |
| Formula weight                              | 244.32   |
| Temperature/K                               | 100.0  |
| Crystal system                              | orthorhombic   |
| Space group                                 | Pna2 <sub>1</sub>  |
| a/Å   | 18.9371(4)   |
| b/Å   | 9.1172(2)  |
| c/Å   | 7.2212(2)  |
| α/°   | 90   |
| β/°   | 90   |
| γ/°   | 90   |
| Volume/Å <sup>3</sup>                       | 1246.76(5)   |
| Z   | 4  |
| ρ <sub>calc</sub> /cm <sup>3</sup>          | 1.302  |
| μ/mm <sup>-1</sup>                          | 0.073  |
| F(000)                                      | 520.0  |
| Crystal size/mm <sup>3</sup>                | 0.15 × 0.15 × 0.15   |
| Radiation                                   | MoKα (λ = 0.71073)   |
| 2θ range for data collection/°              | 4.958 to 54.202  |
| Index ranges                                | -24 ≤ h ≤ 24, -11 ≤ k ≤ 11, -9 ≤ l ≤ 9   |
| Reflections collected                       | 17356  |
| Independent reflections                     | 2748 [2624 with I > 2σI; R <sub>int</sub> = 0.0525, R <sub>sigma</sub> = 0.0290] |
| Data/restraints/parameters                  | 2748/46/202  |
| Goodness-of-fit on F <sup>2</sup>           | 1.042  |
| Final R indexes [I ≥ 2σ (I)]                | R <sub>1</sub> = 0.0438, wR <sub>2</sub> = 0.1038                                |
| Final R indexes [all data]                  | R <sub>1</sub> = 0.0460, wR <sub>2</sub> = 0.1059                                |
| Largest diff. peak/hole / e Å <sup>-3</sup> | 0.20/-0.22   |
| Flack parameter                             | -5.1(10)   |

Numbering Scheme (and numbered model with 50% displacement ellipsoids)

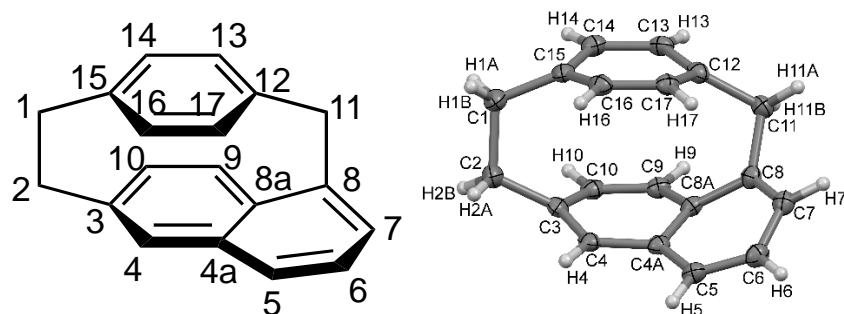


**Table A1-2:** Fractional Atomic Coordinates ( $\times 10^4$ ) and Equivalent Isotropic Displacement Parameters ( $\text{\AA}^2 \times 10^3$ ) for MUN1118.  $U_{\text{eq}}$  is defined as 1/3 of the trace of the orthogonalised  $U_{\text{ij}}$  tensor.

| Atom | <i>x</i>    | <i>y</i> | <i>z</i> | <i>U</i> (eq) |
|------|-------------|----------|----------|---------------|
| C1   | 3102.2 (15) | 6360 (3) | 4331 (4) | 29.7 (6)      |
| C2   | 3740.3 (14) | 6567 (3) | 5730 (4) | 26.7 (6)      |
| C3   | 4047.0 (14) | 5137 (3) | 6425 (4) | 23.0 (5)      |
| C4   | 4693.3 (13) | 4617 (3) | 5866 (3) | 21.6 (5)      |
| C4A  | 4830.2 (12) | 3065 (3) | 5825 (3) | 21.1 (5)      |
| C5   | 5452.5 (13) | 2457 (3) | 5039 (4) | 23.8 (5)      |
| C6   | 5455.1 (13) | 1027 (3) | 4451 (4) | 24.9 (5)      |
| C7   | 4812.1 (13) | 221 (3)  | 4389 (4) | 24.2 (5)      |
| C8   | 4215.5 (13) | 764 (3)  | 5209 (4) | 22.6 (5)      |
| C8A  | 4260.9 (12) | 2117 (3) | 6223 (3) | 21.0 (5)      |
| C9   | 3693.1 (13) | 2680 (3) | 7286 (3) | 21.5 (5)      |
| C10  | 3596.4 (13) | 4165 (3) | 7424 (4) | 23.3 (5)      |
| C11  | 3479.1 (13) | 307 (3)  | 4523 (4) | 24.2 (5)      |
| C12  | 3156.5 (13) | 1722 (3) | 3717 (4) | 23.3 (5)      |
| C13  | 2557.9 (13) | 2368 (3) | 4474 (4) | 23.9 (5)      |
| C14  | 2475.1 (13) | 3896 (3) | 4459 (4) | 24.7 (5)      |
| C15  | 2993.3 (13) | 4783 (3) | 3702 (4) | 23.2 (5)      |
| C16  | 3499.1 (13) | 4107 (3) | 2566 (4) | 23.6 (5)      |
| C17  | 3576.4 (13) | 2597 (3) | 2565 (3) | 22.5 (5)      |

**Table A1-3:** Anisotropic Displacement Parameters ( $\text{\AA}^2 \times 10^3$ ) for MUN1118. The Anisotropic displacement factor exponent takes the form:  $-2\pi^2[h^2a^2U_{11}+2hka^*b^*U_{12}+\dots]$ .

| Atom | $U_{11}$  | $U_{22}$  | $U_{33}$  | $U_{23}$  | $U_{13}$   | $U_{12}$  |
|------|-----------|-----------|-----------|-----------|------------|-----------|
| C1   | 33.5 (14) | 24.5 (13) | 31.1 (13) | 0.0 (12)  | -10.0 (12) | 2.9 (10)  |
| C2   | 28.2 (13) | 21.3 (12) | 30.6 (13) | -2.7 (11) | -4.7 (11)  | 1.2 (10)  |
| C3   | 26.6 (13) | 22.4 (12) | 20.1 (12) | -5.1 (10) | -4.7 (10)  | 0.3 (10)  |
| C4   | 22.3 (11) | 23.0 (11) | 19.5 (12) | 0.4 (10)  | -5.3 (10)  | -3.3 (9)  |
| C4A  | 21.0 (11) | 25.3 (11) | 17.2 (11) | -0.6 (10) | -2.9 (10)  | 1.2 (9)   |
| C5   | 19.5 (11) | 28.2 (12) | 23.8 (12) | 1.8 (10)  | -1.5 (10)  | 0.3 (10)  |
| C6   | 23.1 (11) | 28.6 (12) | 23.2 (12) | -1.2 (11) | 2.3 (11)   | 4.4 (10)  |
| C7   | 29.5 (13) | 22.7 (12) | 20.5 (12) | 0.7 (10)  | 1.7 (11)   | 2.6 (10)  |
| C8   | 24.9 (12) | 20.6 (11) | 22.2 (12) | 3.3 (10)  | 0.6 (10)   | 0.3 (10)  |
| C8A  | 20.2 (11) | 24.1 (12) | 18.7 (12) | 3.0 (9)   | -1.2 (9)   | 3.6 (10)  |
| C9   | 21.3 (11) | 26.7 (12) | 16.7 (11) | 1.6 (10)  | 0.8 (9)    | 0.3 (10)  |
| C10  | 22.7 (12) | 29.3 (13) | 18.0 (12) | -2.6 (10) | -2.5 (10)  | 3.6 (10)  |
| C11  | 25.3 (13) | 21.0 (12) | 26.4 (13) | -1.1 (11) | -0.5 (11)  | -3.0 (9)  |
| C12  | 26.0 (13) | 23.3 (12) | 20.7 (11) | -1.5 (10) | -3.3 (10)  | -3.2 (10) |
| C13  | 19.8 (11) | 29.3 (12) | 22.6 (12) | 2.3 (11)  | -3.1 (10)  | -4.0 (10) |
| C14  | 21.3 (11) | 30.8 (12) | 22.0 (12) | 0.1 (11)  | -2.2 (10)  | 2.7 (10)  |
| C15  | 23.7 (12) | 25.0 (12) | 20.8 (12) | 1.1 (11)  | -6.9 (10)  | 1.9 (10)  |
| C16  | 24.1 (12) | 25.9 (13) | 20.8 (12) | 2.6 (10)  | -2.5 (10)  | -3.2 (9)  |
| C17  | 22.6 (12) | 25.9 (12) | 18.9 (12) | -1.6 (11) | -0.1 (10)  | 0.1 (9)   |

**Table A1-4:** Bond Lengths for MUN1118.

| Atom | Atom | Length/Å | Atom | Atom | Length/Å |
|------|------|----------|------|------|----------|
| C1   | C2   | 1.586(4) | C8   | C8A  | 1.437(3) |
| C1   | C15  | 1.521(3) | C8   | C11  | 1.537(3) |
| C2   | C3   | 1.513(3) | C8A  | C9   | 1.417(3) |
| C3   | C4   | 1.373(4) | C9   | C10  | 1.369(4) |
| C3   | C10  | 1.426(4) | C11  | C12  | 1.542(3) |
| C4   | C4A  | 1.438(3) | C12  | C13  | 1.389(4) |
| C4A  | C5   | 1.421(3) | C12  | C17  | 1.400(4) |
| C4A  | C8A  | 1.412(3) | C13  | C14  | 1.401(3) |
| C5   | C6   | 1.371(3) | C14  | C15  | 1.385(4) |
| C6   | C7   | 1.423(4) | C15  | C16  | 1.404(4) |
| C7   | C8   | 1.368(4) | C16  | C17  | 1.385(4) |

**Table A1-5:** Bond Angles for MUN1118.

| Atom | Atom | Atom | Angle/°  | Atom | Atom | Atom | Angle/°    |
|------|------|------|----------|------|------|------|------------|
| C15  | C1   | C2   | 113.9(2) | C4A  | C8A  | C9   | 117.9(2)   |
| C3   | C2   | C1   | 113.7(2) | C9   | C8A  | C8   | 122.8(2)   |
| C4   | C3   | C2   | 122.8(2) | C10  | C9   | C8A  | 120.0(2)   |
| C4   | C3   | C10  | 117.9(2) | C9   | C10  | C3   | 119.8(2)   |
| C10  | C3   | C2   | 118.3(2) | C8   | C11  | C12  | 104.73(19) |
| C3   | C4   | C4A  | 120.4(2) | C13  | C12  | C11  | 122.0(2)   |
| C5   | C4A  | C4   | 122.8(2) | C13  | C12  | C17  | 117.1(2)   |
| C8A  | C4A  | C4   | 117.4(2) | C17  | C12  | C11  | 118.4(2)   |
| C8A  | C4A  | C5   | 118.4(2) | C12  | C13  | C14  | 120.6(2)   |
| C6   | C5   | C4A  | 119.9(2) | C15  | C14  | C13  | 120.3(2)   |
| C5   | C6   | C7   | 119.9(2) | C14  | C15  | C1   | 122.0(2)   |
| C8   | C7   | C6   | 120.4(2) | C14  | C15  | C16  | 117.2(2)   |
| C7   | C8   | C8A  | 118.8(2) | C16  | C15  | C1   | 119.8(2)   |
| C7   | C8   | C11  | 120.8(2) | C17  | C16  | C15  | 120.6(2)   |
| C8A  | C8   | C11  | 116.8(2) | C16  | C17  | C12  | 120.4(2)   |
| C4A  | C8A  | C8   | 117.9(2) |      |      |      |            |

**Table A1-6:** Hydrogen Atom Coordinates ( $\text{\AA}\times 10^4$ ) and Isotropic Displacement Parameters ( $\text{\AA}^2\times 10^3$ ) for MUN1118.

| <b>Atom</b> | <b>x</b>  | <b>y</b>  | <b>z</b>  | <b>U(eq)</b> |
|-------------|-----------|-----------|-----------|--------------|
| H1A         | 2663.53   | 6709.89   | 4931.24   | 36           |
| H1B         | 3186.36   | 6980.31   | 3227.5    | 36           |
| H2A         | 4117.92   | 7132.79   | 5106.61   | 32           |
| H2B         | 3575.72   | 7148.96   | 6803.46   | 32           |
| H4          | 5051 (13) | 5290 (30) | 5340 (40) | 26           |
| H5          | 5860 (12) | 3090 (30) | 4830 (50) | 29           |
| H6          | 5885 (12) | 630 (30)  | 3850 (40) | 30           |
| H7          | 4809 (15) | -660 (30) | 3620 (40) | 29           |
| H9          | 3335 (13) | 1980 (30) | 7780 (40) | 26           |
| H10         | 3166 (12) | 4570 (30) | 8010 (40) | 28           |
| H11A        | 3188.42   | -69.89    | 5558.15   | 29           |
| H11B        | 3515.47   | -461.89   | 3559.62   | 29           |
| H13         | 2259 (14) | 1750 (30) | 5250 (40) | 29           |
| H14         | 2097 (13) | 4350 (30) | 5190 (40) | 30           |
| H16         | 3867 (13) | 4700 (30) | 1970 (40) | 28           |
| H17         | 4011 (12) | 2200 (30) | 1980 (40) | 27           |

**Table A1-7:** Torsion Angles for MUN1118.

| <b>A</b> | <b>B</b> | <b>C</b> | <b>D</b> | <b>Angle/°</b> | <b>A</b> | <b>B</b> | <b>C</b> | <b>D</b> | <b>Angle/°</b> |
|----------|----------|----------|----------|----------------|----------|----------|----------|----------|----------------|
| C1       | C2       | C3       | C4       | 107.6 (3)      | C7       | C8       | C8AC9    |          | -172.9 (2)     |
| C1       | C2       | C3       | C10      | -60.5 (3)      | C7       | C8       | C11      | C12      | -113.9 (3)     |
| C1       | C15      | C16      | C17      | 154.2 (2)      | C8       | C8AC9    | C10      |          | -146.4 (3)     |
| C2       | C1       | C15      | C14      | 100.6 (3)      | C8       | C11      | C12      | C13      | -116.3 (3)     |
| C2       | C1       | C15      | C16      | -68.0 (3)      | C8       | C11      | C12      | C17      | 45.2 (3)       |
| C2       | C3       | C4       | C4A      | -151.2 (2)     | C8AC4AC5 | C6       |          |          | 9.0 (4)        |
| C2       | C3       | C10      | C9       | 147.3 (2)      | C8AC8    | C11      | C12      |          | 44.4 (3)       |
| C3       | C4       | C4AC5    |          | 171.7 (2)      | C8AC9    | C10      | C3       |          | 3.1 (4)        |
| C3       | C4       | C4AC8A   |          | 5.3 (4)        | C10      | C3       | C4       | C4A      | 16.9 (4)       |
| C4       | C3       | C10      | C9       | -21.4 (4)      | C11      | C8       | C8AC4A   |          | -137.6 (2)     |
| C4       | C4AC5    | C6       |          | -157.3 (2)     | C11      | C8       | C8AC9    |          | 28.4 (3)       |
| C4       | C4AC8AC8 |          |          | 143.2 (2)      | C11      | C12      | C13      | C14      | 146.6 (3)      |
| C4       | C4AC8AC9 |          |          | -23.5 (3)      | C11      | C12      | C17      | C16      | -146.6 (2)     |
| C4AC5    | C6       | C7       |          | 8.8 (4)        | C12      | C13      | C14      | C15      | -0.6 (4)       |
| C4AC8AC9 | C10      |          |          | 19.5 (4)       | C13      | C12      | C17      | C16      | 15.9 (4)       |
| C5       | C4AC8AC8 |          |          | -23.8 (3)      | C13      | C14      | C15      | C1       | -153.3 (3)     |
| C5       | C4AC8AC9 |          |          | 169.5 (2)      | C13      | C14      | C15      | C16      | 15.6 (4)       |
| C5       | C6       | C7       | C8       | -11.5 (4)      | C14      | C15      | C16      | C17      | -15.0 (4)      |
| C6       | C7       | C8       | C8A      | -3.6 (4)       | C15      | C1       | C2       | C3       | -9.5 (4)       |
| C6       | C7       | C8       | C11      | 154.2 (2)      | C15      | C16      | C17      | C12      | -0.8 (4)       |
| C7       | C8       | C8AC4A   |          | 21.2 (4)       | C17      | C12      | C13      | C14      | -15.2 (4)      |

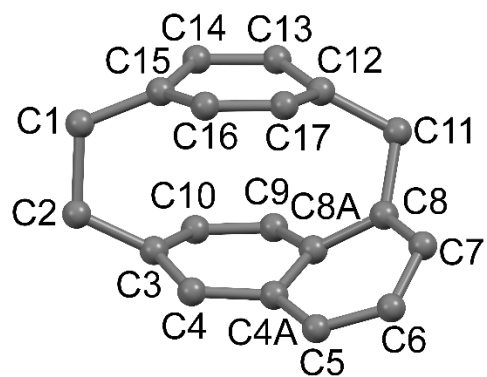


**Figure A1-1:** Ball-and-stick model with systematic numbering (H-atoms omitted for clarity.)

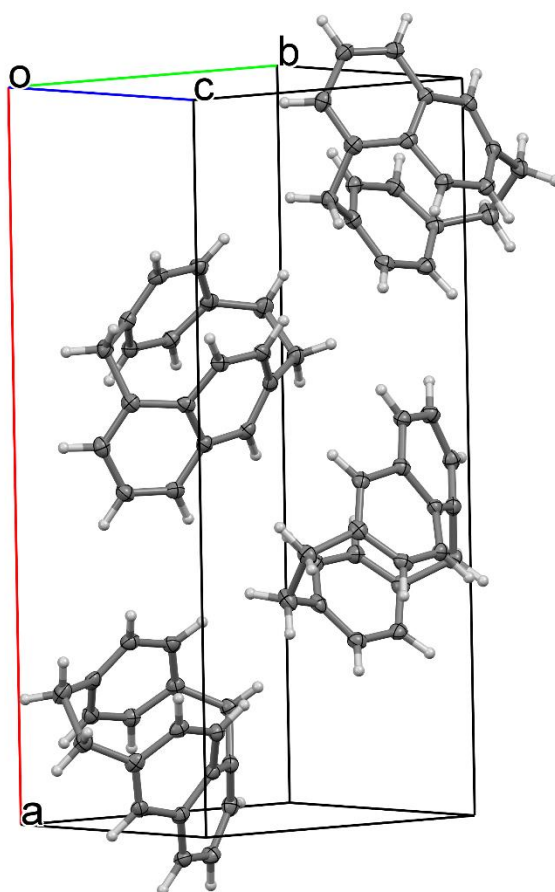


**Figure A1-2:** Packing diagram with 50% probability ellipsoids. No significant intermolecular short contacts are present.

#### 4. Computational Data

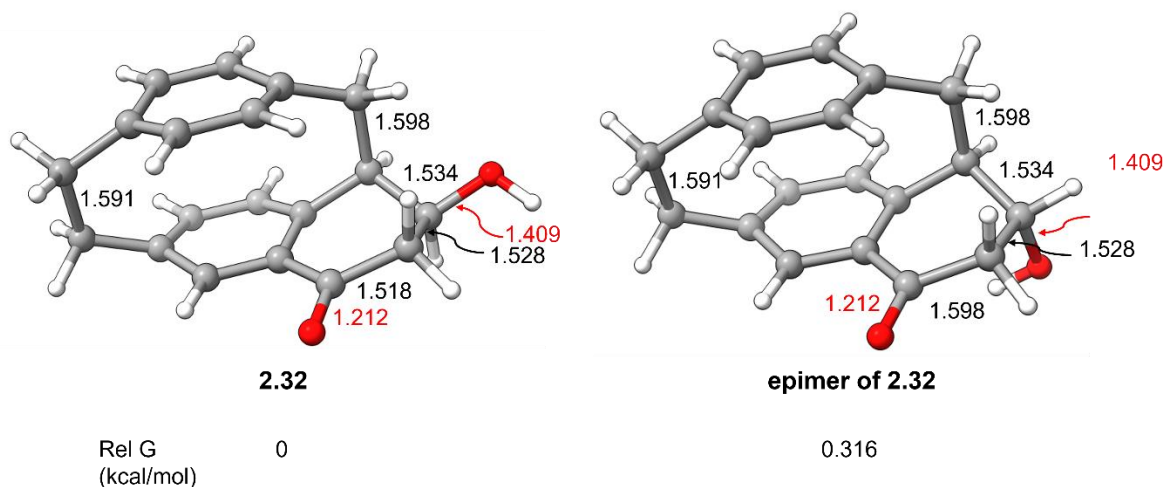
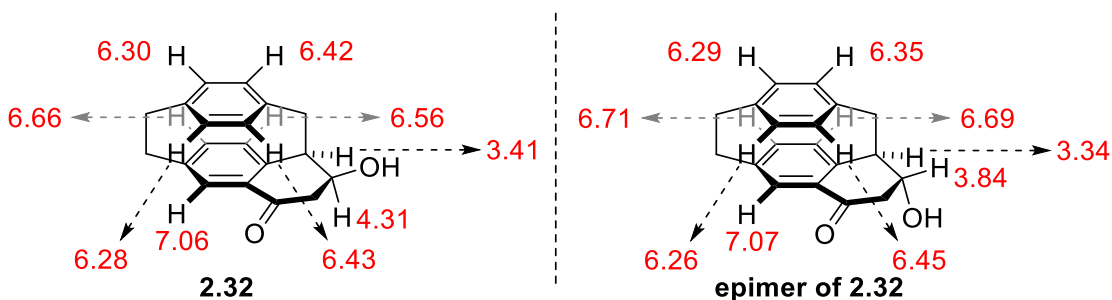


**Figure A1-3:** Optimized geometries of **2.32** and its epimer in chloroform at the M06-2X/Def2SVP level of theory.



\* Note: The chemical shift of residual chloroform at 7.26 ppm was used as the reference.

**Figure A1-4:**  $^1\text{H}$  NMR chemical Shifts (in red) of **2.32** and its epimer calculated at the GIAO-B3LYP/6-311+G(2d,p) level of theory.

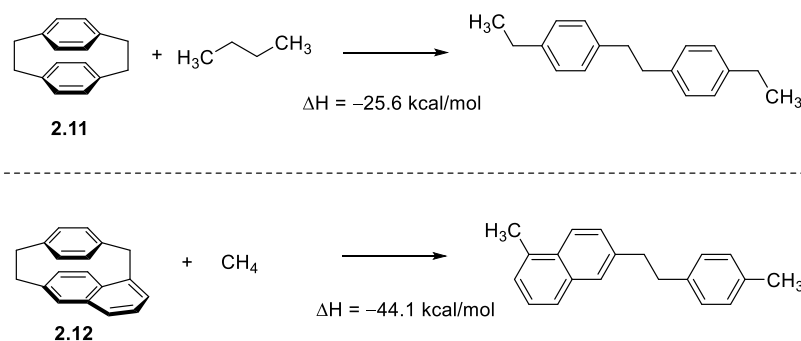
Geometry optimization of cyclophane **2.12** and other compounds was performed at the M06-2X/Def2TZVP level, and the optimized structures were validated as ground-state energy minima by frequency calculations at the same level of theory (zero imaginary frequency).

Cartesian coordinate of optimized **2.12** ( $E = -733.561843$  Hartree, dipole moment = 0.905320 Debye)

|   |             |            |             |
|---|-------------|------------|-------------|
| H | 0.93310994  | 3.11540027 | 1.12795906  |
| C | 0.95507596  | 2.40470922 | 0.30871700  |
| C | 1.03853404  | 0.47135808 | -1.64932314 |
| C | -0.23191011 | 2.02402215 | -0.30279204 |
| C | 2.13946107  | 1.71307821 | 0.04851098  |
| C | 2.15049411  | 0.62603313 | -0.81796008 |

|   |             |             |             |
|---|-------------|-------------|-------------|
| C | -0.12840007 | 1.16698109  | -1.40415012 |
| H | 3.01164113  | 1.91898826  | 0.65937702  |
| H | -1.02351713 | 0.89464904  | -1.95278316 |
| H | 1.03982106  | -0.30803697 | -2.40369420 |
| C | 3.16129522  | -0.49065991 | -0.70052407 |
| H | 3.50401226  | -0.79410692 | -1.69082315 |
| H | 4.03534427  | -0.12615785 | -0.16035403 |
| C | -1.59162821 | 2.14379811  | 0.40368901  |
| H | -2.31135628 | 2.74989413  | -0.14890403 |
| H | -1.44372722 | 2.61050015  | 1.37975907  |
| C | -2.11775220 | 0.70496799  | 0.48589501  |
| C | 2.62061723  | -1.80097002 | 0.03925598  |
| H | 2.60820326  | -2.62611308 | -0.67283607 |
| H | 3.34144429  | -2.05887302 | 0.81721804  |
| C | -1.18551910 | -0.29381205 | 0.91901004  |
| C | 1.24466712  | -1.62756806 | 0.62810902  |
| C | -1.15396305 | -1.52922013 | 0.23930799  |
| C | -0.09831303 | 0.01296701  | 1.77261010  |
| C | 1.07895508  | -0.65473599 | 1.64652209  |
| C | 0.11055706  | -2.16438614 | 0.07518698  |
| H | -0.16915807 | 0.86465607  | 2.43735115  |
| H | 1.94478613  | -0.33751594 | 2.21695214  |
| H | 0.18371809  | -2.96969119 | -0.64883207 |
| C | -2.31183512 | -1.92207920 | -0.48708206 |
| H | -2.33879409 | -2.90258728 | -0.94739809 |
| C | -3.34675623 | -1.04639718 | -0.65202407 |
| H | -4.22637328 | -1.34291922 | -1.20857011 |
| C | -3.19992626 | 0.30608393  | -0.24806504 |
| H | -3.89107534 | 1.04689196  | -0.63378307 |

The strain energies of cyclophanes **2.11** and **2.12** were calculated by the following isodesmic reactions (Scheme A1-1) at the M06-2X/Def2TZVP level of theory.



**Scheme A1-1:** Isodesmic reactions for the calculation of the strain energies of cyclophanes **2.11** and **2.12**.

The optimized Cartesian coordinates of compound **2.12** were subjected to TD-M06 2X/def2TZVP (singlets, nstates = 10) calculations to compute its UV-vis absorption spectrum in the gas phase.

**Table A1-8:** Summary of TD-M06-2X/def2TZVP computed UV-Vis absorption spectral data of cyclophane **2.12**.

| $\lambda_{\text{abs}}$ (nm) | $f$    | Major MO contributions  |
|-----------------------------|--------|---|
| 301.1                       | 0.0044 | H-1 $\rightarrow$ (54%), HOMO $\rightarrow$ L+1 (27%)   |
| 297.5                       | 0.0273 | HOMO $\rightarrow$ LUMO (87%)   |
| 265.7                       | 0.0251 | H-2 $\rightarrow$ LUMO (23%), H-1 $\rightarrow$ LUMO (23%), HOMO $\rightarrow$ L+1 (19%),<br>HOMO $\rightarrow$ L+2 (16%) |
| 247.3                       | 0.0636 | H-1 $\rightarrow$ LUMO (10%), HOMO $\rightarrow$ L+1 (32%), HOMO $\rightarrow$ L+2 (20%)                                  |
| 239.8                       | 0.0055 | H-1 $\rightarrow$ L+1 (56%), HOMO $\rightarrow$ L+2 (21%)   |
| 234.3                       | 0.1192 | H-3 $\rightarrow$ LUMO (10%), H-2 $\rightarrow$ LUMO (43%), HOMO $\rightarrow$ L+3 (18%)                                  |
| 231.1                       | 0.1465 | H-2 $\rightarrow$ LUMO (19%), H-1 $\rightarrow$ L+1 (25%), HOMO $\rightarrow$ L+2 (30%)                                   |
| 223.4                       | 0.0288 | H-1 $\rightarrow$ L+2 (62%)   |
| 216.9                       | 0.053  | H-2 $\rightarrow$ L+1 (11%), H-1 $\rightarrow$ L+3 (26%), HOMO $\rightarrow$ L+3 (13%)                                    |
| 216.2                       | 0.0014 | H-3 $\rightarrow$ LUMO (31%), HOMO $\rightarrow$ L+3 (47%)  |

## 5. Bond Lengths for Naphthalene

From a search of the CCDC, 31 structures of naphthalene were found with R1 < 7.5%. Mean values of these 31 structures are shown below and were used as the reference bond lengths for naphthalene.

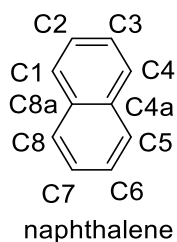


**Table A1-9:** Summary of the bond lengths in Å for the 31 structures of naphthalene from a search of the CCDC.

| <b>Bond</b> | <b>Minimum</b> | <b>Maximum</b> | <b>Mean</b> | <b>Std. Dev.</b> | <b>Mean Dev.</b> |
|-------------|----------------|----------------|-------------|------------------|------------------|
| C1–C2       | 1.35           | 1.388          | 1.374       | 0.006            | 0.004            |
| C1–C8a      | 1.404          | 1.427          | 1.42        | 0.005            | 0.004            |
| C8–C8a      | 1.413          | 1.426          | 1.42        | 0.003            | 0.002            |
| C7–C8       | 1.359          | 1.387          | 1.374       | 0.006            | 0.004            |
| C6–C7       | 1.386          | 1.425          | 1.413       | 0.009            | 0.006            |
| C5–C6       | 1.35           | 1.388          | 1.374       | 0.006            | 0.004            |
| C4a–C5      | 1.404          | 1.427          | 1.42        | 0.005            | 0.004            |
| C4–C4a      | 1.413          | 1.426          | 1.42        | 0.003            | 0.002            |
| C3–C4       | 1.359          | 1.387          | 1.374       | 0.006            | 0.004            |
| C2–C3       | 1.386          | 1.425          | 1.413       | 0.009            | 0.006            |
| C4a–C8a     | 1.4            | 1.438          | 1.42        | 0.008            | 0.005            |

## Chapter 3: Synthesis of [1](1,6)Naphthaleno[1](1,6)naphthalenophane by Double Contractive Annulation of [2.2]Paracyclophane

### Statement of Contributions

Sourav Biswas: Performed the synthetic work, physical data collection, data analysis.

Dr. Zahra A. Tabasi: Measured UV/vis absorption, excitation, and emission spectra of cyclophane **3.3**.

Dr. Louise N. Dawe: Solved the crystal structures of cyclophanes (**3.3**, **3.13**, **3.24**, **3.25**, and **3.27**) and provided publishable crystal structure reports.

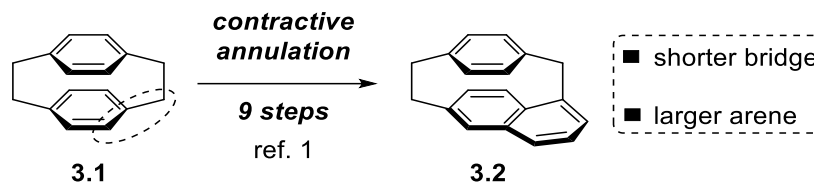
Prof. Yuming Zhao: Performed all computational work, interpreted the results, guided to writing of the corresponding sections.

Prof. Graham J. Bodwell: Principal investigator (PI) of the work, who led the project and majorly contributed to the interpretation/analysis of data.

The work described in this Chapter includes everyone's contributions for the purpose of a complete discussion.

### 3.1 Introduction

As discussed in Chapter 2, contractive annulation was recently introduced as a new strategy for the synthesis of small, strained cyclophanes.<sup>1</sup> The strategy involves the benzannulation of an existing cyclophane using a set of three contiguous carbon atoms consisting of a benzylic C(sp<sup>3</sup>) atom, the bridgehead (*ipso*) C(sp<sup>2</sup>) atom to which it is bonded and a neighboring (*ortho*) C(sp<sup>2</sup>) atom (Scheme 3.1). The use of a bridge C(sp<sup>3</sup>) atom in the benzannulation means that the growth of the aromatic system is necessarily accompanied by a shortening of the bridge. The utility of contractive annulation was first demonstrated in the synthesis of the structurally unusual cyclophane [2](6,1)naphthaleno[1]paracyclophane (**3.2**) from [2.2]paracyclophane (**3.1**).<sup>1</sup> Reported in this Chapter are the details of a double contractive annulation of **3.1** to afford a [1.1]naphthalenophane.



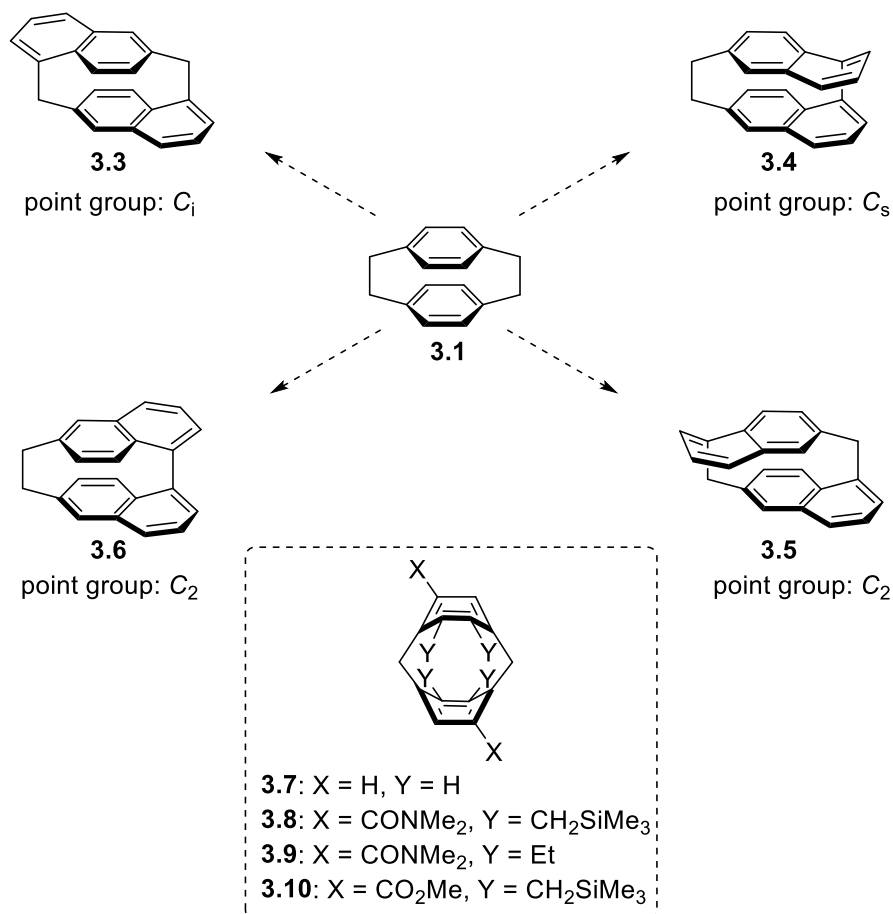
**Scheme 3.1:** Contractive annulation for the synthesis of [2](6,1)naphthaleno[1]paracyclophane (**3.2**).

### 3.2 Objective

Application of the contractive annulation strategy to both aromatic rings of [2.2]paracyclophane could conceivably be done in four different ways to afford a set of four structurally interesting compounds **3.3–3.6**. Compounds **3.3** and **3.5** are [1.1]naphthalenophanes, or more precisely, *anti* and *syn* conformers of [1](1,6)naphthaleno[1](1,6)naphthalenophane, respectively. Compounds **3.4** and **3.6** can either be viewed as *syn* and *anti* conformers of [2](6,1)naphthaleno[0](1,6)naphthalenophane, respectively, or C<sub>s</sub> and C<sub>2</sub>-symmetric conformers

of [2](6,6')1,1'-binaphthylphane, respectively. All of these compounds are exciting synthetic targets, but **3.3** was chosen for initial study due to its high symmetry ( $C_i$ ).

For the synthesis of **3.3**, a two-directional synthetic approach using the chemistry established (see Chapter 2) earlier for the synthesis of **3.2** was an obvious choice. A point of concern with this approach is that each step in a two-directional synthesis is necessarily performed on a bifunctional molecule and this can have a major impact on the yield of each step (compared to the analogous one-directional synthesis). [1.1]Cyclophane **3.3** would be expected to be more strained than **3.2** and the first major question to be answered was whether the contractive annulation strategy is powerful enough to enable the synthesis of **3.3**. If the strategy is powerful enough, **3.3** would join a very small family of [1.1]cyclophanes. [1.1]Paracyclophane **3.7** (Scheme 3.2, inset) was reported by the Tsuji group in 1993, but it lacked sufficient stability for its isolation.<sup>2</sup> Later, the same group reported kinetically stabilized [1.1]paracyclophane derivatives **3.8–3.10**.<sup>3</sup> The larger aromatic systems in **3.3** (naphthalene *vs.* benzene) may result in greater stability than for **3.7**, so the successful synthesis of **3.3** would provide opportunities to study not only its spectroscopic properties, but also its chemical reactivity.



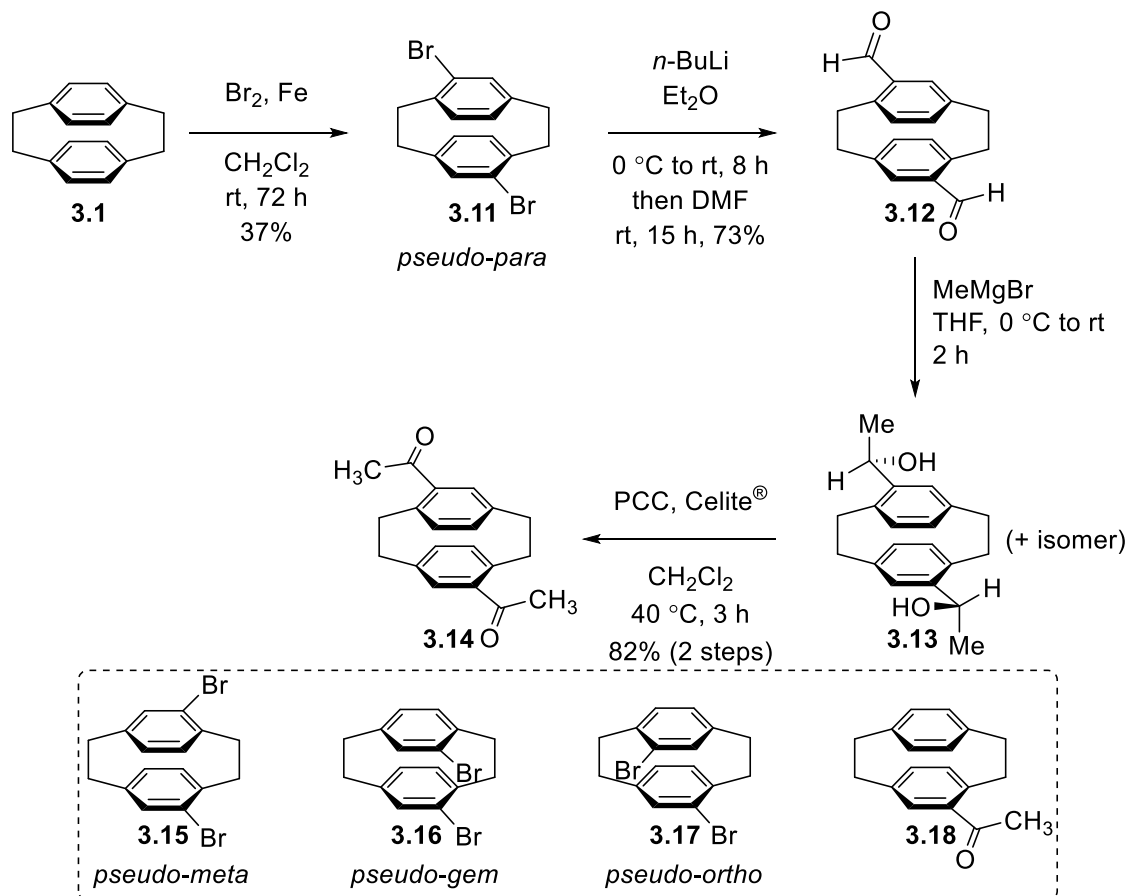
**Scheme 3.2:** Possible products from the double contractive annulation of [2.2]paracyclophane (**3.1**). Inset: selected examples of [1.1]paracyclophanes.

### 3.3 Results and Discussion

#### 3.3.1 Synthesis

The contractive annulation of [2.2]paracyclophane (**3.1**) to access **3.2** commenced with a Friedel-Crafts acylation reaction,<sup>1</sup> so the two-directional synthesis of **3.3** would require access to the *pseudo-para*-diacetyl[2.2]paracyclophane (**3.14**) (Scheme 3.3). The direct synthesis of **3.14** from [2.2]paracyclophane (**3.1**) by the Friedel–Crafts acylation reaction is, however, not a viable process because the first acylation to give 4-acetyl[2.2]paracyclophane (**3.18**) (Scheme 3.3, inset) deactivates the system toward further reaction (see Chapter 1, Section 1.3.3).<sup>4</sup> Hence, adoption of

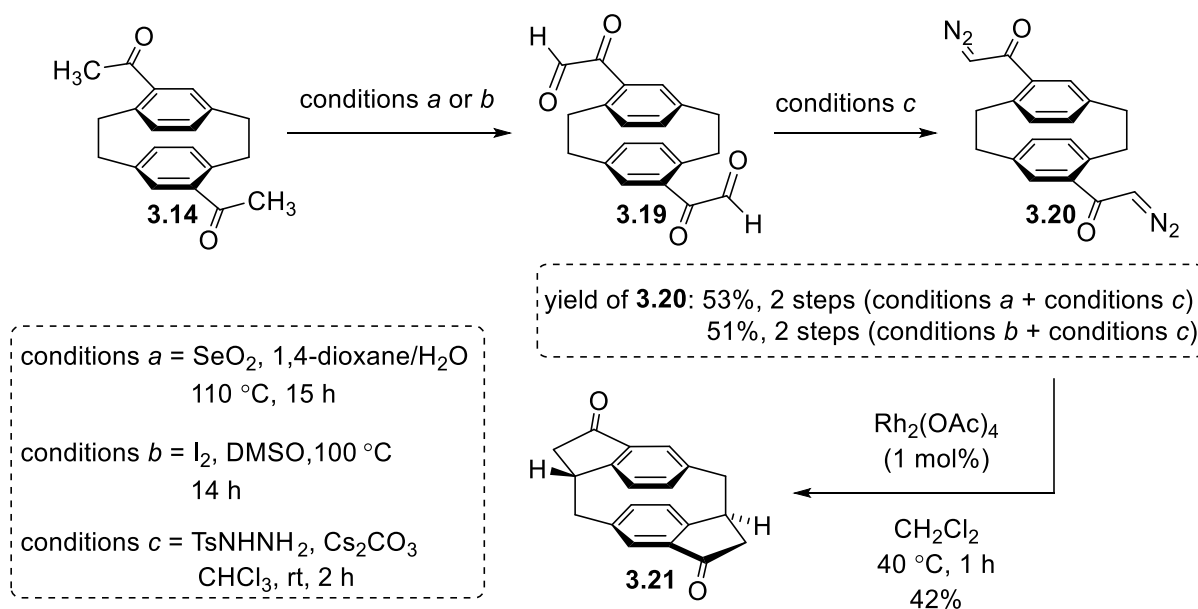
a different, indirect route was required. The most common and practical way for the synthesis of *pseudo-para* disubstituted [2.2]paracyclophane derivatives commences with the bromination of [2.2]paracyclophane (**3.1**) to afford a mixture of all four isomers (**3.11**, **3.15**, **3.16**, and **3.17**) of dibromo[2.2]paracyclophane.<sup>5</sup> The low solubility of **3.11** (*pseudo-para* isomer) in dichloromethane facilitates its isolation and purification from the other isomers. In this regard, [2.2]paracyclophane (**3.1**) was subjected to bromination conditions (2.1 equiv Br<sub>2</sub> and Fe catalyst)<sup>4a</sup> and dibromo[2.2]paracyclophane **3.11** was isolated in 37% yield (Scheme 2). Lithium-halogen exchange of **3.11** followed by quenching of the corresponding dilithiated species with DMF afforded *pseudo-para*-diformyl[2.2]paracyclophane (**3.12**) (73%).<sup>6</sup> A double Grignard reaction of **3.12** with MeMgBr afforded a *ca.* 78:22 mixture of diastereomeric diols. For analytical purposes, the major isomer **3.13** could be isolated in *ca.* 95% purity and its structure was unequivocally established by X-ray crystallographic analysis (see Appendix 2). The major isomer **3.13** is a *meso* compound arising from the attack of MeMgBr from the less hindered faces of **3.12** in the conformation shown. A subsequent PCC-mediated oxidation of **3.13** resulted in the formation of the required diacetyl[2.2]paracyclophane **3.14** (82%, 2 steps), thereby accomplishing the fulfillment of “Stage 1” (see Chapter 2, Section 3.2) of the contractive annulation strategy.



**Scheme 3.3:** 4-Step synthesis of diacetyl[2.2]paracyclophane **3.14** from [2.2]paracyclophane (**3.1**). Inset: structures of dibromo[2.2]paracyclophanes **3.15–3.17**, and 4-acetyl[2.2]paracyclophane (**3.18**).

From this point, the synthetic approach mirrored the one used for the synthesis of **3.2** from **3.18**. Riley oxidation of diacetyl[2.2]paracyclophane **3.14** yielded the corresponding bis(glyoxal) **3.19** presumably with its mono- and dihydrated forms (Scheme 3.4). Treatment of **3.19** with TsNHNH<sub>2</sub> in the presence of Cs<sub>2</sub>CO<sub>3</sub> as base resulted in the formation of the bis(diazoketone) **3.20** (53%, 2 steps; 73% per functional group). Bis(glyoxal) **3.19** was found to have better solubility in THF than in chloroform. Hence, an attempt was made to improve the yield of **3.20** by switching the solvent from chloroform to THF. Nonetheless, the reaction proceeded smoothly providing **3.20**, albeit in lower yield (49%, 2 steps; 70% per functional group). The conversion of **3.14** to **3.19** was also explored under Kornblum oxidation conditions.<sup>7</sup> The use of 3.0 equiv of I<sub>2</sub> (3.0

equiv) and DMSO as solvent (and reagent) resulted in the formation of glyoxal **3.19**, which upon reaction with TsNHNH<sub>2</sub>/Cs<sub>2</sub>CO<sub>3</sub> furnished **3.20** (51%, 2 steps, 71% per functional group). Compound **3.20** was found to be unstable to silica gel chromatography and was found to be poorly soluble in common organic solvents (dichloromethane, chloroform, ethyl acetate, and hexanes). Analytically pure samples of **3.20** could be obtained by trituration of the crude reaction mixture with ice-cold methanol. Having set the stage for the key ring-forming reaction, the bis(diazoketone) **3.20** was subjected to C–H insertion reaction conditions (1 mol% Rh<sub>2</sub>(OAc)<sub>4</sub>, CH<sub>2</sub>Cl<sub>2</sub>, 40 °C) to afford bis(indanone) **3.21** (42%; 65% per functional group).

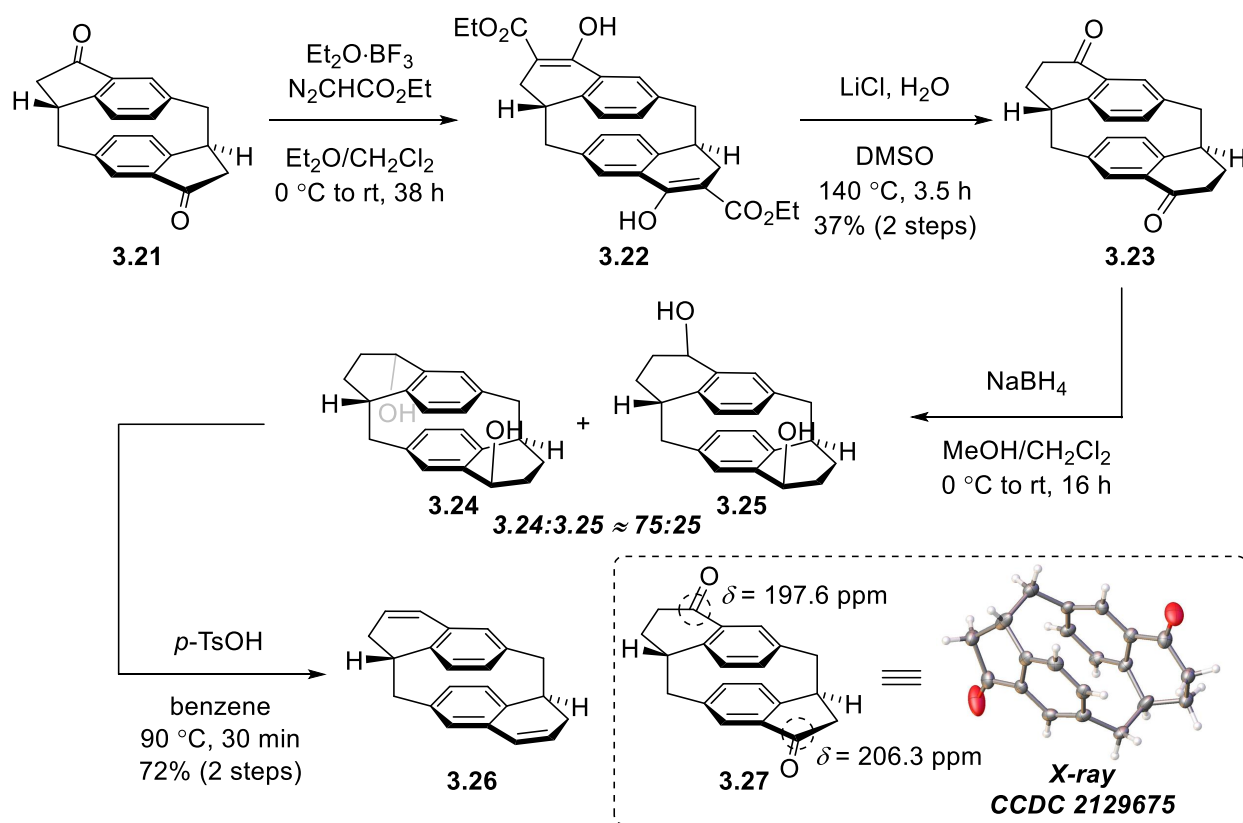


**Scheme 3.4:** Synthesis of the key intermediate **3.21** from diacetyl[2.2]paracyclophane **3.14**.

The newly formed bis(indanone) **3.21** contains two five-membered rings, hence a two-fold ring-expansion reaction was required to prepare for the aromatization stage of the contractive annulation process. The use of Et<sub>2</sub>O (solvent used in the analogous ring expansion reaction<sup>1</sup> in the synthesis of **3.2**) as the sole solvent for the ring-expansion reaction of **3.21** at room temperature or at reflux was found to be fruitless, as no progress of the reaction was evident from TLC analysis. The use of a binary solvent system consisting of Et<sub>2</sub>O/CH<sub>2</sub>Cl<sub>2</sub> (1:1 v/v) for the Büchner–Curtius–

Schlotterbeck reaction was explored. Accordingly, the Büchner–Curtius–Schlotterbeck reaction of **3.21** with ethyl diazoacetate (9.0 equiv) in the presence of Et<sub>2</sub>O·BF<sub>3</sub> (9.0 equiv) in Et<sub>2</sub>O/CH<sub>2</sub>Cl<sub>2</sub> furnished enol ester **3.22** (Scheme 3.5). Subsequent treatment of **3.22** with LiCl under Krapcho dealkoxycarbonylation conditions afforded bis(tetralone) **3.23** (37%, 2 steps; 61% per functional group). No evidence of isomeric tetralones (containing one or two  $\beta$ -tetralone units) was evident in the <sup>1</sup>H NMR spectrum of the crude product. It is important to note that when the ring-expansion reaction was carried out in dichloromethane with 9.0 equiv of each of the reagents, a significant amount of the partial ring-expanded product **3.27** (31%) and trace amounts of **3.23** were obtained over two steps. Increasing the amounts of the reagents (Et<sub>2</sub>O·BF<sub>3</sub>, ethyl diazoacetate) did not improve the 2-step yield of the desired product **3.23**, rather resulted in the formation of more undesired side products. Owing to the presence of a center of inversion in bis(tetralone) **3.23**, the <sup>13</sup>C NMR spectrum features only one signal at  $\delta = 197.8$  ppm for the two carbonyl groups. In contrast, due to the nonsymmetric structure, the <sup>13</sup>C NMR spectrum of diketone **3.27** shows two signals at  $\delta = 197.6$  ppm and  $\delta = 206.3$  ppm for the carbonyl groups of the  $\alpha$ -tetralone and indanone moieties, respectively. The assignments were made based on the known <sup>13</sup>C NMR chemical shifts of the carbonyl groups of the similar [2.2]paracyclophane derivatives with tetralone and indanone moieties.<sup>1</sup> The third element of the contractive annulation strategy was initiated by reduction of **3.23** with NaBH<sub>4</sub> in MeOH/CH<sub>2</sub>Cl<sub>2</sub> (1:2 v/v) to provide a mixture of *meso*-diol **3.24** and its epimer **3.25**. The ratio of the two isomers formed in the reaction could not be obtained from the <sup>1</sup>H NMR analysis of the crude reaction mixture with a high degree of accuracy because of the overlap of most of the peaks of both the isomers. Hence, the diols **3.24** and **3.25** were separated by silica gel column chromatography and based on the isolated yields, the ratio of **3.24** to **3.25** corresponds to *ca.* 75:25. The benzylic protons in *meso*-diol **3.24** appear as a multiplet centered at  $\delta = 4.67$  ppm

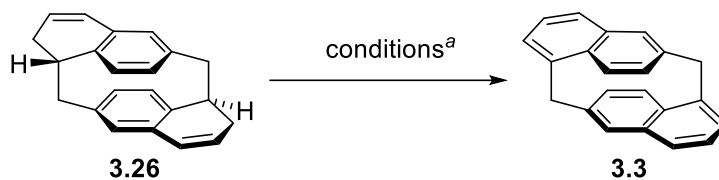
with an integral value corresponding to two protons, whereas the benzylic protons in diol **3.25** appear as a multiplet centered at  $\delta = 4.66$  ppm with an integral value corresponding to one proton and as a doublet at  $\delta = 4.54$  ppm with an integral value corresponding to one proton. The structures of the two diols were further unambiguously determined by X-ray analysis (see Appendix 2). The stereochemical outcome of the reduction was of no consequence as it proved to be more practical to use the crude mixture consisting of **3.24** and **3.25** in the ensuing dehydration reaction. Treatment of the diol mixture with *p*-TsOH afforded bis(dihydronaphthalene) **3.26** (72%, 2 steps; 85% per functional group).



**Scheme 3.5:** Synthesis of bis(dihydronaphthalene) **3.26** from bis(indanone) **3.21** over four steps. Inset: structure of diketone **3.27**.

Finally, dehydrogenation of **3.26** was carried out using DDQ under different conditions. The use of  $\text{K}_2\text{CO}_3$  as additive and halogenated solvents (1,2-DCE and  $\text{CH}_2\text{Cl}_2$ ) led to complete

consumption of the starting material (**3.26**) to afford TLC-immobile material (Table 3.1, Entries 1 and 2). This observation is in line with the incompatibility of the dehydrogenation reaction of [2](6,1)naphthaleno[1]paracyclophane (**3.2**) in halogenated solvents (see Chapter 2, Table 2.2). Changing the solvent to toluene and carrying out the reaction of **3.26** at room temperature failed to promote the dehydrogenation reaction (TLC analysis), and near quantitative recovery of **3.26** was possible after passing the crude reaction mixture through a short pad of silica gel using hexanes as eluent (Table 3.1, Entry 3). Increasing the amount of DDQ to 9.0 equiv and elevating the temperature to 70 °C led to the formation of the desired [1.1]naphthalenophane **3.3** only in trace quantities (Table 3.1, Entry 4). Decreasing the temperature to 40 °C led to the formation of **3.3** in 5% yield (Table 3.1, Entry 5). The yield was further improved to 7% by the portionwise addition of DDQ (Table 3.1, Entry 6). A slight improvement in yield was observed when the reaction was performed on a 0.17 mmol scale (8% yield of **3.3**; 28% per functional group). Changing the oxidant to *o*-chloranil led to the decomposition of **3.26**, producing a complex mixture from which **3.3** could not be isolated/detected (Table 3.1, Entry 7). No apparent reaction was observed when *p*-chloranil was used under different reaction conditions (Table 3.1, Entries 8–10).

**Table 3.1:** Conditions screened for the dehydrogenation of hydrocarbon **3.26**.

| Entry | Conditions  | Yield <sup>b</sup>   |
|-------|---|----------------------|
| 1     | DDQ (4.0 equiv), K <sub>2</sub> CO <sub>3</sub> (2.1 equiv), 1,2-DCE, rt, 16 h  | not detected         |
| 2     | DDQ (4.0 equiv), K <sub>2</sub> CO <sub>3</sub> (2.1 equiv), CH <sub>2</sub> Cl <sub>2</sub> , rt, 16 h                     | not detected         |
| 3     | DDQ (4.0 equiv), K <sub>2</sub> CO <sub>3</sub> (2.1 equiv), toluene, rt, 20 h  | no reaction          |
| 4     | DDQ (9.0 equiv), K <sub>2</sub> CO <sub>3</sub> (2.1 equiv), toluene, 70 °C, 9 h  | trace                |
| 5     | DDQ (9.0 equiv), K <sub>2</sub> CO <sub>3</sub> (2.1 equiv), toluene, 40 °C, 27 h   | 5%                   |
| 6     | DDQ (9.0 equiv) <sup>c</sup> , K <sub>2</sub> CO <sub>3</sub> (2.1 equiv), toluene, 40 °C, 40 h                             | 7% (8%) <sup>d</sup> |
| 7     | <i>o</i> -chloranil (4.0) equiv, toluene, rt, 16 h  | not detected         |
| 8     | <i>p</i> -chloranil (4.0 equiv), 1,2-DCE, rt, 16 h  | no reaction          |
| 9     | <i>p</i> -chloranil (4.0 equiv), 1,2-DCE, 70 °C, 26 h   | no reaction          |
| 10    | <i>p</i> -chloranil (10.0 equiv), toluene, 100 °C, 17 h   | no reaction          |
| 11    | Br <sub>2</sub> (2.4 equiv), CHCl <sub>3</sub> , 0 °C to rt, 16 h; then <i>t</i> -BuOK (6.1 equiv)<br>THF, 0 °C to rt, 13 h | not detected         |

<sup>a</sup>Reaction conditions: **3.26** (0.12 mmol), reagents (as per table), solvent (10 mL). <sup>b</sup>Isolated yields.

<sup>c</sup>Portionwise addition of DDQ. <sup>d</sup>0.17 mmol of **3.26**, solvent (15 mL).

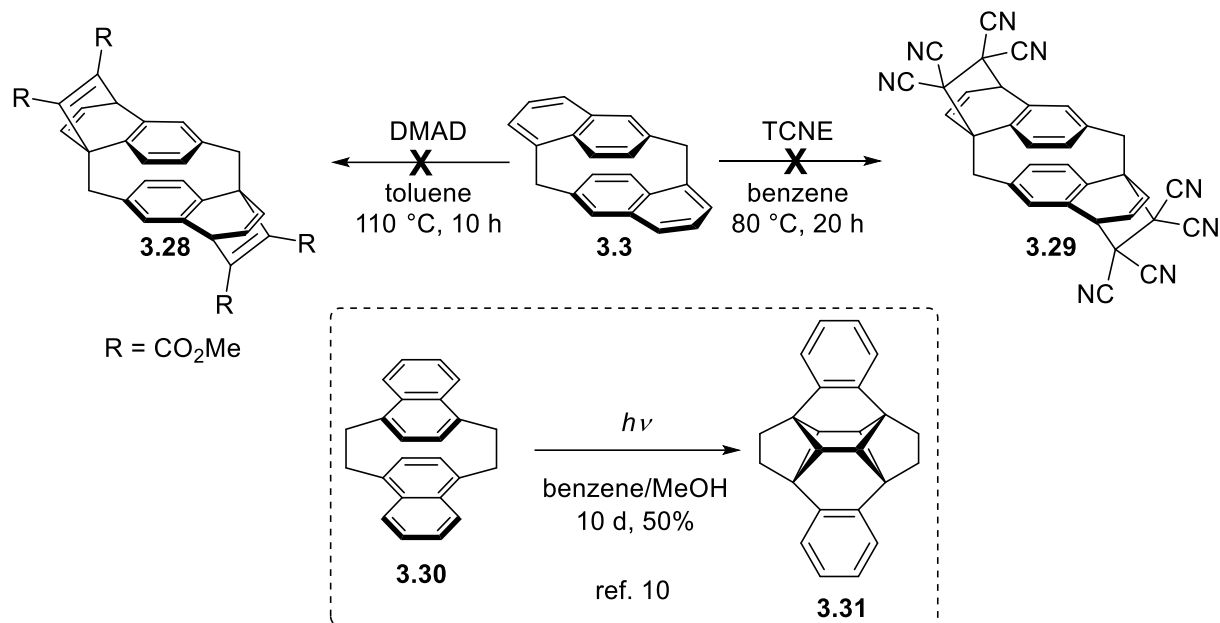
A two-step transformation comprising bromination/elimination reactions was screened with the aim of improving the yield for the dehydrogenation step (Table 3.1, Entry 11). Treatment of **3.26** with Br<sub>2</sub> (2.4 equiv) resulted in an insoluble material. Due to the very poor solubility of the resulting product in common deuterated solvents (CD<sub>2</sub>Cl<sub>2</sub>, CDCl<sub>3</sub>, benzene-*d*<sub>6</sub>, and DMSO-*d*<sub>6</sub>), no <sup>1</sup>H NMR spectrum could be recorded. No conclusion could be made about the identity of the of the insoluble material from high-resolution mass spectrometry (HRMS) analysis.

Nevertheless, assuming the material as the expected two-fold brominated product (bromination of two conjugated olefinic double bonds), it was treated with 4.1 equiv of *t*-BuOK, which was deemed to effect a four-fold elimination of HBr to afford the target **3.3**. As evident from TLC analysis, the reaction generated several spots, none of which correspond to the desired cyclophane **3.3**. The appearance of several spots on TLC plate could be due to the formation of partially eliminated products. Further addition of 2.0 equiv of *t*-BuOK was found to be ineffective to result in the formation of **3.3**. Comparison of the results of the two TLC analyses, one after the addition of 4.1 equiv of *t*-BuOK and another after the addition of an extra 2.0 equiv (total 6.1 equiv) of *t*-BuOK seemed to suggest no apparent changes. As TLC analysis revealed no formation of **3.3**, no efforts to isolate and characterize the products of the bromination/elimination reactions were made.

The use of chlorinated solvents in the reaction (Table 3.1, Entries 1 and 2, *vide supra*) or at any stage during the purification led to a substantial or complete loss of product. Once isolated, [1.1]naphthalenophane **3.3** was found to be stable for at least several months in the solid state and also in solution in chlorinated (dichloromethane and chloroform) and non-chlorinated solvents (hexanes, benzene, and ethyl acetate). The overall yield of the 12-step synthesis of **3.3** from [2.2]paracyclophane (**3.1**) is 0.1%. Since every reaction was a twofold reaction, this corresponds to 3.2% per functional group. For the sake of comparison to the synthesis of [2.1]cyclophane **3.2**, the overall yield of **3.3** from *pseudo-para*-diacetyl[2.2]paracyclophane (**3.14**) is 0.5% (6.8% per functional group). By comparison, the overall yield of **3.2** from 4-acetyl[2.2]paracyclophane (**3.18**) was 5.7%.

The low overall yield of **3.3** meant that only a few mg of material (as much as 7 mg) were isolated per batch. This limited the extent to which the chemistry of **3.3** could be studied. Cycloaddition reactions have been well-documented for distorted aromatic systems,<sup>8</sup> so an attempt

was made to react **3.3** with 5.0 equiv of tetracyanoethylene (TCNE) at room temperature (Scheme 3.6). Surprisingly, no reaction took place under the reaction conditions (TLC and  $^1\text{H}$  NMR analysis). Elevation of the of temperature to 80 °C proved to be fruitless (TLC analysis), providing no traces of Diels–Alder adduct **3.29** or any other cycloaddition products. Both at room temperature and 80 °C, the reaction mixture was deep green in colour, which suggested that a charge-transfer complex had formed. TCNE is known to form deep-colored complexes with aromatic hydrocarbons.<sup>9</sup> An attempted Diels–Alder reaction of **3.3** with 3.5 equiv of a different dienophile, dimethyl acetylenedicarboxylate (DMAD) also met with failure, resulting in no sign of reaction (TLC analysis). Irradiation of a  $\text{CDCl}_3$  solution of **3.3** at 302–312 nm in an NMR tube for 19 h led to no change in the  $^1\text{H}$  NMR spectrum of **3.3**, indicating no observable reaction under the photochemical conditions. In this context, it is worth mentioning that Wasserman and Keehn found *anti*-[2.2](1,4)naphthalenophane (**3.30**) underwent intramolecular cycloaddition to afford cage hydrocarbon **3.31** (50%) under UV irradiation (Scheme 3.6, inset).<sup>10</sup> The unexpectedly defiant behavior of [1.1]naphthalenophane **3.3** toward the above-mentioned dienophiles (TCNE, DMAD), even under heating, and the failure of **3.3** to undergo any reaction under the photochemical conditions speaks to remarkable chemical stability of this strained cyclophane.



**Scheme 3.6:** Attempted cycloaddition of [1.1]naphthalenophane **3.3**. Inset: formation of cage hydrocarbon **3.31** from [2.2]naphthalenophane **3.30** under photochemical conditions.

### 3.3.2 X-Ray Crystallographic Analysis

The structure of **3.3** was confirmed using single crystal X-ray diffraction (XRD) (Figures 3.1, *vide infra*). The naphthalene units are highly twisted,<sup>11</sup> as quantified by the torsion angles C3–C4–C8–C9 [ $-34.1(1)^\circ$ ] and C4–C3–C9–C8 [ $-34.2(1)^\circ$ ]. These values are *ca.*  $1^\circ$  smaller than the corresponding values in [2](6,1)naphthaleno[1]paracyclophane (**3.2**). The aromatic rings that originated from [2.2]paracyclophane (**3.1**) are no longer situated in a perfect face-to-face orientation with an average separation of  $3.09\text{ \AA}$ ,<sup>5</sup> but rather are slipped sideways from one another and forced even closer together. The centroid of the C9–C10 bond lies directly over the centroid of the C6<sup>i</sup>–C7<sup>i</sup>–C8<sup>i</sup>–C9<sup>i</sup>–C10<sup>i</sup>–C11<sup>i</sup> ring (Ring B<sup>i</sup>) beneath it with a distance of  $2.96\text{ \AA}$ . Just considering the directly overlapping portions of the naphthalene systems, the shortest distance between the planes defined by C8–C9–C10–C11 and C8<sup>i</sup>–C9<sup>i</sup>–C10<sup>i</sup>–C(11<sup>i</sup>) is  $2.74\text{ \AA}$ . The bridgehead to bridgehead distance (distance between C8 and C2<sup>i</sup>) in **3.3** is ever shorter ( $2.45\text{ \AA}$ ). It is worth noting that the bridgehead to bridgehead distance and the distance between the two

mean planes defined by the two aromatic rings in [1.1]paracyclophane **3.8** are 2.38 Å (almost 1 Å less than sum of van der Waals radii) and 2.80 Å, respectively.

Local distortions from planarity in small cyclophanes are typically quantified using the angles  $\alpha$  and  $\beta$  and/or their sum (see Chapter 1). For **3.3**, the angles in the vicinity of the C2 bridgehead are  $\alpha = 11.2^\circ$  and  $\beta = 19.3^\circ$  ( $\alpha + \beta = 30.5^\circ$ ). A slightly larger value of  $\alpha = 16.9^\circ$  and a slightly smaller value of  $\beta = 14.9^\circ$  are observed in the vicinity of the C8 bridgehead. However the sum of the values of  $\alpha$  and  $\beta$  ( $\alpha + \beta = 31.8^\circ$ ) at C8 is higher than that in the vicinity of the C2 bridgehead. These values substantially exceed those for **3.1** ( $\alpha = 12.6^\circ$ ,  $\beta = 11.2^\circ$ ,  $\alpha + \beta = 23.8^\circ$ )<sup>12</sup> and significantly exceed those (average values) for **3.2** ( $\alpha = 13.7^\circ$ ,  $\beta = 13.4^\circ$ ,  $\alpha + \beta = 27.1^\circ$ ).<sup>1</sup>

The two bond lengths associated with the methano bridge of **3.3** are 1.536(2) (C1–C2) and 1.537(2) Å (C1–C8<sup>i</sup>). These values are comparable to the bond lengths [1.542(3) and 1.537(3) Å] associated with the methano bridge in **3.2**.<sup>1</sup> The methano bridge (C1) for **3.3** has a compressed bond angle of 105.69(12)°, which is comparable (*ca.* 1° larger) to the bond angle<sup>1</sup> of 104.73(19)° for the analogous methano bridge in **3.2**.

The bond lengths of the naphthalene systems are within normal ranges,<sup>13</sup> except for C6–C7 [1.430(2) Å] and C2–C11 [1.439(2) Å], which are a little longer than the corresponding bonds in naphthalene (1.420 Å).<sup>13</sup> In this regard, it is important to note that the crystal structure of cyclophane **3.2** also reveals similar elongation of the analogous bonds compared to those of naphthalene.<sup>1</sup> In both cases, the stretching of these bonds is presumably a consequence of their location on the bridgehead-to-bridgehead pathway (C8 to C2 in case of **3.3**).

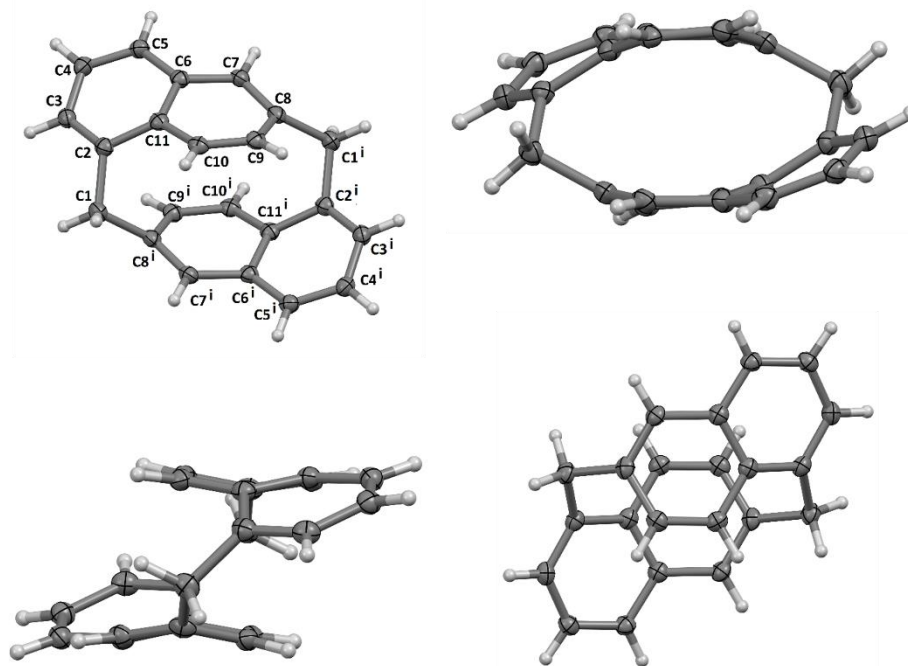


**Figure 3.1:** Four views of the structure of [1.1]naphthalenophane **3.3** with 50% displacement ellipsoids. CCDC 2105261 contains the crystallographic data for **3.3**.

### 3.3.3 Density Functional Theory (DFT) Calculations

The high degree of distortion in the molecular framework of **3.3** translates into a large strain energy (56.6 kcal/mol). By comparison, the strain energies for **3.1** and **3.2** are 25.6 and 44.1 kcal/mol, respectively.<sup>1</sup> Thus, each successive contractive annulation of **3.1** leads to a substantial increase in molecular strain. This is true not only for the total strain energy, but also for the amount of strain per skeletal atom (**3.1**: 1.60 kcal/mol/C; **3.2**: 2.32 kcal/mol/C; **3.3**: 2.57 kcal/mol/C). Molecular electrostatic potential (MEP) analysis suggests repulsion would occur between the electron-rich central regions of naphthalene (Figure 3.2A). More details about these non-covalent interactions can be visualized by the NCI plot based on reduced density gradient (RDG) analysis (Figure 3.2B). There is a RDG isosurface located between the two naphthalene moieties with significant repulsive (red colored) domains near the methylene linkages.

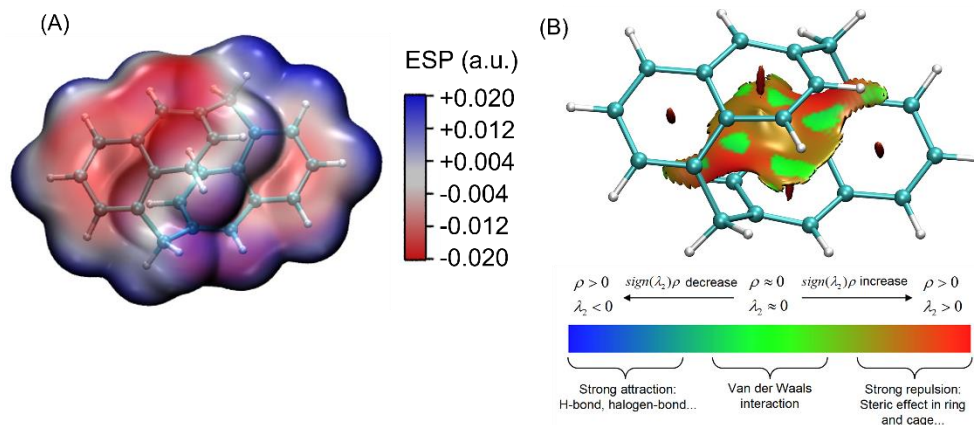


**Figure 3.2:** (A) MEP map of **3.3**. (B) Non-covalent interaction (NCI) plot of **3.3** (isovalue = 0.50 a.u.). Calculations were performed at the M06-2x/Def2SVP level of theory.

To assess the degree of aromaticity of the individual rings of the naphthalene unit in [1.1]naphthalenophane **3.3**, NICS(-1), NICS(0), and NICS(1) calculations were performed on **3.3** (Figure 3.3, Table 3.2, *vide infra*). For NICS(0) calculations, the dummy atom was placed at the centroid of the individual benzene rings. For NICS(-1) calculations, the dummy atom was placed at a distance of 1 Å toward the interior of the cyclophane from the centroid of each individual benzene ring in the naphthalene unit. Conversely, for NICS(1), the dummy atom was placed at a distance of 1 Å toward the exterior of the naphthalene unit from the centroid of each individual benzene ring in the naphthalene unit. For comparison purposes, NICS calculations were also performed on planar 1,6-dimethylnaphthalene (**3.32**) and distorted 1,6-dimethylnaphthalene **3.33**, the geometry of which comes from the deletion of one of the naphthalene units in **3.3** and the addition of H atoms to the dangling bonds of the methylene bridges. Due to its planar structure, the NICS(1) and NICS(-1) values for **3.32** are equivalent.

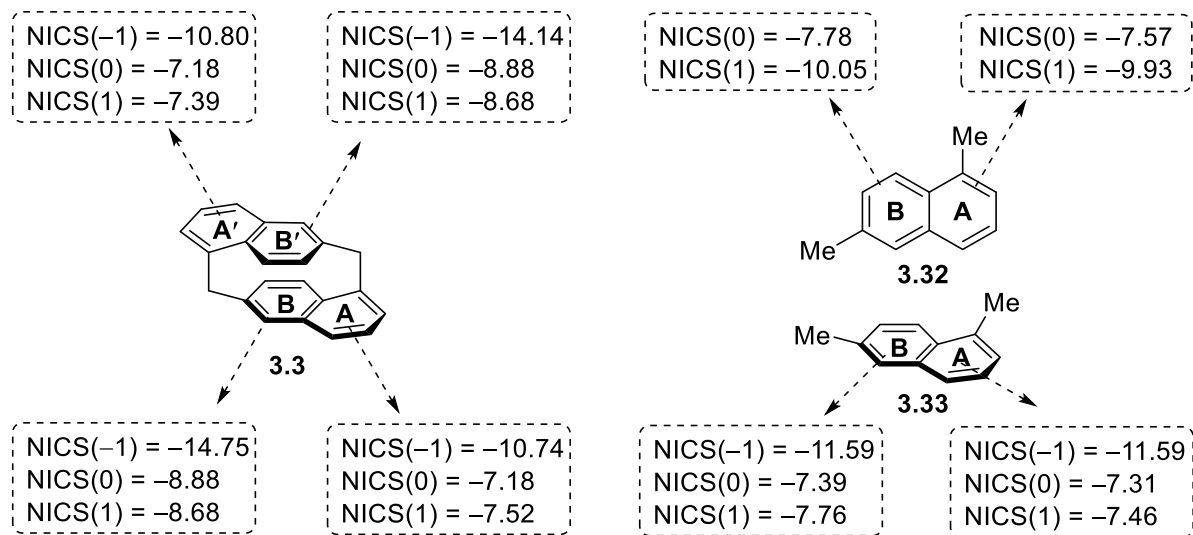


**Figure 3.3:** DFT-calculated NICS values for the naphthalene units in **3.3**, **3.32**, and **3.33**.

The analysis starts with compound **3.32**, for which the two different rings would be expected to exhibit essentially the same NICS values. In line with this expectation, both the NICS(1) and NICS(0) values of the B ring are only slightly more negative than those of the A ring ( $\Delta\text{NICS} = -0.12$  and  $-0.21$ , respectively) (Figure 3.3, Table 3.2). Moving to [1.1]naphthalenophane **3.3**, it can be seen that the values for the A and B rings now differ substantially. The NICS(1), NICS(0) and NICS(-1) values of the B ring are now substantially more negative than those of the A ring ( $\Delta\text{NICS} = -1.24$ ,  $-1.70$  and  $-3.68$ , respectively). The increasing magnitude of this difference in moving from the exterior of the cyclophane to the interior indicates a strong magnetic effect of one naphthalene unit on the other. The same conclusion comes from comparing the values for the individual rings in **3.3** and **3.32**. For the A rings, the NICS(1) and NICS(0) values for the A rings in **3.3** are less negative than those in **3.32** ( $\Delta\text{NICS} = 2.41$  and  $0.39$ , respectively), whereas the NICS(-1) value is more negative ( $\Delta\text{NICS} = -0.83$ ). The  $\Delta\text{NICS}$  value becomes substantially more negative upon moving from the exterior of the cyclophane to the interior (range = 3.25 ppm), which is consistent with a shielding effect of

the opposite naphthalene system. For the B rings, the same trend is observed, but it is more pronounced. The  $\Delta$ NICS values for NICS(1), NICS(0) and NICS(-1) are 1.37, -1.10 and -4.40, respectively (range = 5.77 ppm).

Consideration of the NICS values for the nonplanar model compound **3.33** provided a means to evaluate the effects of distorting 1,6-dimethylnaphthalene without any interference from the effects a proximate naphthalene system. For **3.33**, the two different rings have similar NICS(-1), NICS(0), and NICS(1) values with the B ring having slightly more negative values ( $\Delta$ NICS = -0.30, -0.08 and 0.00, respectively) (Table 3.2, *vide infra*). Distortion from planarity has a roughly equal effect on the aromaticity of the A and B rings. A comparison between **3.32** and **3.33** revealed that bending the naphthalene system out of planarity causes a dummy atom on the concave face to experience greater shielding ( $\Delta$ NICS(-1) = -1.56 and -1.64 for the A and B rings, respectively). Conversely, dummy atoms on the convex face experience less shielding ( $\Delta$ NICS(1) = 2.47 and 2.29 for the A and B rings, respectively). This makes intuitive sense and is in line with precedent in other bent aromatic systems. The NICS(0) values also become less negative ( $\Delta$ NICS(0) = 0.26 and 0.39 for the A and B rings, respectively), which may be a reflection of the loss of some aromatic character due to distortion from planarity.

Finally, a comparison of **3.33** to **3.3** provides an estimate of the magnitude of the effect of one naphthalene system on the other. For the A ring, the change in going from **3.33** to **3.3** is minimal for NICS(1) ( $\Delta$ NICS = 0.00) and NICS(0) ( $\Delta$ NICS = +0.13), while there is a significant deshielding for NICS(-1) ( $\Delta$ NICS = +0.82) (Table 3.2, *vide infra*). Conversely, the NICS values for the B ring become progressively more negative upon moving from the convex face of the concave face ( $\Delta$ NICS(1) = -0.92,  $\Delta$ NICS(0) = -1.49,  $\Delta$ NICS(-1) = -2.86). Greater shielding is experienced by the dummy atom as it moves toward the opposite naphthalene system.

**Table 3.2:** Comparison of the NICS values for compounds **3.3**, **3.32**, and **3.33**.

| NICS              | Compound 3.32 |        | Compound 3.33 |        | Compound 3.3        |                     |
|-------------------|---------------|--------|---------------|--------|---------------------|---------------------|
|                   | Ring A        | Ring B | Ring A        | Ring B | Ring A <sup>a</sup> | Ring B <sup>a</sup> |
| NICS(1)           | -9.93         | -10.05 | -7.46         | -7.76  | -7.46               | -8.68               |
| NICS(0)           | -7.57         | -7.78  | -7.32         | -7.39  | -7.18               | -8.88               |
| NICS(-1)          | -9.93         | -10.05 | -11.59        | -11.59 | -10.77              | -14.45              |
| $\Delta$ NICS(1)  | —             | —      | +2.47         | +2.29  | +2.47<br>+0.00      | +1.37<br>-0.92      |
| $\Delta$ NICS(0)  | —             | —      | +0.26         | +0.39  | +0.39<br>+0.13      | -1.10<br>-1.49      |
| $\Delta$ NICS(-1) | —             | —      | -1.66         | -1.54  | -0.84<br>+0.82      | -4.40<br>-2.86      |

<sup>a</sup>NICS numbers for **3.3** are averages values. Blue numbers indicate the change relative to **3.32**. Red numbers indicate the change relative to **3.33**.

### 3.3.4 NMR Analysis

The assignments of the proton resonances of **3.3** were corroborated by 1D and 2D NMR (COSY, HSQC, and NOESY) experiments. All the 1D and 2D NMR spectra are shown in Appendix 2 (*vide infra*). A detailed description of how the assignments were made is given below. The numbering of protons in the description indicates that of the protons shown in Figure 3.4 (*vide infra*).

1. Aromatic protons with a coupling constant ( $J$ ) of 1.6 Hz can only be H(7) as none of the other aromatic protons are expected to exhibit solely such a small coupling constant (*meta*-coupling). All other aromatic protons have at least one *ortho*-coupled magnetically non-equivalent hydrogen to them. Hence, the signal at  $\delta = 7.48$  ppm is attributed to H(7).
2. H(7) exhibits a NOESY correlation with the bridge proton appearing at  $\delta = 4.19$  ppm. As H(7) is closer to H(1A) than H(1B) in space, the signal at  $\delta = 4.19$  ppm is attributed to H(1A).

- The other bridge proton appearing at  $\delta = 3.96$  ppm is attributed to H(1B), which exhibits a NOESY correlation with the signal at  $\delta = 4.88$  ppm. This signal at  $\delta = 4.88$  ppm also shows a weak COSY correlation with H(7). Hence, the signal at  $\delta = 4.88$  ppm is attributed to H(9).
- A strong COSY correlation can be observed between H(9) and the signal at  $\delta = 6.24$  ppm. Hence the signal at  $\delta = 6.24$  ppm is attributed to H(10).
- The left half of the multiplet at  $\delta = 7.20$ – $7.13$  ppm shows NOESY correlations between both the bridge protons. Hence the left half of the multiplet is attributed to H(3).
- H(7) exhibits a NOESY correlation with the multiplet at  $\delta = 7.40$ – $7.35$  ppm. Hence this multiplet is attributed to H(5).
- The only other proton that is left is H(4), which is attributed to the right half of the multiplet at  $\delta = 7.20$ – $7.13$  ppm.

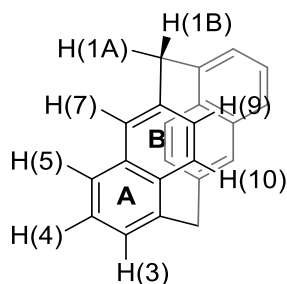


**Figure 3.4:** Numbering of the protons in [1.1]naphthalenophane **3.3**.

The  $^1\text{H}$  NMR spectrum of  $C_i$  symmetric **3.3** consists of just eight signals (Figure 3.5). The slipped stacking juxtaposition of the two naphthalene systems places H(9) and (H10) in the shielding zone of the opposite deck, especially the former. Consequently, H(9) gives rise to the highest field aromatic signal ( $\delta 4.88$  ppm). This resonance is at slightly higher field than the highest field aromatic signal in **3.2** ( $\delta 4.97$  ppm), but the shielding effect is actually more substantial in **3.3**. For **3.2**, the proton in question is part of a benzene system while H(9) in **3.3** is

part of a naphthalene system. Using *p*-xylene ( $\delta$  7.07 ppm) (see Appendix 2 for the  $^1\text{H}$  NMR spectrum) and 1,6-dimethylnaphthalene (**3.32**) ( $\delta$  7.38 ppm) (see Appendix 2 for the  $^1\text{H}$  NMR and COSY NMR spectra) as comparison compounds, the  $\Delta\delta$  values for the highest field aromatic protons in **3.2** and **3.3** are 2.10 and 2.50 ppm, respectively.

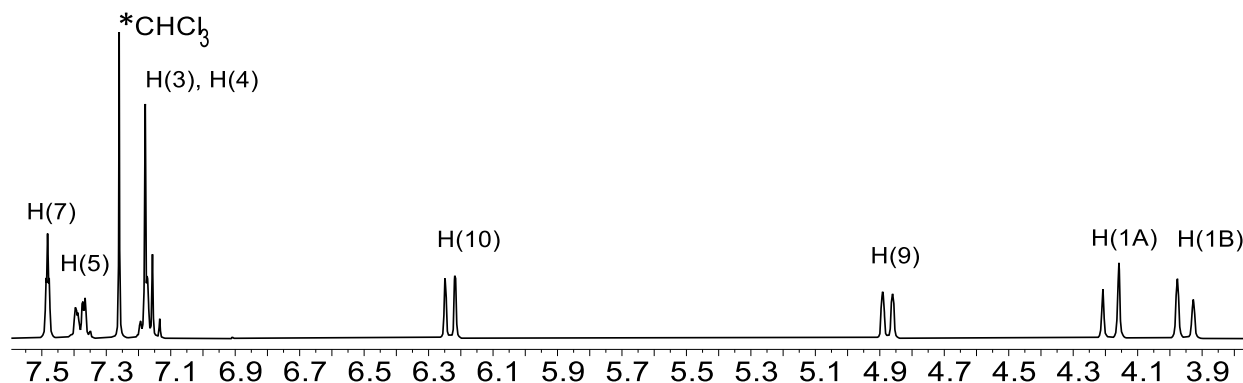


**Figure 3.5:** 300 MHz  $^1\text{H}$  NMR spectrum of **3.3** in  $\text{CDCl}_3$ .

### 3.3.5 UV/Vis Absorption and Fluorescence Spectroscopy

The UV/vis absorption spectra of **3.3** were measured in various organic media, ranging from nonpolar to polar solvents (see Appendix 2, Figure A2-7). The results indicate little solvatochromic effects, which is consistent with the nonpolar ( $\mu = 0$  Debye) and rigid molecular structure of **3.3**. The UV/vis absorption spectrum of **3.3** in cyclohexane is shown in Figure 3.6A. The spectrum features peaks at 236, 261, and 307 nm. TD-DFT analysis indicates that the  $S_0 \rightarrow S_1$  (*i.e.*, HOMO to LUMO) transition occurs at 369 nm, but it is symmetry forbidden and hence not experimentally observed. A transition band at 335 nm (HOMO-1 to LUMO) is predicted by TD-DFT, which accounts for the broad tail in the UV/vis spectrum. The absorption spectrum of **3.3** in cyclohexane was measured at varying concentrations (see Appendix 2, Figure A2-8). All spectra exhibit similar line shapes. The absorbance of **3.3** was found to disobey the Beer-Lambert

law above the concentration of  $ca. 10^{-4}$  M (Appendix 2, Figure A2-9), suggesting the occurrence of aggregation in solution.

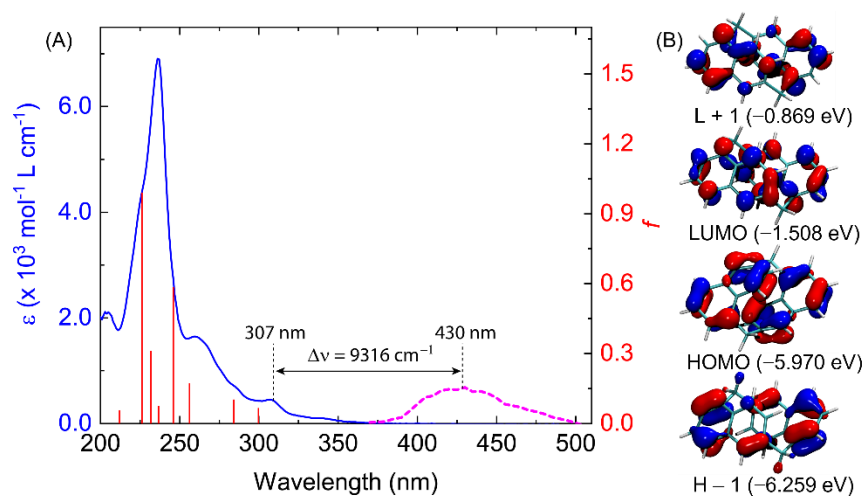


**Figure 3.6:** (A) UV/vis absorption and fluorescence ( $\lambda_{\text{exc}} = 350$  nm,  $\Phi_{\text{F}} = 0.033$ ) spectra of **3.3** measured in cyclohexane. TD-DFT simulated UV/vis spectrum (red color bar graph) calculated at the M06/Def2-TZVPP level (cyclohexane). (B) Contour plots for FMOs of **3.3** calculated at M06-2X/Def2SVP level.

The fluorescence spectra of **3.3** in various solvents also show insignificant solvent effects (see Appendix 2, Figure A2-10). It is noteworthy that the maximum emission peak (e.g.,  $\lambda_{\text{em}} = 430$  nm in cyclohexane) appears to be considerably redshifted compared to typical naphthalene monomer emission<sup>14</sup> ( $\lambda_{\text{em}} = 324$  nm in cyclohexane) and naphthalene excimer emission ( $\lambda_{\text{em}} = 391$  nm in *n*-heptane)<sup>15</sup> by  $ca. 106$  nm and  $39$  nm, respectively (Figure 3.6A, *vide supra*). The emission behavior of **3.3** can be attributed to an excimer mechanism based on the observed large Stokes shift of  $9316 \text{ cm}^{-1}$ . Since no naphthalene monomer emission bands are observed at a concentration of  $ca. 10^{-4}$  M, the excimer is believed to be solely formed *via* an intramolecular approach. The X-ray structure of **3.3** clearly shows that the two naphthalene units are in a close distance and their surfaces eclipse to a significant degree. This molecular geometry favors the intramolecular excimer formation. Such instances of the formation of intramolecular excimers [*m.n*]naphthalenophanes ( $m \leq 4$ ,  $n \leq 4$ ) were previously documented in the literature.<sup>16</sup>

### 3.3.6 Cyclic Voltammetry

The electrochemical redox properties of 1,6-dimethylnaphthalene (**3.32**) and [1.1]naphthalenophane (**3.3**) were studied by cyclic voltammetry (CV) (Figure 3.7). Both compounds exhibit irreversible CV behavior in the positive potential window. Compound **3.3** shows an anodic peak at 1.74 V, which is 0.20 V lower than that of compound **3.32** ( $E_{pa} = 1.94$  V). These results indicate that compound **3.3** is easier to oxidize than compound **3.32**. The onset oxidation potentials ( $E_{\text{onset}}^{\text{ox}}$ ) show a difference of 0.11 V. Onset potentials can be correlated with the DFT-calculated HOMO energies.<sup>17</sup> From the onset potential values, the HOMOs of **3.3** and **3.32** were calculated to be  $-5.97$  and  $-6.08$  eV, respectively. This is in line with DFT calculations, which estimated the energy of the HOMOs as  $-5.97$  and  $-6.10$  eV for **3.3** and **3.32**, respectively (see Figure 3.6B for HOMO of **3.3**).

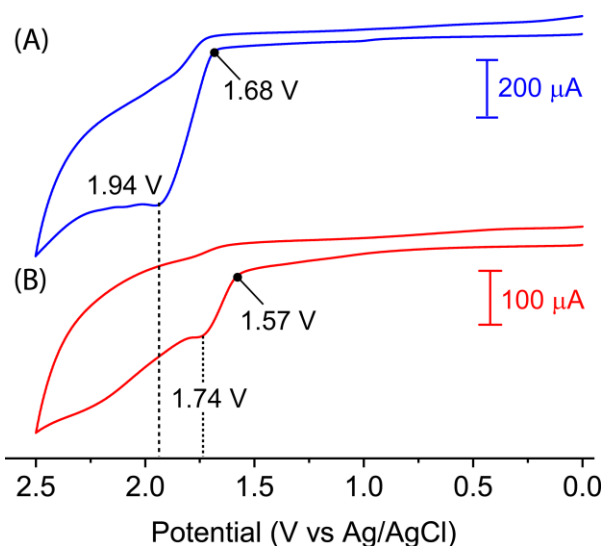


**Figure 3.7:** Cyclic voltammograms of (A) 1,6-dimethylnaphthalene (**3.32**) and (B) [1.1]naphthalenophane **3.3** measured in CH<sub>3</sub>CN. Experimental conditions: electrolyte: *n*-Bu<sub>4</sub>NBF<sub>4</sub>, 0.1 M, working electrode: glassy carbon, reference electrode: Ag/AgCl, counter electrode: Pt wire. Scan rate = 0.5 V/s.

### 3.4 Conclusions

The synthesis of the first [1.1]naphthalenophane (**3.3**) by double contractive annulation demonstrates the power and efficacy of the contractive annulation strategy and provides reason for optimism that this strategy would allow access to other structurally unusual aromatic systems. The overall yield for the 12-step synthesis of **3.3** from commercially available [2.2]paracyclophane (**3.1**) is 0.1% (3.2% per functional group). In terms of yield, the synthetic route (from **3.1** to **3.3**) suffered mostly from the low-yielding last step (aromatization). The main challenge here is to develop superior aromatization methods. As revealed by the crystal structure, the two naphthalene units in **3.3** are forced very close to one another. Preliminary attempted cycloaddition reactions illustrates surprising, yet remarkable stability of the [1.1]naphthalenophane **3.3**. A detailed investigation of the chemical behavior of **3.3** will have to await the synthesis of large quantities of **3.3**. The emission behavior of **3.3** is attributed to the emission of the intramolecularly formed excimers.

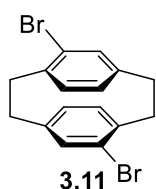
### 3.5 Experimental Section

#### General

Reactions were performed under a balloon containing nitrogen gas unless otherwise indicated. All reactions were performed with oven-dried (120 °C) glassware. All reactions under heating conditions were performed in an oil bath. Dry diethyl ether of ACS grade and used as received. THF, dichloromethane, and toluene used in reactions were dry and obtained from an MBraun solvent purification system (SPS). Commercially available DDQ was recrystallized from benzene prior to use. Solvents were removed from reaction mixtures under reduced pressure using a rotary evaporator. Chromatographic separations were achieved using Silicycle silica gel 60, particle size of 40–63 µm. Column dimensions are recorded as height × diameter. Thin-layer chromatography (TLC) was performed using precoated plastic-backed POLYGRAM® SIL G/UV254 silica gel plates with a layer thickness of 200 µm. Compounds on TLC plates were visualized using a UV lamp (254 and 365 nm) or cerium molybdate stain (Hanessian's stain). Melting points were recorded using an OptiMelt automated or a MEL-TEMP II melting point instrument and are uncorrected. Infrared (IR) spectra were recorded using neat samples on a Bruker Alpha spectrometer. <sup>1</sup>H and <sup>13</sup>C NMR spectra were recorded on Bruker AVANCE spectrometers at 300 MHz or 500 MHz and 75 MHz, respectively. Chemical shifts of the NMR spectra are reported relative to the residual solvent peak (CDCl<sub>3</sub>: 7.26 ppm for <sup>1</sup>H NMR, 77.16 ppm for <sup>13</sup>C NMR). High resolution mass spectrometry (HRMS) data were obtained using an Agilent 6200 series instrument, employing a TOF mass analyzer. UV/vis absorption spectra were recorded on a Varian Cary 6000i spectrophotometer. The Fluorescence spectrum was measured on a Photon Technology International (PTI) QuantaMaster spectrofluorometer. Commercially available [2.2]paracyclophane (**3.1**) was used as received. Cyclic voltammetric (CV) analysis was carried

out in a standard three electrode setup. A glassy carbon electrode was used as the working electrode, a Pt wire was used as the counter electrode, and Ag/AgCl was used as the reference electrode. The experiments were controlled by a BASi Epsilon potentiostat. Samples were first dissolved in acetonitrile together with *n*-Bu<sub>4</sub>BF<sub>4</sub> (0.1 M) as the electrolyte and then subjected to measurements.

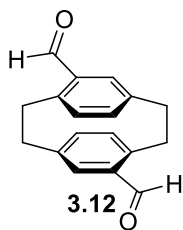
#### 4,16-Dibromo[2.2]paracyclophane (**3.11**)<sup>4a</sup>



A solution of bromine (1.80 mL, 35.1 mmol) in dichloromethane (15 mL) was added dropwise to a stirred room temperature suspension of iron filings (270 mg, 4.8 mmol) in dichloromethane (30 mL). After stirring for 1 h at room temperature, the reaction mixture was diluted with dichloromethane (100 mL) and [2.2]paracyclophane (**3.1**) (20.00 g, 96.01 mmol) was added. After stirring the mixture for 30 min, a solution of bromine (8.50 mL, 166 mmol) in dichloromethane (70 mL) was added dropwise over 4 h and then the reaction mixture was stirred for 72 h during which a precipitate was formed. The reaction mixture was cooled to 0 °C (ice/water) for 20 min. The precipitate was isolated by suction filtration and washed with cold dichloromethane (50 mL). The filtrate was concentrated under reduced pressure and dichloromethane (50 mL) was added to precipitate the rest of the product, isolated by suction filtration, and washed the precipitate with ice-cold dichloromethane (10 mL). The combined precipitate was air-dried and recrystallized from toluene to afford **3.11** (12.90 g, 37%) as an off-white fluffy solid.  $R_f = 0.48$  (1% ethyl acetate/hexanes); mp 251–252 °C (lit. mp<sup>4a</sup> 249 °C); <sup>1</sup>H NMR (300 MHz, CDCl<sub>3</sub>)  $\delta$  7.15 (dd,  $J = 7.8, 1.8$  Hz, 2H), 6.52 (d,  $J = 1.7$  Hz, 2H), 6.44 (d,  $J = 7.8$  Hz, 2H), 3.50 (ddd,  $J = 12.5, 10.4, 2.1$  Hz, 2H), 3.16 (ddd,  $J = 13.6, 9.1, 3.4$  Hz, 2H), 2.99–2.80 (m, 4H); <sup>13</sup>C NMR (75 MHz, CDCl<sub>3</sub>)  $\delta$  141.3, 138.7, 137.5, 134.3, 128.4, 126.9, 35.5, 33.0;

IR  $\nu$  2951 (w), 2935 (w), 2852 (w), 1583 (w), 1535 (w), 1475 (w), 1391 (w), 1189 (w), 1029 (s), 898 (m), 831 (m), 703 (s), 669 (m)  $\text{cm}^{-1}$ ; HRMS [APPI-(+)] calcd for  $\text{C}_{16}\text{H}_{14}^{79}\text{Br}^{81}\text{Br}$   $[\text{M}+\text{H}]^+$  365.9442, found 365.9423. ; HRMS [APPI-(+)] calcd for  $\text{C}_{16}\text{H}_{14}^{79}\text{Br}_2$   $[\text{M}+\text{H}]^+$  363.9462, found 363.9439.

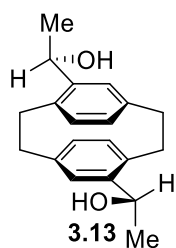
#### 4,16-Diformyl[2.2]paracyclophane (**3.12**)<sup>6</sup>



A 1.50 M solution of *n*-butyllithium (54.6 mL, 81.9 mmol) in hexanes was added dropwise using a dropping funnel to a stirred 0 °C (ice/water) suspension of **3.11** (5.00 g, 13.7 mmol) in dry diethyl ether (300 mL). The reaction mixture was allowed to warm up to room temperature and then stirred at room temperature for 8 h. Then the reaction mixture was cooled to 0 °C (ice/water) and dry dimethylformamide (20.0 mL, 258 mmol) was added dropwise using the funnel. The reaction mixture was again allowed to warm up to room temperature and stirred for 15 h. The reaction mixture was cooled to 0 °C (ice/water). A 6 M aqueous solution of HCl (15 mL) was added to the reaction mixture at 0 °C (ice/water) and the resulting mixture was warmed to room temperature and stirred for 1 h. The majority of the solvent was evaporated, and the reaction mixture was diluted with dichloromethane (150 mL) and water (100 mL) and the layers were separated. The aqueous layer was extracted with dichloromethane (100 mL) and the combined organic layers were washed with saturated sodium bicarbonate solution (150 mL), washed with water (2 × 100 mL), dried over  $\text{Na}_2\text{SO}_4$ , filtered, and concentrated under reduced pressure. The residue was recrystallized from toluene to afford **3.12** (2.64 g, 73%) as a white crystalline solid.  $R_f = 0.58$  (40% ethyl acetate/hexanes); mp 235–238 °C (dec.) (lit. mp<sup>6</sup> 240 °C (dec.));  $^1\text{H NMR}$  (300 MHz,  $\text{CDCl}_3$ )  $\delta$  9.94 (s, 2H), 7.05 (d,  $J = 2.0$  Hz, 2H), 6.63 (dd,  $J = 7.8, 2.0$  Hz, 2H), 6.52 (d,  $J = 7.8$  Hz, 2H), 4.13 (ddd,  $J = 12.9, 10.3, 2.6$  Hz, 2H), 3.29 (ddd,  $J = 13.2, 10.6, 2.5$  Hz, 2H), 3.15 (ddd,  $J = 14.6, 8.8, 4.4$  Hz, 2H), 3.01

(ddd,  $J = 14.8, 9.0, 4.1$  Hz, 2H);  $^{13}\text{C}$  NMR (75 MHz,  $\text{CDCl}_3$ )  $\delta$  192.1, 143.1, 140.7, 137.1, 136.9, 136.7, 135.4, 34.5, 32.9; IR  $\nu$  2931 (w), 2856 (w), 2751 (w), 1673 (s), 1588 (w), 1550 (w), 1225 (w), 1139 (w), 974 (w), 791 (w), 753 (w), 722 (w)  $\text{cm}^{-1}$ ; HRMS [APPI-(+)] calcd for  $\text{C}_{18}\text{H}_{16}\text{O}_2$   $[\text{M}]^+$  264.1150, found 264.1149.

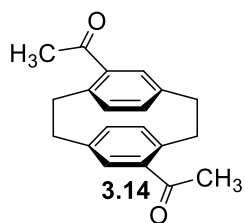
#### 4,16-Bis(hydroxyethyl)[2.2]paracyclophane (**3.13**)



A 2.40 M solution of methylmagnesium bromide (15.7 mL, 37.7 mmol) in diethyl ether was added dropwise to a stirred 0 °C (ice/water) suspension of **3.12** (2.50 g, 9.46 mmol) in THF (100 mL). The cold bath was removed, and the reaction mixture was stirred for 2 h as it warmed to room temperature. Then the reaction mixture was cooled to 0 °C (ice/water) and saturated  $\text{NH}_4\text{Cl}$  solution (50 mL) was added and stirred for 5 min. The majority of the solvent was evaporated under reduced pressure and the reaction mixture was diluted with ethyl acetate (100 mL) and water (100 mL). The layers were separated, and the aqueous layer was extracted with ethyl acetate ( $2 \times 100$  mL). The combined organic layers were washed with water (100 mL), saturated  $\text{NaCl}$  solution ( $2 \times 100$  mL), dried over  $\text{Na}_2\text{SO}_4$ , filtered, and concentrated under reduced pressure to afford a *ca.* 3.6:1 mixture ( $^1\text{H}$  NMR analysis) of diastereomeric diols (2.64 g, 94%) as a white solid. A nearly pure sample (*ca.* 95% by  $^1\text{H}$  NMR) of the major isomer **3.13** was obtained by preparative thin layer chromatography (PTLC, 50% ethyl acetate/hexanes as eluent) followed by crystallization from dichloromethane/pentane (1:2 v/v) in a refrigerator (4 °C). The other isomer could not be obtained in pure form. Major isomer (**3.13**):  $R_f = 0.51$  (50% ethyl acetate/hexanes); mp 217–220 °C;  $^1\text{H}$  NMR (300 MHz,  $\text{CDCl}_3$ )  $\delta$  6.62–6.58 (m, 4H), 6.38 (d,  $J = 7.5$  Hz, 2H), 4.95 (qd,  $J = 6.3, 3.9$  Hz, 2H), 3.32 (ddd,  $J = 13.4, 9.8, 2.6$  Hz, 2H), 3.20–3.02 (m, 4H), 2.84 (ddd,  $J = 13.5, 10.6, 5.7$  Hz, 2H), 1.76 (d,  $J = 4.0$  Hz, 2H), 1.29 (d,  $J = 6.4$  Hz, 6H);  $^{13}\text{C}$  NMR (75 MHz,  $\text{CDCl}_3$ )  $\delta$  145.5, 140.2, 135.1, 134.2, 128.6,

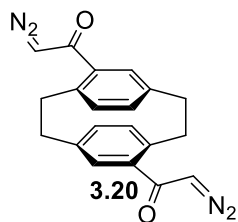
128.4, 68.2, 34.0, 32.9, 25.8; IR  $\nu$  3415 (w), 2973 (m), 2889 (w), 1451 (w), 1252 (m), 1139 (m), 1103 (m), 1056 (s), 893 (s), 732 (w)  $\text{cm}^{-1}$ ; HRMS [APPI-(+)] calcd for  $\text{C}_{20}\text{H}_{21}$   $[\text{M}+\text{H}-2\text{H}_2\text{O}]^+$  261.1643, found 261.1631; HRMS [APPI-(+)] calcd for  $\text{C}_{20}\text{H}_{23}\text{O}$   $[\text{M}+\text{H}-\text{H}_2\text{O}]^+$  279.1749, found 279.1735.

#### 4,16-Diacetyl[2.2]paracyclophane (**3.14**)<sup>4a</sup>



Celite<sup>®</sup> (10.00 g) and pyridinium chlorochromate (9.09 g, 42.2 mmol) were added to a stirred room temperature solution of the mixture of the diastereomeric diols (contains **3.13** as the major isomer) (2.50 g, 8.43 mmol) in dichloromethane (170 mL). The reaction mixture was heated at 40 °C for 3 h. Then the reaction mixture was cooled to room temperature, filtered through a small pad of Celite<sup>®</sup>, washed with dichloromethane (100 mL), concentrated under reduced pressure, and the residue was subjected to column chromatography (10 cm  $\times$  5.5 cm, 80–100% dichloromethane/hexanes) to a white solid, which was further recrystallized from chloroform/hexanes (1:3 v/v) to afford **3.14** (2.14 g, 87%) as white crystals.  $R_f = 0.30$  (dichloromethane); mp 176–178 °C;  $^1\text{H}$  NMR (300 MHz,  $\text{CDCl}_3$ )  $\delta$  6.92 (d,  $J = 1.9$  Hz, 2H), 6.67 (dd,  $J = 7.8, 1.9$  Hz, 2H), 6.39 (d,  $J = 7.8$  Hz, 2H), 3.90 (ddd,  $J = 12.5, 10.3, 2.2$  Hz, 2H), 3.27 (ddd,  $J = 14.5, 8.6, 4.2$  Hz, 2H), 3.12 (ddd,  $J = 12.8, 10.3, 2.3$  Hz, 2H), 2.85 (ddd,  $J = 14.4, 8.5, 4.1$  Hz, 2H), 2.44 (s, 6H);  $^{13}\text{C}$  NMR (75 MHz,  $\text{CDCl}_3$ )  $\delta$  200.9, 140.9, 140.4, 138.2, 135.4, 134.4, 133.8, 35.0, 34.5, 29.0; IR  $\nu$  2928 (w), 1669 (s), 1354 (w), 1261 (m), 736 (w)  $\text{cm}^{-1}$ ; HRMS [APPI-(+)] calcd for  $\text{C}_{20}\text{H}_{21}\text{O}_2$   $[\text{M}+\text{H}]^+$  293.1542, found 293.1541.

### 1,1'-([2.2]paracyclophane-4,16-diyl)bis(2-diazoethanone) (**3.20**)



Compound **3.14** (2.00 g, 6.84 mmol) was added to a stirred 50 °C solution of selenium dioxide (4.55 g, 41.0 mmol) in 1,4-dioxane/water (70 mL, 10:1 v/v). The resulting mixture was then heated at 110 °C for 15 h. Then the reaction mixture was cooled to room temperature, gravity filtered, washed with ethyl acetate (50 mL). The organic layer was dried over Na<sub>2</sub>SO<sub>4</sub>, concentrated under reduced pressure and the residue was subjected to column chromatography (10 cm × 5.5 cm, ethyl acetate) to afford crude glyoxal **3.19** (1.98 g, presumably with hydrated forms) as a yellow sticky solid.  $R_f = 0.57$ – $0.33$  (60% ethyl acetate/hexanes); <sup>1</sup>H NMR (300 MHz, CDCl<sub>3</sub>)  $\delta$  9.63 (s), the remainder of the spectrum is complex; IR  $\nu$  3425 (br, w), 2928 (w), 2858 (w), 1677 (s), 1592 (w), 1550 (w), 1090 (m), 988 (m) cm<sup>-1</sup>; HRMS [ESI-(+)] calcd for C<sub>20</sub>H<sub>17</sub>O<sub>4</sub> [M+H]<sup>+</sup> 321.1127, found 321.1127; HRMS [APPI-(+)] calcd for C<sub>20</sub>H<sub>19</sub>O<sub>5</sub> [M+H<sub>2</sub>O+H]<sup>+</sup> 339.1232, found 339.1258.

Tosyl hydrazide (2.42 g, 12.9 mmol) and cesium carbonate (12.08 g, 37.08 mmol) were added to a stirred room temperature solution of **3.19** (1.98 g, 6.18 mmol based on **3.19**) in chloroform (60 mL). The resulting mixture was stirred for 2 h. Deionized water (50 mL) was added to the reaction mixture and stirred vigorously for 5 min. The two layers were separated, and the aqueous layer was further extracted with chloroform (2 × 50 mL). The combined organic layers were washed with saturated aqueous NaCl solution (2 × 100 mL), dried over Na<sub>2</sub>SO<sub>4</sub>, filtered, and concentrated under reduced pressure. The residue was triturated with ice-cold methanol (3 × 10 mL) to afford **3.20** (1.25 g, 53% over two steps) as a beige solid.  $R_f = 0.49$  (40% ethyl acetate/hexanes); mp 245–248 °C (dec.); <sup>1</sup>H NMR (300 MHz, CDCl<sub>3</sub>)  $\delta$  6.82 (dd,  $J = 7.9, 1.9$  Hz, 2H), 6.70 (d,  $J = 1.9$  Hz, 2H), 6.41 (d,  $J = 7.9$  Hz, 2H), 5.43 (s, 2H), 3.78 (t,  $J = 11.5, 2H$ ), 3.33 (ddd,  $J = 12.7, 10.5, 4.9$  Hz, 2H), 3.10–3.02 (m, 2H), 2.91 (ddd,  $J = 12.5, 10.5, 4.9$  Hz, 2H);

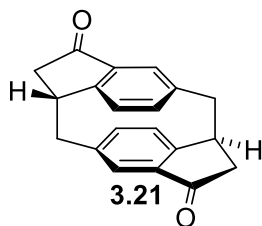
$^{13}\text{C}$  NMR (75 MHz,  $\text{CDCl}_3$ )  $\delta$  189.2, 140.6, 139.6, 136.9, 135.6, 134.8, 131.6, 55.9, 35.1, 34.3; IR  $\nu$  3058 (w), 2940 (w), 2095 (s), 1593 (s), 1533 (w), 1485 (w), 1351 (s), 1243 (w), 1195 (w), 1166 (w), 1017 (m), 820 (w), 729 (w), 668 (w)  $\text{cm}^{-1}$ ; HRMS [APPI-(+)] calcd for  $\text{C}_{20}\text{H}_{17}\text{O}_2$   $[\text{M}+\text{H}-2\text{N}_2]^+$  289.1229, found 289.1235.  $[\text{M}]^+$  or  $[\text{M}+\text{H}]^+$  peak was not observed.

The conversion of **3.14** to **3.19** was also explored under the Kornblum oxidation conditions described below.

$\text{I}_2$  (5.20 g, 20.5 mmol) was added to a stirred room temperature suspension of **3.14** (2.00 g, 6.84 mmol) in DMSO (30 mL). The resulting mixture was heated at 100 °C for 14 h. The reaction mixture was cooled to room temperature and then poured into ice-cold water (100 mL). The mixture was stirred for 5 min after which ethyl acetate (100 mL) was added to the mixture. The two layers were separated and the aqueous layer was extracted with ethyl acetate (3  $\times$  100 mL). The combined organic layers were washed with saturated  $\text{Na}_2\text{S}_2\text{O}_3$  (100 mL), saturated aqueous NaCl solution (2  $\times$  200 mL), dried over  $\text{Na}_2\text{SO}_4$ , filtered, and concentrated under reduced pressure. The residue was subjected to column chromatography (10 cm  $\times$  5.5 cm, ethyl acetate) to afford crude glyoxal **3.19** (1.81 g, presumably with hydrated forms) as a yellow sticky solid.

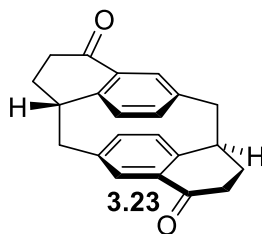
Following the same procedure described above for the conversion of **3.19** to **3.20**, using **3.19** (1.81 g, 5.65 mmol based on **3.19**), tosyl hydrazide (2.10 g, 11.3 mmol), cesium carbonate (11.05 g, 33.90 mmol) and chloroform (55 mL), **3.20** (1.21 g, 51% over 2 steps) was obtained as a beige solid after trituration of the crude residue with ice-cold methanol (3  $\times$  10 mL).

### Bis(indanone) **3.21**



$\text{Rh}_2(\text{OAc})_4$  (0.014 g, 0.032 mmol) was added to a stirred 40 °C solution of **3.20** (1.10 g, 3.19 mmol) in dichloromethane (80 mL). The resulting mixture was stirred at this temperature for 1 h. The solvent was removed under reduced pressure and the residue was directly subjected to column chromatography (12 cm  $\times$  4.5 cm, 0–6% ethyl acetate/dichloromethane) to afford **3.21** (0.386 g, 42%) as an off-white solid.  $R_f = 0.28$  (8% ethyl acetate/ dichloromethane); mp 293–296 °C (dec.);  $^1\text{H}$  NMR (500 MHz,  $\text{CDCl}_3$ )  $\delta$  6.92 (d,  $J = 2.0$  Hz, 2H), 6.75 (dd,  $J = 8.0, 2.1$  Hz, 2H), 6.68 (d,  $J = 8.0$  Hz, 2H), 4.06 (t,  $J = 8.1$  Hz, 2H), 3.37 (dd,  $J = 13.7, 8.7$  Hz, 2H), 3.20 (d,  $J = 13.8$  Hz, 2H), 3.17 (dd,  $J = 18.5, 7.7$  Hz, 2H), 2.62 (d,  $J = 18.5$  Hz, 2H);  $^{13}\text{C}$  NMR (75 MHz,  $\text{CDCl}_3$ )  $\delta$  206.1, 157.4, 141.8, 139.3, 135.5, 130.6, 130.0, 47.3, 45.2, 41.0; IR  $\nu$  2933 (w), 1694 (s), 1596 (w), 1280 (m), 967 (w), 835 (m), 718 (w), 688 (w)  $\text{cm}^{-1}$ ; HRMS [APPI-(+)] calcd for  $\text{C}_{20}\text{H}_{17}\text{O}_2$   $[\text{M}+\text{H}]^+$  289.1229, found 289.1225.

### Bis(tetralone) **3.23**



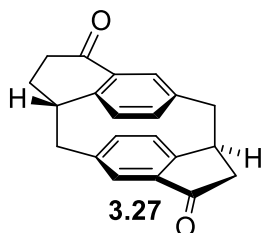
$\text{Et}_2\text{O}\cdot\text{BF}_3$  (1.35 mL, 10.9 mmol) was added to a stirred 0 °C (ice/water) suspension of **3.21** (0.350 g, 1.21 mmol) in diethyl ether (25 mL). The resulting mixture was stirred at this temperature for 5 min, after which dichloromethane (25 mL) was added *via* a cannula to the reaction mixture. Then a solution of ethyl diazoacetate (1.24 g, 10.9 mmol) in diethyl ether/dichloromethane (5 mL) was added dropwise to the mixture at 0 °C (ice/water). The cold bath was removed and the mixture was stirred for 38 h as it warmed to room temperature. An aqueous solution of saturated sodium bicarbonate (10 mL) was added dropwise to the reaction mixture. The solvents were removed under reduced pressure and the residue was diluted with dichloromethane (50 mL) and water (50

mL). The layers were separated, and the aqueous layer was extracted with dichloromethane (2 × 30 mL). The combined organic layers were washed with saturated aqueous NaCl solution (100 mL), dried over Na<sub>2</sub>SO<sub>4</sub>, filtered, and concentrated under reduced pressure. The residue was subjected to column chromatography (12 cm × 4.5 cm, 0–5% ethyl acetate/dichloromethane) to afford **3.22** (0.520 g) as a brown gummy solid. Attempted purification of the enol ester **3.22** failed. The <sup>1</sup>H NMR spectrum is too complex to extract any meaningful information. HRMS [APPI(+)] calcd for C<sub>28</sub>H<sub>29</sub>O<sub>6</sub> [M+H]<sup>+</sup> 461.1964, found 461.1963.

Lithium chloride (0.479 g, 11.3 mmol) and deionized water (0.30 mL, 18 mmol) were added to a stirred room temperature solution of **3.22** (0.520 g, 1.13 mmol based on **3.22**) in dimethyl sulfoxide (15 mL). The resulting mixture was stirred at 140 °C for 3.5 h. The reaction mixture was cooled to room temperature, poured into ice-cold water (50 mL) and stirred for 5 min. Dichloromethane (50 mL) was added to the mixture and the layers were separated. The aqueous layer was extracted with dichloromethane (3 × 30 mL) and the combined organic layers were washed with water (100 mL), washed with saturated aqueous NaCl solution (100 mL), dried over Na<sub>2</sub>SO<sub>4</sub>, filtered, and concentrated under reduced pressure. The residue was subjected to column chromatography (18 cm × 4.5 cm, 4% ethyl acetate/dichloromethane) to afford a yellow solid, which was further triturated with diethyl ether (2 × 2.5 mL) to afford **3.23** (0.142 g, 37% over 2 steps) as an off-white solid. *R*<sub>f</sub> = 0.35 (5% ethyl acetate/dichloromethane); mp 266–268 °C (dec.); <sup>1</sup>H NMR (300 MHz, CDCl<sub>3</sub>) δ 7.23 (d, *J* = 2.1, 2H), 6.67 (dd, *J* = 7.9, 2.1 Hz, 2H), 6.47 (d, *J* = 7.9 Hz, 2H), 3.65–3.58 (m, 2H), 3.47 (dd, *J* = 13.3, 10.7 Hz, 2H), 3.07 (dd, *J* = 13.3, 3.1 Hz, 2H), 3.02–2.91 (m, 2H), 2.79–2.56 (m, 4H), 2.29–2.21 (m, 2H); <sup>13</sup>C NMR (75 MHz, CDCl<sub>3</sub>) δ 197.8, 146.7, 141.1, 136.7, 135.7, 132.3, 132.1, 40.6, 39.8, 34.0, 29.6; IR ν 2929 (w), 2867 (w), 1663 (s),

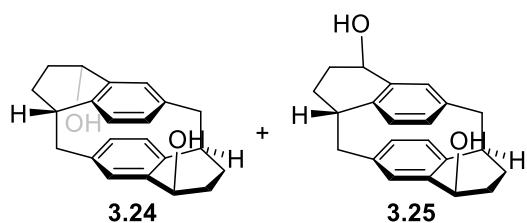
1592 (w), 1254 (m), 1225 (w), 1146 (w), 809 (m), 746 (w)  $\text{cm}^{-1}$ ; HRMS [APPI-(+)] calcd for  $\text{C}_{22}\text{H}_{21}\text{O}_2$   $[\text{M}+\text{H}]^+$  317.1542, found 317.1526.

### Diketone **3.27**



Changing the solvent system from  $\text{Et}_2\text{O}/\text{CH}_2\text{Cl}_2$  to  $\text{CH}_2\text{Cl}_2$  in the above-described Büchner–Curtius–Schlotterbeck reaction (conversion of **3.21** to **3.22**) of **3.21** and following the same procedures described for the Büchner–Curtius–Schlotterbeck and the ensuing Krapcho dealkoxycarbonylation reactions, diketone **3.27** was isolated in 31% yield as a yellow solid by column chromatography (18 cm  $\times$  4.5 cm, 1–3% ethyl acetate/dichloromethane) on the same reaction scale. An analytically pure sample of **3.27** was obtained by recrystallization from  $\text{CH}_2\text{Cl}_2$ /hexanes.  $R_f = 0.39$  (5% ethyl acetate/dichloromethane); mp 251–254  $^\circ\text{C}$  (dec.),  $^1\text{H}$  NMR (300 MHz,  $\text{CDCl}_3$ )  $\delta$  7.17 (d,  $J = 2.1$  Hz, 1H), 6.96 (br s, 1H), 6.77–6.71 (m, 2H), 6.68 (dd,  $J = 8.0, 1.8$  Hz, 1H), 6.44 (d,  $J = 8.0$  Hz, 1H), 4.05 (t,  $J = 7.7$ , 1H), 3.61–3.48 (m, 2H), 3.29–2.94 (m, 5H), 2.76 (dddd,  $J = 18.6, 5.6, 2.0, 0.8$  Hz, 1H), 2.67–2.55 (m, 2H), 2.27 (ddt,  $J = 13.4, 6.2, 2.2$  Hz, 1H);  $^{13}\text{C}$  NMR (75 MHz,  $\text{CDCl}_3$ )  $\delta$  206.3, 197.6, 156.8, 147.4, 142.9, 139.8, 139.6, 138.4, 135.5, 133.5, 133.1, 132.3, 130.3, 128.9, 46.8, 44.6, 41.0, 40.3, 39.8, 33.7, 29.1; IR  $\nu$  2923 (m), 2855 (w), 1704 (s), 1670 (s), 1591 (w), 1402 (w), 1282 (m), 1039 (w), 826 (w), 671 (w)  $\text{cm}^{-1}$ ; HRMS [APPI-(+)] calcd for  $\text{C}_{21}\text{H}_{19}\text{O}_2$   $[\text{M}+\text{H}]^+$  303.1385, found 303.1392.

### Diols **3.24** and **3.25**

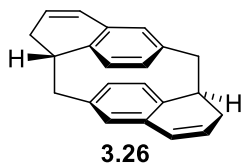


Sodium borohydride (0.053 g, 1.39 mmol) was added to a stirred 0 °C (ice/water) solution of bis(tetralone) **3.23** (0.110 g, 0.348 mmol) in methanol/dichloromethane (9 mL, 2:1 v/v). The cold

bath was removed, and the resulting mixture was stirred for 16 h as it warmed to room temperature. After cooling to 0 °C (ice/water), water (3 mL) was added to the reaction mixture. The majority of the solvent was removed under reduced pressure. The resulting residue was diluted with dichloromethane (30 mL) and water (30 mL). The layers were separated, and the aqueous layer was extracted with dichloromethane (2 × 30 mL). The combined organic layers were washed with saturated aqueous NaCl solution (50 mL), dried over Na<sub>2</sub>SO<sub>4</sub>, filtered, and concentrated under reduced pressure. The residue was subjected to column chromatography (15 cm × 3.0 cm, 15–25% ethyl acetate/dichloromethane) to afford the *meso*-diol **3.24** (0.073 g, 66%) and its epimer **3.25** (0.023 g, 21%) as white solids. Major (*meso*) isomer **3.24**: *R*<sub>f</sub> = 0.57 (30% ethyl acetate/dichloromethane); mp 227–229 °C; <sup>1</sup>H NMR (300 MHz, CDCl<sub>3</sub>) δ 6.79 (d, *J* = 1.9 Hz, 2H), 6.49 (dd, *J* = 7.8, 1.9 Hz, 2H), 6.30 (d, *J* = 7.8 Hz, 2H), 4.70–4.63 (m, 2H), 3.51–3.46 (m, 2H), 3.29 (dd, *J* = 13.2, 10.3 Hz, 2H), 2.92 (dd, *J* = 13.3, 2.4 Hz, 2H), 2.41–2.26 (m, 4H), 2.22–2.13 (m, 2H), 2.05–1.98 (m, 2H), 1.85 (d, *J* = 6.3 Hz, 2H); <sup>13</sup>C NMR (75 MHz, CDCl<sub>3</sub>) δ 140.2, 139.4, 137.7, 133.0, 132.4, 128.4, 69.7, 43.9, 40.6, 29.9, 29.7; IR ν 3321 (br, w), 2919 (m), 2849 (w), 2812 (w), 1454 (w), 1272 (w), 1245 (m), 1042 (s), 900 (m), 813 (m), 675 (m) cm<sup>-1</sup>; HRMS [APPI-(+)] calcd for C<sub>22</sub>H<sub>23</sub>O [M+H-H<sub>2</sub>O]<sup>+</sup> 303.1749, found 303.1760; Minor isomer **3.25**: *R*<sub>f</sub> = 0.35 (30% ethyl acetate/dichloromethane); mp 182–184 °C; <sup>1</sup>H NMR (300 MHz, CDCl<sub>3</sub>) δ 6.78 (d, *J* = 1.5 Hz, 1H), 6.55 (dd, *J* = 7.9, 2.0 Hz, 1H), 6.46 (d, *J* = 2.1 Hz, 1H), 6.44–6.42 (m, 1H), 6.34 (d,

$J = 7.9$  Hz, 1H), 6.22 (d,  $J = 7.8$  Hz, 1H), 4.69–4.62 (m, 1H), 4.54 (dd,  $J = 8.0, 3.9$  Hz, 1H), 3.54–3.43 (m, 2H), 3.29–3.19 (m, 2H), 2.90 (dd,  $J = 13.3, 2.4$  Hz, 2H), 2.52–2.45 (m, 2H), 2.35–2.29 (m, 2H), 2.22–2.13 (m, 1H), 2.05–1.92 (m, 3H), 1.82–1.75 (m, 1H), 1.30 (d,  $J = 5.0$ , 1H);  $^{13}\text{C}$  NMR (75 MHz,  $\text{CDCl}_3$ )  $\delta$  140.4, 140.2, 139.5, 139.1, 138.2, 137.6, 133.7, 133.3, 133.2, 132.8, 130.1, 128.9, 69.7, 69.0, 43.6, 43.0, 40.6, 40.1, 29.9, 29.6, 27.9, 26.8; IR  $\nu$  3350 (br, w), 2924 (w), 2854 (w), 1086 (w), 1034 (m), 898 (m), 823 (w), 715 (w), 677 (w)  $\text{cm}^{-1}$ ; HRMS [APPI-(+)] calcd for  $\text{C}_{22}\text{H}_{23}\text{O}$   $[\text{M}+\text{H}-\text{H}_2\text{O}]^+$  303.1749, found 303.1755.

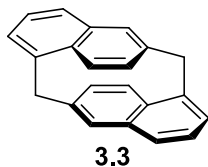
### Bis(dihydronaphthalene) **3.26**



*p*-Toluenesulfonic acid (0.004 g, 0.02 mmol) was added to a stirred room temperature suspension of a mixture of **3.24** (0.063 g, 0.20 mmol) and **3.25** (0.013 g, 0.041 mmol) in benzene (5 mL). The reaction flask was equipped with a Barrett apparatus and the mixture was heated at 90 °C for 30 min. After cooling to room temperature, saturated sodium bicarbonate solution (5 mL) was added to the reaction mixture and stirring was continued for 5 min. The majority of the solvent was evaporated under reduced pressure. The residue was diluted with dichloromethane (30 mL) and water (30 mL). The layers were separated, and the aqueous layer was extracted with dichloromethane (2 × 20 mL) and the combined organic layers were washed with saturated aqueous NaCl solution (50 mL), dried over  $\text{Na}_2\text{SO}_4$ , filtered, and concentrated under reduced pressure. The residue was triturated with diethyl ether (2 × 2 mL) to afford **3.26** (0.056 g, 83%) as a white solid (*Note: Owing to the very poor solubility of 3.26, to avoid a significant loss of the material, hot dichloromethane was used for rinsing the flask where the combined organic layers were dried and for rinsing the funnel used for filtration.*)  $R_f = 0.42$  (8% dichloromethane/hexanes), 0.73 (3% acetone/hexanes); mp 228–230 °C (dec.);  $^1\text{H}$  NMR (300 MHz,  $\text{CDCl}_3$ )  $\delta$  6.92 (dd,  $J = 7.6, 1.9$  Hz, 2H), 6.30 (d,  $J = 7.6$  Hz, 2H), 6.17

(dd,  $J = 9.5, 3.0$  Hz, 2H), 5.95–5.88 (m, 4H), 3.26–3.09 (m, 4H), 2.90–2.80 (m, 4H), 2.46 (ddd,  $J = 17.8, 6.1, 1.6$  Hz, 2H);  $^{13}\text{C}$  NMR (75 MHz,  $\text{CDCl}_3$ )  $\delta$  140.7, 136.2, 135.5, 132.9, 131.2, 129.9, 128.6, 125.5, 42.1, 39.4, 33.6; IR  $\nu$  2920 (w), 1591 (w), 1426 (w), 891 (m), 797 (w), 769 (w), 704 (s)  $\text{cm}^{-1}$ ; HRMS [APPI-(+)] calcd for  $\text{C}_{22}\text{H}_{21}$   $[\text{M}+\text{H}]^+$  285.1643, found 285.1640.

### [1.1]Naphthalenophane 3.3



DDQ (0.1598 g, 0.7040 mmol) and anhydrous  $\text{K}_2\text{CO}_3$  (0.0510 g, 0.369 mmol) were added to a stirred nitrogen-purged room temperature solution of **3.26** (0.0500 g, 0.176 mmol) in toluene (15 mL). The resulting mixture was heated at 40 °C for 20 h after which the reaction mixture was cooled to room temperature and DDQ (0.1199 g, 0.5280 mmol) was added. After stirring the mixture at 40 °C for another 2 h, it was cooled to room temperature and the last portion of DDQ (0.0799 g, 0.352 mmol) was added. The reaction was stirred at 40 °C for another 18 h. The solvent was evaporated under reduced pressure and the residue was subjected directly to column chromatography (11 cm  $\times$  2.0 cm, 15% benzene/hexanes) to afford **3.3** (0.0041 g, 8%) as a white solid (*Note: Chlorinated solvents such as dichloromethane should be avoided during the transfer of the crude reaction mixture. Benzene or toluene is recommended as solvent for this transfer*).  $R_f = 0.53$  (20% benzene/hexanes), 0.65 (3% acetone/hexanes); mp 207–209 °C (dec.);  $^1\text{H}$  NMR (300 MHz,  $\text{CDCl}_3$ )  $\delta$  7.48 (t,  $J = 1.6$  Hz, 2H), 7.40–7.35 (m, 2H), 7.20–7.13 (m, 4H), 6.24 (dd,  $J = 9.2, 0.7$  Hz, 2H), 4.88 (d,  $J = 9.3$  Hz, 2H), 4.19 (d,  $J = 14.8$  Hz, 2H), 3.96 (br d,  $J = 14.8$  Hz, 2H);  $^{13}\text{C}$  NMR (75 MHz,  $\text{CDCl}_3$ )  $\delta$  144.3, 144.2, 135.3, 135.1, 130.1, 129.9, 126.5, 125.7, 125.0, 124.6, 43.7; IR  $\nu$  2957 (w), 2922 (w), 2853 (w), 1462 (w), 1261 (w), 1096 (w), 1019 (w), 801 (w), 764 (w)  $\text{cm}^{-1}$ ; HRMS [APPI-(+)] calcd for  $\text{C}_{22}\text{H}_{16}$   $[\text{M}]^+$  280.1252, found 280.1244.

### 3.6 References

1. Biswas, S.; Qiu, C. S.; Dawe, L. N.; Zhao, Y.; Bodwell, G. J. *Angew. Chem. Int. Ed.* **2019**, *58*, 9166–9170.
2. Tsuji, T.; Ohkita, M.; Konno, T.; Nishida, S. *J. Am. Chem. Soc.* **1997**, *119*, 8425–8431.
3. (a) Kawai, H.; Suzuki, T.; Ohkita, M.; Tsuji, T. *Chem. Eur. J.* **2000**, *6*, 4177–4187. (b) Kawai, H.; Suzuki, T.; Ohkita, M.; Tsuji, T. *Angew. Chem. Int. Ed.* **1998**, *37*, 817–819.
4. (a) Braun, C.; Nieger, M.; Thiel, W. R.; Bräse, S. *Chem. Eur. J.* **2017**, *23*, 15474–15483. (b) Cram, D. J.; Allinger, N. L. *J. Am. Chem. Soc.* **1955**, *77*, 6289–6294.
5. (a) Hassan, Z.; Spuling, E.; Knoll, D. M.; Bräse, S. *Angew. Chem. Int. Ed.* **2020**, *59*, 2156–2170. (b) Hassan, Z.; Spuling, E.; Knoll, D. M.; Lahann, J.; Bräse, S. *Chem. Soc. Rev.* **2018**, *47*, 6947–6963.
6. Delcourt, M.-L.; Felder, S.; Benedetti, E.; Micouin, L. *ACS Catal.* **2018**, *8*, 6612–6616.
7. For a recent review on the application of the Kornblum oxidation of aryl methyl ketones, see: Rajai-Daryasarei, S.; Gohari, M. H.; Mohammadi, N. *New J. Chem.* **2021**, *45*, 20486–20518.
8. (a) Bodwell, G. J.; Fleming, J. J.; Mannion, M. R.; Miller, D. O. *J. Org. Chem.* **2000**, *65*, 5360–5370. (b) Bodwell, G. J.; Bridson, J. N.; Houghton, T. J.; Kennedy, J. W. J.; Mannion, M. R. *Chem. Eur. J.* **1999**, *5*, 1823–1827. (c) Misumi, S. *Pure Appl. Chem.* **1987**, *59*, 1627–1636.
9. Biasutti, M. A.; Silber, J. J. *Can. J. Chem.* **1996**, *74*, 1603–1608.
10. Wasserman, H. H.; Keehn, P. M. *J. Am. Chem. Soc.* **1967**, *89*, 2770–2772.
11. Pascal, R. A., Jr. *Chem. Rev.* **2006**, *106*, 4809–4819.
12. Hope, H.; Bernstein, J.; Trueblood, K. N. *Acta Crystallogr. Sect. B* **1972**, *28*, 1733–1743.

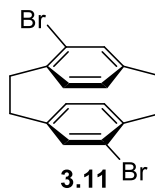
13. From a search of the CCDC, 31 structures of naphthalene were found with  $R1 < 7.5\%$ . Mean values of these 31 structures (see Chapter 2, Appendix 1) were used as the reference bond lengths for naphthalene.
14. Maeda, H.; Maeda, T.; Mizuno, K. *Molecules* **2012**, *17*, 5108–5125.
15. Aladekomo, J. B.; Birks, J. B. *Proc. R. Soc. London, Ser. A* **1965**, *284*, 551–565.
16. (a) Yanagidate, M.; Takayama, K.; Takeuchi, M.; Nishimura, J.; Shizuka, H. *J. Phys. Chem.* **1993**, *97*, 8881–8888. (b) Froines, J. R.; Hagerman, P. J. *Chem. Phys. Lett.* **1969**, *4*, 135–138.
17. The energy of the HOMOs was calculated using the equation:  $E_{\text{HOMO}} = -4.4 - (E_{\text{onset}}^{\text{ox}})$ . For more information, see: de Leeuw, D. M.; Simenon, M. M. J.; Brown, A. R.; Einerhand, R. E. F. *Synth. Met.* **1997**, *87*, 53–59.

## **Appendix 2**

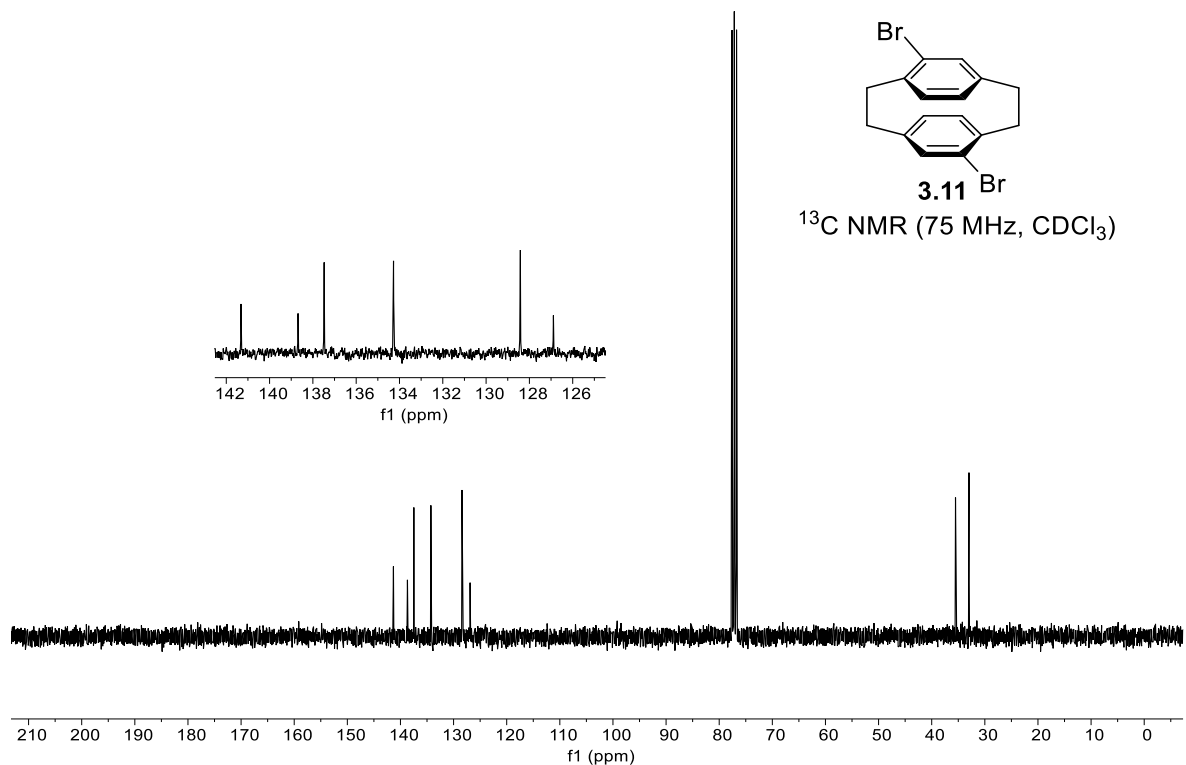
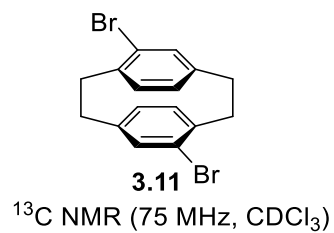
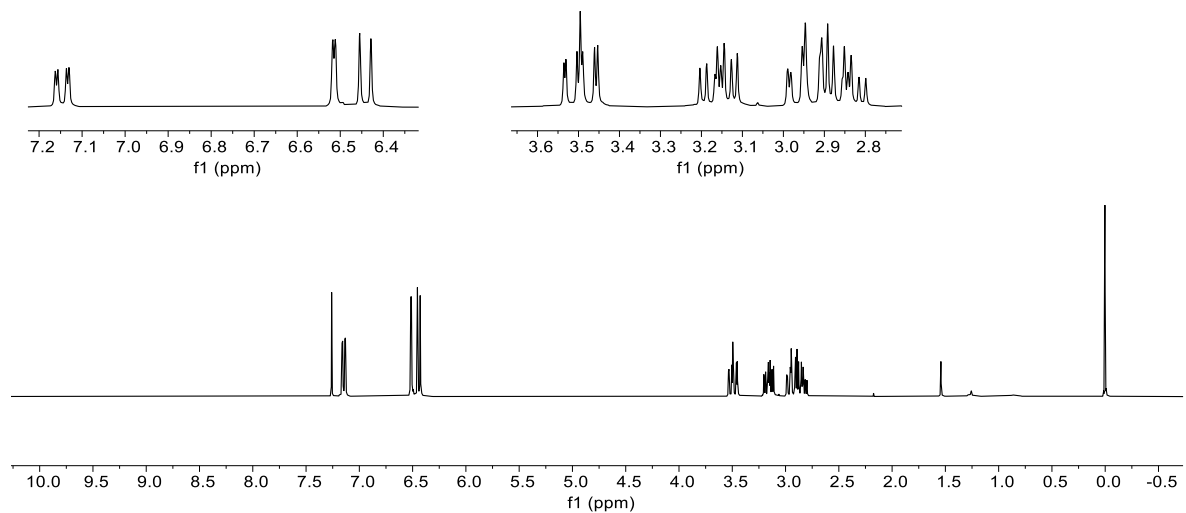
**$^1\text{H}$ ,  $^{13}\text{C}$  NMR Spectra, Two-Dimensional NMR Spectra, X-ray Crystallographic Data, UV/Vis Absorption and Emission Spectra, and DFT Calculations for**

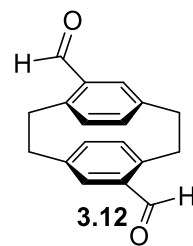
## **Chapter 3**

# 1. $^1\text{H}$ and $^{13}\text{C}$ NMR Spectra

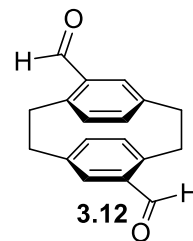
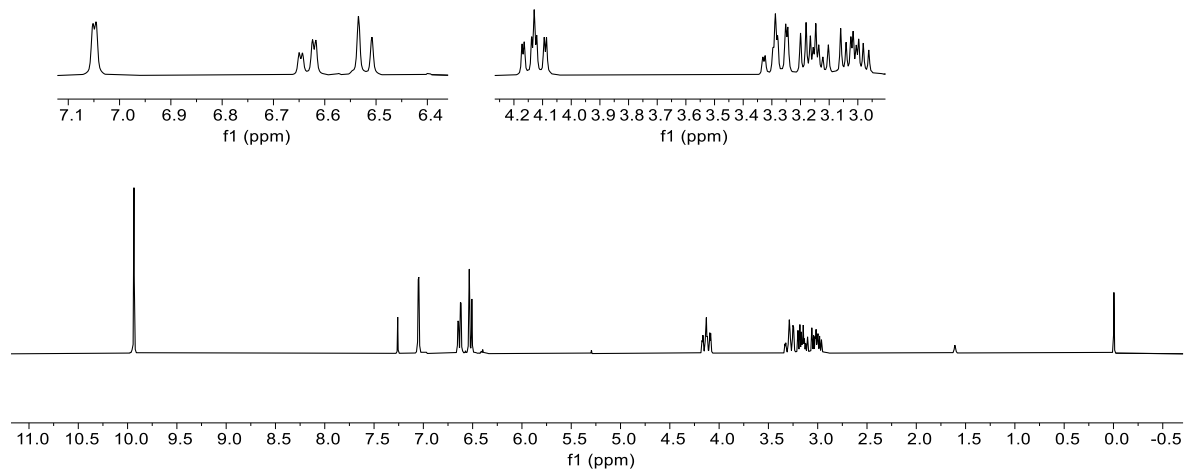


$^1\text{H}$  NMR (300 MHz,  $\text{CDCl}_3$ )

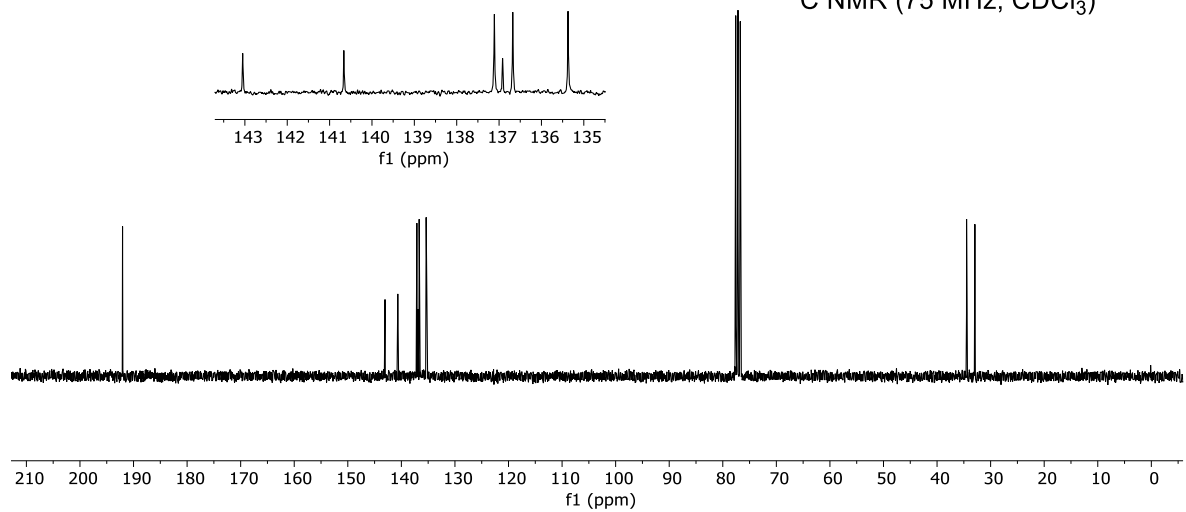


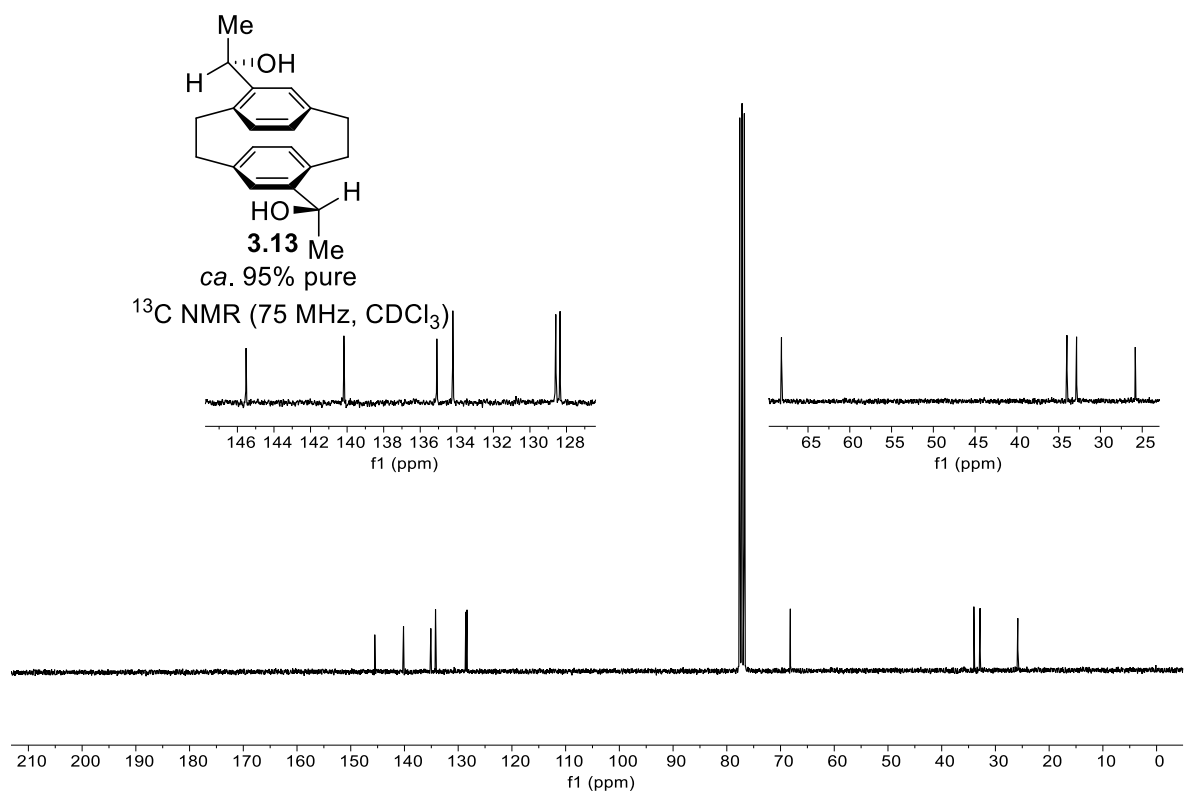
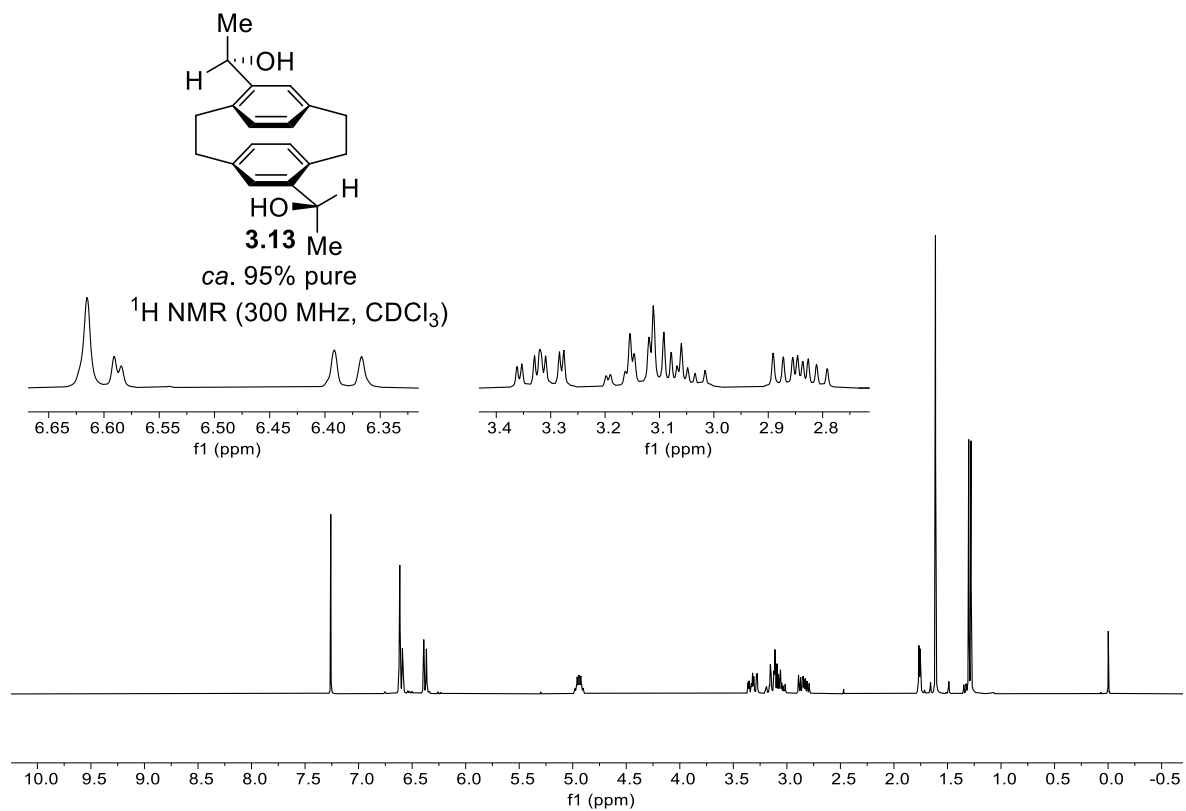


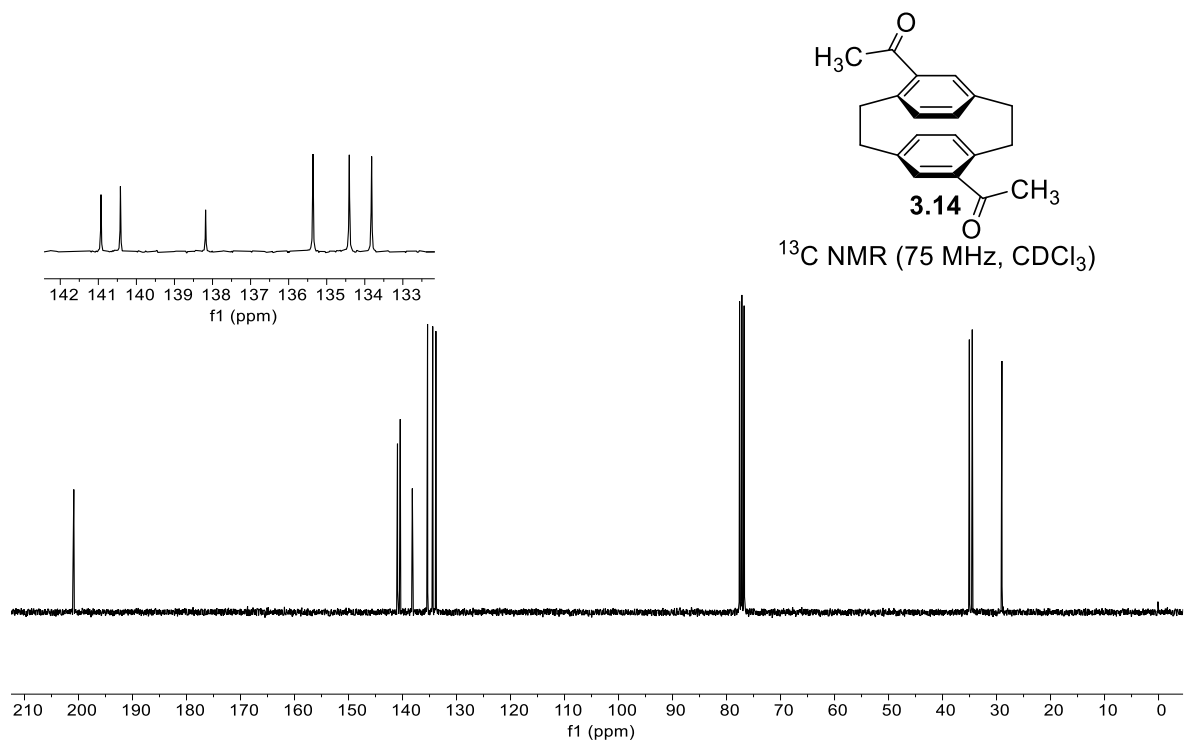
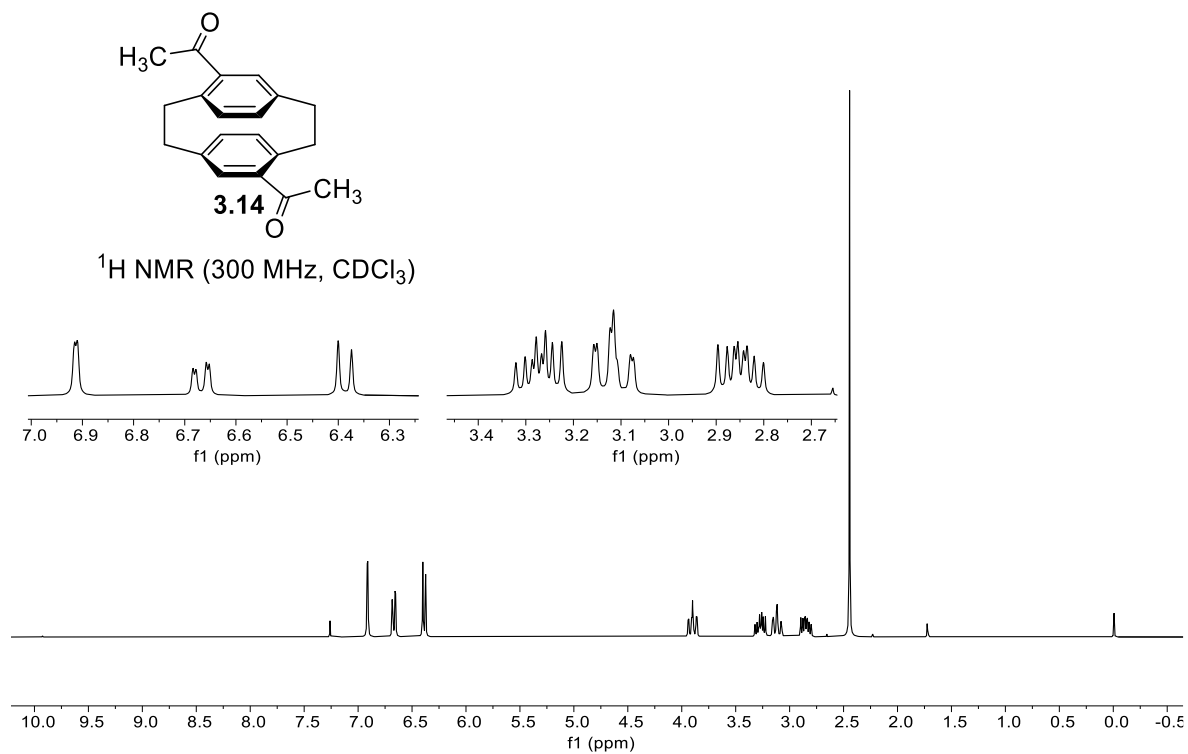
<sup>1</sup>H NMR (300 MHz, CDCl<sub>3</sub>)

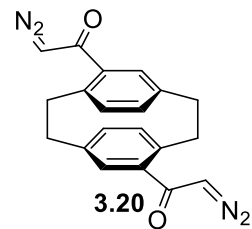


<sup>13</sup>C NMR (75 MHz, CDCl<sub>3</sub>)

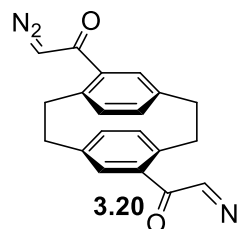
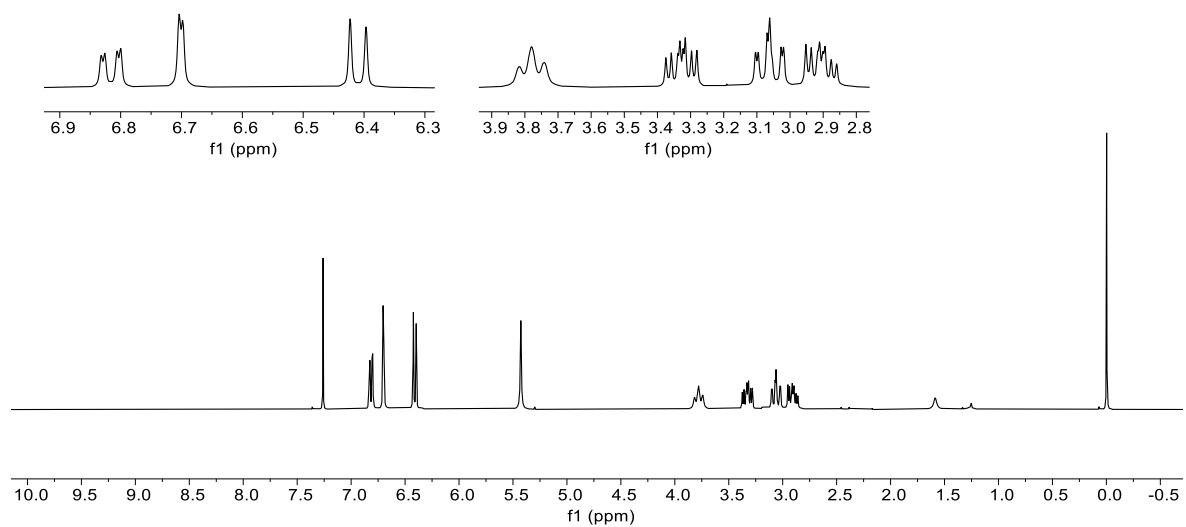




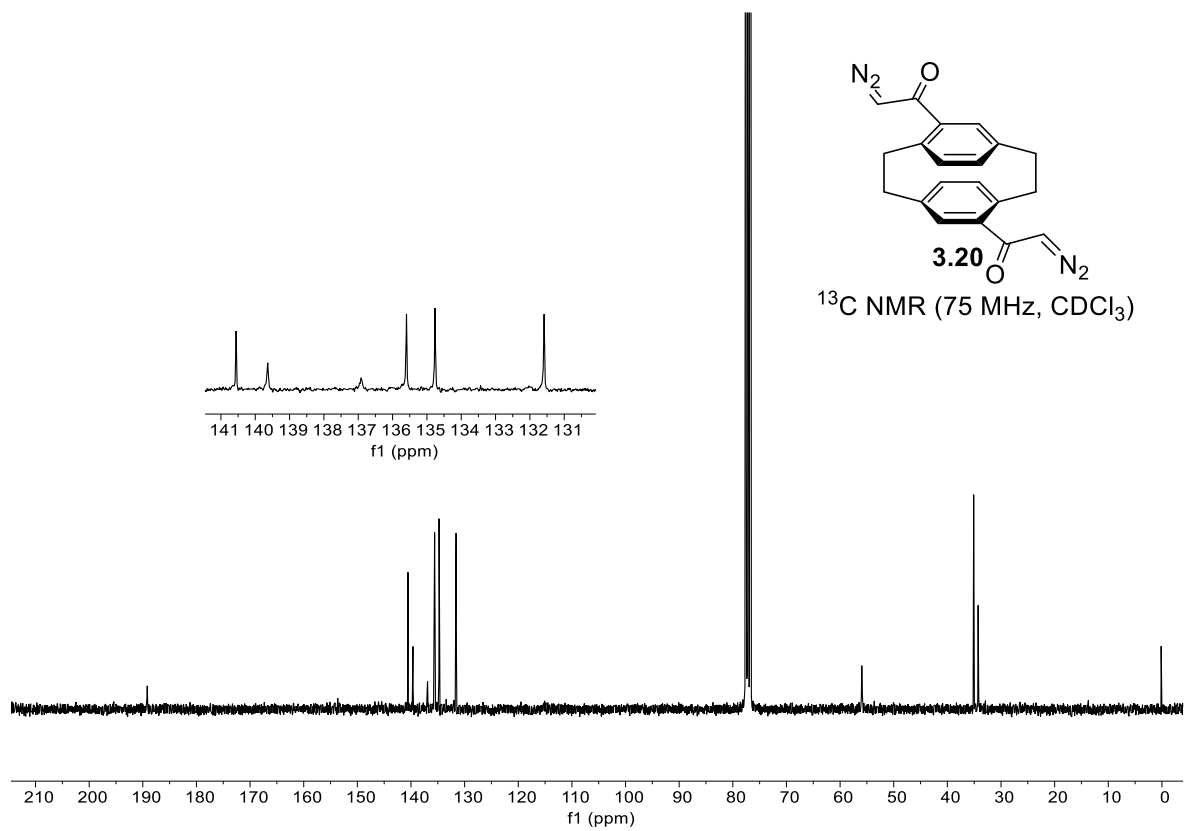


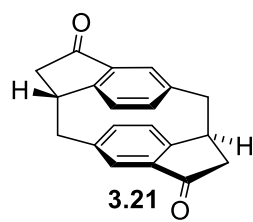


<sup>1</sup>H NMR (300 MHz, CDCl<sub>3</sub>)

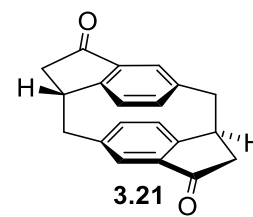
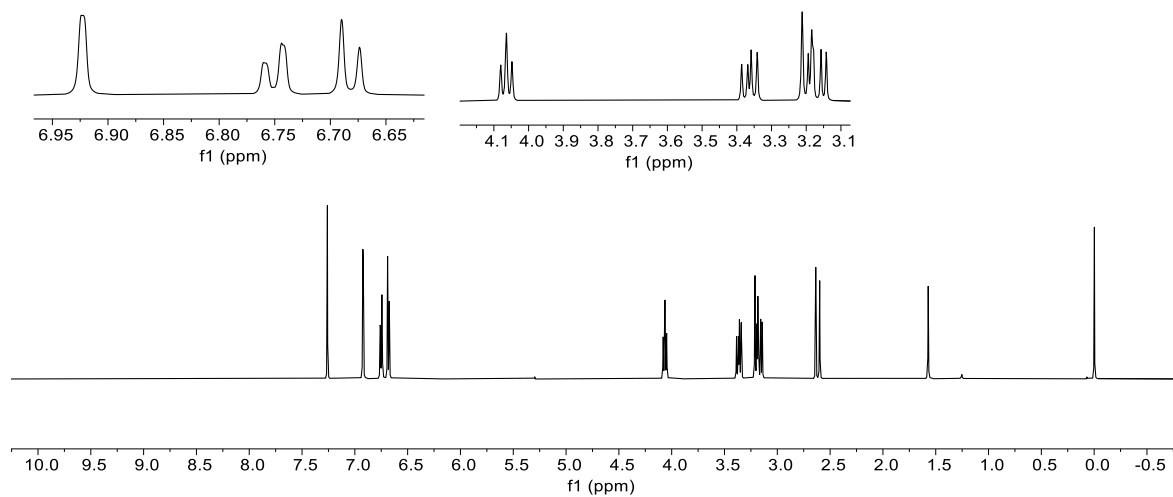


<sup>13</sup>C NMR (75 MHz, CDCl<sub>3</sub>)

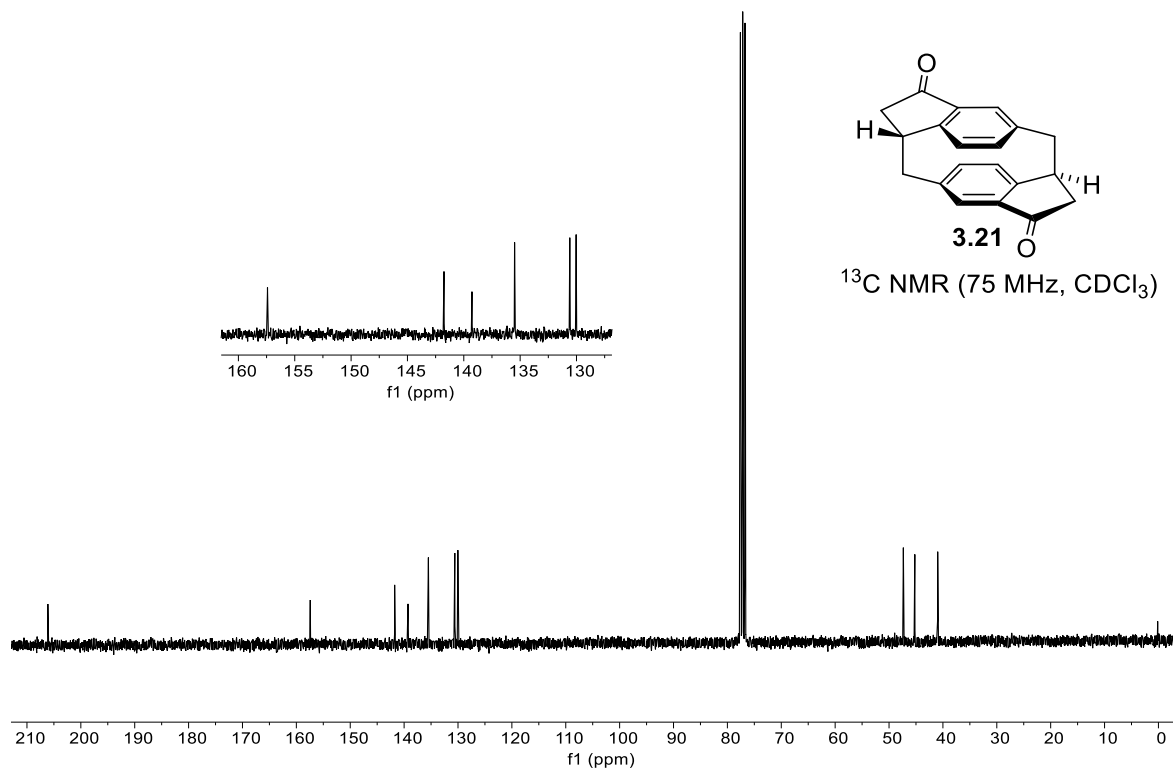


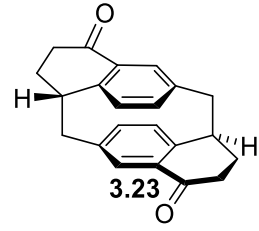


<sup>1</sup>H NMR (500 MHz, CDCl<sub>3</sub>)

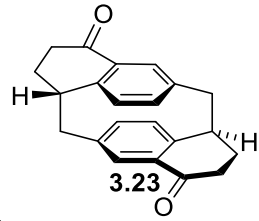
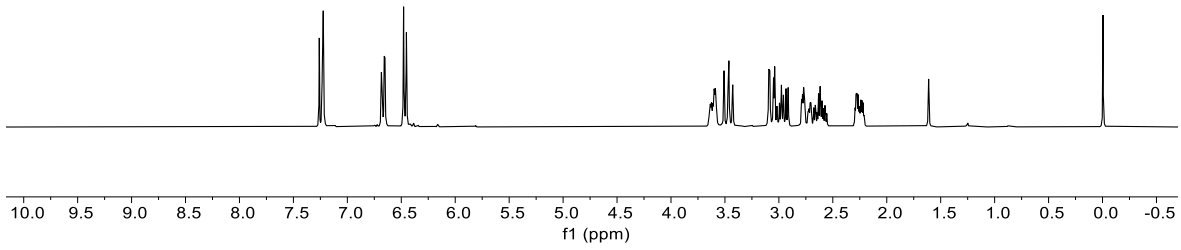
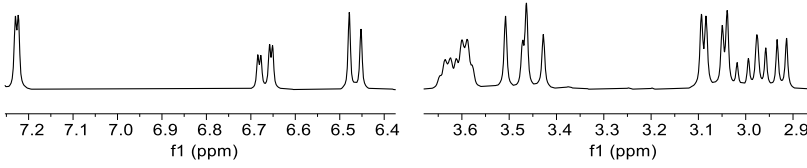


<sup>13</sup>C NMR (75 MHz, CDCl<sub>3</sub>)

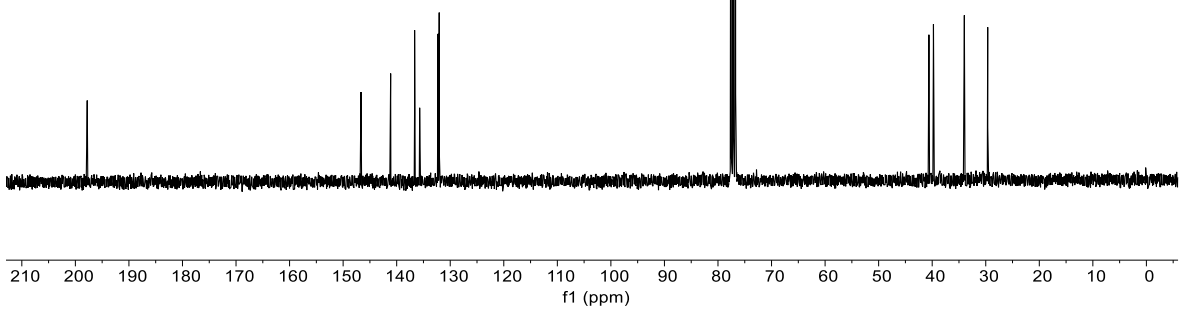
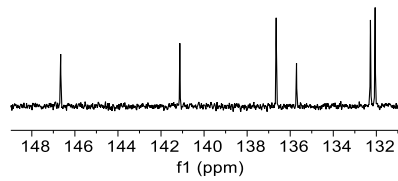


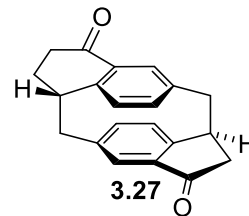


<sup>1</sup>H NMR (300 MHz, CDCl<sub>3</sub>)

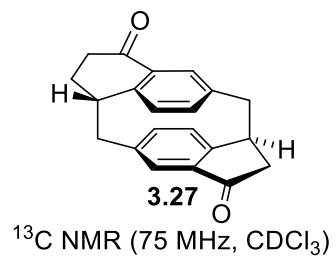
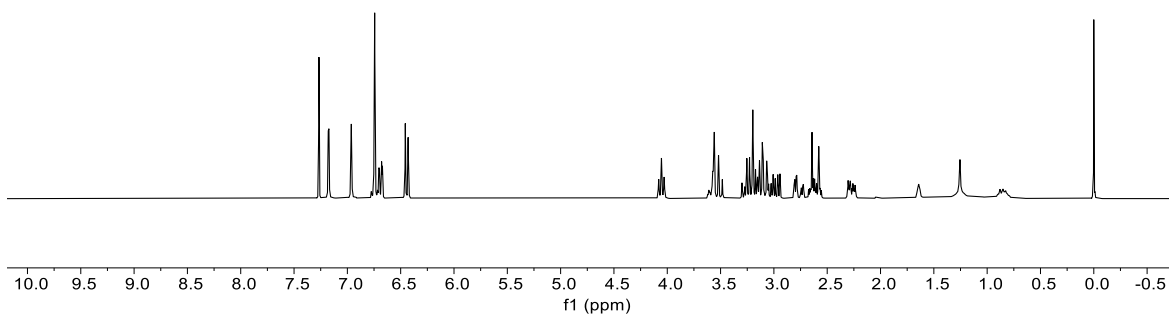
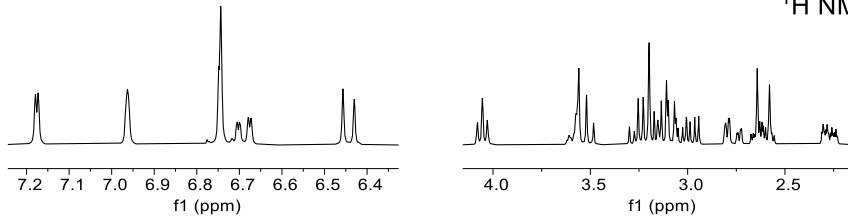


<sup>13</sup>C NMR (75 MHz, CDCl<sub>3</sub>)

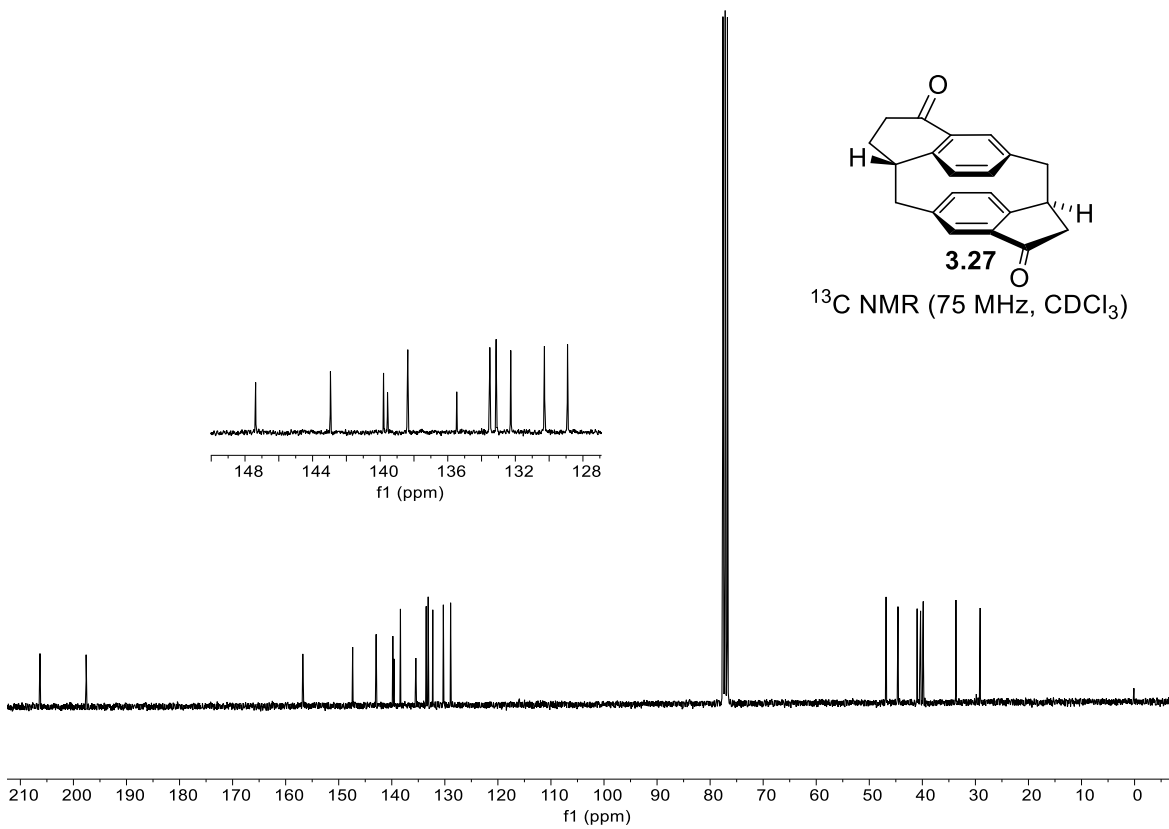
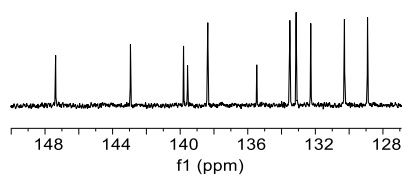


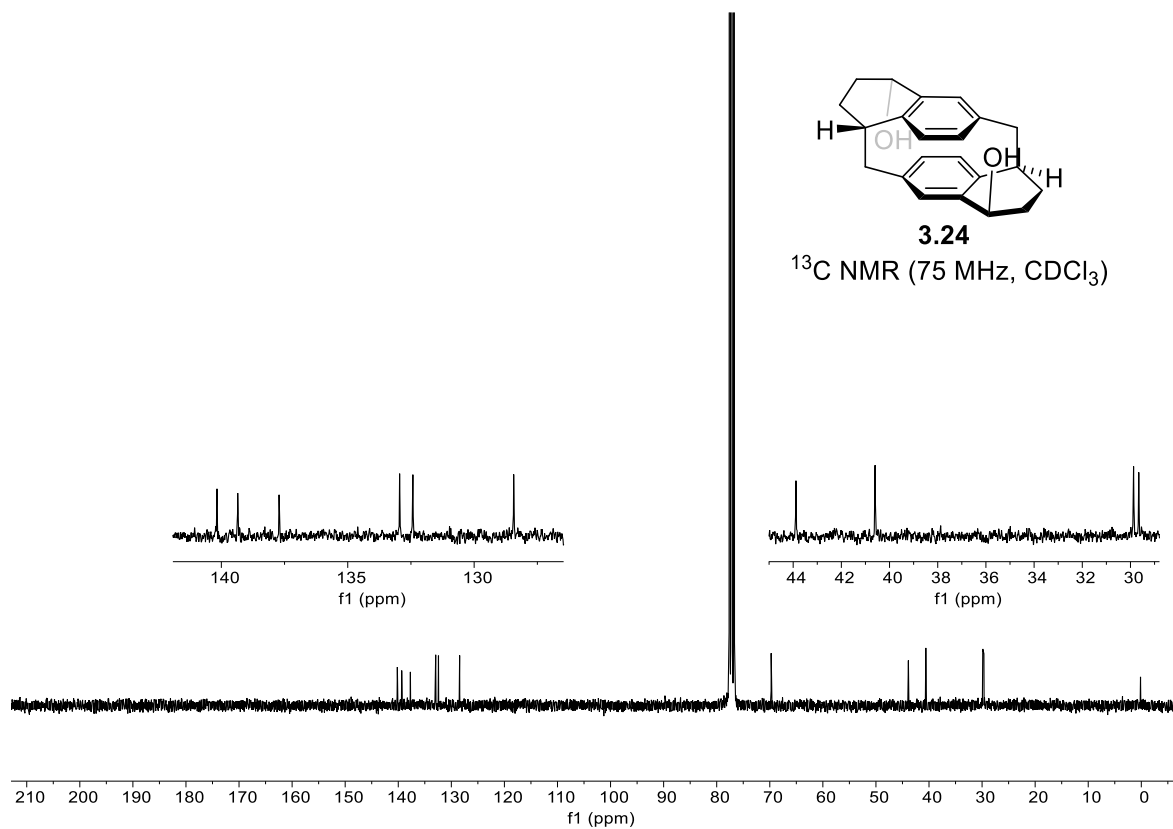
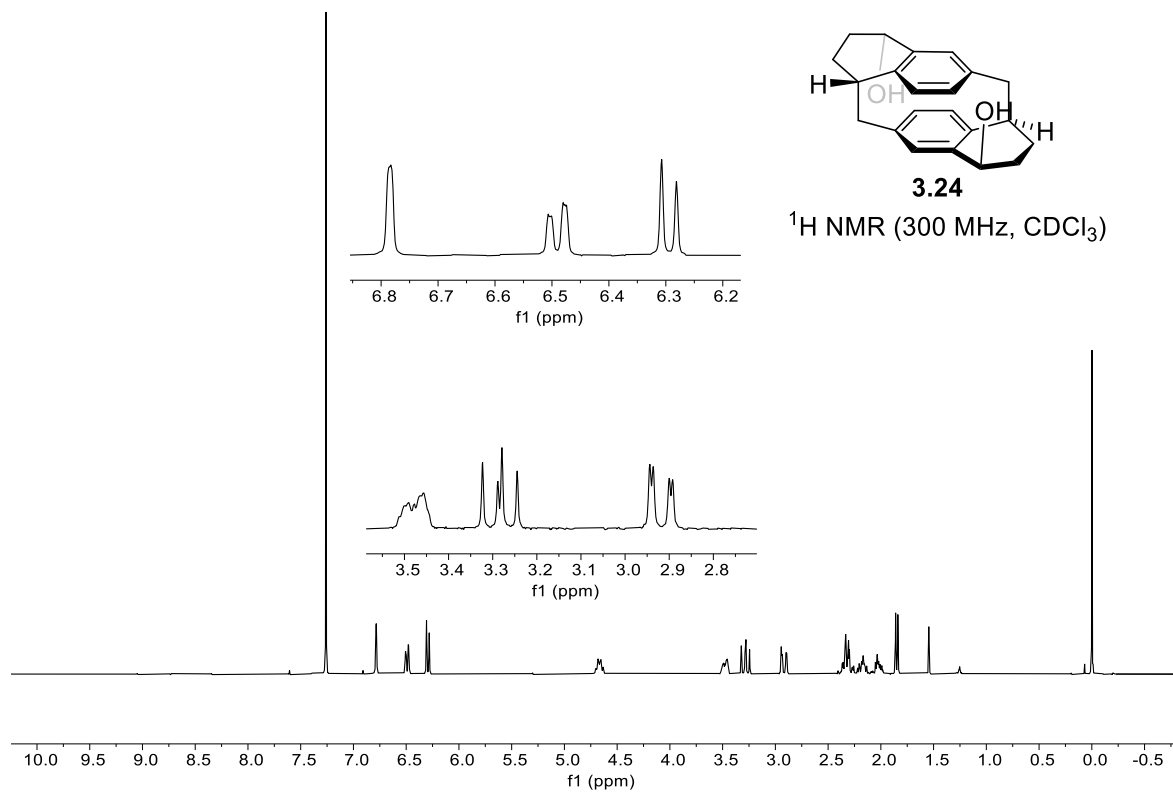


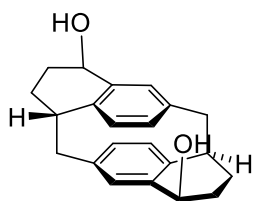
$^1\text{H}$  NMR (300 MHz,  $\text{CDCl}_3$ )



$^{13}\text{C}$  NMR (75 MHz,  $\text{CDCl}_3$ )

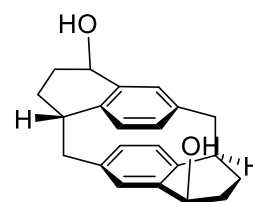
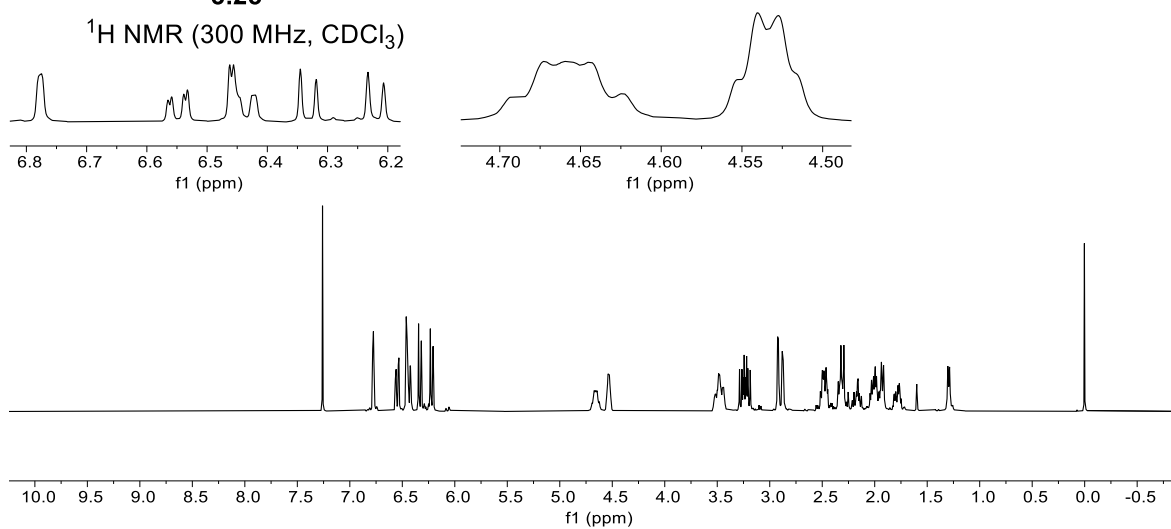






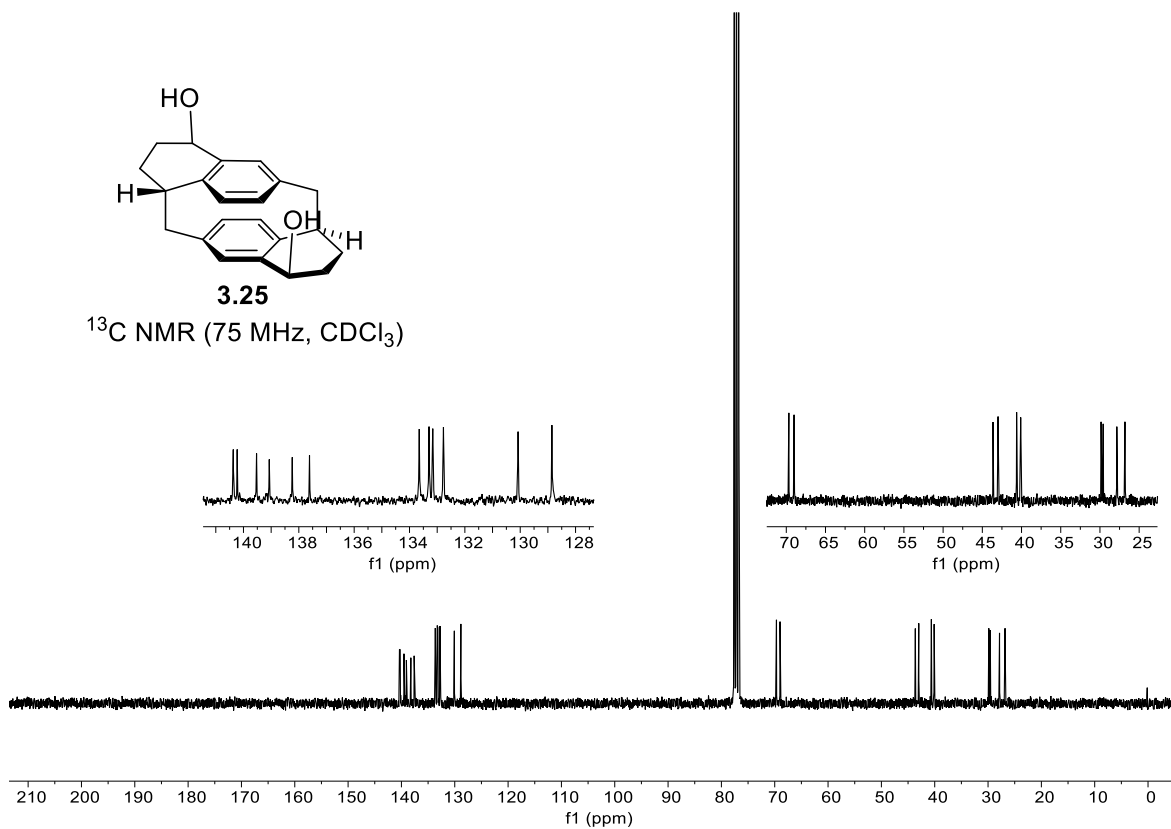
3.25

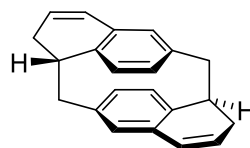
$^1\text{H NMR}$  (300 MHz,  $\text{CDCl}_3$ )



3.25

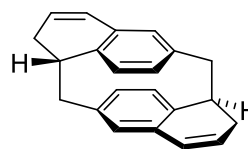
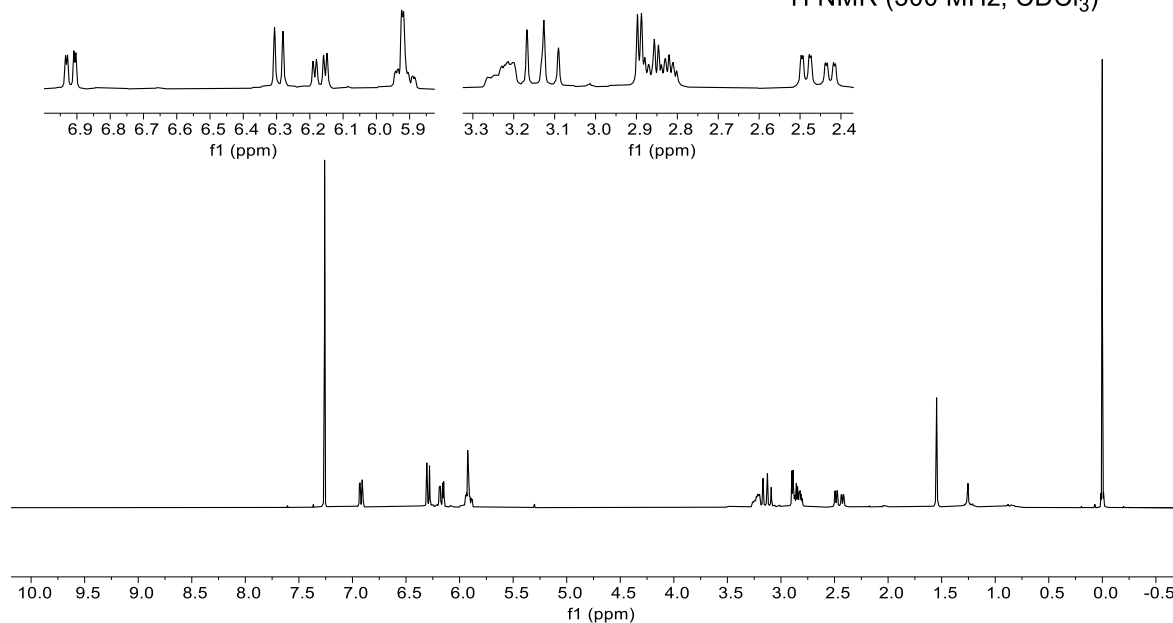
$^{13}\text{C NMR}$  (75 MHz,  $\text{CDCl}_3$ )





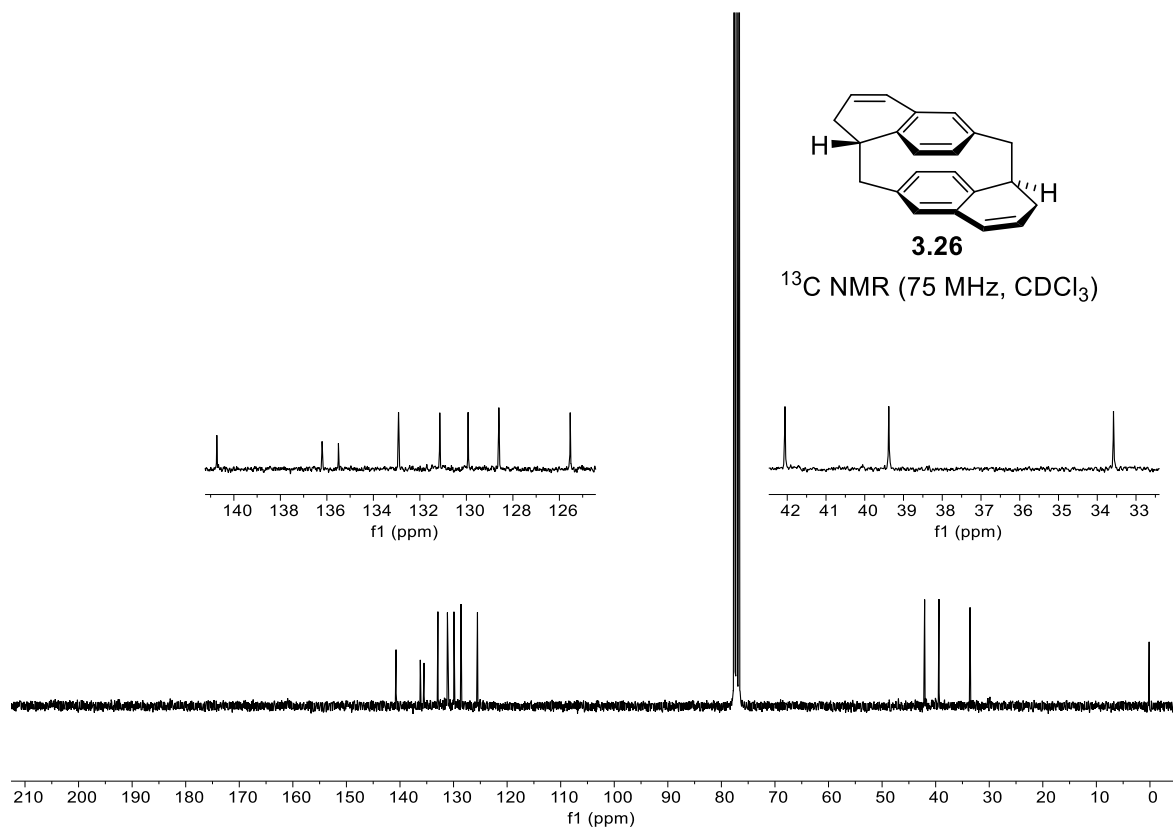
**3.26**

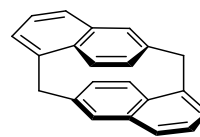
$^1\text{H NMR}$  (300 MHz,  $\text{CDCl}_3$ )



**3.26**

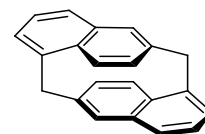
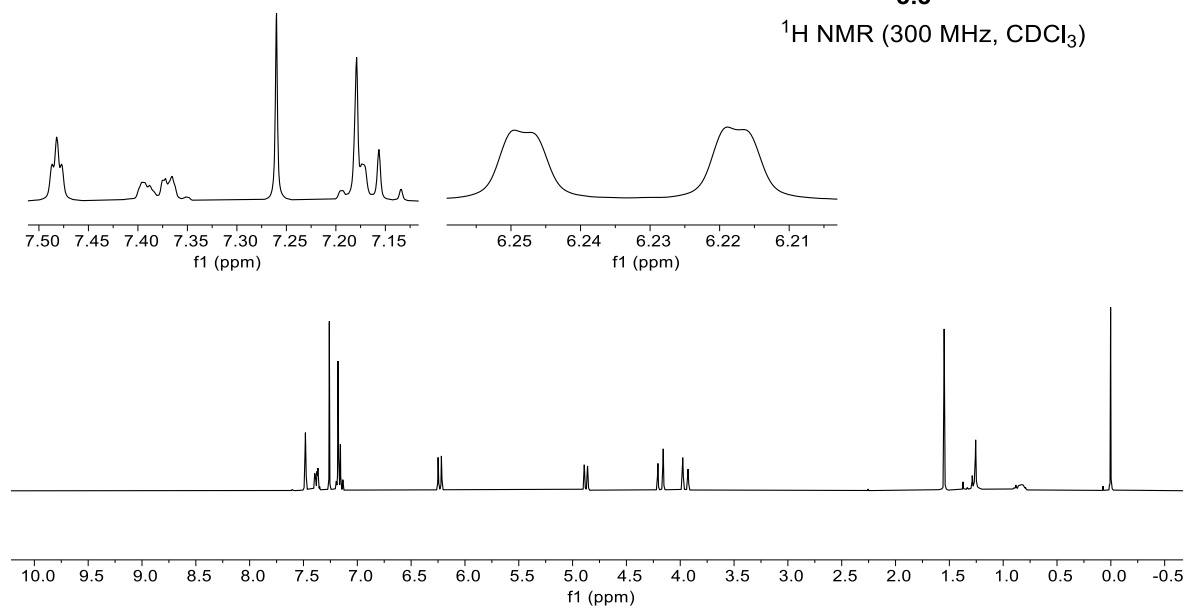
$^{13}\text{C NMR}$  (75 MHz,  $\text{CDCl}_3$ )





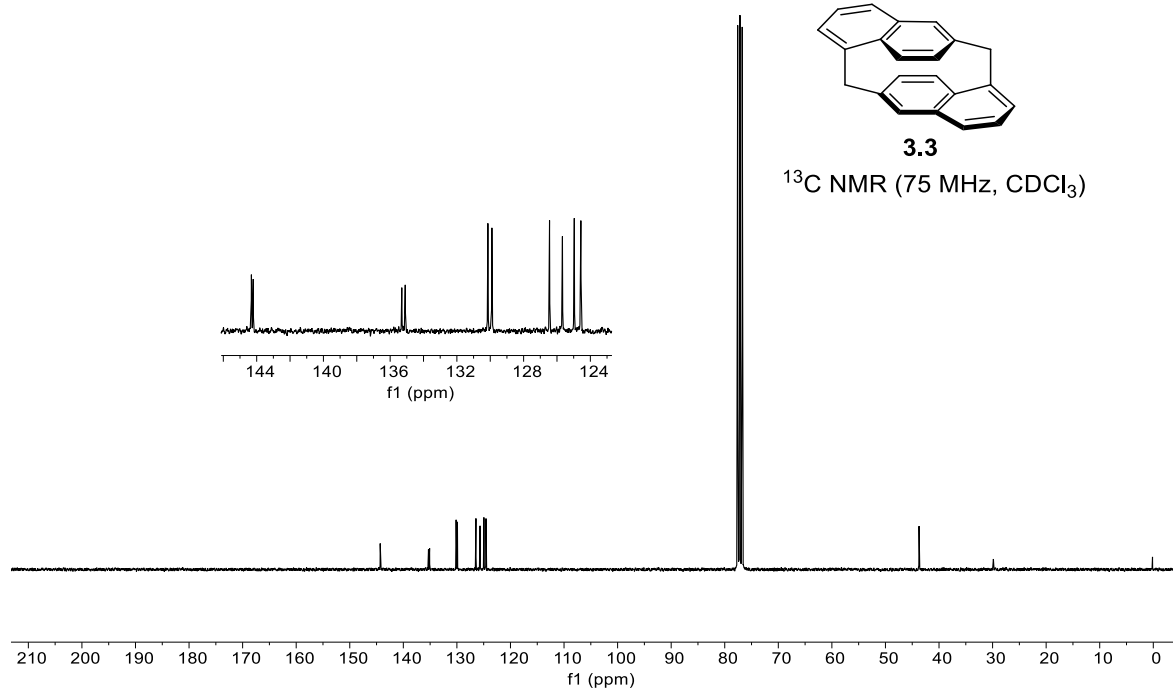
**3.3**

<sup>1</sup>H NMR (300 MHz, CDCl<sub>3</sub>)



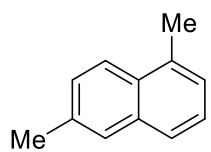
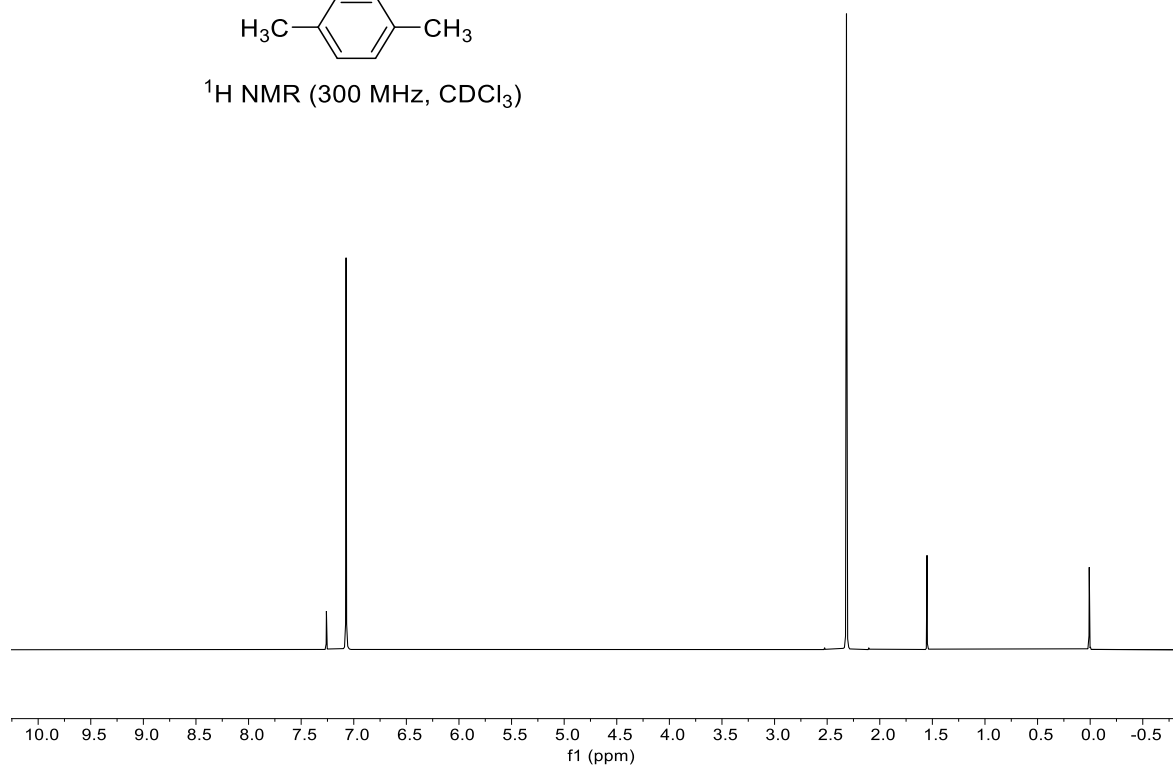
**3.3**

<sup>13</sup>C NMR (75 MHz, CDCl<sub>3</sub>)



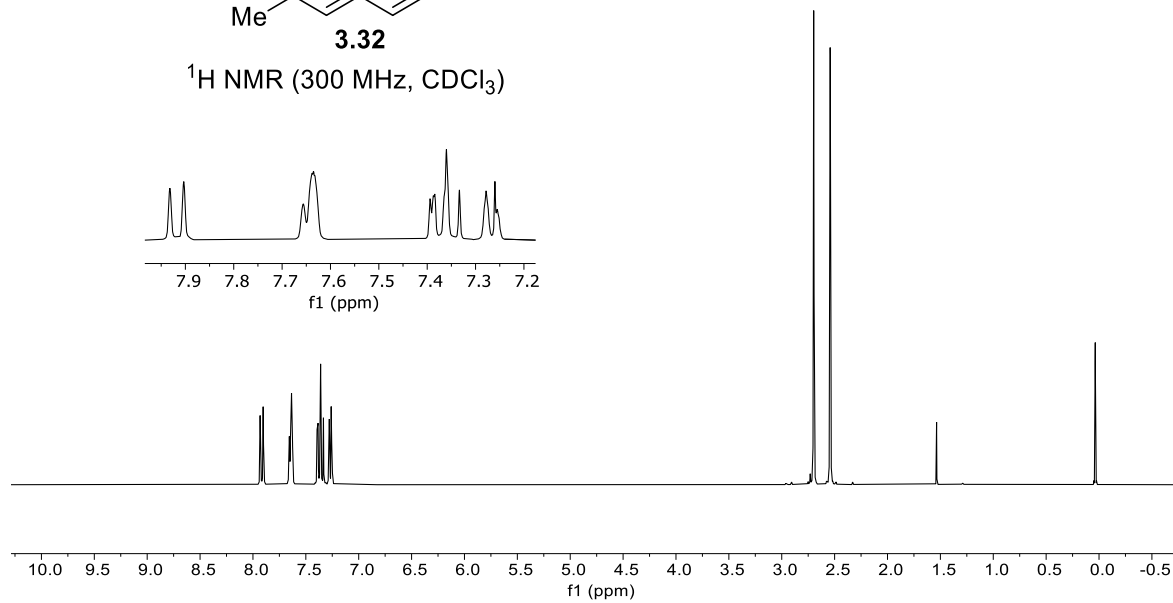
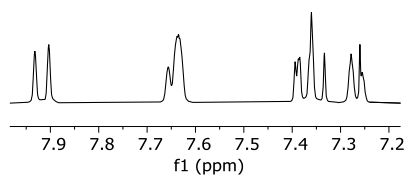


<sup>1</sup>H NMR (300 MHz, CDCl<sub>3</sub>)

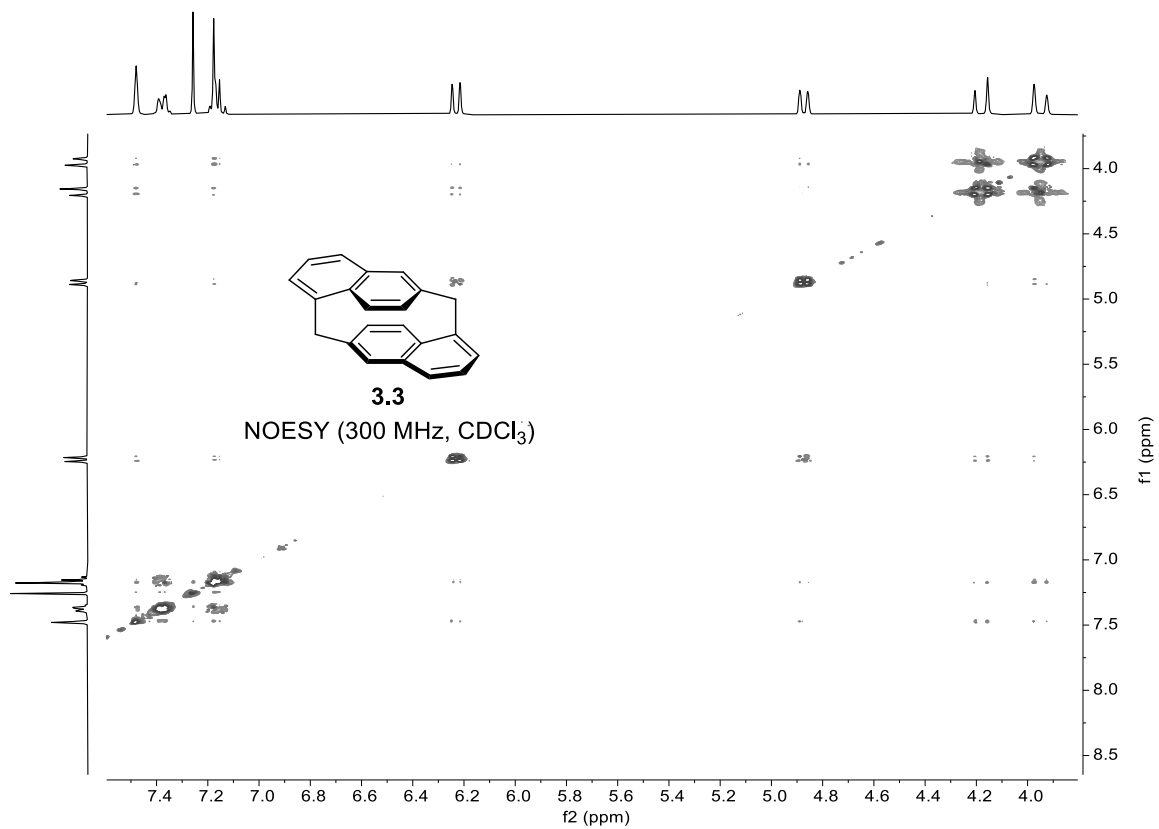
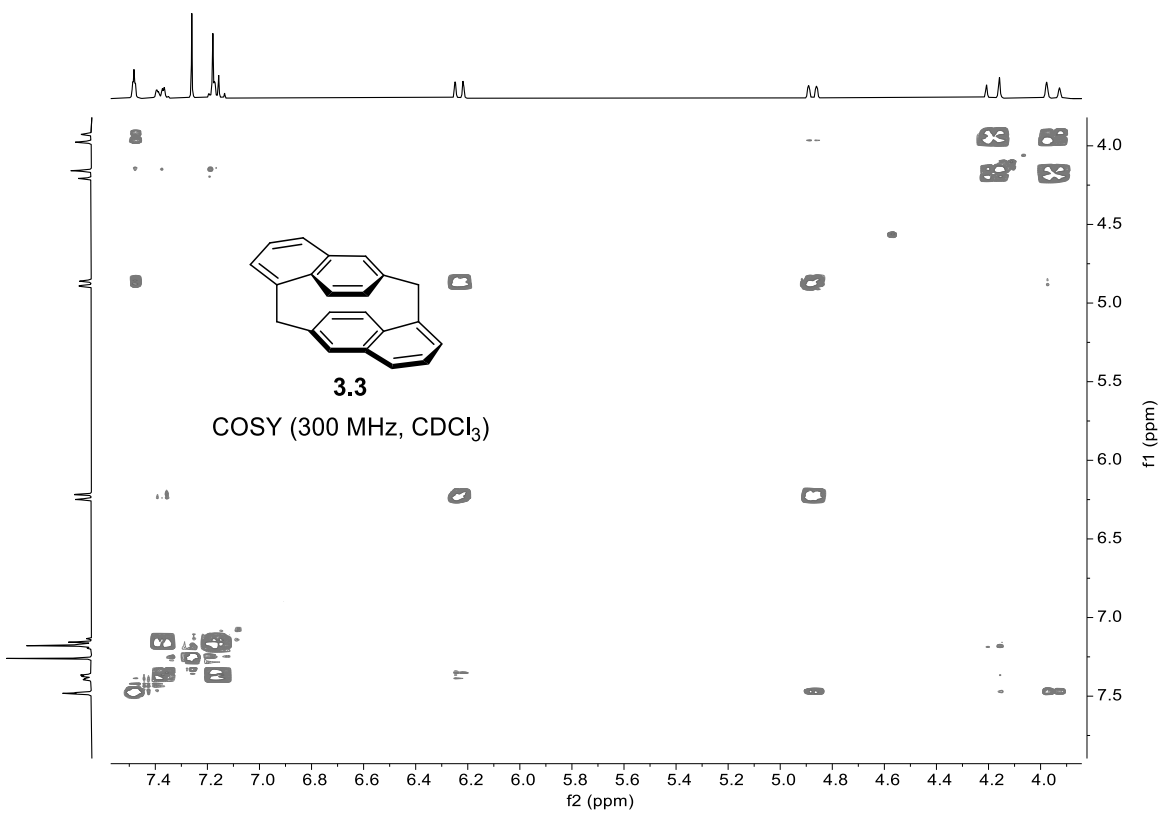


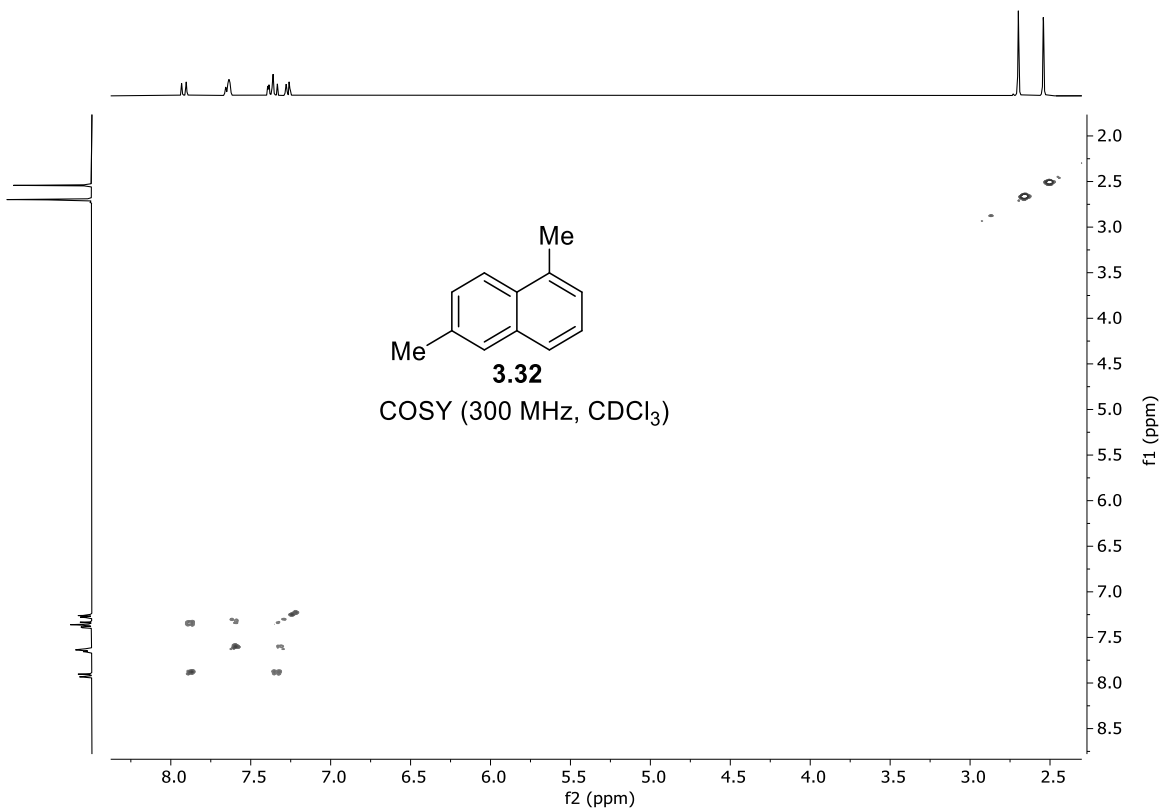
**3.32**

<sup>1</sup>H NMR (300 MHz, CDCl<sub>3</sub>)



## 2. Two-Dimensional NMR Spectra





### **3. X-Ray Structure Details for Compounds 3.13, 3.27, 3.24, 3.25, and 3.3**

#### **Crystallization Procedure:**

##### **Diol 3.13**

Crystals suitable for single crystal X-ray diffraction (XRD) were grown by recrystallization of **3.13** from diethyl ether/dichloromethane (1:1 v/v) at  $-20\text{ }^{\circ}\text{C}$ .

##### **Diketone 3.27**

Crystals suitable for single crystal X-ray diffraction (XRD) were grown by slow evaporation of the solvent from a saturated solution of **3.27** in dichloromethane at room temperature.

##### **Diol 3.24**

Crystals suitable for single crystal X-ray diffraction (XRD) were grown by vapor diffusion of hexanes into a solution of **3.24** in chloroform at room temperature.

##### **Diol 3.25**

Crystals suitable for single crystal X-ray diffraction (XRD) were grown by vapor diffusion of hexanes into a solution of **3.25** in chloroform at room temperature.

##### **[1.1]Naphthalenophane 3.3**

Crystals suitable for single crystal X-ray diffraction (XRD) were grown by vapor diffusion of methanol into a solution of **3.3** in chloroform at room temperature.

### 3.1 Compound 3.13

Sample: SB-002-123-mix

X-ray Structure Report

for

Prof. G. Bodwell

Prepared by

Louise N. Dawe, PhD

Department of Chemistry and Biochemistry  
Wilfrid Laurier University  
Science Building  
75 University Ave. W.  
Waterloo, ON, ON  
ldawe@wlu.ca

September 4, 2020

[Introduction](#)

Data for this structure was collected by Dr. Jian-Bin Lin, Centre for Chemical Analysis, Research and Training (C-CART), Memorial University of Newfoundland.

H-atoms, except H1, were introduced in calculated positions and refined on a riding model. H1 was introduced in its difference map positions and refined positionally and isotropically, without restraints. All other atoms were introduced in difference map positions and refined anisotropically.

## Experimental

A single crystal of C<sub>20</sub>H<sub>24</sub>O<sub>2</sub> was selected and collected on a XtaLAB Synergy, Dualflex, HyPix diffractometer. The crystal was kept at 100.0(2) K during data collection. Using Olex2 [1], the structure was solved with the SHELXT [2] structure solution program using Intrinsic Phasing and refined with the SHELXL [3] refinement package using Least Squares minimisation.

1. Dolomanov, O.V., Bourhis, L.J., Gildea, R.J, Howard, J.A.K. & Puschmann, H. (2009), J. Appl. Cryst. 42, 339-341.
2. Sheldrick, G.M. (2015). Acta Cryst. A71, 3-8.
3. Sheldrick, G.M. (2015). Acta Cryst. C71, 3-8.

### Crystal structure determination

**Crystal Data** for C<sub>20</sub>H<sub>24</sub>O<sub>2</sub> ( $M = 296.39$  g/mol): tetragonal, space group P4<sub>2</sub>/n (no. 86),  $a = 10.63070(10)$  Å,  $c = 13.41230(10)$  Å,  $V = 1515.75(3)$  Å<sup>3</sup>,  $Z = 4$ ,  $T = 100.0(2)$  K,  $\mu(\text{Cu K}\alpha) = 0.639$  mm<sup>-1</sup>,  $D_{\text{calc}} = 1.299$  g/cm<sup>3</sup>, 18911 reflections measured ( $10.618^\circ \leq 2\theta \leq 154.408^\circ$ ), 1611 unique (1528 with  $I > 2\sigma(I)$ );  $R_{\text{int}} = 0.0434$ ,  $R_{\text{sigma}} = 0.0212$ ) which were used in all calculations. The final  $R_1$  was 0.0555 ( $I > 2\sigma(I)$ ) and  $wR_2$  was 0.1450 (all data).

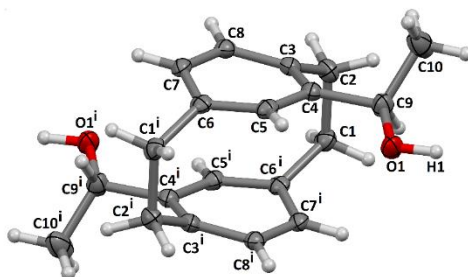


Figure A2-1: Crystal structure of **3.13** with 50% displacement ellipsoids. CCDC 2106465 contains the crystallographic data for **3.13**.

**Table A2-1:** Crystal data and structure refinement for **3.13**.

|   |   |
|---|---|
| Identification code                         | SB-002-123-mix  |
| Empirical formula                           | C <sub>20</sub> H <sub>24</sub> O <sub>2</sub>                |
| Formula weight                              | 296.39  |
| Temperature/K                               | 100.0(2)  |
| Crystal system                              | tetragonal  |
| Space group                                 | P4 <sub>2</sub> /n  |
| a/Å   | 10.63070(10)  |
| b/Å   | 10.63070(10)  |
| c/Å   | 13.41230(10)  |
| α/°   | 90  |
| β/°   | 90  |
| γ/°   | 90  |
| Volume/Å <sup>3</sup>                       | 1515.75(3)  |
| Z   | 4   |
| ρ <sub>calc</sub> /cm <sup>3</sup>          | 1.299   |
| μ/mm <sup>-1</sup>                          | 0.639   |
| F(000)                                      | 640.0   |
| Crystal size/mm <sup>3</sup>                | 0.08 × 0.06 × 0.04  |
| Radiation                                   | Cu Kα (λ = 1.54184)   |
| 2θ range for data collection/°              | 10.618 to 154.408   |
| Index ranges                                | -13 ≤ h ≤ 13, -13 ≤ k ≤ 9, -16 ≤ l ≤ 16                       |
| Reflections collected                       | 18911   |
| Independent reflections                     | 1611 [R <sub>int</sub> = 0.0434, R <sub>sigma</sub> = 0.0212] |
| Data/restraints/parameters                  | 1611/0/105  |
| Goodness-of-fit on F <sup>2</sup>           | 1.119   |
| Final R indexes [I ≥ 2σ (I)]                | R <sub>1</sub> = 0.0555, wR <sub>2</sub> = 0.1434             |
| Final R indexes [all data]                  | R <sub>1</sub> = 0.0588, wR <sub>2</sub> = 0.1450             |
| Largest diff. peak/hole / e Å <sup>-3</sup> | 0.40/-0.33  |

**Table A2-2:** Fractional atomic coordinates ( $\times 10^4$ ) and equivalent isotropic displacement parameters ( $\text{\AA}^2 \times 10^3$ ) for **3.13**.  $U_{eq}$  is defined as 1/3 of the trace of the orthogonalised  $U_{ij}$  tensor.

| Atom | x           | y           | z           | U(eq)    |
|------|-------------|-------------|-------------|----------|
| O1   | 7310.5 (12) | 5739.2 (13) | 2871.8 (10) | 28.1 (4) |
| C1   | 6971.9 (17) | 5796.0 (16) | 6378.9 (14) | 24.2 (4) |
| C2   | 7389.7 (16) | 4459.9 (17) | 5960.8 (14) | 23.7 (4) |
| C3   | 6506.0 (16) | 3950.8 (16) | 5171.7 (13) | 20.4 (4) |
| C4   | 6500.8 (16) | 4381.4 (15) | 4177.7 (13) | 20.5 (4) |
| C5   | 5406.5 (17) | 4281.2 (16) | 3617.9 (13) | 21.3 (4) |
| C6   | 4299.6 (16) | 3787.9 (15) | 4019.0 (13) | 20.4 (4) |
| C7   | 4398.5 (16) | 3139.0 (15) | 4915.6 (14) | 21.3 (4) |
| C8   | 5489.8 (16) | 3217.3 (15) | 5482.5 (13) | 20.9 (4) |
| C9   | 7639.0 (17) | 5072.5 (18) | 3766.8 (14) | 26.0 (4) |
| C10  | 8718 (2)    | 4187 (2)    | 3592.7 (17) | 40.6 (6) |

**Table A2-3:** Anisotropic displacement parameters ( $\text{\AA}^2 \times 10^3$ ) for **3.13**. The anisotropic displacement factor exponent takes the form:  $-2\pi^2[h^2a^2U_{11}+2hka*b*U_{12}+\dots]$ .

| Atom | $U_{11}$  | $U_{22}$  | $U_{33}$  | $U_{23}$  | $U_{13}$ | $U_{12}$ |
|------|-----------|-----------|-----------|-----------|----------|----------|
| O1   | 23.4 (7)  | 28.7 (7)  | 32.3 (7)  | 11.7 (5)  | 2.3 (5)  | 0.1 (5)  |
| C1   | 24.1 (9)  | 20.2 (8)  | 28.4 (9)  | -0.6 (7)  | -3.5 (7) | -3.8 (7) |
| C2   | 19.9 (8)  | 26.8 (9)  | 24.6 (9)  | 0.1 (7)   | -0.5 (7) | 2.1 (7)  |
| C3   | 19.0 (8)  | 17.8 (8)  | 24.5 (9)  | -1.1 (6)  | 1.6 (7)  | 3.6 (6)  |
| C4   | 20.3 (8)  | 16.8 (8)  | 24.4 (9)  | -1.7 (6)  | 3.4 (7)  | 1.4 (6)  |
| C5   | 25.5 (9)  | 17.3 (8)  | 21.0 (8)  | -1.5 (6)  | 1.4 (7)  | 0.1 (6)  |
| C6   | 22.2 (8)  | 15.1 (7)  | 23.8 (8)  | -4.6 (6)  | -1.8 (7) | -0.9 (6) |
| C7   | 21.3 (8)  | 14.8 (8)  | 27.7 (9)  | -1.4 (6)  | 3.4 (7)  | -1.6 (6) |
| C8   | 22.9 (8)  | 16.5 (8)  | 23.4 (8)  | 0.5 (6)   | 3.7 (7)  | 2.8 (6)  |
| C9   | 22.5 (9)  | 28.0 (9)  | 27.4 (9)  | 7.5 (7)   | 0.2 (7)  | -0.9 (7) |
| C10  | 33.7 (11) | 46.8 (13) | 41.2 (12) | 17.1 (10) | 12.1 (9) | 12.0 (9) |

**Table A2-4: Bond Lengths for 3.13.**

| Atom | Atom            | Length/Å  | Atom | Atom | Length/Å  |
|------|-----------------|-----------|------|------|-----------|
| O1   | C9              | 1.437 (2) | C4   | C5   | 1.389 (2) |
| C1   | C2              | 1.590 (2) | C4   | C9   | 1.519 (2) |
| C1   | C6 <sup>1</sup> | 1.519 (2) | C5   | C6   | 1.396 (2) |
| C2   | C3              | 1.515 (2) | C6   | C7   | 1.390 (2) |
| C3   | C4              | 1.410 (2) | C7   | C8   | 1.390 (3) |
| C3   | C8              | 1.396 (2) | C9   | C10  | 1.503 (3) |

<sup>1</sup>I-X,I-Y,I-Z**Table A2-5: Bond Angles for 3.13.**

| Atom            | Atom | Atom | Angle/°     | Atom | Atom | Atom            | Angle/°     |
|-----------------|------|------|-------------|------|------|-----------------|-------------|
| C6 <sup>1</sup> | C1   | C2   | 112.62 (14) | C5   | C6   | C1 <sup>1</sup> | 120.35 (16) |
| C3              | C2   | C1   | 113.08 (14) | C7   | C6   | C1 <sup>1</sup> | 121.04 (16) |
| C4              | C3   | C2   | 123.17 (16) | C7   | C6   | C5              | 117.12 (16) |
| C8              | C3   | C2   | 118.08 (16) | C8   | C7   | C6              | 120.44 (16) |
| C8              | C3   | C4   | 117.44 (16) | C7   | C8   | C3              | 121.07 (17) |
| C3              | C4   | C9   | 119.80 (15) | O1   | C9   | C4              | 110.36 (15) |
| C5              | C4   | C3   | 119.32 (16) | O1   | C9   | C10             | 111.40 (16) |
| C5              | C4   | C9   | 120.55 (16) | C10  | C9   | C4              | 111.19 (16) |
| C4              | C5   | C6   | 121.77 (17) |      |      |                 |             |

<sup>1</sup>I-X,I-Y,I-Z

**Table A2-6:** Torsion Angles for **3.13**.

| A               | B  | C  | D   | Angle/°      | A               | B  | C  | D               | Angle/°      |
|-----------------|----|----|-----|--------------|-----------------|----|----|-----------------|--------------|
| C1              | C2 | C3 | C4  | 77.1 (2)     | C4              | C5 | C6 | C1 <sup>1</sup> | 151.87 (16)  |
| C1              | C2 | C3 | C8  | -89.50 (19)  | C4              | C5 | C6 | C7              | -14.4 (2)    |
| C1 <sup>1</sup> | C6 | C7 | C8  | -152.70 (16) | C5              | C4 | C9 | O1              | 10.4 (2)     |
| C2              | C3 | C4 | C5  | -154.12 (16) | C5              | C4 | C9 | C10             | -113.8 (2)   |
| C2              | C3 | C4 | C9  | 19.4 (2)     | C5              | C6 | C7 | C8              | 13.4 (2)     |
| C2              | C3 | C8 | C7  | 153.86 (16)  | C6 <sup>1</sup> | C1 | C2 | C3              | 6.3 (2)      |
| C3              | C4 | C5 | C6  | 1.3 (2)      | C6              | C7 | C8 | C3              | 0.4 (3)      |
| C3              | C4 | C9 | O1  | -163.05 (15) | C8              | C3 | C4 | C5              | 12.5 (2)     |
| C3              | C4 | C9 | C10 | 72.8 (2)     | C8              | C3 | C4 | C9              | -173.96 (15) |
| C4              | C3 | C8 | C7  | -13.5 (2)    | C9              | C4 | C5 | C6              | -172.11 (16) |

<sup>1</sup>1-X,1-Y,1-Z**Table A2-7:** Hydrogen Atom Coordinates ( $\text{\AA}\times 10^4$ ) and Isotropic Displacement Parameters ( $\text{\AA}^2\times 10^3$ ) for **3.13**.

| Atom | x         | y         | z         | U(eq)  |
|------|-----------|-----------|-----------|--------|
| H1   | 8040 (30) | 6100 (30) | 2630 (20) | 49 (8) |
| H1A  | 6934.97   | 5758.68   | 7100.88   | 29     |
| H1B  | 7600.32   | 6416.71   | 6197.46   | 29     |
| H2A  | 8227.39   | 4529.94   | 5679.45   | 28     |
| H2B  | 7429.46   | 3866.95   | 6509.59   | 28     |
| H5   | 5411.18   | 4549.95   | 2958.06   | 26     |
| H7   | 3729.81   | 2649.15   | 5137.44   | 26     |
| H8   | 5544.06   | 2773.93   | 6078.72   | 25     |
| H9   | 7904.63   | 5692.61   | 4264.83   | 31     |
| H10A | 8502.66   | 3606.94   | 3071.17   | 61     |
| H10B | 8891.7    | 3729.4    | 4194.41   | 61     |
| H10C | 9449.9    | 4657.64   | 3401.23   | 61     |

## 3.2 Compound 3.27

Sample: SB-002-bis-2-teralone

X-ray Structure Report

for  
Prof. G. Bodwell

Prepared by

Louise N. Dawe, PhD

Department of Chemistry and Biochemistry  
Wilfrid Laurier University  
Science Building  
75 University Ave. W.  
Waterloo, ON, ON  
ldawe@wlu.ca

June 27, 2021

[Introduction](#)

Data for this structure was collected by Dr. JB Lin, Memorial University of Newfoundland.

SB-002-bis-2-teralone crystallized in the centrosymmetric space group *Pbca*. All non-hydrogen atoms were refined anisotropically. All hydrogen atoms were introduced in calculated positions and refined on a riding model. The asymmetric unit contains half of the molecule, which results in positional disorder for the 50:50 occupancy aliphatic ring, one which is five-membered, and the other, six-membered. Other characterizations are consistent with each molecule containing one five-member ring and one six-membered ring.

## Experimental

A single crystal of C<sub>21</sub>H<sub>18</sub>O<sub>2</sub> [**3.27**] was selected and diffraction data collected on a XtaLAB Synergy, Dualflex, HyPix diffractometer. The crystal was kept at 100.0(2) K during data collection. Using Olex2 [1], the structure was solved with the SHELXT [2] structure solution program using Intrinsic Phasing and refined with the SHELXL [3] refinement package using Least Squares minimisation.

1. Dolomanov, O.V., Bourhis, L.J., Gildea, R.J, Howard, J.A.K. & Puschmann, H. (2009), J. Appl. Cryst. 42, 339-341.
2. Sheldrick, G.M. (2015). Acta Cryst. A71, 3-8.
3. Sheldrick, G.M. (2015). Acta Cryst. C71, 3-8.

## Crystal Structure Determination

**Crystal Data for C<sub>21</sub>H<sub>18</sub>O<sub>2</sub> (*M* = 302.35 g/mol):** orthorhombic, space group Pbc<sub>a</sub> (no. 61), *a* = 7.53630(10) Å, *b* = 17.2036(2) Å, *c* = 11.25990(10) Å, *V* = 1459.86(3) Å<sup>3</sup>, *Z* = 4, *T* = 100.0(2) K,  $\mu(\text{Cu K}\alpha) = 0.687 \text{ mm}^{-1}$ , *D*<sub>calc</sub> = 1.376 g/cm<sup>3</sup>, 17056 reflections measured (10.284° ≤ 2θ ≤ 159.178°), 1576 unique (1514 with *I* > 2σ(*I*); *R*<sub>int</sub> = 0.0451, *R*<sub>sigma</sub> = 0.0182) which were used in all calculations. The final *R*<sub>1</sub> was 0.0664 (*I* > 2σ(*I*)) and *wR*<sub>2</sub> was 0.1485 (all data).

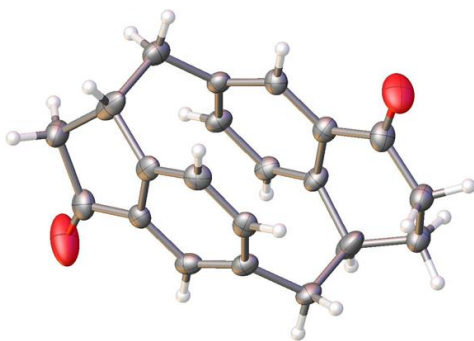


**Figure A2-2:** Crystal structure of **3.27** with 50% displacement ellipsoids. CCDC 2129675 contains the crystallographic data for **3.27**.

**Table A2-8:** Crystal data and structure refinement for **3.27**.

|   |  |
|---|--|
| Identification code                         | SB-002-bis-2-teralone  |
| Empirical formula                           | C <sub>21</sub> H <sub>18</sub> O <sub>2</sub>                                     |
| Formula weight                              | 302.35   |
| Temperature/K                               | 100.0(2)   |
| Crystal system                              | orthorhombic   |
| Space group                                 | Pbca   |
| a/Å   | 7.53630(10)  |
| b/Å   | 17.2036(2)   |
| c/Å   | 11.25990(10)   |
| α/°   | 90   |
| β/°   | 90   |
| γ/°   | 90   |
| Volume/Å <sup>3</sup>                       | 1459.86(3)   |
| Z   | 4  |
| ρ <sub>calc</sub> /cm <sup>3</sup>          | 1.376  |
| μ/mm <sup>-1</sup>                          | 0.687  |
| F(000)                                      | 640.0  |
| Crystal size/mm <sup>3</sup>                | 0.227 × 0.147 × 0.051  |
| Radiation                                   | Cu Kα (λ = 1.54184)  |
| 2θ range for data collection/°              | 10.284 to 159.178  |
| Index ranges                                | -8 ≤ h ≤ 9, -21 ≤ k ≤ 21, -14 ≤ l ≤ 14   |
| Reflections collected                       | 17056  |
| Independent reflections                     | 1576 [1514 with I > 2σ(I); R <sub>int</sub> = 0.0451, R <sub>sigma</sub> = 0.0182] |
| Data/restraints/parameters                  | 1576/52/145  |
| Goodness-of-fit on F <sup>2</sup>           | 1.262  |
| Final R indexes [I >= 2σ (I)]               | R <sub>1</sub> = 0.0664, wR <sub>2</sub> = 0.1478                                  |
| Final R indexes [all data]                  | R <sub>1</sub> = 0.0680, wR <sub>2</sub> = 0.1485                                  |
| Largest diff. peak/hole / e Å <sup>-3</sup> | 0.20/-0.22   |

**Table A2-9:** Fractional atomic coordinates ( $\times 10^4$ ) and equivalent isotropic displacement parameters ( $\text{\AA}^2 \times 10^3$ ) for **3.27**.  $U_{eq}$  is defined as 1/3 of the trace of the orthogonalised  $U_{ij}$  tensor.

| Atom | x         | y           | z           | U(eq)     |
|------|-----------|-------------|-------------|-----------|
| O1   | 5629 (16) | 6684 (5)    | 7479 (8)    | 43.3 (19) |
| O1A  | 5782 (16) | 6486 (5)    | 7773 (7)    | 37.4 (17) |
| C1   | 6290 (40) | 6406 (7)    | 6591 (16)   | 31 (4)    |
| C1A  | 6440 (40) | 6370 (6)    | 6799 (15)   | 21 (3)    |
| C2   | 6463 (3)  | 5569.6 (13) | 6292 (2)    | 24.3 (5)  |
| C3   | 5452 (3)  | 4972.7 (13) | 6801 (2)    | 24.9 (5)  |
| C4   | 5405 (3)  | 4246.6 (13) | 6267.0 (19) | 23.7 (5)  |
| C5   | 6674 (3)  | 4096.4 (13) | 5381 (2)    | 24.5 (5)  |
| C6   | 7669 (3)  | 4685.6 (13) | 4869 (2)    | 24.8 (5)  |
| C7   | 7400 (3)  | 5449.8 (13) | 5243 (2)    | 25.1 (5)  |
| C8   | 7780 (20) | 6105 (5)    | 4355 (9)    | 23.2 (17) |
| C8A  | 7640 (20) | 6228 (5)    | 4634 (11)   | 34 (2)    |
| C9   | 8366 (7)  | 6828 (3)    | 5043 (4)    | 27.2 (9)  |
| C9A  | 7288 (9)  | 6833 (4)    | 5627 (6)    | 35.1 (14) |
| C10  | 7039 (11) | 7042 (4)    | 6027 (6)    | 34.5 (15) |
| C11  | 3831 (3)  | 3712.3 (14) | 6450 (2)    | 27.6 (5)  |

**Table A2-10:** Anisotropic Displacement Parameters ( $\text{\AA}^2 \times 10^3$ ) for **3.27**. The Anisotropic displacement factor exponent takes the form:  $-2\pi^2[h^2a^{*2}U_{11}+2hka^*b^*U_{12}+\dots]$ .

| Atom | U <sub>11</sub> | U <sub>22</sub> | U <sub>33</sub> | U <sub>23</sub> | U <sub>13</sub> | U <sub>12</sub> |
|------|-----------------|-----------------|-----------------|-----------------|-----------------|-----------------|
| O1   | 45 (4)          | 38 (4)          | 47 (5)          | -9 (3)          | 8 (4)           | -8 (3)          |
| O1A  | 47 (3)          | 39 (5)          | 25 (3)          | -3 (2)          | 9 (3)           | 2 (3)           |
| C1   | 24 (5)          | 36 (5)          | 31 (6)          | -3 (3)          | -11 (5)         | 0 (4)           |
| C1A  | 19 (5)          | 23 (4)          | 21 (5)          | 0 (2)           | -3 (5)          | 2 (3)           |
| C2   | 18.9 (10)       | 26.3 (11)       | 27.7 (11)       | 0.5 (9)         | -3.9 (9)        | 1.4 (8)         |
| C3   | 20.6 (10)       | 28.7 (11)       | 25.5 (11)       | 3.5 (9)         | -1.4 (9)        | 2.7 (9)         |
| C4   | 20.8 (10)       | 25.2 (11)       | 25.0 (11)       | 6.5 (9)         | -1.1 (9)        | 2.9 (8)         |
| C5   | 22.0 (10)       | 23.4 (11)       | 28.2 (11)       | 4.8 (9)         | -1.2 (9)        | 5.6 (8)         |
| C6   | 16.5 (9)        | 30.1 (11)       | 27.7 (11)       | 3.1 (9)         | 0.9 (9)         | 4.5 (9)         |
| C7   | 15.6 (9)        | 28.1 (11)       | 31.4 (11)       | 4.2 (9)         | -1.9 (9)        | -0.6 (8)        |
| C8   | 25 (4)          | 18 (3)          | 27 (4)          | 0 (2)           | 0 (3)           | -1 (3)          |
| C8A  | 21 (4)          | 34 (4)          | 47 (6)          | 7 (3)           | -1 (5)          | -3 (4)          |
| C9   | 28 (2)          | 27 (2)          | 27 (2)          | -1.8 (18)       | 5 (2)           | -6.7 (19)       |
| C9A  | 25 (3)          | 28 (3)          | 52 (4)          | 6 (3)           | -8 (3)          | -9 (3)          |
| C10  | 44 (3)          | 29 (3)          | 31 (3)          | -11 (2)         | 12 (3)          | -7 (3)          |
| C11  | 27.5 (11)       | 27.1 (11)       | 28.2 (11)       | 4.4 (9)         | 5.0 (10)        | -0.1 (9)        |

**Table A2-11:** Bond lengths for **3.27**.

| Atom | Atom | Length/ $\text{\AA}$ | Atom | Atom             | Length/ $\text{\AA}$ |
|------|------|----------------------|------|------------------|----------------------|
| O1   | C1   | 1.214 (18)           | C4   | C11              | 1.514 (3)            |
| O1A  | C1A  | 1.220 (15)           | C5   | C6               | 1.387 (3)            |
| C1   | C2   | 1.484 (13)           | C6   | C7               | 1.395 (3)            |
| C1   | C9A  | 1.512 (14)           | C7   | C8               | 1.533 (10)           |
| C1A  | C2   | 1.491 (11)           | C7   | C8A              | 1.514 (11)           |
| C1A  | C10  | 1.516 (10)           | C8   | C9               | 1.532 (9)            |
| C2   | C3   | 1.402 (3)            | C8   | C11 <sup>1</sup> | 1.548 (17)           |
| C2   | C7   | 1.392 (3)            | C8A  | C9A              | 1.550 (10)           |
| C3   | C4   | 1.387 (3)            | C8A  | C11 <sup>1</sup> | 1.650 (17)           |
| C4   | C5   | 1.406 (3)            | C9   | C10              | 1.537 (6)            |

<sup>1</sup>I-X,I-Y,I-Z

**Table A-12:** Bond angles for **3.27**.

| <b>Atom</b> | <b>Atom</b> | <b>Atom</b> | <b>Angle/°</b> | <b>Atom</b>     | <b>Atom</b> | <b>Atom</b>      | <b>Angle/°</b> |
|-------------|-------------|-------------|----------------|-----------------|-------------|------------------|----------------|
| O1          | C1          | C2          | 127.3 (10)     | C2              | C7          | C6               | 118.0 (2)      |
| O1          | C1          | C9A         | 127.1 (10)     | C2              | C7          | C8               | 122.7 (4)      |
| C2          | C1          | C9A         | 105.3 (11)     | C2              | C7          | C8A              | 108.2 (4)      |
| O1A         | C1A         | C2          | 120.0 (9)      | C6              | C7          | C8               | 117.9 (4)      |
| O1A         | C1A         | C10         | 120.8 (9)      | C6              | C7          | C8A              | 132.8 (4)      |
| C2          | C1A         | C10         | 118.8 (9)      | C7              | C8          | C11 <sup>1</sup> | 112.6 (9)      |
| C3          | C2          | C1          | 124.7 (8)      | C9              | C8          | C7               | 108.7 (7)      |
| C3          | C2          | C1A         | 120.9 (6)      | C9              | C8          | C11 <sup>1</sup> | 110.9 (8)      |
| C7          | C2          | C1          | 112.4 (6)      | C7              | C8A         | C9A              | 104.3 (7)      |
| C7          | C2          | C1A         | 117.9 (5)      | C7              | C8A         | C11 <sup>1</sup> | 108.2 (8)      |
| C7          | C2          | C3          | 121.0 (2)      | C9A             | C8A         | C11 <sup>1</sup> | 112.3 (9)      |
| C4          | C3          | C2          | 119.7 (2)      | C8              | C9          | C10              | 111.8 (6)      |
| C3          | C4          | C5          | 117.1 (2)      | C1              | C9A         | C8A              | 106.0 (8)      |
| C3          | C4          | C11         | 120.5 (2)      | C1A             | C10         | C9               | 115.1 (8)      |
| C5          | C4          | C11         | 121.2 (2)      | C4              | C11         | C8 <sup>1</sup>  | 114.3 (4)      |
| C6          | C5          | C4          | 121.9 (2)      | C4              | C11         | C8A <sup>1</sup> | 112.7 (4)      |
| C5          | C6          | C7          | 119.0 (2)      | C8 <sup>1</sup> | C11         | C8A <sup>1</sup> | 13.7 (6)       |

<sup>1</sup>I-X,I-Y,I-Z

**Table A2-13:** Torsion angles for **3.27**.

| A   | B   | C   | D                | Angle/°     | A                | B   | C   | D                | Angle/°     |
|-----|-----|-----|------------------|-------------|------------------|-----|-----|------------------|-------------|
| O1  | C1  | C2  | C3               | 20 (4)      | C3               | C4  | C11 | C8 <sup>1</sup>  | 81.4 (4)    |
| O1  | C1  | C2  | C7               | -176 (2)    | C3               | C4  | C11 | C8A <sup>1</sup> | 96.2 (4)    |
| O1  | C1  | C9A | C8A              | -173 (3)    | C4               | C5  | C6  | C7               | -0.1 (3)    |
| O1A | C1A | C2  | C3               | 12 (3)      | C5               | C4  | C11 | C8 <sup>1</sup>  | -85.8 (4)   |
| O1A | C1A | C2  | C7               | -172.9 (18) | C5               | C4  | C11 | C8A <sup>1</sup> | -71.0 (5)   |
| O1A | C1A | C10 | C9               | 161 (2)     | C5               | C6  | C7  | C2               | 14.7 (3)    |
| C1  | C2  | C3  | C4               | 164.3 (14)  | C5               | C6  | C7  | C8               | -152.0 (8)  |
| C1  | C2  | C7  | C6               | 179.5 (13)  | C5               | C6  | C7  | C8A              | -152.3 (10) |
| C1  | C2  | C7  | C8A              | -10.4 (15)  | C6               | C7  | C8  | C9               | -150.3 (6)  |
| C1A | C2  | C3  | C4               | 175.7 (13)  | C6               | C7  | C8  | C11 <sup>1</sup> | 86.4 (7)    |
| C1A | C2  | C7  | C6               | 169.8 (13)  | C6               | C7  | C8A | C9A              | -173.9 (4)  |
| C1A | C2  | C7  | C8               | -24.1 (15)  | C6               | C7  | C8A | C11 <sup>1</sup> | 66.4 (11)   |
| C2  | C1  | C9A | C8A              | 13 (2)      | C7               | C2  | C3  | C4               | 1.2 (3)     |
| C2  | C1A | C10 | C9               | -27 (3)     | C7               | C8  | C9  | C10              | -52.5 (12)  |
| C2  | C3  | C4  | C5               | 13.3 (3)    | C7               | C8A | C9A | C1               | -19.0 (17)  |
| C2  | C3  | C4  | C11              | -154.4 (2)  | C8               | C9  | C10 | C1A              | 47.0 (15)   |
| C2  | C7  | C8  | C9               | 43.6 (13)   | C9A              | C1  | C2  | C3               | -166.4 (9)  |
| C2  | C7  | C8  | C11 <sup>1</sup> | -79.7 (6)   | C9A              | C1  | C2  | C7               | -2 (2)      |
| C2  | C7  | C8A | C9A              | 18.1 (11)   | C10              | C1A | C2  | C3               | -160.4 (13) |
| C2  | C7  | C8A | C11 <sup>1</sup> | -101.6 (5)  | C10              | C1A | C2  | C7               | 14 (3)      |
| C3  | C2  | C7  | C6               | -15.5 (3)   | C11              | C4  | C5  | C6               | 153.5 (2)   |
| C3  | C2  | C7  | C8               | 150.6 (8)   | C11 <sup>1</sup> | C8  | C9  | C10              | 71.8 (8)    |
| C3  | C2  | C7  | C8A              | 154.6 (7)   | C11 <sup>1</sup> | C8A | C9A | C1               | 97.9 (15)   |
| C3  | C4  | C5  | C6               | -14.1 (3)   |                  |     |     |                  |             |

<sup>1</sup>I-X,I-Y,I-Z

**Table A2-14:** Hydrogen Atom Coordinates ( $\text{\AA}\times 10^4$ ) and Isotropic Displacement Parameters ( $\text{\AA}^2\times 10^3$ ) for **3.27**.

| Atom | <i>x</i> | <i>y</i> | <i>z</i> | U(eq) |
|------|----------|----------|----------|-------|
| H3   | 4800.47  | 5065.18  | 7509.8   | 30    |
| H5   | 6855.05  | 3576.04  | 5126.54  | 29    |
| H6   | 8520.15  | 4570.65  | 4272.18  | 30    |
| H8   | 8787.64  | 5937.23  | 3835.76  | 28    |
| H8A  | 8868.63  | 6281.64  | 4316.84  | 41    |
| H9A  | 8482.04  | 7270.74  | 4486.43  | 33    |
| H9B  | 9545.04  | 6732.5   | 5402.67  | 33    |
| H9C  | 8422.88  | 7038.97  | 5938.52  | 42    |
| H9D  | 6574.38  | 7271.49  | 5318.28  | 42    |
| H10A | 7587.47  | 7441.67  | 6542.46  | 41    |
| H10B | 5979.67  | 7278.94  | 5652.9   | 41    |
| H11A | 3451.43  | 3746.51  | 7290.27  | 33    |
| H11B | 4213.51  | 3170.48  | 6300.75  | 33    |
| H11C | 3245.33  | 3845.51  | 7210.37  | 33    |
| H11D | 4259.11  | 3169.55  | 6508.88  | 33    |

**Table A2-15:** Atomic occupancy for **3.27**.

| Atom | Occupancy | Atom | Occupancy | Atom | Occupancy |
|------|-----------|------|-----------|------|-----------|
| O1   | 0.5       | O1A  | 0.5       | C1   | 0.5       |
| C1A  | 0.5       | C8   | 0.5       | H8   | 0.5       |
| C8A  | 0.5       | H8A  | 0.5       | C9   | 0.5       |
| H9A  | 0.5       | H9B  | 0.5       | C9A  | 0.5       |
| H9C  | 0.5       | H9D  | 0.5       | C10  | 0.5       |
| H10A | 0.5       | H10B | 0.5       | H11A | 0.5       |
| H11B | 0.5       | H11C | 0.5       | H11D | 0.5       |

### 3.3 Compound 3.24

Sample: SB-bistetralol-1

X-ray Structure Report

for  
Prof. G. Bodwell

Prepared by

Louise N. Dawe, PhD

Department of Chemistry and Biochemistry  
Wilfrid Laurier University  
Science Building  
75 University Ave. W.  
Waterloo, ON, ON  
ldawe@wlu.ca

June 26, 2021

[Introduction](#)

Data for this structure was collected by Dr. JB Lin, Memorial University of Newfoundland.

SB-bistetralol-1 crystallized in the centrosymmetric space group  $P4_2/n$ . The asymmetric unit contains half of the molecule, with chiral centres at C1 and C8, both with *R*-configuration. The (*S,S*)-isomer is also present in the unit cell, generated by space group symmetry operations.

All non-hydrogen atoms were refined anisotropically. All hydrogen atoms were introduced in calculated positions and refined on a riding model, except H1A which was introduced in its difference map position and refined isotropically.

## Experimental

A single crystal of C<sub>22</sub>H<sub>24</sub>O<sub>2</sub> [**3.24**] was selected and diffraction data collected on a XtaLAB Synergy, Dualflex, HyPix diffractometer. The crystal was kept at 100.0(1) K during data collection. Using Olex2 [1], the structure was solved with the SHELXT [2] structure solution program using Intrinsic Phasing and refined with the SHELXL [3] refinement package using Least Squares minimisation.

1. Dolomanov, O.V., Bourhis, L.J., Gildea, R.J, Howard, J.A.K. & Puschmann, H. (2009), *J. Appl. Cryst.* 42, 339-341.
2. Sheldrick, G.M. (2015). *Acta Cryst.* A71, 3-8.
3. Sheldrick, G.M. (2015). *Acta Cryst.* C71, 3-8.

## Crystal structure determination

**Crystal Data for C<sub>22</sub>H<sub>24</sub>O<sub>2</sub> (*M* = 320.41 g/mol):** tetragonal, space group P4<sub>2</sub>/n (no. 86), *a* = 11.65420(10) Å, *c* = 11.99110(10) Å, *V* = 1628.64(3) Å<sup>3</sup>, *Z* = 4, *T* = 100.0(1) K,  $\mu(\text{Cu K}\alpha) = 0.639 \text{ mm}^{-1}$ , *D*<sub>calc</sub> = 1.307 g/cm<sup>3</sup>, 20468 reflections measured (10.586° ≤ 2θ ≤ 159.28°), 1757 unique (1644 with *I* > 2σ(*I*); *R*<sub>int</sub> = 0.0514, *R*<sub>sigma</sub> = 0.0204) which were used in all calculations. The final *R*<sub>1</sub> was 0.0448 (*I* > 2σ(*I*)) and *wR*<sub>2</sub> was 0.1236 (all data).

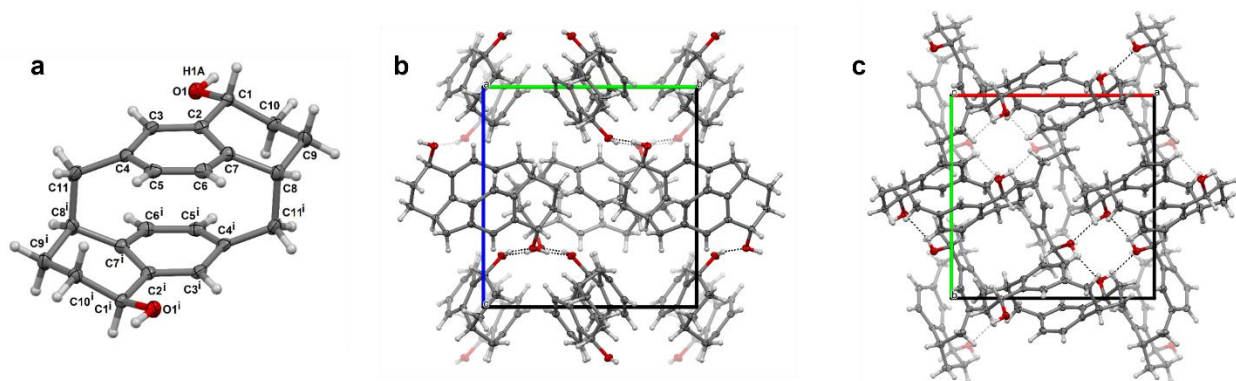


**Figure A2-3:** (a) Crystal structure of **3.24** with 50% displacement ellipsoids. (b) Packing for **3.24** with 50% displacement ellipsoids, viewed down the *a*-axis. (c) Packing for **3.24** with 50% displacement ellipsoids, viewed down the *c*-axis. CCDC 2106466 contains the crystallographic data for **3.24**.

**Table A2-16:** Crystal data and structure refinement for **3.24**.

|   |  |
|---|--|
| Identification code                         | SB-bistetralol-1   |
| Empirical formula                           | C <sub>22</sub> H <sub>24</sub> O <sub>2</sub>                                     |
| Formula weight                              | 320.41   |
| Temperature/K                               | 100.0(1)   |
| Crystal system                              | tetragonal   |
| Space group                                 | P4 <sub>2</sub> /n   |
| a/Å   | 11.65420(10)   |
| b/Å   | 11.65420(10)   |
| c/Å   | 11.99110(10)   |
| α/°   | 90   |
| β/°   | 90   |
| γ/°   | 90   |
| Volume/Å <sup>3</sup>                       | 1628.64(3)   |
| Z   | 4  |
| ρ <sub>calc</sub> /cm <sup>3</sup>          | 1.307  |
| μ/mm <sup>-1</sup>                          | 0.639  |
| F(000)                                      | 688.0  |
| Crystal size/mm <sup>3</sup>                | 0.5 × 0.2 × 0.1  |
| Radiation                                   | Cu Kα (λ = 1.54184)  |
| 2θ range for data collection/°              | 10.586 to 159.28   |
| Index ranges                                | -14 ≤ h ≤ 11, -14 ≤ k ≤ 14, -15 ≤ l ≤ 15   |
| Reflections collected                       | 20468  |
| Independent reflections                     | 1757 [1644 with I > 2σ(I); R <sub>int</sub> = 0.0514, R <sub>sigma</sub> = 0.0204] |
| Data/restraints/parameters                  | 1757/0/113   |
| Goodness-of-fit on F <sup>2</sup>           | 1.079  |
| Final R indexes [I >= 2σ (I)]               | R <sub>1</sub> = 0.0448, wR <sub>2</sub> = 0.1216                                  |
| Final R indexes [all data]                  | R <sub>1</sub> = 0.0466, wR <sub>2</sub> = 0.1236                                  |
| Largest diff. peak/hole / e Å <sup>-3</sup> | 0.27/-0.23   |

**Table A2-17:** Fractional atomic coordinates ( $\times 10^4$ ) and equivalent isotropic displacement Parameters ( $\text{\AA}^2 \times 10^3$ ) for **3.24**.  $U_{eq}$  is defined as 1/3 of the trace of the orthogonalised  $U_{ij}$  tensor.

| Atom | x           | y           | z           | U(eq)    |
|------|-------------|-------------|-------------|----------|
| C1   | 5055.4 (10) | 7569.0 (10) | 3537.6 (9)  | 17.8 (3) |
| C2   | 4531.5 (10) | 6465.5 (10) | 3966.2 (10) | 17.3 (3) |
| C3   | 4566.6 (10) | 5455.7 (10) | 3343.2 (10) | 19.2 (3) |
| C4   | 4109.5 (10) | 4428.6 (10) | 3753.6 (10) | 19.8 (3) |
| C5   | 3394.9 (10) | 4509.5 (11) | 4681.7 (11) | 20.8 (3) |
| C6   | 3376.0 (10) | 5500.6 (10) | 5324.1 (10) | 20.4 (3) |
| C7   | 4049.9 (10) | 6443.4 (10) | 5041.7 (10) | 19.0 (3) |
| C8   | 4439.6 (11) | 7267.9 (10) | 5944.9 (10) | 22.0 (3) |
| C9   | 4776.4 (12) | 8429.6 (11) | 5441.3 (11) | 24.9 (3) |
| C10  | 5599.4 (11) | 8275.5 (10) | 4463.4 (10) | 20.8 (3) |
| C11  | 4524.9 (12) | 3270.5 (11) | 3345.8 (10) | 24.0 (3) |
| O1   | 5868.7 (7)  | 7312.3 (7)  | 2674.7 (7)  | 20.0 (2) |

**Table A2-18:** Anisotropic displacement parameters ( $\text{\AA}^2 \times 10^3$ ) for **3.24**. The anisotropic displacement factor exponent takes the form:  $-2\pi^2[h^2a^2U_{11}+2hka*b*U_{12}+\dots]$ .

| Atom | $U_{11}$ | $U_{22}$ | $U_{33}$ | $U_{23}$ | $U_{13}$ | $U_{12}$ |
|------|----------|----------|----------|----------|----------|----------|
| C1   | 18.8 (5) | 19.7 (6) | 14.8 (5) | 0.2 (4)  | 2.1 (4)  | 2.3 (4)  |
| C2   | 15.8 (5) | 20.9 (6) | 15.0 (6) | 1.1 (4)  | -1.4 (4) | 0.5 (4)  |
| C3   | 21.3 (6) | 23.0 (6) | 13.2 (5) | 0.9 (4)  | -2.6 (4) | -1.9 (4) |
| C4   | 22.0 (6) | 22.1 (6) | 15.3 (6) | -0.7 (4) | -5.9 (4) | -3.2 (4) |
| C5   | 17.9 (5) | 22.9 (6) | 21.7 (6) | 4.5 (5)  | -3.1 (5) | -3.1 (4) |
| C6   | 17.1 (5) | 25.6 (6) | 18.5 (6) | 3.4 (5)  | 2.4 (4)  | 2.1 (4)  |
| C7   | 18.9 (6) | 20.9 (6) | 17.1 (6) | 1.0 (4)  | 1.1 (4)  | 2.8 (4)  |
| C8   | 29.9 (7) | 20.1 (6) | 16.0 (6) | -1.4 (4) | 6.2 (5)  | 1.2 (5)  |
| C9   | 37.7 (7) | 18.2 (6) | 18.8 (6) | -2.1 (5) | 4.5 (5)  | 0.8 (5)  |
| C10  | 26.6 (6) | 17.7 (5) | 18.0 (6) | -0.2 (4) | 0.3 (5)  | -2.2 (4) |
| C11  | 36.2 (7) | 21.3 (6) | 14.4 (6) | -2.0 (4) | -1.9 (5) | -5.2 (5) |
| O1   | 22.4 (5) | 20.1 (4) | 17.5 (5) | 0.0 (3)  | 5.7 (3)  | -0.7 (3) |

**Table A2-19: Bond lengths for 3.24.**

| Atom | Atom | Length/Å    | Atom | Atom             | Length/Å    |
|------|------|-------------|------|------------------|-------------|
| C1   | C2   | 1.5135 (16) | C4   | C11              | 1.5150 (17) |
| C1   | C10  | 1.5206 (16) | C5   | C6               | 1.3885 (17) |
| C1   | O1   | 1.4347 (13) | C6   | C7               | 1.3925 (17) |
| C2   | C3   | 1.3946 (16) | C7   | C8               | 1.5174 (16) |
| C2   | C7   | 1.4067 (16) | C8   | C9               | 1.5335 (17) |
| C3   | C4   | 1.3996 (16) | C8   | C11 <sup>1</sup> | 1.6042 (18) |
| C4   | C5   | 1.3932 (17) | C9   | C10              | 1.5255 (17) |

<sup>1</sup>I-X, I-Y, I-Z**Table A2-20: Bond angles for 3.24.**

| Atom | Atom | Atom | Angle/°     | Atom | Atom | Atom             | Angle/°     |
|------|------|------|-------------|------|------|------------------|-------------|
| C2   | C1   | C10  | 112.35 (9)  | C5   | C6   | C7               | 120.83 (11) |
| O1   | C1   | C2   | 109.52 (9)  | C2   | C7   | C8               | 121.55 (10) |
| O1   | C1   | C10  | 111.34 (9)  | C6   | C7   | C2               | 117.55 (11) |
| C3   | C2   | C1   | 121.56 (10) | C6   | C7   | C8               | 119.66 (10) |
| C3   | C2   | C7   | 119.16 (11) | C7   | C8   | C9               | 110.77 (10) |
| C7   | C2   | C1   | 119.20 (10) | C7   | C8   | C11 <sup>1</sup> | 110.85 (10) |
| C2   | C3   | C4   | 121.49 (11) | C9   | C8   | C11 <sup>1</sup> | 111.19 (10) |
| C3   | C4   | C11  | 121.79 (11) | C10  | C9   | C8               | 111.08 (10) |
| C5   | C4   | C3   | 116.77 (11) | C1   | C10  | C9               | 111.27 (10) |
| C5   | C4   | C11  | 120.61 (11) | C4   | C11  | C8 <sup>1</sup>  | 114.69 (10) |
| C6   | C5   | C4   | 120.60 (11) |      |      |                  |             |

<sup>1</sup>I-X, I-Y, I-Z**Table A2-21: Hydrogen bonds for 3.24.**

| D  | H   | A               | d(D-H)/Å | d(H-A)/Å | d(D-A)/Å    | D-H-A/° |
|----|-----|-----------------|----------|----------|-------------|---------|
| O1 | H1A | O1 <sup>1</sup> | 0.89 (2) | 1.87 (2) | 2.7386 (12) | 163 (2) |

<sup>1</sup>+Y, 3/2-X, 1/2-Z

**Table A2-22:** Torsion angles for **3.24**.

| A  | B  | C   | D                | Angle/°      | A                | B  | C   | D                | Angle/°      |
|----|----|-----|------------------|--------------|------------------|----|-----|------------------|--------------|
| C1 | C2 | C3  | C4               | 178.23 (11)  | C5               | C6 | C7  | C2               | 14.60 (17)   |
| C1 | C2 | C7  | C6               | 167.28 (10)  | C5               | C6 | C7  | C8               | -152.91 (11) |
| C1 | C2 | C7  | C8               | -25.45 (16)  | C6               | C7 | C8  | C9               | -159.56 (11) |
| C2 | C1 | C10 | C9               | -50.12 (13)  | C6               | C7 | C8  | C11 <sup>1</sup> | 76.51 (14)   |
| C2 | C3 | C4  | C5               | 14.28 (17)   | C7               | C2 | C3  | C4               | 1.52 (18)    |
| C2 | C3 | C4  | C11              | -155.38 (11) | C7               | C8 | C9  | C10              | -49.85 (14)  |
| C2 | C7 | C8  | C9               | 33.44 (16)   | C8               | C9 | C10 | C1               | 60.53 (14)   |
| C2 | C7 | C8  | C11 <sup>1</sup> | -90.49 (13)  | C10              | C1 | C2  | C3               | -143.90 (11) |
| C3 | C2 | C7  | C6               | -15.93 (17)  | C10              | C1 | C2  | C7               | 32.81 (15)   |
| C3 | C2 | C7  | C8               | 151.34 (11)  | C11              | C4 | C5  | C6               | 154.04 (12)  |
| C3 | C4 | C5  | C6               | -15.75 (17)  | C11 <sup>1</sup> | C8 | C9  | C10              | 73.89 (13)   |
| C3 | C4 | C11 | C8 <sup>1</sup>  | 91.08 (14)   | O1               | C1 | C2  | C3               | -19.61 (15)  |
| C4 | C5 | C6  | C7               | 1.45 (18)    | O1               | C1 | C2  | C7               | 157.10 (10)  |
| C5 | C4 | C11 | C8 <sup>1</sup>  | -78.19 (14)  | O1               | C1 | C10 | C9               | -173.39 (9)  |

<sup>1</sup>I-X,I-Y,I-Z**Table A2-23:** Hydrogen atom coordinates ( $\text{\AA}\times 10^4$ ) and isotropic displacement parameters ( $\text{\AA}^2\times 10^3$ ) for **3.24**.

| Atom | x         | y         | z         | U(eq)  |
|------|-----------|-----------|-----------|--------|
| H1   | 4438.87   | 8028.21   | 3206.31   | 21     |
| H3   | 4901.23   | 5464.94   | 2639.19   | 23     |
| H5   | 2926.36   | 3894.17   | 4872.69   | 25     |
| H6   | 2907.23   | 5535.11   | 5950.85   | 24     |
| H8   | 3792.75   | 7394.57   | 6452.33   | 26     |
| H9A  | 4092.07   | 8825.32   | 5188.28   | 30     |
| H9B  | 5138.61   | 8898.65   | 6009.29   | 30     |
| H10A | 5813.86   | 9022.39   | 4173.6    | 25     |
| H10B | 6291.18   | 7895.89   | 4720.67   | 25     |
| H11A | 4770.13   | 3347.37   | 2576.37   | 29     |
| H11B | 3885.32   | 2738.02   | 3359.56   | 29     |
| H1A  | 6219 (18) | 7970 (20) | 2494 (18) | 49 (5) |

### 3.4 Compound 3.25

Sample: SB-tetralol-2

X-ray Structure Report

for  
Prof. G. Bodwell

Prepared by

Louise N. Dawe, PhD

Department of Chemistry and Biochemistry  
Wilfrid Laurier University  
Science Building  
75 University Ave. W.  
Waterloo, ON, ON  
ldawe@wlu.ca

June 27, 2021

[Introduction](#)

Data for this structure was collected by Dr. JB Lin, Memorial University of Newfoundland.

SB-bistetralol-2 crystallized in the polar space group  $Pna2_1$ . The asymmetric unit contains the fully molecule, however, two areas of disorder are present (both aliphatic rings). The occupancy of the two components are 0.765(5): 0.235(5). Four stereocentres are present (C1, C8, C11, and C18). For the major occupancy component, these are (*S,S,S,R*) and for the minor component (*R,S,R,R*). Note that while the space group lacks an inversion centre, it does contain glide planes, and so the opposite isomers are generated by symmetry operations.

All non-hydrogen atoms were refined anisotropically, however, the minor component did exhibit some ellipsoids that were not physically reasonable, and so their displacements were either treated with an isotropic displacement restraint or were constrained to be identical to their corresponding major component. All hydrogen atoms were introduced in calculated positions and refined on a riding model, except H1 and H2 which were introduced in its difference map positions and refined isotropically.

## Experimental

A single crystal of C<sub>22</sub>H<sub>24</sub>O<sub>2</sub> [**3.25**] was selected and diffraction data collected on a XtaLAB Synergy, Dualflex, HyPix diffractometer. The crystal was kept at 100(2) K during data collection. Using Olex2 [1], the structure was solved with the SHELXT [2] structure solution program using Intrinsic Phasing and refined with the SHELXL [3] refinement package using Least Squares minimisation.

1. Dolomanov, O.V., Bourhis, L.J., Gildea, R.J., Howard, J.A.K. & Puschmann, H. (2009), *J. Appl. Cryst.* 42, 339-341.
2. Sheldrick, G.M. (2015). *Acta Cryst.* A71, 3-8.
3. Sheldrick, G.M. (2015). *Acta Cryst.* C71, 3-8.

## Crystal structure determination

**Crystal Data for C<sub>22</sub>H<sub>24</sub>O<sub>2</sub> (*M* = 320.41 g/mol):** orthorhombic, space group Pna2<sub>1</sub> (no. 33), *a* = 7.4774(2) Å, *b* = 17.6070(5) Å, *c* = 12.2773(3) Å, *V* = 1616.36(7) Å<sup>3</sup>, *Z* = 4, *T* = 100(2) K,  $\mu(\text{Cu K}\alpha) = 0.644 \text{ mm}^{-1}$ , *D*<sub>calc</sub> = 1.317 g/cm<sup>3</sup>, 19272 reflections measured (8.78° ≤ 2θ ≤ 148.978°), 2962 unique (2744 with *I* > 2σ(*I*)); *R*<sub>int</sub> = 0.0666, *R*<sub>sigma</sub> = 0.0405) which were used in all calculations. The final *R*<sub>1</sub> was 0.0690 (*I* > 2σ(*I*)) and *wR*<sub>2</sub> was 0.1898 (all data).

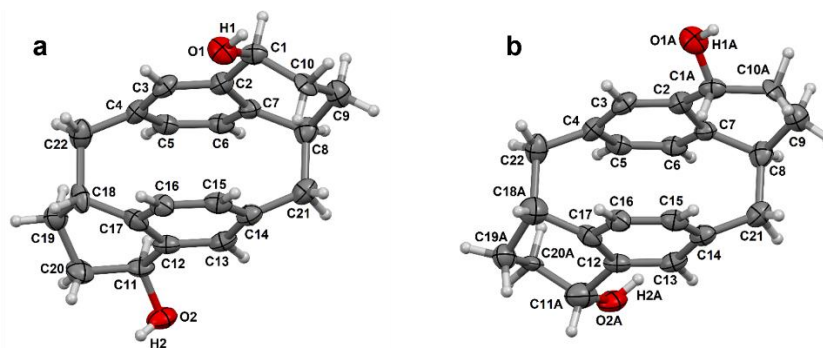


**Figure A2-4:** (a) Crystal structure of **3.25** with 50% displacement ellipsoids. (a) Major occupancy conformer. (b) Minor occupancy conformer. CCDC 2106467 contains the crystallographic data for **3.25**.

**Table A2-24:** Crystal data and structure refinement for **3.25**.

|   |  |
|---|--|
| Identification code                         | SB-tetralol-2  |
| Empirical formula                           | C <sub>22</sub> H <sub>24</sub> O <sub>2</sub>                                     |
| Formula weight                              | 320.41   |
| Temperature/K                               | 100(2)   |
| Crystal system                              | orthorhombic   |
| Space group                                 | Pna2 <sub>1</sub>  |
| a/Å   | 7.4774(2)  |
| b/Å   | 17.6070(5)   |
| c/Å   | 12.2773(3)   |
| α/°   | 90   |
| β/°   | 90   |
| γ/°   | 90   |
| Volume/Å <sup>3</sup>                       | 1616.36(7)   |
| Z   | 4  |
| ρ <sub>calc</sub> /cm <sup>3</sup>          | 1.317  |
| μ/mm <sup>-1</sup>                          | 0.644  |
| F(000)                                      | 688.0  |
| Crystal size/mm <sup>3</sup>                | 0.227 × 0.147 × 0.051  |
| Radiation                                   | Cu Kα (λ = 1.54184)  |
| 2θ range for data collection/°              | 8.78 to 148.978  |
| Index ranges                                | -9 ≤ h ≤ 9, -22 ≤ k ≤ 21, -15 ≤ l ≤ 13   |
| Reflections collected                       | 19272  |
| Independent reflections                     | 2962 [2744 with I > 2σ(I); R <sub>int</sub> = 0.0666, R <sub>sigma</sub> = 0.0405] |
| Data/restraints/parameters                  | 2962/30/266  |
| Goodness-of-fit on F <sup>2</sup>           | 1.071  |
| Final R indexes [I >= 2σ (I)]               | R <sub>1</sub> = 0.0690, wR <sub>2</sub> = 0.1865                                  |
| Final R indexes [all data]                  | R <sub>1</sub> = 0.0728, wR <sub>2</sub> = 0.1898                                  |
| Largest diff. peak/hole / e Å <sup>-3</sup> | 0.33/-0.34   |
| Flack parameter                             | 0.2(3)   |

**Table A2-25:** Fractional atomic coordinates ( $\times 10^4$ ) and equivalent isotropic displacement parameters ( $\text{\AA}^2 \times 10^3$ ) for **3.25**.  $U_{eq}$  is defined as 1/3 of the trace of the orthogonalised  $U_{ij}$  tensor.

| Atom | x          | y         | z         | U(eq)     |
|------|------------|-----------|-----------|-----------|
| O1   | 6701 (7)   | 3211 (3)  | 2709 (4)  | 46.5 (12) |
| O1A  | 5640 (20)  | 3310 (9)  | 2486 (16) | 46.5 (12) |
| O2   | 9508 (7)   | 6677 (3)  | 7312 (4)  | 46.4 (11) |
| O2A  | 8220 (20)  | 6765 (9)  | 6909 (13) | 46.4 (11) |
| C1   | 5307 (9)   | 3489 (4)  | 3424 (7)  | 36.1 (16) |
| C1A  | 5880 (40)  | 3450 (11) | 3570 (30) | 36.1 (16) |
| C2   | 5715 (6)   | 4303 (3)  | 3737 (4)  | 35.1 (11) |
| C3   | 6795 (7)   | 4784 (3)  | 3112 (4)  | 36.8 (11) |
| C4   | 7081 (6)   | 5538 (3)  | 3407 (4)  | 35.3 (11) |
| C5   | 5968 (6)   | 5840 (3)  | 4215 (4)  | 33.8 (11) |
| C6   | 4953 (6)   | 5371 (3)  | 4858 (4)  | 33.6 (10) |
| C7   | 4981 (6)   | 4585 (3)  | 4707 (4)  | 30.7 (10) |
| C8   | 4566 (7)   | 4069 (3)  | 5657 (4)  | 40.3 (11) |
| C9   | 3902 (7)   | 3298 (3)  | 5256 (5)  | 46.8 (13) |
| C10  | 5213 (10)  | 2993 (5)  | 4439 (7)  | 39 (2)    |
| C10A | 4780 (50)  | 2913 (18) | 4290 (30) | 39 (2)    |
| C11  | 9118 (14)  | 6558 (6)  | 6187 (6)  | 35.3 (19) |
| C11A | 9670 (50)  | 6500 (20) | 6180 (30) | 60 (14)   |
| C12  | 9115 (6)   | 5719 (3)  | 5853 (4)  | 34.5 (11) |
| C13  | 8085 (6)   | 5209 (3)  | 6454 (4)  | 36.5 (11) |
| C14  | 7841 (6)   | 4457 (3)  | 6116 (4)  | 35.4 (10) |
| C15  | 8990 (6)   | 4197 (3)  | 5294 (4)  | 37.5 (12) |
| C16  | 9983 (6)   | 4708 (3)  | 4685 (4)  | 36.3 (11) |
| C17  | 9895 (6)   | 5481 (3)  | 4878 (5)  | 37.3 (12) |
| C18  | 10188 (13) | 6050 (6)  | 3961 (7)  | 40 (3)    |
| C18A | 10400 (40) | 5935 (18) | 3860 (20) | 62 (18)   |
| C19  | 10017 (9)  | 6910 (4)  | 4293 (6)  | 43.1 (15) |
| C19A | 11120 (30) | 6668 (11) | 4480 (20) | 43.1 (15) |
| C20  | 10411 (12) | 7013 (4)  | 5501 (7)  | 46.7 (18) |
| C20A | 9630 (30)  | 7031 (12) | 5213 (19) | 32 (5)    |
| C21  | 6252 (7)   | 3996 (3)  | 6445 (5)  | 41.2 (11) |
| C22  | 8733 (7)   | 5960 (3)  | 3033 (5)  | 45.7 (13) |

**Table A2-26:** Anisotropic displacement parameters ( $\text{\AA}^2 \times 10^3$ ) for **3.25**. The anisotropic displacement factor exponent takes the form:  $-2\pi^2[h^2a^2U_{11}+2hka*b*U_{12}+\dots]$ .

| Atom | U <sub>11</sub> | U <sub>22</sub> | U <sub>33</sub> | U <sub>23</sub> | U <sub>13</sub> | U <sub>12</sub> |
|------|-----------------|-----------------|-----------------|-----------------|-----------------|-----------------|
| O1   | 47 (3)          | 40 (2)          | 52 (3)          | -14 (2)         | 5 (2)           | 3 (2)           |
| O1A  | 47 (3)          | 40 (2)          | 52 (3)          | -14 (2)         | 5 (2)           | 3 (2)           |
| O2   | 64 (3)          | 43 (2)          | 32 (2)          | -11 (2)         | -10 (2)         | 2 (2)           |
| O2A  | 64 (3)          | 43 (2)          | 32 (2)          | -11 (2)         | -10 (2)         | 2 (2)           |
| C1   | 33 (4)          | 40 (3)          | 35 (4)          | -6 (2)          | -6 (4)          | 7 (3)           |
| C1A  | 33 (4)          | 40 (3)          | 35 (4)          | -6 (2)          | -6 (4)          | 7 (3)           |
| C2   | 37 (2)          | 37 (2)          | 31 (3)          | 0 (2)           | -2 (2)          | 2.6 (18)        |
| C3   | 47 (3)          | 38 (2)          | 25 (2)          | -2 (2)          | 0 (2)           | 8 (2)           |
| C4   | 41 (2)          | 37 (2)          | 28 (3)          | 6 (2)           | 1 (2)           | 5.5 (18)        |
| C5   | 31 (2)          | 33 (2)          | 38 (3)          | -6 (2)          | -8 (2)          | 3.3 (17)        |
| C6   | 30 (2)          | 39 (2)          | 32 (3)          | -10.9 (19)      | -2.7 (19)       | 5.4 (16)        |
| C7   | 31 (2)          | 36 (2)          | 25 (2)          | -2.4 (19)       | -3.1 (18)       | -1.8 (16)       |
| C8   | 46 (3)          | 42 (2)          | 34 (3)          | -4 (2)          | 10 (2)          | 0 (2)           |
| C9   | 44 (3)          | 42 (3)          | 54 (3)          | 2 (2)           | 2 (3)           | -4.9 (19)       |
| C10  | 49 (5)          | 22 (3)          | 46 (4)          | -10 (3)         | -7 (4)          | -15 (3)         |
| C10A | 49 (5)          | 22 (3)          | 46 (4)          | -10 (3)         | -7 (4)          | -15 (3)         |
| C11  | 39 (4)          | 38 (4)          | 29 (4)          | -13 (3)         | -6 (3)          | 4 (3)           |
| C11A | 71 (19)         | 53 (15)         | 56 (17)         | -3 (10)         | -19 (12)        | 1 (12)          |
| C12  | 34 (2)          | 39 (2)          | 31 (3)          | -9 (2)          | -8.5 (19)       | 4.1 (17)        |
| C13  | 40 (2)          | 44 (3)          | 25 (2)          | -5 (2)          | -3 (2)          | 10 (2)          |
| C14  | 36 (2)          | 41 (2)          | 28 (3)          | -4 (2)          | -1 (2)          | 5.8 (18)        |
| C15  | 35 (2)          | 38 (2)          | 40 (3)          | -10 (2)         | -6 (2)          | 6.0 (17)        |
| C16  | 32 (2)          | 43 (2)          | 34 (3)          | -10 (2)         | 3 (2)           | -0.9 (17)       |
| C17  | 25 (2)          | 43 (3)          | 44 (3)          | -9 (2)          | 1 (2)           | -4.4 (17)       |
| C18  | 41 (4)          | 37 (4)          | 42 (5)          | -8 (3)          | 21 (4)          | -9 (3)          |
| C18A | 60 (20)         | 70 (20)         | 50 (20)         | -2 (12)         | -2 (12)         | -13 (11)        |
| C19  | 48 (3)          | 34 (3)          | 47 (4)          | 4 (3)           | -5 (3)          | -5 (2)          |
| C19A | 48 (3)          | 34 (3)          | 47 (4)          | 4 (3)           | -5 (3)          | -5 (2)          |
| C20  | 52 (4)          | 40 (4)          | 47 (5)          | -12 (3)         | -5 (4)          | -10 (3)         |
| C20A | 33 (9)          | 34 (8)          | 31 (10)         | -3 (7)          | -17 (8)         | -5 (7)          |
| C21  | 49 (3)          | 42 (2)          | 32 (2)          | 3 (2)           | 2 (2)           | 6 (2)           |
| C22  | 45 (3)          | 39 (2)          | 53 (3)          | 12 (2)          | 8 (3)           | 4 (2)           |

**Table A2-27: Bond lengths for 3.25.**

| <b>Atom</b> | <b>Atom</b> | <b>Length/Å</b> | <b>Atom</b> | <b>Atom</b> | <b>Length/Å</b> |
|-------------|-------------|-----------------|-------------|-------------|-----------------|
| O1          | C1          | 1.448 (9)       | C11         | C12         | 1.534 (11)      |
| O1A         | C1A         | 1.37 (4)        | C11         | C20         | 1.511 (11)      |
| O2          | C11         | 1.427 (9)       | C11A        | C12         | 1.50 (5)        |
| O2A         | C11A        | 1.48 (2)        | C11A        | C20A        | 1.51 (2)        |
| C1          | C2          | 1.515 (8)       | C12         | C13         | 1.393 (7)       |
| C1          | C10         | 1.524 (10)      | C12         | C17         | 1.396 (8)       |
| C1A         | C2          | 1.52 (2)        | C13         | C14         | 1.401 (7)       |
| C1A         | C10A        | 1.53 (2)        | C14         | C15         | 1.403 (7)       |
| C2          | C3          | 1.400 (7)       | C14         | C21         | 1.494 (7)       |
| C2          | C7          | 1.402 (7)       | C15         | C16         | 1.385 (7)       |
| C3          | C4          | 1.392 (7)       | C16         | C17         | 1.383 (6)       |
| C4          | C5          | 1.400 (7)       | C17         | C18         | 1.523 (9)       |
| C4          | C22         | 1.514 (7)       | C17         | C18A        | 1.53 (2)        |
| C5          | C6          | 1.371 (7)       | C18         | C19         | 1.573 (12)      |
| C6          | C7          | 1.396 (6)       | C18         | C22         | 1.583 (10)      |
| C7          | C8          | 1.512 (7)       | C18A        | C19A        | 1.59 (2)        |
| C8          | C9          | 1.525 (7)       | C18A        | C22         | 1.61 (2)        |
| C8          | C21         | 1.595 (7)       | C19         | C20         | 1.523 (11)      |
| C9          | C10         | 1.502 (9)       | C19A        | C20A        | 1.57 (2)        |
| C9          | C10A        | 1.52 (2)        |             |             |                 |

**Table A2-28: Bond angles for 3.25.**

| Atom Atom Atom | Angle/°    | Atom Atom Atom | Angle/°    |
|----------------|------------|----------------|------------|
| O1 C1 C2       | 109.2 (5)  | O2A C11A C20A  | 106 (2)    |
| O1 C1 C10      | 109.5 (5)  | C12 C11A C20A  | 110 (3)    |
| C2 C1 C10      | 110.2 (6)  | C13 C12 C11    | 118.7 (5)  |
| O1A C1A C2     | 107 (2)    | C13 C12 C11A   | 127.2 (11) |
| O1A C1A C10A   | 112 (2)    | C13 C12 C17    | 119.5 (4)  |
| C2 C1A C10A    | 119 (2)    | C17 C12 C11    | 121.1 (5)  |
| C3 C2 C1       | 123.3 (5)  | C17 C12 C11A   | 113.0 (11) |
| C3 C2 C1A      | 118.5 (13) | C12 C13 C14    | 121.6 (5)  |
| C3 C2 C7       | 118.5 (4)  | C13 C14 C15    | 116.2 (5)  |
| C7 C2 C1       | 118.2 (5)  | C13 C14 C21    | 122.5 (4)  |
| C7 C2 C1A      | 119.7 (13) | C15 C14 C21    | 120.3 (4)  |
| C4 C3 C2       | 121.5 (5)  | C16 C15 C14    | 120.3 (4)  |
| C3 C4 C5       | 117.1 (4)  | C17 C16 C15    | 121.4 (4)  |
| C3 C4 C22      | 120.9 (4)  | C12 C17 C18    | 119.8 (6)  |
| C5 C4 C22      | 120.9 (4)  | C12 C17 C18A   | 130.2 (15) |
| C6 C5 C4       | 120.6 (4)  | C16 C17 C12    | 117.5 (5)  |
| C5 C6 C7       | 120.8 (4)  | C16 C17 C18    | 121.0 (6)  |
| C2 C7 C8       | 121.5 (4)  | C16 C17 C18A   | 111.3 (14) |
| C6 C7 C2       | 118.0 (4)  | C17 C18 C19    | 115.5 (8)  |
| C6 C7 C8       | 119.4 (4)  | C17 C18 C22    | 111.5 (5)  |
| C7 C8 C9       | 110.7 (4)  | C19 C18 C22    | 103.1 (7)  |
| C7 C8 C21      | 110.7 (4)  | C17 C18A C19A  | 96.8 (16)  |
| C9 C8 C21      | 112.5 (4)  | C17 C18A C22   | 109.8 (17) |
| C10 C9 C8      | 108.8 (4)  | C19A C18A C22  | 123 (2)    |
| C10A C9 C8     | 120.6 (11) | C20 C19 C18    | 110.6 (6)  |
| C9 C10 C1      | 111.7 (7)  | C20A C19A C18A | 111 (2)    |
| C9 C10A C1A    | 114 (2)    | C11 C20 C19    | 110.8 (7)  |
| O2 C11 C12     | 113.6 (7)  | C11A C20A C19A | 100.7 (18) |
| O2 C11 C20     | 109.3 (7)  | C14 C21 C8     | 114.9 (4)  |
| C20 C11 C12    | 111.3 (7)  | C4 C22 C18     | 113.0 (5)  |
| O2A C11A C12   | 104 (3)    | C4 C22 C18A    | 115.2 (10) |

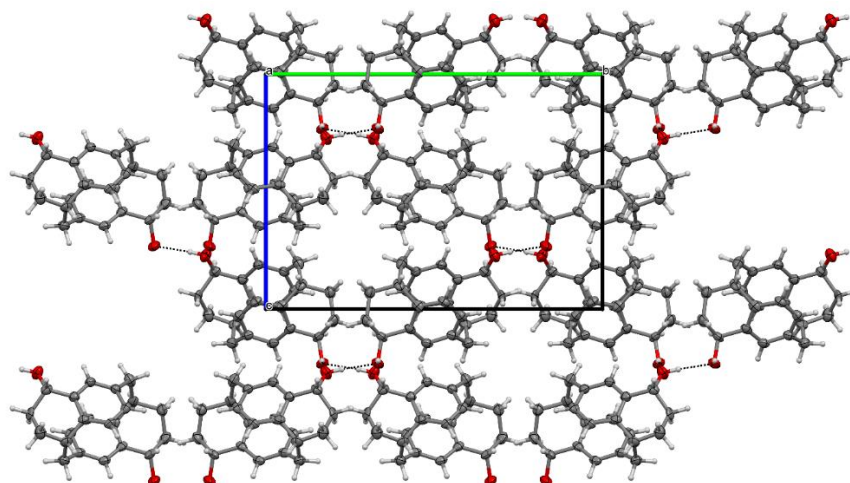


**Figure A2-5:** Extended packing diagram of **3.25** (major conformer only) with 50% displacement ellipsoids, viewed down the *a*-axis. Hydrogen bonds indicated with dashed lines. The same motif is observed for the minor occupancy conformer.

**Table A2-29:** Hydrogen bonds for **3.25**.

| D  | H  | A               | d(D-H)/Å | d(H-A)/Å | d(D-A)/Å  | D-H-A/°  |
|----|----|-----------------|----------|----------|-----------|----------|
| O1 | H1 | O2 <sup>1</sup> | 0.85 (3) | 2.04 (3) | 2.889 (6) | 172 (8)  |
| O2 | H2 | O1 <sup>2</sup> | 0.85 (3) | 2.10 (5) | 2.883 (7) | 153 (10) |

<sup>1</sup>3/2-X,-1/2+Y,-1/2+Z; <sup>2</sup>2-X,1-Y,1/2+Z

**Table A2-30: Torsion angles for 3.25.**

| A   | B            | C      | D    | Angle/°     | A                | B            | C        | D    | Angle/°     |
|-----|--------------|--------|------|-------------|------------------|--------------|----------|------|-------------|
| O1  | C1           | C2     | C3   | 23.4 (8)    | C11              | C12          | C13      | C14  | 171.9 (6)   |
| O1  | C1           | C2     | C7   | -156.1 (5)  | C11              | C12          | C17      | C16  | 174.1 (6)   |
| O1  | C1           | C10    | C9   | 174.8 (5)   | C11              | C12          | C17      | C18  | -20.9 (8)   |
| O1A | C1A          | C2     | C3   | -54 (2)     | C11AC12          | C13          | C14      |      | -171.9 (17) |
| O1A | C1A          | C2     | C7   | 146.7 (14)  | C11AC12          | C17          | C16      |      | 158.6 (15)  |
| O1A | C1A          | C10AC9 |      | -139 (2)    | C11AC12          | C17          | C18A     |      | -34 (2)     |
| O2  | C11          | C12    | C13  | 51.8 (9)    | C12              | C11          | C20      | C19  | 54.6 (10)   |
| O2  | C11          | C12    | C17  | -137.9 (6)  | C12              | C11AC20AC19A |          |      | -64 (3)     |
| O2  | C11          | C20    | C19  | -179.1 (7)  | C12              | C13          | C14      | C15  | 13.9 (7)    |
| O2A | C11AC12      | C13    |      | -29 (3)     | C12              | C13          | C14      | C21  | -154.9 (5)  |
| O2A | C11AC12      | C17    |      | 157.0 (14)  | C12              | C17          | C18      | C19  | 14.6 (9)    |
| O2A | C11AC20AC19A |        |      | -176 (3)    | C12              | C17          | C18      | C22  | -102.7 (8)  |
| C1  | C2           | C3     | C4   | 177.5 (5)   | C12              | C17          | C18AC19A |      | 39 (2)      |
| C1  | C2           | C7     | C6   | -163.6 (4)  | C12              | C17          | C18AC22  |      | -89.4 (19)  |
| C1  | C2           | C7     | C8   | 28.3 (7)    | C13              | C12          | C17      | C16  | -15.6 (7)   |
| C1A | C2           | C3     | C4   | -162.6 (14) | C13              | C12          | C17      | C18  | 149.4 (5)   |
| C1A | C2           | C7     | C6   | 176.2 (13)  | C13              | C12          | C17      | C18A | 152.1 (13)  |
| C1A | C2           | C7     | C8   | 8.2 (14)    | C13              | C14          | C15      | C16  | -15.0 (7)   |
| C2  | C1           | C10    | C9   | 54.6 (7)    | C13              | C14          | C21      | C8   | 88.6 (6)    |
| C2  | C1A          | C10AC9 |      | -12 (4)     | C14              | C15          | C16      | C17  | 1.0 (7)     |
| C2  | C3           | C4     | C5   | -12.9 (7)   | C15              | C14          | C21      | C8   | -79.8 (6)   |
| C2  | C3           | C4     | C22  | 155.7 (5)   | C15              | C16          | C17      | C12  | 14.6 (7)    |
| C2  | C7           | C8     | C9   | -35.9 (6)   | C15              | C16          | C17      | C18  | -150.2 (6)  |
| C2  | C7           | C8     | C21  | 89.5 (5)    | C15              | C16          | C17      | C18A | -155.4 (12) |
| C3  | C2           | C7     | C6   | 16.9 (6)    | C16              | C17          | C18      | C19  | 179.0 (5)   |
| C3  | C2           | C7     | C8   | -151.2 (5)  | C16              | C17          | C18      | C22  | 61.7 (10)   |
| C3  | C4           | C5     | C6   | 15.1 (7)    | C16              | C17          | C18AC19A |      | -152.5 (14) |
| C3  | C4           | C22    | C18  | -103.7 (7)  | C16              | C17          | C18AC22  |      | 79 (2)      |
| C3  | C4           | C22    | C18A | -92.9 (16)  | C17              | C12          | C13      | C14  | 1.4 (7)     |
| C4  | C5           | C6     | C7   | -1.3 (7)    | C17              | C18          | C19      | C20  | 25.2 (9)    |
| C5  | C4           | C22    | C18  | 64.4 (7)    | C17              | C18          | C22      | C4   | 19.1 (10)   |
| C5  | C4           | C22    | C18A | 75.3 (16)   | C17              | C18AC19AC20A |          |      | -59 (2)     |
| C5  | C6           | C7     | C2   | -14.9 (6)   | C17              | C18AC22      | C4       |      | -1 (3)      |
| C5  | C6           | C7     | C8   | 153.4 (5)   | C18              | C19          | C20      | C11  | -59.9 (9)   |
| C6  | C7           | C8     | C9   | 156.2 (4)   | C18AC19AC20AC11A |              |          |      | 79 (3)      |
| C6  | C7           | C8     | C21  | -78.4 (5)   | C19              | C18          | C22      | C4   | -105.5 (6)  |
| C7  | C2           | C3     | C4   | -3.0 (7)    | C19AC18AC22      | C4           |          |      | -113 (2)    |
| C7  | C8           | C9     | C10  | 51.9 (7)    | C20              | C11          | C12      | C13  | 175.7 (6)   |
| C7  | C8           | C9     | C10A | 41 (2)      | C20              | C11          | C12      | C17  | -14.0 (10)  |

**Table A2-30:** Torsion angles for **3.25**.

| <b>A</b> | <b>B</b> | <b>C</b> | <b>D</b> | <b>Angle/°</b> | <b>A</b> | <b>B</b> | <b>C</b> | <b>D</b> | <b>Angle/°</b> |
|----------|----------|----------|----------|----------------|----------|----------|----------|----------|----------------|
| C7       | C8       | C21      | C14      | 1.6 (6)        | C20A     | C11A     | C12      | C13      | -142.3 (14)    |
| C8       | C9       | C10      | C1       | -64.4 (7)      | C20A     | C11A     | C12      | C17      | 44 (2)         |
| C8       | C9       | C10A     | C1A      | -19 (4)        | C21      | C8       | C9       | C10      | -72.5 (7)      |
| C9       | C8       | C21      | C14      | 126.0 (5)      | C21      | C8       | C9       | C10A     | -83 (2)        |
| C10      | C1       | C2       | C3       | 143.8 (6)      | C21      | C14      | C15      | C16      | 154.0 (5)      |
| C10      | C1       | C2       | C7       | -35.7 (7)      | C22      | C4       | C5       | C6       | -153.5 (5)     |
| C10A     | C1A      | C2       | C3       | 177 (2)        | C22      | C18      | C19      | C20      | 147.1 (6)      |
| C10A     | C1A      | C2       | C7       | 17 (3)         | C22      | C18A     | C19A     | C20A     | 60 (3)         |

**Table A2-31:** Hydrogen atom coordinates ( $\text{\AA}\times 10^4$ ) and isotropic displacement parameters ( $\text{\AA}^2\times 10^3$ ) for 3.25.

| Atom | <i>x</i>   | <i>y</i>  | <i>z</i>  | U(eq) |
|------|------------|-----------|-----------|-------|
| H1   | 6440 (110) | 2750 (20) | 2570 (80) | 70    |
| H1A  | 5610.98    | 2839.31   | 2378.9    | 70    |
| H2   | 10640 (40) | 6660 (50) | 7200 (90) | 70    |
| H2A  | 7332.4     | 6473.75   | 6844.84   | 70    |
| H1B  | 4133.04    | 3469.67   | 3034.67   | 43    |
| H1C  | 7155.71    | 3325.13   | 3723.3    | 43    |
| H3   | 7346.04    | 4591.99   | 2471.33   | 44    |
| H5   | 5914.78    | 6373.87   | 4319.15   | 41    |
| H6   | 4222.33    | 5583.32   | 5413.11   | 40    |
| H8   | 3574.53    | 4307.75   | 6082.54   | 48    |
| H9A  | 3792.82    | 2942.56   | 5876.62   | 56    |
| H9B  | 2709.66    | 3354.3    | 4914.56   | 56    |
| H9C  | 3980.07    | 2942.11   | 5877.83   | 56    |
| H9D  | 2616.74    | 3355.69   | 5080.54   | 56    |
| H10A | 4855.11    | 2471.65   | 4227.98   | 47    |
| H10B | 6413.6     | 2964.11   | 4776.9    | 47    |
| H10C | 3839.37    | 2673.1    | 3836.02   | 47    |
| H10D | 5573.25    | 2503.93   | 4557.78   | 47    |
| H11  | 7892.14    | 6762.65   | 6047.48   | 42    |
| H11A | 10860.84   | 6508.48   | 6554.38   | 72    |
| H13  | 7535.59    | 5376.89   | 7108.82   | 44    |
| H15  | 9087.67    | 3667.59   | 5153.42   | 45    |
| H16  | 10740.1    | 4523.15   | 4123.22   | 44    |
| H18  | 11399.35   | 5963.51   | 3639.29   | 48    |
| H18A | 11428.82   | 5677.9    | 3496.27   | 74    |
| H19A | 10867.44   | 7216.86   | 3859.32   | 52    |
| H19B | 8792.21    | 7091.34   | 4132.16   | 52    |
| H19C | 12153.13   | 6524.91   | 4945.09   | 52    |
| H19D | 11536.6    | 7046      | 3943.66   | 52    |
| H20A | 11649.08   | 6846.34   | 5656.48   | 56    |
| H20B | 10313.01   | 7557.46   | 5692.96   | 56    |
| H20C | 9928.81    | 7558.78   | 5420.68   | 39    |
| H20D | 8449.12    | 7022.65   | 4846.57   | 39    |
| H21A | 5886.54    | 4152.14   | 7187.15   | 49    |
| H21B | 6611.58    | 3455.6    | 6480.52   | 49    |
| H22A | 8378.67    | 6470.4    | 2772.86   | 55    |
| H22B | 9271.28    | 5684.3    | 2410.97   | 55    |
| H22C | 8407.63    | 6497.57   | 2905.15   | 55    |
| H22D | 9121.85    | 5744.04   | 2326.83   | 55    |

**Table A2-32: Atomic occupancy for 3.25.**

| <b>Atom</b> | <b>Occupancy</b> | <b>Atom</b> | <b>Occupancy</b> | <b>Atom</b> | <b>Occupancy</b> |
|-------------|------------------|-------------|------------------|-------------|------------------|
| O1          | 0.765 (5)        | H1          | 0.765 (5)        | O1A         | 0.235 (5)        |
| H1A         | 0.235 (5)        | O2          | 0.765 (5)        | H2          | 0.765 (5)        |
| O2A         | 0.235 (5)        | H2A         | 0.235 (5)        | C1          | 0.765 (5)        |
| H1B         | 0.765 (5)        | C1A         | 0.235 (5)        | H1C         | 0.235 (5)        |
| H9A         | 0.765 (5)        | H9B         | 0.765 (5)        | H9C         | 0.235 (5)        |
| H9D         | 0.235 (5)        | C10         | 0.765 (5)        | H10A        | 0.765 (5)        |
| H10B        | 0.765 (5)        | C10A        | 0.235 (5)        | H10C        | 0.235 (5)        |
| H10D        | 0.235 (5)        | C11         | 0.765 (5)        | H11         | 0.765 (5)        |
| C11A        | 0.235 (5)        | H11A        | 0.235 (5)        | C18         | 0.765 (5)        |
| H18         | 0.765 (5)        | C18A        | 0.235 (5)        | H18A        | 0.235 (5)        |
| C19         | 0.765 (5)        | H19A        | 0.765 (5)        | H19B        | 0.765 (5)        |
| C19A        | 0.235 (5)        | H19C        | 0.235 (5)        | H19D        | 0.235 (5)        |
| C20         | 0.765 (5)        | H20A        | 0.765 (5)        | H20B        | 0.765 (5)        |
| C20A        | 0.235 (5)        | H20C        | 0.235 (5)        | H20D        | 0.235 (5)        |
| H22A        | 0.765 (5)        | H22B        | 0.765 (5)        | H22C        | 0.235 (5)        |
| H22D        | 0.235 (5)        |             |                  |             |                  |

### 3.5 Compound 3.3

Sample: SB-003-79

#### X-ray Structure Report

for

Prof. G. Bodwell

Prepared by

Louise N. Dawe, PhD

Department of Chemistry and Biochemistry  
Wilfrid Laurier University  
Science Building  
75 University Ave. W.  
Waterloo, ON, ON  
ldawe@wlu.ca

August 26, 2020

[Introduction](#)

Data for this structure was collected by Dr. Jian-Bin Lin, Centre for Chemical Analysis, Research and Training (C-CART), Memorial University of Newfoundland.

H-atoms were introduced in calculated positions and refined on a riding model, while all other atoms were introduced in difference map positions and refined anisotropically.

## Experimental

A single crystal of C<sub>22</sub>H<sub>16</sub> was selected and collected on a XtaLAB Synergy, Dualflex, HyPix diffractometer. The crystal was kept at 100(2) K during data collection. Using Olex2 [1], the structure was solved with the SHELXT [2] structure solution program using Intrinsic Phasing and refined with the SHELXL [3] refinement package using Least Squares minimisation.

4. Dolomanov, O.V., Bourhis, L.J., Gildea, R.J, Howard, J.A.K. & Puschmann, H. (2009), *J. Appl. Cryst.* 42, 339-341.
5. Sheldrick, G.M. (2015). *Acta Cryst.* A71, 3-8.
6. Sheldrick, G.M. (2015). *Acta Cryst.* C71, 3-8.

### Crystal structure determination

**Crystal Data** for C<sub>22</sub>H<sub>16</sub> ( $M = 280.35$  g/mol): monoclinic, space group P2<sub>1</sub>/n (no. 14),  $a = 6.96850(10)$  Å,  $b = 11.5185(3)$  Å,  $c = 8.5135(2)$  Å,  $\beta = 94.649(2)^\circ$ ,  $V = 681.10(3)$  Å<sup>3</sup>,  $Z = 2$ ,  $T = 100(2)$  K,  $\mu(\text{Cu K}\alpha) = 0.584$  mm<sup>-1</sup>,  $D_{\text{calc}} = 1.367$  g/cm<sup>3</sup>, 8777 reflections measured ( $12.958^\circ \leq 2\theta \leq 153.996^\circ$ ), 1425 unique (1248 with  $I > 2\sigma(I)$ );  $R_{\text{int}} = 0.0550$ ,  $R_{\text{sigma}} = 0.0338$ ) which were used in all calculations. The final  $R_1$  was 0.0482 ( $I > 2\sigma(I)$ ) and  $wR_2$  was 0.1294 (all data).

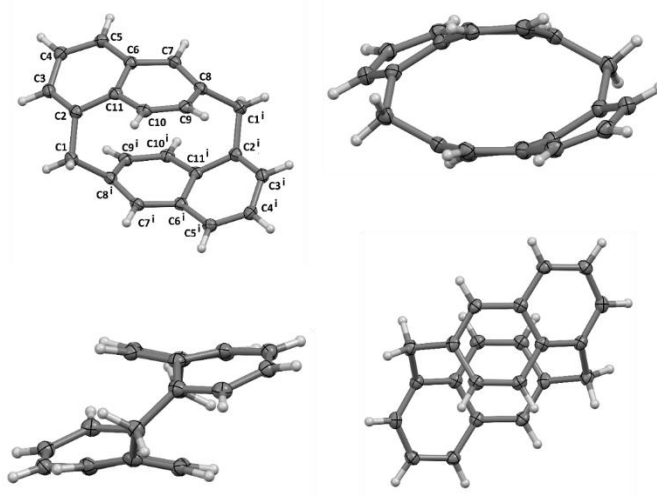


**Figure A2-6:** Four views of the structure of **3.3** with 50% displacement ellipsoids. CCDC 2105261 contains the crystallographic data for **3.3**.

**Table A2-33:** Crystal data and structure refinement for **3.3**.

|   |  |
|---|--|
| Identification code                         | SB-003-79  |
| Empirical formula                           | C <sub>22</sub> H <sub>16</sub>  |
| Formula weight                              | 280.35   |
| Temperature/K                               | 100(2)   |
| Crystal system                              | monoclinic   |
| Space group                                 | P2 <sub>1</sub> /n   |
| a/Å   | 6.96850(10)  |
| b/Å   | 11.5185(3)   |
| c/Å   | 8.5135(2)  |
| α/°   | 90   |
| β/°   | 94.649(2)  |
| γ/°   | 90   |
| Volume/Å <sup>3</sup>                       | 681.10(3)  |
| Z   | 2  |
| ρ <sub>calc</sub> /cm <sup>3</sup>          | 1.367  |
| μ/mm <sup>-1</sup>                          | 0.584  |
| F(000)                                      | 296.0  |
| Crystal size/mm <sup>3</sup>                | 0.11 × 0.07 × 0.05   |
| Radiation                                   | Cu Kα (λ = 1.54184)  |
| 2θ range for data collection/°              | 12.958 to 153.996  |
| Index ranges                                | -8 ≤ h ≤ 7, -14 ≤ k ≤ 13, -10 ≤ l ≤ 10   |
| Reflections collected                       | 8777   |
| Independent reflections                     | 1425 [1248 with I > 2σ(I); R <sub>int</sub> = 0.0550, R <sub>sigma</sub> = 0.0338] |
| Data/restraints/parameters                  | 1425/0/100   |
| Goodness-of-fit on F <sup>2</sup>           | 1.082  |
| Final R indexes [I ≥ 2σ (I)]                | R <sub>1</sub> = 0.0482, wR <sub>2</sub> = 0.1252                                  |
| Final R indexes [all data]                  | R <sub>1</sub> = 0.0546, wR <sub>2</sub> = 0.1294                                  |
| Largest diff. peak/hole / e Å <sup>-3</sup> | 0.30/-0.25   |

**Table A2-34:** Fractional atomic coordinates ( $\times 10^4$ ) and equivalent isotropic displacement parameters ( $\text{\AA}^2 \times 10^3$ ) for **3.3**.  $U_{\text{eq}}$  is defined as 1/3 of the trace of the orthogonalised  $U_{\text{ij}}$  tensor.

| Atom | <i>x</i> | <i>y</i>    | <i>z</i>    | $U(\text{eq})$ |
|------|----------|-------------|-------------|----------------|
| C1   | 4617 (2) | 5727.5 (13) | 1747.5 (17) | 24.0 (4)       |
| C2   | 4084 (2) | 6685.5 (13) | 2889.3 (17) | 21.2 (4)       |
| C3   | 4777 (2) | 7794.6 (14) | 2760.5 (18) | 23.2 (4)       |
| C4   | 4987 (2) | 8537.8 (14) | 4079.5 (18) | 23.1 (4)       |
| C5   | 4779 (2) | 8111.7 (13) | 5561.0 (18) | 22.7 (4)       |
| C6   | 4131 (2) | 6955.4 (13) | 5756.5 (17) | 20.8 (3)       |
| C7   | 4545 (2) | 6314.0 (13) | 7182.4 (17) | 22.0 (4)       |
| C8   | 4147 (2) | 5144.0 (14) | 7247.9 (17) | 22.1 (4)       |
| C9   | 2848 (2) | 4680.6 (14) | 6026.6 (18) | 21.8 (4)       |
| C10  | 2566 (2) | 5237.4 (13) | 4615.2 (18) | 21.2 (3)       |
| C11  | 3461 (2) | 6328.4 (13) | 4385.8 (17) | 20.3 (3)       |

**Table A2-35:** Anisotropic displacement parameters ( $\text{\AA}^2 \times 10^3$ ) for **3.3**. The anisotropic displacement factor exponent takes the form:  $-2\pi^2[h^2a^2U_{11}+2hka*b*U_{12}+\dots]$ .

| Atom | $U_{11}$ | $U_{22}$ | $U_{33}$ | $U_{23}$ | $U_{13}$ | $U_{12}$ |
|------|----------|----------|----------|----------|----------|----------|
| C1   | 28.3 (8) | 25.9 (8) | 17.8 (7) | 0.0 (6)  | 2.4 (6)  | 1.6 (6)  |
| C2   | 20.2 (7) | 24.6 (8) | 18.8 (7) | -0.4 (6) | 0.3 (5)  | 2.7 (6)  |
| C3   | 23.9 (7) | 25.6 (8) | 20.4 (7) | 3.2 (6)  | 3.3 (6)  | 3.0 (6)  |
| C4   | 22.7 (7) | 20.2 (7) | 26.4 (8) | 1.7 (6)  | 2.5 (6)  | 1.5 (6)  |
| C5   | 23.7 (7) | 21.4 (8) | 22.9 (7) | -2.3 (6) | 1.5 (6)  | 1.4 (6)  |
| C6   | 19.1 (7) | 22.5 (8) | 21.0 (7) | -1.0 (6) | 3.7 (5)  | 1.9 (6)  |
| C7   | 23.2 (7) | 25.1 (8) | 17.9 (7) | -2.8 (6) | 3.5 (5)  | 1.5 (6)  |
| C8   | 23.6 (8) | 25.8 (8) | 17.5 (7) | 0.3 (6)  | 6.2 (6)  | 2.9 (6)  |
| C9   | 19.4 (7) | 22.4 (8) | 24.4 (7) | -0.2 (6) | 6.6 (6)  | 0.2 (5)  |
| C10  | 16.8 (7) | 24.4 (8) | 22.6 (7) | -2.0 (6) | 2.1 (5)  | 0.9 (6)  |
| C11  | 16.8 (7) | 23.0 (8) | 21.3 (7) | 0.0 (6)  | 1.9 (5)  | 3.3 (6)  |

**Table A2-36: Bond lengths for 3.3.**

| Atom | Atom            | Length/Å  | Atom | Atom | Length/Å  |
|------|-----------------|-----------|------|------|-----------|
| C1   | C2              | 1.536 (2) | C6   | C7   | 1.430 (2) |
| C1   | C8 <sup>1</sup> | 1.537 (2) | C6   | C11  | 1.419 (2) |
| C2   | C3              | 1.373 (2) | C7   | C8   | 1.378 (2) |
| C2   | C11             | 1.439 (2) | C8   | C9   | 1.426 (2) |
| C3   | C4              | 1.410 (2) | C9   | C10  | 1.362 (2) |
| C4   | C5              | 1.372 (2) | C10  | C11  | 1.424 (2) |
| C5   | C6              | 1.421 (2) |      |      |           |

<sup>1</sup>I-X,I-Y,I-Z**Table A2-37: Bond angles for 3.3.**

| Atom | Atom | Atom            | Angle/°     | Atom | Atom | Atom            | Angle/°     |
|------|------|-----------------|-------------|------|------|-----------------|-------------|
| C2   | C1   | C8 <sup>1</sup> | 105.69 (12) | C8   | C7   | C6              | 120.80 (14) |
| C3   | C2   | C1              | 120.89 (13) | C7   | C8   | C1 <sup>1</sup> | 123.77 (14) |
| C3   | C2   | C11             | 118.02 (13) | C7   | C8   | C9              | 117.04 (14) |
| C11  | C2   | C1              | 117.44 (13) | C9   | C8   | C1 <sup>1</sup> | 117.08 (14) |
| C2   | C3   | C4              | 121.04 (14) | C10  | C9   | C8              | 120.33 (14) |
| C5   | C4   | C3              | 120.20 (14) | C9   | C10  | C11             | 120.20 (14) |
| C4   | C5   | C6              | 120.09 (14) | C6   | C11  | C2              | 118.69 (14) |
| C5   | C6   | C7              | 122.65 (14) | C6   | C11  | C10             | 117.07 (13) |
| C11  | C6   | C5              | 117.87 (13) | C10  | C11  | C2              | 122.74 (13) |
| C11  | C6   | C7              | 117.74 (14) |      |      |                 |             |

<sup>1</sup>I-X,I-Y,I-Z

**Table A2-38:** Torsion angles for **3.3**.

| A               | B  | C   | D   | Angle/°      | A               | B   | C   | D               | Angle/°      |
|-----------------|----|-----|-----|--------------|-----------------|-----|-----|-----------------|--------------|
| C1              | C2 | C3  | C4  | -153.97 (14) | C6              | C7  | C8  | C1 <sup>1</sup> | 145.78 (14)  |
| C1              | C2 | C11 | C6  | 138.70 (14)  | C6              | C7  | C8  | C9              | -17.2 (2)    |
| C1              | C2 | C11 | C10 | -26.9 (2)    | C7              | C6  | C11 | C2              | -143.12 (14) |
| C1 <sup>1</sup> | C8 | C9  | C10 | -141.68 (15) | C7              | C6  | C11 | C10             | 23.3 (2)     |
| C2              | C3 | C4  | C5  | 9.9 (2)      | C7              | C8  | C9  | C10             | 22.5 (2)     |
| C3              | C2 | C11 | C6  | -20.0 (2)    | C8 <sup>1</sup> | C1  | C2  | C3              | 113.44 (15)  |
| C3              | C2 | C11 | C10 | 174.37 (14)  | C8 <sup>1</sup> | C1  | C2  | C11             | -44.61 (17)  |
| C3              | C4 | C5  | C6  | -7.4 (2)     | C8              | C9  | C10 | C11             | -4.4 (2)     |
| C4              | C5 | C6  | C7  | 156.01 (15)  | C9              | C10 | C11 | C2              | 147.21 (15)  |
| C4              | C5 | C6  | C11 | -8.6 (2)     | C9              | C10 | C11 | C6              | -18.6 (2)    |
| C5              | C6 | C7  | C8  | -170.09 (14) | C11             | C2  | C3  | C4              | 4.0 (2)      |
| C5              | C6 | C11 | C2  | 22.2 (2)     | C11             | C6  | C7  | C8              | -5.5 (2)     |
| C5              | C6 | C11 | C10 | -171.32 (13) |                 |     |     |                 |              |

<sup>1</sup>1-X,1-Y,1-Z**Table A2-39:** Hydrogen atom coordinates ( $\text{\AA}\times 10^4$ ) and isotropic displacement parameters ( $\text{\AA}^2\times 10^3$ ) for **3.3**.

| Atom | x       | y       | z       | U(eq) |
|------|---------|---------|---------|-------|
| H1A  | 5338.79 | 6047.77 | 921.34  | 29    |
| H1B  | 3467.86 | 5354.29 | 1266.55 | 29    |
| H3   | 5112.76 | 8059.85 | 1788.08 | 28    |
| H4   | 5266.08 | 9319.27 | 3944.7  | 28    |
| H5   | 5063.92 | 8580.36 | 6438.51 | 27    |
| H7   | 5089.05 | 6691.27 | 8076.12 | 26    |
| H9   | 2190.65 | 3994.84 | 6194.26 | 26    |
| H10  | 1785.57 | 4903.75 | 3799.01 | 25    |

#### 4. UV/Vis Absorption and Emission Spectra of 3.3 in Different Solvents

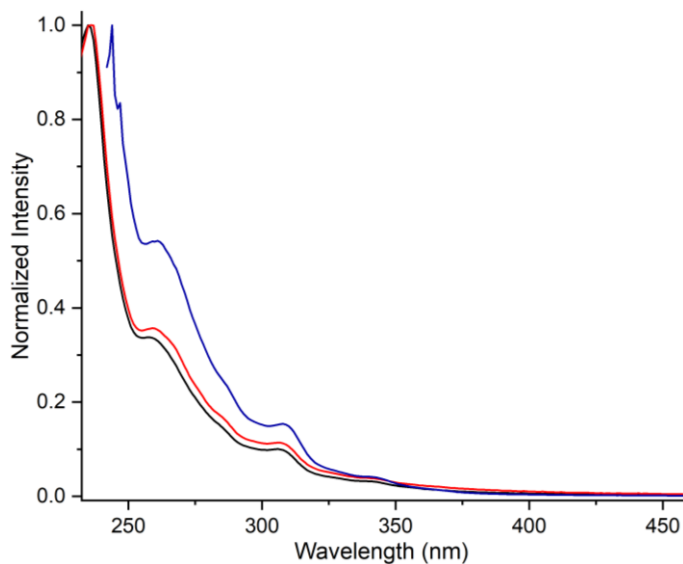


**Figure A2-7:** Normalized UV/vis absorption spectra of **3.3** in acetonitrile (black line), dichloromethane ( $\lambda_{\text{cut-off}} \approx 235$  nm) (blue line), and cyclohexane (red line).

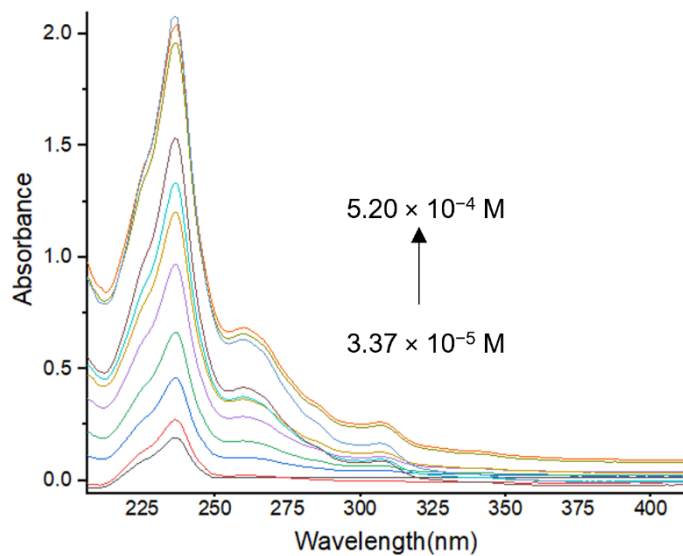


**Figure A2-8:** UV/vis absorption spectra of **3.3** at different concentrations in cyclohexane.

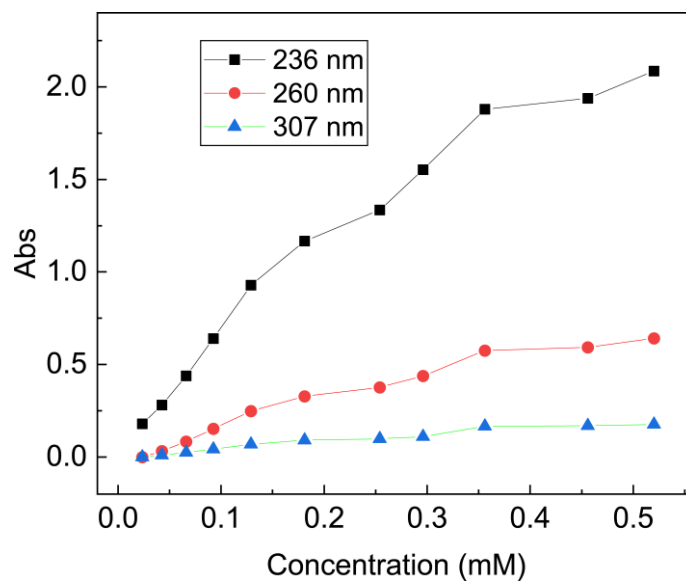


**Figure A2-9:** Plot of UV/vis absorbance of **3.3** at 236, 260, and 307 nm in cyclohexane in correlation with its concentration.

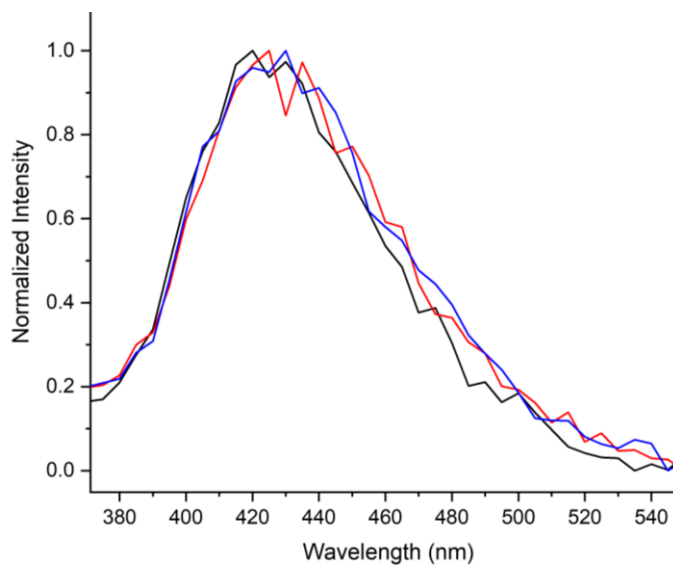
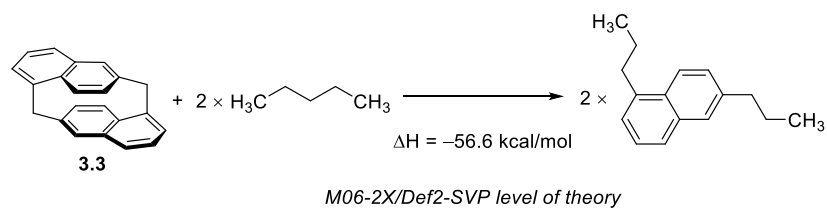


**Figure A2-10:** Normalized emission ( $\lambda_{exc} = 350$  nm) spectra of **3.3** in acetonitrile (black line), dichloromethane (blue line), and cyclohexane (red line).

## 5. DFT Calculations



**Scheme A4-1:** Isodesmic reaction for the calculation of the strain energy of [1.1]naphthalenophane **3.3**.

## Chapter 4: Synthesis of [2.2]Paracyclophane/9-Alkylfluorene Hybrids and the Discovery of a Solvent-assisted Rearrangement

### Statement of Co-Authorship

The majority of this chapter has been published in *Org. Lett.* **2021**, *23*, 5461–5465.

Authors: Sourav Biswas, Dr. Zahra A. Tabasi, Dr. Jian-Bin Lin, Prof. Yuming Zhao, and Prof. Graham J. Bodwell.

Sourav Biswas (listed as 1<sup>st</sup> author): Performed the synthetic work, physical data collection, data analysis, wrote the first draft of the manuscript, and contributed significantly to the preparation of the manuscript.

Zahra A. Tabasi: Measured UV/vis absorption, excitation, and emission spectra of cyclophanes **4.20** and **4.22**.

Jian-Bin Lin: Solved the crystal structures of cyclophanes **4.11**, **4.18**, **4.20**, and **4.22** of this Chapter and provided publishable crystal structure reports.

Yuming Zhao: Performed all computational work, interpreted the results, contributed to writing of the corresponding sections of the manuscript.

Graham J. Bodwell: Principal investigator (PI) of the work, who led the project and majorly contributed to the interpretation/analysis of data and writing of the manuscript.

The article has been reproduced in this chapter in an adapted form that includes the contributions of all the co-authors for the purpose of a complete discussion.

## 4.1 Introduction

Planar and non-planar polynuclear aromatic hydrocarbons (PAH) have garnered considerable interest from the synthetic community for years owing to not only their aesthetically pleasing structures but also their distinctive chemical and physical properties.<sup>1</sup> A workhorse for the synthesis of large PAHs is the Diels–Alder reaction of an aryl-substituted cyclopentadieneone with an appropriate alkyne followed by intramolecular Scholl reactions. The recent synthesis of a plethora of both planar<sup>2</sup> and non-planar<sup>3</sup> large PAHs showcase the synthetic utility of the Diels–Alder / Scholl approach. A few selected examples of structurally interesting PAHs (**4.1–4.3**) are shown in (Figure 4.1).

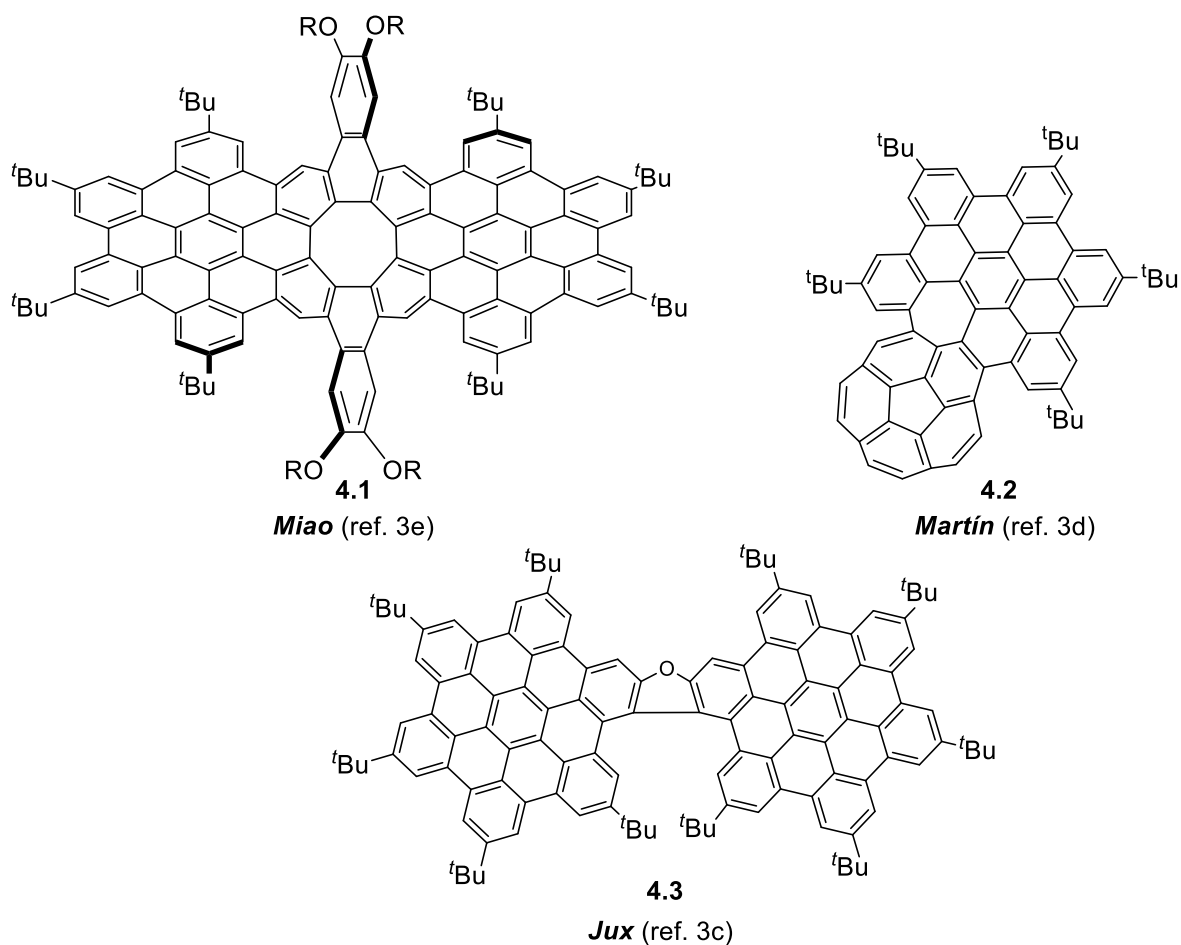
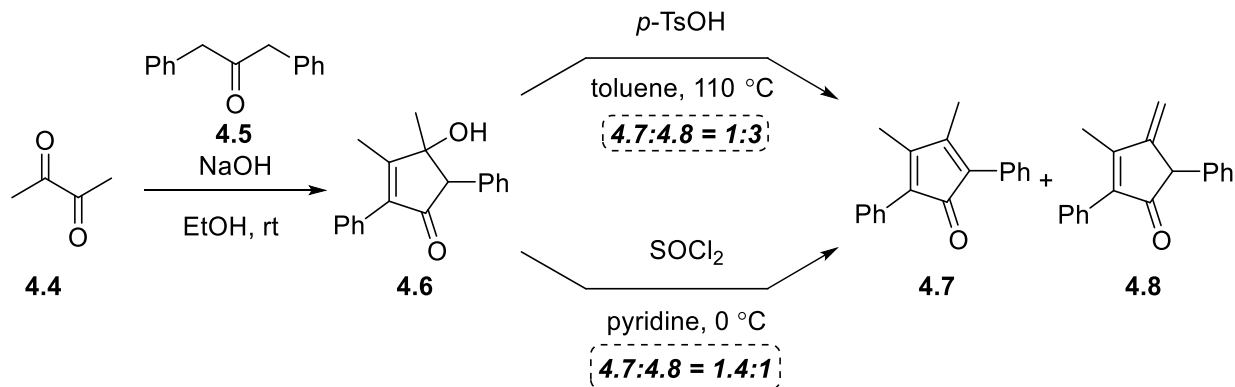


**Figure 4.1:** Recently reported PAHs **4.1–4.3** synthesized using the Diels–Alder / Scholl approach.

Diketones previously employed in the synthesis of large PAHs are commonly diaryl 1,2-diketones. Therefore, it appears to be a limitation of the Diels–Alder / Scholl approach that the cyclopentadienone system cannot have any  $sp^3$ -hybridized carbon atoms attached to it. The scarcity of such examples is presumably associated with the low yield of such cyclopentadienones obtained from a classical double aldol condensation as a consequence of the low selectivity toward the formation of the desired cyclopentadienones. A competitive dehydration resulting from the loss of water from an intermediate hydroxycyclopentenone leads to the undesired methylenecyclopentenone. For example, Mackenzie and Greenfield reported that treatment of a mixture of butanedione (**4.4**) and 1,3-diphenylacetone (**4.5**) with sodium hydroxide in ethanol at room temperature brought about the formation of the corresponding hydroxycyclopentenone **4.6**.<sup>4</sup> Hydroxycyclopentenone **4.6** was further exposed to  $\text{SOCl}_2$  in pyridine at 0 °C to afford the corresponding cyclopentadienone **4.7** and the methylenecyclopentenone **4.8** in a ratio of 1.4:1 (Scheme 4.1). The preference toward the formation of the desired cyclopentadienone **4.7** deteriorated further upon the treatment of hydroxycyclopentenone **4.6** with *p*-TsOH in toluene at reflux, leading to the formation of **4.7** and **4.8** in a ratio of 1:3.<sup>5</sup> In this Chapter, the synthesis a [2.2]paracyclophane-based cyclopentadienone system, wherein the cyclopentadienone system is attached to an  $sp^3$ -hybridized carbon atom, will be discussed. In addition, the synthesis of two [2.2]paracyclophane / 9-alkylfluorene hybrids by Diels–Alder reactions of the cyclopentadienone with the appropriate dienophiles, the electronic properties of the two hybrids, and an unusual solvent-assisted rearrangement that was discovered *en route* to the preparation of the [2.2]paracyclophane-based cyclopentadienone will be presented in detail.

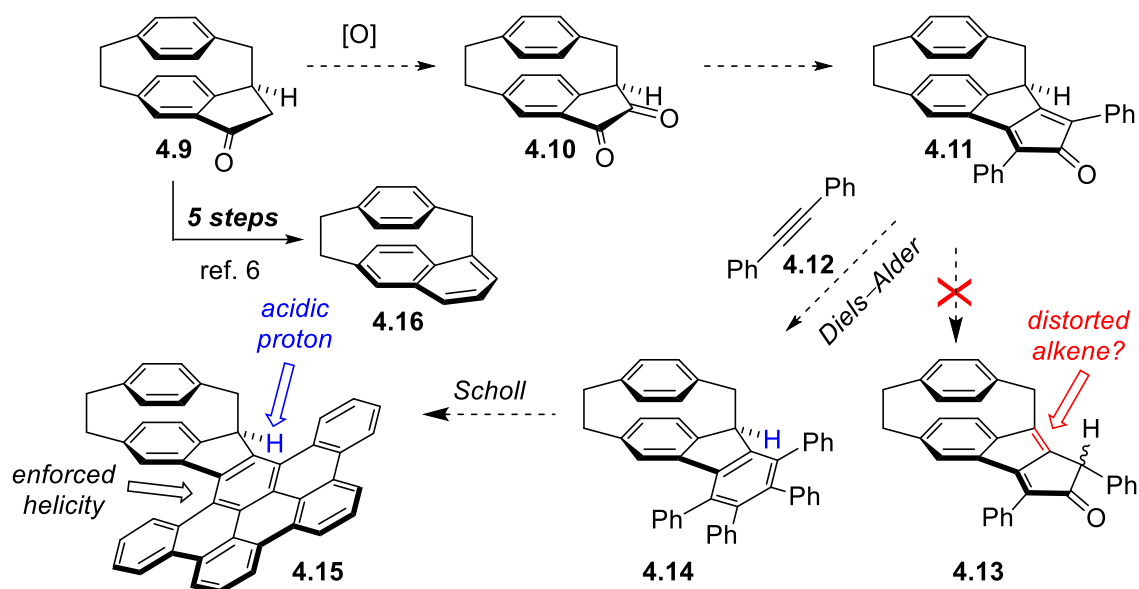


**Scheme 4.1:** Double aldol condensation of 2,3-butanedione (**4.4**) with 1,3-diphenylacetone (**4.5**).

## 4.2 Objective

Indanone **4.9** (Scheme 4.2), which featured as a key intermediate in the recent synthesis of [2](6,1)naphthaleno[1]paracyclophane (**4.16**) (Scheme 4.2),<sup>6</sup> appeared to offer an opportunity to exploit the Diels-Alder / Scholl approach on a system that contains an *sp*<sup>3</sup>-hybridized carbon atom. Specifically, oxidation of **4.9** to dione **4.10** would set the stage for an aldol condensation leading to cyclopentadienone **4.11** (Scheme 4.2). In this case, migration of one of the alkenes out of the cyclopentadienone system, resulting in the formation of the side product **4.13**, might be disfavored (the B3LYP-D3/6-31G(d)-optimized structure of **4.13** is 13.45 kcal/mol higher in energy than that of **4.11**, Appendix 3) because of the strained nature of the new alkene. Subjection of **4.11** to the Diels–Alder reaction with diphenylacetylene (**4.12**) would afford the very unusual fluorene derivative **4.14**. Such systems would be interesting due to their chirality and the presence of an acidic fluorenyl proton.<sup>7</sup> The chirality in **4.14** arises from a combination of point chirality at the stereogenic 9 position of the fluorene system and the planar chirality of the monosubstituted [2.2]paracyclophane system. Together, these elements of asymmetry enforce helicity in the fluorene system, even without additional  $\pi$ -extension. These systems are likely to be fluorescent, which imbues them with the potential to exhibit circularly polarized luminescence (CPL). 9-

Alkylfluorenes have an acidic proton [ $pK_a$  (DMSO) for 9-methylfluorene = 22.3],<sup>8</sup> so cyclophane **4.14** can be reasonably expected to be acidic, albeit to a somewhat lesser extent due to the distortion from planarity of the resulting fluorenyl anion. Considering that neutral aromatic systems are known to tolerate a large amount of distortion from planarity without losing a substantial amount of their “aromaticity”,<sup>9</sup> the effect on the acidity of **4.14** is not expected to be large. Moreover, the Scholl reaction of **4.14** would afford  $\pi$ -extended fluorene **4.15**. The anions obtained from deprotonation of such a system would be of great interest.



**Scheme 4.2:** Intended synthesis of [2.2]paracyclophane-PAH hybrid **4.15**.

## 4.3 Results and Discussion

### 4.3.1 Synthesis

Indanone **4.9** was synthesized from [2.2]paracyclophane (**4.17**) in 31% overall yield following the recently reported four-step protocol (Chapter 2, Scheme 2.5, Table 2.1).<sup>6</sup> Subjection of **4.9** to Riley oxidation conditions<sup>10</sup> afforded dione **4.10** (63%) (Scheme 4.3, *vide infra*). Exposure of **4.10** and 1,3-diphenylacetone (**4.5**) to the typical double aldol condensation conditions (KOH, ethanol,

80 °C) led to the complete consumption of the starting materials within 15 min. After purification by column chromatography, a blood red solid was isolated. The HRMS spectrum of the product showed a peak at  $m/z = 437.1888$ , which is consistent with a  $[M+H]^+$  peak for the desired cyclopentadienone **4.11** (Scheme 4.2, *vide supra*). However, careful inspection of the  $^1\text{H}$  NMR spectrum of the product revealed that one of the signals clearly did not agree with the structure of **4.11**. Specifically, the singlet at  $\delta$  6.24 ppm would not be expected for the cyclopentadienone **4.11**. Subsequently, a cross-peak was observed between the singlet at  $\delta = 6.24$  ppm and a carbon signal at  $\delta = 125.4$  ppm in the HSQC spectrum, suggesting that the

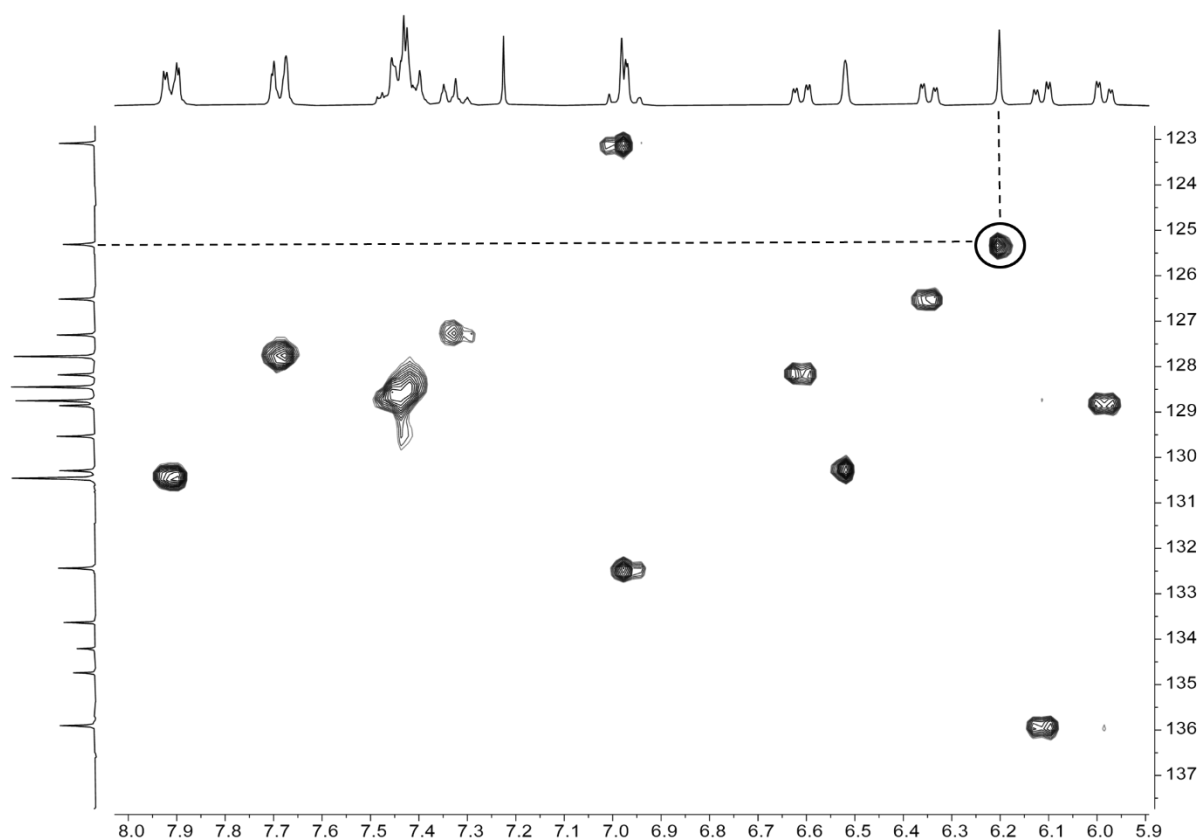
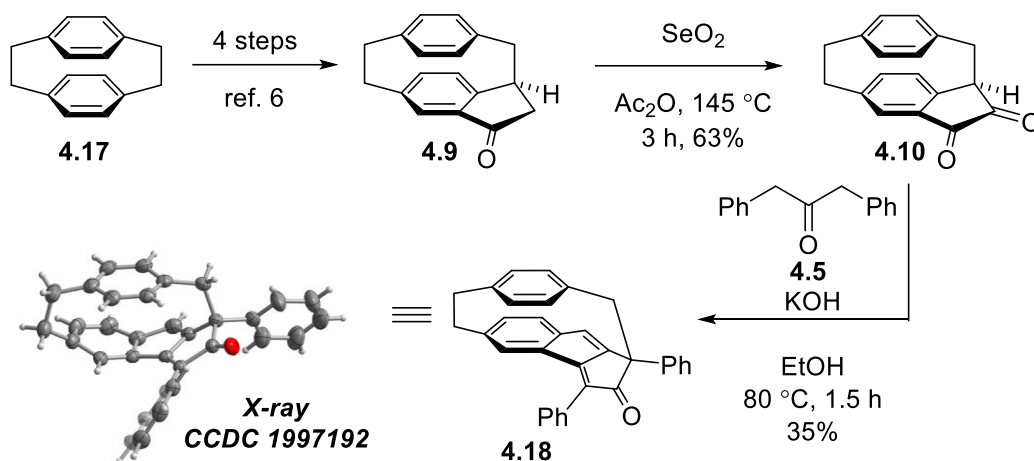


**Figure 4.2:** Aromatic regions ( $\delta_{\text{H}} = 8.0\text{--}5.9$  ppm and  $\delta_{\text{C}} = 137\text{--}123$  ppm) of the HSQC spectrum of cyclophane **4.18**.

proton in question was attached to an  $sp^2$ -hybridized carbon atom (Figure 4.2, see Appendix 3 for the full spectrum).

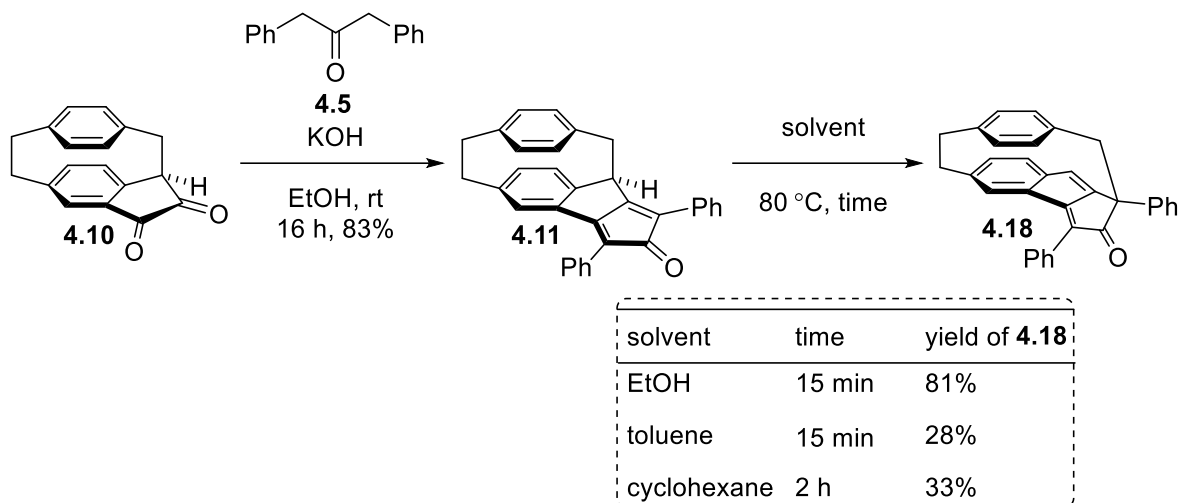
At this juncture, it was clear that a rearrangement had occurred. Several possibilities were considered, but none could be fully supported to the exclusion of others using an array of 2D NMR experiments. The structure of the product was then determined unequivocally using single crystal X-ray analysis. Crystals suitable for X-ray crystallographic analysis were obtained by recrystallization from hexane. Analysis of the X-ray data disclosed the unknown compound to be the rearranged cyclophane **4.18**. A slightly better yield (35%) was obtained if the reaction was allowed to run for 1.5 h (*cf.* 26% yield after 15 min).



**Scheme 4.3:** Serendipitous synthesis of cyclophane **4.18**.

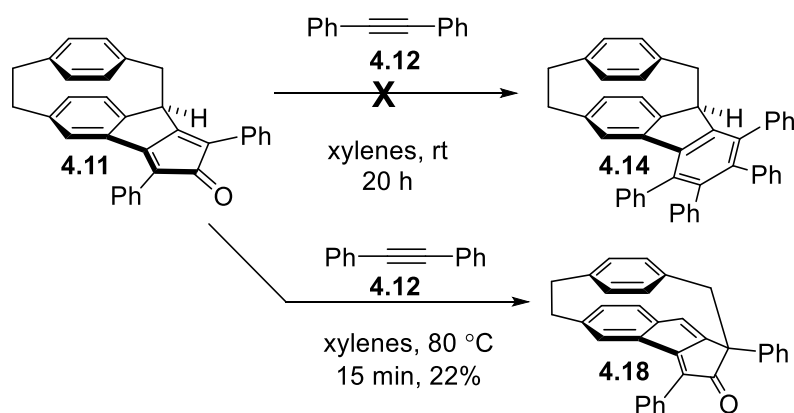
When the double aldol condensation reaction was carried out at room temperature, the desired cyclopentadienone **4.11** was isolated in 83% yield as a purple solid (Scheme 4.4). The structure of the product was unequivocally assigned by single crystal X-ray diffraction analysis. Cyclopentadienone **4.11** was found to be stable in the solid state at  $-20\text{ }^\circ\text{C}$  for several months, but it decomposes (not to the rearrangement product **4.18** as analyzed by TLC) in solution under ambient conditions over the period of one week, as other cyclopentadienones are known to do.<sup>11</sup> It was found that the use of 0.95 equiv (substoichiometric) instead of 1.00 equiv of compound **4.5**

was advantageous to ensure the complete consumption of 1,3-diphenylacetone (**4.5**). In some instances, when the dione **4.10** and 1,3-diphenylacetone (**4.5**) were used in a 1:1 molar ratio, even the presence of a small amount of unreacted 1,3-diphenylacetone (**4.5**) rendered purification of the cyclopentadienone **4.11** difficult. The difference between the  $R_f$  values of **4.11** ( $R_f = 0.24$  in 6% ethyl acetate/hexanes) and **4.10** ( $R_f = 0.05$  in 6% ethyl acetate/hexanes) on silica gel is significant whereas the difference between the cyclopentadienone **4.11** and 1,3-diphenylacetone (**4.5**) ( $R_f = 0.23$  in 6% ethyl acetate/hexanes) is negligibly small. Although, TLC analysis showed the complete consumption of the limiting starting material (**4.10**) within 1 h, it was necessary to let the reaction run for 16 h to achieve a high yield of the product (25% yield after 1 h vs 83% yield after 16 h). The initial formation of the intermediate  $\beta$ -hydroxycyclopentanones (not shown), which slowly disappeared and converged to the cyclopentadienone **4.11** over time might account for the time-dependent yields. A control experiment was then performed to shed light on the mechanism of the rearrangement (specifically to verify the involvement of **4.11** in the rearrangement). A solution of the cyclopentadienone **4.11** in ethanol was heated at 80 °C for 15 min and after column chromatographic purification, the rearrangement product **4.18** was obtained in 81% yield. This indicates the involvement of the cyclopentadienone **4.11** as a transient intermediate in the one-pot conversion of **4.10** to cyclophane **4.18**. In terms of yield, this two-step conversion was found to be better than the one-pot conversion. Heating a solution of **4.11** in toluene at 80 °C for 15 minutes also led to the formation of **4.18** (28%), but now several other more polar side products were prominent (TLC analysis). In cyclohexane at 80 °C, the conversion of **4.11** to **4.18** (33% yield) appeared to give the same set of more polar side products (TLC analysis), but required 2 h for **4.11** to be fully consumed. Despite considerable effort, none of the side products could be identified.



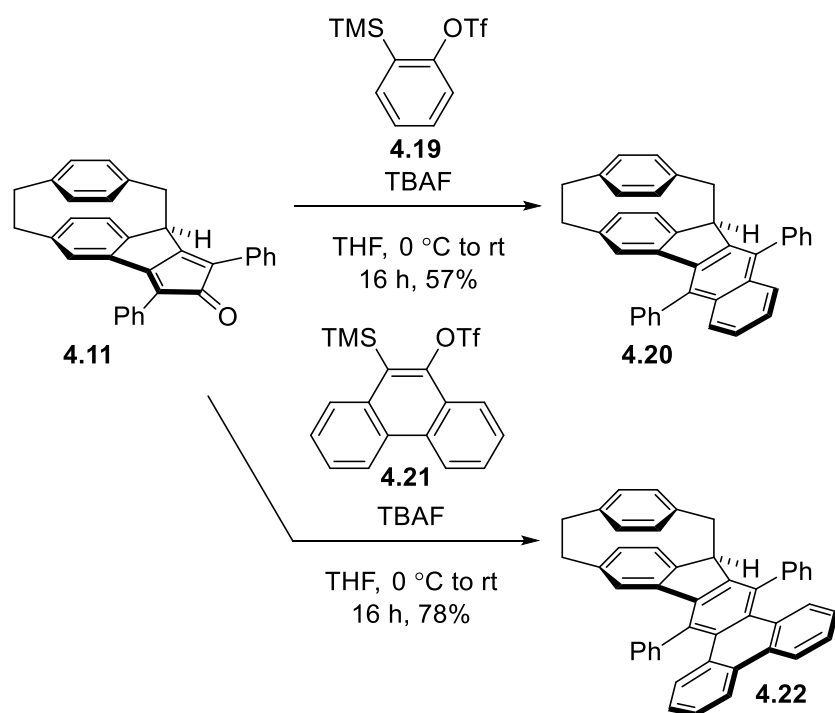
**Scheme 4.4:** Two-step conversion of dione **4.10** to cyclophane **4.18**.

Diels–Alder reactions between aryl-substituted cyclopentadienones and diarylacetylenes often require high temperatures (above 200 °C).<sup>12</sup> The observation of rearrangement of cyclopentadienone **4.11** at 80 °C in three solvents did not bode well for using **4.11** to generate larger arenes using Diels–Alder reactions. Indeed, the reaction of **4.11** with diphenylacetylene (**4.12**) in xylenes did not proceed at room temperature after 20 h (TLC analysis) and at 80 °C produced essentially the same result as heating **4.11** in toluene, giving cyclophane **4.18** (22%) and the recovered alkyne **4.12** (94%) (Scheme 4.5).



**Scheme 4.5:** Attempted synthesis of fluorene-containing cyclophane **4.14**.

Arynes are much more reactive dienophiles than normal alkynes, so their use as reaction partners for cyclopentadienone **4.11** was investigated with the expectation that the cycloadditions would proceed at room temperature. To test the hypothesis, a test reaction was run between a relatively simple aryne precursor, 2-(trimethylsilyl)phenyl trifluoromethanesulfonate (**4.19**) and **4.11** (Scheme 4.6). Reaction of **4.11** with benzyne precursor **4.19** proceeded smoothly at 0 °C to rt to afford benzofluorene derivative **4.20** (57%). Similarly, the use of phenanthryne precursor **4.21**<sup>13</sup> under the same conditions afforded larger cyclophane **4.22** (78%). Cyclophane **4.22** is a precursor to the desired  $\pi$ -extended fluorene **4.15**, which could be formed *via* a two-fold intramolecular Scholl reaction.

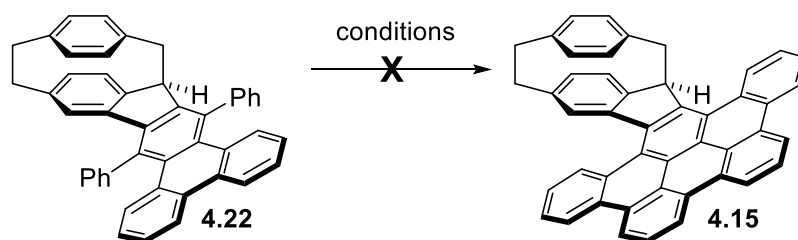


**Scheme 4.6:** Reactions of cyclopentadienone **4.11** with *in-situ* generated arynes.

Finally, the Scholl reaction was attempted with the precursor (**4.22**) under various conditions (Table 4.1). Benzofluorene derivative **4.22** underwent rapid decomposition under the classical Scholl reaction conditions ( $\text{FeCl}_3$ ,  $\text{CH}_2\text{Cl}_2/\text{MeNO}_2$ )<sup>14</sup> to produce TLC-immobile material

(Table 4.1, Entry 1). A similar observation was also made when the Scholl reaction was attempted under slightly modified Rathore's conditions (DDQ, Me<sub>3</sub>SO<sub>3</sub>H, CH<sub>2</sub>Cl<sub>2</sub>)<sup>15</sup> (Table 4.1, Entry 2). Attempts to achieve the Scholl reaction with only DDQ as oxidant met with failure, and led solely to the recovery of the starting material (Table 4.1, Entries 3 and 4). The use of DDQ in combination with a Lewis acid (Et<sub>2</sub>O·BF<sub>3</sub>)<sup>16</sup> was also found to be inefficacious, resulting in the formation of TLC-immobile material (Table 4.1, Entry 5). Attempts to achieve the  $\pi$ -extension in **4.22** under photochemical conditions also met with failure (Table 4.1, Entries 6 and 7).

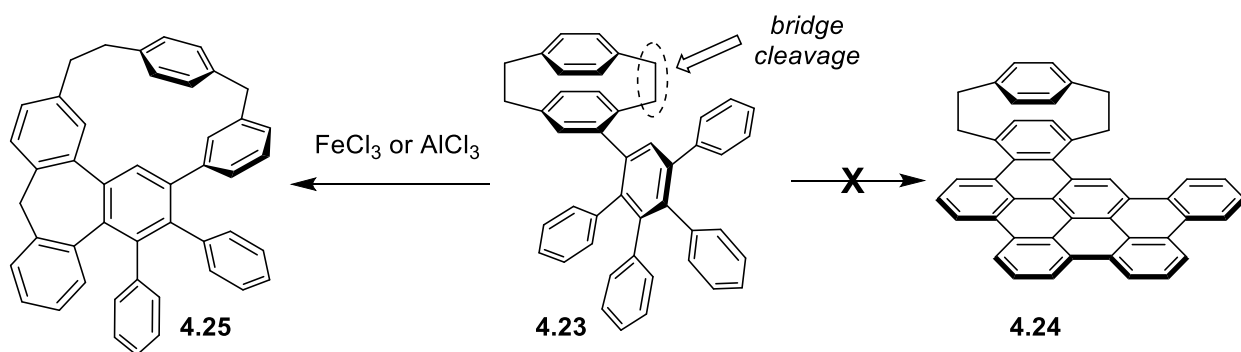
**Table 4.1:** Attempted Scholl and photocyclization reactions for the synthesis of cyclophane **4.15**.



| Entry | Conditions   | Result                    |
|-------|--|---------------------------|
| 1     | FeCl <sub>3</sub> (3 equiv), CH <sub>2</sub> Cl <sub>2</sub> /MeNO <sub>2</sub> , 0 °C, 20 min               | TLC immobile <sup>a</sup> |
| 2     | DDQ (2 equiv), Me <sub>3</sub> SO <sub>3</sub> H (2 equiv), CH <sub>2</sub> Cl <sub>2</sub> , -15 °C, 10 min | TLC immobile <sup>a</sup> |
| 3     | DDQ (3 equiv), CH <sub>2</sub> Cl <sub>2</sub> , rt, 5 h   | no reaction <sup>b</sup>  |
| 4     | DDQ (3 equiv), CH <sub>2</sub> Cl <sub>2</sub> , 40 °C, 15 h   | no reaction <sup>b</sup>  |
| 5     | DDQ (3 equiv), Et <sub>2</sub> O·BF <sub>3</sub> (2 equiv), CH <sub>2</sub> Cl <sub>2</sub> , 0 °C, 5 min    | TLC immobile <sup>a</sup> |
| 6     | Irradiation at 302–312 nm, CDCl <sub>3</sub> , 17 h  | no reaction <sup>c</sup>  |
| 7     | Irradiation at 302–312 nm, I <sub>2</sub> (2 equiv), propylene oxide, benzene, 17 h                          | no reaction <sup>b</sup>  |

<sup>a</sup>TLC analysis. <sup>b</sup>Analysis of the reaction by <sup>1</sup>H NMR spectroscopy. <sup>c</sup>Recovery of **4.22**.

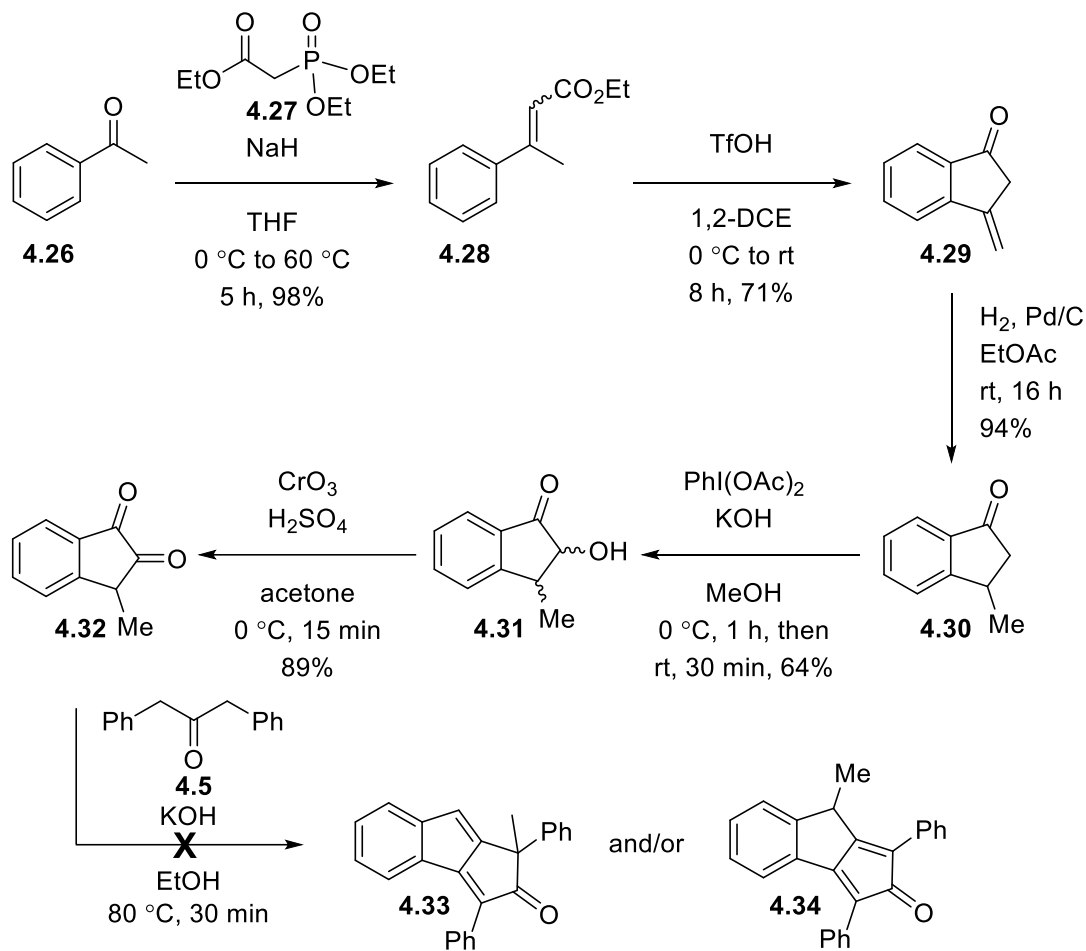
[2.2]Paracyclophanes are known to undergo bridge cleavage upon chemical oxidation to give a benzyl radical / benzyl cation pair<sup>17</sup> and Hopf and co-workers reported that that oligophenyl-substituted [2.2]paracyclophane **4.23** underwent bridge cleavage followed by reclosure to give cyclophane **4.25** upon attempted Scholl reaction instead of giving nanographenophane **4.24** (Scheme 4.7).<sup>18</sup> Despite this precedent, the attempt to convert **4.22** to **4.15** was worthwhile because the presence of the triphenylene unit in **4.22** was expected to enable the formation of a more stable arenium radical cation (compared to **4.23**) and this pointed to the possibility that cyclodehydrogenation might now become favored over (or at least competitive with) bridge cleavage. Clearly, this was not the case. The failure of the Scholl reactions (Table 4.1, *vide supra*) may be due to the occurrence of a similar bridge cleavage phenomenon to generate benzyl cation radical from the precursor **4.22**, which presumably underwent rapid polymerization. Although, the formation of the desired cyclophane **4.15** and its subsequent fragmentation by a similar pathway under the conditions of its formation cannot be ruled out. This might demonstrate a significant drawback of the Diels–Alder/Scholl approach in view of its application to the synthesis of targeted  $\pi$ -expanded cyclophanes from smaller cyclophanes.



**Scheme 4.7:** Hopf and co-workers' attempt to synthesize nanographenophane **4.24**.

In order to have a better understanding of the mechanism of the conversion of **4.10** to **4.18**, a similar dione, 3-methyl-1,2-indandione (**4.32**) (Scheme 4.8), was necessary to be accessed for a

comparison purpose. The dione **4.32** was prepared in five steps from acetophenone (Scheme 4.8). The Horner–Wadsworth–Emmons olefination of acetophenone (**4.26**) with triethyl phosphonoacetate (**4.27**) furnished the unsaturated ester **4.28** (98%) as an inseparable mixture of diastereomers (*E:Z*  $\approx$  83:17,  $^1\text{H}$  NMR analysis). Treatment of **4.28** with TfOH induced intramolecular Friedel–Crafts acylation followed by isomerization of the double bond to give indenone **4.29** (71%),<sup>19</sup> which was hydrogenated using a catalytic amount of Pd/C under an atmosphere of  $\text{H}_2$  to provide indanone **4.30** (94%).  $\alpha$ -Hydroxylation<sup>20</sup> of **4.30** was effected by (diacetoxyiodo)benzene (PIDA) in the presence of KOH to afford  $\alpha$ -hydroxyindanone **4.31** (64%) as a mixture of two diastereomers in a ratio of *ca.* 80:20 ( $^1\text{H}$  NMR analysis). However, the stereochemistry at the  $\alpha$ -position to the carbonyl group was of no consequence, as the stereochemistry was destroyed in the next step. Oxidation of **4.31** with the Jones reagent ( $\text{CrO}_3/\text{H}_2\text{SO}_4$ ) afforded the desired dione **4.32** (89%, >90% purity as judged by  $^1\text{H}$  NMR).<sup>21</sup> Purification of the crude product was avoided as the product was reported to be unstable to heat or column chromatography.<sup>21</sup> Subsequently, **4.32** was subjected to double aldol condensation with 1,3-diphenylacetone (**4.5**). Unfortunately, the reaction resulted in the formation of a complex mixture from which a bright orange solid was isolated. The solid was judged to be a mixture of at least two compounds by  $^1\text{H}$  NMR analysis. The mass spectrum of the solid shows a base peak at  $m/z = 349.1229$ . As judged by  $^1\text{H}$  NMR spectroscopy and mass spectrometry, the solid contained neither the rearrangement product **4.33** (calculated  $m/z = 334.1358$ ) nor the corresponding cyclopentadienone **4.34** (calculated  $m/z = 334.1358$ ). The identity of the components of the solid remains unknown.



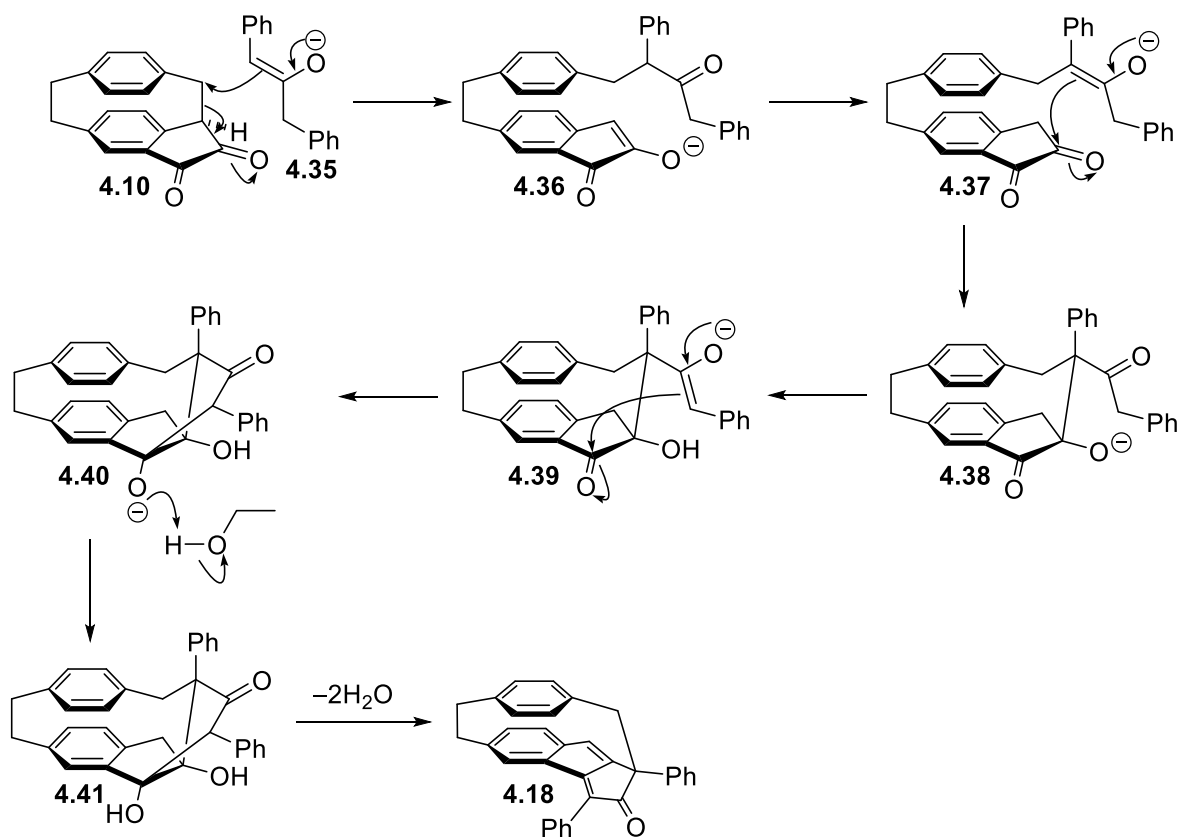
**Scheme 4.8:** Attempted synthesis of compound **4.33**.

### 4.3.2 Reaction Mechanism of the Rearrangement of Cyclopentadienone **4.11** to Cyclophane **4.18**

The rearrangement of cyclopentadienone **4.11** to cyclophane **4.18** is formally a [1,3]-alkyl shift. This type of thermal sigmatropic rearrangement is forbidden by the Woodward-Hofmann rules, so other mechanisms were considered.

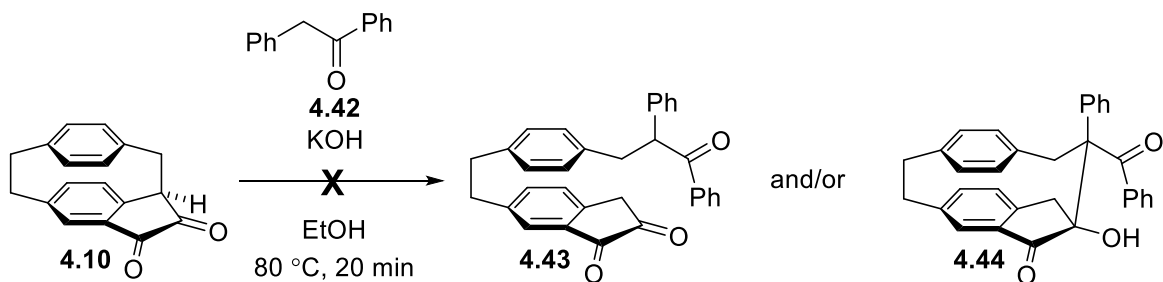
An initially considered plausible mechanism for the formation of **4.18** is depicted in Scheme 4.9. A hand-held molecular model of dione **4.10** suggested that the CH–CH<sub>2</sub> bond in **4.10** was aligned with the π\*(C=O) of the neighboring carbonyl group (bonded to the methine carbon). Hence, the attack of the enolate **4.35** (generated from 1,3-diphenylacetone (**4.5**) under basic

conditions) at the methylene carbon of the CH-CH<sub>2</sub> bond would be reasonable to afford intermediate **4.36**. This would result in the rupture of the cyclophane framework and the relief of a significant amount of strain energy. Intermediate **4.36**, following tautomerization and formation of an enolate by the abstraction of the acidic benzylic methine proton (next to a carbonyl group) by KOH, would form intermediate **4.37**. Intermediate **4.37** could undergo an intramolecular aldol reaction to furnish intermediate **4.38**. Protonation of **4.38** followed by formation of an enolate would give intermediate **4.39**, which following another intramolecular aldol reaction would provide intermediate **4.40**. Finally, protonation to give intermediate **4.41** followed by two-fold dehydration would lead to the formation of cyclophane **4.18**.



**Scheme 4.9:** Initially considered mechanism for the formation of cyclophane **4.18** under aldol condensation conditions.

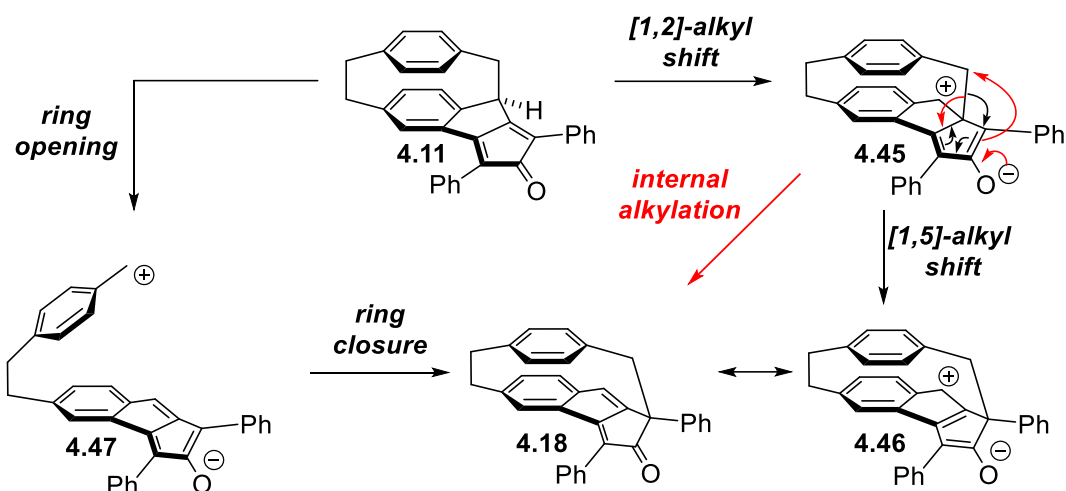
If the proposed mechanism was correct, the reaction of 2-phenylacetophenone (**4.42**) with dione **4.10** under aldol conditions was expected to afford trione **4.43** and/or  $\alpha$ -hydroxyindanone **4.44** (Scheme 4.10). Unlike intermediate **4.38** (Scheme 4.9, *vide supra*),  $\alpha$ -hydroxyindanone **4.44** does not possess any acidic protons ( $\alpha$  to a carbonyl group). Hence, the reaction was supposed to stop at the stage of the formation of **4.44**. With this in mind, **4.10** was treated with **4.42** in the presence of KOH. Unfortunately, **4.10** underwent decomposition within 20 min and a complex mixture of unidentified products was obtained from which none of the expected products (**4.43** and **4.44**) were detected/isolated. As a result, a different mechanism had to be considered.



**Scheme 4.10:** Control experiment with dione **4.10** and 2-phenylacetophenone (**4.43**) to shed light on the mechanism of the formation of cyclophane **4.18**.

A simple ring-opening / ring-closing mechanism was deemed unlikely because zwitterionic intermediate **4.47** contains an antiaromatic benzopentalene system and its closure to give **4.18** would be both entropically and enthalpically challenging (Scheme 4.11). In the crystal structure of cyclopentadienone **4.11**, the CH–CH<sub>2</sub> bond is roughly aligned with the neighboring  $\alpha,\beta$ -unsaturated carbonyl system. Natural bond orbital (NBO) analysis indicated that the  $\sigma(\text{C}–\text{C})$  orbital interacts with  $\pi^*(\text{C}=\text{C})$  of the neighboring C=C bond, affording a stabilization energy  $E(2) = 3.41$  kcal/mol (Appendix 3). These results suggested that the CH–CH<sub>2</sub> bond is slightly delocalized, and supported the notion that a 1,2-alkyl shift to afford zwitterion **4.45** is feasible. On the other hand, **4.45** could conceivably rearrange directly to afford **4.18**. This could be accounted

for by internal alkylation reaction, which could be viewed as another [1,2]-shift, or a thermally allowed [1,5]-alkyl shift. The latter process would afford zwitterion **4.46**, which is simply a resonance structure of **4.18**.



**Scheme 4.11:** Different pathways for the rearrangement of cyclopentadienone **4.11** to cyclophane **4.18**.

To provide support for any of these mechanistic hypotheses, a DFT computational study of the rearrangement was performed. The modeling showed that the [1,2]-alkyl shift pathway from cyclopentadienone **4.11** to intermediate **4.45** needs to overcome a high-energy transition state TS-1 (41.54 kcal/mol in the gas phase, 36.96 kcal/mol in ethanol), rendering it unlikely to be a viable mechanism (Figure 4.3). Moreover, no plausible transition state for the transformation from **4.45** to cyclophane **4.18** could be found despite numerous attempts.

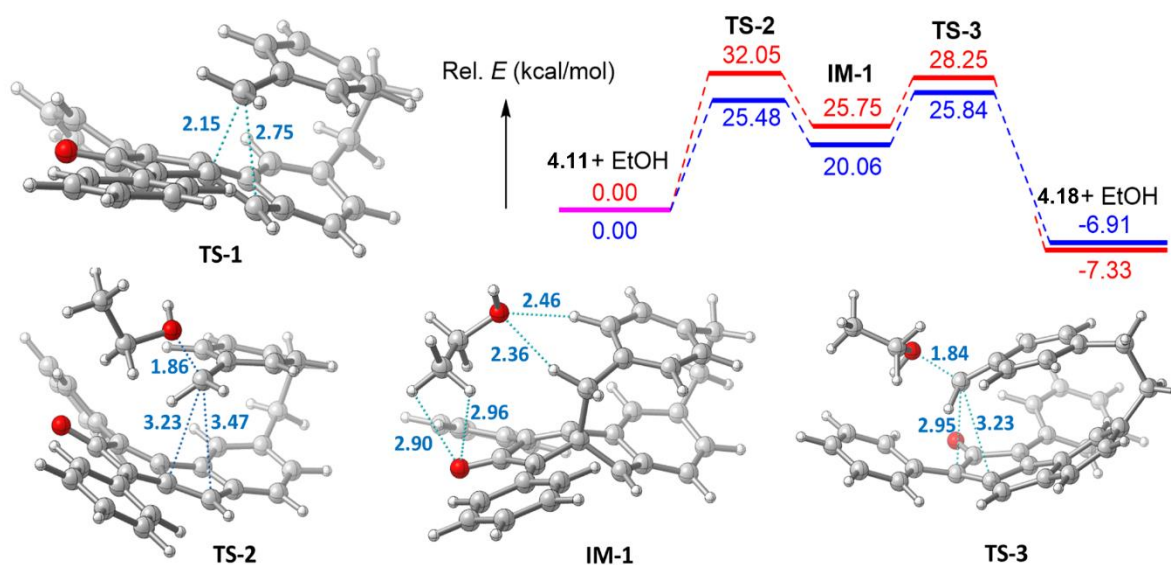


**Figure 4.3:** Optimized geometries of **TS-1**, **TS-2**, **IM-1**, and **TS-3** and energy profiles for the potential energy surface of the ethanol-assisted rearrangement pathway in the gas phase (red) and in ethanol (blue).

Having observed a much cleaner rearrangement in ethanol than in toluene or cyclohexane, the focus was turned to an analogous, solvent-assisted reaction pathway, in which an ethanol molecule participates in the formation of the transition state(s). This pathway was found to involve two transition states (**TS-2** and **TS-3**) and an intermediate (**IM-1**), which is a 1:1 complex of zwitterion **4.45** and ethanol (Figure 4.3, *vide supra*). In comparing **TS-1** to **TS-2**, it can be seen that the involvement of a molecule of ethanol enables the initial 1,2-shift to proceed through a much looser transition state. The migrating carbon atom is much further away from its initial and final bonding partners in **TS-2** (3.47 Å and 3.23 Å, respectively) than it is in **TS-1** (2.75 Å and 2.15 Å, respectively). The longer distances imply lower strain at the transition state. In the gas phase, the relative energy of **TS-2** is higher than that of **TS-3** by 3.80 kcal/mol, which renders the initial 1,2-shift the rate-determining step with an energy barrier of 32.05 kcal/mol. In ethanol solution, both **TS-2** and **TS-3** are significantly lowered in energy. The effect on **TS-3** is more substantial such that it becomes marginally lower in energy than **TS-2** and therefore the rate-determining state.<sup>22</sup> **TS-3** also features long distances between the migrating atom and its initial

and final bonding partners (3.23 Å and 2.95 Å, respectively). The distance between the carbonyl carbon and the migrating carbon in **TS-3** is 3.05 Å, which is consistent with the second step of the rearrangement being a [1,5]-alkyl shift. The overall rearrangement reaction from **4.11** to **4.18** is thermodynamically favored by 7.33 kcal/mol in the gas phase and 6.91 kcal/mol in ethanol solution.

The observation of a relatively fast, but low-yielding rearrangement in toluene suggests that the  $\pi$  system of toluene may also be capable of assisting the rearrangement, but it is not as effective as ethanol at preventing ring opening that enables the formation of other products. Cyclohexane cannot possibly assist the rearrangement in the same way, so the observation of a substantially slower, low-yielding rearrangement in this solvent may point to a ring-opening / ring-closure mechanism within a solvent cage.

### 4.3.3 X-Ray Crystallographic Analysis

The structures of cyclophanes **4.11**, **4.20**, and **4.22** were determined using single-crystal XRD (Figure 4.4, *vide infra*). A common feature is that the CH–CH<sub>2</sub> bond is slightly longer (by 0.07–0.013 Å,  $>3\sigma$ ) than the CH<sub>2</sub>–CH<sub>2</sub> bond in all three structures and this is consistent with the aforementioned alignment of this  $\sigma$  bond with the adjacent  $\pi$  system. The fluorene unit in **4.20** and **4.22** has a helical twist of 16.2° and 13.8°, respectively, as quantified by the *abcd* dihedral angle (Figure 4.4, *vide infra*). The corresponding angle in **4.11** is 25.2°. The triphenylene unit in **4.22** is distorted from planarity with dihedral angles in the bay regions ranging from 14.7° to 22.5°.

### 4.3.4 NMR Analysis

Most of the aromatic signals associated with the [2.2]paracyclophane system in **4.20** are observed at slightly higher field ( $\Delta\delta = 0.00$ – $0.18$  ppm) than those of **4.22**, with the exception of the highest-

field aromatic proton H<sub>x</sub> (**4.20**:  $\delta$  5.50; **4.22**:  $\delta$  5.24 ppm), which appears at significantly lower field ( $\Delta\delta = -0.26$  ppm). The appearance of the H<sub>x</sub> signals at especially high field high is due to the shielding effect of the proximate phenyl ring and the more pronounced effect in **4.22** is due to a difference in how the phenyl group is oriented with respect to H<sub>x</sub>. Although H<sub>x</sub> in **4.20** is closer to the centroid of the phenyl ring (2.60 Å vs. 2.81 Å, Figure 4.4), the phenyl ring in **4.22** has a more face-on relationship to H<sub>x</sub> than in **4.20**. The difference in the orientation of the phenyl ring in **4.22** can be attributed to the presence of the triphenylene system on its other face, which pushes it toward to H<sub>x</sub>. This is reflected by the smaller *cde* bond angle in **4.22** (118.0°, Figure 4.4) than in **4.20** (119.8°, Figure 4.4). The corresponding proton in **4.11** is observed at much lower field ( $\delta$  7.08 ppm,  $\Delta\delta = -1.84$  ppm), presumably due to a combination of a more edge-on orientation of the neighboring phenyl group and the resonance effect of the carbonyl group. For all three cyclophanes, the methine proton of the fluorene system (H<sub>y</sub>) (**4.11**:  $\delta$  5.05 ppm; **4.20**:  $\delta$  4.75; **4.22**:  $\delta$  5.04 ppm) resonates at considerably lower field than the corresponding proton in 9-methylfluorene ( $\delta$  3.94 ppm).<sup>23</sup> This may be due to a deshielding effect of the adjacent phenyl group, which has a roughly edge-on orientation in all three structures. Proton H<sub>z</sub>, which reaches out toward the extended  $\pi$  system, is the second highest field aromatic proton in **4.20** ( $\delta$  5.96 ppm) and **4.22** ( $\delta$  6.07 ppm), but is observed at much lower field in **4.11** ( $\delta$  7.08 ppm,  $\Delta\delta = -0.69$  ppm). This is presumably a consequence of the non-/antiaromatic character of the cyclopentadienone system in **4.11**, which does not exert the same shielding effect as the aromatic systems in **4.20** and **4.22**.

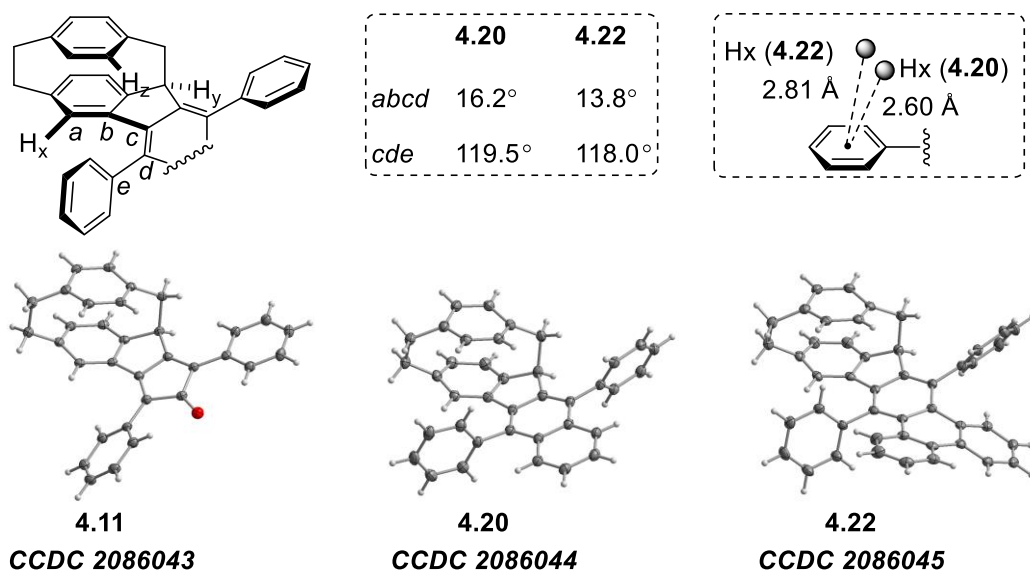


**Figure 4.4:** Crystal structures of cyclophanes **4.11**, **4.20**, and **4.22** with 50% displacement ellipsoids.

A noteworthy feature of the  $^1\text{H}$  NMR spectrum of **4.22** is the broadening of some of the aromatic signals. To address the origin of these broad signals, variable temperature (VT)  $^1\text{H}$  NMR experiments were performed over the temperature range 233–368 K (Figure 4.5). With the aid of 1D and 2D NMR experiments (COSY, HSQC, and NOESY), the broad signals were assigned to one of the phenyl groups attached to the triphenylene moiety of cyclophane **4.22**. Inspection of a hand-held molecular model as well as the crystal structure of **4.22** suggested that the rotation of the phenyl ring situated in the gulf region (closer to the lower benzene deck of the [2.2]paracyclophane framework) would be more hindered than that of the other phenyl ring, resulting in the broadening of  $^1\text{H}$  NMR signals. A 298 K  $^1\text{H}$  NMR spectrum recorded in 1,1,2,2-tetrachloroethane- $d_2$  features a broad multiplet at  $\delta = 8.18\text{--}8.03$  ppm, which slowly started sharpening upon decreasing the temperature of the NMR experiment. At  $T = 273$  K, the signal which was a broad multiplet at 298K turned into a well-resolved doublet ( $J = 7.6$  Hz). The multiplicity became even more apparent upon cooling the NMR sample further. Among all the aromatic protons of the “gulf-region” phenyl group, only the *ortho* (to the substituent) protons

could appear as a doublet. Hence, it is likely that the doublet at  $\delta = 8.12$  ppm is one of the *ortho* protons. However, the determination of the other *ortho* proton proved to be difficult owing to the overlap of several signals in the region  $\delta = 7.65\text{--}7.25$  ppm. The broad multiplet at  $\delta = 7.77\text{--}7.65$  ppm becomes a well-resolved triplet at  $\delta = 7.75$  ( $J = 7.9$  Hz) upon decreasing the temperature from 298 K to 263 K. Based on this observation, the signal at  $\delta = 7.77\text{--}7.65$  ppm (298 K) / 7.75 ppm (263 K) was assigned to one of the *meta* (to the substituent) protons of the gulf-region phenyl ring. An unambiguous assignment of the other *meta* proton also proved to be difficult. The rotational barrier of the phenyl ring was estimated from data obtained from the VT-NMR experiments. The rate constant,  $k_c$  of the interconversion of the two exchanging protons at coalescence temperature,  $T_c$ , was estimated by the Gutowsky–Holm equation using the chemical shift difference ( $\Delta\nu$  in Hz) under slow exchange between the two exchanging protons.<sup>24</sup> From the coalescence temperature,  $T_c$ , and the rate constant,  $k_c$ , the activation energy of rotation ( $\Delta G^\ddagger$ ) was calculated using the Eyring equation.<sup>25</sup> Assuming the center of the multiplet ( $\delta = 7.65\text{--}7.25$  ppm), 7.45 ppm, as the chemical shift of the “difficult-to-assign” *ortho* proton, the barrier to rotation ( $\Delta G^\ddagger$ ) of the phenyl group was determined to be 14.4 kcal/mol [coalescence temperature ( $T_c$ ) = 318 K and  $\Delta\nu = 335$  Hz]. Assuming the same center of the multiplet as the “difficult-to-assign” *meta* proton, the rotational barrier was determined to be 14.9 kcal/mol [coalescence temperature ( $T_c$ ) = 318 K and  $\Delta\nu = 150$  Hz]. The estimated rotational barrier, considering the coalescence temperature to be 328 K and 308 K and the chemical shifts of the *ortho* protons, were 14.9 kcal/mol and 13.9 kcal/mol, respectively. Based on the little variation in the values of the estimated energy barrier at different coalescence temperatures, the barrier to rotation of the phenyl group was concluded to be *ca.*  $14.4 \pm 0.5$  kcal/mol. In any event, the rotational barrier is not of remarkable significance in view of its location in the gulf region.

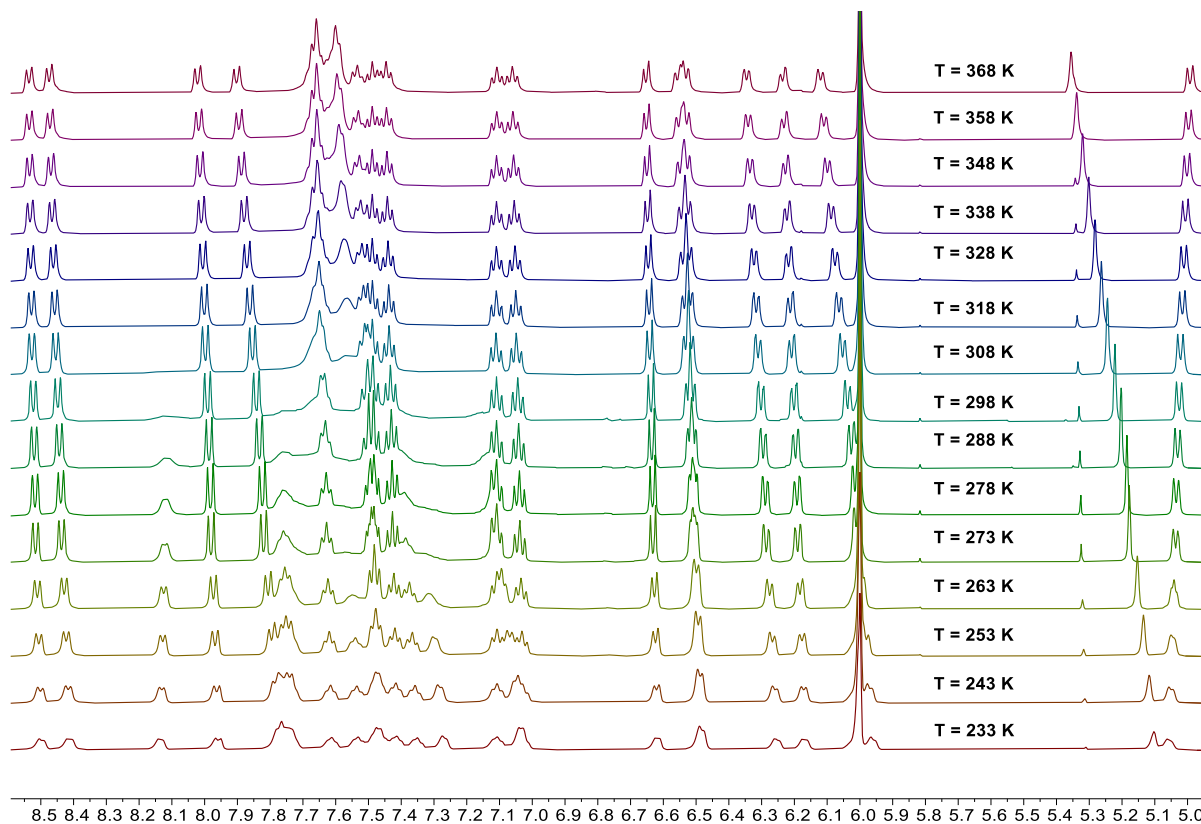


**Figure 4.5:** VT-NMR (500 MHz, C<sub>2</sub>D<sub>2</sub>Cl<sub>4</sub>) spectra of cyclophane **4.22** (aromatic and methine protons).

### 4.3.5 UV/Vis Absorption and Fluorescence Spectroscopy

The UV-Vis absorption spectrum of **4.18** in dichloromethane shows absorption bands at 480 and 375 nm (Figure 4.6, *vide infra*), which can be attributed to HOMO→LUMO and HOMO–1→LUMO transitions, respectively, according to time-dependent density functional theory (TD-DFT) calculations (Appendix 3). The corresponding bands for **4.11** are observed at 550 nm and 379 nm, respectively. The UV-Vis spectrum of cyclophane **4.20** shows a group of peaks at 360, 343, 321, and 290 nm. The first three low-energy bands can be assigned to the HOMO→LUMO transition with a distinct feature of vibronic progression. The spacing values (1377 and 1497 cm<sup>-1</sup>) are in line with the vibrational mode of aromatic C=C bonds. The spectrum of **4.22** shows two absorption peaks at 349 (HOMO→LUMO) and 294 nm, along with two shoulder bands at 379 and 329 nm. The absorbance of **4.22** was found to disobey the Beer-Lambert law in the concentration

range of  $10^{-6}$  to  $10^{-5}$  M (Appendix 3), suggesting the occurrence of aggregation in solution, which may account for the shoulder at 379 nm.

The fluorescence spectrum of **4.20** ( $\Phi_{\text{em}} = 0.23$ ) in dichloromethane shows a relatively sharp emission band at 390 nm without any vibronic features (Figure 4.6). The solvatochromic shift from a nonpolar (hexanes: 385 nm) to a strongly polar solvent (DMSO: 393 nm) is small ( $529 \text{ cm}^{-1}$ ) (Appendix 3), suggesting that the dipole moments of the ground and excited states of cyclophane **4.20** do not differ greatly. Cyclophane **4.22** ( $\Phi_{\text{em}} = 0.14$ ) exhibits dual emissions at 510 and 420 nm in dichloromethane. The shorter-wavelength emission at 420 nm can be assigned to the  $S_1 \rightarrow S_0$  transition of the triphenylene unit, while the origin of the longer-wavelength emission at 510 nm is less clear. Cyclophane **4.22** contains a triphenylene unit. It is well-established that triphenylenes seldom show excimer emission.<sup>26</sup> Excimer emission of triphenylenes in a liquid crystalline or organogel state has been reported, but this appears to require an “eclipsed”  $\pi$ -stacking arrangement.<sup>27</sup> No  $\pi$ -stacking was observed in the crystal structure of **4.22** and only a “staggered” arrangement of triphenylene units appears to be available in solution due to the steric demand of the two phenyl groups. On the other hand, fluorescence spectral analysis of **4.22** at various concentrations revealed that the relative intensity of the emission at 510 nm decreases with decreasing concentration (Appendix 3, Figures A3-7B, A3-7C), which is consistent with excimer formation. It was also found that the solvent has a significant effect on the relative intensities of the two emission bands of **4.22**, but there is no clear correlation with solvent polarity ( $\epsilon_r$ ) (Appendix 3, Figure A3-5, Table A3-1). The excitation spectra of **4.22**, monitored at the short (420 nm) and long (510 nm) wavelengths, show similar profiles that resemble the absorption spectrum. These results are consistent with the dual emission of **4.22** coming from the ground state ( $S_0$ ). Based on the current data, the low-energy emission band in

**4.22** is tentatively assigned to an excimer, which may be another example of an unusual type of excimer arising from edge-to-face interaction. Similar dual emission behavior was recently reported for a hindered  $\pi$ -conjugated organic fluorophore that can only show edge-to-face interaction.<sup>28</sup> Preliminary experiments are not inconsistent with excimer formation in **4.22** (Appendix 3), but a more detailed investigation will be required to firmly establish the origin of the low energy emission.

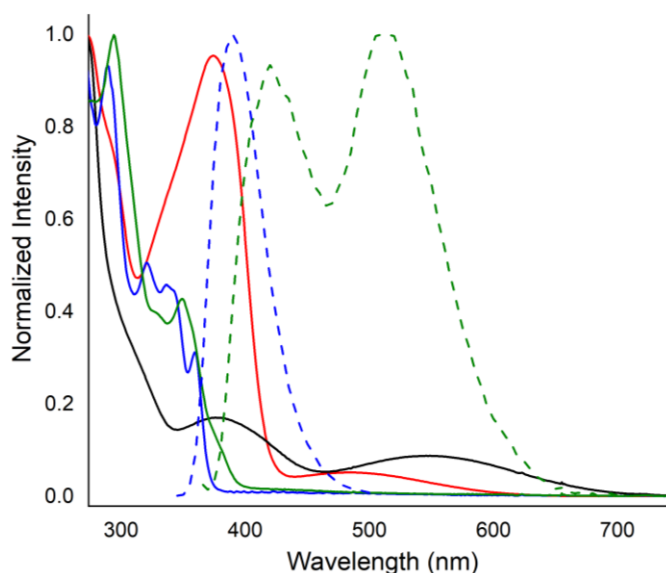


**Figure 4.6:** Normalized electronic absorption spectra of **4.18** (red solid line), **4.11** (black solid line), **4.20** (blue solid line) and **4.22** (solid green line) in dichloromethane, and emission spectra of **4.20** (blue broken line) and **4.22** (green broken line) in dichloromethane ( $\lambda_{\text{exc}}$  (**4.20**) = 320 nm;  $\lambda_{\text{exc}}$  (**4.22**) = 350 nm).

#### 4.4 Conclusions

In conclusion, the rearrangement of cyclopentadienone **4.11** to dienone **4.18** was found to be a two-step process ([1,2]-alkyl shift followed by a [1,5]-alkyl shift) that benefits greatly from the participation of an ethanol solvent molecule. The role of the ethanol molecule is to enable the rearrangement to occur through looser and presumably less strained transition states. The rearrangement could be avoided by forming **4.11** under mild aldol reaction conditions. Diels–Alder/decarbonylation reactions of **4.11** with arynes led to the formation of two fluorescent

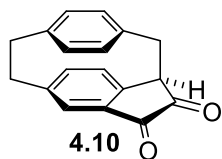
[2.2]paracyclophane/9-alkylfluorene hybrid systems **4.20** and **4.22**. The dual fluorescence emission properties of **4.22** may potentially find application in fluorescence-based sensing and imaging. Attempted cyclodehydrogenation of **4.22** to afford the more highly  $\pi$ -extended system **4.15** was unsuccessful and underscores the sensitivity of [2.2]paracyclophanes under oxidative conditions. Cyclophanes **4.11**, **4.20**, and **4.22** all have a potentially acidic 9-fluorenyl proton, removal of which will complete a contractive annulation process to afford a set of anionic [2.1]cyclophanes related to naphthalenophane **4.16**.

## 4.5 Experimental Section

### General

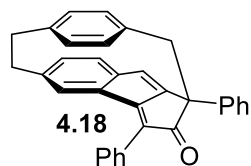
Reactions were performed under a balloon containing nitrogen gas unless otherwise indicated. All reactions were performed with oven-dried (120 °C) glassware. Solvents were removed from reaction mixtures under reduced pressure using a rotary evaporator. Chromatographic separations were achieved using Silicycle silica gel 60, particle size of 40–63 µm. Column dimensions are recorded as height × diameter. Thin-layer chromatography (TLC) was performed using precoated plastic-backed POLYGRAMÒ SIL G/UV254 silica gel plates with a layer thickness of 200 µm. Compounds on TLC plates were visualized using a UV lamp (254 and 365 nm) or cerium molybdate stain (Hanessian's stain). Melting points were recorded using OptiMelt automated melting point instrument and are uncorrected. Infrared (IR) spectra were recorded using neat samples on a Bruker Alpha spectrometer. <sup>1</sup>H and <sup>13</sup>C NMR spectra were recorded on Bruker AVANCE spectrometers at 300 MHz / 500 MHz and 75 MHz, respectively. Chemical shifts of the NMR spectra are reported relative to the residual solvent peak (CDCl<sub>3</sub>: 7.26 ppm for <sup>1</sup>H NMR, 77.16 ppm for <sup>13</sup>C NMR). High resolution mass spectrometry (HRMS) data were obtained using an Agilent 6200 series instrument, employing a TOF mass analyzer. UV/vis absorption spectra were recorded on a Varian Cary 6000i spectrophotometer. The Fluorescence spectrum was measured on a Photon Technology International (PTI) QuantaMaster spectrofluorometer. Indanone **4.9** was synthesized in 4 steps from commercial [2.2]paracyclophane using a literature procedure.<sup>6</sup> Commercial diphenylacetylene (**4.12**), 1,3-diphenylacetone (**4.5**), and 2-phenylacetophenone (**4.42**) were used as received.

### Dione **4.10**



Selenium dioxide (0.214 g, 1.93 mmol) was added to a solution of indanone **4.9** (0.300 g, 1.21 mmol) in acetic anhydride (5 mL). The resulting mixture was heated at 145 °C for 3 h. Then the mixture was cooled to room temperature and suction filtered. The filter cake was washed thoroughly with dichloromethane (20 mL). A 2 M aqueous sodium hydroxide solution (60 mL) followed by dichloromethane (30 mL) were added to the filtrate and two layers were separated. The aqueous layer was extracted with dichloromethane (2 × 20 mL). The combined organic layers were washed with saturated aqueous NaCl solution (2 × 50 mL), dried over Na<sub>2</sub>SO<sub>4</sub>, filtered, and concentrated under reduced pressure. The residue was subjected to column chromatography (15 cm × 3.5 cm, 10–25% ethyl acetate/hexanes) to afford **4.10** (0.199 g, 63%) as an orange solid. *R*<sub>f</sub> = 0.31 (30% ethyl acetate/hexanes); mp 188–190 °C; <sup>1</sup>H NMR (300 MHz, CDCl<sub>3</sub>) δ 7.14 (s, 1H), 6.97 (dd, *J* = 8.0, 1.8 Hz, 1H), 6.89 (d, *J* = 8.0 Hz, 1H), 6.66–6.60 (m, 2H), 6.41 (d, *J* = 8.7 Hz, 1H), 6.16 (d, *J* = 8.5 Hz, 1H), 4.08 (d, *J* = 9.2 Hz, 1H), 3.62 (d, *J* = 13.8 Hz, 1H), 3.35–3.23 (m, 3H), 3.19–3.05 (m, 2H); <sup>13</sup>C NMR (75 MHz, CDCl<sub>3</sub>) δ 205.2, 187.2, 149.9, 144.5, 142.9, 141.6, 140.5, 136.4, 134.9, 133.3, 133.2, 131.2, 131.1, 129.5, 49.6, 42.6, 35.7, 35.1; IR ν 2958 (w), 2927 (w), 2852 (w), 1754 (s), 1712 (s), 1593 (m), 1550 (w), 1288 (m), 992 (m), 913 (m), 723 (m), 619 (m) cm<sup>-1</sup>; HRMS [APPI-(+)] calcd for C<sub>18</sub>H<sub>15</sub>O<sub>2</sub> [M+H]<sup>+</sup> 263.1072, found 263.1077.

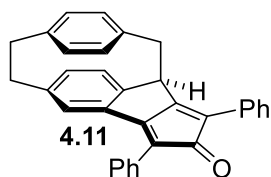
### Cyclophane **4.18**



Dione **4.10** (0.190 g, 0.724 mmol) and 1,3-diphenylacetone (**4.5**) (0.152 g, 0.724 mmol) were suspended in absolute ethanol (4 mL). The mixture was stirred at 80 °C for 30 min to allow for complete dissolution of the solids. A solution of potassium hydroxide (0.041 g, 0.72 mmol) in absolute ethanol (4 mL) was then added

dropwise to the reaction mixture using a dropping funnel over 5 min. The resulting mixture was stirred at 80 °C for additional 1.5 h. Then the mixture was cooled at room temperature and concentrated under reduced pressure. The residue was directly subjected to column chromatography (15 cm × 2.5 cm, 6% ethyl acetate/hexanes) to afford **4.18** (0.110 g, 35%) as a blood red solid.  $R_f = 0.29$  (6% ethyl acetate/hexanes); mp >300 °C;  $^1\text{H NMR}$  (300 MHz,  $\text{CDCl}_3$ )  $\delta$  7.96–7.92 (m, 2H), 7.74–7.71 (m, 2H), 7.52–7.42 (m, 5H), 7.39–7.33 (m, 1H), 7.03 (d,  $J = 7.7$  Hz, 1H), 6.99 (dd,  $J = 7.8, 1.4$  Hz, 1H), 6.65 (dd,  $J = 7.9, 2.2$  Hz, 1H), 6.55 (s, 1H), 6.38 (dd,  $J = 7.8, 2.0$  Hz, 1H), 6.24 (s, 1H), 6.15 (dd,  $J = 7.7, 2.2$  Hz, 1H), 6.02 (dd,  $J = 7.7, 2.0$  Hz, 1H), 3.77 (d,  $J = 12.5$  Hz, 1H), 2.99 (dd,  $J = 13.2, 8.2$  Hz, 1H), 2.97 (d,  $J = 12.5$  Hz, 1H), 2.84 (dd,  $J = 12.4, 8.4$  Hz, 1H), 2.66–2.56 (m, 1H), 2.52–2.42 (m, 1H);  $^{13}\text{C NMR}$  (75 MHz,  $\text{CDCl}_3$ )  $\delta$  207.0, 167.4, 152.5, 150.4, 139.3, 138.5, 138.2, 136.0, 134.8, 134.3, 133.7, 132.5, 130.6, 130.5, 130.4, 129.6, 128.9, 128.8, 128.5, 128.3, 127.9, 127.4, 126.6, 125.4, 123.2, 62.0, 49.1, 35.9, 34.7; IR  $\nu$  2921 (w), 2852 (w), 1753 (w), 1697 (s), 1594 (w), 1444 (w), 1307 (w), 820 (w), 694 (m)  $\text{cm}^{-1}$ ; HRMS [APPI-(+)] calcd for  $\text{C}_{33}\text{H}_{25}\text{O}$   $[\text{M}+\text{H}]^+$  437.1905, found 437.1888.

### Cyclopentadienone **4.11**



Dione **4.10** (0.677 g, 2.58 mmol) and 1,3-diphenylacetone (**4.5**) (0.515 g, 2.45 mmol) were suspended in absolute ethanol (20 mL). A solution of potassium hydroxide (0.144 g, 2.58 mmol) in absolute ethanol (5 mL) was then added dropwise to the reaction mixture over 5 min at room temperature. The resulting mixture was stirred at room temperature for additional 16 h. Then the mixture was concentrated under reduced pressure. The residue was directly subjected to column chromatography (15 cm × 4.5 cm, 6% ethyl acetate/hexanes) to afford **4.11** (0.887 g, 83%) as a sticky purple solid.  $R_f = 0.24$  (6% ethyl acetate/hexanes); mp 156–157 °C (dec.);  $^1\text{H NMR}$  (300 MHz,  $\text{CDCl}_3$ )  $\delta$  8.00–7.96 (m, 2H),

7.75–7.71 (m, 2H), 7.52–7.41 (m, 4H), 7.38–7.32 (m, 2H), 7.08 (d,  $J = 1.6$  Hz, 1H), 6.76 (dd,  $J = 7.8, 1.8$  Hz, 2H), 6.71 (d,  $J = 8.0$  Hz, 1H), 6.65 (dd,  $J = 7.9, 1.9$  Hz, 1H), 6.56 (dd,  $J = 7.8, 2.0$  Hz, 1H), 6.23 (dd,  $J = 7.9, 2.0$  Hz, 1H), 5.05 (d,  $J = 8.2$  Hz, 1H), 3.38 (d,  $J = 13.2$  Hz, 1H), 3.27–3.02 (m, 4H), 3.01–2.90 (m, 1H) (Note: The  $^1\text{H}$  NMR signal at  $\delta = 6.76$  ppm consists of two sets of accidentally degenerate doublet of doublets);  $^{13}\text{C}$  NMR (75 MHz,  $\text{CDCl}_3$ )  $\delta$  203.0, 162.8, 157.9, 149.7, 143.2, 140.6, 138.5, 137.4, 137.1, 134.8, 133.3, 132.5, 131.9, 131.8, 130.2, 129.1, 128.8, 128.6, 128.4, 128.1, 127.7, 127.6, 119.9, 116.6, 46.2, 43.2, 35.4, 35.3; IR  $\nu$  3015 (w), 2924 (w), 2854 (w), 1702 (s), 1595 (w), 1491 (m), 788 (m), 736 (m), 689 (m)  $\text{cm}^{-1}$ ; HRMS [APPI(+)] calcd for  $\text{C}_{33}\text{H}_{25}\text{O}$   $[\text{M}+\text{H}]^+$  437.1905, found 437.1915.

#### **Rearrangement of Cyclopentadienone **4.11** to Cyclophane **4.18** in Ethanol, Toluene, and Cyclohexane**

A solution of cyclopentadienone **4.11** (0.088 g, 0.20 mmol) in absolute ethanol (2 mL) was heated at 80 °C for 15 min. Then the reaction mixture was cooled to room temperature, concentrated, and the residue was subjected to column chromatography (15 cm  $\times$  2.5 cm, 6% ethyl acetate/hexanes) to afford **4.18** (0.071 g, 81%) as a blood red solid.

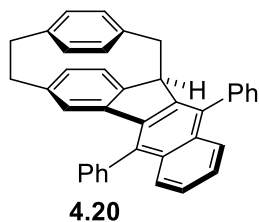
A solution of cyclopentadienone **4.11** (0.020 g, 0.046 mmol) in toluene (0.5 mL) was heated at 80 °C for 15 min. Then the reaction mixture was cooled to room temperature, concentrated, and the residue was subjected to column chromatography (15 cm  $\times$  1.0 cm, 6% ethyl acetate/hexanes) to afford **4.18** (0.0056 g, 28%) as a blood red solid.

A solution of cyclopentadienone **4.11** (0.020 g, 0.046 mmol) in cyclohexane (0.5 mL) was heated at 80 °C for 2 h. Then the reaction mixture was cooled to room temperature, concentrated, and the residue was subjected to column chromatography (15 cm  $\times$  1.0 cm, 6% ethyl acetate/hexanes) to afford **4.18** (0.0065 g, 33%) as a blood red solid.

## Attempted Diels-Alder Cycloaddition of Cyclopentadienone **4.11** and Diphenylacetylene (**4.12**)

A solution of cyclopentadienone **4.11** (0.020 g, 0.046 mmol) and diphenylacetylene (**4.12**) (0.010 g, 0.055 mmol) in xylenes (0.5 mL) was heated at 80 °C for 15 min. Then the reaction mixture was cooled to room temperature and directly subjected to column chromatography (20 cm × 1.0 cm, 1–3% ethyl acetate/hexanes) to afford **4.18** (0.0043 g, 22%) as a blood red solid and **4.12** as an off-white solid (0.0094 g, 94% recovery).

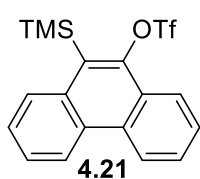
### Cyclophane **4.20**



A 1.0 M solution of tetrabutylammonium fluoride (0.080 mL, 0.080 mmol) in THF was added dropwise to a stirred 0 °C (ice/water bath) mixture of cyclopentadienone **4.11** (0.0298 g, 0.068 mmol) and 2-(trimethylsilyl)phenyl trifluoromethanesulfonate (**4.19**) (0.0185 g, 0.0620 mmol) in dry THF (3 mL). The cold bath was removed and the reaction mixture was stirred for 16 h as it warmed to room temperature. The majority of the solvent was removed under reduced pressure. The remaining mixture was diluted with ethyl acetate (10 mL) and water (10 mL). The layers were separated and the aqueous layer was extracted with ethyl acetate (2 × 10 mL). The combined organic layers were washed with saturated aqueous NaCl solution (30 mL), dried over Na<sub>2</sub>SO<sub>4</sub>, filtered, and concentrated under reduced pressure. The residue was subjected to column chromatography (15 cm × 2.0 cm, 25% dichloromethane/hexanes) to afford a white solid, which was further triturated with diethyl ether (2 × 1 mL) to afford **4.20** (0.0172 g, 57%) as a white solid. *R*<sub>f</sub> = 0.46 (40% dichloromethane/hexanes); mp 216–218 °C; <sup>1</sup>H NMR (300 MHz, CDCl<sub>3</sub>) δ 7.76–7.62 (m, 8H), 7.58–7.52 (m, 2H), 7.48 (td, *J* = 7.5, 1.1 Hz, 1H), 7.43–7.37 (m, 2H), 7.29 (dt, *J* = 7.4, 1.6 Hz, 1H), 6.61 (d, *J* = 7.8 Hz, 1H), 6.52 (dd, *J* = 7.3, 2.2 Hz, 1H), 6.50 (dd, *J* = 7.6, 1.6 Hz,

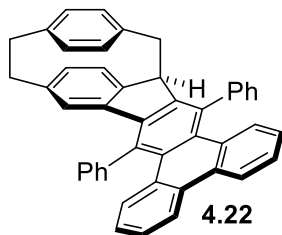
1H), 6.31 (dd,  $J = 7.8, 1.9$  Hz, 1H), 6.03 (dd,  $J = 7.9, 1.9$  Hz, 1H), 5.96 (dd,  $J = 7.9, 1.8$  Hz, 1H), 5.50 (d,  $J = 1.6$  Hz, 1H), 4.75 (d,  $J = 7.8$  Hz, 1H), 3.15 (d,  $J = 12.9$  Hz, 1H), 3.13–3.05 (m, 1H), 2.91–2.60 (m, 4H);  $^{13}\text{C}$  NMR (75 MHz,  $\text{CDCl}_3$ )  $\delta$  146.6, 143.93, 143.90, 141.1, 140.1, 139.1, 138.7, 137.1, 135.5, 135.4, 133.2, 132.8, 132.6, 132.5, 132.4, 132.1, 131.4, 130.5, 130.3, 130.2, 129.7, 129.4, 129.2, 128.7, 128.4, 128.3, 127.8, 127.6, 126.4, 126.2, 125.5, 125.4, 124.3, 49.4, 42.1, 35.7, 35.4 (one signal fewer than expected); IR  $\nu$  3049 (w), 2927 (w), 2853 (w), 1595 (w), 1493 (m), 1376 (m), 769 (m), 746 (m), 703 (s)  $\text{cm}^{-1}$ ; HRMS [APPI-(+)] calcd for  $\text{C}_{38}\text{H}_{29}$   $[\text{M}+\text{H}]^+$  485.2269, found 485.2260.

### 10-(Trimethylsilyl)phenanthrene-9-yl trifluoromethanesulfonate (**4.21**)<sup>13</sup>



10-(Trimethylsilyl)phenanthrene-9-yl trifluoromethanesulfonate (**4.21**) was synthesized from 10-bromo-9-phenanthrol over two steps in 57% yield following a literature procedure.<sup>13</sup>  $R_f = 0.46$  (3% diethyl ether/hexanes); mp 90–92 °C (lit. mp<sup>13</sup> 94 °C);  $^1\text{H}$  NMR (300 MHz,  $\text{CDCl}_3$ )  $\delta$  8.71–8.66 (m, 2H), 8.25–8.22 (m, 1H), 8.13 (d,  $J = 8.2$  Hz, 1H), 7.78–7.62 (m, 4H), 0.62 (s, 9H);  $^{13}\text{C}$  NMR (75 MHz,  $\text{CDCl}_3$ )  $\delta$  148.0, 134.8, 132.9, 130.7, 130.1, 129.9, 128.5, 127.5, 127.3, 126.8, 125.9, 123.5, 122.9, 122.4, 118.9 (q,  $J = 320.4$  Hz), 2.4; IR  $\nu$  2967 (w), 1397 (m), 1205 (s), 1132 (m), 1009 (m), 830 (s), 680 (m)  $\text{cm}^{-1}$ ; HRMS [APPI-(+)] calcd for  $\text{C}_{18}\text{H}_{17}\text{F}_3\text{O}_3\text{SSi}$   $[\text{M}]^+$  398.0620, found 398.0624.

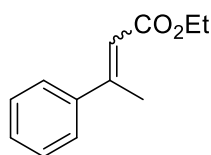
## Cyclophane **4.22**



A 1.0 M solution of tetrabutylammonium fluoride (0.18 mL, 0.18 mmol) in THF was added dropwise to a stirred 0 °C (ice/water bath) mixture of cyclopentadienone **4.11** (0.065 g, 0.15 mmol) and 10-(trimethylsilyl)phenanthrene-9-yl trifluoromethanesulfonate (**4.21**) (0.054 g, 0.14 mmol) in dry THF (7 mL). The cold bath was removed and the reaction mixture was stirred for 16 h as it warmed to room temperature. The majority of the solvent was removed under reduced pressure. The remaining mixture was diluted with ethyl acetate (20 mL) and water (20 mL). The layers were separated and the aqueous layer was extracted with ethyl acetate (2 × 20 mL). The combined organic layers were washed with saturated aqueous NaCl solution (60 mL), dried over Na<sub>2</sub>SO<sub>4</sub>, filtered, and concentrated under reduced pressure. The residue was subjected to column chromatography (15 cm × 2.0 cm, 10–30% dichloromethane/hexanes) to afford **4.22** (0.062 g, 78%) as a white solid.  $R_f = 0.41$  (40% dichloromethane/hexanes); mp 284–286 °C; <sup>1</sup>H NMR (300 MHz, CDCl<sub>3</sub>) δ 8.53 (dd,  $J = 8.3, 1.4$  Hz, 1H), 8.46 (dd,  $J = 8.3, 1.4$  Hz, 1H), 8.30–8.03 (br m, 1H), 7.99 (dd,  $J = 8.6, 1.2$  Hz, 1H), 7.84 (dd,  $J = 8.5, 1.2$  Hz, 1H), 7.78–7.36 (m, 10H), 7.24–7.13 (br m, 1H), 7.09 (ddd,  $J = 8.6, 7.0, 1.5$  Hz, 1H), 7.02 (ddd,  $J = 8.5, 7.0, 1.4$  Hz, 1H), 6.64 (d,  $J = 7.7$  Hz, 1H), 6.52 (dd,  $J = 7.9, 1.8$  Hz, 1H), 6.51 (dd,  $J = 7.7, 1.6$  Hz, 1H), 6.31 (dd,  $J = 7.8, 1.9$  Hz, 1H), 6.21 (dd,  $J = 7.8, 1.9$  Hz, 1H), 6.07 (dd,  $J = 7.9, 1.9$  Hz, 1H), 5.24 (d,  $J = 1.5$  Hz, 1H), 5.04 (d,  $J = 8.0$  Hz, 1H), 3.16–3.07 (m, 1H), 2.89–2.65 (m, 5H); <sup>13</sup>C NMR (75 MHz, CDCl<sub>3</sub>) δ 146.9, 146.2, 144.3, 143.5, 143.2, 141.1, 140.9, 140.1, 137.1, 136.1, 135.6, 134.1, 132.5, 132.32, 132.30, 131.84, 131.76, 130.9, 130.7, 130.6, 130.33, 130.29, 130.0, 129.6, 129.5, 129.1, 127.8, 127.7, 127.2, 126.5, 125.2, 124.7, 124.2, 122.9, 122.8, 50.0, 40.5, 35.8, 35.4 (seven signals fewer than expected); IR  $\nu$  3018 (w), 2924 (w), 2853 (w), 1594 (w), 1494 (m), 1440 (m),

762 (s), 727 (s), 703 (s)  $\text{cm}^{-1}$ ; HRMS [APPI-(+)] calcd for  $\text{C}_{46}\text{H}_{33}$   $[\text{M}+\text{H}]^+$  585.2582, found 585.2578.

### Ethyl 3-phenylbut-2-enoate (**4.28**)<sup>29</sup>

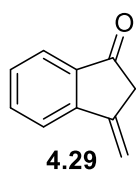


**4.28**

Triethyl phosphonoacetate (**4.27**) (8.40 g, 37.5 mmol) was added dropwise to a stirred 0 °C (ice/water) suspension of sodium hydride (60% dispersion in mineral oil, 0.999 g, 25.0 mmol) in THF (50 mL). The mixture was stirred at the same temperature for 15 min. Then a solution of acetophenone (**4.26**) (1.50 g, 12.5 mmol) in THF (10 mL) was added dropwise to the mixture. The resulting mixture was stirred at 0 °C for another 30 min and then heated at 60 °C for 5 h. A saturated aqueous  $\text{NH}_4\text{Cl}$  solution (50 mL) was added to the reaction mixture. The majority of the solvent was removed under reduced pressure. The reaction mixture was diluted with dichloromethane (50 mL) and water (50 mL) was added. The two layers were separated and the aqueous layer was extracted with dichloromethane (2  $\times$  30 mL). The combined organic layers were washed with saturated aqueous NaCl solution (50 mL), dried over  $\text{Na}_2\text{SO}_4$ , filtered, and concentrated under reduced pressure. The residue was subjected to column chromatography (15 cm  $\times$  4.5 cm, 0–5% ethyl acetate/hexanes) to afford a *ca.* 83:17 mixture of *E*- and *Z*-diastereomers of **4.28** (2.32 g, 98%) as a pale yellow oil.  $R_f = 0.49$  and 0.38 (8% ethyl acetate/hexanes);  $^1\text{H}$  NMR (300 MHz,  $\text{CDCl}_3$ ) distinguishable signals for *E*-isomer:  $\delta$  7.50–7.45 (m, 2H), 7.41–7.30 (m, 3H), 6.14 (q,  $J = 1.3$  Hz, 1H), 4.22 (q,  $J = 7.1$  Hz, 2H), 2.59 (d,  $J = 1.3$  Hz, 3H), 1.32 (t,  $J = 7.1$  Hz, 3H); distinguishable signals for *Z*-isomer:  $\delta$  7.22–7.19 (m, 2H), 5.91 (q,  $J = 1.5$  Hz, 1H), 4.00 (q,  $J = 7.1$  Hz, 2H), 2.18 (d,  $J = 1.5$  Hz, 3H), 1.08 (t,  $J = 7.1$  Hz, 3H);  $^{13}\text{C}$  NMR (75 MHz,  $\text{CDCl}_3$ ) distinguishable signals for *E*-isomer:  $\delta$  167.0, 155.7, 142.4, 129.1, 128.6, 128.0, 126.9, 126.4, 117.3, 60.0, 18.1, 14.5;

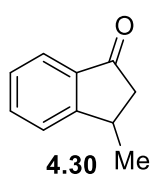
distinguishable signals for *Z*-isomer:  $\delta$  166.1, 155.5, 141.0, 127.9, 117.9, 27.3, 14.1; HRMS [APPI-(+)] calcd for C<sub>12</sub>H<sub>15</sub>O<sub>2</sub> [M+H]<sup>+</sup> 191.1072, found 191.1078.

### 3-Methylene-2,3-dihydro-1*H*-inden-1-one (4.29)<sup>19</sup>



Triflic acid (10.0 mL, 113 mmol) was added dropwise to a stirred 0 °C (ice/water) solution of **4.28** (0.897 g, 4.72 mmol) in 1,2-dichloroethane (50 mL). The resulting mixture was warmed to room temperature and stirred for 8 h. A saturated aqueous sodium bicarbonate solution (50 mL) was added to the reaction mixture. The two layers were separated and the aqueous layer was extracted with dichloromethane (2 × 30 mL). The combined organic layers were washed with saturated aqueous NaCl solution (100 mL), dried over Na<sub>2</sub>SO<sub>4</sub>, filtered, and concentrated under reduced pressure. The residue was subjected to column chromatography (15 cm × 4.5 cm, 5–10% ethyl acetate/hexanes) to afford **4.29** (0.482 g, 71%) as a viscous red oil that solidified on standing in a freezer to afford a waxy red solid.  $R_f$  = 0.45 (15% ethyl acetate/hexanes); <sup>1</sup>H NMR (300 MHz, CDCl<sub>3</sub>)  $\delta$  7.80–7.75 (m, 2H), 7.63 (td,  $J$  = 7.5, 1.1 Hz, 1H), 7.43 (td,  $J$  = 7.5, 0.9 Hz, 1H), 5.83 (t,  $J$  = 2.0 Hz, 1H), 5.32 (t,  $J$  = 1.6 Hz, 1H), 3.28 (t,  $J$  = 1.8 Hz, 2H); <sup>13</sup>C NMR (75 MHz, CDCl<sub>3</sub>)  $\delta$  203.0, 149.9, 139.8, 137.4, 134.9, 129.3, 123.5, 121.4, 108.0, 42.2; HRMS [APPI-(+)] calcd for C<sub>10</sub>H<sub>9</sub>O [M+H]<sup>+</sup> 145.0653, found 145.0645.

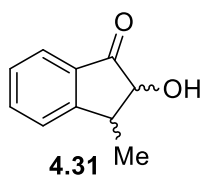
### 3-Methyl-2,3-dihydro-1*H*-inden-1-one (4.30)<sup>30</sup>



Pd/C (10 wt%, 25 mg) was added to a nitrogen-purged stirred solution of **4.29** (0.256 g, 1.78 mmol) in ethyl acetate (15 mL). The resulting mixture was purged with hydrogen (inflated balloon) for 5 min and then stirred under an atmosphere of hydrogen (inflated balloon) for 16 h. The mixture was vacuum filtered through a pad of Celite<sup>®</sup>, washed with ethyl acetate (3 × 10 mL), concentrated under reduced pressure, and the residue was subjected to column chromatography (10 cm × 2.5 cm, 5–10% ethyl acetate/hexanes) to afford

**4.30** (0.244 g, 94%) as a pale yellow oil.  $R_f = 0.36$  (15% ethyl acetate/hexanes);  $^1\text{H NMR}$  (300 MHz,  $\text{CDCl}_3$ )  $\delta$  7.72 (d,  $J = 7.9$  Hz, 1H), 7.60 (td,  $J = 7.4, 1.2$  Hz, 1H), 7.50 (dd,  $J = 7.7, 1.0$  Hz, 1H), 7.36 (td,  $J = 7.4, 1.0$  Hz, 1H), 3.49–3.38 (m, 1H), 2.93 (dd,  $J = 19.0, 7.5$  Hz, 1H), 2.27 (dd,  $J = 19.0, 3.5$  Hz, 1H), 1.40 (d,  $J = 7.1$  Hz, 3H);  $^{13}\text{C NMR}$  (75 MHz,  $\text{CDCl}_3$ )  $\delta$  206.5, 160.1, 136.6, 134.9, 127.5, 125.4, 123.6, 45.5, 32.9, 21.5; HRMS [APPI-(+)] calcd for  $\text{C}_{10}\text{H}_{11}\text{O}$   $[\text{M}+\text{H}]^+$  147.0810, found 147.0806.

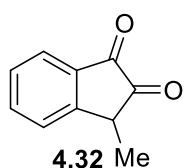
### 2-Hydroxy-3-methyl-2,3-dihydro-1H-inden-1-one (**4.31**)<sup>21</sup>



Pulverized potassium hydroxide (0.805 g, 14.4 mmol) was added to a 0 °C (ice/water) solution of **4.30** (0.189 g, 1.29 mmol) in methanol (8 mL) and the mixture was stirred at that temperature for 10 min. (Diacetoxyiodo)benzene (0.499 g, 1.55 mmol) was added to the mixture and the resulting mixture was stirred at the same temperature for 1 h and then warmed to room temperature and stirred for another 30 min. The majority of the solvent was removed under reduced pressure. The reaction mixture was diluted with diethyl ether (10 mL) and 3% aqueous sodium bicarbonate solution (10 mL) was added. The layers were separated, the organic layer was washed with water ( $2 \times 10$  mL), dried over  $\text{Na}_2\text{SO}_4$ , filtered, and concentrated under reduced pressure. The residue was dissolved in THF (5 mL) and 6 M aqueous hydrochloric acid solution (0.40 mL) was added to the stirred solution. After stirring the mixture for 30 min, the majority of the solvent was removed under reduced pressure. The residue was diluted with diethyl ether (10 mL). The organic solution was washed with saturated aqueous sodium bicarbonate solution (10 mL), water ( $2 \times 10$  mL), dried over  $\text{Na}_2\text{SO}_4$ , filtered, and concentrated under reduced pressure. The residue was subjected to column chromatography (15 cm  $\times$  2.5 cm, 20–35% ethyl acetate/hexanes) to afford a *ca.* 3:1 mixture of diastereomers of **4.31** (0.134 g, 64%) as a white waxy solid.  $R_f = 0.45$  (40% ethyl acetate/hexanes);  $^1\text{H NMR}$  (300 MHz,

CDCl<sub>3</sub>) distinguishable signals for the major diastereomer:  $\delta$  7.77–7.61 (m, 2H), 7.49 (dd,  $J = 7.7$ , 0.8 Hz, 1H), 7.43–7.37 (m, 1H), 4.11 (d,  $J = 5.4$  Hz, 1H), 3.50 (br s, 1H), 3.24–3.15 (m, 1H), 1.60 (d,  $J = 7.0$  Hz, 1H); distinguishable signals for the minor diastereomer:  $\delta$  4.58 (d,  $J = 7.3$  Hz, 1H), 3.71–3.62 (m, 1H), 3.32 (br s, 1H), 1.21 (d,  $J = 7.2$  Hz, 1H); <sup>13</sup>C NMR (75 MHz, CDCl<sub>3</sub>) distinguishable signals for the major diastereomer:  $\delta$  205.7, 154.7, 136.0, 133.4, 128.1, 124.9, 124.1, 82.5, 41.6, 17.1; distinguishable signals for the minor diastereomer:  $\delta$  206.7, 157.5, 135.9, 132.7, 128.2, 126.3, 124.4, 77.0, 38.8, 17.9; HRMS [APPI-(+)] calcd for C<sub>10</sub>H<sub>11</sub>O<sub>2</sub> [M+H]<sup>+</sup> 163.0759, found 163.0748.

### 3-Methyl-1,2-indandione (**4.32**)<sup>21</sup>



Thirty drops of a freshly prepared solution of the Jones reagent (prepared from 1.00 g of chromium trioxide, 0.9 mL of concentrated sulfuric acid, 0.6 mL deionized water) was added to a stirred 0 °C (ice/water) solution of **4.31** (0.095 g, 0.59 mmol) in acetone (10 mL). After the addition was complete, the characteristic orange color of the Jones reagent persisted. The resulting reaction mixture was stirred for 15 min at the same temperature. Isopropanol (0.2 mL) was added to the reaction mixture to destroy the excess Jones reagent. The majority of the solvent was removed under reduced pressure. The reaction mixture was diluted with dichloromethane (20 mL) and saturated aqueous sodium bicarbonate solution (10 mL) was added. The layers were separated and the organic layer was washed with water (2 × 10 mL), dried over Na<sub>2</sub>SO<sub>4</sub>, filtered, and concentrated under reduced pressure to afford **4.32** (0.083 g, 89%, >90% pure as judged by <sup>1</sup>H NMR) as an orange viscous liquid. *Note: Purification was avoided as the product was reported to be unstable to heat or column chromatography.*<sup>21</sup> <sup>1</sup>H NMR (300 MHz, CDCl<sub>3</sub>)  $\delta$  7.92 (d,  $J = 7.8$  Hz, 1H), 7.80 (t,  $J = 7.6$  Hz, 1H), 7.60 (d,  $J = 7.8$  Hz, 1H), 7.51 (t,  $J = 7.6$  Hz, 1H), 3.59 (q,  $J = 7.3$  Hz, 1H), 1.54 (d,  $J = 7.5$  Hz, 3H); <sup>13</sup>C NMR (75 MHz,

CDCl<sub>3</sub>)  $\delta$  203.4, 187.7, 152.4, 138.1, 136.0, 128.8, 126.4, 125.4, 40.9, 16.1; HRMS [APPI(+)]  
calcd for C<sub>10</sub>H<sub>9</sub>O<sub>2</sub> [M+H]<sup>+</sup> 161.0603, found 161.0595.

## 4.6 References

1. (a) Ye, Q.; Chi, C.-Y. *Chem. Mater.* **2014**, *26*, 4046–4056. (b) De, P. K.; Neckers, D. C. *Org. Lett.* **2012**, *14*, 78–81. (c) Chen, L.; Hernandez, Y.; Feng, X.; Müllen, K. *Angew. Chem. Int. Ed.* **2012**, *51*, 7640–7654.
2. (a) Wu, J.; Pisula, W.; Müllen, K. *Chem. Rev.* **2007**, *107*, 718–747. (b) Zhi, L. J.; Müllen, K. *J. Mater. Chem.* **2008**, *18*, 1472–1484. (c) Pun, S. H.; Miao, Q. *Acc. Chem. Res.* **2018**, *51*, 1630–1642.
3. (a) Medel, M. A.; Cruz, C. M.; Miguel, D.; Blanco, V.; Morcillo, S. P.; Campaña, A. G. *Angew. Chem. Int. Ed.* **2021**, *60*, 22051–22056. (b) Medel, M. A.; Tapia, R.; Blanco, V.; Miguel, D.; Morcillo, S. P.; Campaña, A. G. *Angew. Chem. Int. Ed.* **2021**, *60*, 6094–6100. (c) Reger, D.; Haines, P.; Heinemann, F. W.; Guldi, D. M.; Jux, N. *Angew. Chem. Int. Ed.* **2018**, *57*, 5938–5942. (d) Fernandez-García, J. M.; Evans, P. J.; Rivero, S. M.; Fernandez, I.; García-Fresnadillo, D.; Perles, J.; Casado, J.; Martín, N. *J. Am. Chem. Soc.* **2018**, *140*, 17188–17196. (e) Cheung, K. Y.; Chan, C. K.; Liu, Z.; Miao, Q. *Angew. Chem. Int. Ed.* **2017**, *56*, 9003–9007. (f) Cheung, K. Y.; Xu, X.; Miao, Q. *J. Am. Chem. Soc.* **2015**, *137*, 3910–3914.
4. Greenfield, S.; Mackenzie, K. *J. Chem. Soc., Perkin Trans. 2* **1986**, 1651–1666.
5. Barton, J. W.; Shepherd, M. K. *J. Chem. Soc., Perkin Trans. 1* **1986**, 961–966.
6. Biswas, S.; Qiu, C. S.; Dawe, L. N.; Zhao, Y.; Bodwell, G. J. *Angew. Chem. Int. Ed.* **2019**, *58*, 9166–9170.
7. Zhou, Z.; Kawade, R. K.; Wei, Z.; Kuriakose, F.; Üngör, Ö.; Jo, M.; Shatruk, M.; Gershoni-Poranne, R.; Petrukhina, M. A.; Alabugin, I. V. *Angew. Chem. Int. Ed.* **2020**, *59*, 1256–1262

8. Matthews, W. S.; Bares, J. E.; Bartmess, J. E.; Bordwell, F. G.; Cornforth, F. J.; Drucker, G. E.; Margolin, Z.; McCallum, R. J.; McCollum, G. J.; Vanier, N. R. *J. Am. Chem. Soc.* **1975**, *97*, 7006–7014.
9. Dobrowolski, M. A.; Cyranski, M. K.; Merner, B. L.; Bodwell, G. J.; Wu, J.; Schleyer, P. v. R. *J. Org. Chem.* **2008**, *73*, 8001–8009.
10. Gui, Y.; Li, J.; Guo, C.-S.; Li, X.-L.; Lu, Z.-F.; Huang, Z.-Z. *Adv. Synth. Catal.* **2008**, *350*, 2483–2487.
11. Cyclopentadienones are known to decompose slowly. See for example: Potter, R. G.; Hughes, T. S. *J. Org. Chem.* **2008**, *73*, 2995–3004.
12. For a review on Diels–Alder reactions of cyclopentadienones and alkynes, see: Dyan, O. T.; Borodkin, G. I.; Zaikin, P. A. *Eur. J. Org. Chem.* **2019**, 7271–7306.
13. Peña, D.; Cobas, A.; Pérez, D.; Guitián, E. *Synthesis* **2002**, 1454–1458.
14. Koga, Y.; Kaneda, T.; Saito, Y.; Murakami, K.; Itami, K. *Science* **2018**, *359*, 435–439.
15. Zhai, L.; Shukla, R.; Rathore, R. *Org. Lett.* **2009**, *11*, 3474–3477.
16. Waghray, D.; de Vet, C.; Karypidou, K.; Dehaen, W. *J. Org. Chem.* **2013**, *78*, 11147–11154.
17. (a) Adam, W.; Miranda, M. A.; Mojarrad, F.; Sheikh, H. *Chem. Ber.* **1994**, *127*, 875–879. (b) Hopf, H.; Kleinschroth, J. *Angew. Chem. Int. Ed.* **1982**, *21*, 469–480. (c) Sato, T.; Torizuka, K.; Shimizu, M.; Kurihara, N.; Yoda, N. *Bull. Chem. Soc. Jpn.* **1979**, *52*, 2420–2423. (d) Shono, T.; Ikeda, A.; Hayashi, J.; Hakozaiki, S. *J. Am. Chem. Soc.* **1975**, *97*, 4261–4264. (e) Reich, H. J.; Cram, D. J.; *J. Am. Chem. Soc.* **1969**, *91*, 3517–3526. (f) Helgeson, R. C.; Cram, D. J. *J. Am. Chem. Soc.* **1966**, *88*, 509–515.
18. Sankararaman, S.; Hopf, H.; Dix, I.; Jones, P. G. *Eur. J. Org. Chem.* **2000**, 2711–2716.
19. Ramulu, B. V.; Satyanarayana, G. *RSC Adv.* **2015**, *5*, 70972–70976.

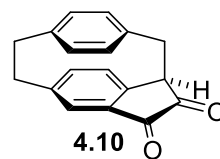
20. Matsuo, K.; Shindo, M. *Org. Lett.* **2010**, *12*, 5346–5349.
21. Dayan, S.; Almog, J.; Khodzhaev, O.; Rozen, S. *J. Org. Chem.* **1998**, *63*, 2752–2754.
22. Kozuch, S.; Martin, J. M. L. *ChemPhysChem* **2011**, *12*, 1413–1418.
23. Bowen, M. E.; Aavula, B. R.; Mash, E. A. *J. Org. Chem.* **2002**, *67*, 9087–9088.
24. Gutowsky–Holm equation used:  $k_c = \pi\Delta\nu/\sqrt{2}$ , where  $k_c$  = rate of the interconversion of the two exchanging protons,  $\Delta\nu$  = chemical shift difference (in Hz) under slow exchange between the two exchanging protons. For more information, see: (a) Friebolin, H. *Basic One- and Two-Dimensional NMR spectroscopy*, 3rd ed.; Wiley: Weinheim, 1998; Chapter 11. (b) Allerhand, A.; Gutowsky, H. S.; Jonas, J.; Meinzer, R. A. *J. Am. Chem. Soc.* **1966**, *88*, 3185–3194.
25. Eyring equation used:  $\Delta G^\ddagger = RT_c[23.76 - \ln(k_c/T_c)]$ , where  $\Delta G^\ddagger$  = activation energy of rotation,  $k_c$  = rate of the interconversion of the two exchanging protons,  $T_c$  = coalescence temperature. For more information, see: Kincaid, J. F.; Eyring, H.; Stearn, A. E. *Chem. Rev.* **1941**, *28*, 301–365.
26. (a) Schwab, M. G.; Qin, T.; Pisula, W.; Mavrinskiy, A.; Feng, X.; Baumgarten, M.; Kim, H.; Laquai, F.; Schuh, S. Trattnig, R.; List, E. J. W.; Müllen, K. *Chem. Asian. J.* **2011**, *6*, 3001–3010. (b) Nandy, R.; Sankararaman, S. *Beilstein J. Org. Chem.* **2010**, *6*, 992–1001. (c) Sasson, R.; Braitbart, O.; Weinreb, A. *J. Lumin.* **1988**, *39*, 223–225. (d) Birks, J. B.; Christophorou, L. G. *Nature* **1962**, *194*, 442–444.
27. Ikeda, M.; Takeuchi, M.; Shinkai, S. *Chem. Commun.* **2003**, 1354–1355.
28. Chen, Y.-H.; Tang, K.-C.; Chen, Y.-T.; Shen, J. Y.; Wu, Y.-S.; Liu, S.-H.; Lee, C.-S.; Chen, C. H.; Lai, T.-Y.; Tung, S.-H. *Chem. Sci.* **2016**, *7*, 3556–3563.
29. Porta, E. O. J.; Vallejos, M. M.; Bracca, A. B. J.; Labadie, G. R. *RSC Adv.* **2017**, *7*, 47527–47538.

30. Kumar, D. R.; Panigrahy, R. S.; Kishore, D. R.; Satyanarayana, G. *ChemistrySelect* **2019**, *4*, 12111–12116.

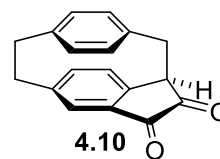
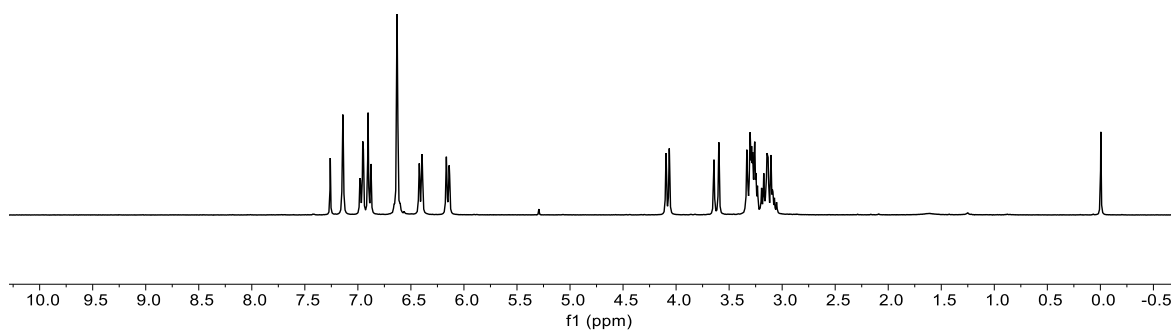
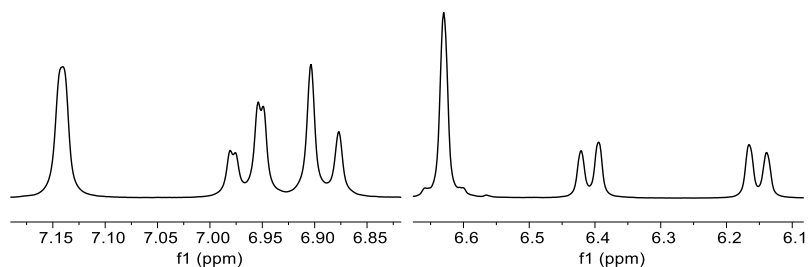
## **Appendix 3**

**$^1\text{H}$ ,  $^{13}\text{C}$  NMR Spectra, Two-Dimensional NMR Spectra, X-ray Crystallographic Data, UV/vis Absorption Spectra, Excitation and Emission Spectra, and Computational Data for Chapter 4**

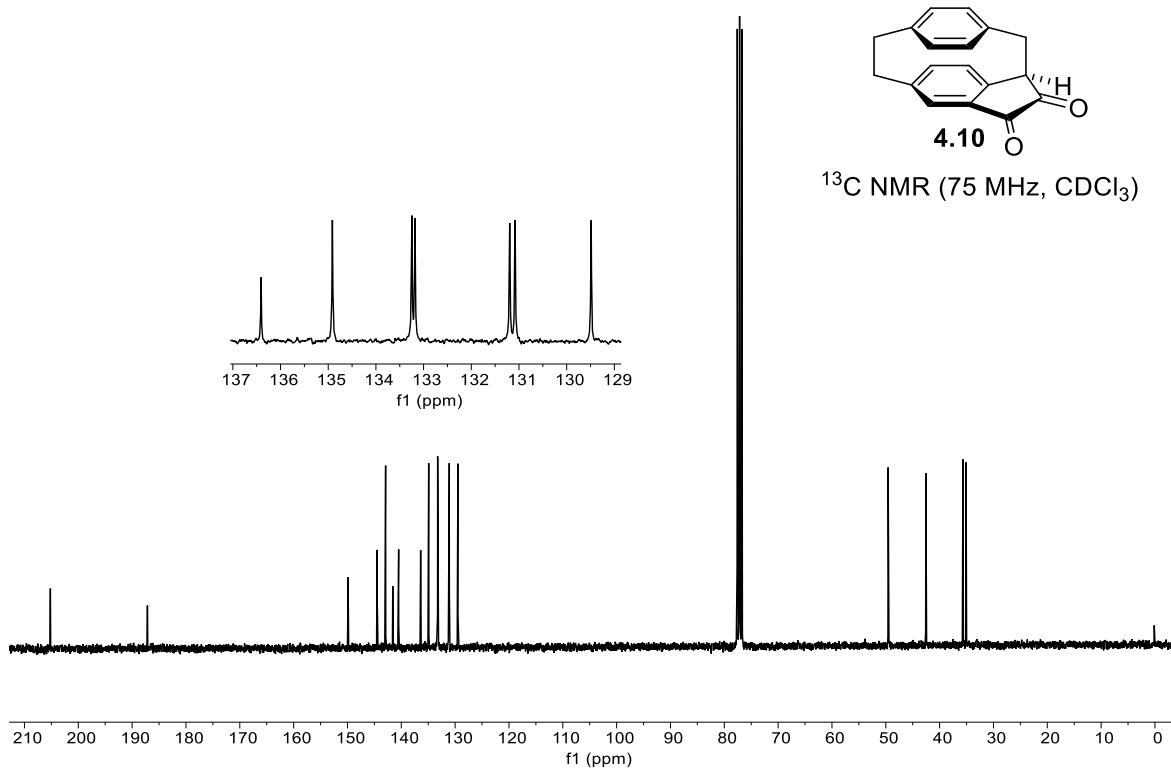
# 1. $^1\text{H}$ and $^{13}\text{C}$ NMR Spectra



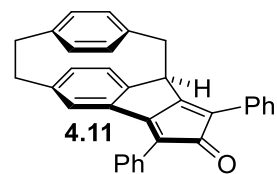
$^1\text{H}$  NMR (300 MHz,  $\text{CDCl}_3$ )



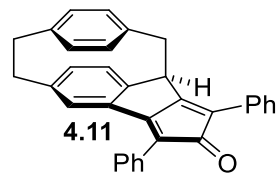
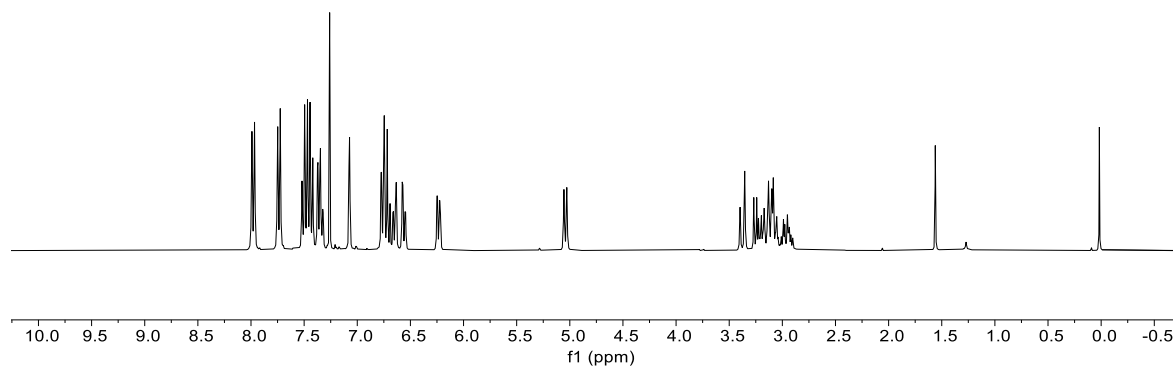
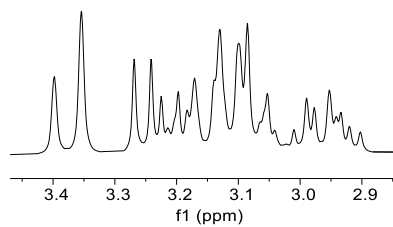
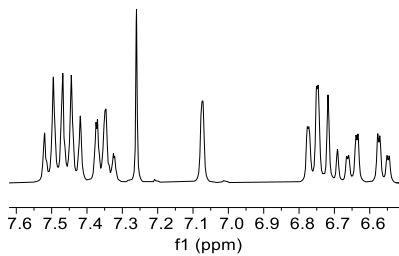
$^{13}\text{C}$  NMR (75 MHz,  $\text{CDCl}_3$ )



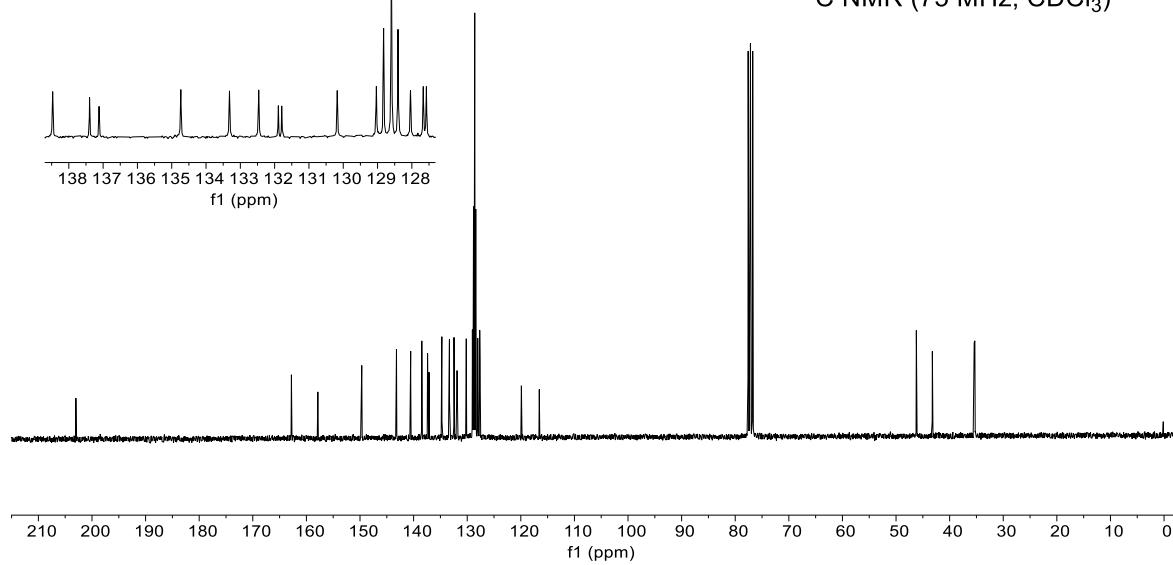
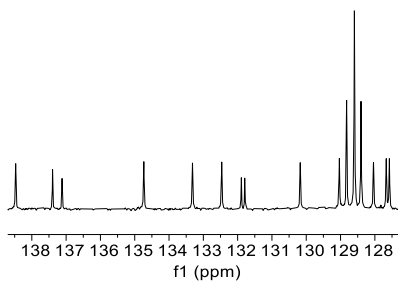


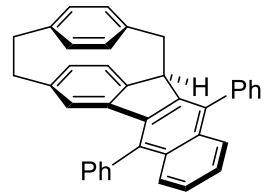


$^1\text{H}$  NMR (300 MHz,  $\text{CDCl}_3$ )



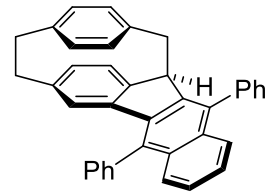
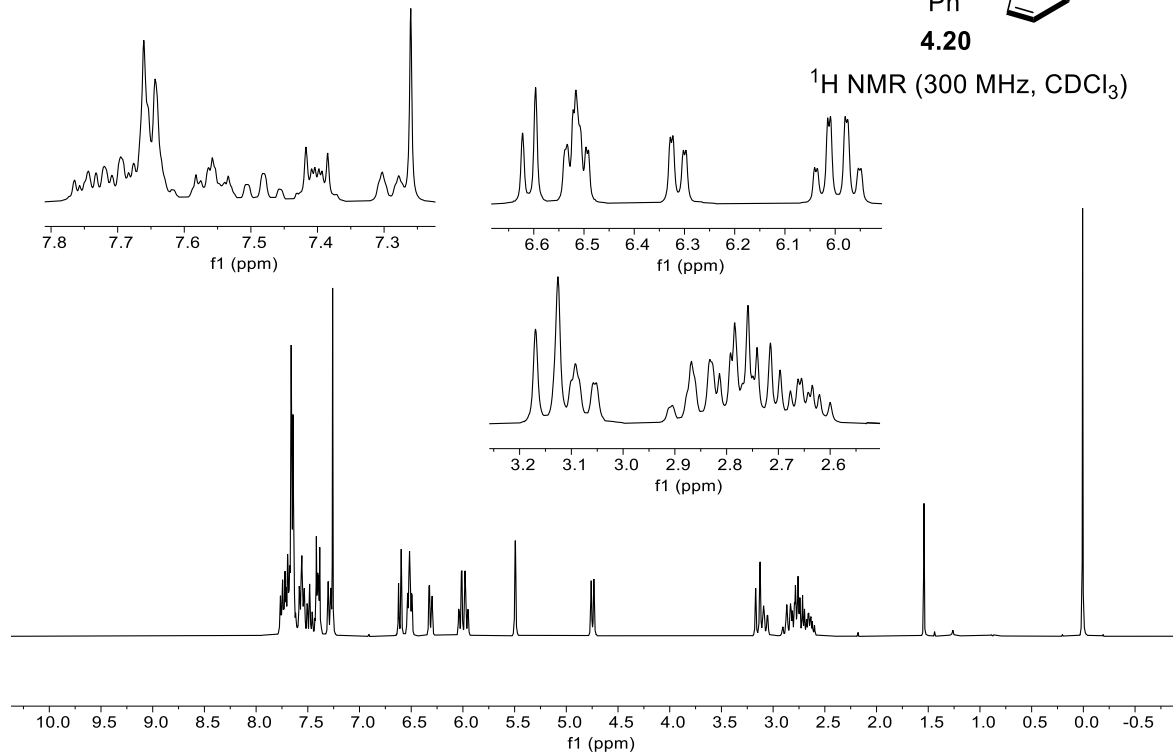
$^{13}\text{C}$  NMR (75 MHz,  $\text{CDCl}_3$ )





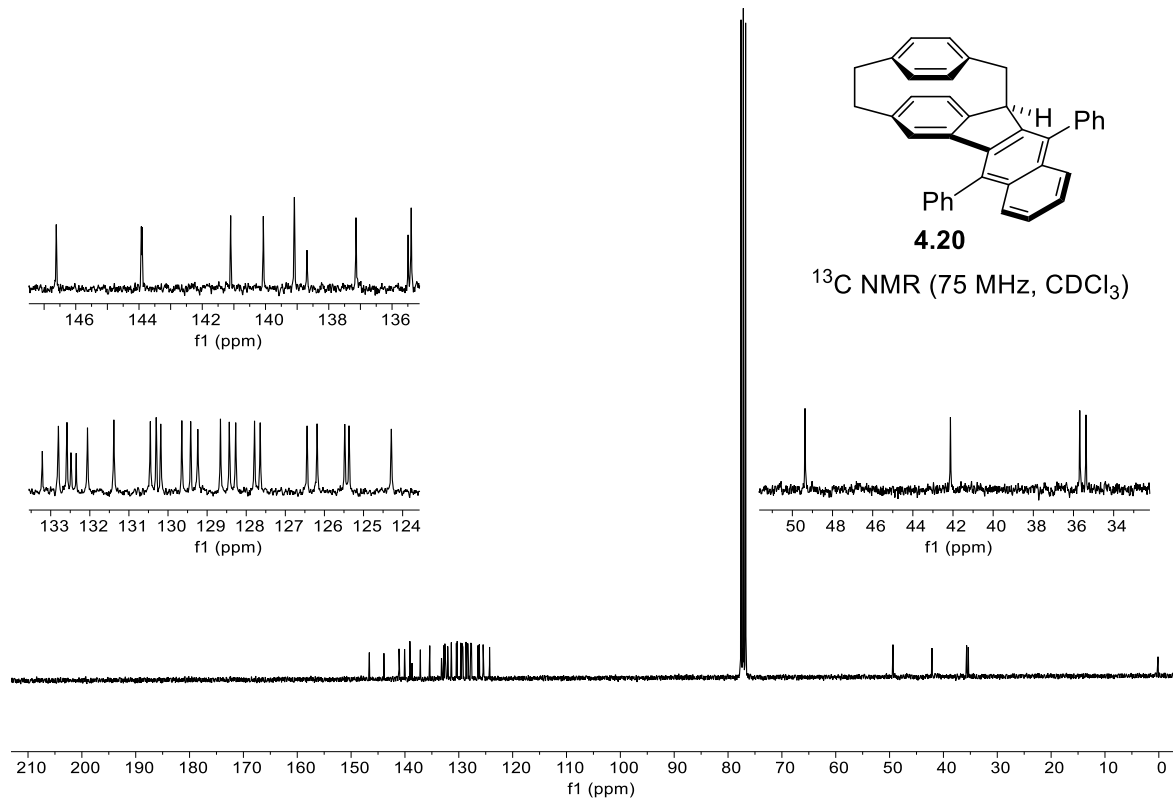
4.20

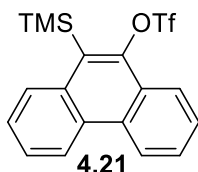
$^1\text{H}$  NMR (300 MHz,  $\text{CDCl}_3$ )



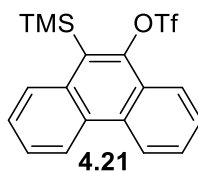
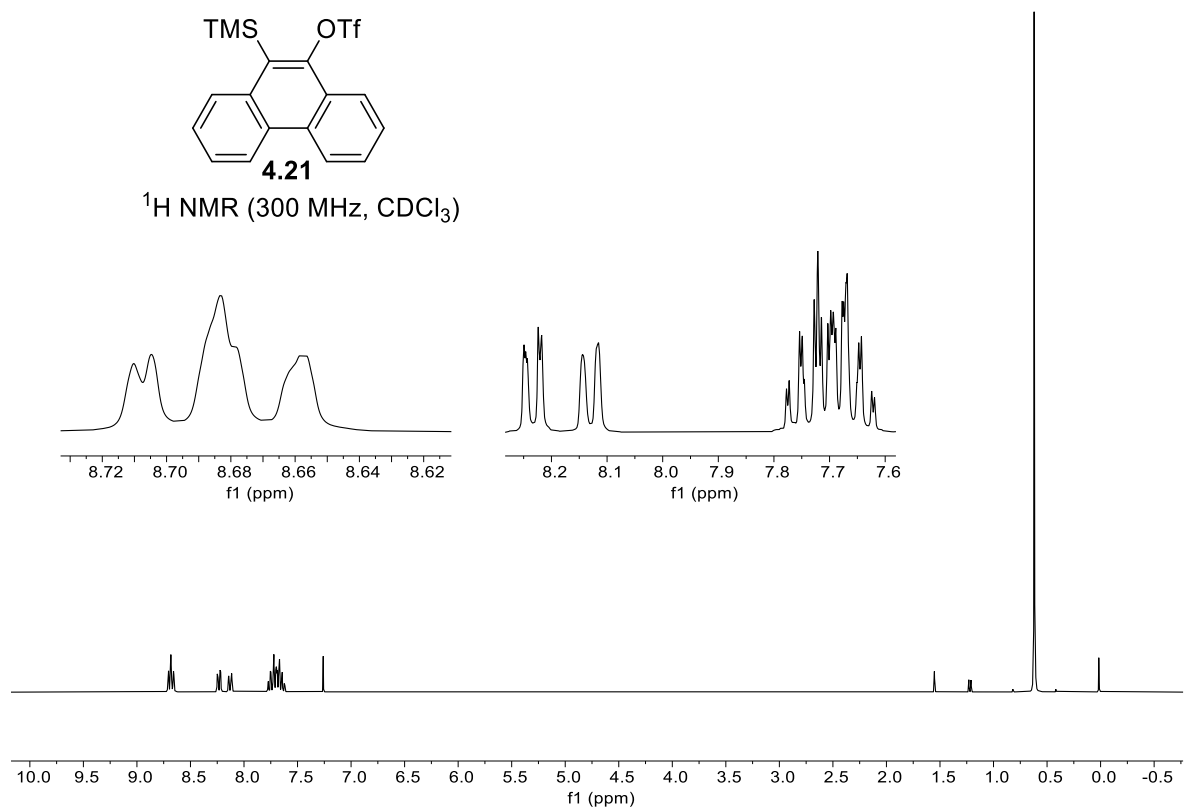
4.20

$^{13}\text{C}$  NMR (75 MHz,  $\text{CDCl}_3$ )

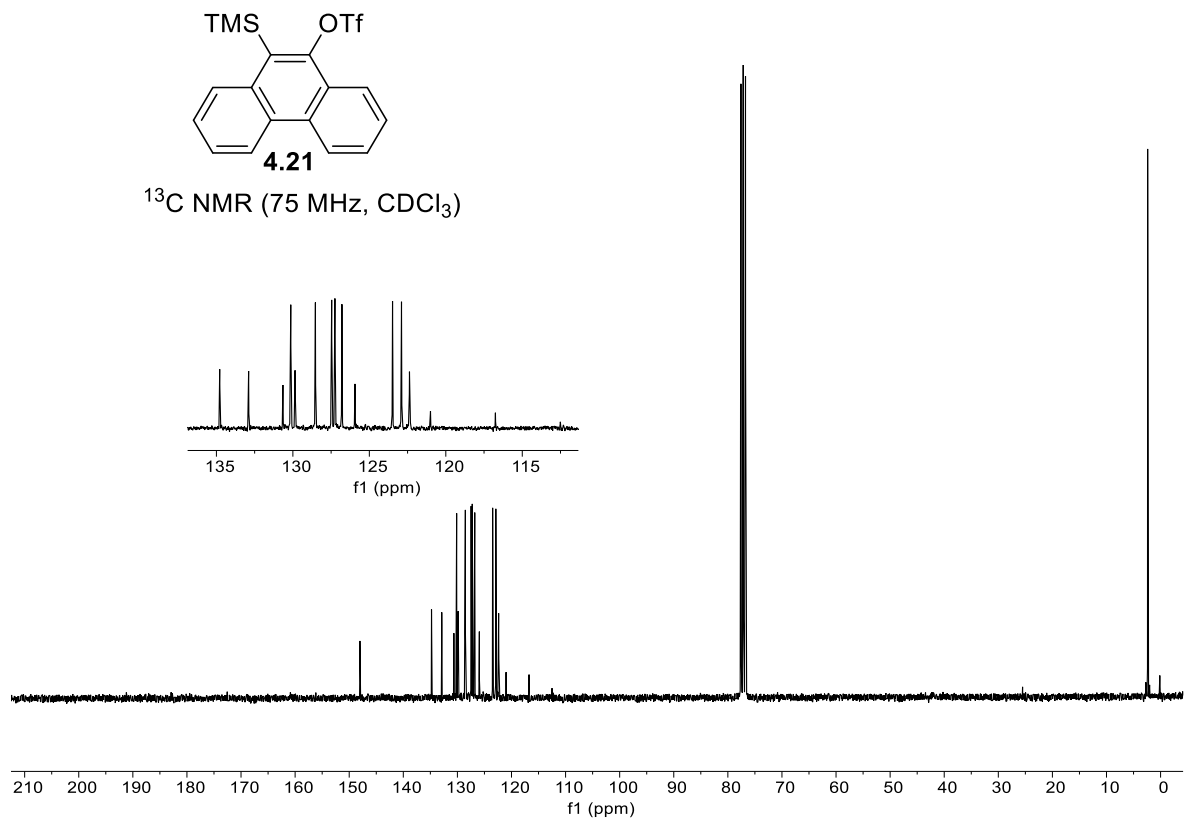


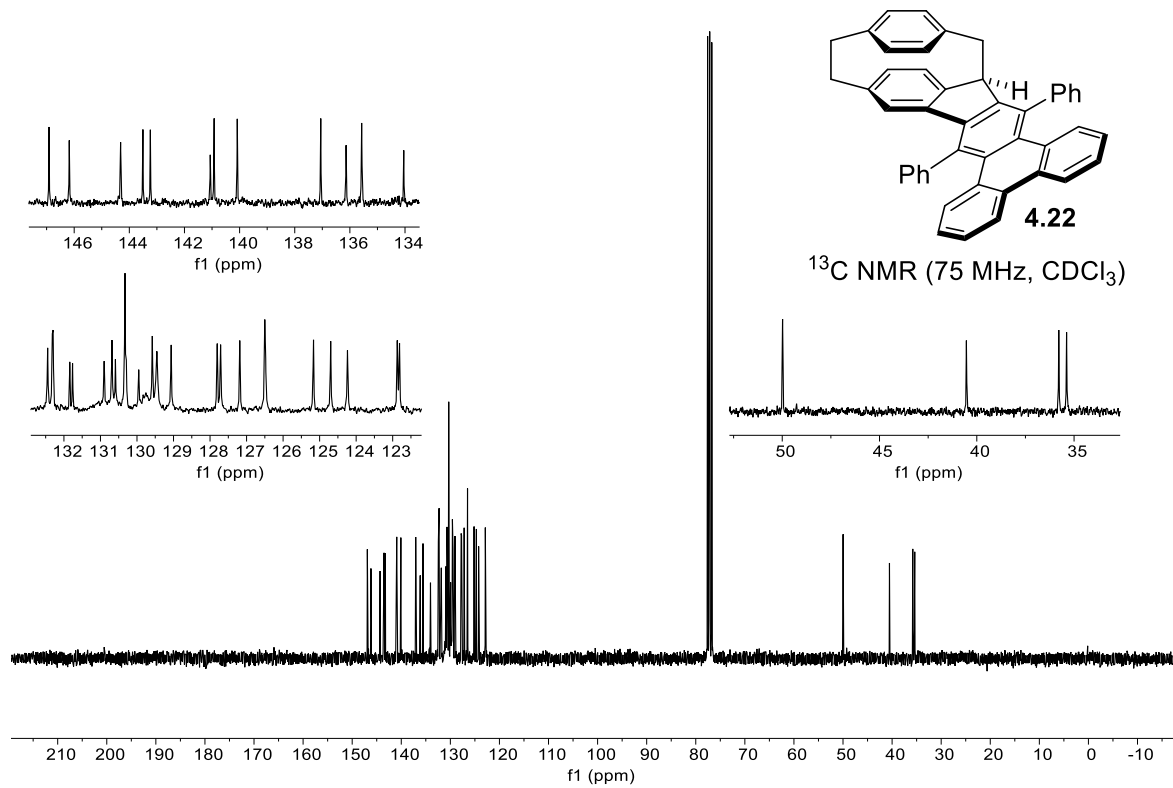
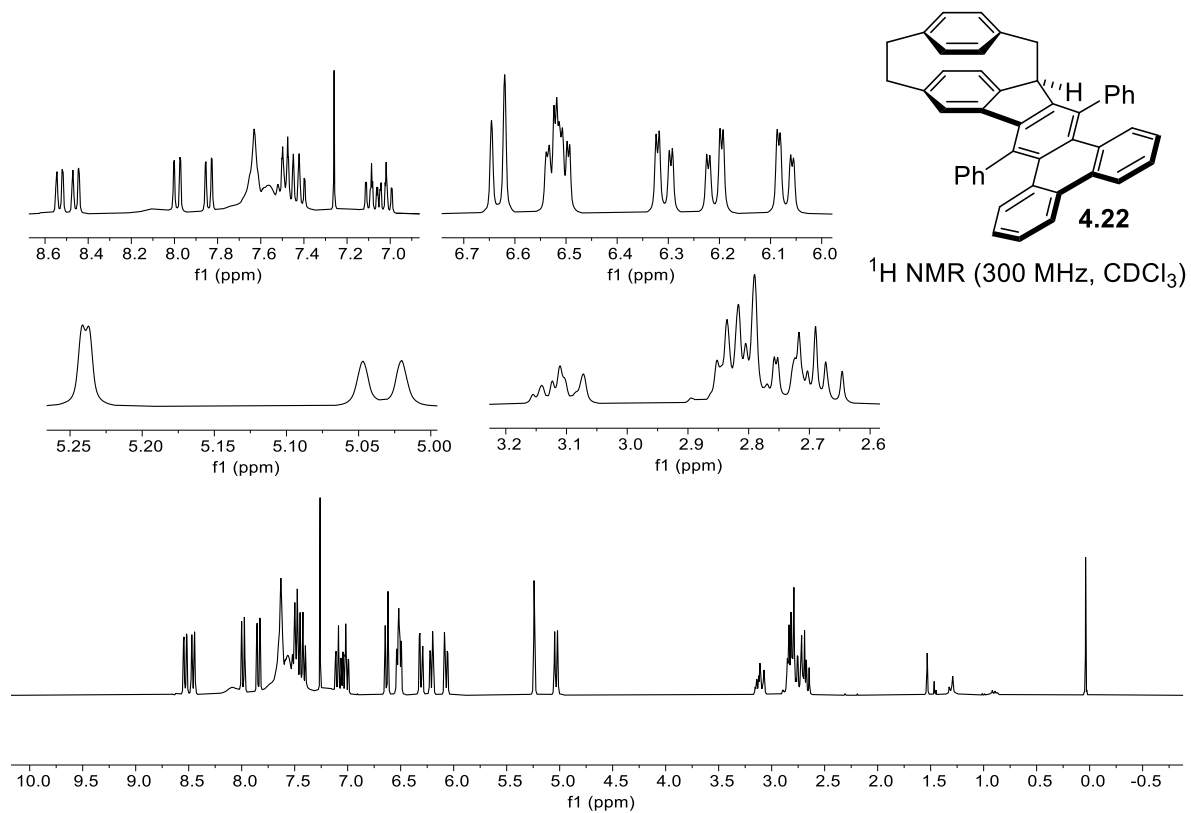


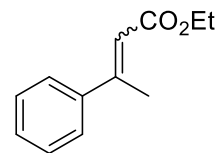
<sup>1</sup>H NMR (300 MHz, CDCl<sub>3</sub>)



<sup>13</sup>C NMR (75 MHz, CDCl<sub>3</sub>)

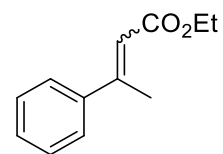
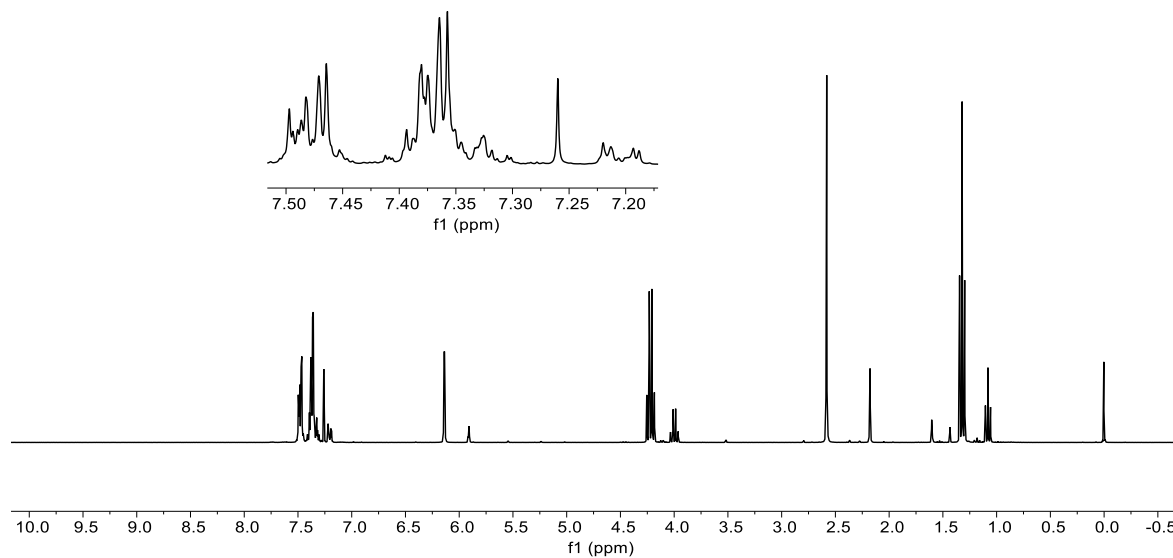






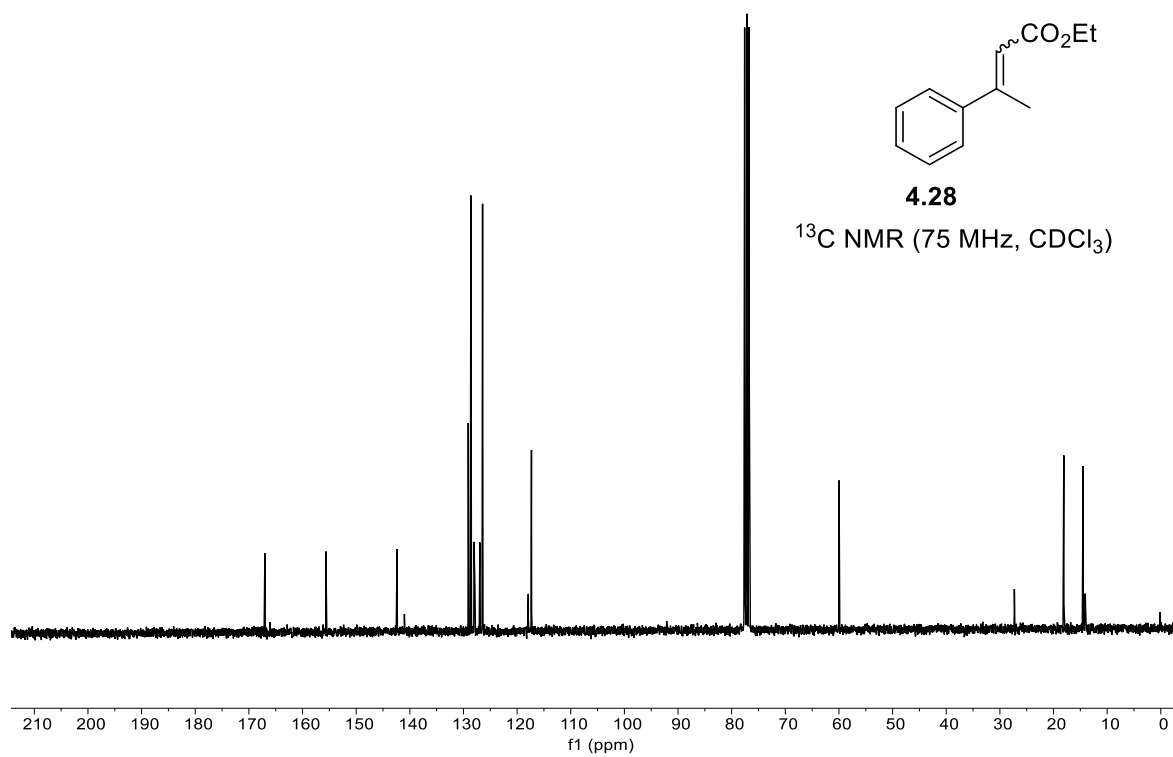
**4.28**

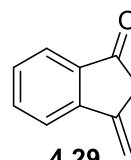
$^1\text{H}$  NMR (300 MHz,  $\text{CDCl}_3$ )



**4.28**

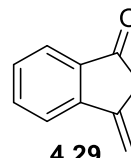
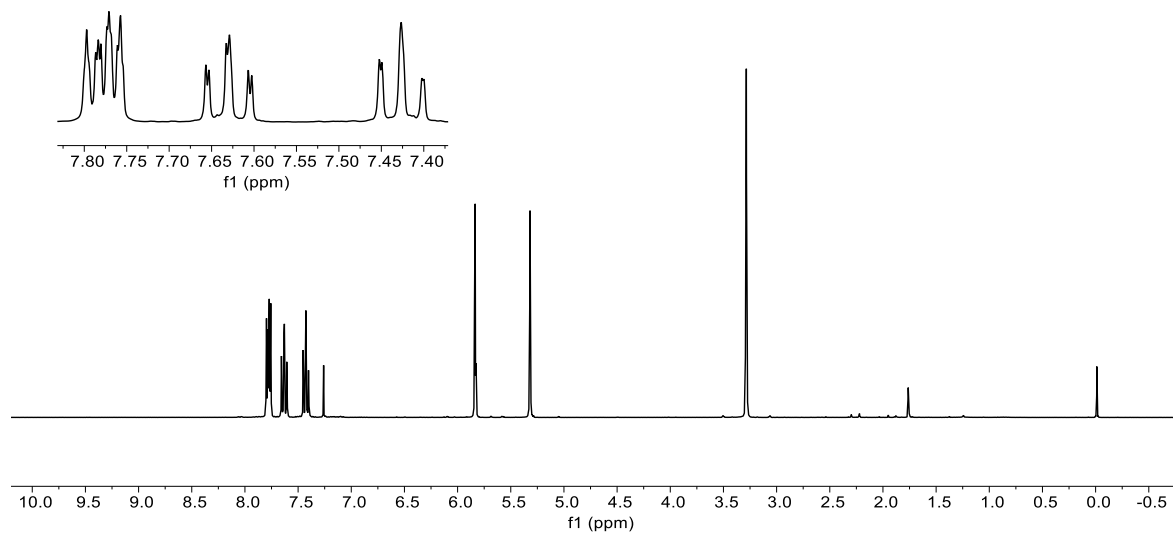
$^{13}\text{C}$  NMR (75 MHz,  $\text{CDCl}_3$ )





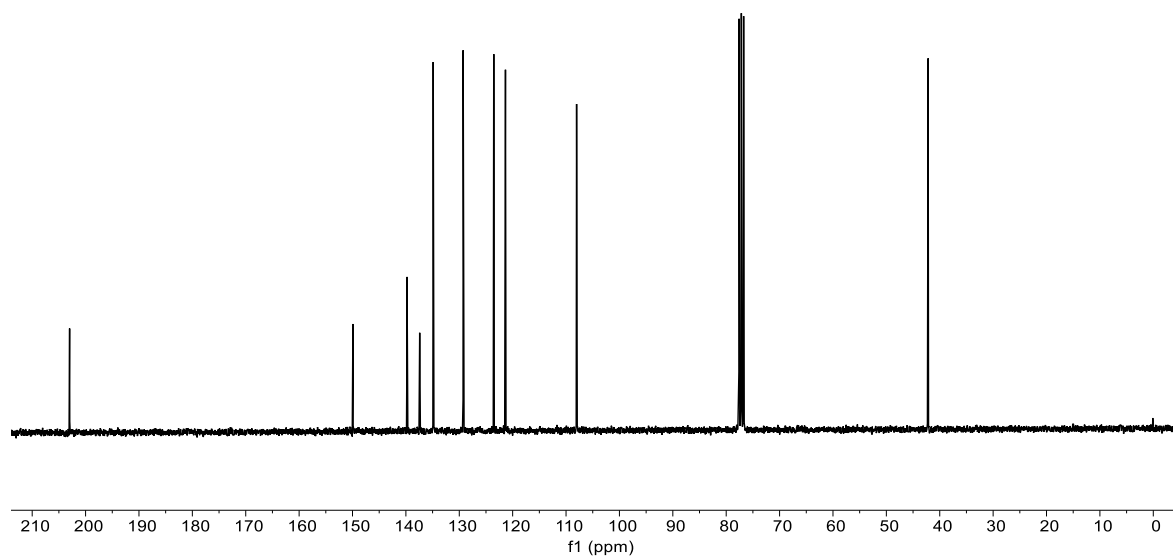
4.29

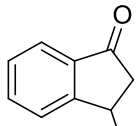
<sup>1</sup>H NMR (300 MHz, CDCl<sub>3</sub>)



4.29

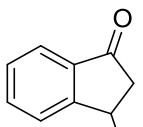
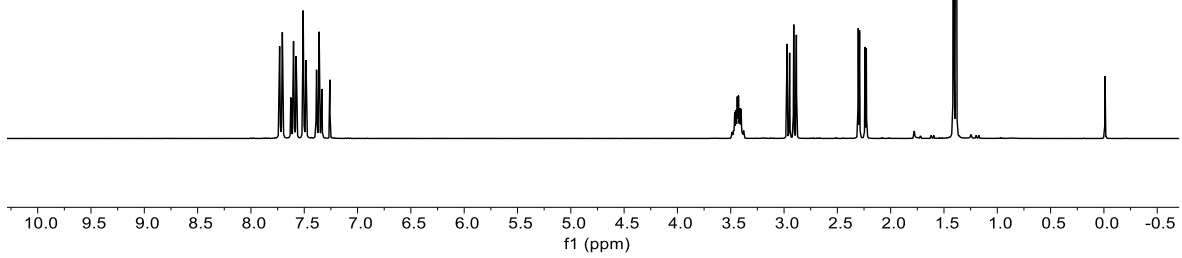
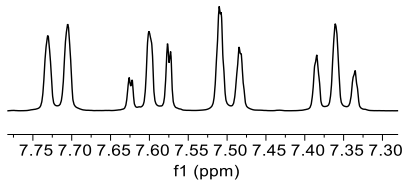
<sup>13</sup>C NMR (75 MHz, CDCl<sub>3</sub>)





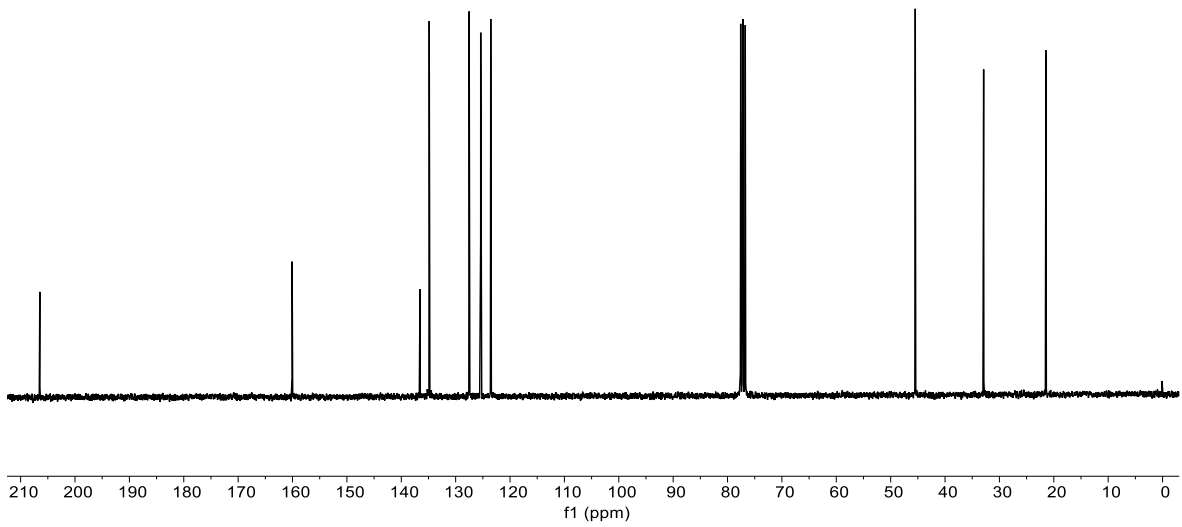
**4.30** Me

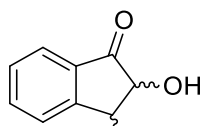
<sup>1</sup>H NMR (300 MHz, CDCl<sub>3</sub>)



**4.30** Me

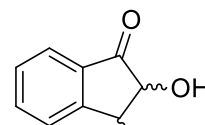
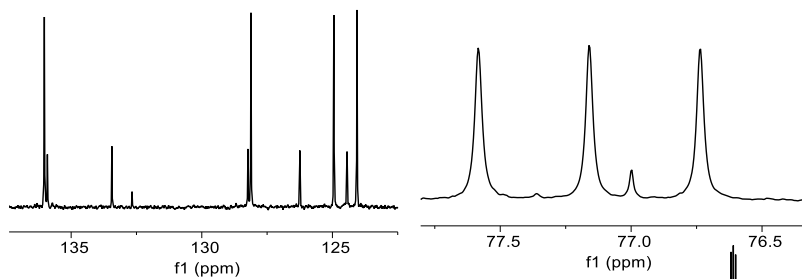
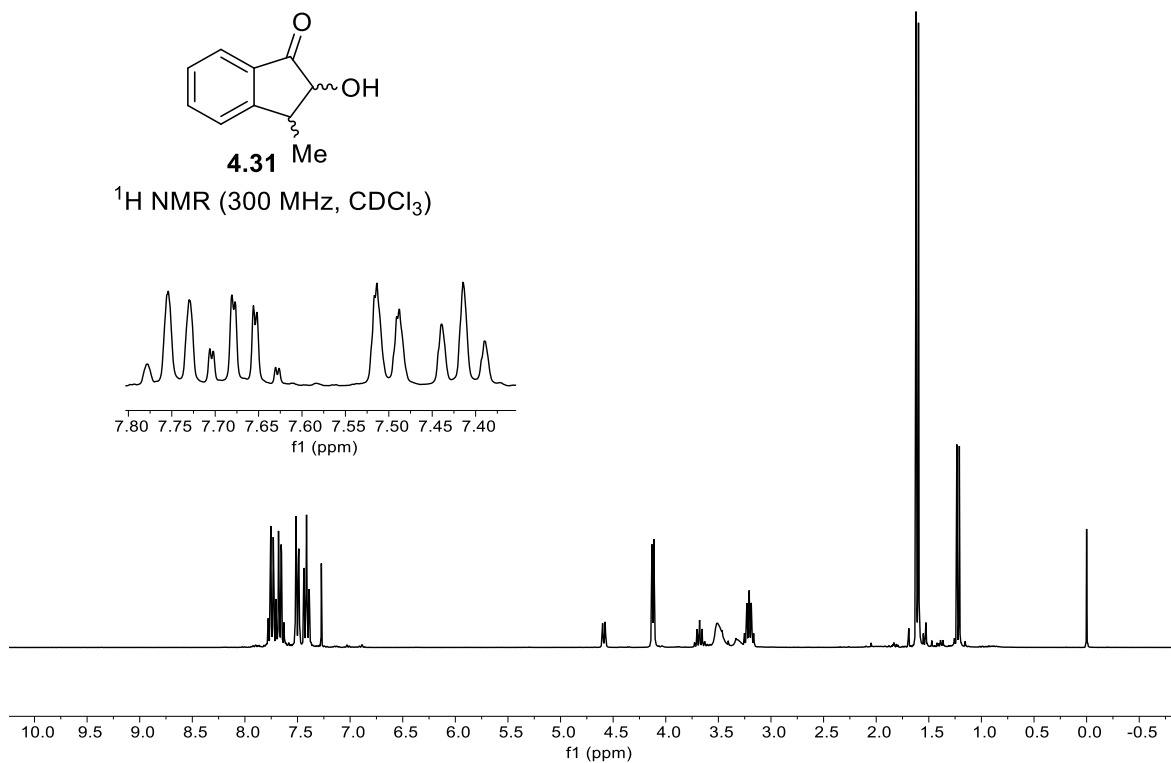
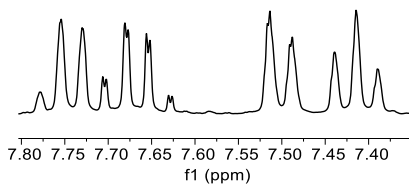
<sup>13</sup>C NMR (75 MHz, CDCl<sub>3</sub>)





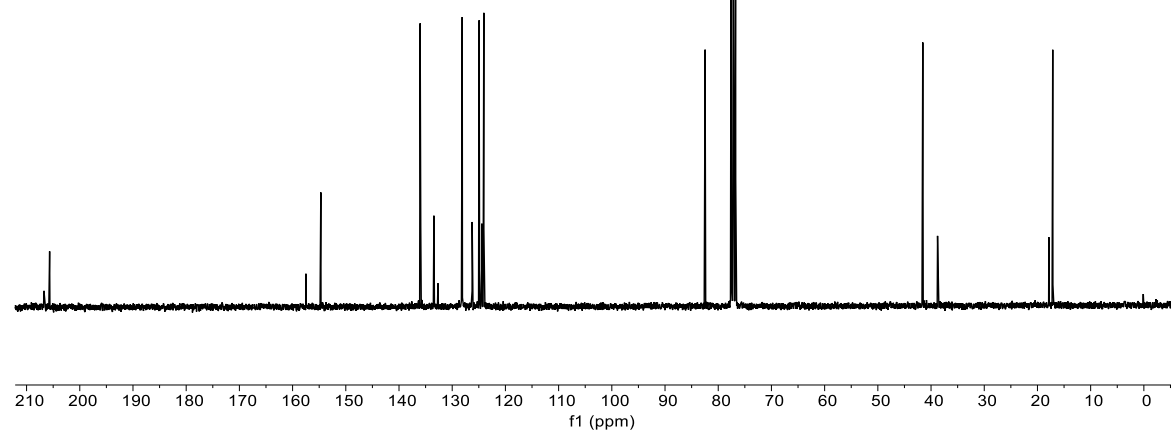
**4.31** Me

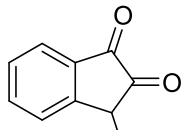
$^1\text{H}$  NMR (300 MHz,  $\text{CDCl}_3$ )



**4.31** Me

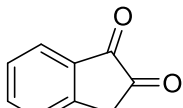
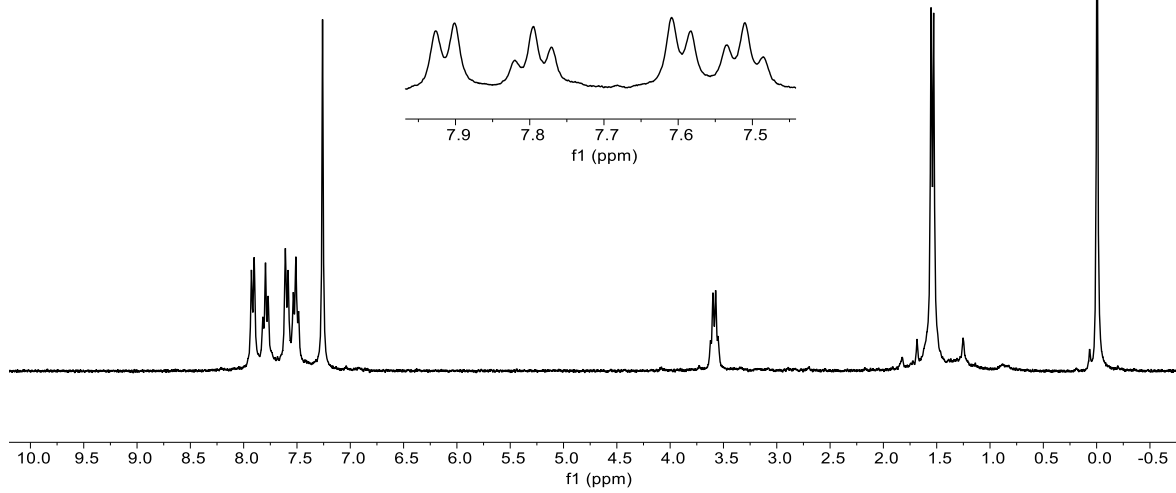
$^{13}\text{C}$  NMR (75 MHz,  $\text{CDCl}_3$ )





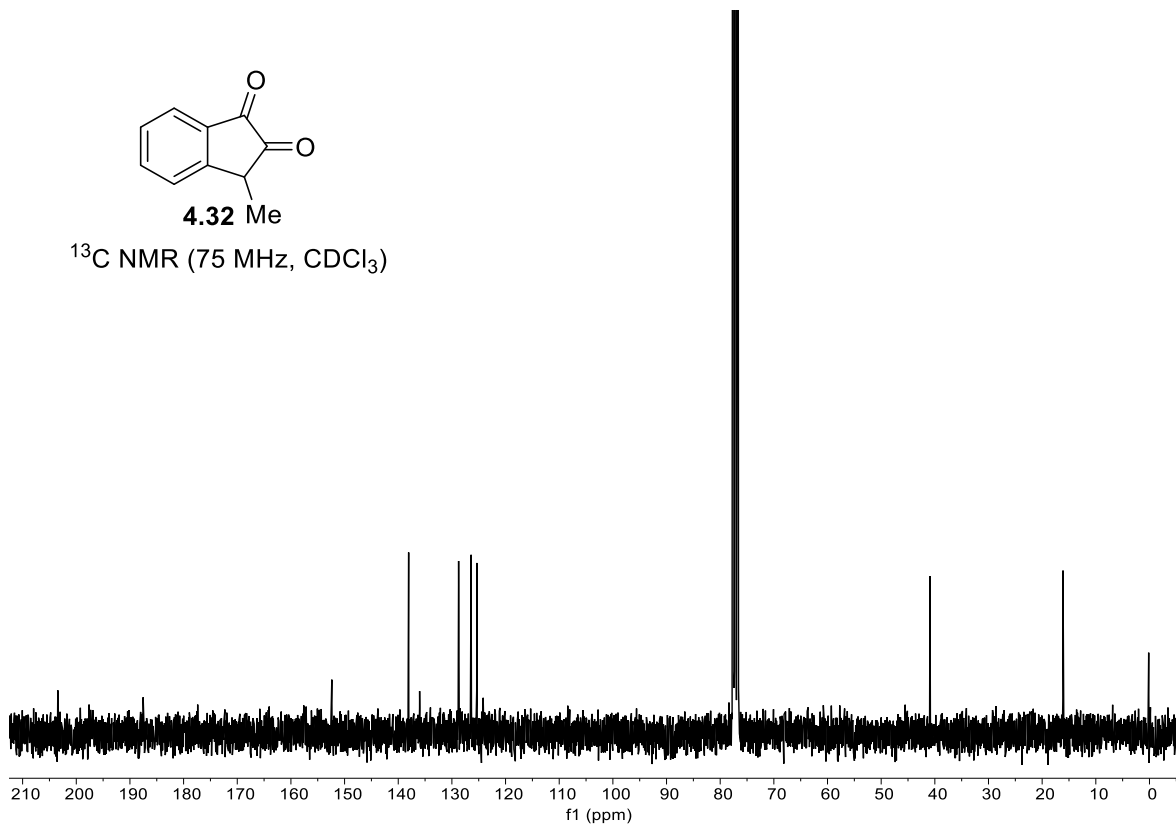
**4.32 Me**

$^1\text{H}$  NMR (300 MHz,  $\text{CDCl}_3$ )

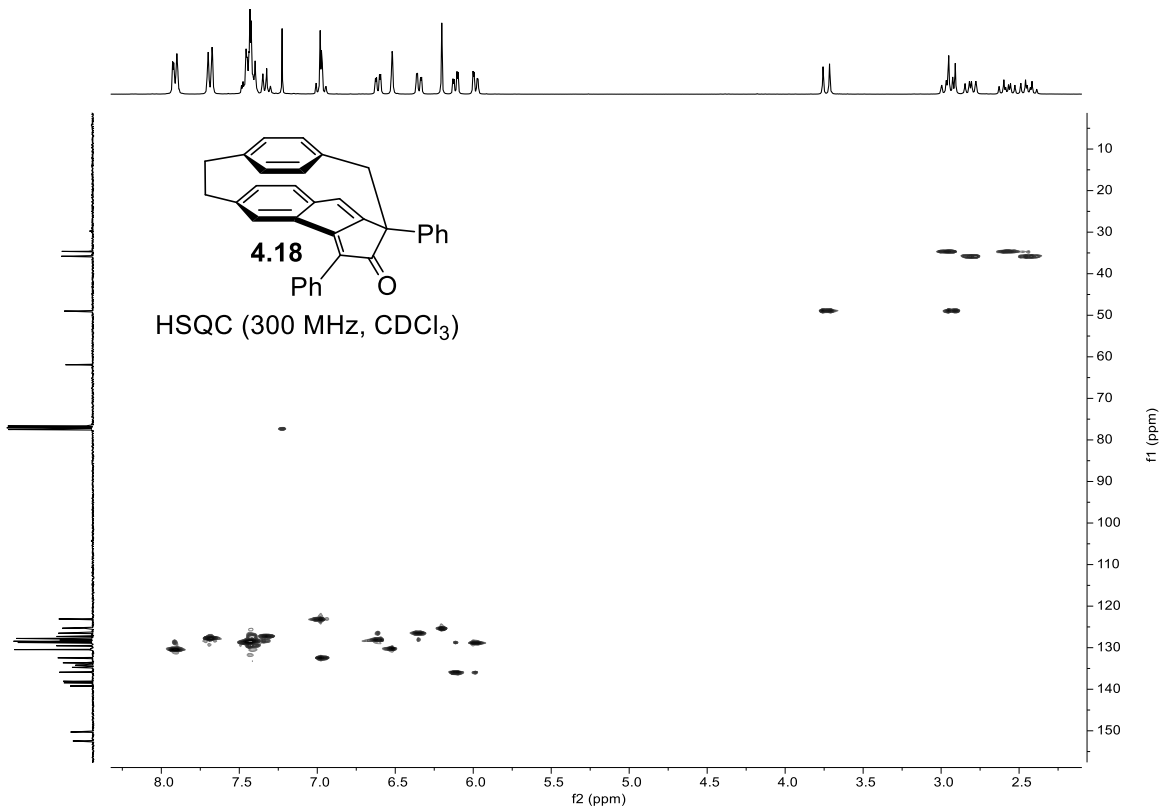
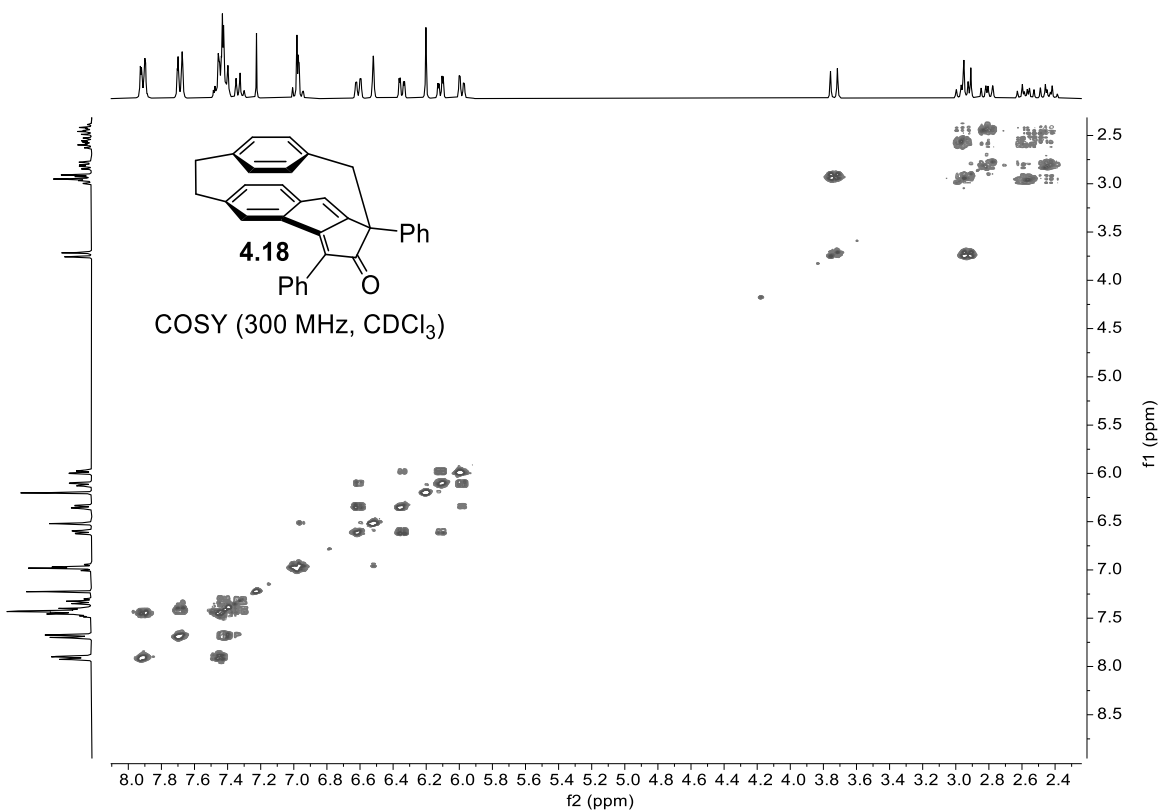


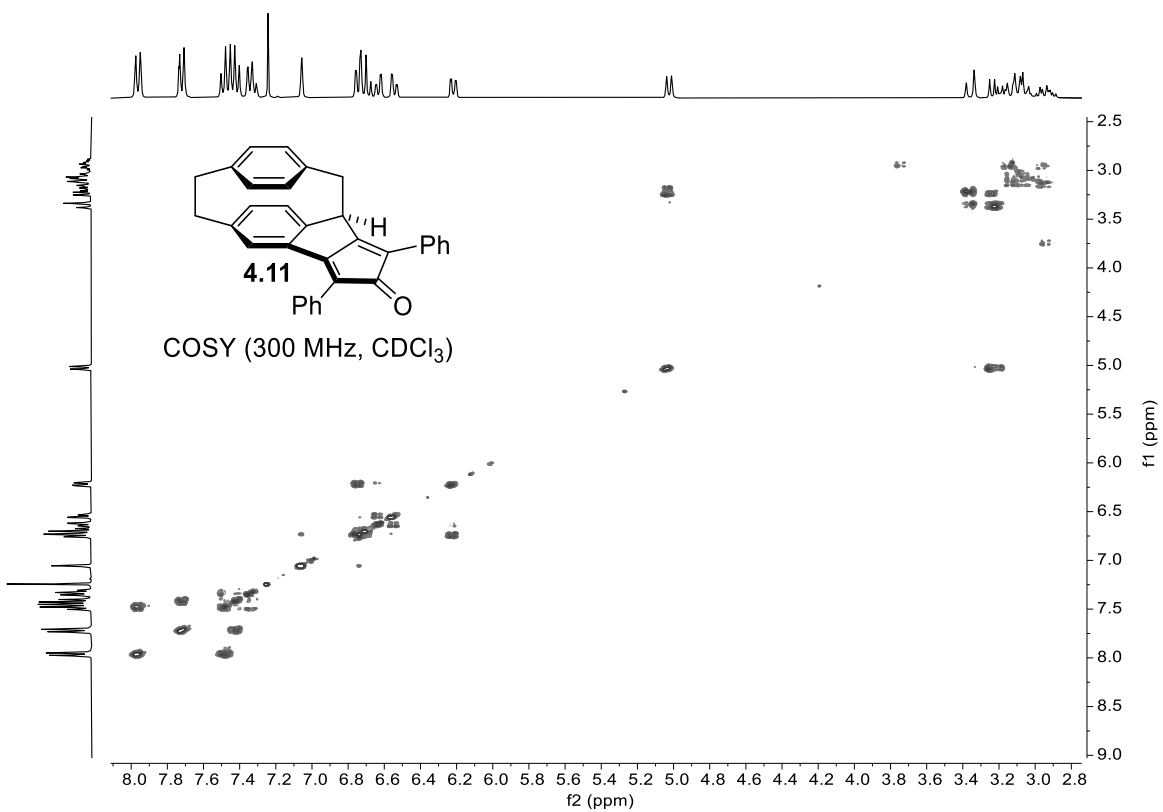
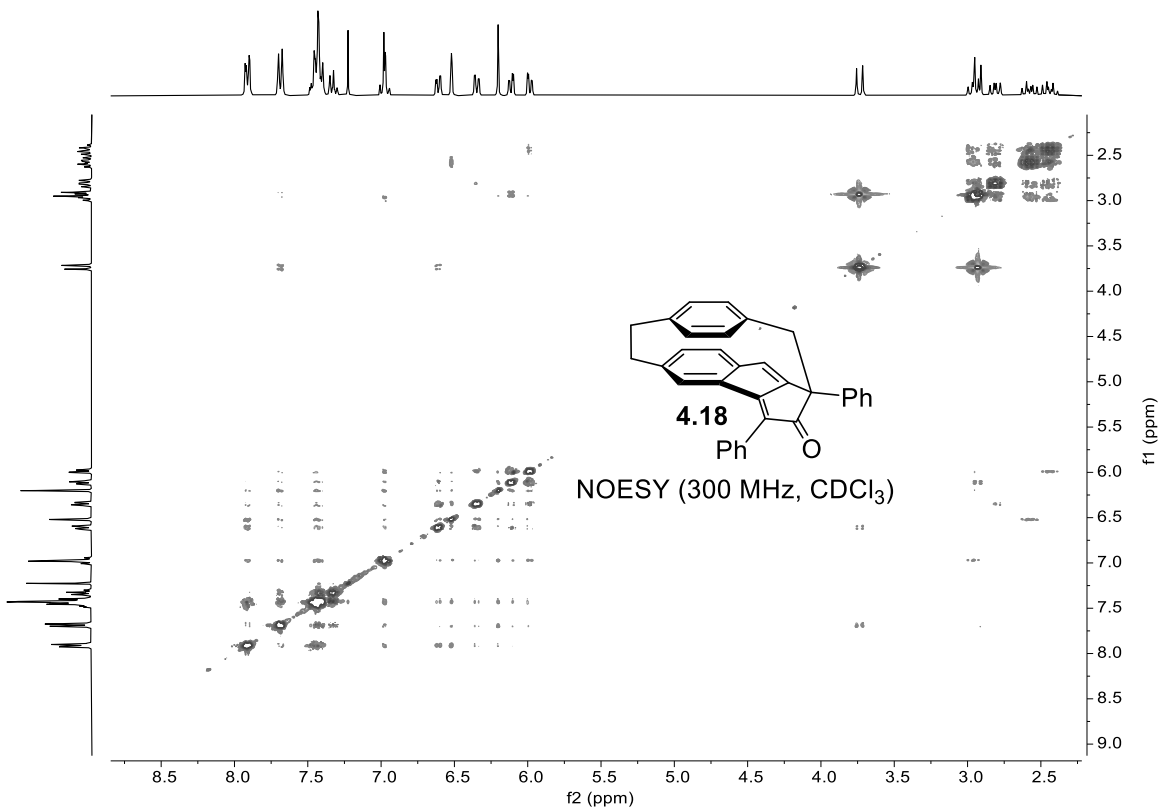
**4.32 Me**

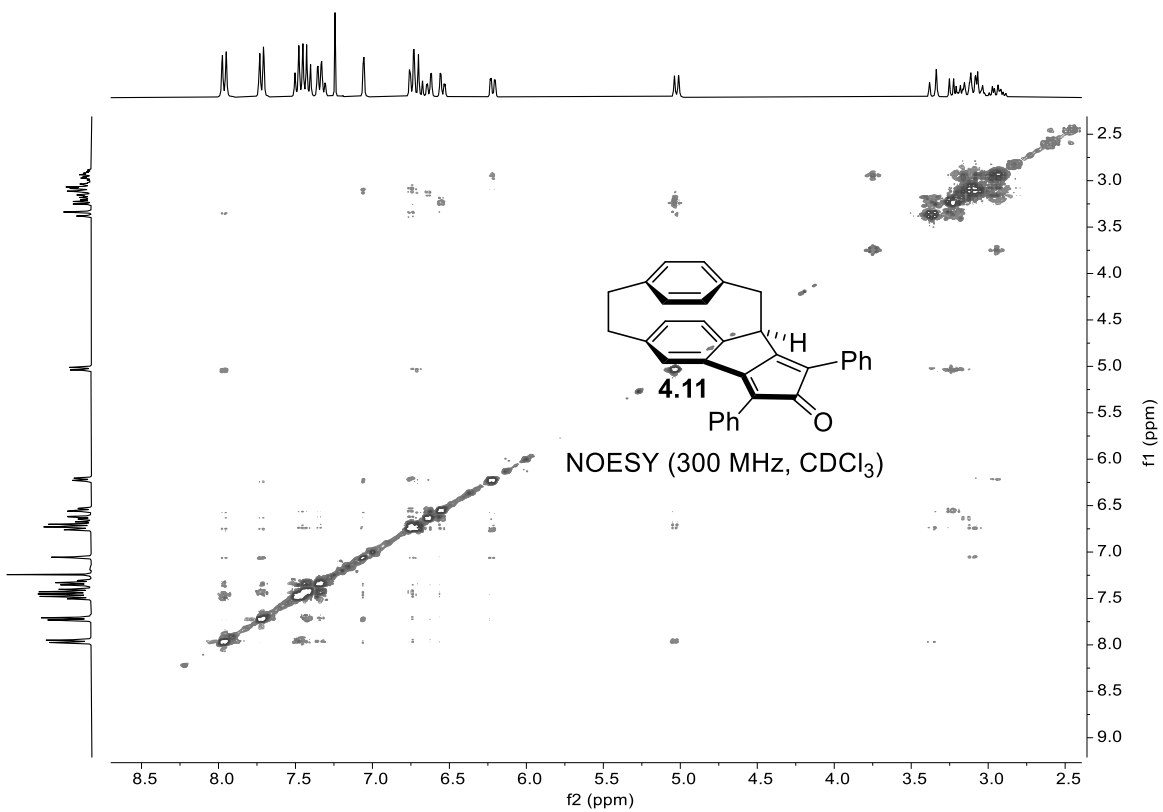
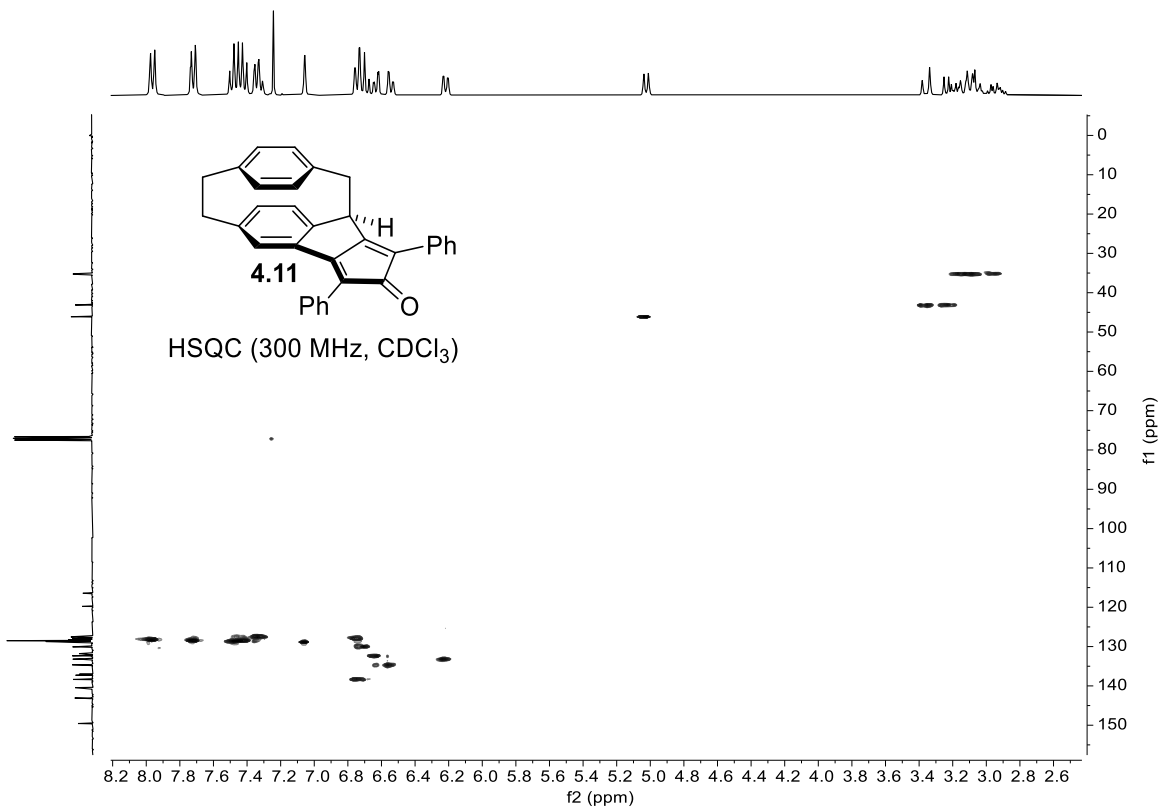
$^{13}\text{C}$  NMR (75 MHz,  $\text{CDCl}_3$ )

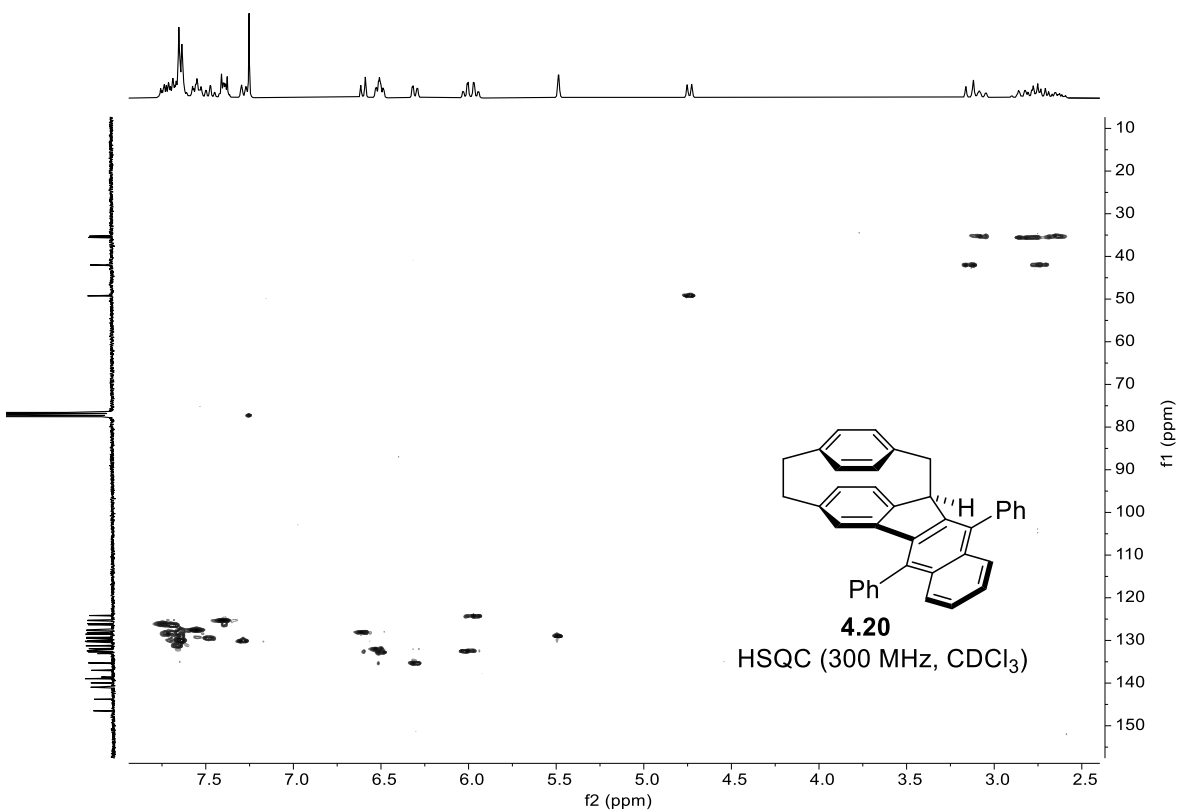
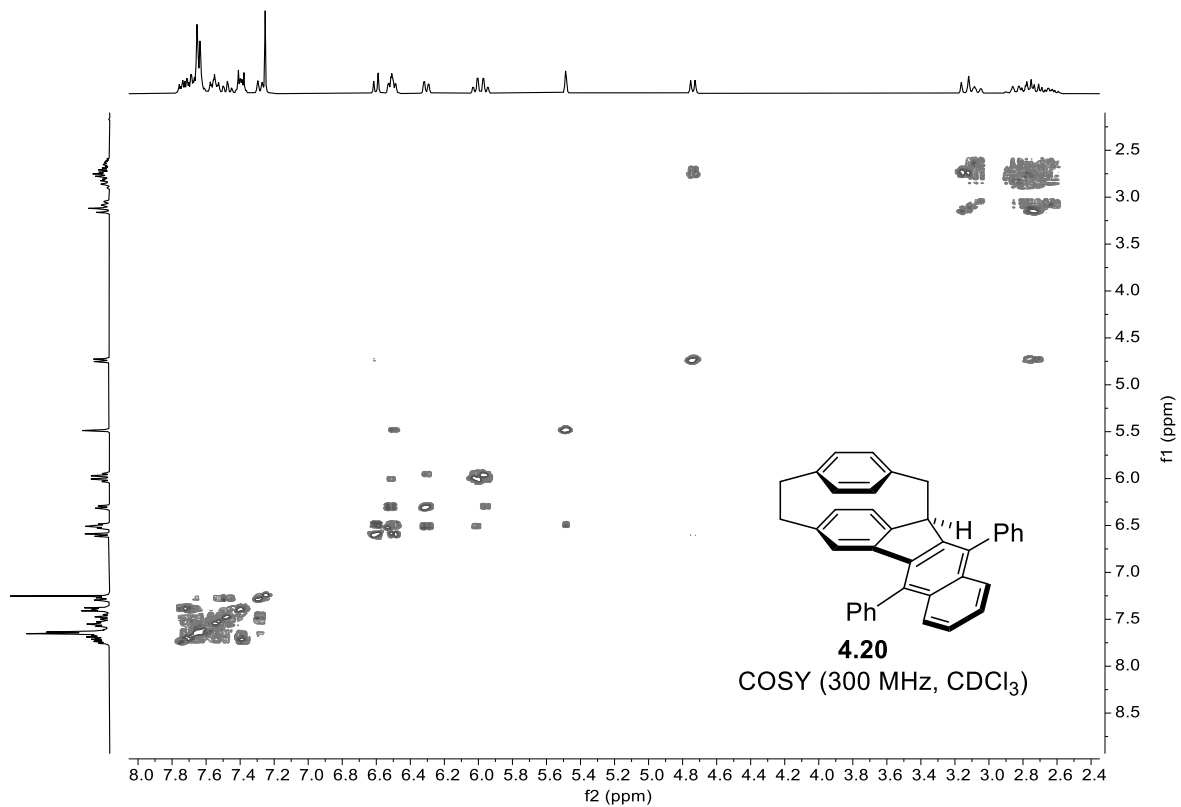


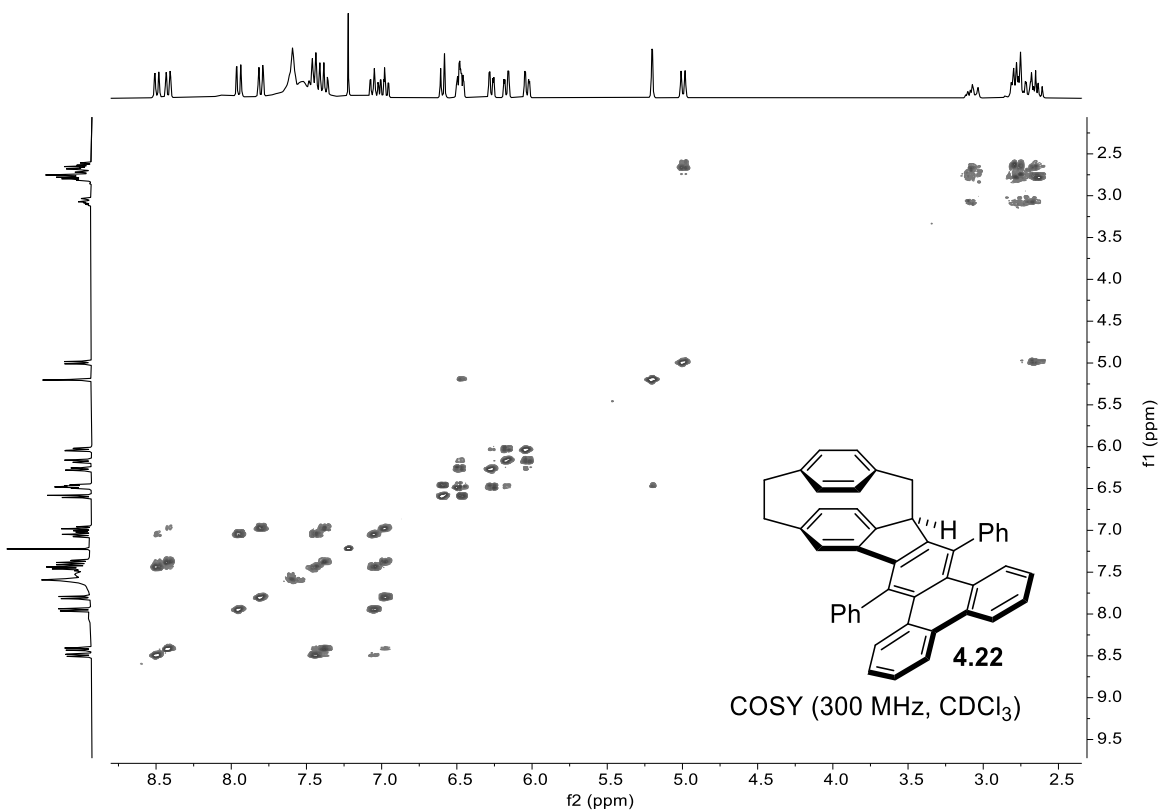
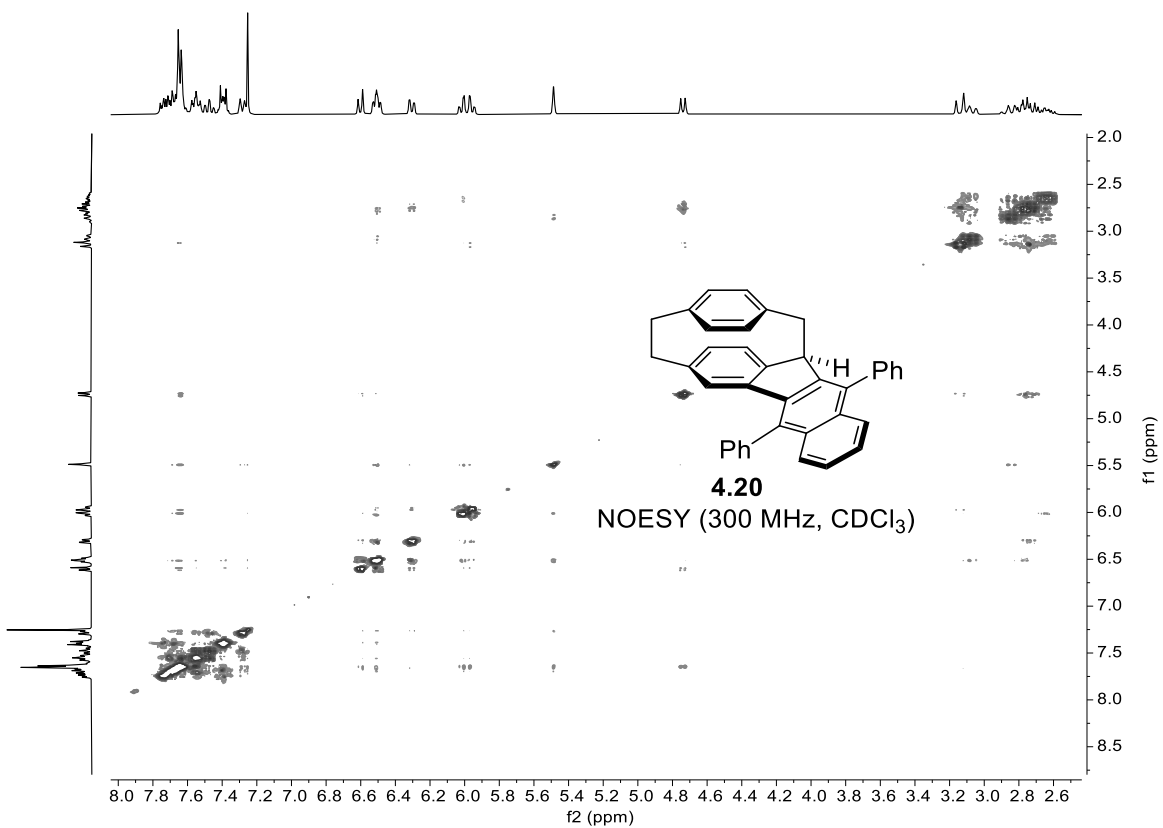
## 2. Two-Dimensional NMR Spectra

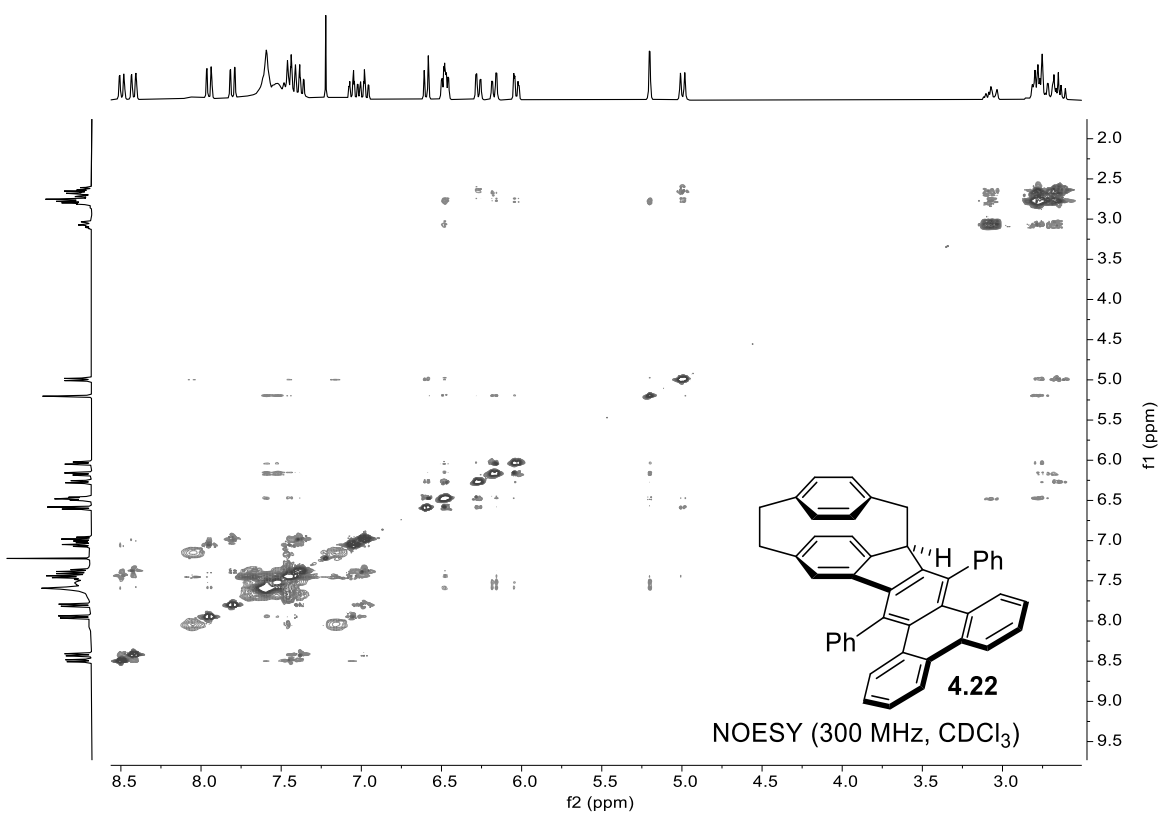
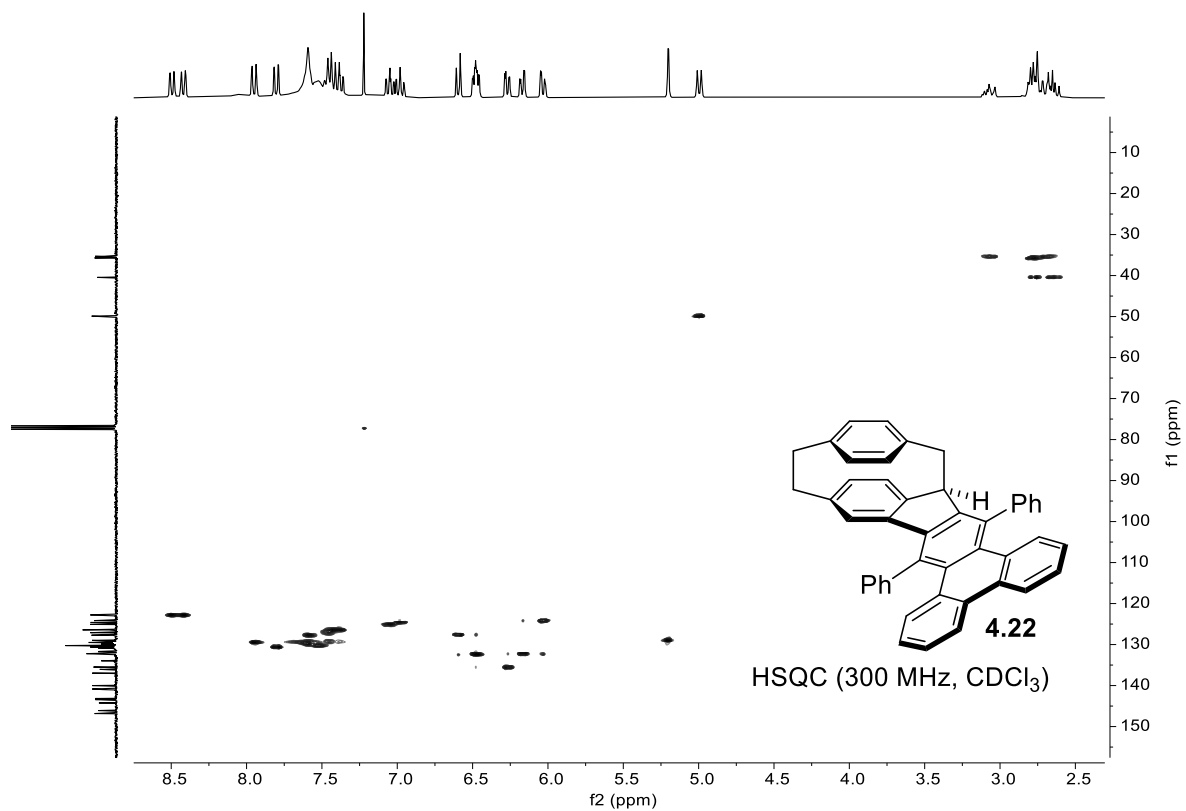












### 3. UV/vis Absorption and Fluorescence Analyses

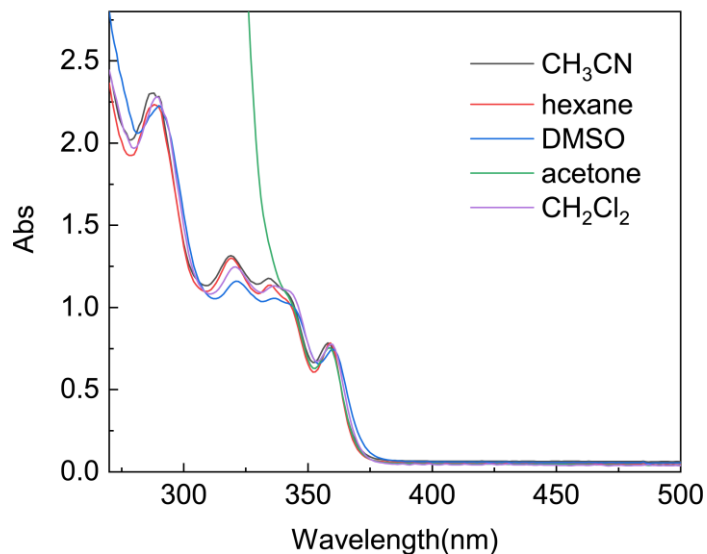


**Figure A3-1:** UV/vis absorption spectra of compound **4.20** ( $3.43 \times 10^{-5}$  M) measured in different solvents.

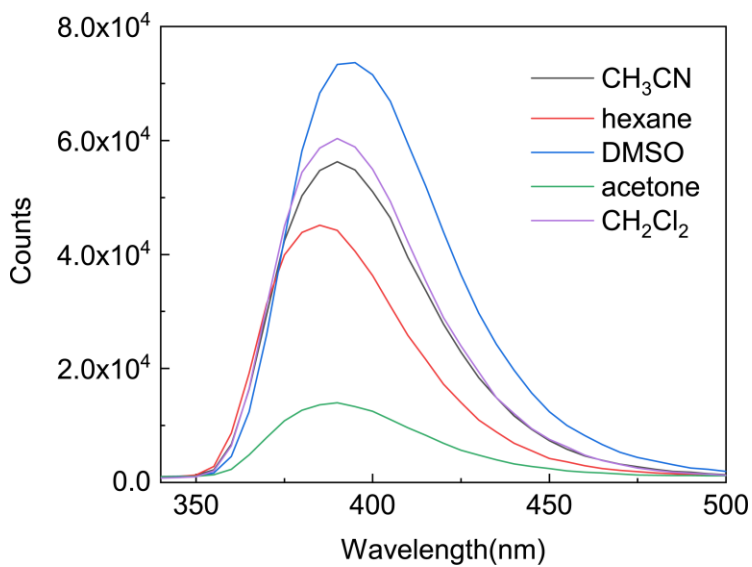


**Figure A3-2:** Fluorescence spectra of compound **4.20** ( $3.43 \times 10^{-5}$  M,  $\lambda_{exc} = 320$  nm) measured in different solvents.

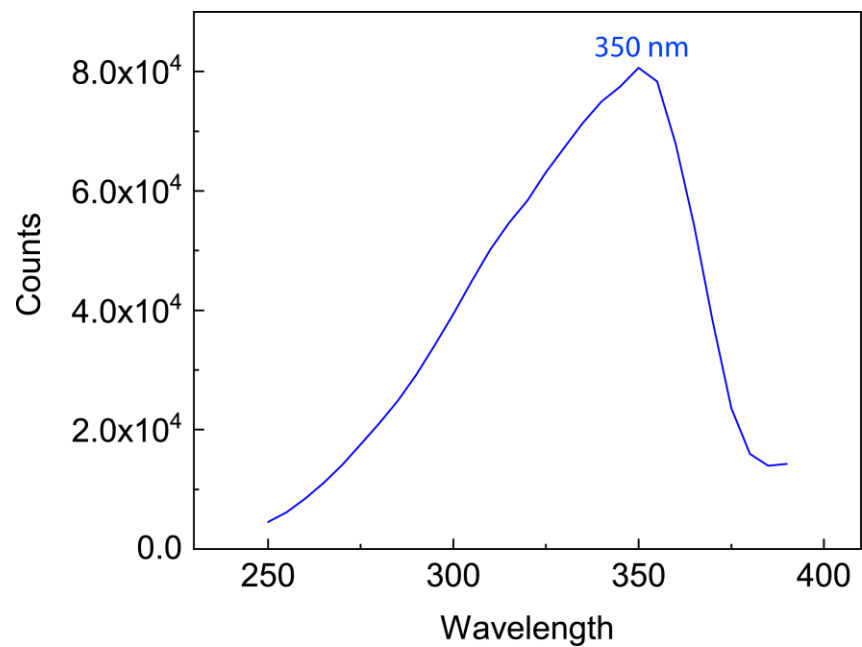


**Figure A3-3:** Excitation spectrum of compound **4.20** ( $3.43 \times 10^{-5}$  M) in  $\text{CH}_2\text{Cl}_2$  monitoring the emission wavelength of 389 nm.

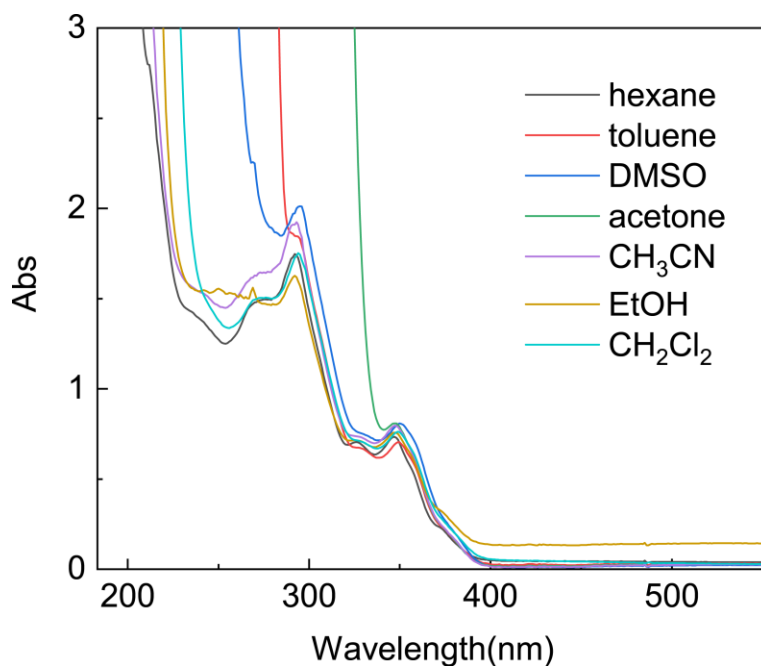


**Figure A3-4:** UV/vis absorption spectra of compound **4.22** ( $3.43 \times 10^{-5}$  M) measured in different solvents.

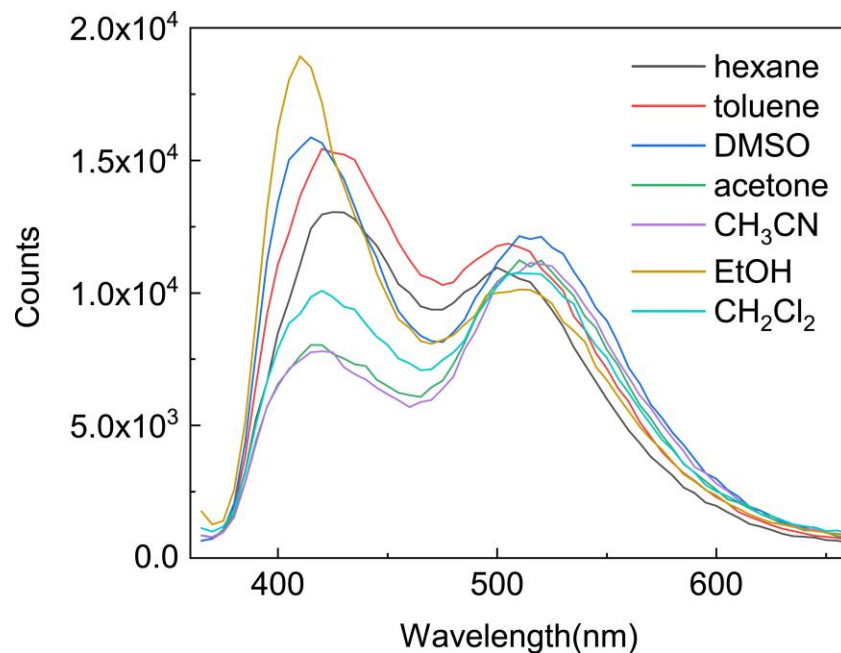


**Figure A3-5:** Fluorescence spectra of compound **4.22** ( $2.13 \times 10^{-5}$  M,  $\lambda_{\text{exc}} = 350$  nm) measured in different solvents.

**Table A3-1:** Summary of emission wavelengths and relative intensities of **4.22** ( $2.13 \times 10^{-5}$  M) in various solvents.

| Solvent                         | $\epsilon_r$ | $\lambda_{\text{em}}^1$ (nm) | $\lambda_{\text{em}}^2$ (nm) | $I(\lambda_{\text{em}}^1)/I(\lambda_{\text{em}}^2)$ |
|---------------------------------|--------------|------------------------------|------------------------------|---|
| hexane                          | 1.88         | 425                          | 502                          | 1.290   |
| toluene                         | 2.38         | 425                          | 505                          | 1.299   |
| CH <sub>2</sub> Cl <sub>2</sub> | 8.93         | 420                          | 510                          | 0.937   |
| CH <sub>3</sub> CN              | 35.94        | 417                          | 517                          | 0.699   |
| acetone                         | 20.56        | 417                          | 513                          | 0.722   |
| DMSO                            | 46.45        | 415                          | 515                          | 1.300   |
| EtOH                            | 24.55        | 410                          | 508                          | 1.862   |

$\epsilon_r$ : Relative permittivity (dielectric constant);  $\lambda_{\text{em}}^1$  and  $\lambda_{\text{em}}^2$ : maximum emission wavelengths;  $I(\lambda_{\text{em}}^1)/I(\lambda_{\text{em}}^2)$ : ratio of emission intensities at  $\lambda_{\text{em}}^1$  and  $\lambda_{\text{em}}^2$ .

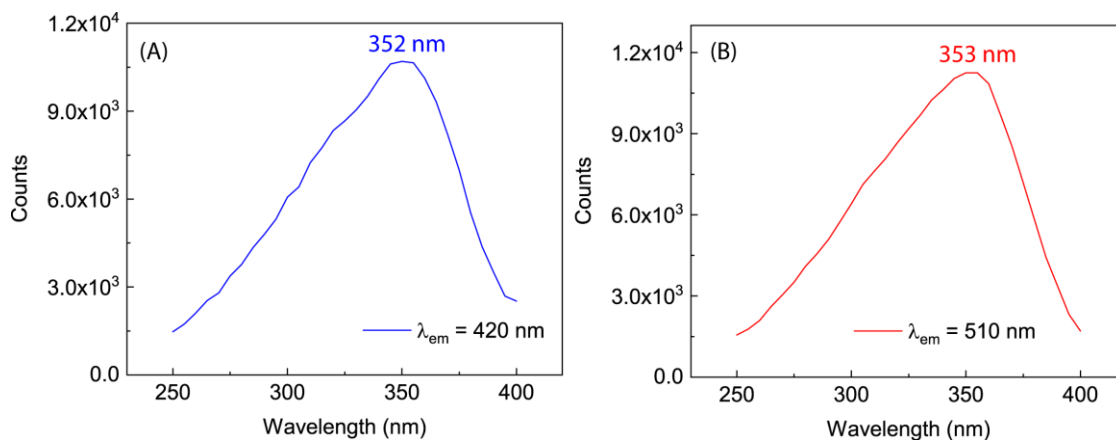


**Figure A3-6:** Excitation spectra of compound **4.22** ( $2.13 \times 10^{-5}$  M,  $\lambda_{\text{exc}} = 350$  nm) in  $\text{CH}_2\text{Cl}_2$  monitoring the emission wavelengths of (A) 420 nm and (B) 510 nm.

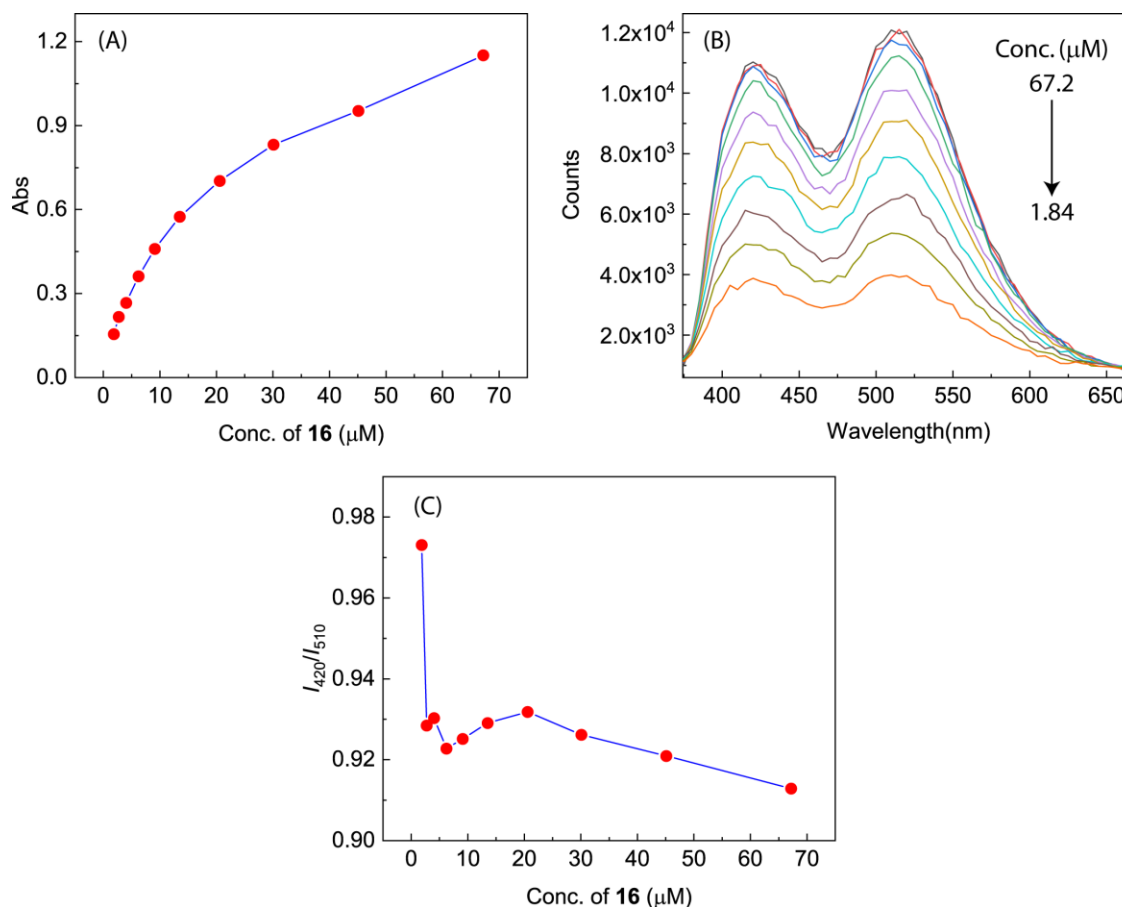


**Figure A3-7:** (A) Plot of UV/vis absorbance of **4.22** at 348 nm in  $\text{CH}_2\text{Cl}_2$  in correlation with its concentration. (B) Fluorescence spectra of **4.22** measured in  $\text{CH}_2\text{Cl}_2$  ( $\lambda_{\text{exc}} = 350$  nm) at different concentrations. The arrow indicates the decreasing trend of concentrations. (C) The ratio of the intensities of emission peaks at 420 nm and 510 nm as a function of the concentration of **4.22**.

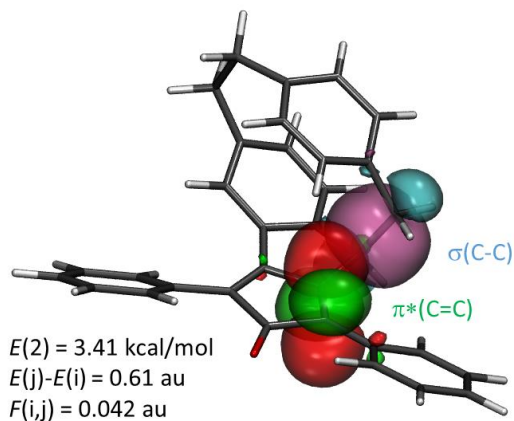
## 4. DFT Computational Studies

### 4.1 Computational Methods

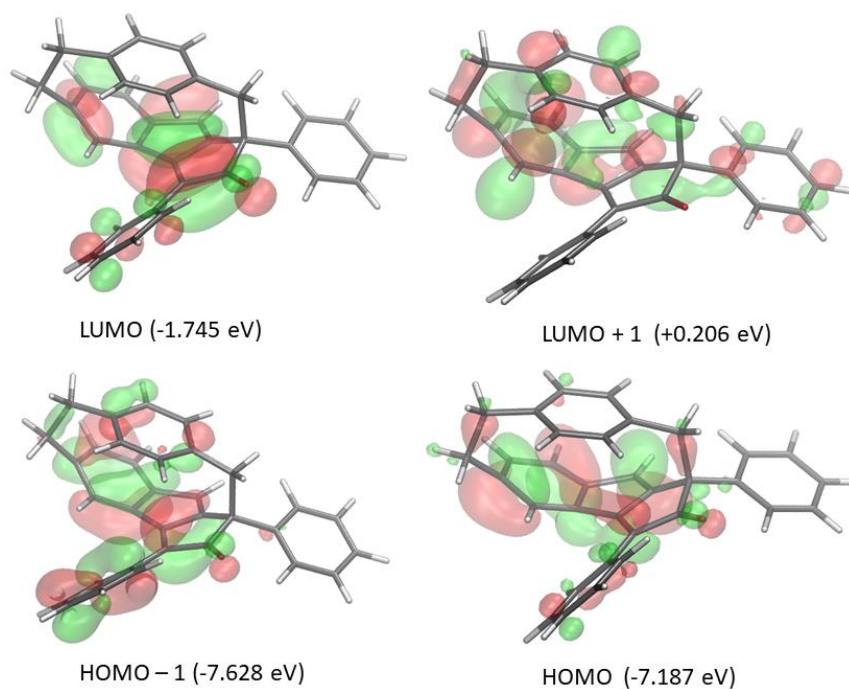
Ground-state molecular geometries were optimized at B3LYP/6-31G(d) level of theory with Grimme's D3 dispersion method included. The optimized geometries were subjected to frequency calculations at the same level of theory to confirm they are energy minima (i.e., zero imaginary frequencies). Transition states were also optimized at the B3LYP-D3/6-31G(d) level and confirmed as saddle points by the presence of only one imaginary frequency in each of their calculated vibrational spectra. All the DTF optimization calculations were performed in the gas phase using the *Gaussian 16* (revision B.01) software package, except that the search and optimization of transition state **TS-2** were performed with *Spartan '18* at the B3LYP-D3/6-31G(d) level. Energies of gas-phase optimized geometries in solvent (ethanol) were calculated at the B3LYP-D3/6-31G(d) level using the polarizable continuum model (PCM) implemented in *Gaussian 16*.

Natural bond orbital (NBO) analysis of **4.11** was conducted its B3LYP-D3/6-31G(d) optimized geometry. Calculations were done at the B3LYP/6-311+G(2d,p) level using the NBO method implemented in Gaussian 09W (revision D.01). Frontier molecular orbital (FMO) calculations were carried out at the B3LYP/6-311+G(2d,p) level using B3LYP-D3/6-31G(d) optimized geometries. Time-dependent density functional theory (TD-DFT) calculations were performed at the CAM-B3LYP/6-311+G(2d,p) level using B3LYP-D3/6-31G(d) optimized geometries. Visualization of molecular structures and orbital contour plots were done using *CYLVView* (version 1.0b) and *VMD* software package.

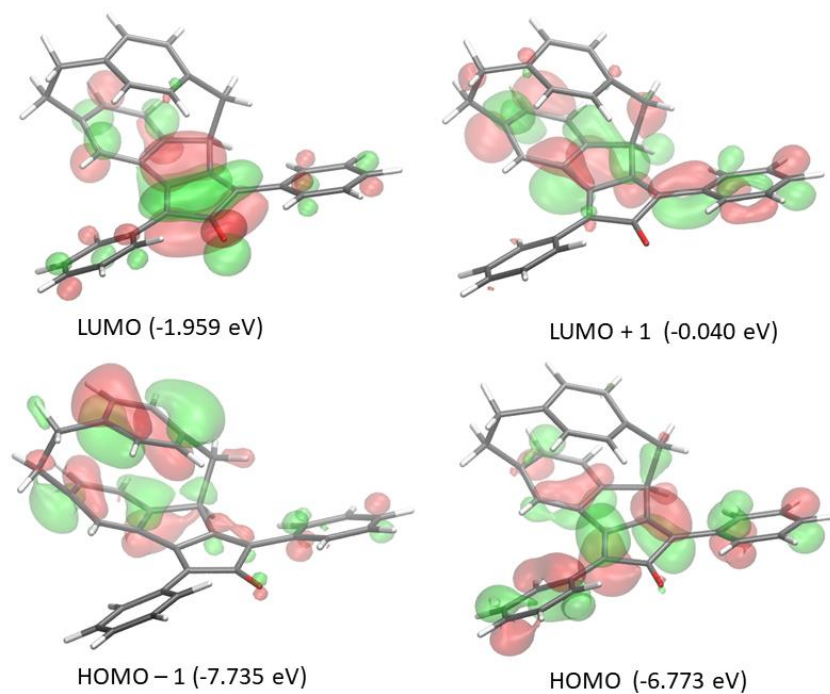
### 4.2 Computational Results



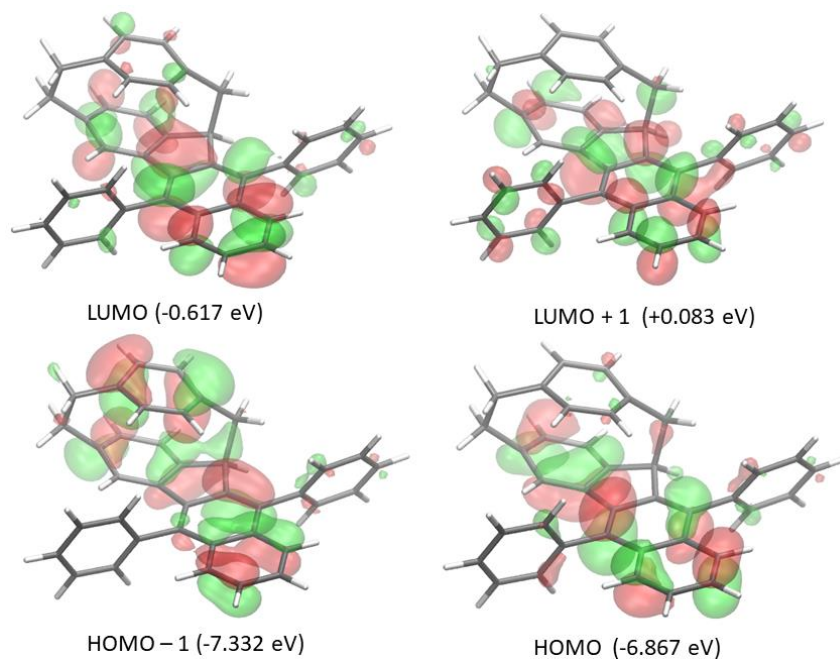
**Figure A3-8:** Contour plots of natural bond orbitals of **4.11** (isovalue = 0.03 au) showing the interactions of C-C bonding orbital ( $\sigma$ ) and neighboring C=C antibonding orbital ( $\pi^*$ ). Single-point calculations done at the B3LYP/6-311+G(2d,p) level using the B3LYP-D3/6-31G(d) optimized geometry.



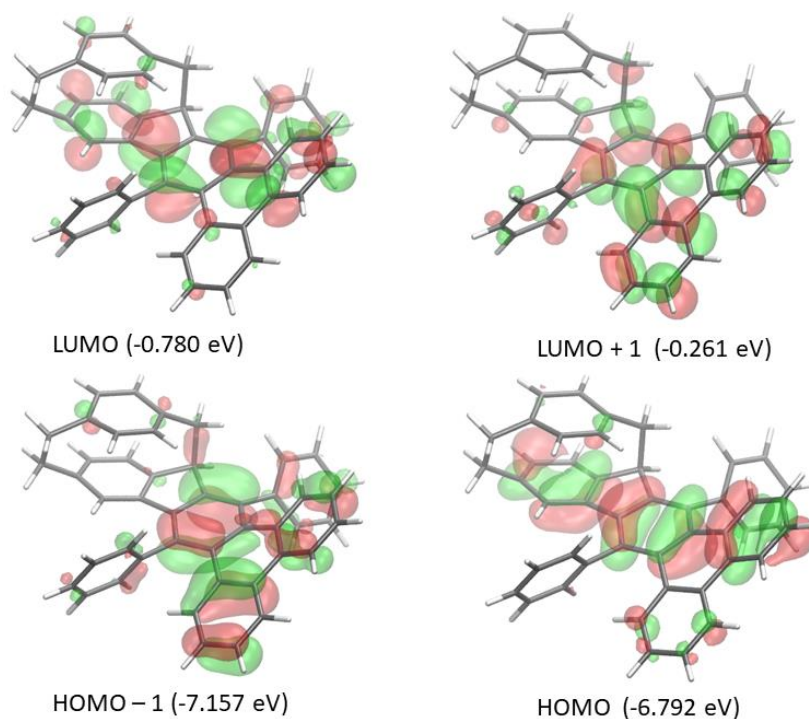
**Figure A3-9:** Contour plots (isovalue = 0.03 au) of frontier molecular orbitals and eigenvalues of **4.18**. Single-point calculations done at the B3LYP/6-311+G(2d,p) level using the B3LYP-D3/6-31G(d) optimized geometry.



**Figure A3-10:** Contour plots (isovalue = 0.03 au) of frontier molecular orbitals and eigenvalues of **4.11**. Single-point calculations done at the B3LYP/6-311+G(2d,p) level using the B3LYP-D3/6-31G(d) optimized geometry.



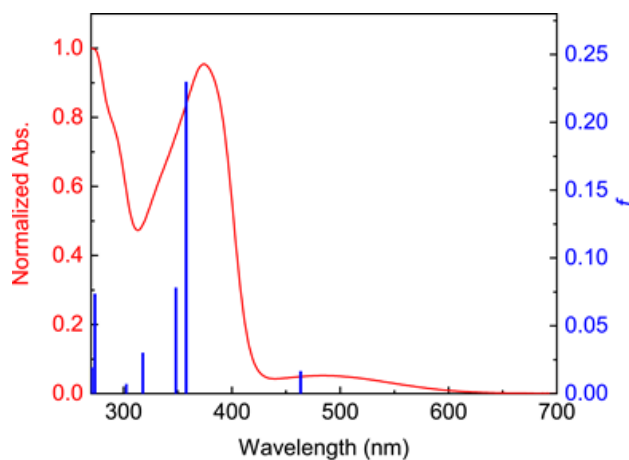
**Figure A3-11:** Contour plots (isovalue = 0.03 au) of frontier molecular orbitals and eigenvalues of **4.20**. Single-point calculations done at the B3LYP/6-311+G(2d,p) level using the B3LYP-D3/6-31G(d) optimized geometry.



**Figure A3-12:** Contour plots (isovalue = 0.03 au) of frontier molecular orbitals and eigenvalues of **4.22**. Single-point calculations done at the B3LYP/6-311+G(2d,p) level using the B3LYP-D3/6-31G(d) optimized geometry.

**Table A3-2:** TD-DFT calculated UV/vis absorption data for compound **4.18**.

| $\lambda$ (nm) | $f$    | Major contribs   |
|----------------|--------|--|
| 463.4          | 0.0165 | H-1 $\rightarrow$ L (10%), H $\rightarrow$ L (87%)   |
| 357.8          | 0.2298 | H-1 $\rightarrow$ L (57%)  |
| 348.3          | 0.0782 | H-7 $\rightarrow$ L (23%), H-2 $\rightarrow$ L (18%), H-1 $\rightarrow$ L (28%)                            |
| 317.8          | 0.0301 | H-7 $\rightarrow$ L (11%), H-2 $\rightarrow$ L (68%)   |
| 302.4          | 0.007  | H-3 $\rightarrow$ L (86%)  |
| 273.5          | 0.0736 | H-8 $\rightarrow$ L (12%), H-7 $\rightarrow$ L (21%), H-6 $\rightarrow$ L (22%), H $\rightarrow$ L+1 (15%) |
| 270.6          | 0.0192 | H-8 $\rightarrow$ L (18%), H-6 $\rightarrow$ L (29%), H-4 $\rightarrow$ L (16%)                            |
| 270.3          | 0.0114 | H-6 $\rightarrow$ L (10%), H-4 $\rightarrow$ L (72%)   |
| 252.5          | 0.0048 | H-5 $\rightarrow$ L (80%)  |
| 250.5          | 0.1582 | H-8 $\rightarrow$ L (38%), H $\rightarrow$ L+1 (38%)   |

**Figure A3-13:** Comparison of UV/vis spectra of **4.18** experimentally determined in CH<sub>2</sub>Cl<sub>2</sub> (red trace) and TD-DFT calculated in the gas phase (blue bar graph).**Table A3-3:** TD-DFT calculated UV/vis absorption data for compound **4.11**.

| $\lambda$ (nm) | $f$    | Major contribs                                       |
|----------------|--------|--|
| 580.8          | 0.0896 | H $\rightarrow$ L (94%)                              |
| 403.1          | 0.0007 | H-7 $\rightarrow$ L (62%), H-4 $\rightarrow$ L (18%) |
| 348.8          | 0.1221 | H-1 $\rightarrow$ L (87%)                            |
| 331.1          | 0.1064 | H-2 $\rightarrow$ L (91%)                            |
| 307.8          | 0.0258 | H-3 $\rightarrow$ L (75%)                            |
| 291.3          | 0.0402 | H-5 $\rightarrow$ L (71%), H-4 $\rightarrow$ L (10%) |
| 286.4          | 0.0018 | H-6 $\rightarrow$ L (13%), H-4 $\rightarrow$ L (58%) |
| 279.1          | 0.0567 | H-6 $\rightarrow$ L (49%), H $\rightarrow$ L+1 (18%) |

|       |        |                                       |
|-------|--------|---------------------------------------|
| 278.2 | 0.0979 | H-6→L (20%), H→L+1 (36%), H→L+2 (21%) |
| 270.9 | 0.07   | H→L+1 (28%), H→L+2 (33%)              |

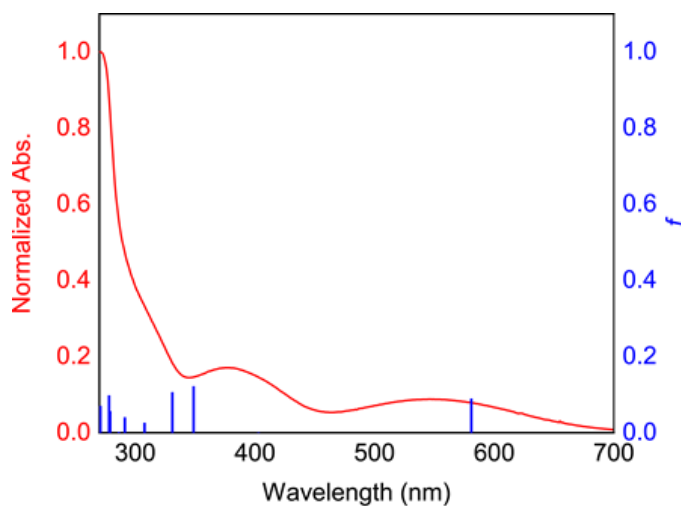


**Figure A3-14:** Comparison of UV/vis spectra of **4.11** experimentally determined in CH<sub>2</sub>Cl<sub>2</sub> (red trace) and TD-DFT calculated in the gas phase (blue bar graph).

**Table A3-4:** TD-DFT calculated UV/vis absorption data for compound **4.20**.

| $\lambda$ (nm) | $f$    | Major contribs                            |
|----------------|--------|---|
| 316.4          | 0.2042 | H→L (83%)                                 |
| 300.1          | 0.0531 | H-1→L (38%), H→L+1 (25%)                  |
| 287.4          | 0.0119 | H-2→L (31%), H-1→L (16%), H→L+2 (10%)     |
| 271.9          | 0.3645 | H-2→L (28%), H-1→L (16%), H→L+1 (38%)     |
| 266.5          | 0.0032 | H-4→L (12%), H-3→L (14%)                  |
| 250.7          | 0.0666 | H-3→L (31%), H→L+1 (13%)                  |
| 244.8          | 0.1985 | H-3→L (13%), H-1→L+1 (12%), H-1→L+2 (17%) |
| 242.8          | 0.0369 | H→L+3 (27%), H→L+4 (17%)                  |
| 241.6          | 0.0262 | H-1→L+1 (22%), H→L+3 (15%)                |
| 238.4          | 0.0027 | H→L+4 (16%), H→L+5 (18%)                  |

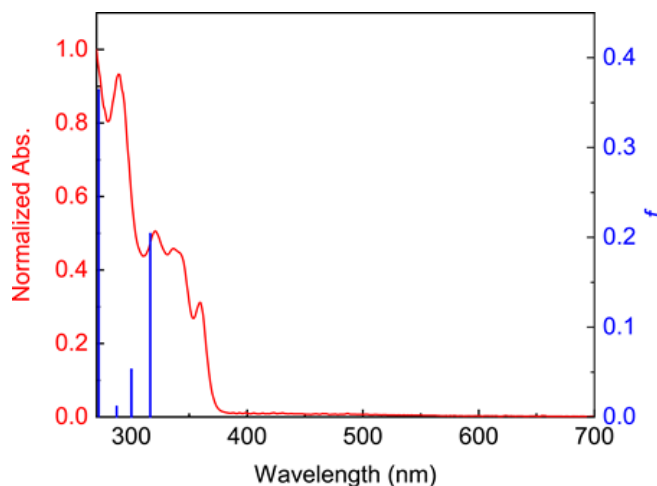


**Figure A3-15:** Comparison of UV/vis spectra of **4.20** experimentally determined in  $\text{CH}_2\text{Cl}_2$  (red trace) and TD-DFT calculated in the gas phase (blue bar graph).

**Table A3-5:** TD-DFT calculated UV/vis absorption data for compound **4.22**.

| $\lambda$ (nm) | $f$    | Major contribs   |
|----------------|--------|--|
| 338.2          | 0.2981 | H $\rightarrow$ L (79%)  |
| 323.4          | 0.0724 | H-1 $\rightarrow$ L (47%), H $\rightarrow$ L (11%), H $\rightarrow$ L+1 (31%)                                |
| 293.0          | 0.0149 | H-2 $\rightarrow$ L (42%)  |
| 283.1          | 0.3043 | H-4 $\rightarrow$ L (14%), H-1 $\rightarrow$ L (22%), H $\rightarrow$ L+1 (32%)                              |
| 282.5          | 0.1007 | H-1 $\rightarrow$ L+1 (18%), H $\rightarrow$ L+1 (14%), H $\rightarrow$ L+2 (29%)                            |
| 275.7          | 0.2467 | H-3 $\rightarrow$ L (24%), H-1 $\rightarrow$ L+1 (26%)   |
| 268.8          | 0.1987 | H-5 $\rightarrow$ L (13%), H-4 $\rightarrow$ L (12%), H-3 $\rightarrow$ L (19%), H-1 $\rightarrow$ L+1 (17%) |
| 266.9          | 0.0057 | H-4 $\rightarrow$ L (19%), H-1 $\rightarrow$ L+2 (30%)   |
| 263.8          | 0.1077 | H-5 $\rightarrow$ L (19%), H-3 $\rightarrow$ L (22%)   |
| 258.3          | 0.3036 | H-4 $\rightarrow$ L (26%), H-1 $\rightarrow$ L+2 (17%), H $\rightarrow$ L+2 (19%)                            |

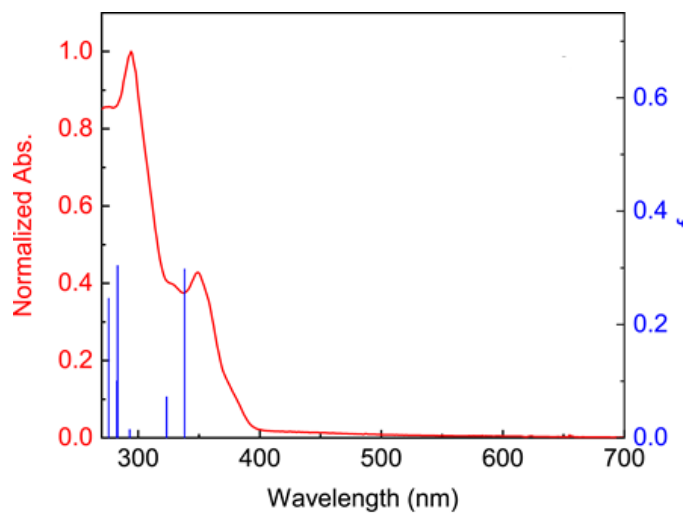


**Figure A3-16:** Comparison of UV/vis spectra of **4.22** experimentally determined in  $\text{CH}_2\text{Cl}_2$  (red trace) and TD-DFT calculated in the gas phase (blue bar graph).

## 5. X-Ray Structure Details for Compounds **4.18**, **4.11**, **4.20**, and **4.22**

### 5.1 Experimental Details

Single-crystal X-ray diffraction data was collected at 293(2) K (compound **4.18**) or 100(2) K (compounds **4.11**, **4.20**, **4.22**) on a XtaLAB Synergy-S, Dualflex, HyPix-6000HE diffractometer using Cu  $K\alpha$  radiation ( $\lambda = 1.5406 \text{ \AA}$ ). A crystal was mounted on nylon CryoLoops with Paraton-N. The data collection and reduction were processed within *CrysAlisPro* (Rigaku OD, 2019 (compounds **4.18** and **4.20**) or 2021 (compounds **4.11** and **4.22**). A Gaussian absorption correction was applied to the collected reflections. Using Olex2, the structure was solved with the ShelXT structure solution program using Intrinsic Phasing and refined with the ShelXL refinement package using Least Squares minimisation. All non-hydrogen atoms were refined anisotropically. The organic hydrogen atoms were generated geometrically.

#### Crystallization Procedures:

##### Cyclophane **4.18**

Crystals suitable for single crystal X-ray diffraction (XRD) were grown by recrystallization of **4.18** from hexanes at  $-20 \text{ }^\circ\text{C}$ .

##### Cyclopentadienone **4.11**

Crystals suitable for single crystal X-ray diffraction (XRD) were grown by slow diffusion of hexanes into a solution of **4.11** in dichloromethane at  $-20 \text{ }^\circ\text{C}$ .

##### Cyclophane **4.20**

Crystals suitable for single crystal X-ray diffraction (XRD) were grown by vapor diffusion of methanol into a solution of **4.20** in chloroform at room temperature.

##### Cyclophane **4.22**

Crystals suitable for single crystal X-ray diffraction (XRD) were grown by vapor diffusion of methanol into a solution of **4.22** in benzene at room temperature.

## 5.2 Compound 4.18

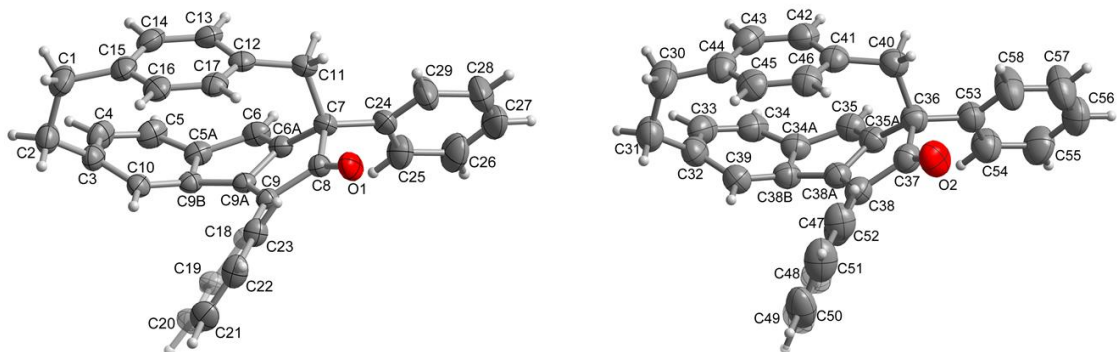


**Figure A3-17:** Molecules A and B of compound **4.18** in the crystal. Non-hydrogen atoms are represented by displacement ellipsoids at the 30% probability level. CCDC-1997192.

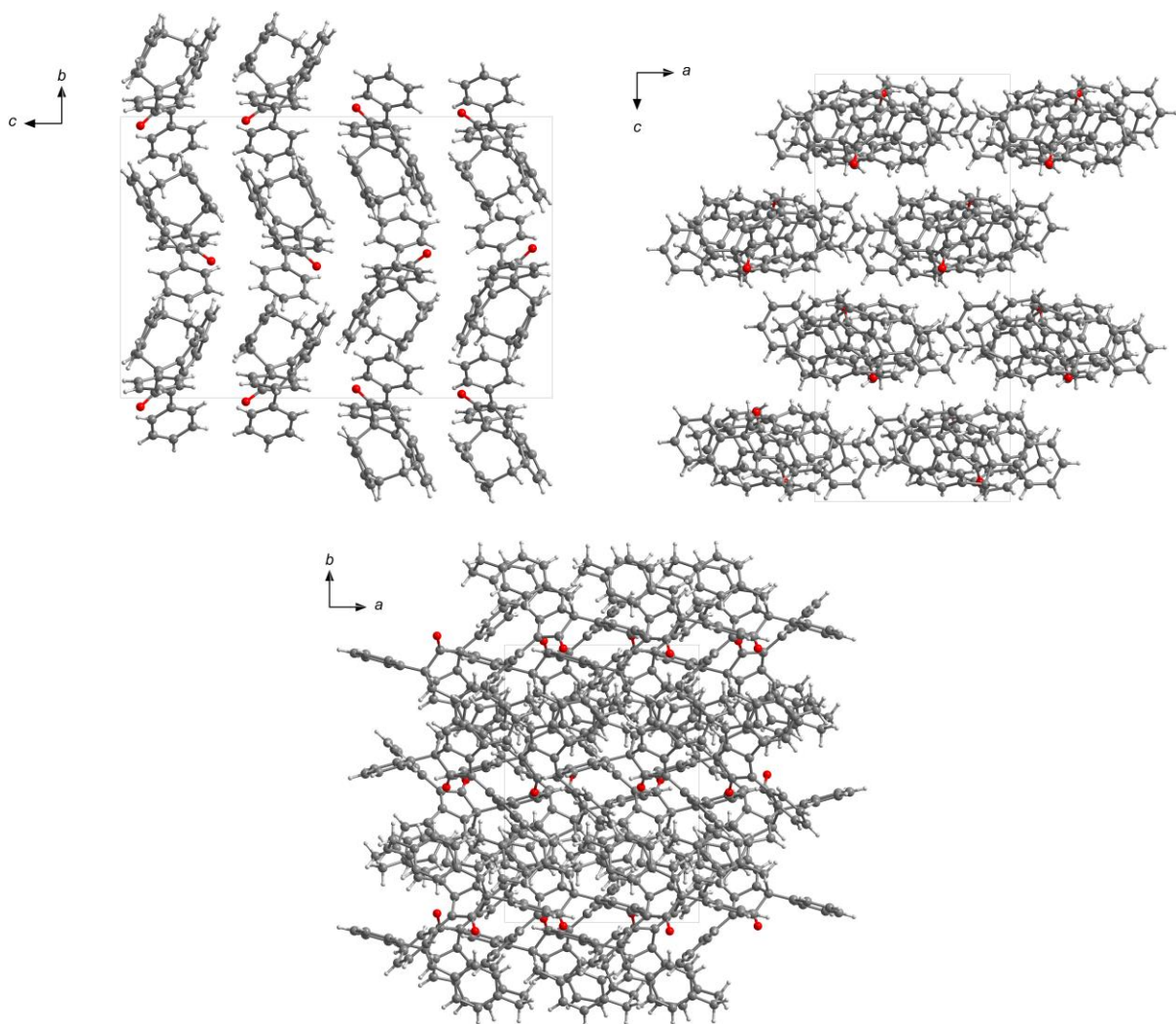


**Figure A3-18:** Crystal packing diagram for compound **4.18** from different perspectives.

**Table A3-6:** Crystal data and structure refinement for compound **4.18**.

|  |  |
|--|--|
| Empirical formula                                    | C <sub>33</sub> H <sub>24</sub> O  |
| Formula weight                                       | 436.52   |
| Temperature/K  | 293(2)   |
| Crystal system                                       | orthorhombic   |
| Space group  | <i>P</i> 2 <sub>1</sub> 2 <sub>1</sub> 2 <sub>1</sub>                        |
| <i>a</i> /Å  | 11.47420(10)   |
| <i>b</i> /Å  | 16.34440(10)   |
| <i>c</i> /Å  | 25.0767(2)   |
| Volume/Å <sup>3</sup>                                | 4702.86(6)   |
| <i>Z</i>   | 8  |
| $\rho_{\text{calc}}$ /cm <sup>3</sup>                | 1.233  |
| $\mu$ /mm <sup>-1</sup>                              | 0.559  |
| F(000)   | 1840.0   |
| Crystal size/mm <sup>3</sup>                         | 0.232 × 0.186 × 0.14   |
| Radiation  | Cu <i>K</i> α ( $\lambda$ = 1.54184)   |
| 2 $\theta$ range for data collection/°               | 6.456 to 154.894   |
| Index ranges   | -14 ≤ <i>h</i> ≤ 14, -20 ≤ <i>k</i> ≤ 19, -31 ≤ <i>l</i> ≤ 31                |
| Reflections collected                                | 47091  |
| Independent reflections                              | 9763 [ <i>R</i> <sub>int</sub> = 0.0449, <i>R</i> <sub>sigma</sub> = 0.0349] |
| Data/restraints/parameters                           | 9763/0/614   |
| Goodness-of-fit on F <sup>2</sup>                    | 1.046  |
| Final <i>R</i> indexes [ <i>I</i> ≥ 2σ ( <i>I</i> )] | <i>R</i> <sub>1</sub> = 0.0418, <i>wR</i> <sub>2</sub> = 0.1133              |
| Final <i>R</i> indexes [all data]                    | <i>R</i> <sub>1</sub> = 0.0462, <i>wR</i> <sub>2</sub> = 0.1177              |
| Largest diff. peak/hole / e Å <sup>-3</sup>          | 0.18/-0.14   |
| Flack parameter                                      | 0.09(15)   |

**Table A3-7:** Fractional atomic coordinates ( $\times 10^4$ ) and equivalent isotropic displacement parameters ( $\text{\AA}^2 \times 10^3$ ) for compound **4.18**  $U_{\text{eq}}$  is defined as 1/3 of the trace of the orthogonalised  $U_{\text{IJ}}$  tensor.

| Atom | <i>x</i>   | <i>y</i>    | <i>z</i>   | <b>U(eq)</b> |
|------|------------|-------------|------------|--------------|
| O1   | 6523.5(19) | 10318.0(12) | 4541.9(8)  | 77.6(5)      |
| C1   | 10755(4)   | 7040(3)     | 4013.1(15) | 105.6(12)    |
| C2   | 10997(3)   | 7356(2)     | 3437.6(14) | 92.1(9)      |
| C3   | 9881(3)    | 7586.9(18)  | 3163.8(11) | 73.9(7)      |
| C4   | 9138(3)    | 7007.5(18)  | 2945.0(12) | 84.6(9)      |
| C5   | 7953(3)    | 7140.9(17)  | 2886.0(11) | 81.1(8)      |
| C5A  | 7494(3)    | 7870.0(15)  | 3071.1(9)  | 64.6(6)      |
| C6   | 6339(2)    | 8031.4(15)  | 3302.5(10) | 67.4(6)      |
| C6A  | 6434(2)    | 8690.6(13)  | 3618.6(9)  | 56.3(5)      |
| C7   | 5914(2)    | 9037.4(14)  | 4120.6(10) | 60.8(5)      |
| C8   | 6688(2)    | 9805.6(13)  | 4199.0(9)  | 56.8(5)      |
| C9   | 7706.6(19) | 9764.5(12)  | 3833.9(8)  | 49.9(4)      |
| C9A  | 7567.2(19) | 9074.0(12)  | 3540.1(8)  | 49.7(4)      |
| C9B  | 8257(2)    | 8502.0(13)  | 3227.0(8)  | 53.9(5)      |
| C10  | 9442(2)    | 8374.4(15)  | 3261.3(9)  | 61.3(5)      |
| C11  | 6258(3)    | 8437.9(18)  | 4593.8(11) | 72.5(7)      |
| C12  | 7441(3)    | 8036.2(16)  | 4541.6(10) | 67.7(6)      |
| C13  | 7534(3)    | 7251.9(17)  | 4337.9(12) | 78.2(7)      |
| C14  | 8611(3)    | 6921.3(18)  | 4202.8(13) | 85.1(9)      |
| C15  | 9635(3)    | 7353(2)     | 4259.0(12) | 81.2(8)      |
| C16  | 9553(3)    | 8110(2)     | 4512.8(11) | 78.1(7)      |
| C17  | 8478(3)    | 8438.1(18)  | 4653.1(9)  | 70.2(6)      |
| C18  | 8680(2)    | 10338.7(12) | 3824.6(8)  | 52.6(4)      |
| C19  | 9283(2)    | 10468.2(16) | 3350.4(10) | 65.6(6)      |
| C20  | 10190(3)   | 11016(2)    | 3329.1(14) | 85.9(8)      |
| C21  | 10492(3)   | 11461(2)    | 3778.2(16) | 88.9(9)      |
| C22  | 9932(3)    | 11322.5(18) | 4249.1(14) | 80.5(8)      |
| C23  | 9023(2)    | 10770.2(15) | 4277.2(11) | 65.7(6)      |
| C24  | 4628(2)    | 9250.9(17)  | 4120.4(13) | 74.0(7)      |
| C25  | 4027(3)    | 9328(2)     | 3646.1(16) | 95.1(9)      |
| C26  | 2865(4)    | 9558(3)     | 3635(2)    | 121.7(15)    |
| C27  | 2282(4)    | 9698(3)     | 4099(3)    | 125.2(16)    |
| C28  | 2863(5)    | 9657(4)     | 4571(3)    | 149(2)       |
| C29  | 4042(4)    | 9427(4)     | 4587.5(19) | 126.0(17)    |
| O2   | 8001.8(18) | 5135.3(12)  | 2902.4(7)  | 75.3(5)      |
| C30  | 3732(3)    | 1962(2)     | 3533.5(13) | 90.1(9)      |
| C31  | 3372(3)    | 2380(2)     | 4069.8(12) | 76.1(7)      |
| C32  | 4430(2)    | 2669.8(15)  | 4370.6(9)  | 62.0(5)      |
| C33  | 5124(2)    | 2134.3(14)  | 4655.3(9)  | 63.5(6)      |
| C34  | 6301(2)    | 2290.5(14)  | 4749.5(9)  | 60.2(5)      |
| C34A | 6788(2)    | 2990.7(13)  | 4529.5(8)  | 52.6(4)      |
| C35  | 7980(2)    | 3110.6(13)  | 4327.8(8)  | 54.5(5)      |

|      |            |            |            |           |
|------|------------|------------|------------|-----------|
| C35A | 7941.1(19) | 3705.7(13) | 3956.1(8)  | 50.9(4)   |
| C36  | 8552(2)    | 3959.6(13) | 3455.4(8)  | 54.3(5)   |
| C37  | 7792(2)    | 4697.9(13) | 3282.1(9)  | 55.8(5)   |
| C38  | 6718.5(19) | 4725.7(13) | 3614.0(8)  | 52.4(4)   |
| C38A | 6799.4(19) | 4098.0(12) | 3968.5(8)  | 49.1(4)   |
| C38B | 6054.0(19) | 3585.6(12) | 4303.1(8)  | 50.8(4)   |
| C39  | 4879(2)    | 3441.1(14) | 4235.6(9)  | 56.1(5)   |
| C40  | 8323(2)    | 3271.4(15) | 3019.6(9)  | 60.8(5)   |
| C41  | 7137(2)    | 2870.3(14) | 3054.7(8)  | 57.0(5)   |
| C42  | 7003(2)    | 2142.3(14) | 3330.1(9)  | 62.8(5)   |
| C43  | 5918(3)    | 1828.6(15) | 3449.9(10) | 68.5(6)   |
| C44  | 4900(2)    | 2235.5(17) | 3312.8(10) | 68.0(6)   |
| C45  | 5023(2)    | 2924.4(17) | 2994.0(10) | 66.9(6)   |
| C46  | 6116(2)    | 3232.2(16) | 2861.9(9)  | 62.1(5)   |
| C47  | 5758(2)    | 5313.2(13) | 3541.0(9)  | 57.1(5)   |
| C48  | 5201(2)    | 5650.3(15) | 3980.0(11) | 65.7(6)   |
| C49  | 4338(3)    | 6236.2(19) | 3919.8(14) | 80.7(8)   |
| C50  | 4005(3)    | 6473(2)    | 3426.0(16) | 88.5(9)   |
| C51  | 4513(3)    | 6141(2)    | 2983.5(14) | 86.0(9)   |
| C52  | 5406(3)    | 5568.1(18) | 3036.2(11) | 73.2(7)   |
| C53  | 9833(2)    | 4186.4(14) | 3500.7(10) | 60.1(5)   |
| C54  | 10323(3)   | 4357.5(19) | 3992.4(11) | 74.2(7)   |
| C55  | 11482(3)   | 4593(2)    | 4034.8(13) | 84.6(8)   |
| C56  | 12159(3)   | 4648(2)    | 3585.9(13) | 80.9(8)   |
| C57  | 11690(3)   | 4476(3)    | 3105.4(14) | 106.9(13) |
| C58  | 10531(3)   | 4249(3)    | 3059.3(12) | 97.5(11)  |

**Table A3-8:** Selected bond distances (Å) for compound **4.18**.

| Atom | Atom | Length/Å | Atom | Atom | Length/Å |
|------|------|----------|------|------|----------|
| O1   | C8   | 1.215(3) | O2   | C37  | 1.214(3) |
| C1   | C2   | 1.558(5) | C30  | C31  | 1.564(4) |
| C1   | C15  | 1.515(5) | C30  | C44  | 1.517(4) |
| C2   | C3   | 1.501(5) | C31  | C32  | 1.506(4) |
| C3   | C4   | 1.387(5) | C32  | C33  | 1.382(4) |
| C3   | C10  | 1.403(4) | C32  | C39  | 1.403(3) |
| C4   | C5   | 1.385(5) | C33  | C34  | 1.395(4) |
| C5   | C5A  | 1.383(4) | C34  | C34A | 1.388(3) |
| C5A  | C6   | 1.471(4) | C34A | C35  | 1.471(3) |
| C5A  | C9B  | 1.410(3) | C34A | C38B | 1.406(3) |
| C6   | C6A  | 1.342(3) | C35  | C35A | 1.348(3) |
| C6A  | C7   | 1.504(3) | C35A | C36  | 1.497(3) |
| C6A  | C9A  | 1.457(3) | C35A | C38A | 1.459(3) |

|     |     |          |      |      |          |
|-----|-----|----------|------|------|----------|
| C7  | C8  | 1.550(3) | C36  | C37  | 1.551(3) |
| C7  | C11 | 1.589(3) | C36  | C40  | 1.590(3) |
| C7  | C24 | 1.517(4) | C36  | C53  | 1.520(3) |
| C8  | C9  | 1.486(3) | C37  | C38  | 1.488(3) |
| C9  | C9A | 1.357(3) | C38  | C38A | 1.361(3) |
| C9  | C18 | 1.459(3) | C38  | C47  | 1.473(3) |
| C9A | C9B | 1.455(3) | C38A | C38B | 1.462(3) |
| C9B | C10 | 1.378(4) | C38B | C39  | 1.379(3) |
| C11 | C12 | 1.513(4) | C40  | C41  | 1.513(3) |
| C12 | C13 | 1.384(4) | C41  | C42  | 1.384(3) |
| C12 | C17 | 1.388(4) | C41  | C46  | 1.399(4) |
| C13 | C14 | 1.390(5) | C42  | C43  | 1.379(4) |
| C14 | C15 | 1.378(5) | C43  | C44  | 1.387(4) |
| C15 | C16 | 1.395(5) | C44  | C45  | 1.388(4) |
| C16 | C17 | 1.391(4) | C45  | C46  | 1.391(4) |
| C18 | C19 | 1.392(3) | C47  | C48  | 1.388(4) |
| C18 | C23 | 1.393(3) | C47  | C52  | 1.393(3) |
| C19 | C20 | 1.373(4) | C48  | C49  | 1.385(4) |
| C20 | C21 | 1.385(5) | C49  | C50  | 1.353(5) |
| C21 | C22 | 1.363(5) | C50  | C51  | 1.366(5) |
| C22 | C23 | 1.381(4) | C51  | C52  | 1.394(4) |
| C24 | C25 | 1.380(5) | C53  | C54  | 1.384(4) |
| C24 | C29 | 1.380(5) | C53  | C58  | 1.370(4) |
| C25 | C26 | 1.386(5) | C54  | C55  | 1.388(4) |
| C26 | C27 | 1.361(7) | C55  | C56  | 1.370(5) |
| C27 | C28 | 1.360(8) | C56  | C57  | 1.349(5) |
| C28 | C29 | 1.406(6) | C57  | C58  | 1.386(4) |

**Table A3-9:** Selected bond angles (°) for compound **4.18**.

| Atom | Atom | Atom | Angle/°  | Atom | Atom | Atom | Angle/°    |
|------|------|------|----------|------|------|------|------------|
| C15  | C1   | C2   | 114.6(3) | C44  | C30  | C31  | 114.7(2)   |
| C3   | C2   | C1   | 110.8(3) | C32  | C31  | C30  | 110.8(2)   |
| C4   | C3   | C2   | 122.3(3) | C33  | C32  | C31  | 121.6(2)   |
| C4   | C3   | C10  | 118.3(3) | C33  | C32  | C39  | 118.8(2)   |
| C10  | C3   | C2   | 117.1(3) | C39  | C32  | C31  | 117.3(2)   |
| C5   | C4   | C3   | 122.6(3) | C32  | C33  | C34  | 122.0(2)   |
| C5A  | C5   | C4   | 118.3(3) | C34A | C34  | C33  | 118.2(2)   |
| C5   | C5A  | C6   | 129.1(3) | C34  | C34A | C35  | 128.4(2)   |
| C5   | C5A  | C9B  | 119.2(3) | C34  | C34A | C38B | 119.3(2)   |
| C9B  | C5A  | C6   | 108.6(2) | C38B | C34A | C35  | 109.02(18) |
| C6A  | C6   | C5A  | 107.7(2) | C35A | C35  | C34A | 107.66(19) |
| C6   | C6A  | C7   | 139.9(2) | C35  | C35A | C36  | 139.9(2)   |

|     |     |     |            |      |      |      |            |
|-----|-----|-----|------------|------|------|------|------------|
| C6  | C6A | C9A | 109.7(2)   | C35  | C35A | C38A | 109.38(19) |
| C9A | C6A | C7  | 107.74(19) | C38A | C35A | C36  | 108.47(17) |
| C6A | C7  | C8  | 100.63(18) | C35A | C36  | C37  | 100.80(17) |
| C6A | C7  | C11 | 107.12(19) | C35A | C36  | C40  | 107.64(17) |
| C6A | C7  | C24 | 118.2(2)   | C35A | C36  | C53  | 117.26(18) |
| C8  | C7  | C11 | 105.2(2)   | C37  | C36  | C40  | 105.36(17) |
| C24 | C7  | C8  | 111.8(2)   | C53  | C36  | C37  | 112.01(18) |
| C24 | C7  | C11 | 112.6(2)   | C53  | C36  | C40  | 112.56(18) |
| O1  | C8  | C7  | 124.0(2)   | O2   | C37  | C36  | 124.5(2)   |
| O1  | C8  | C9  | 126.1(2)   | O2   | C37  | C38  | 125.8(2)   |
| C9  | C8  | C7  | 109.61(18) | C38  | C37  | C36  | 109.42(17) |
| C9A | C9  | C8  | 106.21(19) | C38A | C38  | C37  | 106.62(18) |
| C9A | C9  | C18 | 128.1(2)   | C38A | C38  | C47  | 128.6(2)   |
| C18 | C9  | C8  | 125.65(18) | C47  | C38  | C37  | 124.74(19) |
| C9  | C9A | C6A | 112.93(19) | C35A | C38A | C38B | 106.60(17) |
| C9  | C9A | C9B | 139.7(2)   | C38  | C38A | C35A | 112.26(19) |
| C9B | C9A | C6A | 106.40(18) | C38  | C38A | C38B | 140.1(2)   |
| C5A | C9B | C9A | 106.4(2)   | C34A | C38B | C38A | 106.11(19) |
| C10 | C9B | C5A | 121.3(2)   | C39  | C38B | C34A | 121.1(2)   |
| C10 | C9B | C9A | 126.9(2)   | C39  | C38B | C38A | 126.8(2)   |
| C9B | C10 | C3  | 118.8(3)   | C38B | C39  | C32  | 118.9(2)   |
| C12 | C11 | C7  | 115.2(2)   | C41  | C40  | C36  | 114.52(18) |
| C13 | C12 | C11 | 120.2(3)   | C42  | C41  | C40  | 120.1(2)   |
| C13 | C12 | C17 | 116.5(3)   | C42  | C41  | C46  | 116.3(2)   |
| C17 | C12 | C11 | 123.1(3)   | C46  | C41  | C40  | 123.4(2)   |
| C12 | C13 | C14 | 121.3(3)   | C43  | C42  | C41  | 121.9(2)   |
| C15 | C14 | C13 | 122.3(3)   | C42  | C43  | C44  | 121.9(2)   |
| C14 | C15 | C1  | 120.6(3)   | C43  | C44  | C30  | 120.8(3)   |
| C14 | C15 | C16 | 116.4(3)   | C43  | C44  | C45  | 116.5(2)   |
| C16 | C15 | C1  | 122.9(4)   | C45  | C44  | C30  | 122.6(3)   |
| C17 | C16 | C15 | 121.1(3)   | C44  | C45  | C46  | 121.5(2)   |
| C12 | C17 | C16 | 121.9(3)   | C45  | C46  | C41  | 121.3(2)   |
| C19 | C18 | C9  | 119.5(2)   | C48  | C47  | C38  | 120.4(2)   |
| C19 | C18 | C23 | 118.6(2)   | C48  | C47  | C52  | 117.9(2)   |
| C23 | C18 | C9  | 121.9(2)   | C52  | C47  | C38  | 121.7(2)   |
| C20 | C19 | C18 | 120.6(3)   | C49  | C48  | C47  | 121.2(3)   |
| C19 | C20 | C21 | 120.0(3)   | C50  | C49  | C48  | 120.0(3)   |
| C22 | C21 | C20 | 119.9(3)   | C49  | C50  | C51  | 120.6(3)   |
| C21 | C22 | C23 | 120.6(3)   | C50  | C51  | C52  | 120.2(3)   |
| C22 | C23 | C18 | 120.2(3)   | C47  | C52  | C51  | 120.0(3)   |
| C25 | C24 | C7  | 120.5(3)   | C54  | C53  | C36  | 120.6(2)   |
| C25 | C24 | C29 | 118.0(3)   | C58  | C53  | C36  | 121.5(2)   |
| C29 | C24 | C7  | 121.4(3)   | C58  | C53  | C54  | 117.8(2)   |
| C24 | C25 | C26 | 121.4(4)   | C53  | C54  | C55  | 120.9(3)   |
| C27 | C26 | C25 | 120.1(5)   | C56  | C55  | C54  | 119.8(3)   |

|     |     |     |          |     |     |     |          |
|-----|-----|-----|----------|-----|-----|-----|----------|
| C28 | C27 | C26 | 119.7(4) | C57 | C56 | C55 | 119.7(3) |
| C27 | C28 | C29 | 120.7(5) | C56 | C57 | C58 | 120.8(3) |
| C24 | C29 | C28 | 120.0(5) | C53 | C58 | C57 | 120.9(3) |

**Table A3-10:** Selected torsion angles for compound **4.18**.

| A   | B   | C   | D   | Angle/°     | A    | B    | C    | D    | Angle/°      |
|-----|-----|-----|-----|-------------|------|------|------|------|--------------|
| O1  | C8  | C9  | C9A | 176.6 (2)   | O2   | C37  | C38  | C38A | 175.6 (2)    |
| O1  | C8  | C9  | C18 | -0.4 (4)    | O2   | C37  | C38  | C47  | -2.2 (4)     |
| C1  | C2  | C3  | C4  | -78.4 (4)   | C30  | C31  | C32  | C33  | -77.7 (3)    |
| C1  | C2  | C3  | C10 | 84.3 (4)    | C30  | C31  | C32  | C39  | 84.8 (3)     |
| C1  | C15 | C16 | C17 | 169.0 (3)   | C30  | C44  | C45  | C46  | 170.3 (2)    |
| C2  | C1  | C15 | C14 | 91.1 (4)    | C31  | C30  | C44  | C43  | 90.3 (4)     |
| C2  | C1  | C15 | C16 | -83.6 (4)   | C31  | C30  | C44  | C45  | -85.7 (4)    |
| C2  | C3  | C4  | C5  | 153.6 (3)   | C31  | C32  | C33  | C34  | 153.3 (2)    |
| C2  | C3  | C10 | C9B | -152.0 (3)  | C31  | C32  | C39  | C38B | -151.2 (2)   |
| C3  | C4  | C5  | C5A | -2.4 (5)    | C32  | C33  | C34  | C34A | -2.7 (3)     |
| C4  | C3  | C10 | C9B | 11.4 (4)    | C33  | C32  | C39  | C38B | 11.7 (3)     |
| C4  | C5  | C5A | C6  | -146.8 (3)  | C33  | C34  | C34A | C35  | -146.0 (2)   |
| C4  | C5  | C5A | C9B | 10.7 (4)    | C33  | C34  | C34A | C38B | 11.1 (3)     |
| C5  | C5A | C6  | C6A | 154.5 (3)   | C34  | C34A | C35  | C35A | 153.5 (2)    |
| C5  | C5A | C9B | C9A | -163.8 (2)  | C34  | C34A | C38B | C38A | -162.80 (18) |
| C5  | C5A | C9B | C10 | -8.1 (4)    | C34  | C34A | C38B | C39  | -8.2 (3)     |
| C5A | C6  | C6A | C7  | -148.4 (3)  | C34A | C35  | C35A | C36  | -149.5 (3)   |
| C5A | C6  | C6A | C9A | 9.9 (3)     | C34A | C35  | C35A | C38A | 10.4 (2)     |
| C5A | C9B | C10 | C3  | -3.2 (3)    | C34A | C38B | C39  | C32  | -3.4 (3)     |
| C6  | C5A | C9B | C9A | -2.0 (2)    | C35  | C34A | C38B | C38A | -1.6 (2)     |
| C6  | C5A | C9B | C10 | 153.7 (2)   | C35  | C34A | C38B | C39  | 152.9 (2)    |
| C6  | C6A | C7  | C8  | 174.8 (3)   | C35  | C35A | C36  | C37  | 174.9 (3)    |
| C6  | C6A | C7  | C11 | 65.1 (4)    | C35  | C35A | C36  | C40  | 64.8 (3)     |
| C6  | C6A | C7  | C24 | -63.3 (4)   | C35  | C35A | C36  | C53  | -63.3 (4)    |
| C6  | C6A | C9A | C9  | 177.70 (19) | C35  | C35A | C38A | C38  | 177.83 (18)  |
| C6  | C6A | C9A | C9B | -11.2 (2)   | C35  | C35A | C38A | C38B | -11.4 (2)    |
| C6A | C7  | C8  | O1  | 174.2 (2)   | C35A | C36  | C37  | O2   | 175.7 (2)    |
| C6A | C7  | C8  | C9  | -11.8 (2)   | C35A | C36  | C37  | C38  | -10.4 (2)    |
| C6A | C7  | C11 | C12 | 34.0 (3)    | C35A | C36  | C40  | C41  | 34.3 (3)     |
| C6A | C7  | C24 | C25 | -16.5 (4)   | C35A | C36  | C53  | C54  | -16.4 (3)    |
| C6A | C7  | C24 | C29 | 167.9 (3)   | C35A | C36  | C53  | C58  | 165.3 (3)    |
| C6A | C9A | C9B | C5A | 7.7 (2)     | C35A | C38A | C38B | C34A | 7.6 (2)      |
| C6A | C9A | C9B | C10 | -146.2 (2)  | C35A | C38A | C38B | C39  | -145.0 (2)   |
| C7  | C6A | C9A | C9  | -16.8 (2)   | C36  | C35A | C38A | C38  | -15.7 (2)    |

| <b>A</b> | <b>B</b> | <b>C</b> | <b>D</b> | <b>Angle/°</b> | <b>A</b> | <b>B</b> | <b>C</b> | <b>D</b> | <b>Angle/°</b> |
|----------|----------|----------|----------|----------------|----------|----------|----------|----------|----------------|
| C7       | C6A      | C9A      | C9B      | 154.33 (17)    | C36      | C35A     | C38A     | C38B     | 155.02 (17)    |
| C7       | C8       | C9       | C9A      | 2.6 (2)        | C36      | C37      | C38      | C38A     | 1.8 (2)        |
| C7       | C8       | C9       | C18      | -174.30 (19)   | C36      | C37      | C38      | C47      | -176.03 (19)   |
| C7       | C11      | C12      | C13      | -97.4 (3)      | C36      | C40      | C41      | C42      | -95.5 (2)      |
| C7       | C11      | C12      | C17      | 77.7 (3)       | C36      | C40      | C41      | C46      | 78.5 (3)       |
| C7       | C24      | C25      | C26      | -177.1 (4)     | C36      | C53      | C54      | C55      | -177.7 (3)     |
| C7       | C24      | C29      | C28      | 177.3 (5)      | C36      | C53      | C58      | C57      | 178.4 (4)      |
| C8       | C7       | C11      | C12      | -72.5 (3)      | C37      | C36      | C40      | C41      | -72.6 (2)      |
| C8       | C7       | C24      | C25      | 99.6 (3)       | C37      | C36      | C53      | C54      | 99.4 (3)       |
| C8       | C7       | C24      | C29      | -76.0 (4)      | C37      | C36      | C53      | C58      | -78.9 (3)      |
| C8       | C9       | C9A      | C6A      | 8.6 (2)        | C37      | C38      | C38A     | C35A     | 8.4 (2)        |
| C8       | C9       | C9A      | C9B      | -158.2 (2)     | C37      | C38      | C38A     | C38B     | -157.7 (2)     |
| C8       | C9       | C18      | C19      | -151.8 (2)     | C37      | C38      | C47      | C48      | -140.9 (2)     |
| C8       | C9       | C18      | C23      | 27.6 (3)       | C37      | C38      | C47      | C52      | 37.0 (3)       |
| C9       | C9A      | C9B      | C5A      | 175.0 (2)      | C38      | C38A     | C38B     | C34A     | 174.2 (2)      |
| C9       | C9A      | C9B      | C10      | 21.1 (4)       | C38      | C38A     | C38B     | C39      | 21.5 (4)       |
| C9       | C18      | C19      | C20      | 178.9 (3)      | C38      | C47      | C48      | C49      | 176.5 (2)      |
| C9       | C18      | C23      | C22      | -178.5 (2)     | C38      | C47      | C52      | C51      | -178.4 (2)     |
| C9A      | C6A      | C7       | C8       | 16.3 (2)       | C38A     | C35A     | C36      | C37      | 14.9 (2)       |
| C9A      | C6A      | C7       | C11      | -93.4 (2)      | C38A     | C35A     | C36      | C40      | -95.2 (2)      |
| C9A      | C6A      | C7       | C24      | 138.2 (2)      | C38A     | C35A     | C36      | C53      | 136.8 (2)      |
| C9A      | C9       | C18      | C19      | 31.9 (3)       | C38A     | C38      | C47      | C48      | 41.8 (3)       |
| C9A      | C9       | C18      | C23      | -148.6 (2)     | C38A     | C38      | C47      | C52      | -140.3 (3)     |
| C9A      | C9B      | C10      | C3       | 147.2 (2)      | C38A     | C38B     | C39      | C32      | 145.6 (2)      |
| C9B      | C5A      | C6       | C6A      | -4.9 (3)       | C38B     | C34A     | C35      | C35A     | -5.5 (2)       |
| C10      | C3       | C4       | C5       | -8.8 (5)       | C39      | C32      | C33      | C34      | -8.8 (3)       |
| C11      | C7       | C8       | O1       | -74.6 (3)      | C40      | C36      | C37      | O2       | -72.4 (3)      |
| C11      | C7       | C8       | C9       | 99.4 (2)       | C40      | C36      | C37      | C38      | 101.49 (19)    |
| C11      | C7       | C24      | C25      | -142.3 (3)     | C40      | C36      | C53      | C54      | -142.1 (2)     |
| C11      | C7       | C24      | C29      | 42.1 (4)       | C40      | C36      | C53      | C58      | 39.6 (4)       |
| C11      | C12      | C13      | C14      | 169.1 (3)      | C40      | C41      | C42      | C43      | 168.7 (2)      |
| C11      | C12      | C17      | C16      | -168.3 (2)     | C40      | C41      | C46      | C45      | -167.1 (2)     |
| C12      | C13      | C14      | C15      | -0.6 (4)       | C41      | C42      | C43      | C44      | -1.6 (4)       |
| C13      | C12      | C17      | C16      | 7.0 (3)        | C42      | C41      | C46      | C45      | 7.1 (3)        |
| C13      | C14      | C15      | C1       | -168.3 (3)     | C42      | C43      | C44      | C30      | -168.8 (3)     |
| C13      | C14      | C15      | C16      | 6.7 (4)        | C42      | C43      | C44      | C45      | 7.4 (3)        |
| C14      | C15      | C16      | C17      | -5.9 (4)       | C43      | C44      | C45      | C46      | -5.9 (4)       |
| C15      | C1       | C2       | C3       | -25.0 (5)      | C44      | C30      | C31      | C32      | -24.8 (4)      |
| C15      | C16      | C17      | C12      | -0.9 (4)       | C44      | C45      | C46      | C41      | -1.4 (4)       |
| C17      | C12      | C13      | C14      | -6.3 (4)       | C46      | C41      | C42      | C43      | -5.7 (3)       |
| C18      | C9       | C9A      | C6A      | -174.60 (19)   | C47      | C38      | C38A     | C35A     | -174.0 (2)     |

| <b>A</b> | <b>B</b> | <b>C</b> | <b>D</b> | <b>Angle/°</b> | <b>A</b> | <b>B</b> | <b>C</b> | <b>D</b> | <b>Angle/°</b> |
|----------|----------|----------|----------|----------------|----------|----------|----------|----------|----------------|
| C18      | C9       | C9A      | C9B      | 18.6 (4)       | C47      | C38      | C38A     | C38B     | 20.0 (4)       |
| C18      | C19      | C20      | C21      | -1.7 (5)       | C47      | C48      | C49      | C50      | 1.7 (5)        |
| C19      | C18      | C23      | C22      | 1.0 (4)        | C48      | C47      | C52      | C51      | -0.4 (4)       |
| C19      | C20      | C21      | C22      | 3.7 (5)        | C48      | C49      | C50      | C51      | -0.1 (5)       |
| C20      | C21      | C22      | C23      | -3.3 (5)       | C49      | C50      | C51      | C52      | -1.8 (5)       |
| C21      | C22      | C23      | C18      | 1.0 (4)        | C50      | C51      | C52      | C47      | 2.0 (5)        |
| C23      | C18      | C19      | C20      | -0.6 (4)       | C52      | C47      | C48      | C49      | -1.4 (4)       |
| C24      | C7       | C8       | O1       | 47.8 (3)       | C53      | C36      | C37      | O2       | 50.3 (3)       |
| C24      | C7       | C8       | C9       | -138.1 (2)     | C53      | C36      | C37      | C38      | -135.81 (19)   |
| C24      | C7       | C11      | C12      | 165.6 (2)      | C53      | C36      | C40      | C41      | 165.0 (2)      |
| C24      | C25      | C26      | C27      | -1.3 (7)       | C53      | C54      | C55      | C56      | -0.9 (5)       |
| C25      | C24      | C29      | C28      | 1.5 (7)        | C54      | C53      | C58      | C57      | 0.0 (6)        |
| C25      | C26      | C27      | C28      | 3.8 (8)        | C54      | C55      | C56      | C57      | 0.4 (6)        |
| C26      | C27      | C28      | C29      | -3.6 (9)       | C55      | C56      | C57      | C58      | 0.3 (7)        |
| C27      | C28      | C29      | C24      | 0.9 (9)        | C56      | C57      | C58      | C53      | -0.5 (8)       |
| C29      | C24      | C25      | C26      | -1.3 (6)       | C58      | C53      | C54      | C55      | 0.7 (5)        |

### 5.3 Compound 4.11

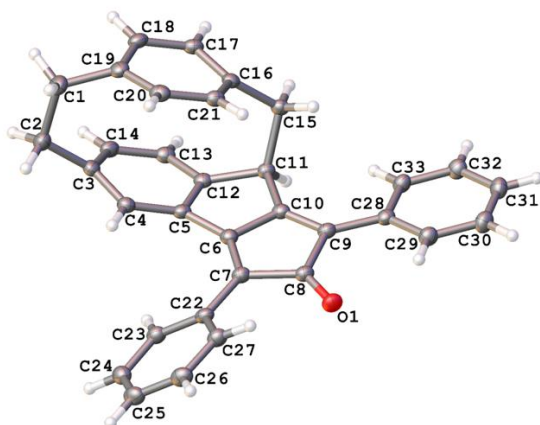


**Figure A3-19:** Crystal structure of compound **4.11**. (Non-hydrogen atoms are represented by displacement ellipsoids at the 50% probability level). CCDC-2086043.

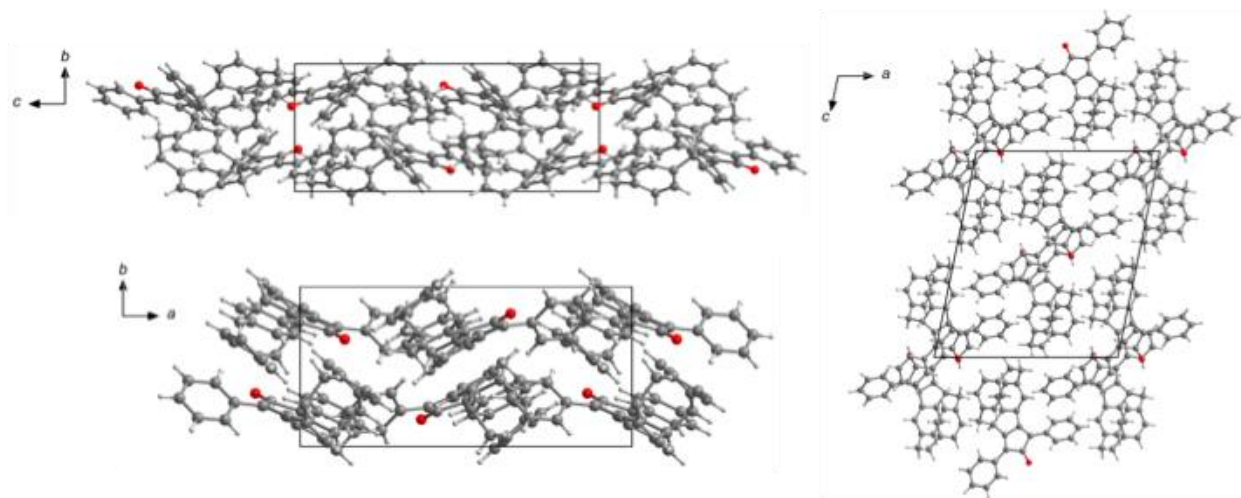


**Figure A3-20:** Crystal packing diagram for compound **4.11** from different perspectives.

**Table A3-11:** Crystal data and structure refinement for compound **4.11**.

|   |  |
|---|--|
| Empirical formula                                   | C <sub>33</sub> H <sub>24</sub> O  |
| Formula weight                                      | 436.52   |
| Temperature/K                                       | 100(2)   |
| Crystal system                                      | monoclinic   |
| Space group   | <i>P</i> 2 <sub>1</sub> / <i>n</i>   |
| <i>a</i> /Å   | 16.1315(2)   |
| <i>b</i> /Å   | 7.63800(10)  |
| <i>c</i> /Å   | 18.4860(2)   |
| $\beta$ /°  | 101.6320(10)   |
| Volume/Å <sup>3</sup>                               | 2230.93(5)   |
| <i>Z</i>  | 4  |
| $\rho_{\text{calc}}$ /cm <sup>3</sup>               | 1.300  |
| $\mu$ /mm <sup>-1</sup>                             | 0.589  |
| <i>F</i> (000)                                      | 920.0  |
| Crystal size/mm <sup>3</sup>                        | 0.31 × 0.29 × 0.06   |
| Radiation   | Cu <i>K</i> α ( $\lambda$ = 1.54184)   |
| 2 $\theta$ range for data collection/°              | 6.642 to 159.798   |
| Index ranges  | -20 ≤ <i>h</i> ≤ 20, -9 ≤ <i>k</i> ≤ 9, -23 ≤ <i>l</i> ≤ 21                  |
| Reflections collected                               | 53709  |
| Independent reflections                             | 4823 [ <i>R</i> <sub>int</sub> = 0.0606, <i>R</i> <sub>sigma</sub> = 0.0261] |
| Data/restraints/parameters                          | 4823/0/307   |
| Goodness-of-fit on <i>F</i> <sup>2</sup>            | 1.070  |
| Final <i>R</i> indexes [ <i>I</i> ≥ 2σ( <i>I</i> )] | <i>R</i> <sub>1</sub> = 0.0415, <i>wR</i> <sub>2</sub> = 0.1104              |
| Final <i>R</i> indexes [all data]                   | <i>R</i> <sub>1</sub> = 0.0454, <i>wR</i> <sub>2</sub> = 0.1137              |
| Largest diff. peak/hole / e Å <sup>-3</sup>         | 0.29/-0.23   |

**Table A3-12:** Fractional atomic coordinates ( $\times 10^4$ ) and equivalent isotropic displacement parameters ( $\text{\AA}^2 \times 10^3$ ) for compound **4.11**.  $U_{\text{eq}}$  is defined as 1/3 of the trace of the orthogonalised  $U_{\text{IJ}}$  tensor.

| Atom | <i>x</i>   | <i>y</i>    | <i>z</i>   | $U(\text{eq})$ |
|------|------------|-------------|------------|----------------|
| O1   | 3654.9 (5) | 1685.2 (12) | 4889.4 (5) | 25.0 (2)       |
| C1   | 5734.5 (8) | 703.8 (18)  | 9449.8 (7) | 28.4 (3)       |
| C2   | 5139.9 (8) | 2384.7 (18) | 9392.3 (7) | 25.9 (3)       |
| C3   | 5173.3 (7) | 3500.7 (16) | 8725.8 (6) | 21.5 (2)       |
| C4   | 4650.7 (7) | 3124.1 (15) | 8048.3 (6) | 20.2 (2)       |
| C5   | 4901.6 (7) | 3626.2 (15) | 7397.6 (6) | 18.6 (2)       |
| C6   | 4579.7 (7) | 3087.4 (15) | 6638.9 (6) | 18.7 (2)       |
| C7   | 3875.9 (7) | 2452.7 (15) | 6193.7 (6) | 19.7 (2)       |
| C8   | 4118.4 (7) | 2205.0 (15) | 5447.3 (6) | 19.9 (2)       |
| C9   | 5037.5 (7) | 2806.4 (15) | 5521.5 (6) | 19.2 (2)       |
| C10  | 5271.5 (7) | 3347.8 (15) | 6228.6 (6) | 18.2 (2)       |
| C11  | 6035.1 (7) | 4133.6 (15) | 6732.1 (6) | 18.3 (2)       |
| C12  | 5681.7 (7) | 4478.6 (15) | 7427.8 (6) | 18.5 (2)       |
| C13  | 6090.6 (7) | 5207.9 (15) | 8092.7 (6) | 20.4 (2)       |
| C14  | 5829.8 (7) | 4714.3 (16) | 8738.1 (6) | 22.5 (2)       |
| C15  | 6811.4 (7) | 2789.0 (15) | 6891.2 (6) | 19.4 (2)       |
| C16  | 6773.1 (7) | 1653.7 (15) | 7551.4 (6) | 18.8 (2)       |
| C17  | 7248.0 (7) | 2069.3 (15) | 8248.7 (7) | 21.0 (2)       |
| C18  | 6983.2 (8) | 1542.6 (16) | 8886.8 (7) | 22.9 (2)       |
| C19  | 6230.4 (8) | 608.4 (16)  | 8838.2 (6) | 23.0 (2)       |
| C20  | 5865.1 (7) | -111.7 (16) | 8152.4 (7) | 22.6 (2)       |
| C21  | 6135.7 (7) | 396.6 (15)  | 7516.2 (6) | 20.2 (2)       |
| C22  | 3017.6 (7) | 2248.3 (16) | 6329.6 (6) | 20.2 (2)       |
| C23  | 2740.6 (7) | 3332.2 (16) | 6844.2 (6) | 22.3 (2)       |
| C24  | 1919.1 (8) | 3211.1 (17) | 6966.9 (7) | 25.0 (3)       |
| C25  | 1363.6 (8) | 1973.1 (18) | 6585.1 (7) | 27.1 (3)       |
| C26  | 1632.2 (8) | 892.4 (17)  | 6076.5 (7) | 26.3 (3)       |
| C27  | 2447.2 (7) | 1030.1 (17) | 5938.6 (7) | 23.3 (2)       |
| C28  | 5515.7 (7) | 2812.8 (15) | 4928.5 (6) | 19.6 (2)       |
| C29  | 5211.5 (8) | 2009.5 (16) | 4243.6 (7) | 23.1 (2)       |
| C30  | 5688.6 (9) | 2026.7 (17) | 3694.7 (7) | 26.1 (3)       |
| C31  | 6474.9 (8) | 2823.3 (17) | 3813.0 (7) | 25.4 (3)       |
| C32  | 6782.9 (8) | 3635.0 (17) | 4486.0 (7) | 24.5 (3)       |
| C33  | 6309.7 (7) | 3639.5 (16) | 5031.6 (6) | 21.8 (2)       |

**Table A3-13:** Selected bond distances (Å) for compound **4.11**.

| Atom | Atom | Length/Å    | Atom | Atom | Length/Å    |
|------|------|-------------|------|------|-------------|
| O1   | C8   | 1.2121 (14) | C13  | C14  | 1.3946 (17) |
| C1   | C2   | 1.5932 (18) | C15  | C16  | 1.5086 (16) |
| C1   | C19  | 1.5127 (17) | C16  | C17  | 1.3968 (16) |
| C2   | C3   | 1.5080 (17) | C16  | C21  | 1.3987 (16) |
| C3   | C4   | 1.3915 (16) | C17  | C18  | 1.3923 (17) |
| C3   | C14  | 1.4041 (18) | C18  | C19  | 1.3957 (17) |
| C4   | C5   | 1.3979 (16) | C19  | C20  | 1.3985 (17) |
| C5   | C6   | 1.4534 (16) | C20  | C21  | 1.3898 (17) |
| C5   | C12  | 1.4080 (16) | C22  | C23  | 1.4006 (17) |
| C6   | C7   | 1.3508 (16) | C22  | C27  | 1.4024 (17) |
| C6   | C10  | 1.4836 (15) | C23  | C24  | 1.3919 (17) |
| C7   | C8   | 1.5200 (16) | C24  | C25  | 1.3928 (19) |
| C7   | C22  | 1.4645 (16) | C25  | C26  | 1.3847 (19) |
| C8   | C9   | 1.5317 (15) | C26  | C27  | 1.3928 (17) |
| C9   | C10  | 1.3504 (16) | C28  | C29  | 1.4034 (16) |
| C9   | C28  | 1.4621 (16) | C28  | C33  | 1.4062 (16) |
| C10  | C11  | 1.5106 (15) | C29  | C30  | 1.3919 (17) |
| C11  | C12  | 1.5310 (15) | C30  | C31  | 1.3838 (19) |
| C11  | C15  | 1.6002 (15) | C31  | C32  | 1.3892 (18) |
| C12  | C13  | 1.3891 (16) | C32  | C33  | 1.3821 (16) |

**Table A3-14:** Selected bond angles (°) for compound **4.11**.

| Atom | Atom | Atom | Angle/°     | Atom | Atom | Atom | Angle/°     |
|------|------|------|-------------|------|------|------|-------------|
| C19  | C1   | C2   | 113.01 (10) | C12  | C13  | C14  | 118.51 (11) |
| C3   | C2   | C1   | 112.94 (10) | C13  | C14  | C3   | 121.42 (11) |
| C4   | C3   | C2   | 120.24 (11) | C16  | C15  | C11  | 111.06 (9)  |
| C4   | C3   | C14  | 117.97 (11) | C17  | C16  | C15  | 120.78 (10) |
| C14  | C3   | C2   | 120.73 (11) | C17  | C16  | C21  | 117.39 (11) |
| C3   | C4   | C5   | 119.33 (11) | C21  | C16  | C15  | 120.44 (10) |
| C4   | C5   | C6   | 130.07 (11) | C18  | C17  | C16  | 120.75 (11) |
| C4   | C5   | C12  | 120.28 (10) | C17  | C18  | C19  | 120.32 (11) |
| C12  | C5   | C6   | 108.16 (10) | C18  | C19  | C1   | 120.78 (11) |
| C5   | C6   | C10  | 107.23 (10) | C18  | C19  | C20  | 117.49 (11) |
| C7   | C6   | C5   | 141.48 (11) | C20  | C19  | C1   | 120.45 (11) |
| C7   | C6   | C10  | 111.29 (10) | C21  | C20  | C19  | 120.69 (11) |
| C6   | C7   | C8   | 105.02 (10) | C20  | C21  | C16  | 120.39 (11) |

| Atom | Atom | Atom | Angle/°    | Atom | Atom | Atom | Angle/°    |
|------|------|------|------------|------|------|------|------------|
| C6   | C7   | C22  | 129.89(11) | C23  | C22  | C7   | 119.72(11) |
| C22  | C7   | C8   | 124.59(10) | C23  | C22  | C27  | 118.44(11) |
| O1   | C8   | C7   | 125.85(10) | C27  | C22  | C7   | 121.81(11) |
| O1   | C8   | C9   | 126.46(11) | C24  | C23  | C22  | 121.07(11) |
| C7   | C8   | C9   | 107.64(9)  | C23  | C24  | C25  | 119.93(12) |
| C10  | C9   | C8   | 104.78(10) | C26  | C25  | C24  | 119.43(11) |
| C10  | C9   | C28  | 129.65(11) | C25  | C26  | C27  | 121.03(12) |
| C28  | C9   | C8   | 125.55(10) | C26  | C27  | C22  | 120.08(12) |
| C6   | C10  | C11  | 110.02(9)  | C29  | C28  | C9   | 122.25(11) |
| C9   | C10  | C6   | 111.20(10) | C29  | C28  | C33  | 117.51(11) |
| C9   | C10  | C11  | 138.78(11) | C33  | C28  | C9   | 120.25(10) |
| C10  | C11  | C12  | 100.97(9)  | C30  | C29  | C28  | 120.62(11) |
| C10  | C11  | C15  | 111.65(9)  | C31  | C30  | C29  | 120.86(11) |
| C12  | C11  | C15  | 111.49(9)  | C30  | C31  | C32  | 119.25(11) |
| C5   | C12  | C11  | 111.62(10) | C33  | C32  | C31  | 120.28(11) |
| C13  | C12  | C5   | 118.79(10) | C32  | C33  | C28  | 121.46(11) |
| C13  | C12  | C11  | 128.43(10) |      |      |      |            |

**Table A3-15:** Selected torsion angles (°) for compound **4.11**.

| A  | B   | C   | D   | Angle/°     | A   | B   | C   | D   | Angle/°     |
|----|-----|-----|-----|-------------|-----|-----|-----|-----|-------------|
| O1 | C8  | C9  | C10 | 176.80(12)  | C9  | C28 | C33 | C32 | 178.67(11)  |
| O1 | C8  | C9  | C28 | -1.50(19)   | C10 | C6  | C7  | C8  | 2.24(13)    |
| C1 | C2  | C3  | C4  | 86.00(14)   | C10 | C6  | C7  | C22 | -169.81(11) |
| C1 | C2  | C3  | C14 | -82.00(15)  | C10 | C9  | C28 | C29 | 172.34(12)  |
| C1 | C19 | C20 | C21 | 153.60(11)  | C10 | C9  | C28 | C33 | -7.59(19)   |
| C2 | C1  | C19 | C18 | 82.48(14)   | C10 | C11 | C12 | C5  | 12.89(12)   |
| C2 | C1  | C19 | C20 | -84.24(15)  | C10 | C11 | C12 | C13 | -179.75(11) |
| C2 | C3  | C4  | C5  | -153.77(11) | C10 | C11 | C15 | C16 | -88.42(11)  |
| C2 | C3  | C14 | C13 | 152.72(11)  | C11 | C12 | C13 | C14 | -151.17(12) |
| C3 | C4  | C5  | C6  | 165.35(11)  | C11 | C15 | C16 | C17 | -97.39(12)  |
| C3 | C4  | C5  | C12 | 1.03(17)    | C11 | C15 | C16 | C21 | 68.82(13)   |
| C4 | C3  | C14 | C13 | -15.55(17)  | C12 | C5  | C6  | C7  | -169.05(15) |
| C4 | C5  | C6  | C7  | 25.2(2)     | C12 | C5  | C6  | C10 | 10.48(12)   |
| C4 | C5  | C6  | C10 | -155.30(12) | C12 | C11 | C15 | C16 | 23.68(13)   |
| C4 | C5  | C12 | C11 | 152.37(10)  | C12 | C13 | C14 | C3  | 0.41(17)    |
| C4 | C5  | C12 | C13 | -16.35(16)  | C14 | C3  | C4  | C5  | 14.56(17)   |
| C5 | C6  | C7  | C8  | -178.24(14) | C15 | C11 | C12 | C5  | -105.81(10) |
| C5 | C6  | C7  | C22 | 9.7(3)      | C15 | C11 | C12 | C13 | 61.55(15)   |

| <b>A</b> | <b>B</b> | <b>C</b> | <b>D</b> | <b>Angle/°</b> | <b>A</b> | <b>B</b> | <b>C</b> | <b>D</b> | <b>Angle/°</b> |
|----------|----------|----------|----------|----------------|----------|----------|----------|----------|----------------|
| C5       | C6       | C10      | C9       | 177.37 (10)    | C15      | C16      | C17      | C18      | 153.26 (11)    |
| C5       | C6       | C10      | C11      | -2.23 (12)     | C15      | C16      | C21      | C20      | -152.56 (11)   |
| C5       | C12      | C13      | C14      | 15.40 (16)     | C16      | C17      | C18      | C19      | -0.87 (18)     |
| C6       | C5       | C12      | C11      | -15.05 (13)    | C17      | C16      | C21      | C20      | 14.10 (16)     |
| C6       | C5       | C12      | C13      | 176.23 (10)    | C17      | C18      | C19      | C1       | -152.81 (11)   |
| C6       | C7       | C8       | O1       | -178.53 (12)   | C17      | C18      | C19      | C20      | 14.30 (17)     |
| C6       | C7       | C8       | C9       | -0.99 (12)     | C18      | C19      | C20      | C21      | -13.55 (17)    |
| C6       | C7       | C22      | C23      | 25.83 (19)     | C19      | C1       | C2       | C3       | 1.90 (16)      |
| C6       | C7       | C22      | C27      | -156.43 (12)   | C19      | C20      | C21      | C16      | -0.69 (17)     |
| C6       | C10      | C11      | C12      | -6.02 (12)     | C21      | C16      | C17      | C18      | -13.35 (17)    |
| C6       | C10      | C11      | C15      | 112.56 (10)    | C22      | C7       | C8       | O1       | -5.93 (19)     |
| C7       | C6       | C10      | C9       | -2.94 (14)     | C22      | C7       | C8       | C9       | 171.61 (11)    |
| C7       | C6       | C10      | C11      | 177.46 (10)    | C22      | C23      | C24      | C25      | 1.27 (18)      |
| C7       | C8       | C9       | C10      | -0.72 (12)     | C23      | C22      | C27      | C26      | -1.32 (17)     |
| C7       | C8       | C9       | C28      | -179.03 (10)   | C23      | C24      | C25      | C26      | -1.08 (19)     |
| C7       | C22      | C23      | C24      | 177.75 (11)    | C24      | C25      | C26      | C27      | -0.31 (19)     |
| C7       | C22      | C27      | C26      | -179.09 (11)   | C25      | C26      | C27      | C22      | 1.53 (19)      |
| C8       | C7       | C22      | C23      | -144.84 (11)   | C27      | C22      | C23      | C24      | -0.06 (17)     |
| C8       | C7       | C22      | C27      | 32.90 (17)     | C28      | C9       | C10      | C6       | -179.72 (11)   |
| C8       | C9       | C10      | C6       | 2.07 (13)      | C28      | C9       | C10      | C11      | -0.3 (2)       |
| C8       | C9       | C10      | C11      | -178.50 (13)   | C28      | C29      | C30      | C31      | 0.47 (19)      |
| C8       | C9       | C28      | C29      | -9.78 (18)     | C29      | C28      | C33      | C32      | -1.26 (18)     |
| C8       | C9       | C28      | C33      | 170.29 (11)    | C29      | C30      | C31      | C32      | -0.9 (2)       |
| C9       | C10      | C11      | C12      | 174.55 (14)    | C30      | C31      | C32      | C33      | 0.25 (19)      |
| C9       | C10      | C11      | C15      | -66.87 (18)    | C31      | C32      | C33      | C28      | 0.85 (19)      |
| C9       | C28      | C29      | C30      | -179.33 (11)   | C33      | C28      | C29      | C30      | 0.59 (17)      |

## 5.4 Compound 4.20

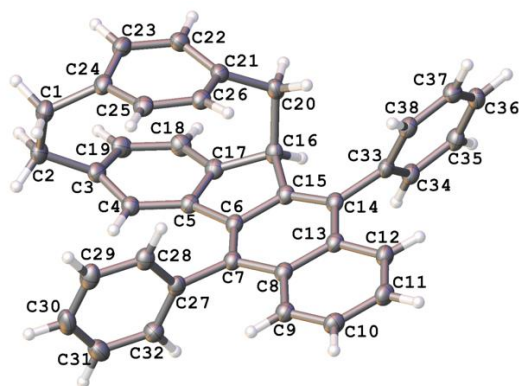


**Figure A3-21:** X-ray crystal structure of compound **4.20** (non-hydrogen atoms are represented by displacement ellipsoids at the 50% probability level). CCDC-2086044.

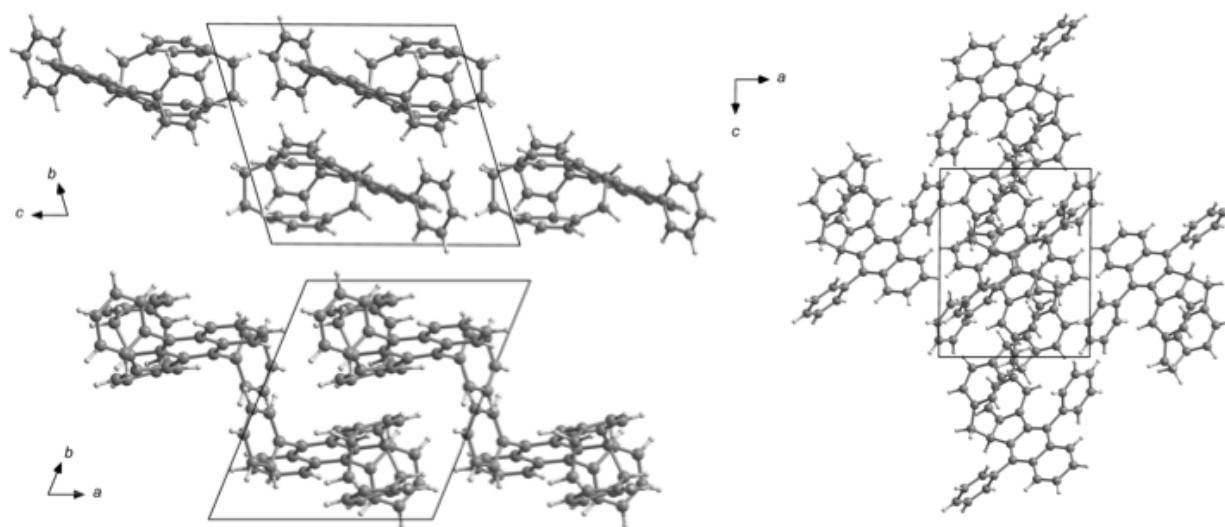


**Figure A3-22.** Crystal packing diagram for compound **4.20** from different perspectives.

**Table A3-16:** Crystal data and structure refinement for compound **4.20**.

|  |  |
|--|--|
| Empirical formula                                    | C <sub>38</sub> H <sub>28</sub>  |
| Formula weight                                       | 484.60   |
| Temperature/K  | 100(2)   |
| Crystal system                                       | triclinic  |
| Space group  | <i>P</i> -1  |
| <i>a</i> /Å  | 10.01109(15)   |
| <i>b</i> /Å  | 12.05612(19)   |
| <i>c</i> /Å  | 12.06975(17)   |
| $\alpha$ /°  | 72.0163(13)  |
| $\beta$ /°   | 83.3365(12)  |
| $\gamma$ /°  | 66.7370(15)  |
| Volume/Å <sup>3</sup>                                | 1272.91(4)   |
| <i>Z</i>   | 2  |
| $\rho_{\text{calc}}$ /cm <sup>3</sup>                | 1.264  |
| $\mu$ /mm <sup>-1</sup>                              | 0.540  |
| <i>F</i> (000)                                       | 512.0  |
| Crystal size/mm <sup>3</sup>                         | 0.189 × 0.11 × 0.056   |
| Radiation  | Cu <i>K</i> α ( $\lambda$ = 1.54184)   |
| 2 $\theta$ range for data collection/°               | 7.702 to 154.844   |
| Index ranges   | -12 ≤ <i>h</i> ≤ 10, -15 ≤ <i>k</i> ≤ 15, -15 ≤ <i>l</i> ≤ 15                |
| Reflections collected                                | 61725  |
| Independent reflections                              | 5337 [ <i>R</i> <sub>int</sub> = 0.0550, <i>R</i> <sub>sigma</sub> = 0.0234] |
| Data/restraints/parameters                           | 5337/0/344   |
| Goodness-of-fit on <i>F</i> <sup>2</sup>             | 1.068  |
| Final <i>R</i> indexes [ <i>I</i> ≥ 2σ ( <i>I</i> )] | <i>R</i> <sub>1</sub> = 0.0414, <i>wR</i> <sub>2</sub> = 0.1072              |
| Final <i>R</i> indexes [all data]                    | <i>R</i> <sub>1</sub> = 0.0465, <i>wR</i> <sub>2</sub> = 0.1111              |
| Largest diff. peak/hole / e Å <sup>-3</sup>          | 0.27/-0.20   |

**Table A3-17:** Fractional atomic coordinates ( $\times 10^4$ ) and equivalent isotropic displacement parameters ( $\text{\AA}^2 \times 10^3$ ) for compound **4.20**.  $U_{\text{eq}}$  is defined as 1/3 of the trace of the orthogonalised  $U_{\text{ij}}$  tensor.

| Atom | <i>x</i>    | <i>y</i>    | <i>z</i>     | $U(\text{eq})$ |
|------|-------------|-------------|--------------|----------------|
| C1   | 5491.4 (15) | 1767.0 (12) | 10607.2 (11) | 29.1 (3)       |
| C2   | 4966.6 (15) | 3258.6 (12) | 10230.7 (11) | 27.9 (3)       |
| C3   | 5050.7 (14) | 3799.7 (11) | 8924.5 (11)  | 24.4 (3)       |
| C4   | 4161.3 (13) | 3681.3 (11) | 8197.5 (10)  | 22.3 (2)       |
| C5   | 4619.8 (13) | 3644.3 (11) | 7067.3 (10)  | 21.5 (2)       |
| C6   | 4082.2 (13) | 3247.6 (11) | 6227.9 (10)  | 21.2 (2)       |
| C7   | 2810.4 (13) | 3069.6 (11) | 6202.2 (10)  | 21.6 (2)       |
| C8   | 2587.9 (13) | 2656.6 (11) | 5271.3 (10)  | 21.7 (2)       |
| C9   | 1264.7 (14) | 2539.6 (11) | 5150.6 (10)  | 24.5 (3)       |
| C10  | 1037.6 (14) | 2151.0 (12) | 4257.5 (11)  | 27.0 (3)       |
| C11  | 2138.9 (15) | 1864.9 (12) | 3433.1 (11)  | 27.9 (3)       |
| C12  | 3430.8 (14) | 1975.4 (12) | 3516.4 (10)  | 25.9 (3)       |
| C13  | 3708.9 (13) | 2368.2 (11) | 4432.7 (10)  | 22.5 (2)       |
| C14  | 5053.0 (13) | 2496.3 (11) | 4524.3 (10)  | 22.0 (2)       |
| C15  | 5201.2 (13) | 2958.6 (11) | 5393.4 (10)  | 22.1 (2)       |
| C16  | 6527.6 (13) | 3118.1 (11) | 5700.0 (10)  | 23.8 (3)       |
| C17  | 5950.5 (14) | 3747.3 (11) | 6664.2 (10)  | 23.5 (3)       |
| C18  | 6671.3 (14) | 4129.7 (12) | 7297.7 (11)  | 26.5 (3)       |
| C19  | 6213.8 (14) | 4144.7 (12) | 8432.2 (11)  | 26.6 (3)       |
| C20  | 7809.4 (13) | 1774.3 (12) | 6186.6 (11)  | 25.7 (3)       |
| C21  | 7592.9 (13) | 1181.8 (11) | 7460.2 (11)  | 24.3 (3)       |
| C22  | 8352.7 (14) | 1272.8 (12) | 8310.4 (11)  | 27.0 (3)       |
| C23  | 7787.1 (14) | 1258.9 (12) | 9419.8 (11)  | 27.8 (3)       |
| C24  | 6427.9 (14) | 1194.1 (11) | 9694.4 (10)  | 25.8 (3)       |
| C25  | 5832.8 (14) | 842.8 (11)  | 8929.6 (11)  | 25.4 (3)       |
| C26  | 6427.5 (14) | 805.7 (11)  | 7832.8 (11)  | 24.1 (3)       |
| C27  | 1731.3 (13) | 3254.2 (12) | 7162.4 (10)  | 22.8 (2)       |
| C28  | 1780.8 (14) | 2216.9 (12) | 8109.6 (11)  | 26.2 (3)       |
| C29  | 932.2 (15)  | 2382.2 (14) | 9088.0 (12)  | 32.1 (3)       |
| C30  | -0.1 (16)   | 3586.3 (15) | 9110.6 (12)  | 36.0 (3)       |
| C31  | -94.6 (15)  | 4615.8 (14) | 8160.2 (13)  | 35.2 (3)       |
| C32  | 770.6 (14)  | 4450.0 (13) | 7187.7 (11)  | 28.7 (3)       |
| C33  | 6287.9 (13) | 2137.3 (11) | 3713.9 (10)  | 22.5 (2)       |
| C34  | 6780.8 (14) | 3052.4 (11) | 3002.0 (10)  | 24.6 (3)       |
| C35  | 8005.6 (14) | 2725.4 (13) | 2312.6 (11)  | 27.5 (3)       |
| C36  | 8753.4 (14) | 1476.6 (13) | 2328.5 (11)  | 28.1 (3)       |
| C37  | 8262.4 (14) | 562.3 (12)  | 3023.0 (11)  | 27.9 (3)       |
| C38  | 7034.0 (14) | 884.1 (12)  | 3710.1 (10)  | 25.6 (3)       |

**Table A3-18:** Selected bond distances (Å) for compound **4.20**.

| Atom | Atom | Length/Å    | Atom | Atom | Length/Å    |
|------|------|-------------|------|------|-------------|
| C1   | C2   | 1.5877 (18) | C16  | C20  | 1.6005 (17) |
| C1   | C24  | 1.5128 (17) | C17  | C18  | 1.3879 (17) |
| C2   | C3   | 1.5151 (17) | C18  | C19  | 1.3958 (17) |
| C3   | C4   | 1.3936 (17) | C20  | C21  | 1.5124 (17) |
| C3   | C19  | 1.3969 (18) | C21  | C22  | 1.4001 (17) |
| C4   | C5   | 1.3963 (16) | C21  | C26  | 1.3926 (18) |
| C5   | C6   | 1.4744 (16) | C22  | C23  | 1.3899 (17) |
| C5   | C17  | 1.4035 (17) | C23  | C24  | 1.3895 (19) |
| C6   | C7   | 1.3774 (17) | C24  | C25  | 1.3982 (18) |
| C6   | C15  | 1.4275 (16) | C25  | C26  | 1.3933 (17) |
| C7   | C8   | 1.4322 (16) | C27  | C28  | 1.3981 (17) |
| C7   | C27  | 1.4962 (16) | C27  | C32  | 1.3891 (18) |
| C8   | C9   | 1.4145 (18) | C28  | C29  | 1.3909 (18) |
| C8   | C13  | 1.4319 (17) | C29  | C30  | 1.388 (2)   |
| C9   | C10  | 1.3733 (17) | C30  | C31  | 1.385 (2)   |
| C10  | C11  | 1.4078 (18) | C31  | C32  | 1.3929 (18) |
| C11  | C12  | 1.3693 (19) | C33  | C34  | 1.3947 (17) |
| C12  | C13  | 1.4226 (16) | C33  | C38  | 1.3974 (17) |
| C13  | C14  | 1.4339 (18) | C34  | C35  | 1.3912 (17) |
| C14  | C15  | 1.3767 (16) | C35  | C36  | 1.3867 (18) |
| C14  | C33  | 1.4935 (16) | C36  | C37  | 1.3860 (19) |
| C15  | C16  | 1.5155 (17) | C37  | C38  | 1.3913 (18) |
| C16  | C17  | 1.5188 (16) |      |      |             |

**Table A3-19:** Selected bond angles (°) for compound **4.20**.

| Atom | Atom | Atom | Angle/°     | Atom | Atom | Atom | Angle/°     |
|------|------|------|-------------|------|------|------|-------------|
| C24  | C1   | C2   | 112.57 (10) | C17  | C16  | C20  | 110.30 (10) |
| C3   | C2   | C1   | 111.83 (10) | C5   | C17  | C16  | 109.96 (10) |
| C4   | C3   | C2   | 119.14 (11) | C18  | C17  | C5   | 119.59 (11) |
| C4   | C3   | C19  | 118.55 (11) | C18  | C17  | C16  | 128.94 (11) |
| C19  | C3   | C2   | 120.65 (11) | C17  | C18  | C19  | 118.35 (12) |
| C3   | C4   | C5   | 119.25 (11) | C18  | C19  | C3   | 121.44 (11) |
| C4   | C5   | C6   | 130.09 (11) | C21  | C20  | C16  | 111.17 (9)  |
| C4   | C5   | C17  | 120.22 (11) | C22  | C21  | C20  | 119.60 (11) |
| C17  | C5   | C6   | 108.45 (10) | C26  | C21  | C20  | 121.56 (11) |
| C7   | C6   | C5   | 130.87 (11) | C26  | C21  | C22  | 117.17 (11) |

| Atom | Atom | Atom | Angle/°     | Atom | Atom | Atom | Angle/°     |
|------|------|------|-------------|------|------|------|-------------|
| C7   | C6   | C15  | 121.43 (11) | C23  | C22  | C21  | 121.02 (12) |
| C15  | C6   | C5   | 107.58 (10) | C24  | C23  | C22  | 120.32 (12) |
| C6   | C7   | C8   | 118.48 (11) | C23  | C24  | C1   | 120.88 (12) |
| C6   | C7   | C27  | 119.83 (10) | C23  | C24  | C25  | 117.12 (11) |
| C8   | C7   | C27  | 121.64 (11) | C25  | C24  | C1   | 120.49 (12) |
| C9   | C8   | C7   | 121.21 (11) | C26  | C25  | C24  | 121.25 (12) |
| C9   | C8   | C13  | 118.76 (11) | C21  | C26  | C25  | 119.87 (11) |
| C13  | C8   | C7   | 120.03 (11) | C28  | C27  | C7   | 119.36 (11) |
| C10  | C9   | C8   | 121.66 (12) | C32  | C27  | C7   | 121.32 (11) |
| C9   | C10  | C11  | 119.69 (12) | C32  | C27  | C28  | 119.04 (11) |
| C12  | C11  | C10  | 120.33 (11) | C29  | C28  | C27  | 120.63 (12) |
| C11  | C12  | C13  | 121.59 (12) | C30  | C29  | C28  | 119.61 (13) |
| C8   | C13  | C14  | 119.93 (11) | C31  | C30  | C29  | 120.20 (12) |
| C12  | C13  | C8   | 117.97 (11) | C30  | C31  | C32  | 120.08 (13) |
| C12  | C13  | C14  | 122.09 (11) | C27  | C32  | C31  | 120.37 (12) |
| C13  | C14  | C33  | 122.03 (10) | C34  | C33  | C14  | 119.62 (11) |
| C15  | C14  | C13  | 118.49 (11) | C34  | C33  | C38  | 118.80 (11) |
| C15  | C14  | C33  | 119.48 (11) | C38  | C33  | C14  | 121.42 (11) |
| C6   | C15  | C16  | 110.10 (10) | C35  | C34  | C33  | 120.81 (11) |
| C14  | C15  | C6   | 121.46 (11) | C36  | C35  | C34  | 120.00 (12) |
| C14  | C15  | C16  | 128.19 (11) | C37  | C36  | C35  | 119.61 (12) |
| C15  | C16  | C17  | 101.88 (10) | C36  | C37  | C38  | 120.66 (12) |
| C15  | C16  | C20  | 110.59 (10) | C37  | C38  | C33  | 120.10 (12) |

**Table A3-20:** Selected torsion angles (°) for compound **4.20**.

| A  | B   | C   | D   | Angle/°      | A   | B   | C   | D   | Angle/°      |
|----|-----|-----|-----|--------------|-----|-----|-----|-----|--------------|
| C1 | C2  | C3  | C4  | 64.92 (15)   | C13 | C14 | C33 | C34 | 118.37 (13)  |
| C1 | C2  | C3  | C19 | -100.18 (13) | C13 | C14 | C33 | C38 | -66.29 (16)  |
| C1 | C24 | C25 | C26 | 153.62 (12)  | C14 | C15 | C16 | C17 | 176.21 (12)  |
| C2 | C1  | C24 | C23 | 65.89 (15)   | C14 | C15 | C16 | C20 | -66.55 (15)  |
| C2 | C1  | C24 | C25 | -99.70 (14)  | C14 | C33 | C34 | C35 | 174.48 (11)  |
| C2 | C3  | C4  | C5  | -151.98 (11) | C14 | C33 | C38 | C37 | -174.09 (11) |
| C2 | C3  | C19 | C18 | 152.46 (12)  | C15 | C6  | C7  | C8  | -3.76 (17)   |
| C3 | C4  | C5  | C6  | 164.57 (12)  | C15 | C6  | C7  | C27 | 173.60 (10)  |
| C3 | C4  | C5  | C17 | -1.08 (17)   | C15 | C14 | C33 | C34 | -62.01 (16)  |
| C4 | C3  | C19 | C18 | -12.73 (18)  | C15 | C14 | C33 | C38 | 113.32 (13)  |
| C4 | C5  | C6  | C7  | 16.2 (2)     | C15 | C16 | C17 | C5  | 14.27 (13)   |
| C4 | C5  | C6  | C15 | -159.65 (12) | C15 | C16 | C17 | C18 | 179.93 (12)  |

| <b>A</b> | <b>B</b> | <b>C</b> | <b>D</b> | <b>Angle/°</b> | <b>A</b> | <b>B</b> | <b>C</b> | <b>D</b> | <b>Angle/°</b> |
|----------|----------|----------|----------|----------------|----------|----------|----------|----------|----------------|
| C4       | C5       | C17      | C16      | 154.66 (11)    | C15      | C16      | C20      | C21      | -81.34 (12)    |
| C4       | C5       | C17      | C18      | -12.55 (17)    | C16      | C17      | C18      | C19      | -151.19 (12)   |
| C5       | C6       | C7       | C8       | -179.11 (11)   | C16      | C20      | C21      | C22      | -98.91 (13)    |
| C5       | C6       | C7       | C27      | -1.75 (19)     | C16      | C20      | C21      | C26      | 65.91 (15)     |
| C5       | C6       | C15      | C14      | 176.67 (10)    | C17      | C5       | C6       | C7       | -176.86 (12)   |
| C5       | C6       | C15      | C16      | 2.03 (13)      | C17      | C5       | C6       | C15      | 7.30 (13)      |
| C5       | C17      | C18      | C19      | 13.29 (18)     | C17      | C16      | C20      | C21      | 30.59 (14)     |
| C6       | C5       | C17      | C16      | -13.81 (13)    | C17      | C18      | C19      | C3       | -0.71 (19)     |
| C6       | C5       | C17      | C18      | 178.98 (11)    | C19      | C3       | C4       | C5       | 13.44 (17)     |
| C6       | C7       | C8       | C9       | -175.62 (11)   | C20      | C16      | C17      | C5       | -103.18 (12)   |
| C6       | C7       | C8       | C13      | 3.62 (17)      | C20      | C16      | C17      | C18      | 62.49 (16)     |
| C6       | C7       | C27      | C28      | -93.62 (14)    | C20      | C21      | C22      | C23      | 151.88 (12)    |
| C6       | C7       | C27      | C32      | 80.22 (15)     | C20      | C21      | C26      | C25      | -149.15 (12)   |
| C6       | C15      | C16      | C17      | -9.62 (12)     | C21      | C22      | C23      | C24      | -2.06 (19)     |
| C6       | C15      | C16      | C20      | 107.62 (11)    | C22      | C21      | C26      | C25      | 16.03 (17)     |
| C7       | C6       | C15      | C14      | 0.36 (18)      | C22      | C23      | C24      | C1       | -151.07 (12)   |
| C7       | C6       | C15      | C16      | -174.28 (10)   | C22      | C23      | C24      | C25      | 14.98 (18)     |
| C7       | C8       | C9       | C10      | 179.64 (11)    | C23      | C24      | C25      | C26      | -12.50 (18)    |
| C7       | C8       | C13      | C12      | -179.30 (11)   | C24      | C1       | C2       | C3       | 20.28 (15)     |
| C7       | C8       | C13      | C14      | -0.16 (17)     | C24      | C25      | C26      | C21      | -3.14 (18)     |
| C7       | C27      | C28      | C29      | 170.96 (11)    | C26      | C21      | C22      | C23      | -13.60 (18)    |
| C7       | C27      | C32      | C31      | -171.72 (12)   | C27      | C7       | C8       | C9       | 7.07 (17)      |
| C8       | C7       | C27      | C28      | 83.65 (15)     | C27      | C7       | C8       | C13      | -173.69 (10)   |
| C8       | C7       | C27      | C32      | -102.51 (14)   | C27      | C28      | C29      | C30      | 1.7 (2)        |
| C8       | C9       | C10      | C11      | -0.30 (19)     | C28      | C27      | C32      | C31      | 2.15 (19)      |
| C8       | C13      | C14      | C15      | -3.21 (17)     | C28      | C29      | C30      | C31      | 0.6 (2)        |
| C8       | C13      | C14      | C33      | 176.40 (10)    | C29      | C30      | C31      | C32      | -1.5 (2)       |
| C9       | C8       | C13      | C12      | -0.05 (17)     | C30      | C31      | C32      | C27      | 0.1 (2)        |
| C9       | C8       | C13      | C14      | 179.10 (10)    | C32      | C27      | C28      | C29      | -3.03 (19)     |
| C9       | C10      | C11      | C12      | -0.17 (19)     | C33      | C14      | C15      | C6       | -176.46 (10)   |
| C10      | C11      | C12      | C13      | 0.53 (19)      | C33      | C14      | C15      | C16      | -2.87 (18)     |
| C11      | C12      | C13      | C8       | -0.41 (18)     | C33      | C34      | C35      | C36      | -0.06 (19)     |
| C11      | C12      | C13      | C14      | -179.53 (11)   | C34      | C33      | C38      | C37      | 1.29 (18)      |
| C12      | C13      | C14      | C15      | 175.89 (11)    | C34      | C35      | C36      | C37      | 0.79 (19)      |
| C12      | C13      | C14      | C33      | -4.49 (18)     | C35      | C36      | C37      | C38      | -0.49 (19)     |
| C13      | C8       | C9       | C10      | 0.40 (18)      | C36      | C37      | C38      | C33      | -0.57 (19)     |
| C13      | C14      | C15      | C6       | 3.17 (17)      | C38      | C33      | C34      | C35      | -0.98 (18)     |
| C13      | C14      | C15      | C16      | 176.75 (11)    |          |          |          |          |                |

## 5.5 Compound 4.22

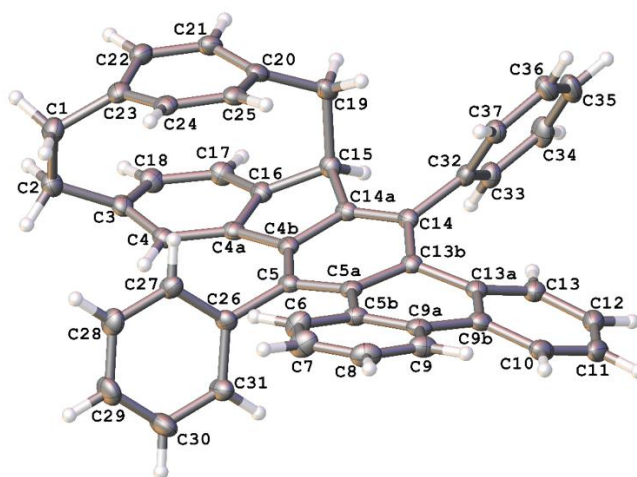


**Figure A3-23:** Crystal structure of compound **4.22**. Non-hydrogen atoms are represented by displacement ellipsoids at the 50% probability level). CCDC-2086045.

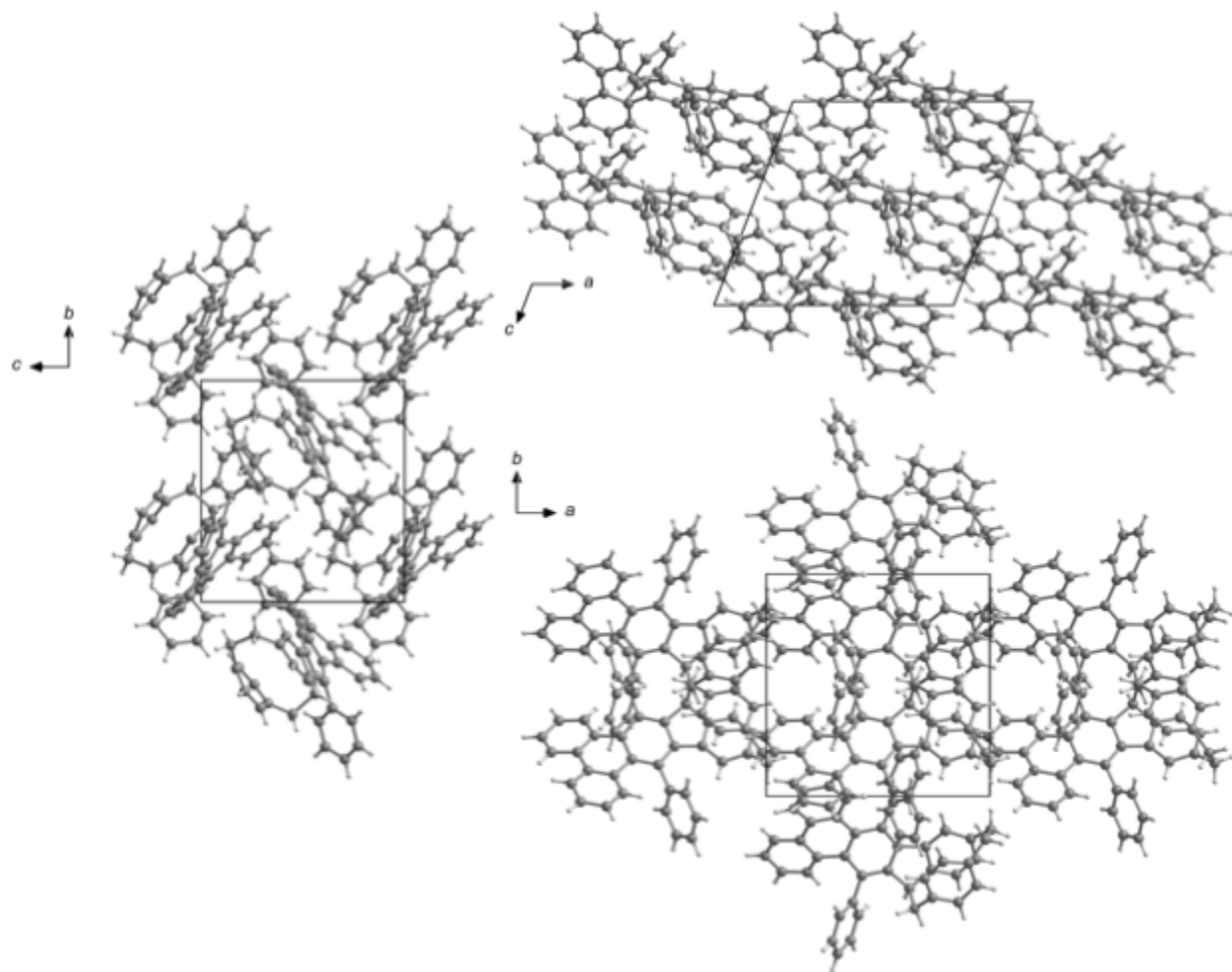


**Figure A3-24:** Crystal packing diagram for compound **4.22** from different perspectives.

**Table A3-21:** Crystal data and structure refinement for compound **4.22**.

|  |   |
|--|---|
| Empirical formula  | C <sub>46</sub> H <sub>32</sub>                                 |
| Formula weight   | 584.71  |
| Temperature/K  | 100(2)  |
| Crystal system   | monoclinic  |
| Space group  | <i>Pc</i>   |
| <i>a</i> /Å  | 12.52070(10)  |
| <i>b</i> /Å  | 11.58530(10)  |
| <i>c</i> /Å  | 11.45110(10)  |
| $\beta$ /°   | 111.1430(10)  |
| Volume/Å <sup>3</sup>  | 1549.23(2)  |
| <i>Z</i>   | 2   |
| $\rho_{\text{calc}}$ /mg/mm <sup>3</sup>                     | 1.253   |
| $\mu$ /mm <sup>-1</sup>                                      | 0.537   |
| <i>F</i> (000)   | 616.0   |
| Crystal size/mm <sup>3</sup>                                 | 0.177 × 0.148 × 0.124   |
| 2 $\theta$ range for data collection                         | 7.57 to 159.512°  |
| Index ranges   | -15 ≤ <i>h</i> ≤ 15, -14 ≤ <i>k</i> ≤ 14, -13 ≤ <i>l</i> ≤ 14   |
| Reflections collected  | 70048   |
| Independent reflections                                      | 6557 [ <i>R</i> (int) = 0.0602]                                 |
| Data/restraints/parameters                                   | 6557/2/416  |
| Goodness-of-fit on <i>F</i> <sup>2</sup>                     | 1.053   |
| Final <i>R</i> indexes [ <i>I</i> ≥ 2 $\sigma$ ( <i>I</i> )] | <i>R</i> <sub>1</sub> = 0.0320, <i>wR</i> <sub>2</sub> = 0.0797 |
| Final <i>R</i> indexes [all data]                            | <i>R</i> <sub>1</sub> = 0.0326, <i>wR</i> <sub>2</sub> = 0.0801 |
| Largest diff. peak/hole / e Å <sup>-3</sup>                  | 0.14/-0.17  |

**Table A3-22:** Fractional atomic coordinates ( $\times 10^4$ ) and equivalent isotropic displacement parameters ( $\text{\AA}^2 \times 10^3$ ) for compound **4.22**.  $U_{\text{eq}}$  is defined as 1/3 of the trace of the orthogonalised  $U_{ij}$  tensor.

| Atom | x           | y           | z          | U(eq)   |
|------|-------------|-------------|------------|---------|
| C1   | 9804.8(17)  | 8052.9(18)  | 8546(2)    | 28.4(4) |
| C2   | 10052.6(17) | 8498.6(17)  | 7358(2)    | 26.3(4) |
| C3   | 9156.9(16)  | 8089.1(16)  | 6143.3(18) | 22.4(4) |
| C4   | 8020.1(16)  | 8443.2(15)  | 5840.3(18) | 20.7(4) |
| C4A  | 7128.2(16)  | 7733.9(15)  | 5111.0(17) | 19.5(4) |
| C4B  | 5880.4(15)  | 7748.8(15)  | 4857.2(17) | 18.7(3) |
| C5   | 5171.1(16)  | 8580.6(15)  | 5067.0(17) | 19.2(4) |
| C5A  | 3976.2(15)  | 8336.6(15)  | 4713.1(17) | 18.7(4) |
| C5B  | 3181.2(16)  | 9052.1(16)  | 5103.5(18) | 21.2(4) |
| C6   | 3570.2(18)  | 9873.8(18)  | 6078(2)    | 28.2(4) |
| C7   | 2831.4(19)  | 10457.8(19) | 6512(2)    | 31.8(5) |
| C8   | 1664.2(18)  | 10246.5(18) | 6011(2)    | 29.4(4) |
| C9   | 1256.3(18)  | 9434.4(17)  | 5072(2)    | 26.8(4) |
| C9A  | 1986.4(16)  | 8838.1(16)  | 4602.0(19) | 22.1(4) |
| C9B  | 1529.3(16)  | 8013.8(16)  | 3574.4(19) | 22.5(4) |
| C10  | 356.7(16)   | 8013.5(16)  | 2814(2)    | 26.2(4) |
| C11  | -54.2(17)   | 7326.9(17)  | 1766(2)    | 28.8(4) |
| C12  | 692.8(17)   | 6603.2(17)  | 1456(2)    | 27.3(4) |
| C13  | 1840.3(17)  | 6573.2(16)  | 2203.2(19) | 24.0(4) |
| C13A | 2281.0(15)  | 7262.9(15)  | 3290.6(18) | 20.5(4) |
| C13B | 3523.1(15)  | 7316.8(15)  | 4016.3(17) | 18.6(3) |
| C14  | 4278.8(15)  | 6419.9(15)  | 3950.1(17) | 19.0(3) |
| C14A | 5439.8(16)  | 6657.5(15)  | 4365.3(17) | 19.0(3) |
| C15  | 6400.5(16)  | 5850.6(15)  | 4395.3(18) | 21.3(4) |
| C16  | 7394.0(16)  | 6678.6(16)  | 4664.8(17) | 20.5(4) |
| C17  | 8501.9(17)  | 6462.7(16)  | 4727.4(19) | 23.6(4) |
| C18  | 9380.5(17)  | 7171.8(17)  | 5470.0(19) | 24.7(4) |
| C19  | 6638.1(17)  | 4938.5(16)  | 5508(2)    | 24.3(4) |
| C20  | 7427.8(16)  | 5432.1(16)  | 6737.1(19) | 22.6(4) |
| C21  | 8600.9(17)  | 5220.3(16)  | 7095.9(19) | 24.7(4) |
| C22  | 9406.8(16)  | 5980.6(17)  | 7857.4(19) | 25.4(4) |
| C23  | 9056.3(16)  | 6991.4(17)  | 8268.7(18) | 24.6(4) |
| C24  | 7906.7(17)  | 7057.4(17)  | 8154.6(18) | 23.4(4) |
| C25  | 7093.9(16)  | 6284.6(16)  | 7395.8(18) | 22.2(4) |
| C26  | 5684.1(15)  | 9733.3(15)  | 5565.6(18) | 20.2(4) |
| C27  | 6364.9(17)  | 9886.8(17)  | 6824.4(19) | 23.7(4) |
| C28  | 6846.5(18)  | 10956.9(18) | 7266(2)    | 28.4(4) |
| C29  | 6650(2)     | 11886.1(18) | 6449(2)    | 34.2(5) |
| C30  | 5975(2)     | 11745.7(18) | 5200(2)    | 34.9(5) |
| C31  | 5497.7(18)  | 10670.7(17) | 4755.8(19) | 27.0(4) |
| C32  | 3879.5(15)  | 5209.2(15)  | 3562.5(18) | 20.8(4) |
| C33  | 4116.5(17)  | 4645.8(17)  | 2606.1(19) | 24.8(4) |

| Atom | <i>x</i>   | <i>y</i>   | <i>z</i>   | U(eq)   |
|------|------------|------------|------------|---------|
| C34  | 3774.2(18) | 3506.6(19) | 2302(2)    | 31.2(5) |
| C35  | 3198.6(18) | 2912.5(18) | 2946(2)    | 33.4(5) |
| C36  | 2961.6(18) | 3464.5(17) | 3900(2)    | 30.3(4) |
| C37  | 3290.0(16) | 4607.0(17) | 4199.1(19) | 23.9(4) |

**Table A3-23:** Selected bond distances (Å) for compound **4.22**.

| Atom | Atom | Length/Å | Atom | Atom | Length/Å |
|------|------|----------|------|------|----------|
| C1   | C2   | 1.587(3) | C13B | C14  | 1.426(2) |
| C1   | C23  | 1.509(3) | C14  | C14A | 1.384(3) |
| C2   | C3   | 1.514(3) | C14  | C32  | 1.501(2) |
| C3   | C4   | 1.399(3) | C14A | C15  | 1.514(3) |
| C3   | C18  | 1.399(3) | C15  | C16  | 1.512(3) |
| C4   | C4A  | 1.395(3) | C15  | C19  | 1.599(3) |
| C4A  | C4B  | 1.483(2) | C16  | C17  | 1.386(3) |
| C4A  | C16  | 1.410(3) | C17  | C18  | 1.390(3) |
| C4B  | C5   | 1.389(2) | C19  | C20  | 1.510(3) |
| C4B  | C14A | 1.413(2) | C20  | C21  | 1.397(3) |
| C5   | C5A  | 1.430(3) | C20  | C25  | 1.395(3) |
| C5   | C26  | 1.502(2) | C21  | C22  | 1.385(3) |
| C5A  | C5B  | 1.483(2) | C22  | C23  | 1.391(3) |
| C5A  | C13B | 1.424(2) | C23  | C24  | 1.400(3) |
| C5B  | C6   | 1.413(3) | C24  | C25  | 1.398(3) |
| C5B  | C9A  | 1.418(3) | C26  | C27  | 1.396(3) |
| C6   | C7   | 1.376(3) | C26  | C31  | 1.392(3) |
| C7   | C8   | 1.386(3) | C27  | C28  | 1.392(3) |
| C8   | C9   | 1.380(3) | C28  | C29  | 1.389(3) |
| C9   | C9A  | 1.399(3) | C29  | C30  | 1.383(3) |
| C9A  | C9B  | 1.462(3) | C30  | C31  | 1.396(3) |
| C9B  | C10  | 1.411(3) | C32  | C33  | 1.396(3) |
| C9B  | C13A | 1.403(3) | C32  | C37  | 1.397(3) |
| C10  | C11  | 1.376(3) | C33  | C34  | 1.393(3) |
| C11  | C12  | 1.394(3) | C34  | C35  | 1.386(3) |
| C12  | C13  | 1.382(3) | C35  | C36  | 1.387(3) |
| C13  | C13A | 1.413(3) | C36  | C37  | 1.392(3) |
| C13A | C13B | 1.477(2) |      |      |          |

**Table A3-24:** Selected bond angles (°) for compound **4.22**.

| Atom | Atom | Atom | Angle/°    | Atom | Atom | Atom | Angle/°    |
|------|------|------|------------|------|------|------|------------|
| C23  | C1   | C2   | 112.55(17) | C13B | C14  | C32  | 122.68(16) |
| C3   | C2   | C1   | 112.12(16) | C14A | C14  | C13B | 118.14(16) |

| Atom | Atom | Atom | Angle/°    | Atom | Atom | Atom | Angle/°    |
|------|------|------|------------|------|------|------|------------|
| C4   | C3   | C2   | 119.09(18) | C14A | C14  | C32  | 118.93(15) |
| C18  | C3   | C2   | 121.00(17) | C4B  | C14A | C15  | 110.53(16) |
| C18  | C3   | C4   | 118.28(17) | C14  | C14A | C4B  | 121.71(16) |
| C4A  | C4   | C3   | 119.91(17) | C14  | C14A | C15  | 127.75(16) |
| C4   | C4A  | C4B  | 132.05(17) | C14A | C15  | C19  | 110.14(15) |
| C4   | C4A  | C16  | 119.01(17) | C16  | C15  | C14A | 101.61(14) |
| C16  | C4A  | C4B  | 107.98(16) | C16  | C15  | C19  | 110.72(15) |
| C5   | C4B  | C4A  | 131.95(16) | C4A  | C16  | C15  | 109.86(16) |
| C5   | C4B  | C14A | 120.52(16) | C17  | C16  | C4A  | 120.02(17) |
| C14A | C4B  | C4A  | 107.46(15) | C17  | C16  | C15  | 129.09(17) |
| C4B  | C5   | C5A  | 118.86(16) | C16  | C17  | C18  | 118.78(18) |
| C4B  | C5   | C26  | 118.04(16) | C17  | C18  | C3   | 120.95(17) |
| C5A  | C5   | C26  | 122.92(16) | C20  | C19  | C15  | 111.32(15) |
| C5   | C5A  | C5B  | 123.47(16) | C21  | C20  | C19  | 118.24(18) |
| C13B | C5A  | C5   | 119.17(16) | C25  | C20  | C19  | 123.27(17) |
| C13B | C5A  | C5B  | 117.23(16) | C25  | C20  | C21  | 116.98(18) |
| C6   | C5B  | C5A  | 122.48(17) | C22  | C21  | C20  | 121.56(18) |
| C6   | C5B  | C9A  | 116.78(17) | C21  | C22  | C23  | 120.08(18) |
| C9A  | C5B  | C5A  | 120.34(17) | C22  | C23  | C1   | 120.63(18) |
| C7   | C6   | C5B  | 122.1(2)   | C22  | C23  | C24  | 116.99(18) |
| C6   | C7   | C8   | 120.6(2)   | C24  | C23  | C1   | 120.99(18) |
| C9   | C8   | C7   | 118.80(18) | C25  | C24  | C23  | 121.10(18) |
| C8   | C9   | C9A  | 121.78(19) | C20  | C25  | C24  | 119.76(18) |
| C5B  | C9A  | C9B  | 119.32(17) | C27  | C26  | C5   | 121.58(17) |
| C9   | C9A  | C5B  | 119.88(18) | C31  | C26  | C5   | 119.62(17) |
| C9   | C9A  | C9B  | 120.78(18) | C31  | C26  | C27  | 118.79(17) |
| C10  | C9B  | C9A  | 120.98(18) | C28  | C27  | C26  | 120.78(19) |
| C13A | C9B  | C9A  | 119.39(17) | C29  | C28  | C27  | 119.8(2)   |
| C13A | C9B  | C10  | 119.50(18) | C30  | C29  | C28  | 119.94(19) |
| C11  | C10  | C9B  | 121.12(18) | C29  | C30  | C31  | 120.2(2)   |
| C10  | C11  | C12  | 119.73(18) | C26  | C31  | C30  | 120.43(19) |
| C13  | C12  | C11  | 120.02(19) | C33  | C32  | C14  | 121.76(17) |
| C12  | C13  | C13A | 121.31(19) | C33  | C32  | C37  | 118.55(17) |
| C9B  | C13A | C13  | 118.25(17) | C37  | C32  | C14  | 119.65(17) |
| C9B  | C13A | C13B | 120.11(17) | C34  | C33  | C32  | 120.40(19) |
| C13  | C13A | C13B | 121.12(16) | C35  | C34  | C33  | 120.6(2)   |
| C5A  | C13B | C13A | 118.44(16) | C34  | C35  | C36  | 119.35(19) |
| C5A  | C13B | C14  | 119.78(16) | C35  | C36  | C37  | 120.3(2)   |
| C14  | C13B | C13A | 121.58(16) | C36  | C37  | C32  | 120.76(19) |

**Table A3-25:** Selected torsion angles (°) for compound **4.22**.

| <b>A</b> | <b>B</b> | <b>C</b> | <b>D</b> | <b>Angle/°</b> | <b>A</b> | <b>B</b> | <b>C</b> | <b>D</b> | <b>Angle/°</b> |
|----------|----------|----------|----------|----------------|----------|----------|----------|----------|----------------|
| C1       | C2       | C3       | C4       | 62.7(2)        | C10      | C9B      | C13A     | C13B     | 175.21(17)     |
| C1       | C2       | C3       | C18      | -102.5(2)      | C10      | C11      | C12      | C13      | 0.3(3)         |
| C1       | C23      | C24      | C25      | 151.39(19)     | C11      | C12      | C13      | C13A     | 0.2(3)         |
| C2       | C1       | C23      | C22      | 60.2(2)        | C12      | C13      | C13A     | C9B      | -2.1(3)        |
| C2       | C1       | C23      | C24      | -105.9(2)      | C12      | C13      | C13A     | C13B     | -173.82(17)    |
| C2       | C3       | C4       | C4A      | -150.57(18)    | C13      | C13A     | C13B     | C5A      | 152.31(18)     |
| C2       | C3       | C18      | C17      | 150.94(19)     | C13      | C13A     | C13B     | C14      | -22.5(3)       |
| C3       | C4       | C4A      | C4B      | 165.70(18)     | C13A     | C9B      | C10      | C11      | -3.0(3)        |
| C3       | C4       | C4A      | C16      | -1.6(3)        | C13A     | C13B     | C14      | C14A     | 162.63(17)     |
| C4       | C3       | C18      | C17      | -14.4(3)       | C13A     | C13B     | C14      | C32      | -23.1(3)       |
| C4       | C4A      | C4B      | C5       | 13.8(3)        | C13B     | C5A      | C5B      | C6       | 161.16(18)     |
| C4       | C4A      | C4B      | C14A     | -163.11(19)    | C13B     | C5A      | C5B      | C9A      | -11.4(2)       |
| C4       | C4A      | C16      | C15      | 156.27(17)     | C13B     | C14      | C14A     | C4B      | 0.7(3)         |
| C4       | C4A      | C16      | C17      | -13.2(3)       | C13B     | C14      | C14A     | C15      | 179.61(17)     |
| C4A      | C4B      | C5       | C5A      | -179.99(18)    | C13B     | C14      | C32      | C33      | 127.1(2)       |
| C4A      | C4B      | C5       | C26      | 4.7(3)         | C13B     | C14      | C32      | C37      | -55.3(3)       |
| C4A      | C4B      | C14A     | C14      | -175.52(17)    | C14      | C14A     | C15      | C16      | 168.08(18)     |
| C4A      | C4B      | C14A     | C15      | 5.4(2)         | C14      | C14A     | C15      | C19      | -74.5(2)       |
| C4A      | C16      | C17      | C18      | 13.9(3)        | C14      | C32      | C33      | C34      | 177.41(18)     |
| C4B      | C4A      | C16      | C15      | -13.8(2)       | C14      | C32      | C37      | C36      | -176.74(18)    |
| C4B      | C4A      | C16      | C17      | 176.76(17)     | C14A     | C4B      | C5       | C5A      | -3.4(3)        |
| C4B      | C5       | C5A      | C5B      | 167.95(17)     | C14A     | C4B      | C5       | C26      | -178.71(16)    |
| C4B      | C5       | C5A      | C13B     | -7.9(3)        | C14A     | C14      | C32      | C33      | -58.7(2)       |
| C4B      | C5       | C26      | C27      | -77.0(2)       | C14A     | C14      | C32      | C37      | 118.93(19)     |
| C4B      | C5       | C26      | C31      | 101.9(2)       | C14A     | C15      | C16      | C4A      | 16.2(2)        |
| C4B      | C14A     | C15      | C16      | -12.9(2)       | C14A     | C15      | C16      | C17      | -175.6(2)      |
| C4B      | C14A     | C15      | C19      | 104.45(17)     | C14A     | C15      | C19      | C20      | -84.09(19)     |
| C5       | C4B      | C14A     | C14      | 7.1(3)         | C15      | C16      | C17      | C18      | -153.2(2)      |
| C5       | C4B      | C14A     | C15      | -171.92(16)    | C15      | C19      | C20      | C21      | -93.6(2)       |
| C5       | C5A      | C5B      | C6       | -14.7(3)       | C15      | C19      | C20      | C25      | 71.9(2)        |
| C5       | C5A      | C5B      | C9A      | 172.71(17)     | C16      | C4A      | C4B      | C5       | -177.88(19)    |
| C5       | C5A      | C13B     | C13A     | -159.14(16)    | C16      | C4A      | C4B      | C14A     | 5.2(2)         |
| C5       | C5A      | C13B     | C14      | 15.7(3)        | C16      | C15      | C19      | C20      | 27.5(2)        |
| C5       | C26      | C27      | C28      | 179.07(18)     | C16      | C17      | C18      | C3       | -0.1(3)        |
| C5       | C26      | C31      | C30      | -179.5(2)      | C18      | C3       | C4       | C4A      | 15.0(3)        |
| C5A      | C5       | C26      | C27      | 107.9(2)       | C19      | C15      | C16      | C4A      | -100.77(18)    |
| C5A      | C5       | C26      | C31      | -73.3(2)       | C19      | C15      | C16      | C17      | 67.4(3)        |
| C5A      | C5B      | C6       | C7       | -173.89(19)    | C19      | C20      | C21      | C22      | 152.00(19)     |
| C5A      | C5B      | C9A      | C9       | 173.25(17)     | C19      | C20      | C25      | C24      | -150.93(18)    |
| C5A      | C5B      | C9A      | C9B      | -8.3(3)        | C20      | C21      | C22      | C23      | -1.0(3)        |
| C5A      | C13B     | C14      | C14A     | -12.1(3)       | C21      | C20      | C25      | C24      | 14.8(3)        |
| C5A      | C13B     | C14      | C32      | 162.17(17)     | C21      | C22      | C23      | C1       | -151.00(19)    |

| <b>A</b> | <b>B</b> | <b>C</b> | <b>D</b> | <b>Angle/°</b> | <b>A</b> | <b>B</b> | <b>C</b> | <b>D</b> | <b>Angle/°</b> |
|----------|----------|----------|----------|----------------|----------|----------|----------|----------|----------------|
| C5B      | C5A      | C13B     | C13A     | 24.8(2)        | C21      | C22      | C23      | C24      | 15.7(3)        |
| C5B      | C5A      | C13B     | C14      | -160.34(16)    | C22      | C23      | C24      | C25      | -15.2(3)       |
| C5B      | C6       | C7       | C8       | 0.8(3)         | C23      | C1       | C2       | C3       | 22.4(2)        |
| C5B      | C9A      | C9B      | C10      | -161.52(17)    | C23      | C24      | C25      | C20      | -0.1(3)        |
| C5B      | C9A      | C9B      | C13A     | 14.3(3)        | C25      | C20      | C21      | C22      | -14.4(3)       |
| C6       | C5B      | C9A      | C9       | 0.3(3)         | C26      | C5       | C5A      | C5B      | -17.0(3)       |
| C6       | C5B      | C9A      | C9B      | 178.78(18)     | C26      | C5       | C5A      | C13B     | 167.22(17)     |
| C6       | C7       | C8       | C9       | 0.4(3)         | C26      | C27      | C28      | C29      | 0.0(3)         |
| C7       | C8       | C9       | C9A      | -1.2(3)        | C27      | C26      | C31      | C30      | -0.6(3)        |
| C8       | C9       | C9A      | C5B      | 0.8(3)         | C27      | C28      | C29      | C30      | 0.1(3)         |
| C8       | C9       | C9A      | C9B      | -177.62(18)    | C28      | C29      | C30      | C31      | -0.5(4)        |
| C9       | C9A      | C9B      | C10      | 17.0(3)        | C29      | C30      | C31      | C26      | 0.8(4)         |
| C9       | C9A      | C9B      | C13A     | -167.20(17)    | C31      | C26      | C27      | C28      | 0.2(3)         |
| C9A      | C5B      | C6       | C7       | -1.1(3)        | C32      | C14      | C14A     | C4B      | -173.75(17)    |
| C9A      | C9B      | C10      | C11      | 172.87(18)     | C32      | C14      | C14A     | C15      | 5.1(3)         |
| C9A      | C9B      | C13A     | C13      | -172.49(17)    | C32      | C33      | C34      | C35      | -0.3(3)        |
| C9A      | C9B      | C13A     | C13B     | -0.7(3)        | C33      | C32      | C37      | C36      | 1.0(3)         |
| C9B      | C10      | C11      | C12      | 1.1(3)         | C33      | C34      | C35      | C36      | 0.2(3)         |
| C9B      | C13A     | C13B     | C5A      | -19.2(2)       | C34      | C35      | C36      | C37      | 0.6(3)         |
| C9B      | C13A     | C13B     | C14      | 165.96(17)     | C35      | C36      | C37      | C32      | -1.1(3)        |
| C10      | C9B      | C13A     | C13      | 3.4(3)         | C37      | C32      | C33      | C34      | -0.3(3)        |

## Chapter 5: Synthetic Utility of a [2.2]Paracyclophane-derived Tetralone and Indanone

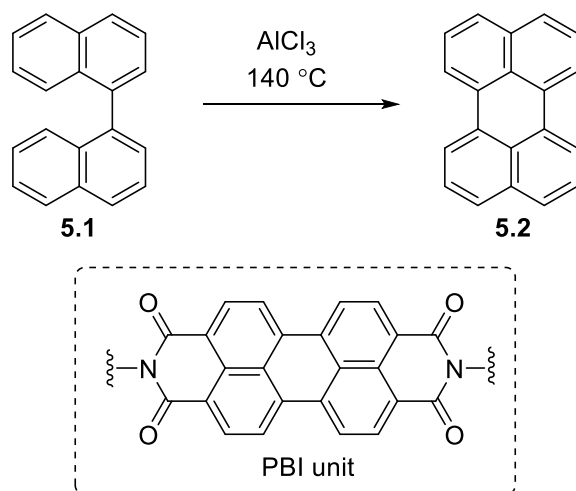
### 5.1 Introduction

The Scholl reaction of polybenzenoid hydrocarbons is a highly efficient method for forging multiple carbon–carbon bonds in a single operation, leading to the construction of small to large-sized planar and non-planar polynuclear aromatic hydrocarbons (PAH).<sup>1</sup> A number of theoretical and experimental studies have been conducted to elucidate the mechanism of the Scholl reaction.<sup>2</sup> Studies have led to primarily two mechanistic pathways, namely, radical-cation and arenium ion pathways, for the Scholl reaction. The intermediates in a Scholl reaction, namely, radical cation and arenium ion intermediates have similar reactivity, which presumably makes it difficult to comment on the exact mechanism of the Scholl reaction. Scholl reactions have occasionally surprised chemists with unexpected reaction outcomes, such as those arising from aryl group migration,<sup>3</sup> skeletal rearrangements.<sup>4</sup>

Perylene (**5.2**) (see structure in Scheme 5.1, *vide infra*) and its derivatives have gained increasing popularity among the scientific community owing to their application as dyes and in materials science.<sup>5</sup> The X-ray structure of **5.2** shows longer *peri*-bond lengths than the other bond lengths.<sup>6</sup> Consequently, **5.2** can be considered as two *peri*-conjoined naphthalene units. As expected, **5.2** exhibits characteristics (<sup>1</sup>H NMR chemical shifts) and reactivity (electrophilic aromatic substitution reactions, such as nitration)<sup>7</sup> that are typical for aromatic compounds.<sup>8</sup> Perylene (**5.2**) is a lucrative candidate for optoelectronic applications due to its high absorbance in the UV/vis region, small Stokes shift, and high quantum yield ( $\phi = 0.98$  in the absence of air).<sup>9</sup>

In 1910, Scholl and co-workers synthesized perylene (**5.2**) for the first time by the Scholl reaction of 1,1'-binaphthalene (**5.1**) in the presence of AlCl<sub>3</sub> as oxidant at high temperature (Scheme 5.1).<sup>10</sup> Although a few examples of cyclophanes bearing the perylene bisimide (PBI)

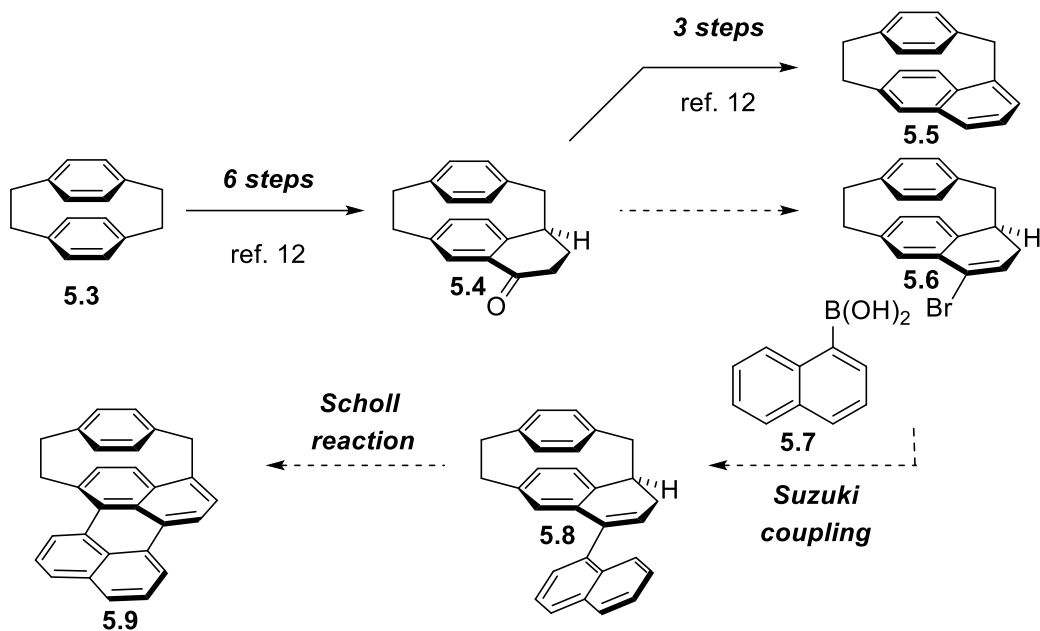
unit (Scheme 5.1, inset) are reported in the literature,<sup>11</sup> examples of cyclophanes with the bare perylene unit could not be found. In this regard, bearing the intriguing photophysical properties in mind, the synthesis of cyclophanes with perylene unit(s) would be highly desirable.



**Scheme 5.1:** Scholl reaction of 1,1'-binaphthalene (**5.1**) for the synthesis of perylene (**5.2**). Inset: structure of the perylene bisimide (PBI) unit.

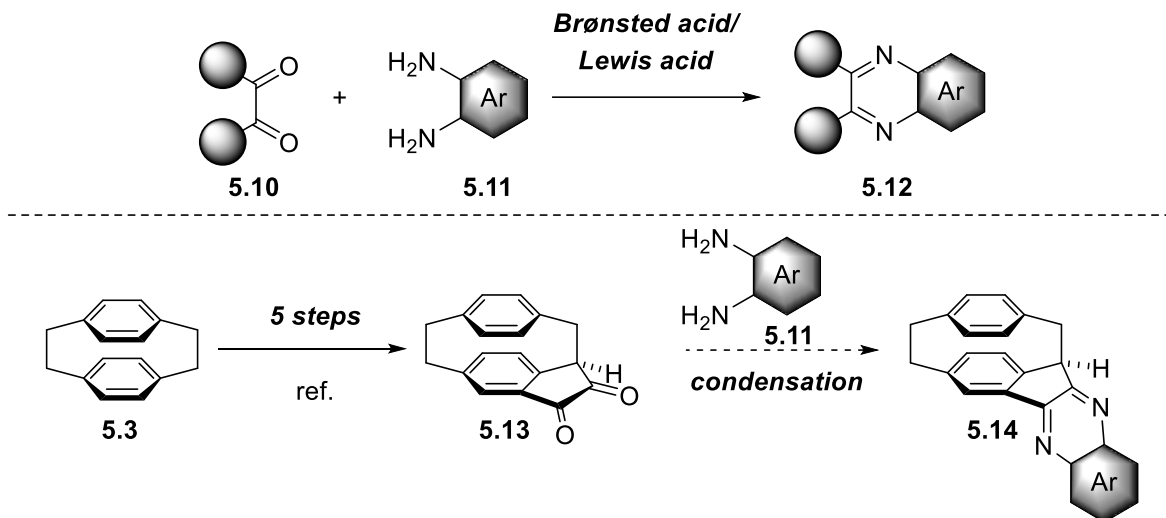
## 5.2 Objective

$\alpha$ -Tetralone **5.4**, which featured as a key intermediate in the synthesis of [2.1]cyclophane **5.5**,<sup>12</sup> seemed to offer an opportunity for the three-step synthesis of a [2.1]cyclophane featuring perylene as one of its aromatic systems. Conversion of tetralone **5.4** to vinyl bromide **5.6** followed by the Suzuki coupling of **5.6** with naphthalene-1-boronic acid (**5.7**) would furnish dihydronaphthalene **5.8** (Scheme 5.2). Finally, the cyclodehydrogenation (Scholl) reaction of **5.8** could provide the targeted [2.1]cyclophane **5.9**.



**Scheme 5.2:** Intended synthesis of [2](1,4)perylene[1]paracyclophane **5.9**.

Quinoxaline derivatives have gained considerable attention in the areas of both materials<sup>13</sup> and biological sciences.<sup>14</sup> One of the major reasons for their widespread application across various fields is due to their easy synthetic accessibility. The most widely used method to construct a quinoxaline framework is by a condensation reaction between a 1,2-diketone (**5.10**) and an appropriate 1,2-arylenediamine (**5.11**), leading to the formation of an quinoxaline derivative (**5.12**) (Scheme 5.3).<sup>15</sup> Dione **5.13** could serve as the 1,2-diketone component in the reactions with a set of 1,2-diarylamines **5.11** to afford [2.2]paracyclophane/quinoxaline hybrids **5.14**. Cyclophanes **5.14** would represent interesting examples of chiral [2.2]paracyclophane derivatives containing an electron-deficient quinoxaline moiety. In particular, it would be interesting to know information about the acidity ( $pK_a$ ) of the methine proton by UV/vis and NMR titration studies. As cyclophanes **5.14** can be considered as a hybrid containing an electron-withdrawing (quinoxaline moiety) and a moderately electron rich ([2.2]paracyclophane moiety), its electronic properties would be of interest.

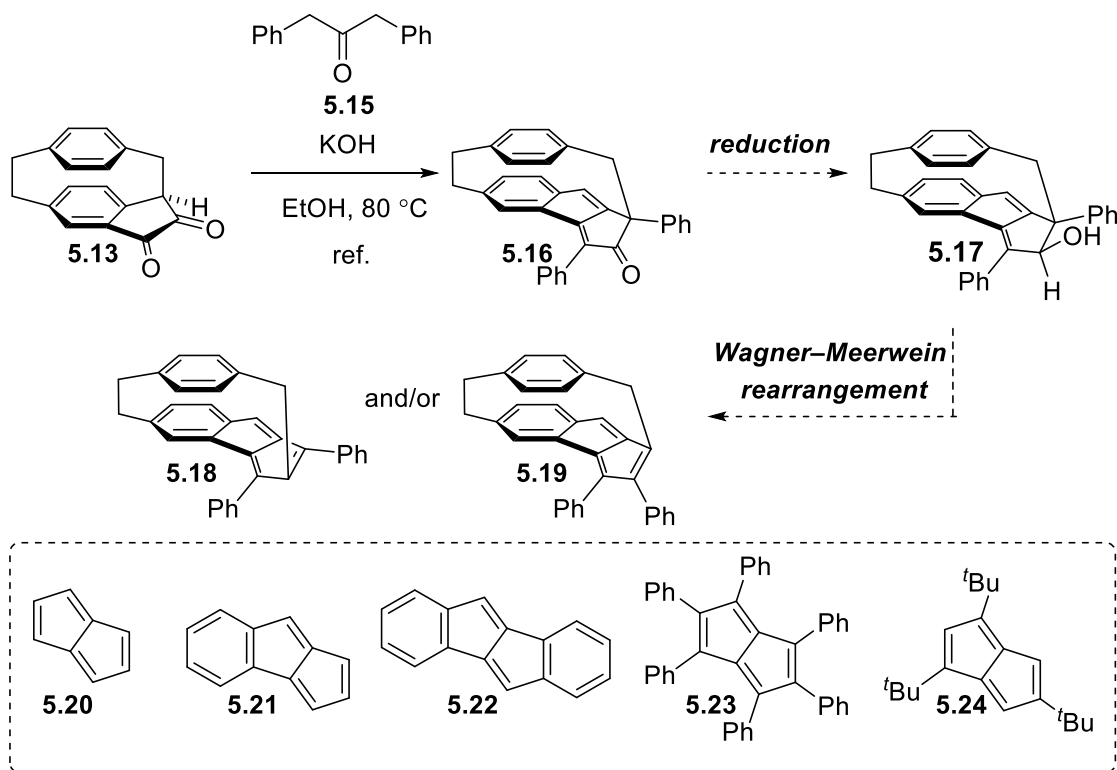


**Scheme 5.3:** Proposed route to [2.2]paracyclophane/quinoxaline hybrids **5.14**.

Pentalene (**5.20**), a hydrocarbon composed of two fused cyclopentadiene rings, is a  $8\pi$  electron system, which is antiaromatic according to Hückel's rule (Scheme 5.4, inset, *vide infra*). Compound **5.20** is a thermally unstable compound, which undergoes dimerization above  $-198\text{ }^{\circ}\text{C}$ .<sup>16</sup> Placement of bulky substituents along the periphery of the pentalene moiety can lead to significant kinetic stabilization as observed for hexaphenylpentalene (**5.23**)<sup>17</sup> and 1,3,5-tri-*tert*-butylpentalene (**5.24**).<sup>18</sup> Another way to enhance the stabilization of the pentalene moiety is to fuse benzene ring(s) to it. Benzopentalene (**5.21**) itself undergoes dimerization at room temperature but is stable at temperatures as high as  $-70\text{ }^{\circ}\text{C}$ .<sup>19</sup> However, introduction of substituents either on the alkene or aromatic positions in the benzopentalene moiety gives rise to derivatives with improved stability.<sup>20</sup> Dibenzo[*a,e*]pentalene (**5.22**) and its derivatives are fairly bench-stable stable  $\pi$ -conjugated compounds with narrow HOMO–LUMO gaps.<sup>21</sup> Presumably, owing to the greater stability and greater ease of handling of dibenzopentalenes, the chemistry of dibenzopentalenes is well-explored compared to benzopentalenes.

Cyclophane **5.16**, isolated serendipitously from an intended double aldol condensation between dione **5.13** and 1,3-diphenylacetone (**5.15**) by the rearrangement<sup>22</sup> of the *in-situ* generated

desired cyclopentadienone (not shown) appeared to offer an opportunity to prepare benzopentalenophanes **5.18** and/or **5.19** by a two-step protocol consisting of reduction (conversion of **5.16** to allylic alcohol **5.17**) and an ensuing Wagner–Meerwein rearrangement (Scheme 5.4). As opposed to a planar benzopentalene moiety, the forced non-planar geometry of the benzopentalene moiety in compounds **5.18** and **5.19** would be expected to decrease the antiaromatic character of the benzopentalene moiety. In addition, the top face of the tetra-substituted benzopentalene moiety in **5.18** and **5.19** is sterically shielded by a 1,4-disubstituted benzene ring. Overall, compounds **5.18** and **5.19** might be sufficiently stable to be isolated and characterized, which would enable the study their photophysical and electrochemical behavior.



**Scheme 5.4:** Proposed synthesis of benzopentalenophanes. Inset: structures of pentalene (**5.20**), benzopentalene (**5.21**), and dibenzo[*a,e*]pentalene (**5.22**), and pentalenes **5.23** and **5.24**.

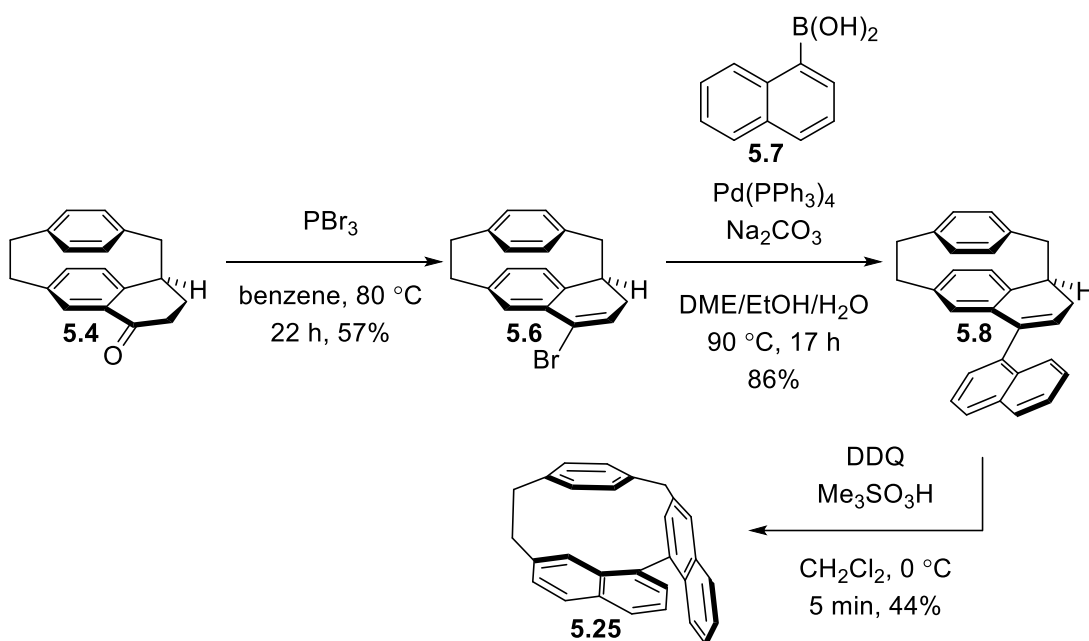
### 5.3 Results and Discussion

### 5.3.1 Synthesis

#### 5.3.1.1 Attempted Synthesis of Cyclophane 5.9

$\alpha$ -Tetralone **5.4** was synthesized from commercially available [2.2]paracyclophane **5.3** over six steps following the recently reported protocol.<sup>12</sup> In 2005, Panda and co-workers developed a mild method for the preparation of 4-bromo-1,2-dihydronaphthalenes from the corresponding  $\alpha$ -tetralone derivatives by using PBr<sub>3</sub>.<sup>23</sup> To accomplish the first step toward the synthesis of the perylene moiety bearing cyclophane **5.9**, conversion of **5.4** to vinyl bromide **5.6** was necessary (see Scheme 5.2, *vide supra*). Reaction of tetralone **5.4** with PBr<sub>3</sub> under heating conditions underwent smoothly to furnish the required vinyl bromide **5.6** (57%) (Scheme 5.5). Vinyl bromides are an important class of coupling partners in the Suzuki reaction.<sup>24</sup> By harnessing the reactivity of the vinyl bromide **5.6**, a Suzuki cross-coupling between **5.6** and naphthalene-1-boronic acid (**5.7**) was carried out. The Suzuki coupling between **5.6** and **5.7** in the presence of a catalytic amount of Pd(PPh<sub>3</sub>)<sub>4</sub> afforded dihydronaphthalene **5.8** (86%), thereby accomplishing the installment of the required naphthalene moiety. Finally, a Scholl reaction was attempted to access the targeted [2.1]cyclophane **5.9** (see Scheme 5.2, *vide supra*). Treatment of **5.8** with DDQ/Me<sub>3</sub>SO<sub>3</sub>H in CH<sub>2</sub>Cl<sub>2</sub> (Rathore's Scholl conditions)<sup>25</sup> resulted in the consumption of the starting material (**5.8**) within 5 min and the formation of one major mobile spot. Column chromatography of the product mixture on silica gel afforded a white solid. The <sup>1</sup>H NMR spectrum (Appendix 4) did not match what was expected for the perylenophane **5.9**. In particular, two slightly broad 1H singlets at  $\delta$  7.74 and 6.08 ppm, and one 1H doublet at  $\delta$  6.69 ( $J = 1.8$  Hz) ppm stood out as being inconsistent with **5.9**. The small coupling constant of 1.8 Hz for the doublet at  $\delta$  6.69 is typical for a *meta*-coupled aromatic proton. The slight broadening of the two singlets also hinted at *meta* coupling. The HMRS spectrum shows a peak at  $m/z = 370.1715$ , which again

did not match the calculated value for the desired cyclophane **5.9** ( $m/z = 368.1565$ ). Based on the available 1D, 2D NMR (see Appendix 4 for COSY, HSQC, NOESY spectra), and HRMS data, the identity of the solid in question could not be determined. Hence, for an unambiguous determination of the identity of the product, crystallographic analysis was indispensable. Crystals suitable for single-crystal X-ray diffraction (SCXRD) analysis (see Appendix 4) were grown by vapor diffusion of methanol into a saturated solution of the product in chloroform.<sup>26</sup> [2](7,3')1,1'-Binaphthaleno[1]paracyclophane (**5.25**) was identified as the unexpected product. From the substitution patterns of the two naphthalene moieties in **5.25**, it was clear that under the reaction conditions the skeleton of the precursor **5.8** had undergone rearrangement. A possible mechanism for the formation of **5.25** in Scheme 5.9 (*vide infra*).

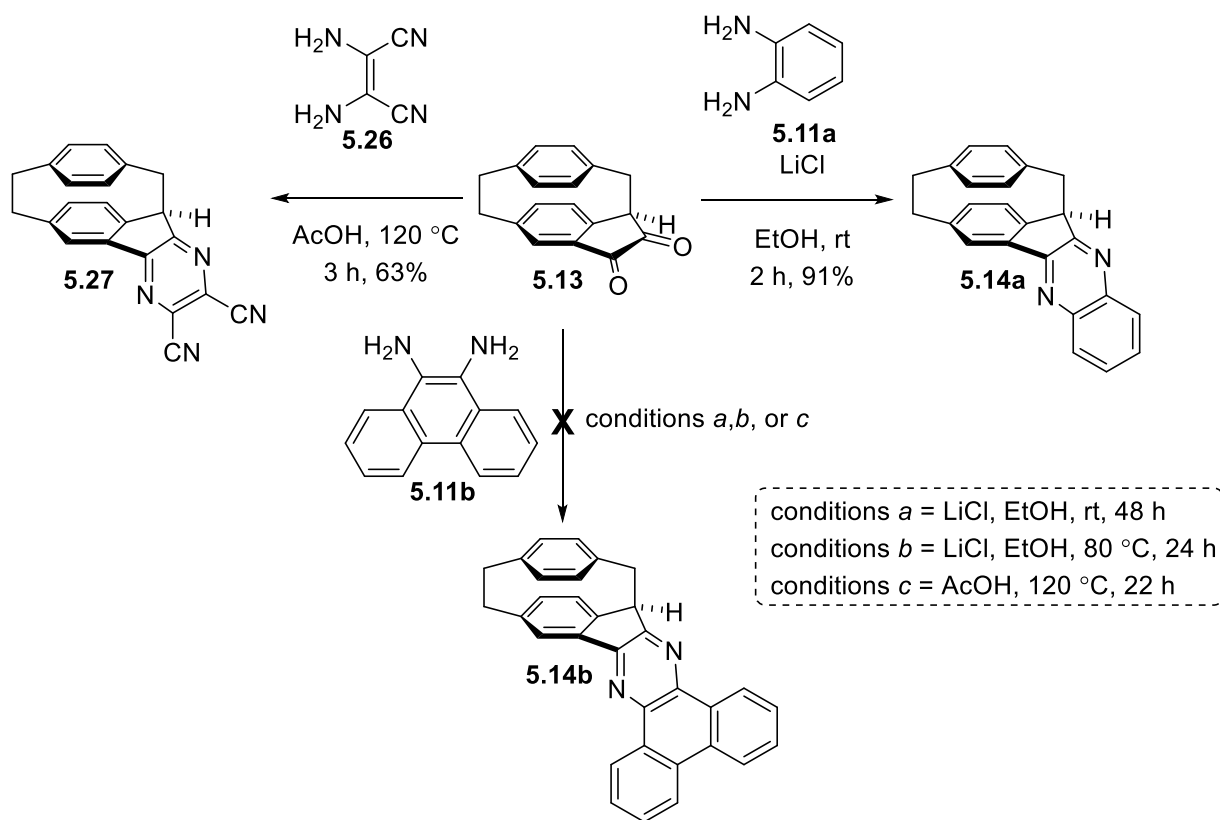


**Scheme 5.5:** Serendipitous synthesis of cyclophane **5.25** over three steps from  $\alpha$ -tetralone **5.4**.

### 5.3.1.2 Synthesis of Quinoxalines **5.14a** and **5.27**

In 2012, Karami and co-workers reported a mild protocol for the condensation of 1,2-diketones and 1,2-aryldiamines in the presence of LiCl as catalyst to afford quinoxalines.<sup>27</sup> Due to the

advantages of operational simplicity and simple work-up procedure, the reaction conditions of Karami and co-workers were initially considered for the synthesis of [2.2]paracyclophane/quinoxaline hybrids. Condensation of dione **5.13** with the quintessential 1,2-diarylamine, *o*-phenylenediamine (**5.11a**), proceeded smoothly under the mild reaction conditions to provide quinoxaline **5.14a** in an excellent yield of 91% (Scheme 5.6). The methine proton in **5.14a** resonates at  $\delta$ 4.66 ppm (d,  $J = 8.1$  Hz), which is downfield shifted by 0.58 ppm from that in dione **5.13** [4.08 ppm (d,  $J = 9.2$  Hz)].<sup>22</sup>



**Scheme 5.6:** Successful and attempted condensation reactions of dione **5.13** with different diamines.

Tetrapyrazinoporphyrazines are a family of macrocycles that are known to form complexes with different metals.<sup>28</sup> Tetrapyrazinoporphyrazines and their alkali metal complexes are promising candidates for optoelectronic applications.<sup>29</sup> 2,3-Dicyanopyrazines are valuable

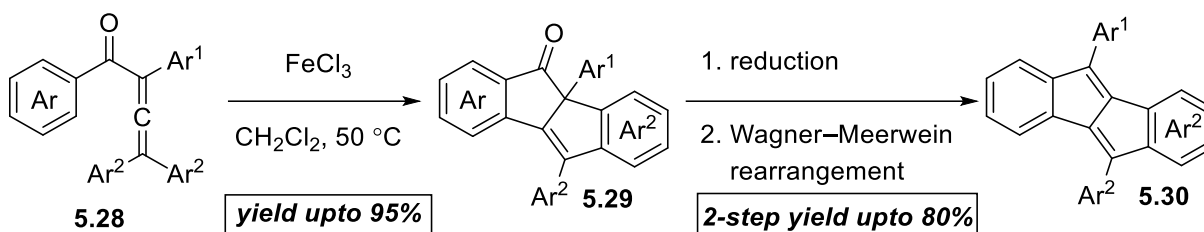
precursors for the synthesis of tetrapyrazinoporphyrins. It was envisaged that dione **5.13** could engage in a condensation reaction with diaminomaleonitrile (**5.26**) to afford [2.2]paracyclophane/pyrazine hybrid **5.27** (Scheme 5.6, *vide supra*). As compound **5.27** possesses a 2,3-dicyanopyrazine unit, compound **5.27** could then serve as a potential precursor to hitherto unknown [2.2]paracyclophane bearing tetrapyrazinoporphyrins. Accordingly, an attempt was made to generate **5.27** by treatment of dione **5.13** with **5.26** in the presence of LiCl (Scheme 5.6, conditions *a*). Unfortunately, the reaction met with failure as no progress of the reaction was observed by TLC analysis. Elevation of the reaction temperature to 80 °C (Scheme 5.6, conditions *b*) was also found to be ineffective to promote the reaction. The use of harsher classical acidic conditions was then explored. Accordingly, reaction of dione **5.13** with **5.26** in AcOH afforded the desired pyrazine **5.27** in 63% yield. The methine proton in **5.27** resonates at  $\delta$  4.65 ppm (d,  $J = 7.6$  Hz), which is at essentially the same place as the corresponding methine proton of **5.14a**.

To incorporate a larger  $\pi$ -system, 9,10-diaminophenanthrene (**5.11b**) was selected as the 1,2-aryldiamine component for the synthesis of [2.2]paracyclophane/quinoxaline hybrid **5.14b**. However, despite several attempts (conditions *a*, *b*, or *c*), **5.11b** was found to be unreactive toward the condensation reaction with dione **5.13**, and thereby the synthesis of **5.14b** was not successful. The reasons for the failure of this reaction are not clear at this time.

### 5.3.1.3 Attempted Synthesis of Benzopentalenophanes **5.18** and **5.19**

In 2019, Miao, Ren, and co-workers disclosed a method consisting of Nazarov cyclization/ $4\pi$  ring closure reactions for the construction of polycyclic compounds (**5.29**) bearing indanone and indene moieties from 1,2-allenyl aryl ketones (**5.28**) in the presence of FeCl<sub>3</sub> (Scheme 5.7).<sup>30</sup> The synthetic utility of the method was demonstrated by the conversion of the polycyclic compounds

(products of the Nazarov/ $4\pi$  ring closure reactions) to unsymmetrically substituted dibenzo[*a,e*]pentalenes (**5.30**) over two steps.

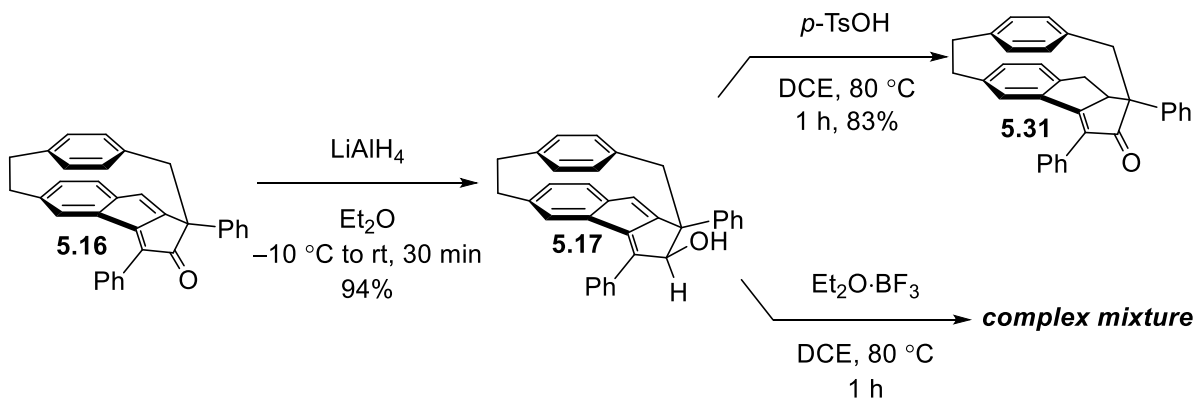


**Scheme 5.7:** Three-step transformation of allenyl aryl ketone **5.28** into dibenzopentalenes **5.30** by Miao, Ren, and co-workers.

With an aim of synthesizing benzopentalenophanes **5.18** and/or **5.19** following a similar 2-step pathway to that reported by Miao, Ren, and co-workers (see Scheme 5.7, conversion of indenones **5.29** to **5.30**), cyclophane **5.16** was first reduced with LiAlH<sub>4</sub> (Scheme 5.8). Reduction of **5.16** yielded allylic alcohol **5.17** (94%) as the sole diastereomer. It is highly likely that the reducing agent attacked from the less hindered bottom face of the carbonyl group to provide the isomer shown in Scheme 5.8. To effect a 1,2-shift of the methano bridge and/or the phenyl ring attached to the quaternary aliphatic carbon atom to afford benzopentalenophane **5.18** and/or **5.19**, respectively, compound **5.17** was exposed to *p*-TsOH. Within 1 h, consumption of the starting material was observed (TLC analysis), and the reaction was quenched with aqueous NaHCO<sub>3</sub> solution. Following column chromatography, a yellow solid was isolated. The HMRS spectrum displays a peak at  $m/z = 439.2044$ , which is 19.0166 units higher than the calculated  $m/z$  value of 420.1878 (M<sup>+</sup>) for the desired benzopentalenophanes **5.18** or **5.19**. Finally, with the assistance of 1D and 2D NMR (see Appendix 4 for COSY, HSQC spectra) experiments, the isolated product was assigned as cyclophane **5.31**, which is a partially hydrogenated product of cyclophane **5.16**. The yield for the conversion of **5.17** to **5.31** was calculated to be 83%. The <sup>1</sup>H NMR spectrum (300 MHz, CDCl<sub>3</sub>) of **5.31** displays several characteristic signals. The diastereotopic protons of

the methano bridge appears as an AX system consisting of two doublets at  $\delta$  3.53 ppm ( $J = 14.1$  Hz) and 3.02 ppm ( $J = 13.6$  Hz), the latter of which overlaps with a multiplet at  $\delta$  3.09–2.99 ppm. Another notable feature is the appearance of the ABX system, which consists of two benzylic geminal protons of the five membered ring fused to the lower benzene ring and the adjacent proton that is attached to a tertiary carbon atom. The two benzylic protons of the five membered ring resonate at  $\delta$  3.46 ppm (dd,  $J = 17.8, 8.6$  Hz) and 3.29 ppm (dd,  $J = 17.8, 4.1$  Hz). The proton attached to the tertiary carbon appears as a doublet of doublets at  $\delta$  4.00 ppm ( $J = 8.6, 4.0$  Hz), which is downfield shifted compared to all benzylic protons in **5.31**.

The use of the Lewis acid  $\text{Et}_2\text{O}\cdot\text{BF}_3$  was screened for the Wagner–Meerwein rearrangement. The reaction led to the formation of a complex mixture of several spots (TLC analysis). An attempted separation of the mixture met with failure. Unfortunately, none of the products could be identified.



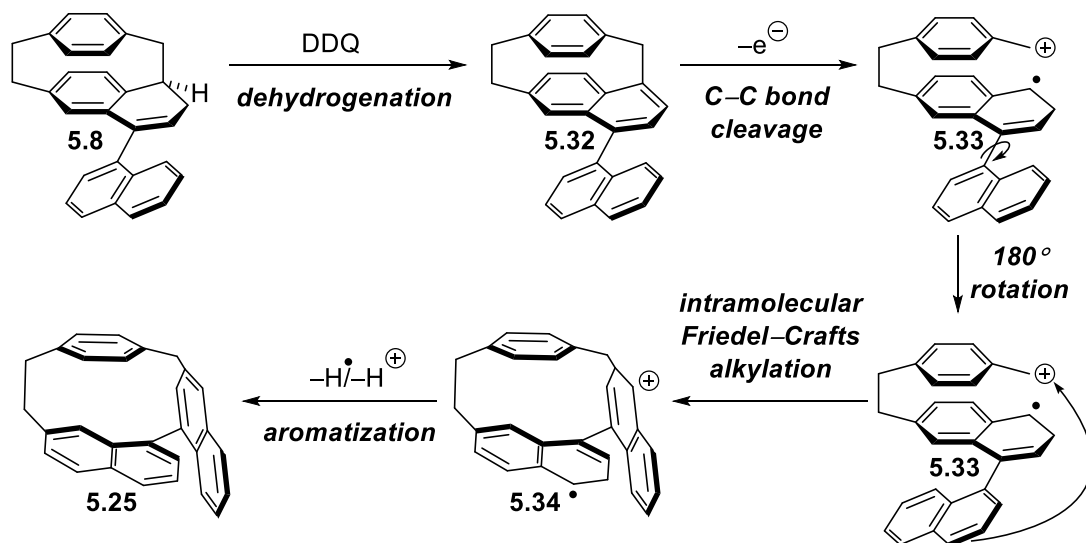
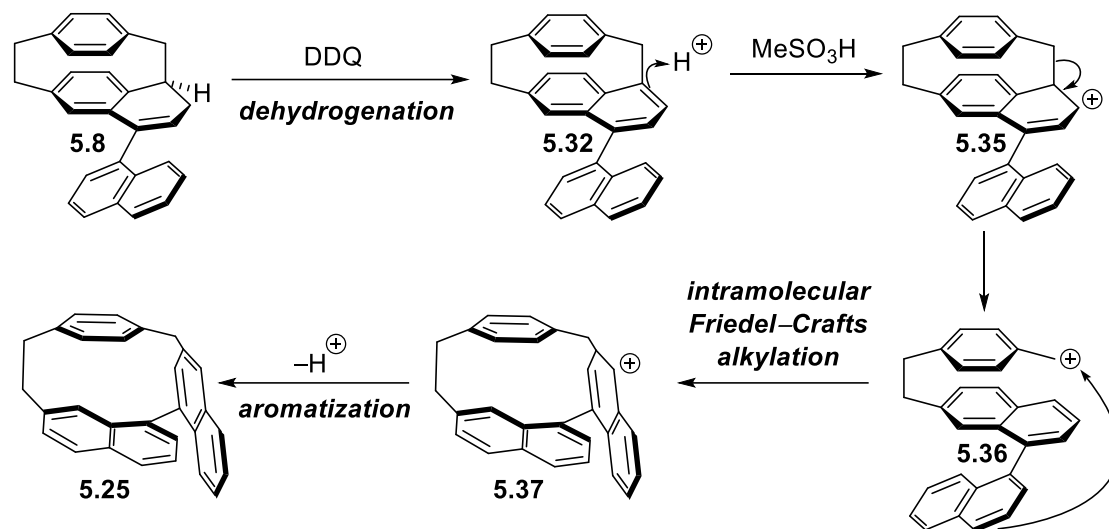
**Scheme 5.8:** Reduction of cyclophane **5.16** followed by attempted Wagner–Meerwein rearrangement under Brønsted/Lewis acidic conditions.

## 5.3.2 Proposed Reaction Mechanisms

### 5.3.2.1 Proposed Mechanism for the Formation of Cyclophane **5.25** under Scholl Conditions

Two different pathways, namely a radical-cation (Scheme 5.9, top, *vide infra*) and an arenium-ion pathway (Scheme 5.9, bottom)<sup>2</sup> have been considered for the surprising outcome (formation of cyclophane **5.25**) under the Scholl conditions.

The first step in the radical-cation pathway commences with the classical oxidation of the dihydronaphthalene moiety in **5.8** to afford [2.1]cyclophane **5.32** as an intermediate. Compound **5.32** undergoes single-electron oxidation followed by cleavage of the CH<sub>2</sub>–CH bond to furnish radical cation **5.33**. The radical cation forming step resembles to the first step of the well-known radical cation mechanistic pathway of the Scholl reaction.<sup>2</sup> Following a 180° rotation of the naphthalene moiety in **5.33** as shown in Scheme 5.9, the 3-position of the naphthalene moiety could attack the carbocationic site (benzylic) in an intramolecular fashion to afford radical cation intermediate **5.34**. Loss of a hydrogen radical and a proton gives [2.1]cyclophane **5.25**. A similar observation of a rearrangement of an oligo-phenyl-substituted [2.2]paracyclophane under Scholl conditions was made by Hopf and co-workers (see Chapter 4, Scheme 4.7).

**radical-cation pathway****arenium-ion pathway**

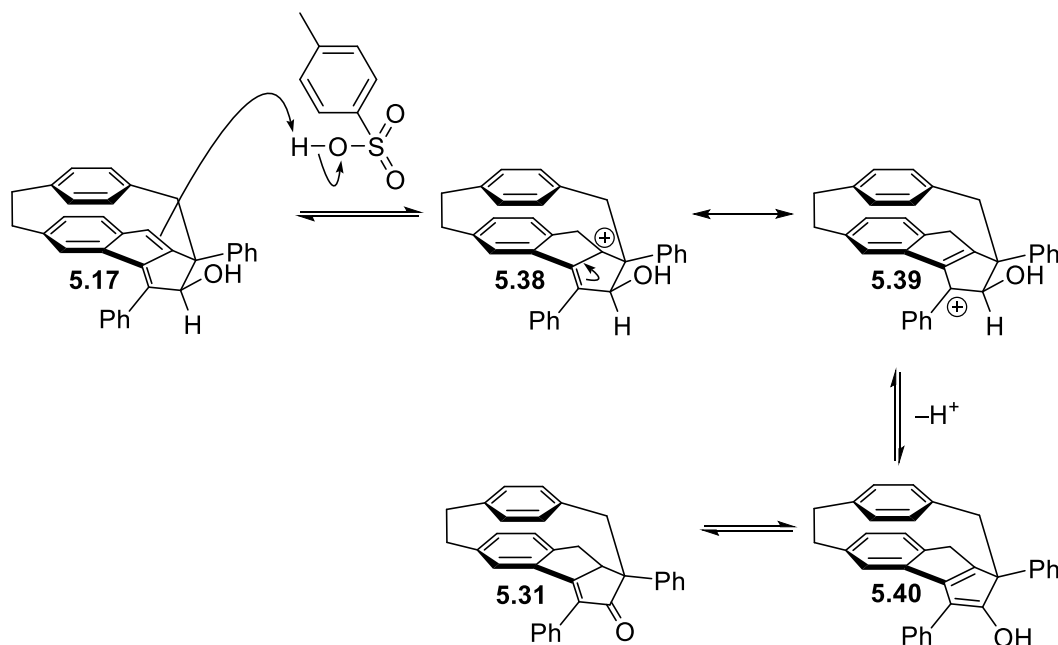
**Scheme 5.9:** Proposed pathways for the formation of cyclophane **5.25** under Scholl conditions.

Another possible pathway that could account for the formation of **5.25** from **5.8** is the arenium-ion pathway, wherein the first step mirrors that of the aforementioned radical cation pathway to afford **5.32** (Scheme 5.9, bottom, *vide supra*). Cyclophane **5.32** could undergo a retro-Friedel-Crafts ring opening reaction to produce cationic intermediate **5.36** via the intermediacy of carbocation species **5.35**. Carbocation intermediate **5.36** could undergo intramolecular Friedel-

Crafts alkylation to give carbocation intermediate **5.37**, which would collapse to [2.1]cyclophane **5.25** following loss of a proton.

### 5.3.2.2 Proposed Mechanism for the Formation of Cyclophane **5.31** under Acidic Conditions

The endocyclic double bond of the five membered ring fused to the lower benzene ring in cyclophane **5.17** could undergo protonation to afford allylic carbocation species **5.38** (Scheme 5.10). Translocation of the double bond in **5.38** would lead to presumably more stable benzylic/allylic carbocation intermediate **5.39**, which is a canonical structure of **5.38**. Loss of a proton would result in the formation of the intermediate cyclophane **5.40**. Intermediate **5.40** upon tautomerization would afford cyclophane **5.31**.



**Scheme 5.10:** Possible mechanism for the formation of cyclophane **5.31** from cyclophane **5.17** in the presence of *p*-TsOH.

### 5.3.3 X-Ray Crystallographic Analysis

The methano bridge (C19) (Figure 5.1) for cyclophane **5.25** has a compressed bond angle of  $106.01(10)^\circ$ , which is close to the angle<sup>12</sup> [ $104.73(19)$ ] at the methano bridge in

[2](6,1)naphthaleno[1]paracyclophane (**5.5**). The ethano bridge has bond angles of  $114.76(11)^\circ$  (C2) and  $110.89(11)^\circ$  (C1). The bond angle at C2 is comparable to the bond angles at the ethano bridge in **5.5** [ $113.9(2)^\circ$  and  $113.7(2)^\circ$ ] and [2.2]paracyclophane (**5.3**) ( $113.7^\circ$ ).<sup>31</sup> The dihedral angle between the two average planes of the two naphthalene moieties in **5.25** is  $66.08^\circ$ , which is *ca.*  $2^\circ$  less than the analogous angle ( $68.19^\circ$ ) found from the crystal structure<sup>32</sup> of 1,1'-binaphthalene (**5.1**).

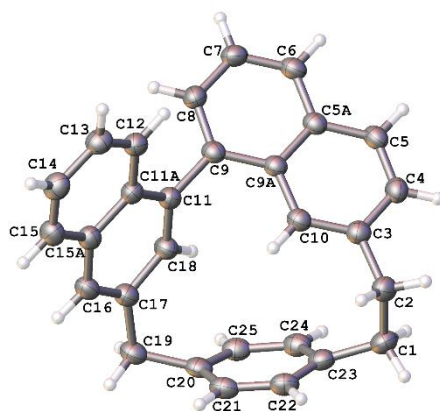


**Figure 5.1:** X-ray crystal structure of **5.25** (non-hydrogen atoms are represented by displacement ellipsoids at the 50% probability level).

As discussed in Chapter 1, the degree of distortion from planarity of bent benzene rings can be determined by two parameters  $\alpha$  and  $\beta$ . The sum of these two parameters ( $\alpha+\beta$ ) can be used as a measure of local distortion. There are four sets of  $\alpha$  and  $\beta$  associated with the four bridgehead carbon atoms, C3, C17, C20, and C23 (Table 5.1). As indicated by the  $\alpha+\beta$  values, it is evident that there is higher degree of local distortion in the vicinity of C20 and C23. As expected, the highest distortion is in the vicinity of the bridgehead carbon (C20) of the methano bridge. However, all  $\alpha+\beta$  values for **5.25** are significantly lower than those of **5.5**, which suggests that the cyclophane framework of **5.25** is substantially less strained than that of **5.5** owing to a presence of a larger aromatic system (1,1'-binaphthalene moiety *vs.* naphthalene moiety).

**Table 5.1:** Experimentally determined values of  $\alpha$ ,  $\beta$  and  $\alpha+\beta$  for **5.25**.

| Bridgehead | $\alpha$  | $\beta$    | $\alpha+\beta$ |
|------------|-----------|------------|----------------|
| C3         | 0.52(9)°  | 1.06(11)°  | 1.58(14)°      |
| C17        | 4.22(14)° | 5.30(13)°  | 9.52(19)°      |
| C20        | 5.99(10)° | 11.78(10)° | 17.77(14)°     |
| C23        | 5.61(10)° | 7.15(11)°  | 12.76(15)°     |

The 1,7-disubstituted naphthalene and the 1,3-disubstituted naphthalene moieties in **5.25** have a twist<sup>33</sup> of just  $-2.00^\circ$  (C3–C4–C7–C8) and  $-3.87^\circ$  (C17–C18–C13–C14), respectively. These values are comparable to the analogous twist angle of the naphthalene moieties in 1,1'-binaphthalene (**5.1**), which is negligibly small ( $0.97^\circ$ ).<sup>32</sup> The slightly higher twist of the naphthalene moieties in **5.25** is presumably brought by the aliphatic bridges due to the inclusion of the 1,1'-binaphthalene moiety into the cyclophane framework.

The C1–C23 and C1–C2 bonds, which are part of the ethano bridge in **5.25**, have bond lengths of 1.508(2) and 1.5515(19) Å, respectively. These values for the bond lengths are smaller than the analogous C(*sp*<sup>2</sup>)–C(*sp*<sup>3</sup>) (see C1–C15 bond in Chapter 2, Figure 2.1) and C(*sp*<sup>3</sup>)–C(*sp*<sup>3</sup>) (see C1–C2 bond in Chapter 2, Figure 2.1) bond lengths of 1.521(3) and 1.586(4) Å, respectively, for **5.5**. The bond length of C2–C3 in **5.25** is 1.5138(18) Å, which is comparable to that [1.513(3) Å] of the analogous C(*sp*<sup>2</sup>)–C(*sp*<sup>3</sup>) (see C2–C3 bond in Chapter 2, Figure 2.1) in **5.5**. The methano bridge in **5.25** has bond lengths of 1.5151(19) and 1.5210(17) Å, which are smaller than those of **5.5**. The C9–C11 has a bond length of 1.4945(17) Å, which is comparable to that (bond connecting two naphthalene moieties) of 1,1'-binaphthalene (**5.1**).<sup>32</sup>

### 5.3.4 NMR Analysis

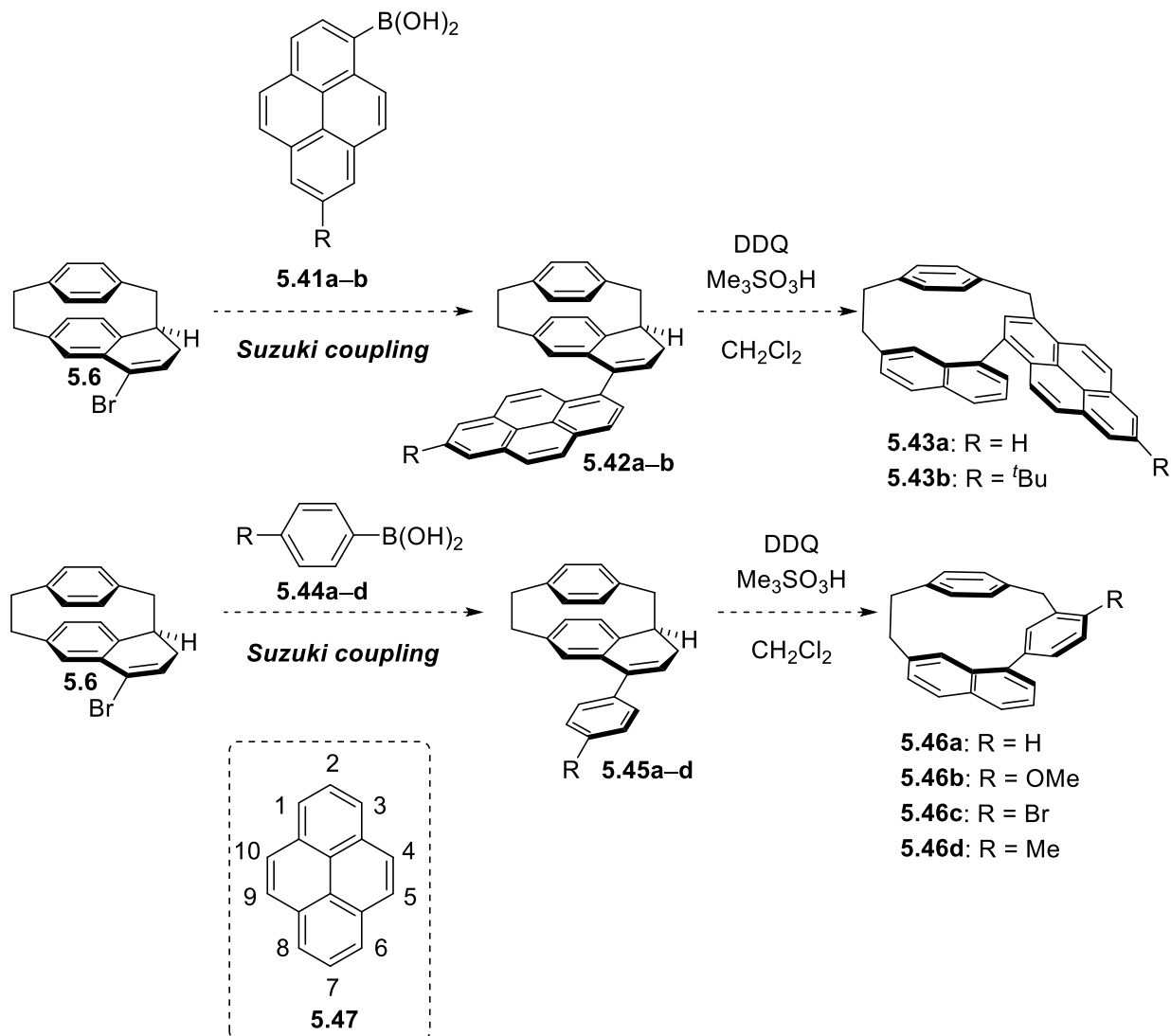
The  $^1\text{H}$  NMR spectrum of **5.25** features aromatic signals that are spread over a broad range ( $\delta$  7.94–6.08 ppm) (see Appendix 4). The highest field aromatic proton resonates at  $\delta$  6.08 ppm and appears as a slightly broad singlet. The proton was assigned to C10 (see crystal structure in Figure 5.1 for numbering) based on a COSY experiment (see Appendix 4 for COSY spectrum). The crystal structure of **5.25** shows a conformation in which C10 is oriented toward the interior of the cyclophane framework. Consequently, C10 experiences magnetic shielding from the 1,4-disubstituted benzene unit and the 1,3-disubstituted naphthalene unit. The diastereotopic protons of the methano bridge (C19) appears as an AB system at  $\delta$  4.13 and 4.05 ppm ( $J = 13.3$  Hz). These protons are downfield shifted compared to the protons of the ethano bridge (C1 and C2), as would be expected for a diarylmethane. The protons of the ethano bridge appears as three discrete multiplets at  $\delta$  3.35–3.22 (1H), 3.09–2.99 (1H), and 2.61–2.48 (2H).

#### 5.4 Future Outlook

The selectivity for the formation of cyclophane **5.25** is noteworthy. Cyclization of radical cation **5.33** or arenium ion **5.36** could conceivably occur at several other positions to give various other cyclophanes. It may be that one or more of these other cyclophanes were among the cluster of more polar minor compounds that were observed by TLC, but no evidence for the formation of any such compounds was obtained. Even if one or more of them was present, none of them were formed to nearly the same extent as **5.25**. Whatever the case, the observed selectivity suggests that this rearrangement reaction might be used for the tailored synthesis of a variety of other unusual [2.1]cyclophanes that would be difficult, if not impossible, to access, using conventional synthetic methods. Scheme 5.11 highlights a few selected examples of [2.1]cyclophanes bearing a pyrenyl or phenyl unit as part of their aromatic systems. A 1-pyrenyl unit is an especially attractive system to use because, according to the proposed mechanism, the 3 position of the pyrene

unit would be the favoured site of cyclization. The innate favourability of the 1, 3, 6, and 8 positions in pyrene (**5.47**) toward electrophilic aromatic substitution of pyrene (**5.47**)<sup>34</sup> may then serve to enhance the selectivity of the rearrangement (Scheme 5.11, inset). Suzuki coupling of dihydronaphthalene **5.6** with pyrene-based boronic acids **5.41a** and **5.41b** would afford dihydronaphthalenes **5.42a** and **5.42b**, respectively. Subsequent subjection of **5.42a** or **5.42b** to the Scholl reaction conditions would result in the formation of the targeted cyclophanes **5.43a** and **5.43b**, respectively.

The use of phenylboronic acids **5.44a–d** for the Suzuki coupling reaction would be expected to furnish [2.1]cyclophanes **5.46a–d** via the intermediacy of the dihydronaphthalenes **5.45a–d**, respectively. The expected site of cyclization on the benzene unit is the 3 position, so the presence of *ortho-/para*-directing substituents at the 4 position, *i.e.* **5.45b–d** would be expected to be advantageous for the intramolecular Friedel–Crafts reactions of the intermediate radical cations or cationic intermediates (not shown, *cf.* **5.33** and **5.36**). In this context it would be interesting to probe what effect an electron-withdrawing group on the phenyl unit would have on the outcome of the rearrangement reaction and the placement of substituents at other positions.



**Scheme 5.11:** Potential utility of dihydronaphthalene **5.6** for the synthesis of [2.1]cyclophanes **5.43a–b** and **5.46a–d** over two steps. Inset: numbering for pyrene (**5.47**).

[2.1]Cyclophane **5.25** was found to be weakly fluorescent (TLC analysis) under 365 nm UV irradiation. Given that pyrene (**5.47**) has a higher quantum yield of 0.32 (cyclohexane) vs. 0.23 (cyclohexane) for unsubstituted parent naphthalene,<sup>9</sup> replacement of the naphthyl unit in **5.25** with a pyrenyl unit would be expected to lead to a cyclophane, which would be a better fluorophore. Comprehensive UV/vis absorption and fluorescence spectroscopic studies with the aid of theoretical calculations on cyclophane **5.25** and similar structurally unusual synthetically

accessible (under the same rearrangement conditions) cyclophanes would be worth pursuing once the scope and limitations of the rearrangement reaction have been explored.

[2.2]Paracyclophane/quinoxaline hybrids bearing heteroaromatic units larger than those in **5.14a–b** might be interesting systems for the UV/vis and NMR titration studies to probe the effects of larger heteroaromatic systems on the acidity ( $pK_a$ ) of the methine proton in such chiral systems.

## 5.5 Conclusions

A serendipitous reaction (rearrangement) of dihydronaphthalene **5.8** was discovered under Scholl conditions. The formation of the product, [2](7,3')1,1'-binaphthaleno[1]paracyclophane (**5.25**), was rationalized by considering two alternative pathways (radical-cation and arenium-ion) that have resemblance to the two commonly accepted mechanisms, namely, radical-cation and arenium-ion mechanisms, for the classical Scholl reaction. The rearrangement reaction could potentially afford a wide variety of unusual [2.1]cyclophanes consisting of a 1,4-disubstituted benzene ring and an aromatic system of choice. However, the aromatic system of choice depends on the availability of the boronic acids (or boronic esters) for their use in the Suzuki coupling with dihydronaphthalene **5.6** to afford the precursors for rearrangement reactions.

Reactions of dione **5.13** with diamines **5.11a** and **5.26** led to the formation of [2.2]paracyclophane/quinoxaline hybrids **5.14a** and **5.27**, respectively. The use of 1,2-diarylamines having larger aromatic units might prove to be useful for the preparation of [2.2]paracyclophane/quinoxaline hybrids with larger heteroaromatic systems.

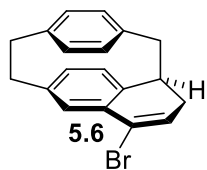
## 5.6 Experimental Section

### General

Reactions were performed under a balloon containing nitrogen gas unless otherwise indicated. All reactions were performed with oven-dried (120 °C) glassware. Solvents were removed from

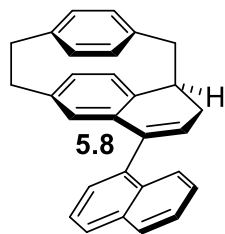
reaction mixtures under reduced pressure using a rotary evaporator. Chromatographic separations were achieved using Silicycle silica gel 60, particle size of 40–63  $\mu\text{m}$ . Column dimensions are recorded as height  $\times$  diameter. Thin-layer chromatography (TLC) was performed using precoated plastic-backed POLYGRAMÒ SIL G/UV254 silica gel plates with a layer thickness of 200  $\mu\text{m}$ . Compounds on TLC plates were visualized using a UV lamp (254 and 365 nm) or cerium molybdate stain (Hanessian's stain). Melting points were recorded using an OptiMelt automated melting point instrument and are uncorrected. Infrared (IR) spectra were recorded using neat samples on a Bruker Alpha spectrometer.  $^1\text{H}$  and  $^{13}\text{C}$  NMR spectra were recorded on Bruker AVANCE spectrometers at 300 MHz / 500 MHz and 75 MHz, respectively. Chemical shifts of the NMR spectra are reported relative to the residual solvent peak ( $\text{CDCl}_3$ : 7.26 ppm for  $^1\text{H}$  NMR, 77.16 ppm for  $^{13}\text{C}$  NMR). High resolution mass spectrometry (HRMS) data were obtained using an Agilent 6200 series instrument, employing a TOF mass analyzer. The synthesis of dione **5.13** is reported in Chapter 4.

### Dihydronaphthalene 5.6



Phosphorous tribromide (0.19 mL, 2.0 mmol) was added dropwise to a stirred room temperature solution of  $\alpha$ -tetralone **5.4** (0.150 g, 0.572 mmol) in benzene (10 mL). The resulting reaction mixture was heated at 80 °C for 22 h. Then, the mixture was cooled to room temperature and a saturated solution of sodium bicarbonate (10 mL) was added into the mixture. After stirring for 5 min, the reaction mixture was diluted with ethyl acetate (10 mL) and the two layers were separated. The aqueous layer was extracted with ethyl acetate (2  $\times$  10 mL). The combined organic layers were washed with saturated aqueous NaCl solution (2  $\times$  40 mL), dried over Na<sub>2</sub>SO<sub>4</sub>, filtered, and concentrated under reduced pressure. The residue was subjected to column chromatography (15 cm  $\times$  2.5 cm, 0–2% ethyl acetate/hexanes) to afford **5.6** (0.106 g, 57%) as a beige solid.  $R_f$  = 0.45 (2% ethyl acetate/hexanes); mp 117–119 °C; <sup>1</sup>H NMR (300 MHz, CDCl<sub>3</sub>)  $\delta$  6.94–6.91 (m, 1H), 6.62 (d,  $J$  = 1.8 Hz, 1H), 6.55 (dd,  $J$  = 7.6, 1.8 Hz, 1H), 6.52–6.49 (m, 2H), 6.42–6.37 (m, 3H), 3.31–2.86 (m, 8H), 2.50 (ddd,  $J$  = 17.9, 6.7, 1.4 Hz, 1H); <sup>13</sup>C NMR (75 MHz, CDCl<sub>3</sub>)  $\delta$  140.9, 140.0, 139.9, 137.0, 134.5, 133.2, 133.0, 132.8, 132.7, 132.5, 131.7, 130.1, 128.4, 123.4, 41.8, 40.0, 35.6, 35.4, 34.9; IR  $\nu$  2922 (w), 2854 (w), 1595 (w), 837 (s), 812 (s), 713 (w) cm<sup>-1</sup>; HRMS [APPI(+)] calcd for C<sub>19</sub>H<sub>17</sub><sup>79</sup>Br [M]<sup>+</sup> 324.0514, found 324.0517; calcd for C<sub>19</sub>H<sub>17</sub><sup>81</sup>Br [M]<sup>+</sup> 326.0493, found 326.0502.

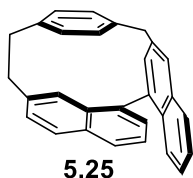
### Dihydronaphthalene 5.8



A degassed (nitrogen bubbled for 15 min) room temperature solution of dihydronaphthalene **5.6** (0.085 g, 0.26 mmol) in dimethoxyethane (2 mL) was added to Pd(PPh<sub>3</sub>)<sub>4</sub> (0.030 g, 0.026 mmol). The resulting mixture was stirred for 5 min at room temperature. A degassed (nitrogen bubbled for 15 min) solution of naphthalene-1-boronic acid (**5.7**) (0.067 g, 0.39 mmol) in ethanol (1 mL) was added to

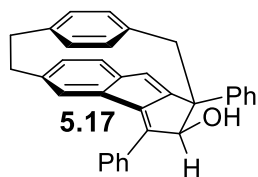
the mixture and the resulting mixture was stirred for 1 min at the same temperature. A degassed (nitrogen bubbled for 15 min) solution of sodium carbonate (0.235 g, 2.22 mmol) in deionized water (2 mL) was added to the mixture and the resulting mixture was stirred at 90 °C for 17 h. After cooling to room temperature, the majority of the solvents were removed under reduced pressure. The residue was diluted with dichloromethane (10 mL) and passed through a small pad of Celite<sup>®</sup>. The filter cake was washed thoroughly with dichloromethane (20 mL). The filtrate was transferred to a separatory funnel and water (30 mL) was added. The two layers were separated and the aqueous layer was extracted with dichloromethane (2 × 10 mL). The combined organic layers were washed with saturated aqueous NaCl solution (50 mL), dried over Na<sub>2</sub>SO<sub>4</sub>, filtered, and concentrated under reduced pressure. The residue was subjected to column chromatography (15 cm × 2.5 cm, 0–2% ethyl acetate/hexanes) to afford **5.8** (0.084 g, 86%) as an off-white solid. The material was judged to be *ca.* 90% pure by <sup>1</sup>H NMR analysis. *R*<sub>f</sub> = 0.44 (4% ethyl acetate/hexanes); mp 183–186 °C; <sup>1</sup>H NMR (300 MHz, CDCl<sub>3</sub>) δ 7.90 (t, *J* = 8.8 Hz, 2H), 7.74 (d, *J* = 7.0 Hz, 1H), 7.65 (t, *J* = 7.4 Hz, 1H), 7.52 (d, *J* = 8.5 Hz, 1H), 7.43 (t, *J* = 7.5 Hz, 1H), 7.27–7.19 (m, 2H), 6.57–6.45 (m, 4H), 6.29 (d, *J* = 7.8 Hz, 1H), 5.98 (d, *J* = 6.1 Hz, 1H), 5.61 (s, 1H), 3.51–3.34 (m, 2H), 3.20–3.11 (m, 2H), 2.97–2.88 (m, 3H), 2.73–2.60 (m, 2H); <sup>13</sup>C NMR (75 MHz, CDCl<sub>3</sub>) δ 140.2, 140.1, 139.2, 139.0, 136.4, 135.8, 133.6, 133.01, 132.98, 132.7, 132.2, 131.8, 131.6, 130.5, 128.1, 127.7, 127.0, 126.8, 126.4, 125.8, 125.7, 42.6, 40.2, 35.32, 35.27, 33.5 (three signals fewer than expected); IR ν 2916 (w), 2851 (w), 2815 (w), 1588 (w), 800 (s), 778 (s) cm<sup>-1</sup>; HRMS [APPI-(+)] calcd for C<sub>19</sub>H<sub>25</sub> [M+H]<sup>+</sup> 373.1956, found 373.1960.

## Cyclophane **5.25**



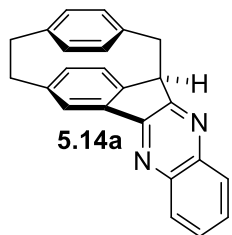
Methanesulfonic acid (1.35 mL, 20.8 mmol) was added to a stirred 0 °C solution of dihydronaphthalene **5.8** (0.0503 g, 0.135 mmol) in dichloromethane (13.5 mL). DDQ (0.0307 g, 0.135 mmol) was added to the 0 °C solution and the resulting mixture was stirred for 5 min at the same temperature. A saturated aqueous solution of sodium bicarbonate (20 mL) was added to the mixture at 0 °C and the mixture was stirred for 5 min. The two layers were separated and the aqueous layer was extracted with dichloromethane (2 × 15 mL). The combined organic layers were washed with water (40 mL), washed with saturated aqueous NaCl solution (40 mL), dried over Na<sub>2</sub>SO<sub>4</sub>, filtered, and concentrated under reduced pressure. The residue was subjected to column chromatography (15 cm × 2 cm, 20% dichloromethane/hexanes) to afford **5.25** (0.0221 g, 44%) as a white solid. *R*<sub>f</sub> = 0.25 (20% dichloromethane/hexanes); mp 227–229 °C; <sup>1</sup>H NMR (300 MHz, CDCl<sub>3</sub>) δ 7.94–7.89 (m, 2H), 7.82 (br d, *J* = 7.7 Hz, 1H), 7.81 (d, *J* = 8.4 Hz, 1H), 7.74 (br s, 1H), 7.52–7.42 (m, 3H), 7.35 (ddd, *J* = 8.4, 6.9, 1.4 Hz, 1H), 7.30 (dd, *J* = 8.4, 1.7 Hz, 1H), 7.21 (dd, *J* = 8.0, 2.0 Hz, 1H), 7.13 (dd, *J* = 7.6, 1.9 Hz, 1H), 7.06 (dd, *J* = 8.0, 1.9 Hz, 1H), 6.69 (d, *J* = 1.8 Hz, 1H), 6.66 (dd, *J* = 7.5, 2.0 Hz, 1H), 6.08 (br s, 1H), 4.13, 4.05 (AB system, *J* = 13.3 Hz, 2H), 3.35–3.22 (m, 1H), 3.09–2.99 (m, 1H), 2.61–2.48 (m, 2H); <sup>13</sup>C NMR (75 MHz, CDCl<sub>3</sub>) δ 141.3, 140.0, 139.6, 137.6, 137.4, 136.5, 134.5, 133.3, 133.2, 133.1, 131.0, 130.4, 130.0, 129.9, 129.2, 128.5, 128.3, 128.1, 128.0, 127.5, 126.3, 126.0, 125.6, 125.5, 124.4, 124.0, 42.2, 39.6, 36.9; IR ν 2922 (w), 2850 (w), 1592 (w), 1504 (w), 824 (s), 750 (m) cm<sup>-1</sup>; HRMS [APPI-(+)] calcd for C<sub>29</sub>H<sub>22</sub> [M]<sup>+</sup> 370.1722, found 370.1715.

## Cyclophane **5.17**



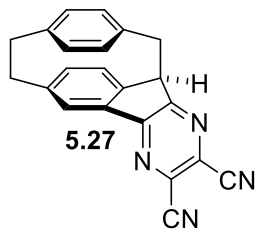
Lithium aluminum hydride (0.013 g, 0.344 mmol) was added to a stirred  $-10\text{ }^{\circ}\text{C}$  (ice/salt) solution of cyclophane **5.16** (0.100 g, 0.228 mmol) in diethyl ether (5 mL). The cold bath was removed and the resulting mixture was stirred for 30 min as it warmed to room temperature. To quench the reaction, a saturated aqueous solution of Rochelle's salt (potassium sodium tartrate) (5 mL) was added to the reaction mixture at  $0\text{ }^{\circ}\text{C}$  (ice/water). The resulting mixture was stirred for 15 min. The two layers were separated and the aqueous layer was extracted with diethyl ether ( $2 \times 10\text{ mL}$ ). The combined organic layers were washed with water ( $2 \times 20\text{ mL}$ ), washed with saturated aqueous NaCl solution (20 mL), dried over  $\text{Na}_2\text{SO}_4$ , filtered, and concentrated under reduced pressure. The residue was subjected to column chromatography ( $10\text{ cm} \times 2.5\text{ cm}$ , 3–8% ethyl acetate/hexanes) to afford **5.17** (0.094 g, 94%) as an orange crystalline solid.  $R_f = 0.34$  (10% ethyl acetate/hexanes); mp  $163\text{--}166\text{ }^{\circ}\text{C}$  (dec.);  $^1\text{H NMR}$  (300 MHz,  $\text{CDCl}_3$ )  $\delta$  8.04–8.00 (m, 2H), 7.74–7.70 (m, 2H), 7.49–7.41 (m, 5H), 7.39–7.33 (m, 1H), 7.13 (dd,  $J = 7.9, 2.1\text{ Hz}$ , 1H), 7.05 (d,  $J = 7.8\text{ Hz}$ , 1H), 6.93 (dd,  $J = 7.9, 1.6\text{ Hz}$ , 1H), 6.45 (br s, 1H), 6.40 (dd,  $J = 7.9, 2.0\text{ Hz}$ , 1H), 6.16 (s, 1H), 6.06 (dd,  $J = 7.7, 2.1\text{ Hz}$ , 1H), 5.85 (dd,  $J = 7.7, 2.0\text{ Hz}$ , 1H), 4.26 (d,  $J = 12.5\text{ Hz}$ , 1H), 2.97 (dd,  $J = 12.5, 8.9\text{ Hz}$ , 1H), 2.78 (dd,  $J = 12.5, 8.6\text{ Hz}$ , 1H), 2.70 (d,  $J = 6.5\text{ Hz}$ , 1H), 2.56 (dd,  $J = 12.6, 9.1\text{ Hz}$ , 1H), 2.51 (d,  $J = 12.6\text{ Hz}$ , 1H), 2.36 (dt,  $J = 12.5, 9.2\text{ Hz}$ , 1H);  $^{13}\text{C NMR}$  (75 MHz,  $\text{CDCl}_3$ )  $\delta$  155.4, 150.9, 147.8, 144.8, 141.8, 137.1, 136.2, 135.06, 135.05, 134.3, 133.7, 130.2, 130.1, 129.8, 129.5, 128.9, 128.6, 127.3, 126.9, 126.7, 126.0, 121.8, 121.0, 88.7, 60.4, 42.6, 35.7, 34.9 (one signal fewer than expected); IR  $\nu$  3544 (br, w), 2923 (w), 2853 (w), 1594 (w), 1495 (w), 1113 (w), 1053 (w), 698 (s)  $\text{cm}^{-1}$ ; HRMS [APPI-(+)] calcd for  $\text{C}_{33}\text{H}_{27}\text{O}$   $[\text{M}+\text{H}]^+$  439.2062, found 439.2057.

### Quinoxaline 5.14a



Lithium chloride (0.0011 g, 0.026 mmol) was added to a stirred room temperature solution of dione **5.13** (0.0172 g, 0.0656 mmol) in ethanol (1.5 mL). The resulting mixture was stirred for 5 min at the same temperature. *o*-Phenylenediamine (**5.11a**) (0.0078 g, 0.072 mmol) was added to the mixture and the mixture was stirred at room temperature for 2 h. The solvent was removed under reduced pressure and the residue was subjected to column chromatography (15 cm × 1.5 cm, 10–20% ethyl acetate/hexanes) to afford **5.14a** (0.0199 g, 91%) as a white solid.  $R_f = 0.45$  (30% ethyl acetate/hexanes); mp 173–175 °C;  $^1\text{H NMR}$  (300 MHz,  $\text{CDCl}_3$ )  $\delta$  8.22–8.17 (m, 2H), 7.81–7.73 (m, 2H), 7.27 (br s, 1H), 6.90 (d,  $J = 7.9$  Hz, 1H), 6.84 (dd,  $J = 7.9, 1.6$  Hz, 1H), 6.68 (dd,  $J = 7.8, 1.9$  Hz, 1H), 6.58 (dd,  $J = 7.9, 2.0$  Hz, 1H), 6.17 (dd,  $J = 8.0, 1.9$  Hz, 1H), 5.45 (dd,  $J = 8.0, 2.0$  Hz, 1H), 4.66 (d,  $J = 8.1$  Hz, 1H), 3.81 (d,  $J = 13.2$  Hz, 1H), 3.45 (dd,  $J = 13.2, 8.2$  Hz, 1H), 3.38–3.20 (m, 2H), 3.13–2.94 (m, 2H);  $^{13}\text{C NMR}$  (75 MHz,  $\text{CDCl}_3$ )  $\delta$  163.9, 156.2, 146.3, 143.3, 142.6, 142.1, 141.0, 140.3, 136.8, 136.5, 135.2, 132.9, 132.8, 130.0, 129.43, 129.38, 129.3, 128.8, 128.3, 125.7, 49.4, 42.9, 35.6, 35.5; IR  $\nu$  2922 (w), 2853 (w), 2362 (w), 2335 (w), 1193 (w), 1024 (w), 765 (s), 711 (w)  $\text{cm}^{-1}$ ; HRMS [APPI-(+)] calcd for  $\text{C}_{24}\text{H}_{19}\text{N}_2$   $[\text{M}+\text{H}]^+$  335.1548, found 335.1556.

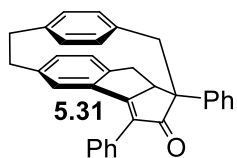
### Quinoxaline 5.27



Diaminomaleonitrile (**5.26**) (0.0157 g, 0.145 mmol) was added to a stirred room temperature suspension of dione **5.13** (0.0254 g, 0.0968 mmol) in acetic acid (3 mL). The resulting mixture was heated at 120 °C for 3 h. The reaction mixture was cooled to room temperature and a saturated aqueous solution of sodium bicarbonate (10 mL) was added to neutralize the acid. Dichloromethane (15 mL) was added to the mixture and the resulting two layers were separated. The aqueous layer was

extracted with dichloromethane ( $2 \times 15$  mL) and the combined organic layers were washed with water (40 mL), washed with saturated aqueous NaCl solution (40 mL), dried over  $\text{Na}_2\text{SO}_4$ , filtered, and concentrated under reduced pressure. The residue was subjected to column chromatography (15 cm  $\times$  2 cm, 80% dichloromethane/hexanes) to afford **5.27** (0.0204 g, 63%) as a greenish-yellow solid.  $R_f = 0.46$  (dichloromethane); mp 121–124 °C;  $^1\text{H}$  NMR (300 MHz,  $\text{CDCl}_3$ )  $\delta$  7.19 (d,  $J = 0.7$  Hz, 1H), 6.98–6.91 (m, 2H), 6.68 (dd,  $J = 7.9, 2.0$  Hz, 1H), 6.59 (dd,  $J = 7.8, 2.0$  Hz, 1H), 6.16 (dd,  $J = 8.1, 2.0$  Hz, 1H), 5.39 (dd,  $J = 8.1, 2.1$  Hz, 1H), 4.65 (d,  $J = 7.6$  Hz, 1H), 3.69 (d,  $J = 13.4$  Hz, 1H), 3.46 (dd,  $J = 13.4, 8.5$  Hz, 1H), 3.39–3.25 (m, 2H), 3.15–3.05 (m, 1H), 3.00 (ddd,  $J = 12.7, 10.5, 5.6$  Hz, 1H);  $^{13}\text{C}$  NMR (75 MHz,  $\text{CDCl}_3$ )  $\delta$  166.8, 158.8, 147.0, 144.6, 140.8, 139.3, 138.2, 135.6, 135.2, 133.2, 132.9, 132.7, 130.1, 129.9, 129.2, 125.1, 114.2, 114.0, 49.7, 41.9, 35.5, 35.4; IR  $\nu$  2926 (w), 2857 (w), 2235 (w), 1550 (m), 1325 (s), 801 (m), 708 (w)  $\text{cm}^{-1}$ ; HRMS [ESI-(+)] calcd for  $\text{C}_{22}\text{H}_{15}\text{N}_4$  [M+H] $^+$  335.1297, found 335.1287.

### Cyclophane **5.31**



*p*-Toluenesulfonic acid (0.016 g, 0.091 mmol) was added to a stirred room temperature solution of cyclophane **5.17** (0.080 g, 0.18 mmol) in 1,2-dichloroethane (3 mL). The resulting mixture was heated at 80 °C for 1 h.

After cooling to room temperature, saturated sodium bicarbonate solution (5 mL) was added to the reaction mixture and stirring was continued for 5 min. Dichloromethane (10 mL) was added to the mixture and the layers were separated. The aqueous layer was extracted with dichloromethane ( $2 \times 10$  mL) and the combined organic layers were washed with water (30 mL), washed with saturated aqueous NaCl solution (30 mL), dried over  $\text{Na}_2\text{SO}_4$ , filtered, and concentrated under reduced pressure. The residue was subjected to column chromatography (15 cm  $\times$  2.5 cm, 0–6% ethyl acetate/hexanes) to afford **5.31** (0.066 g, 83%) as a pale yellow solid.  $R_f = 0.32$  (8% ethyl

acetate/hexanes); mp 278–279 °C (dec.); <sup>1</sup>H NMR (300 MHz, CDCl<sub>3</sub>) δ 7.88–7.81 (m, 4H), 7.49–7.30 (m, 6H), 7.16 (dd, *J* = 8.0, 1.6 Hz, 1H), 7.07 (d, *J* = 8.0 Hz, 1H), 6.81 (dd, *J* = 8.0, 2.1 Hz, 1H), 6.43 (d, *J* = 1.6 Hz, 1H), 6.19 (dd, *J* = 7.7, 2.1 Hz, 1H), 6.13 (dd, *J* = 8.0, 2.0, 1H), 5.83 (dd, *J* = 7.7, 2.0 Hz, 1H), 4.00 (dd, *J* = 8.6, 4.0 Hz, 1H), 3.53 (d, *J* = 14.1 Hz, 1H), 3.46 (dd, *J* = 17.8, 8.6 Hz, 1H), 3.29 (dd, *J* = 17.8, 4.1 Hz, 1H), 3.09–2.99 (m, 2H), 2.86–2.76 (m, 1H), 2.53–2.37 (m, 2H); <sup>13</sup>C NMR (75 MHz, CDCl<sub>3</sub>) δ 207.1, 180.2, 151.2, 144.0, 138.6, 138.5, 138.2, 135.0, 132.8, 132.4, 132.1, 131.8, 129.2, 129.0, 128.6, 128.5, 128.4, 128.3, 127.5, 126.99, 126.95, 126.9, 126.5, 68.0, 53.1, 47.8, 34.7, 34.0, 32.2; IR ν 2923 (w), 1675 (m), 1595 (m), 810 (w), 696 (s) cm<sup>-1</sup>; HRMS [APPI-(+)] calcd for C<sub>33</sub>H<sub>27</sub>O [M+H]<sup>+</sup> 439.2062, found 439.2044.

## 5.7 References

1. (a) Jassas, R. S.; Mughal, E. U.; Sadiq, A.; Alsantali, R. I.; Al-Rooqi, M. M.; Naeem, N.; Moussa, Z.; Ahmed, S. A. *RSC Adv.* **2021**, *11*, 32158–32202. (b) Grzybowski, M.; Sadowski, B.; Butenschön, H.; Gryko, D. *Angew. Chem. Int. Ed.* **2020**, *59*, 2998–3027. (c) Grzybowski, M.; Skonieczny, K.; Butenschön, H.; Gryko, D. T. *Angew. Chem. Int. Ed.* **2013**, *52*, 9900–9930.
2. (a) Zhai, L.; Shukla, R.; Wadumethrige, S. H.; Rathore, R. *J. Org. Chem.* **2010**, *75*, 4748–4760. (b) King, B. T.; Kroulik, J.; Robertson, C. R.; Rempala, P.; Hilton, C. L.; Korinek, J. D.; Gortari, L. M. *J. Org. Chem.* **2007**, *72*, 2279–2288. (c) Rempala, P.; Kroulík, J.; King, B. T. *J. Org. Chem.* **2006**, *71*, 5067–5081. (d) Rempala, P.; Kroulík, J.; King, B. T. *J. Am. Chem. Soc.* **2004**, *126*, 15002–15003.
3. Selected examples of 1,2-aryl group migration: (a) Krzeszewski, M.; Sahara, K.; Poronik, Y. M.; Kubo, T.; Gryko, D. T. *Org. Lett.* **2018**, *20*, 1517–1520. (b) Liu, J.; Narita, A.; Osella, S.;

- Zhang, W.; Schollmeyer, D.; Beljonne, D.; Feng, X.; Müllen, K. *J. Am. Chem. Soc.* **2016**, *138*, 2602–2608.
4. Venkatakrisnan, P.; Ponugoti, N. *Chem. Eur. J.* **2021**, DOI: 10.1002/chem.202103530.
  5. Wu, J.; Pisula, W.; Müllen, K. *Chem. Rev.* **2007**, *107*, 718–747.
  6. Donaldson, D. M.; Robertson, J. M.; White, J. G. *Proc. R. Soc. London, Ser. A* **1953**, *220*, 311–321.
  7. Dewar, M. J. S.; Mole, T. *J. Chem. Soc.* **1956**, 1441–1443.
  8. Markiewicz, J. T.; Wudl, F. *ACS Appl. Mater. Interfaces* **2015**, *7*, 28063–28085.
  9. Berlman, I. B. *Handbook of Fluorescence Spectra of Aromatic Molecules*; Academic Press: New York, 1971.
  10. Scholl, R.; Seer, C.; Weitzenböck, R. *Ber. Dtsch. Chem. Ges.* **1910**, *43*, 2202–2209.
  11. (a) Rühle, J.; Bialas, D.; Spent, P.; Krause, A.-M.; Würthner, F. *Organic Materials* **2020**, *2*, 149–158. (b) Spent, P.; Young, R. M.; Wasielewski, M. R.; Würthner, F. *Chem. Sci.* **2016**, *7*, 5428–5434.
  12. Biswas, S.; Qiu, C. S.; Dawe, L. N.; Zhao, Y.; Bodwell, G. J. *Angew. Chem. Int. Ed.* **2019**, *58*, 9166–9170.
  13. (a) Thomas, K. R. J.; Velusamy, M.; Lin, J. T.; Chuen, C.-H.; Tao, Y.-T. *Chem. Mater.* **2005**, *17*, 1860–1866. (b) Sessler, J. L.; Maeda, H.; Mizuno, T.; Lynch, V. M.; Furuta, H. *J. Am. Chem. Soc.* **2002**, *124*, 13474–13479. (c) Dailey, S.; Feast, J. W.; Peace, R. J.; Sage, R. C.; Till, S.; Wood, E. L. *J. Mater. Chem.* **2001**, *11*, 2238–2243.
  14. (a) Parhi, A. K.; Zhang, Y.; Saionz, K. W.; Pradhan, P.; Kaul, M.; Trivedi, K.; Pilch, D. S.; LaVoie, E. J. *Bioorg. Med. Chem. Lett.* **2013**, *23*, 4968–4974. (b) Rajule, R.; Bryant, V. C.;

- Lopez, H.; Luo, X.; Natarajan, A. *Bioorg. Med. Chem.* **2012**, *20*, 2227–2234. (c) Kim, Y. B.; Kim, Y.; Park, J. Y.; Kim, S. K. *Bioorg. Med. Chem. Lett.* **2004**, *14*, 541–544.
15. Yashwantrao, G.; Saha, S. *Org. Chem. Front.* **2021**, *8*, 2820–2862.
16. (a) Hafner, K.; Goltz, M. *Angew. Chem. Int. Ed. Engl.* **1982**, *21*, 695–696. (b) Hafner, K.; Suda, M. *Angew. Chem. Int. Ed. Engl.* **1976**, *15*, 314–315.
17. Goff, E. L. *J. Am. Chem. Soc.* **1962**, *84*, 3975–3976.
18. Hafner, K.; Süß, H. U. *Angew. Chem. Int. Ed. Engl.* **1973**, *12*, 575–577.
19. Brown, R. F. C.; Choi, N.; Coulston, K. J.; Eastwood, F. W.; Wiersum, U. E.; Jenneskens, L. W. *Tetrahedron Lett.* **1994**, *35*, 4405–4408.
20. (a) Kato, S.-i.; Kuwako, S.; Takahashi, N.; Kijima, T.; Nakamura, Y. *J. Org. Chem.* **2016**, *81*, 7700–7710. (b) London, G.; von Wantoch Rekowski, M.; Dumele, O.; Schweizer, W. B.; Gisselbrecht, J.-P.; Boudon, C.; Diederich, F. *Chem. Sci.* **2014**, *5*, 965–972. (c) Rivera-Fuentes, P.; Rekowski, M. v. W.; Schweizer, W. B.; Gisselbrecht, J.-P.; Boudon, C.; Diederich, F. *Org. Lett.* **2012**, *14*, 4066–4069.
21. (a) Grenz, D. C.; Schmidt, M.; Kratzert, D.; Esser, B. *J. Org. Chem.* **2018**, *83*, 656–663. (b) Saito, M. *Symmetry* **2010**, *2*, 950–969.
22. Biswas, S.; Tabasi, Z. A.; Lin, J.-B.; Zhao, Y.; Bodwell, G. J. *Org. Lett.* **2021**, *23*, 5461–5465.
23. Shagufta; Raghunandan, R.; Moulik, P. R.; Panda, G. *Tetrahedron Lett.* **2005**, *46*, 5337–5341.
24. Suzuki, A. In *Metal-Catalyzed Cross-Coupling Reactions*; Diederich, F., Stang, P. J., Eds.; Wiley-VCH: Weinheim, Germany, 1998; pp 49–89.
25. Zhai, L.; Shukla, R.; Rathore, R. *Org. Lett.* **2009**, *11*, 3474–3477.
26. CCDC 2144507 contains the supplementary crystallographic data for compound **2.12**. These data can be obtained free of charge from The Cambridge Crystallographic Data Centre.

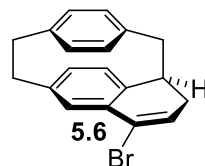
27. Karami, B.; Rooydel, R.; Khodabakhshi, S. *Acta Chim. Slov.* **2012**, *59*, 183–188.
28. Donzello, M. P.; Ercolani, C.; Novakova, V.; Zimcik, P.; Stuzhin, P. A. *Coord. Chem. Rev.* **2016**, *309*, 107–179.
29. Drain, C. M.; Varotto, A.; Radivojevic, I. *Chem. Rev.* **2009**, *109*, 1630–1658.
30. Miao, M.; Jin, M.; Chen, P.; Wang, L.; Zhang, S.; Ren, H. *Org. Lett.* **2019**, *21*, 5957–5961.
31. Hope, H.; Bernstein, J.; Trueblood, K. N. *Acta Crystallogr. Sect. B* **1972**, *28*, 1733–1743.
32. The crystallographic data for compound **5.1** was accessed from the CCDC 604806. The data can be obtained free of charge from The Cambridge Crystallographic Data Centre.
33. Pascal, R. A., Jr. *Chem. Rev.* **2006**, *106*, 4809–4819.
34. Dewar, M. J. S.; Dennington, R. D. *J. Am. Chem. Soc.* **1989**, *111*, 3804–3808.

## **Appendix 4**

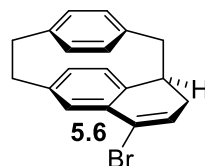
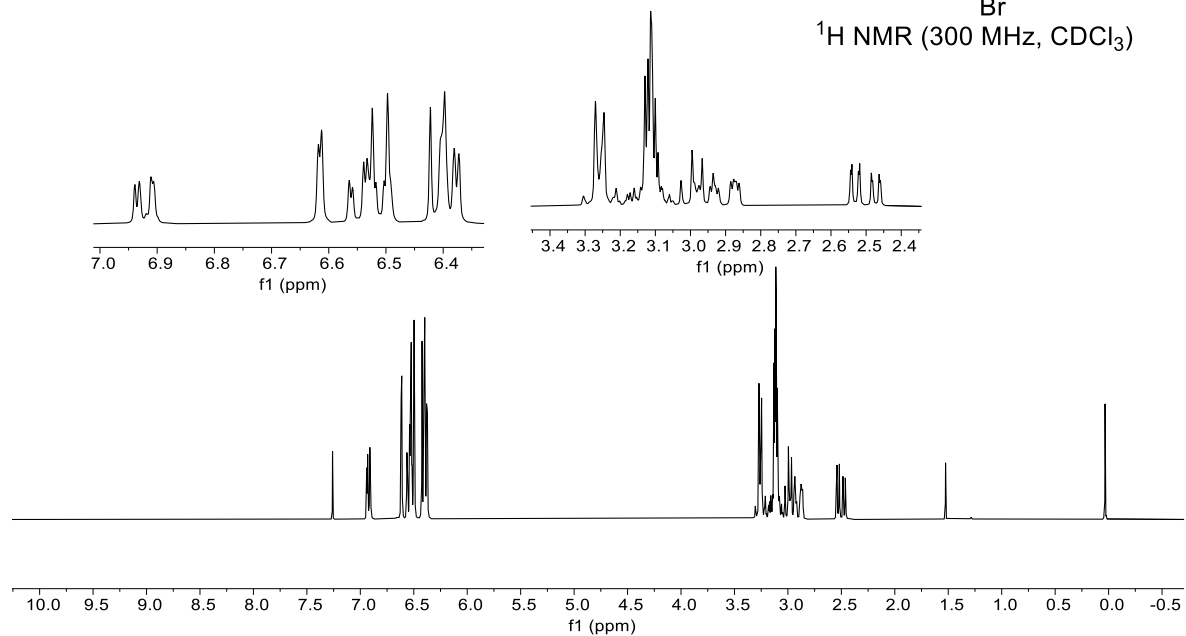
**$^1\text{H}$ ,  $^{13}\text{C}$  NMR Spectra, Two-Dimensional NMR Spectra, X-ray Crystallographic Data for**

## **Chapter 5**

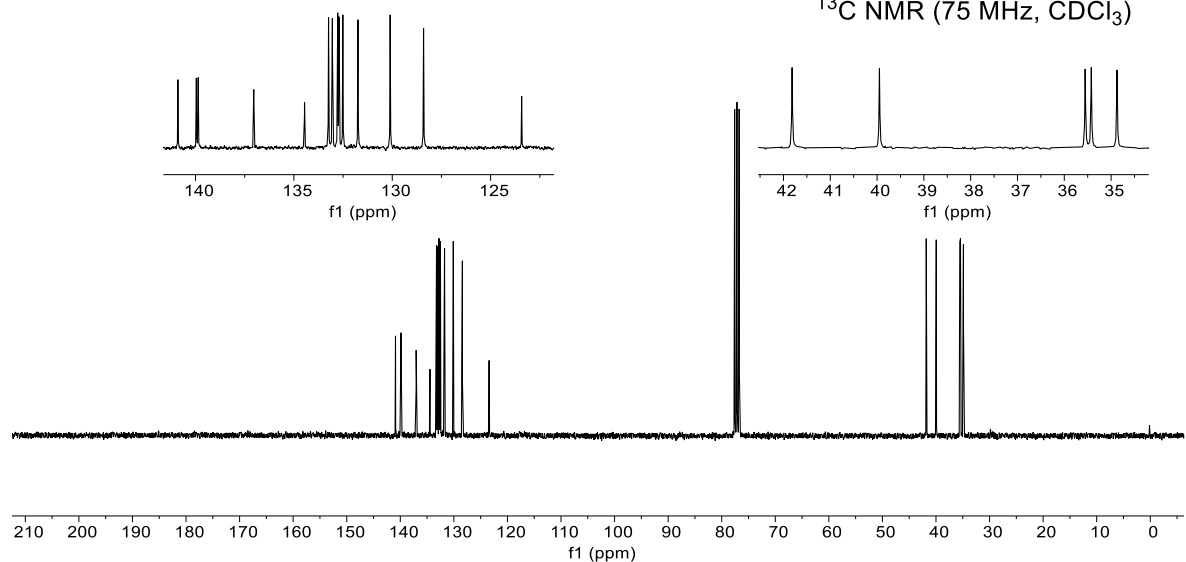
# 1. $^1\text{H}$ and $^{13}\text{C}$ NMR Spectra

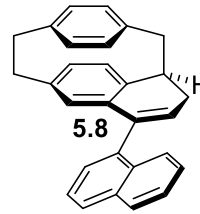


$^1\text{H}$  NMR (300 MHz,  $\text{CDCl}_3$ )



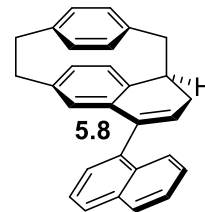
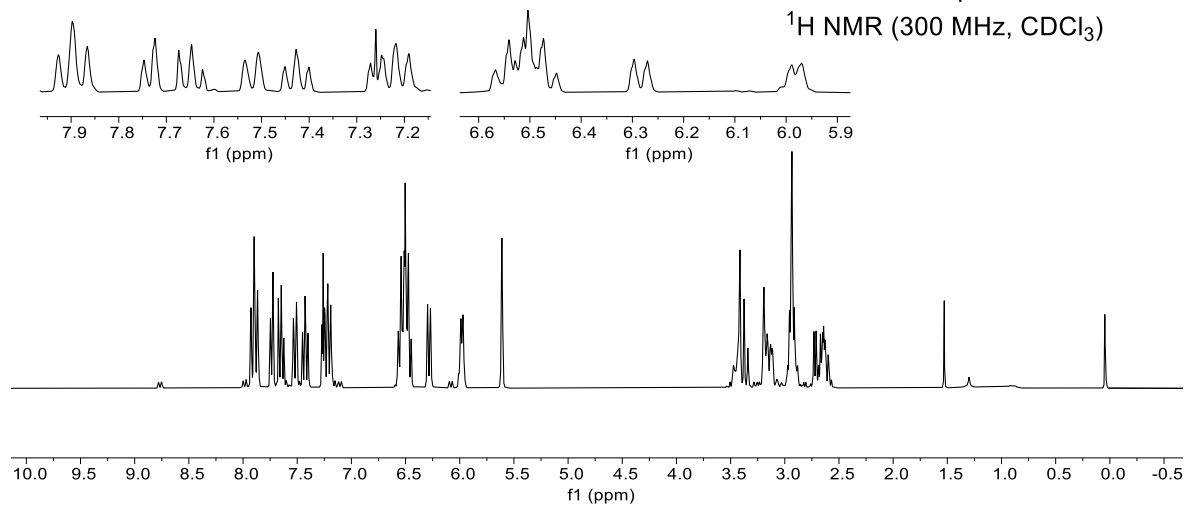
$^{13}\text{C}$  NMR (75 MHz,  $\text{CDCl}_3$ )





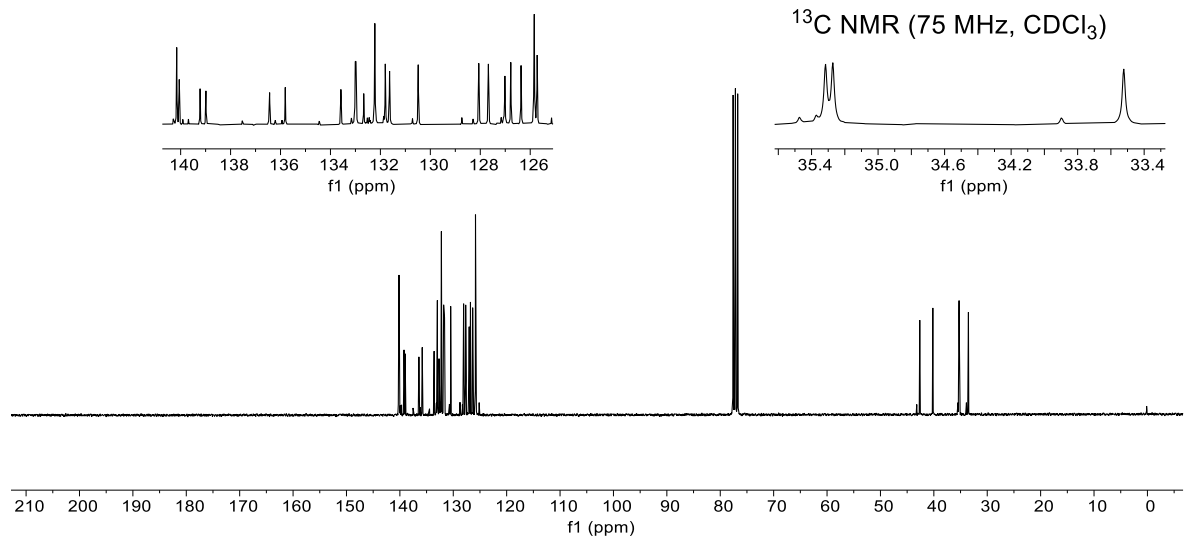
ca. 90% pure

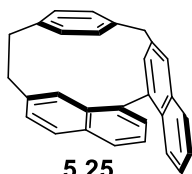
$^1\text{H}$  NMR (300 MHz,  $\text{CDCl}_3$ )



ca. 90% pure

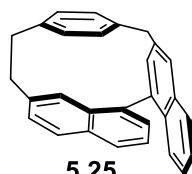
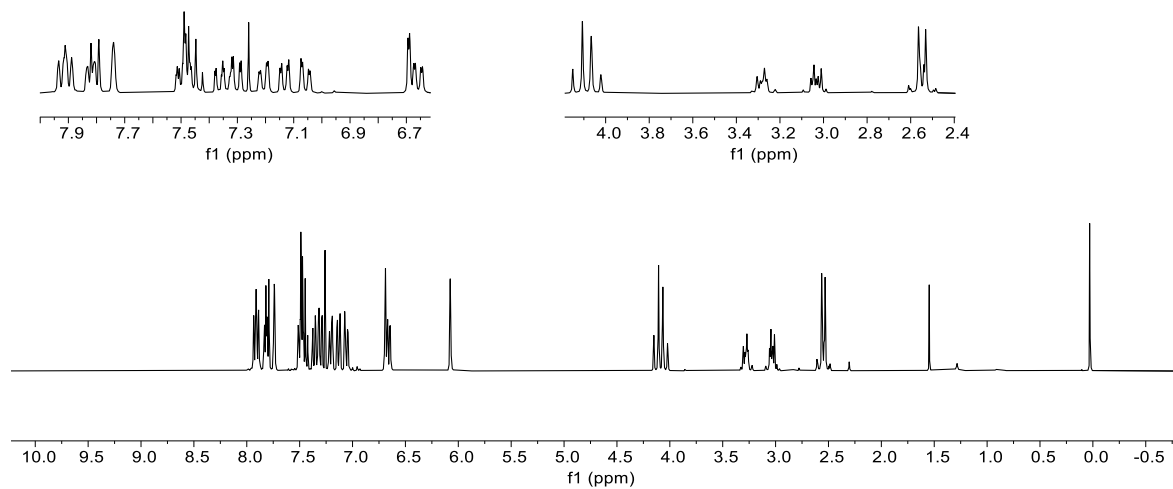
$^{13}\text{C}$  NMR (75 MHz,  $\text{CDCl}_3$ )





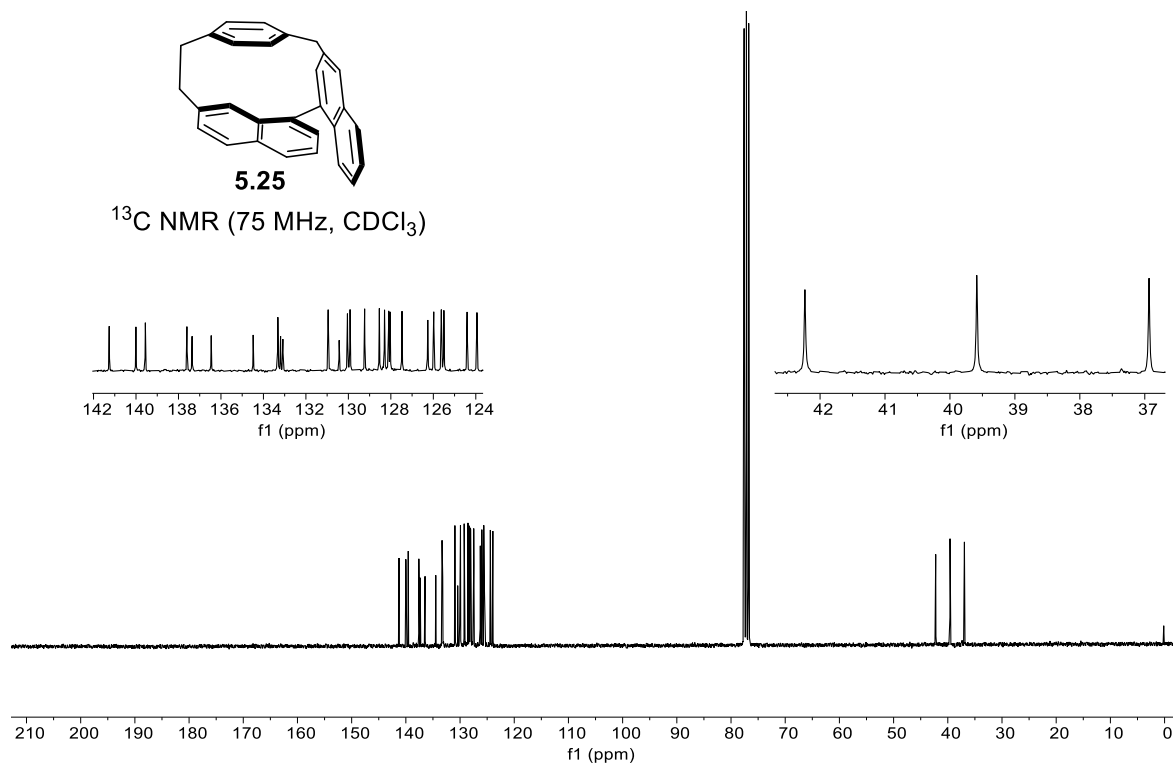
5.25

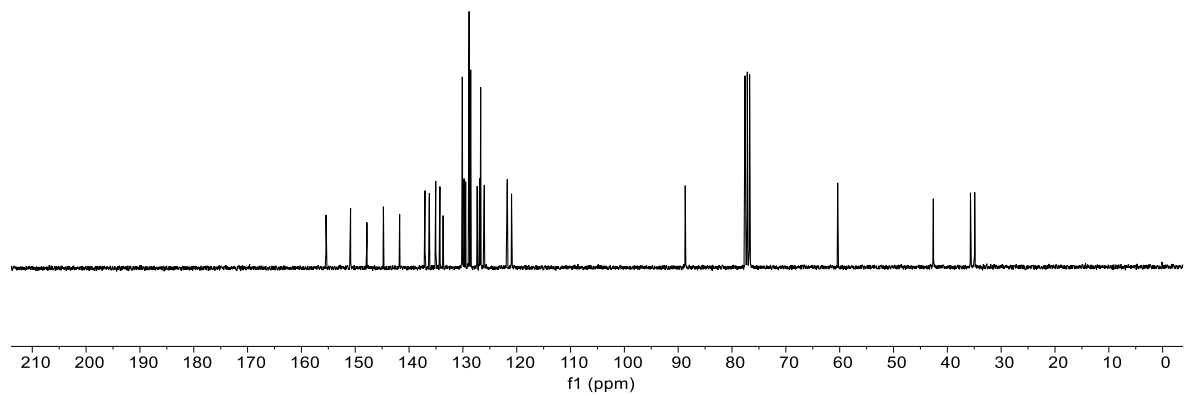
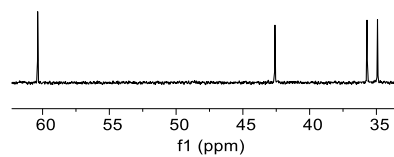
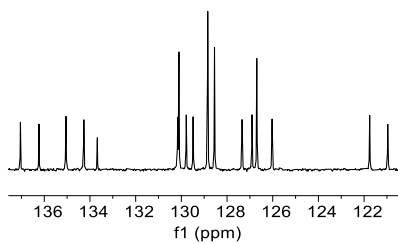
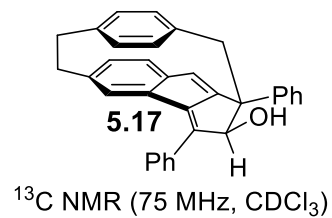
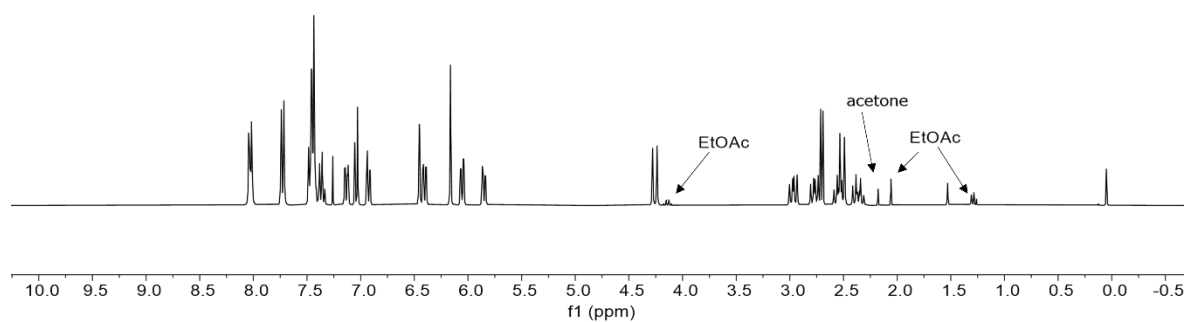
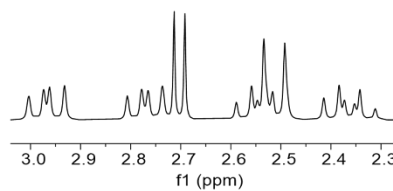
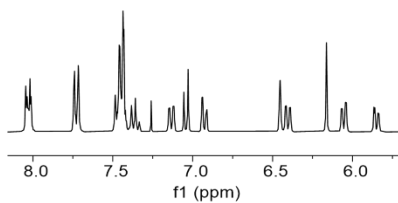
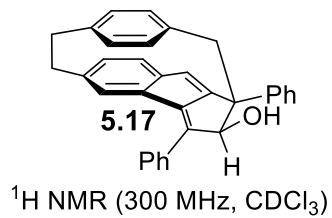
$^1\text{H NMR}$  (300 MHz,  $\text{CDCl}_3$ )

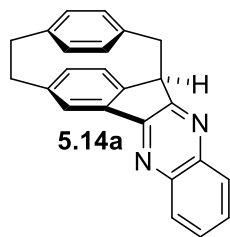


5.25

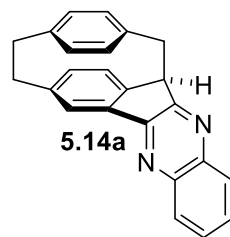
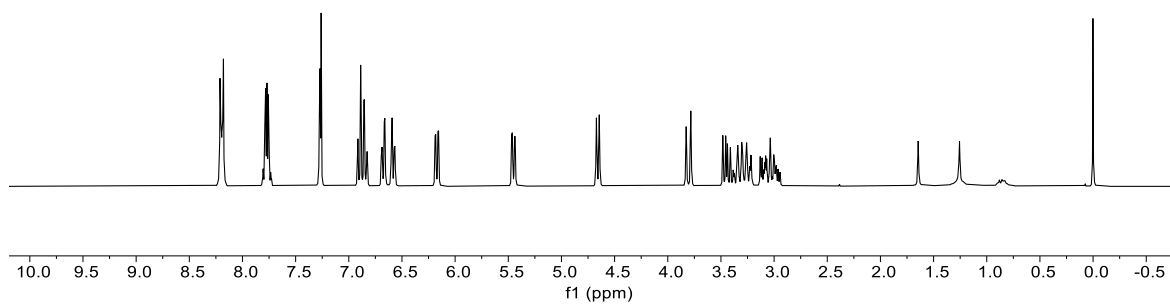
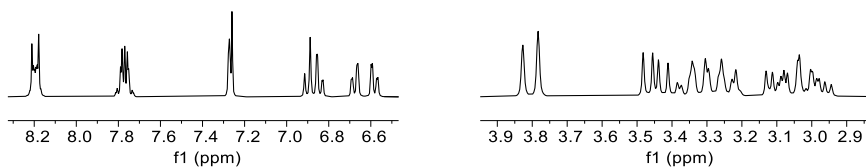
$^{13}\text{C NMR}$  (75 MHz,  $\text{CDCl}_3$ )



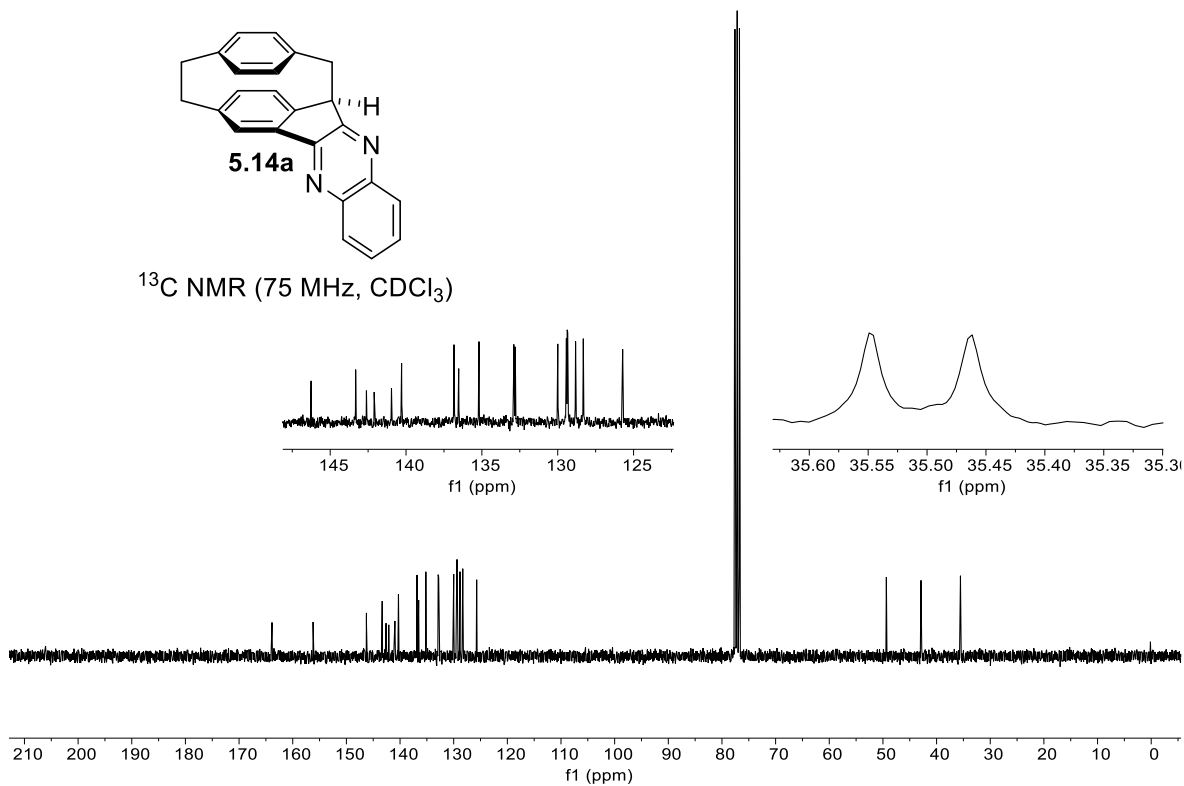


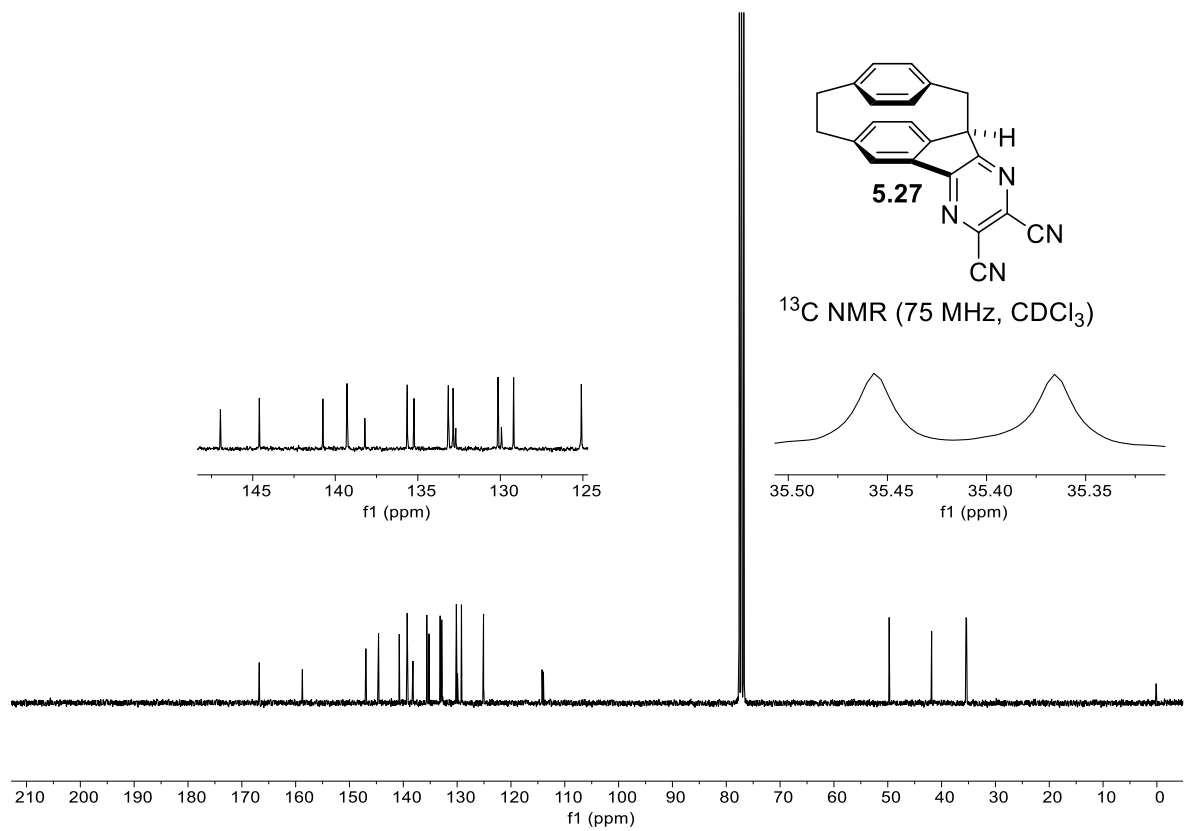
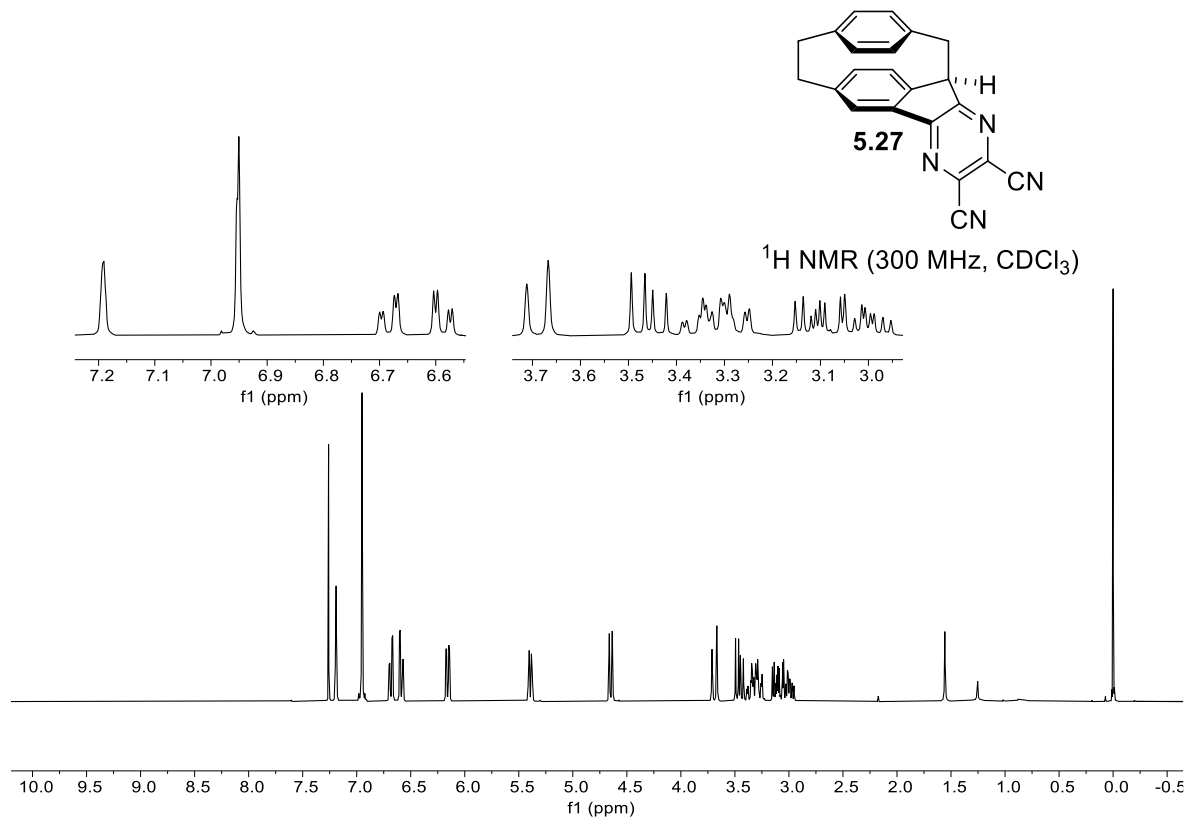


$^1\text{H}$  NMR (300 MHz,  $\text{CDCl}_3$ )



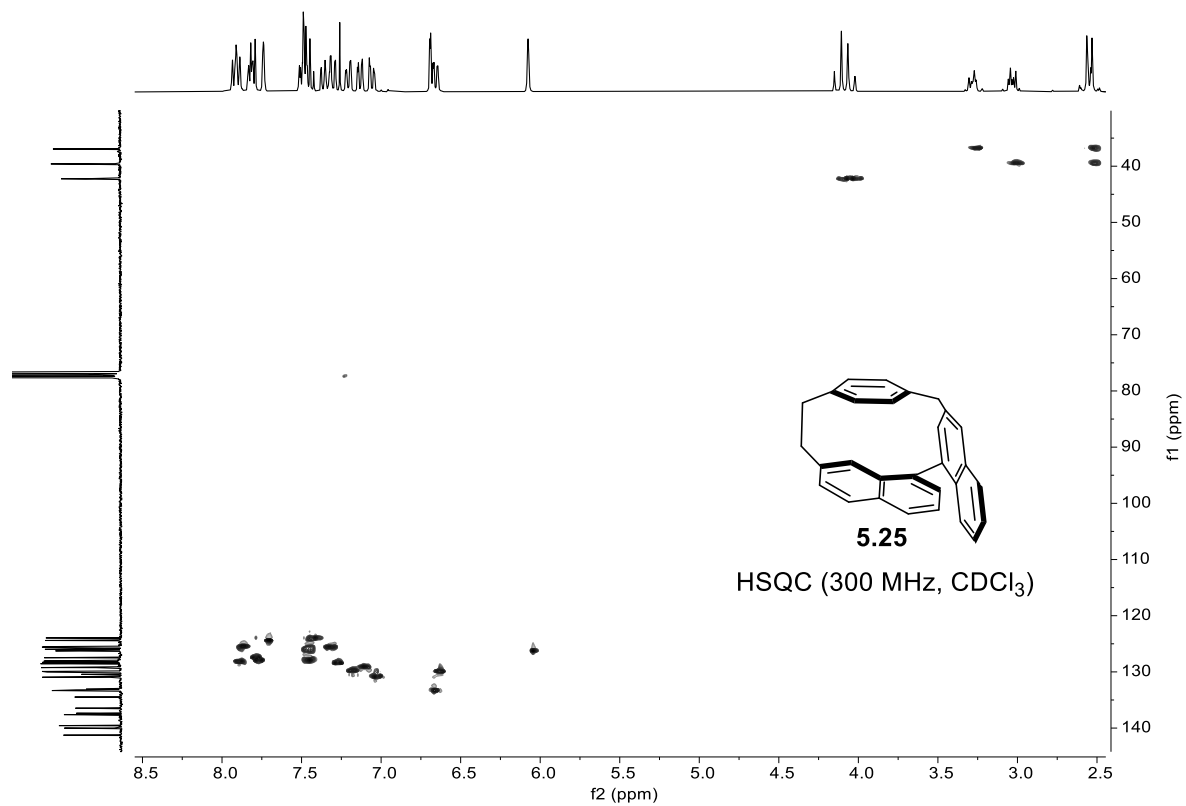
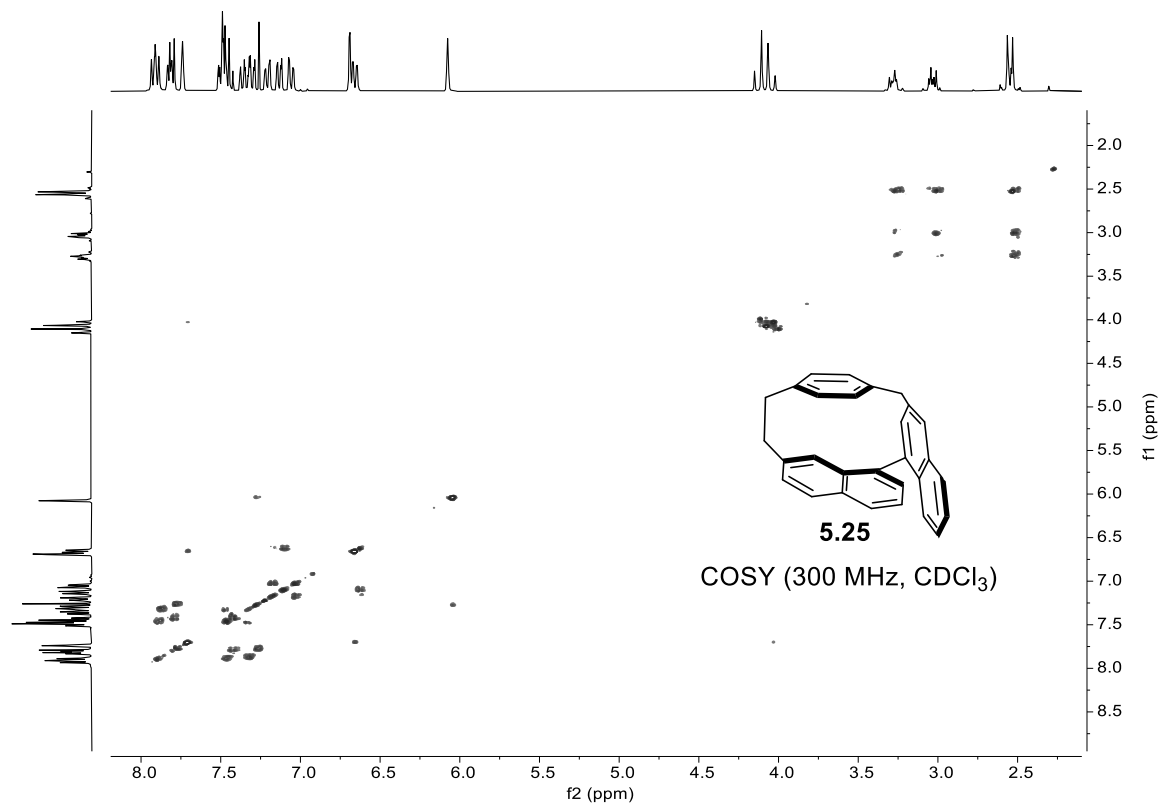
$^{13}\text{C}$  NMR (75 MHz,  $\text{CDCl}_3$ )

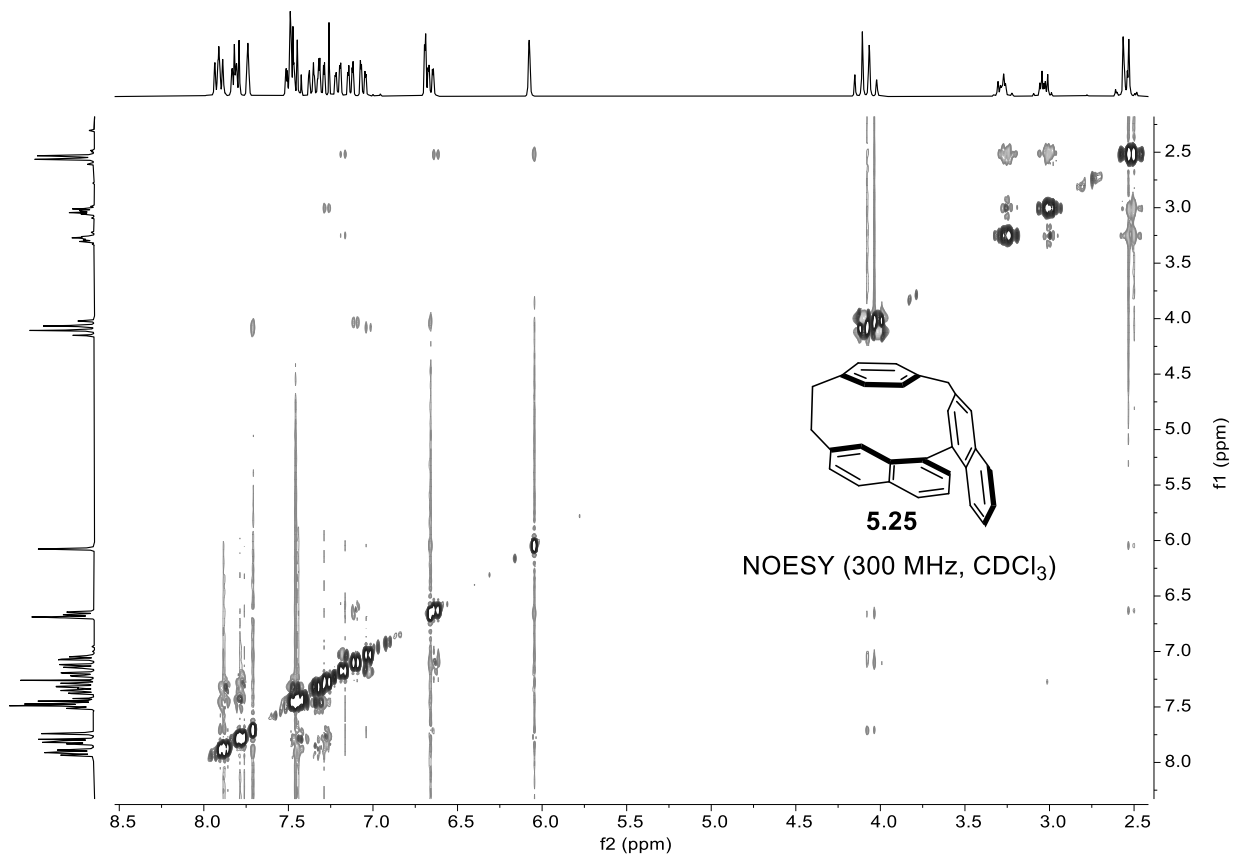


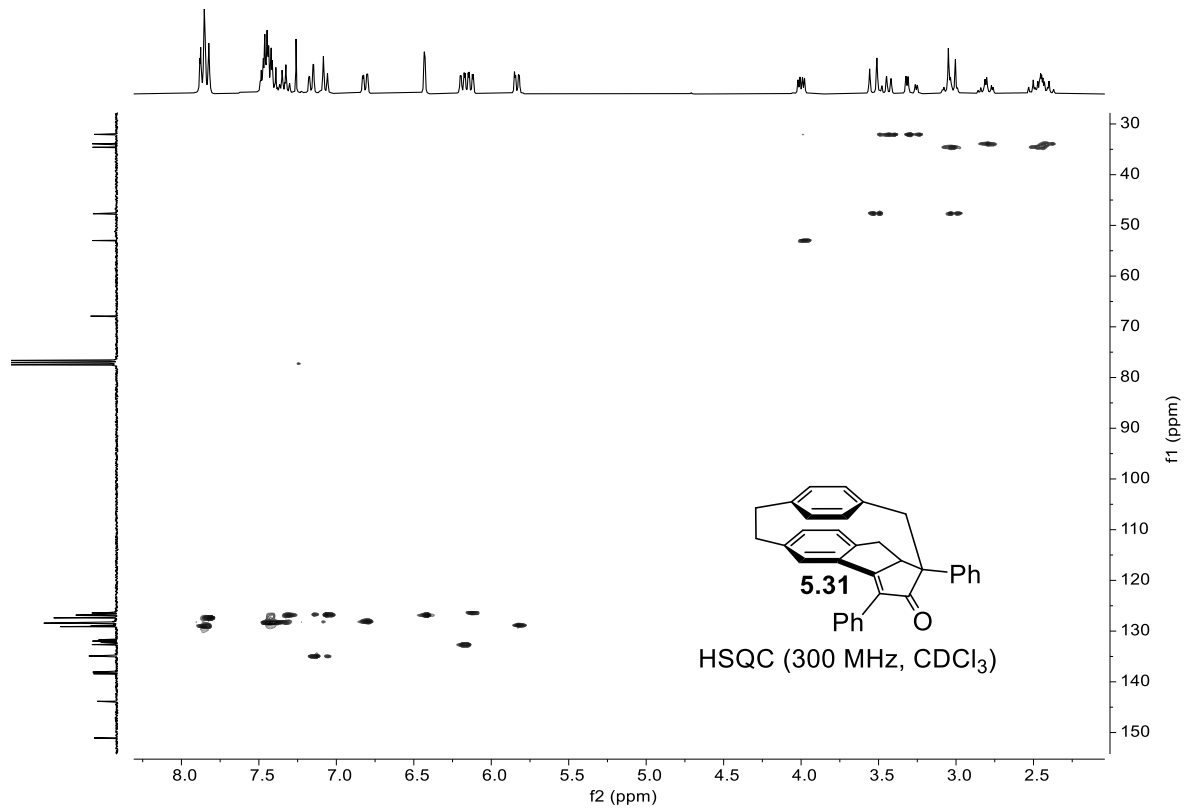
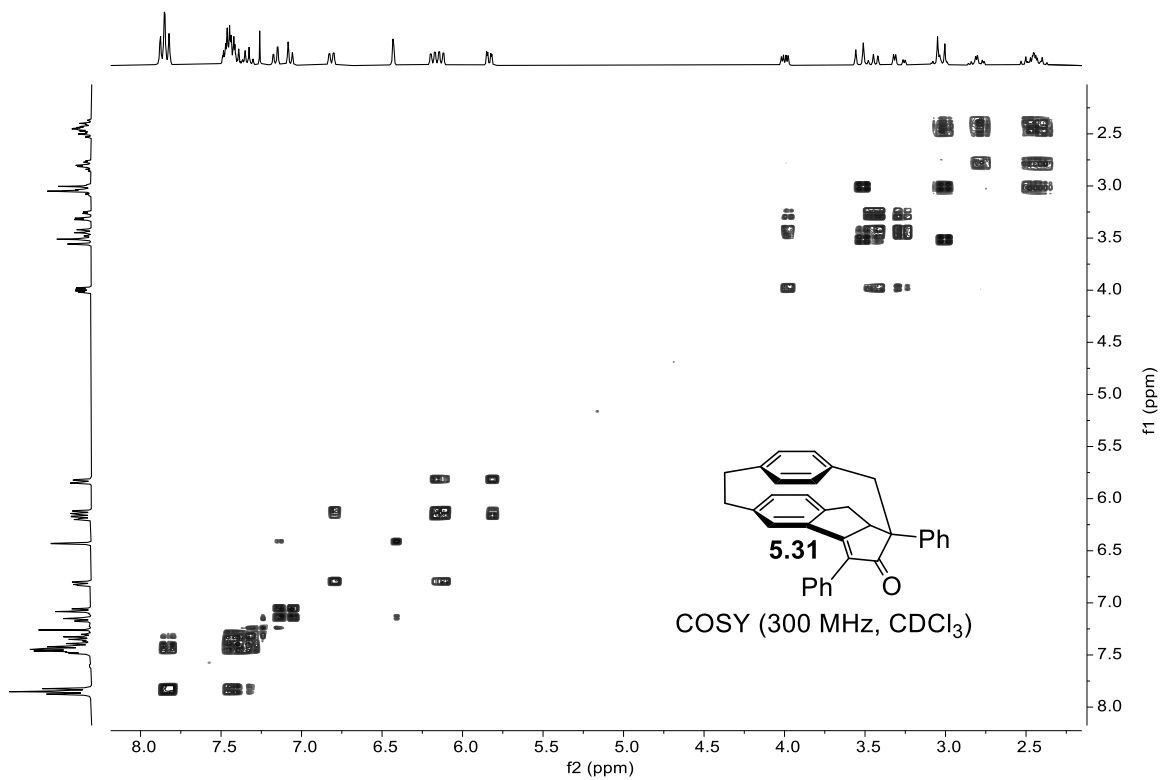




## 2. Two-Dimensional NMR Spectra







### 3. X-Ray Structure Details for Cyclophane 5.25

#### Crystallization Procedure:

#### Cyclophane 5.25

Crystals suitable for single crystal X-ray diffraction (XRD) were grown by vapor diffusion of methanol into a saturated solution of **5.25** in chloroform.

#### Experimental Details

Single-crystal X-ray diffraction data was collected at 100(2) K on a XtaLAB Synergy-S, Dualflex, HyPix-6000HE diffractometer using Cu  $K\alpha$  radiation ( $\lambda = 1.5406 \text{ \AA}$ ). Crystal was mounted on nylon CryoLoops with Paraton-N. The data collection and reduction were processed within *CrysAlisPro* (Rigaku OD, 2021). A multi-scan absorption correction was applied to the collected reflections. Using Olex2 [1], the structure was solved with the ShelXT [2] structure solution program using Intrinsic Phasing and refined with the ShelXL [3] refinement package using Least Squares minimisation. All non-hydrogen atoms were refined anisotropically. The organic hydrogen atoms were generated geometrically.

1. Dolomanov, O.V., Bourhis, L.J., Gildea, R.J, Howard, J.A.K. & Puschmann, H. (2009), *J. Appl. Cryst.* 42, 339-341.
2. Sheldrick, G.M. (2015). *Acta Cryst.* A71, 3-8.
3. Sheldrick, G.M. (2015). *Acta Cryst.* C71, 3-8.

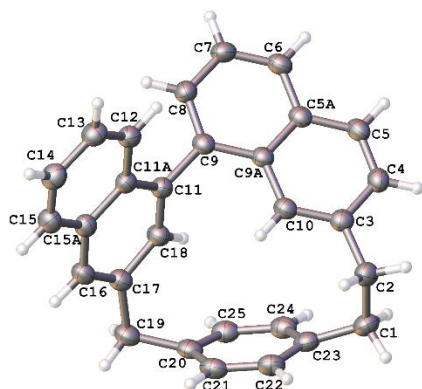


**Figure A4-1:** X-ray crystal structure of **5.25** (CCDC 2144507) (non-hydrogen atoms are represented by displacement ellipsoids at the 50% probability level).

**Table A4-1:** Crystal data and structure refinement for compound **5.25**

|   |  |
|---|--|
| Identification code                                 | SB-002-93  |
| Empirical formula                                   | C <sub>29</sub> H <sub>22</sub>  |
| Formula weight                                      | 370.46   |
| Temperature/K                                       | 100(2)   |
| Crystal system                                      | monoclinic   |
| Space group   | <i>P</i> <sub>2</sub> <sub>1</sub> / <i>n</i>                                |
| <i>a</i> /Å   | 10.5717(2)   |
| <i>b</i> /Å   | 10.9576(2)   |
| <i>c</i> /Å   | 16.7978(3)   |
| $\beta$ /°  | 102.383(2)   |
| Volume/Å <sup>3</sup>                               | 1900.60(6)   |
| <i>Z</i>  | 4  |
| $\rho_{\text{calc}}$ /cm <sup>3</sup>               | 1.295  |
| $\mu$ /mm <sup>-1</sup>                             | 0.552  |
| <i>F</i> (000)                                      | 784.0  |
| Crystal size/mm <sup>3</sup>                        | 0.129 × 0.112 × 0.065  |
| Radiation   | Cu <i>K</i> α ( $\lambda$ = 1.54184)   |
| 2 $\theta$ range for data collection/°              | 9.088 to 158.622   |
| Index ranges  | -13 ≤ <i>h</i> ≤ 12, -13 ≤ <i>k</i> ≤ 13, -21 ≤ <i>l</i> ≤ 20                |
| Reflections collected                               | 36938  |
| Independent reflections                             | 4077 [ <i>R</i> <sub>int</sub> = 0.0569, <i>R</i> <sub>sigma</sub> = 0.0278] |
| Data/restraints/parameters                          | 4077/0/262   |
| Goodness-of-fit on <i>F</i> <sup>2</sup>            | 1.093  |
| Final <i>R</i> indexes [ <i>I</i> ≥ 2σ( <i>I</i> )] | <i>R</i> <sub>1</sub> = 0.0424, <i>wR</i> <sub>2</sub> = 0.1206              |
| Final <i>R</i> indexes [all data]                   | <i>R</i> <sub>1</sub> = 0.0473, <i>wR</i> <sub>2</sub> = 0.1260              |
| Largest diff. peak/hole / e Å <sup>-3</sup>         | 0.29/-0.18   |

**Table A4-2:** Fractional atomic coordinates ( $\times 10^4$ ) and equivalent isotropic displacement parameters ( $\text{\AA}^2 \times 10^3$ ) for cyclophane **5.25**.  $U_{\text{eq}}$  is defined as 1/3 of the trace of the orthogonalised  $U_{ij}$  tensor.

| Atom | <i>x</i>    | <i>y</i>     | <i>z</i>   | $U(\text{eq})$ |
|------|-------------|--------------|------------|----------------|
| C1   | 7438.2 (14) | 3026.2 (14)  | 7863.1 (8) | 41.0 (3)       |
| C2   | 7449.3 (13) | 3729.0 (13)  | 7062.8 (8) | 39.2 (3)       |
| C3   | 6131.8 (12) | 3893.2 (12)  | 6504.6 (8) | 33.3 (3)       |
| C4   | 5701.4 (13) | 3041.5 (12)  | 5872.3 (8) | 36.3 (3)       |
| C5   | 4541.3 (13) | 3178.9 (12)  | 5336.3 (8) | 35.1 (3)       |
| C5A  | 3718.3 (12) | 4174.1 (11)  | 5398.6 (7) | 31.4 (3)       |
| C6   | 2526.9 (13) | 4335.3 (12)  | 4836.3 (8) | 35.9 (3)       |
| C7   | 1757.3 (13) | 5315.0 (13)  | 4904.2 (8) | 36.9 (3)       |
| C8   | 2126.2 (13) | 6157.4 (12)  | 5540.6 (8) | 34.4 (3)       |
| C9   | 3266.1 (12) | 6029.6 (11)  | 6115.1 (7) | 31.0 (3)       |
| C9A  | 4112.2 (12) | 5026.1 (11)  | 6045.6 (7) | 29.4 (3)       |
| C10  | 5341.9 (12) | 4863.2 (11)  | 6581.9 (7) | 31.5 (3)       |
| C11  | 3558.3 (12) | 6851.4 (11)  | 6841.6 (7) | 31.5 (3)       |
| C11A | 3789.1 (12) | 8130.4 (11)  | 6791.1 (7) | 31.3 (3)       |
| C12  | 3857.0 (12) | 8730.9 (12)  | 6051.5 (8) | 34.6 (3)       |
| C13  | 4099.2 (13) | 9956.9 (13)  | 6038.6 (9) | 38.7 (3)       |
| C14  | 4273.7 (14) | 10652.3 (13) | 6760.8 (9) | 40.4 (3)       |
| C15  | 4218.0 (13) | 10100.2 (13) | 7481.2 (9) | 38.4 (3)       |
| C15A | 3984.7 (12) | 8830.7 (12)  | 7521.4 (8) | 33.2 (3)       |
| C16  | 4002.3 (12) | 8249.2 (12)  | 8279.7 (8) | 35.2 (3)       |
| C17  | 3876.1 (12) | 7012.3 (12)  | 8327.5 (7) | 34.0 (3)       |
| C18  | 3611.0 (12) | 6338.6 (12)  | 7589.1 (7) | 33.6 (3)       |
| C19  | 4138.1 (14) | 6316.9 (13)  | 9129.8 (8) | 37.6 (3)       |
| C20  | 5096.6 (13) | 5322.5 (12)  | 9045.4 (7) | 34.6 (3)       |
| C21  | 6386.0 (13) | 5615.7 (13)  | 9064.8 (8) | 37.5 (3)       |
| C22  | 7173.6 (13) | 4827.4 (13)  | 8745.8 (8) | 38.0 (3)       |
| C23  | 6696.4 (13) | 3723.9 (13)  | 8388.1 (8) | 36.5 (3)       |
| C24  | 5450.7 (13) | 3382.3 (12)  | 8444.2 (8) | 36.7 (3)       |
| C25  | 4666.1 (13) | 4164.3 (12)  | 8773.9 (8) | 36.2 (3)       |

**Table A4-3:** Selected bond distances (Å) for cyclophane **5.25**.

| <b>Atom</b> | <b>Atom</b> | <b>Length/Å</b> | <b>Atom</b> | <b>Atom</b> | <b>Length/Å</b> |
|-------------|-------------|-----------------|-------------|-------------|-----------------|
| C1          | C2          | 1.5515 (19)     | C11A        | C12         | 1.4212 (17)     |
| C1          | C23         | 1.508 (2)       | C11A        | C15A        | 1.4240 (17)     |
| C2          | C3          | 1.5138 (18)     | C12         | C13         | 1.3686 (19)     |
| C3          | C4          | 1.4137 (19)     | C13         | C14         | 1.411 (2)       |
| C3          | C10         | 1.3749 (18)     | C14         | C15         | 1.365 (2)       |
| C4          | C5          | 1.3652 (19)     | C15         | C15A        | 1.4169 (19)     |
| C5          | C5A         | 1.4129 (18)     | C15A        | C16         | 1.4207 (18)     |
| C5A         | C6          | 1.4140 (18)     | C16         | C17         | 1.3660 (19)     |
| C5A         | C9A         | 1.4255 (17)     | C17         | C18         | 1.4188 (17)     |
| C6          | C7          | 1.3664 (19)     | C17         | C19         | 1.5210 (17)     |
| C7          | C8          | 1.4030 (19)     | C19         | C20         | 1.5152 (19)     |
| C8          | C9          | 1.3800 (18)     | C20         | C21         | 1.3940 (19)     |
| C9          | C9A         | 1.4379 (17)     | C20         | C25         | 1.3917 (19)     |
| C9          | C11         | 1.4945 (17)     | C21         | C22         | 1.385 (2)       |
| C9A         | C10         | 1.4252 (17)     | C22         | C23         | 1.3955 (19)     |
| C11         | C11A        | 1.4283 (18)     | C23         | C24         | 1.392 (2)       |
| C11         | C18         | 1.3658 (17)     | C24         | C25         | 1.388 (2)       |

**Table A4-4:** Selected bond angles for cyclophane **5.25**.

| <b>Atom</b> | <b>Atom</b> | <b>Atom</b> | <b>Angle/°</b> | <b>Atom</b> | <b>Atom</b> | <b>Atom</b> | <b>Angle/°</b> |
|-------------|-------------|-------------|----------------|-------------|-------------|-------------|----------------|
| C23         | C1          | C2          | 110.89 (11)    | C15A        | C11A        | C11         | 118.21 (11)    |
| C3          | C2          | C1          | 114.76 (11)    | C13         | C12         | C11A        | 120.86 (12)    |
| C4          | C3          | C2          | 119.47 (12)    | C12         | C13         | C14         | 120.46 (13)    |
| C10         | C3          | C2          | 122.02 (12)    | C15         | C14         | C13         | 120.01 (13)    |
| C10         | C3          | C4          | 118.50 (12)    | C14         | C15         | C15A        | 121.22 (13)    |
| C5          | C4          | C3          | 121.44 (12)    | C15         | C15A        | C11A        | 118.85 (12)    |
| C4          | C5          | C5A         | 121.10 (12)    | C15         | C15A        | C16         | 120.94 (12)    |
| C5          | C5A         | C6          | 121.43 (12)    | C16         | C15A        | C11A        | 120.15 (12)    |
| C5          | C5A         | C9A         | 118.57 (11)    | C17         | C16         | C15A        | 121.01 (12)    |
| C6          | C5A         | C9A         | 120.01 (11)    | C16         | C17         | C18         | 117.92 (12)    |
| C7          | C6          | C5A         | 120.23 (12)    | C16         | C17         | C19         | 123.21 (12)    |
| C6          | C7          | C8          | 120.48 (12)    | C18         | C17         | C19         | 118.57 (12)    |
| C9          | C8          | C7          | 121.63 (12)    | C11         | C18         | C17         | 123.45 (12)    |
| C8          | C9          | C9A         | 119.07 (11)    | C20         | C19         | C17         | 106.01 (10)    |
| C8          | C9          | C11         | 120.43 (11)    | C21         | C20         | C19         | 120.15 (12)    |
| C9A         | C9          | C11         | 120.25 (11)    | C25         | C20         | C19         | 120.54 (12)    |
| C5A         | C9A         | C9          | 118.54 (11)    | C25         | C20         | C21         | 117.86 (13)    |
| C10         | C9A         | C5A         | 118.53 (11)    | C22         | C21         | C20         | 120.88 (13)    |
| C10         | C9A         | C9          | 122.92 (11)    | C21         | C22         | C23         | 121.01 (13)    |
| C3          | C10         | C9A         | 121.82 (11)    | C22         | C23         | C1          | 120.39 (13)    |
| C11A        | C11         | C9          | 123.42 (11)    | C24         | C23         | C1          | 121.43 (13)    |
| C18         | C11         | C9          | 117.60 (11)    | C24         | C23         | C22         | 117.64 (13)    |
| C18         | C11         | C11A        | 118.98 (11)    | C25         | C24         | C23         | 121.08 (13)    |
| C12         | C11A        | C11         | 123.20 (12)    | C24         | C25         | C20         | 120.82 (12)    |
| C12         | C11A        | C15A        | 118.58 (12)    |             |             |             |                |

**Table A4-5:** Selected torsion angles for cyclophane **5.25**.

| <b>A</b> | <b>B</b> | <b>C</b> | <b>D</b> | <b>Angle/°</b> | <b>A</b> | <b>B</b> | <b>C</b> | <b>D</b> | <b>Angle/°</b> |
|----------|----------|----------|----------|----------------|----------|----------|----------|----------|----------------|
| C1       | C2       | C3       | C4       | -94.08 (15)    | C11      | C11A     | C12      | C13      | -179.06 (12)   |
| C1       | C2       | C3       | C10      | 87.19 (15)     | C11      | C11A     | C15A     | C15      | 179.84 (12)    |
| C1       | C23      | C24      | C25      | -165.51 (12)   | C11      | C11A     | C15A     | C16      | 2.66 (18)      |
| C2       | C1       | C23      | C22      | -67.64 (16)    | C11A     | C11      | C18      | C17      | 0.46 (19)      |
| C2       | C1       | C23      | C24      | 103.74 (15)    | C11A     | C12      | C13      | C14      | -0.6 (2)       |
| C2       | C3       | C4       | C5       | -177.55 (12)   | C11A     | C15A     | C16      | C17      | 2.16 (19)      |
| C2       | C3       | C10      | C9A      | 178.84 (11)    | C12      | C11A     | C15A     | C15      | 1.01 (18)      |
| C3       | C4       | C5       | C5A      | -0.7 (2)       | C12      | C11A     | C15A     | C16      | -176.17 (11)   |
| C4       | C3       | C10      | C9A      | 0.10 (18)      | C12      | C13      | C14      | C15      | 0.8 (2)        |
| C4       | C5       | C5A      | C6       | 178.77 (12)    | C13      | C14      | C15      | C15A     | -0.1 (2)       |
| C4       | C5       | C5A      | C9A      | -1.21 (19)     | C14      | C15      | C15A     | C11A     | -0.8 (2)       |
| C5       | C5A      | C6       | C7       | -179.12 (12)   | C14      | C15      | C15A     | C16      | 176.32 (12)    |
| C5       | C5A      | C9A      | C9       | -179.17 (11)   | C15      | C15A     | C16      | C17      | -174.95 (13)   |
| C5       | C5A      | C9A      | C10      | 2.44 (17)      | C15A     | C11A     | C12      | C13      | -0.29 (19)     |
| C5A      | C6       | C7       | C8       | -1.3 (2)       | C15A     | C16      | C17      | C18      | -5.53 (19)     |
| C5A      | C9A      | C10      | C3       | -1.92 (18)     | C15A     | C16      | C17      | C19      | 168.12 (12)    |
| C6       | C5A      | C9A      | C9       | 0.85 (17)      | C16      | C17      | C18      | C11      | 4.32 (19)      |
| C6       | C5A      | C9A      | C10      | -177.54 (11)   | C16      | C17      | C19      | C20      | -126.75 (13)   |
| C6       | C7       | C8       | C9       | 0.0 (2)        | C17      | C19      | C20      | C21      | 73.08 (14)     |
| C7       | C8       | C9       | C9A      | 1.75 (19)      | C17      | C19      | C20      | C25      | -92.89 (14)    |
| C7       | C8       | C9       | C11      | -172.56 (12)   | C18      | C11      | C11A     | C12      | 174.88 (11)    |
| C8       | C9       | C9A      | C5A      | -2.12 (17)     | C18      | C11      | C11A     | C15A     | -3.89 (18)     |
| C8       | C9       | C9A      | C10      | 176.20 (11)    | C18      | C17      | C19      | C20      | 46.86 (15)     |
| C8       | C9       | C11      | C11A     | -66.64 (17)    | C19      | C17      | C18      | C11      | -169.64 (12)   |
| C8       | C9       | C11      | C18      | 113.72 (14)    | C19      | C20      | C21      | C22      | -159.83 (12)   |
| C9       | C9A      | C10      | C3       | 179.76 (11)    | C19      | C20      | C25      | C24      | 158.88 (12)    |
| C9       | C11      | C11A     | C12      | -4.76 (19)     | C20      | C21      | C22      | C23      | 0.7 (2)        |
| C9       | C11      | C11A     | C15A     | 176.47 (11)    | C21      | C20      | C25      | C24      | -7.41 (18)     |
| C9       | C11      | C18      | C17      | -179.88 (12)   | C21      | C22      | C23      | C1       | 164.70 (12)    |
| C9A      | C5A      | C6       | C7       | 0.85 (19)      | C21      | C22      | C23      | C24      | -7.00 (19)     |
| C9A      | C9       | C11      | C11A     | 119.12 (13)    | C22      | C23      | C24      | C25      | 6.10 (19)      |
| C9A      | C9       | C11      | C18      | -60.52 (16)    | C23      | C1       | C2       | C3       | -63.98 (16)    |
| C10      | C3       | C4       | C5       | 1.23 (19)      | C23      | C24      | C25      | C20      | 1.11 (19)      |
| C11      | C9       | C9A      | C5A      | 172.20 (11)    | C25      | C20      | C21      | C22      | 6.51 (19)      |
| C11      | C9       | C9A      | C10      | -9.48 (18)     |          |          |          |          |                |